

Characterising the role of 6-O endosulfatases  
in zebrafish vascular development

**A thesis submitted to the University of Manchester for the degree  
of Doctor of philosophy in the Faculty of Medical and Human  
Sciences**

Bushra Gorski

School of Medicine  
University of Manchester

2009

ProQuest Number: U525624

All rights reserved

INFORMATION TO ALL USERS

The quality of this reproduction is dependent upon the quality of the copy submitted.

In the unlikely event that the author did not send a complete manuscript and there are missing pages, these will be noted. Also, if material had to be removed, a note will indicate the deletion.



ProQuest U525624

Published by ProQuest LLC (2019). Copyright of the Dissertation is held by the Author.

All rights reserved.

This work is protected against unauthorized copying under Title 17, United States Code  
Microform Edition © ProQuest LLC.

ProQuest LLC.  
789 East Eisenhower Parkway  
P.O. Box 1346  
Ann Arbor, MI 48106 – 1346

(EX8114)

THE  
LANDS  
PROPERTY  
OFFICE

\*  
T133466

✓

## Table of Contents

<b>Table of contents</b> .....	<b>1</b>
<b>List of Figures</b> .....	<b>6</b>
<b>List of Abbreviations</b> .....	<b>11</b>
<b>Nomenclature</b> .....	<b>14</b>
<b>Abstract</b> .....	<b>15</b>
<b>Declaration</b> .....	<b>16</b>
<b>Copyright</b> .....	<b>16</b>
<b>Acknowledgments</b> .....	<b>17</b>
<b>Chapter 1.0 : Introduction</b> .....	<b>18</b>
<b>1.0 Overview of vascular development</b> .....	<b>19</b>
1.0.1 Vasculogenesis.....	19
1.0.2 Arteriogenesis .....	19
1.0.3 Angiogenesis .....	20
<b>1.1 Therapeutic vasculature targets</b> .....	<b>22</b>
1.1.1 Therapeutic targets of angiogenesis .....	22
1.1.2 Pro angiogenic strategies.....	26
1.1.3 Antiangiogenic therapies.....	27
<b>1.2 Zebrafish as a model organism</b> .....	<b>29</b>
1.2.1 Zebrafish vascular development .....	29
1.2.1.1 Endothelial cell specification and migration.....	31
1.2.1.2 Vascular lumenisation and initiation of circulation .....	31
1.2.1.3 Functional secondary vessels formed by 60hpf .....	33
1.2.1.4 Vessel maintenance.....	37
1.2.2 Zebrafish vascular mutants .....	37
1.2.2.1 Mutants affecting vasculogenesis .....	38
1.2.2.2 Mutants affecting angiogenesis.....	39
1.2.3 Zebrafish as a therapeutic angiogenesis assay .....	40
<b>1.3 Heparan Sulphate Proteoglycans (HSPG)</b> .....	<b>41</b>
1.3.1 Glypicans .....	41
1.3.2 Syndecans.....	42
1.3.3 Perlecan, Agrin and Collagen XVIII.....	45
1.3.4 Role of HSPGs in the endothelium .....	46
1.3.5 Degradation of HSPGs.....	48
1.3.5.1 Endocytosis .....	48
1.3.5.2 Sheddases and Heparanases .....	49
<b>1.4 Heparin/HS binding proteins</b> .....	<b>51</b>
1.4.1 Fibroblast growth factors and receptors .....	51
1.4.1.1.FGFs and heparin/HS interactions .....	53
1.4.1.2 HS structural requirements.....	55
1.4.2 VEGF-A and family of VEGFR .....	56
1.4.2.1 Splice Variants of VEGF-A .....	59
1.4.2.2 Roles of VEGF165 in vascular development.....	62
1.4.2.3 Role of Heparin/HS in VEGF165 mediated angiogenesis.....	63
1.4.2.4 VEGF-VEGFR and HS/heparin interactions .....	64
1.4.3 Heparin/HS oligonucleotides as a therapeutic tool .....	66

<b>1.5 Heparin/HS Biosynthesis</b> .....	<b>67</b>
1.5.1 HS Chain initiation.....	68
1.5.2 Chain Modification .....	71
1.5.3 Epimerisation and 2-O Sulphation .....	72
1.5.4 6-O sulphation.....	74
1.5.5 3-O sulphation.....	75
<b>1.6 6-O endosulfatases (Sulfs)</b> .....	<b>77</b>
1.6.1 Sulf structure and activity .....	77
1.6.2.Molecular mechanism of sulfs .....	78
1.6.3 Role of sulfs during development .....	81
1.6.4 Sulfs in pathological diseases .....	82
1.6.5. 6-O sulphation – a specific code governed by the sulfatases.....	84
<b>1.7 Summary: Aims and Objectives</b> .....	<b>86</b>
<b>Chapter 2.0 Materials</b> .....	<b>87</b>
2.0.1: Purification of Bacterial cultures .....	87
2.0.2: Cloning and Transformation .....	87
2.0.3: PCR reactions.....	88
2.0.4: Agarose gel electrophoresis .....	88
2.0.5: Zebrafish care and maintenance.....	89
2.0.6: Whole mount in-situ hybridisation .....	90
2.0.7: Proliferation assay.....	92
2.0.8: Apoptosis assay.....	93
2.0.9: Imaging of the Zebrafish.....	93
2.0.10:Heparan sulphate extraction.....	93
2.0.11:HPLC Buffers/Solutions .....	94
<b>2.1 Methods</b> .....	<b>95</b>
<b>2.1: Expression and purification of plasmid DNA</b> .....	<b>95</b>
2.1.1: Overnight cultures.....	95
2.1.2: Mini/Midi purification of Plasmid DNA .....	95
2.1.3: Purification of DNA from Agarose slice .....	96
2.1.4: Purification of DNA from enzyme based reactions.....	96
2.1.5: Phenol/Chloroform Extraction.....	96
2.1.6:Ethanol Precipitation.....	96
<b>2.2: Cloning and Transformation</b> .....	<b>97</b>
2.2.1: Producing Agar plates.....	97
2.2.2: Restriction Digests .....	97
2.2.3: Ligation .....	97
2.2.4: PET TOPO <sup>®</sup> Cloning .....	98
2.2.5: Transformation using CaCl <sub>2</sub> treated competent cells.....	98
2.2.6: Analysis of <i>E. coli</i> Transformants.....	98
<b>2.3: Polymerase Chain Reaction</b> .....	<b>98</b>
2.3.1 Primer design for PCR .....	98
2.3.2: Standard PCR.....	99
2.3.3 Long range PCR.....	100
2.3.4: DNA sequencing.....	101
<b>2.4: Preparation and Running agarose gels</b> .....	<b>101</b>
2.4.1 Agarose gel electrophoresis .....	101
<b>2.5: Zebrafish Care and Experimental methods</b> .....	<b>101</b>
2.5.1: Zebrafish care and staging .....	101

2.5.2: Marbling and Collection of Zebrafish embryos.....	102
2.5.3: Preparing microinjection plates- Agarose chambers .....	102
2.5.4: Preparation of morpholinos.....	101
2.5.5: Microinjecting Zebrafish embryos.....	102
2.5.6: Dechorination of Zebrafish embryos .....	103
2.5.7: Microangiography.....	103
2.5.8: DNA extraction from Zebrafish embryos .....	103
2.5.9 Total RNA extraction from zebrafish embryos.....	104
2.5.10: cDNA synthesis .....	104
<b>2.6: Whole mount in situ hybridisation (WISH).....</b>	<b>105</b>
2.6.1 Transcription of DIG-labelled riboprobes.....	104
2.6.2: Fixing Embryos.....	105
2.6.3: Hybridisation.....	105
2.6.4: Post hybridisation washes and preabsorption of antibody .....	106
2.6.5: Removal of Antibody.....	106
2.6.6: Staining and Detection.....	106
<b>2.7: Proliferation assay .....</b>	<b>107</b>
<b>2.8: Apoptosis Assay .....</b>	<b>107</b>
<b>2.9 Imaging of the zebrafish vasculature .....</b>	<b>108</b>
2.9.1: Mounting of embryos.....	108
2.9.2 Confocal imaging.....	108
2.9.3 Widefield imaging.....	109
<b>2.10: Heparan sulphate (HS) extraction and purification.....</b>	<b>109</b>
2.10.1: Degradation of embryos.....	109
2.10.2: Separation and partial purification of HS.....	109
2.10.3: Desalting and digestion of HS.....	109
<b>2.11: SAX High performance liquid chromatography(HPLC).....</b>	<b>110</b>
2.11.1: Loading HS standards and samples.....	110
 <b>Chapter 3: Paper one.....</b>	 <b>111</b>
 <b>Chapter 4.0: Morpholino Knockdown of <i>sulf1c</i> in zebrafish .....</b>	 <b>142</b>
<b>4.1 Introduction.....</b>	<b>142</b>
<b>4.2 Materials and methods .....</b>	<b>144</b>
4.2.1 Morpholino oligonucleotide.....	144
4.2.2 PCR amplification of morpholino target sites.....	147
4.2.3 Preparation and HS Disaccharide analysis of <i>sulf1c</i> morphants.....	147
4.2.4 Analysing the affect of S1c-SBMO on <i>sulf1c</i> transcript.....	148
<b>4.3 Results .....</b>	<b>150</b>
4.3.1 Analysis of HS disaccharide content.....	150
4.3.2 Analysis of S1c-ATGMO injected embryos .....	150
4.3.3 <i>Sulf1c</i> morphants display vascular related morphological defects .....	158
4.3.4 S1c-SBMO affects splicing of <i>sulf1c</i> transcript.....	161
4.3.5 S1c-SBMO morphants exhibit morphological and vascular defects similar to S1c- .....ATG morphants.....	166
4.3.6 Characteristic phenotype of <i>sulf1c</i> morphant has a higher penetrance..... .....in <i>flk</i> :GFP; <i>gata</i> :dsRed line .....	171
4.3.7 Analysis of the <i>sulf1c</i> MO sites .....	173
4.3.8 Injection of <i>sulf1c</i> mRNA partially rescues morphological and..... circulatory phenotype	173

4.3.9 <i>Sulf1c</i> morphants reproducible in p53 <sup>-/-</sup> fish.....	179
<b>4.4 Discussion.....</b>	<b>183</b>
4.4.1 S1c-ATGMO can modify 6-O sulphation levels of the tri-sulfated disaccharide.....	183
4.4.2 S1c-SBMO reduces the expression of the <i>sulf1c</i> wildtype transcript.....	184
4.4.3 S1c-ATGMO and SBMO show consistent phenotypes.....	185
4.4.4 The ATGMO specifically knocks-down <i>sulf1c</i> .....	187
4.4.5 The characteristic features of <i>sulf1c</i> morphants can be partially rescued.....	188
4.4.6 <i>Sulf1c</i> morphant phenotype in comparison to other species.....	190
<b>Chapter 5.0: Paper two.....</b>	<b>193</b>
<b>Chapter 6.0: Continuing the characterisation of <i>sulf1c</i> morphant.....</b>	<b>238</b>
<b>6.1 Introduction.....</b>	<b>238</b>
<b>6.2 Materials and methods.....</b>	<b>239</b>
6.2.1 Proliferation assay.....	239
6.2.2 VEGF165 assay.....	239
6.2.3 Creating I-Sce1 hsp70: <i>VEGF165</i> construct.....	242
6.2.4 Microinjection of <i>I-Sce1</i> construct.....	243
<b>6.3 Results.....</b>	<b>244</b>
6.3.1 <i>Sulf1c</i> morphants display an decrease in cell proliferation in the tail plexus.....	244
6.3.1.2 Discussion.....	247
6.3.2 Creating a VEGF assay.....	249
6.3.3 Ectopic <i>VEGF</i> results in outgrowth of vessels.....	249
6.3.4 Number of Ectopic <i>VEGF</i> sites in mild and moderate class embryo.....	259
6.3.5 Testing the HSP70: <i>VEGF</i> construct in <i>fli1</i> :GFP; <i>gata</i> :ds-Red line.....	263
6.3.6 Analysis of the HSP70: <i>VEGF</i> injected samples reveal mild <i>VEGF</i> overexpression phenotype.....	267
<b>6.4 Discussion.....</b>	<b>268</b>
6.4.1 Microinjection of <i>VEGF</i> plasmid induces phenotypes that are hallmarks of <i>VEGF</i> activity.....	269
<b>Chapter 7.0: Morpholino mediated knockdown of <i>sulf2a</i> and <i>sulf2</i>.....</b>	<b>272</b>
<b>7.1 Introduction.....</b>	<b>272</b>
<b>7.2 Materials and methods.....</b>	<b>274</b>
7.2.1 Morpholino oligonucleotides.....	274
7.2.2 Amplifying the morpholino target sites of <i>sulf2a</i> and <i>sulf2</i> .....	274
7.2.3 RT-PCR analysis of <i>sulf2a</i> and <i>sulf2</i> morphants.....	275
7.2.4 Preparation and HS Disaccharide analysis of <i>sulf2a</i> and <i>sulf2</i> morphants.....	275
<b>7.3 Results.....</b>	<b>278</b>
7.3.1 <i>Sulf2a</i> and <i>sulf2</i> SBMO reduces the level of their respective transcript.....	278
7.3.2 HS Disaccharide analysis of <i>sulf2a</i> and <i>sulf2</i> SBMO injected embryos.....	281
7.3.3 Analysis of S2a-SBMO injected embryos.....	282
7.3.4 Analysis of S2-SBMO injected embryos.....	294
7.3.5 Analysis of ATGMO mediated knockdown of <i>sulf2a</i> and <i>sulf2</i> .....	300
7.3.6 HS Disaccharide analysis of <i>sulf2a</i> and <i>sulf2</i> TBMO injected embryos.....	302
<b>7.4 Discussion.....</b>	<b>308</b>
7.4.1 SBMO can reduce the expression of the wildtype <i>sulf2a</i> and <i>sulf2</i> transcript.....	308
7.4.2 HS disaccharide and phenotype analysis of <i>sulf2a</i> SBMO morphants.....	308
7.4.3 HS disaccharide and phenotype analysis of <i>sulf2</i> SBMO morphants.....	310
7.4.4 True morphant phenotypes v <sub>s</sub> off-target affects.....	311

7.5.5 Future work .....	312
<b>Chapter 8.0 Conclusions.....</b>	<b>313</b>
8.1 Three sulfatases are differentially expressed during zebrafish development.....	313
8.2 Sulfatases have different roles during vascular development.....	313
8.3 Potential cell signalling pathways affected during vascular development in <i>sulf1c</i> morphants.....	314
8.4 Microarray analysis of <i>sulf1/2<sup>-/-</sup></i> embryos .....	316
8.5 Summary .....	317
<b>Chapter 9.0 Appendices.....</b>	<b>318</b>
Appendix I.....	319
Appendix II.....	320
Appendix III.....	321
Appendix IV.....	322
Appendix V.....	323
Appendix VI:.....	324
<b>Chapter 10.0 References.....</b>	<b>330</b>

**Word count-81,001**

## List of Figures

<b>Figure 1.0</b>	An illustration of the angiogenic process	21
<b>Figure 1.1</b>	A partial list of pro-angiogenic and anti-angiogenic factors	23
<b>Figure 1.2</b>	Zebrafish embryos during larval and adult stages	30
<b>Figure 1.3</b>	Signalling molecules required for the formation of embryonic vasculature development	32
<b>Figure 1.4</b>	Vascular development in <i>Fli1</i> :GFP zebrafish embryo	34
<b>Figure 1.5</b>	Functional circulation during zebrafish embryonic development	36
<b>Figure 1.6</b>	Schematic representation of the structures of cell surface and extracellular matrix HSPGs	44
<b>Figure 1.7</b>	Heparin/HS disaccharide structure of a HS chain.	52
<b>Figure 1.8</b>	Crystallographic FGF-FGFR-heparin models	54
<b>Figure 1.9</b>	Schematic representation of VEGF family of growth factors and VEGF receptors	58
<b>Figure 1.10</b>	Alternative splice variants of human VEGF-A gene	61
<b>Figure 1.11</b>	Molecular modelling of a potential heparin disaccharide docked with the VEGF165 heparin binding domain	65
<b>Figure 1.12</b>	A partial list of mutants defective for HS biosynthesis enzyme in different species	69
<b>Figure 1.13</b>	A schematic representation of the enzymes involved in the biosynthesis of Heparin/Heparan sulphate	73
<b>Figure 1.14</b>	A schematic representation of the role of sulfs in modulating HS binding proteins	80
<b>Figure 4.0</b>	A schematic representation of the <i>sulf1c</i> pre-mRNA showing the targeting sites of three <i>sulf1c</i> antisense morpholino	146
<b>Figure 4.1</b>	Picture showing the approximate microinjection target area in yolk of zebrafish embryo at 1 cell stage	146

<b>Figure 4.2</b>	A schematic representation of cleavage sites of three heparan sulphate degrading enzymes	148
<b>Figure 4.3</b>	Heparan sulphate profiling of <i>sulflc</i> ATGMO morphant embryos	151
<b>Figure 4.4</b>	Chart showing the analysis of <i>flil:gata</i> embryos injected with different doses of S1c-ATG Morpholino (MO).	154
<b>Figure 4.5</b>	Brightfield Images of 48hpf embryos classed as non-specific phenotypes	155
<b>Figure 4.6</b>	Defects exhibited by the mild class of <i>sulflc</i> morphant at 28hpf	156
<b>Figure 4.7</b>	Defects exhibited by mild class <i>sulflc</i> morphant at 48hpf.	157
<b>Figure 4.8</b>	Defects exhibited by the moderate class of the <i>sulflc</i> morphant at 1dpf and 2dpf.	160
<b>Figure 4.9</b>	A schematic representation of the possible outcomes of <i>sulflc</i> mRNA transcript by targeting with S1c-SBMO and the position of the primers used in RT-PCR analysis	162
<b>Figure 4.10</b>	RT-PCR analysis at 24hpf to determine the affect of S1c-SBMO on the <i>sulflc</i> pre-mRNA	163
<b>Figure 4.11</b>	Sequence chromatograms of the intron and exon boundaries of the <i>sulflc</i> transcript	164
<b>Figure 4.12</b>	RT-PCR analysis to determine the affect of S1c-SBMO on the <i>sulflc</i> pre-mRNA at later stage during development.	165
<b>Figure 4.13</b>	Chart showing the analysis of <i>flil:gata</i> embryos injected with different doses of S1c-SBMO.	167
<b>Figure 4.14</b>	Defects exhibited by the mild and moderate class of the S1c-SBMO injected embryos	169
<b>Figure 4.15</b>	Chart showing the analysis of <i>flkl:gata</i> embryos injected with S1c-ATGMO.	170
<b>Figure 4.16</b>	Comparison of the S1c-ATGMO injected samples in <i>flil:gata</i> and <i>flkl:gata</i> embryos.	172

<b>Figure 4.17</b>	Sequence chromatograms of the <i>sulf1c</i> morpholino target sites in the different transgenic lines	174
<b>Figure 4.18</b>	Frequencies (%) of the morphological defects of the <i>sulf1c</i> morphants and partial rescue of the mild morphant.	177
<b>Figure 4.19</b>	Graphical depiction of the percentage of axial circulatory defects of the <i>sulf1c</i> morphants and partial rescue of the axial circulation in <i>sulf1c</i> morphants.	179
<b>Figure 4.20</b>	Graphical depiction of cranial circulatory defects of the <i>sulf1c</i> morphants and partial rescue of the cranial circulation in <i>sulf1c</i> morphants.	180
<b>Figure 6.0</b>	Tail vascular defects in <i>sulf1c</i> characteristic morphant	240
<b>Figure 6.1</b>	Anti-phosphohistone H3 (pH3) antibody staining of proliferative cells in tail of 48hpf control injected embryos and <i>sulf1c</i> morphant.	241
<b>Figure 6.2</b>	Region of proliferative cells quantified in control injected and <i>sulf1c</i> characteristic morphant.	245
<b>Figure 6.3</b>	Quantification of the number of proliferating cells in the caudal plexus of control injected and <i>sulf1c</i> characteristic morphant	246
<b>Figure 6.4</b>	A schematic diagram of the frm constructs co-injected at one cell stage and the phenotype at 48hpf	250
<b>Figure 6.5</b>	Chart showing the analysis of <i>fli1</i> :GFP embryos injected with frm: <i>VEGF</i> plasmid.	252
<b>Figure 6.6</b>	Vascular phenotypes observed in mild class of 3dpf embryos injected with frm: <i>VEGF</i> plasmid.	254
<b>Figure 6.7</b>	Vascular phenotypes observed in moderate class of 3dpf embryos injected with Frm: <i>VEGF</i> plasmid	257
<b>Figure 6.8</b>	Vascular phenotypes observed in severe class of 3dpf embryos injected with Frm: <i>VEGF</i> plasmid	260
<b>Figure 6.9</b>	Frequencies (%) of mild and moderate phenotype class following ectopic <i>VEGF</i> expression	263
<b>Figure 6.10</b>	A schematic representation of the functional consequences of the <i>I-SceI</i> meganuclease	265

<b>Figure 6.11</b>	Tg( <i>fli1</i> :GFP; <i>gata</i> :dsRed) embryos co-injected with HSP70:cherry and HSP70: <i>VEGF</i> display mild phenotypes characteristic of ectopic <i>VEGF</i>	266
<b>Figure 7.0</b>	Sequence chromatograms showing the <i>sulf2a</i> and <i>sulf2</i> SBMO target site	276
<b>Figure 7.1</b>	A schematic representation of the possible outcomes of <i>sulf2a</i> and <i>sulf2</i> mRNA transcript by targeting of the <i>sulf2a</i> & <i>sulf2</i> -SBMO	277
<b>Figure 7.2</b>	RT-PCR analysis at 24hpf to determine the affect of S2a-SBMO on the <i>sulf2a</i> pre-mRNA	279
<b>Figure 7.3</b>	RT-PCR analysis at 24hpf to determine the affect of S2-SBMO on the <i>sulf2</i> pre-mRNA.	280
<b>Figure 7.4</b>	Heparan sulphate profiling of <i>sulf2a</i> SBMO morphant embryos	283
<b>Figure 7.5</b>	Heparan sulphate profiling of <i>sulf2</i> SBMO morphant embryos.	285
<b>Figure 7.6</b>	Chart showing the analysis of the <i>fli1</i> :GFP embryos injected with different doses of <i>sulf2a</i> morpholino	288
<b>Figure 7.7</b>	Brightfield images of non-specific phenotypes	289
<b>Figure 7.8</b>	Morphological and vascular defects exhibited by the mild class <i>sulf2a</i> morphants	291
<b>Figure 7.9</b>	Morphological and vascular defects exhibited by the moderate class <i>sulf2a</i> morphants	292
<b>Figure 7.10</b>	Chart showing the analysis of the <i>fli1</i> :GFP embryos injected with different doses of <i>sulf2</i> morpholino	295
<b>Figure 7.11</b>	Morphological defects exhibited by mild class <i>sulf2</i> morphants	296
<b>Figure 7.12</b>	Vascular defects exhibited by the <i>sulf2</i> mild class morphants.	297
<b>Figure 7.13</b>	Morphological and vascular defects exhibited by the <i>sulf2</i> moderate class morphants.	299
<b>Figure 7.14</b>	Heparan sulphate profiling of <i>sulf2a</i> ATGMO morphant embryos	304

<b>Figure 7.15</b>	Heparan sulphate profiling of <i>sulf2</i> ATGMO morphant embryos	306
<b>Figure 8.0</b>	Comparison of HS disaccharide profiling of sulf morphants	315

## List of Abbreviations

°C	Degree Celsius, Temperature
µl	Micro litres
+ve	Positive.
-ve	Negative
3'	Three prime end of DNA sequence
5'	Five Prime end of DNA sequence
A	Adenine
AA	Aortic arches
AMP	Ampere, electrical current
Ang-1	Angiopoietin-1
Approx	Approximate.
ATGMO	ATG codon targeting morpholino
AV	Arterious venous
BA	Basilar artery
BCA	Basilar communicating artery
bp	Base Pair
BMP	Bone morphogenetic protein
C	Cytosine
CA	Caudal artery
CCtA	Cerebellar central arteries
CCV	Common cardinal vein
CtA	Central arteries
CMO	Control morpholino
CV	Caudal vein
Cy5	Cyanine 5
DA	Dorsal Aorta
dATP	Deoxyadenosine triphosphate
dCTP	Deoxycytosine, triphosphate
dGTP	Deoxyguanine triphosphate
dH <sub>2</sub> O	Distilled and sterile water
Di	Diencenphalon

DLAV	Dorsal longitudinal anastomotic vessels
dTTP	Deoxythymidine triphosphate
EDTA	Ethylenediamine tetracetic acid.
EphB2a	Ephrin B2
EphB4	Ephrin B4
EtBr	Ethidium bromide.
eGFP	enhanced green fluorescent protein
FB	Forebrain
FGF	Fibroblast growth factor
Flk	Friendly leukaemia integrated factor
g	Grams
G	Guanine
HCL	H hydrochloric acid
HPLC	High performance liquid chromatography
Hrs	Hours
HS6STs	6-O sulphotransferases
HS3STs	3-O sulphotransferases
HS2STs	2-O sulphotransferases
HS	Heparan sulphate
HSPGs	Heparan sulphate proteoglycans
Hpf	Hours post fertilisation
ISV	Intersegmental vessels
kb	Kilo base
kDa	Kilo Dalton
LDA	Lateral dorsal aortae
MCeV	Mesencephalic vein
Min(s)	Minutes
mM	Millimolar.
MO	Morpholino oligonucleotide
mRNA	Messenger ribonucleic acid
NDSTs	N-deactylase sulphotransferase
OT	Otic vesicle
OV	Optic vein

PBS	Phosphate buffered saline
PCR	Polymerase chain reaction
PCV	Posterior cardinal vein
PDGF	Platelet derived growth factor
PFA	Paraformaldehyde
PHBC	Primordial hindbrain channel
PMBC	Primordial midbrain channel
Pmol	Picomole
PTU	Phenylthiourea
rpm	Revolutions per minute
RT-PCR	Reverse transcriptase polymerase chain reaction
SBMO	Splice-blocking morpholino
SDS	Sodium dodecyl sulphate
Sec(s)	Seconds
Shh	Sonic hedgehog
SIV	Subintestinal basket
Sulf	Sulfatases
T	Thymine
TdT	Terminal deoxynucleotidyl transferase
Te	Telencephalon
Tie-2	Tyrosine Kinase receptor
Tris	Tris-2-amino-2 (hydroxymethyl)-1,3- propanediol.
TUNEL	Terminal deoxynucleotidyl transferase-mediated dUTP nick end labelling
U	Uracil
UMBSF	University of Manchester Biological Services Facility
UTR	Untranslated region
UV	Ultra-violet.
Ve-cad	Ve-cadherin
VEGF	Vascular endothelial growth factor
VEGFR	Vascular endothelial growth factor receptor

## Nomenclature

Standard genetic nomenclature was used throughout this thesis (<http://www.genenames.org/guidelines.html>; [http://zfin.org/zf\\_info/nomen.html](http://zfin.org/zf_info/nomen.html); <http://www.informatics.jax.org/mgihome/nomen/gene.shtml>). When referring to a gene, the gene name is italicised. When referring to a protein, the protein name is not italicised. Human genes and proteins are presented in upper case. Mouse and zebrafish genes and proteins are written in lower case except for the first letter which is a capital letter. When referring to the same gene or protein in a number of species, standard nomenclature for the first species in the list will be used, for example, “sulf in human and mouse”, uses the human nomenclature.

## Abstract

Angiogenesis, the formation of blood vessels from pre-existing vasculature, is an important natural process. Dysregulation of this process leads to numerous disorders and disease states including tumour growth and cardiovascular diseases. One of the major targets for therapy are the growth factors. Research to date has shown several growth factors to require heparan sulphate proteoglycans (HSPGs) as co-receptors for efficient signalling. HSPGs are composed of core protein and heparan sulphate chains (HS). Variations in the size and 6-O sulphation of the HS chains are found to be important for this interaction. HS is a polysaccharide chain that undergoes a series of modifications including C5 epimerisation, N-sulphation, 2-O,6-O and 3-O sulphation. Recently it has been shown HS is further modified at the cell surface by action of 6-O endosulfatases (Sulfs). Sulfs are responsible for removing 6-O sulphate groups from the HS chain, and thereby exert the final control on the level of 6-O sulphation on HS chain. In pathological disease states sulfs modulate tumour growth partly through attenuating growth factors such as VEGF. To fully exploit the therapeutic potential of 6-O endosulfatases in diseases requires the knowledge of sulf function during physiological vascular development. In the current study, characterisation of the three *sulf* transcripts in zebrafish revealed that the sulf predicted proteins are highly conserved when compared to the human and mouse orthologs. Analysis of *Sulfs* expression in zebrafish revealed that the spatial and temporal expression patterns of sulfs are also highly conserved, with *sulf1*, *sulf2a* and *sulf2* expression in the developing vasculature suggesting an *in-vivo* requirement of the *sulfs* during vascular development. Morpholino antisense oligonucleotide mediated knockdown of *sulf1c* in zebrafish induced mild morphological abnormalities associated with cranial and tail vascular defects. Analysis of these morphants by live confocal imaging and whole mount *in-situ* of vascular markers revealed loss of arterial identity and vascular integrity of central arteries. Furthermore HS disaccharide analysis of *sulf1c* morphants conclusively showed an increase in the 6-O sulphated tri-sulfated disaccharides. This indicated a novel role of *sulf1c* in vasculogenesis and angiogenesis *in vivo*. Individual morpholino mediated knockdown of *sulf2a* and *sulf2* revealed defects in intersegmental vessel formation that coincided with defects in notochord shape and chevron shaped somites. The low penetrance of this phenotype with the second set of morpholinos suggests *sulf2a* and *sulf2* may have an indirect affect on the vasculature, and warrants further investigation. The ability to rescue the *sulf1c* phenotype suggests that *sulf1c* has an important role during vascular development that could be further exploited for treatment in vascular related diseases

## **Declaration**

No portion of the work referred to in this thesis has been submitted in support of an application for another degree or qualification of this or any other university or institute of learning.

Bushra Gorski

## **Copyright**

Copyright in text of this thesis rests with the Author. Copies (by any process) either in full, or of extracts, may be made only in accordance with instructions given by the Author and lodged in the John Rylands University Library of Manchester. Details may be obtained from the Librarian. This page must form part of any such copies made. Further copies (by any process) of copies made in accordance with such instructions may not be made without the permission (in writing) of the Author.

The ownership of any intellectual property rights which may be described in this thesis is vested in the University of Manchester, subject to any prior agreement to the contrary, and may not be made available for use by third parties without the written permission of the University, which will prescribe the terms and conditions of any such agreement.

Further information on the conditions under which such disclosures and exploitation may take place is available from the Head of the School of Medicine

## Acknowledgments

Firstly I would like to thank my supervisor Dr Sally Stringer for her patience and support throughout the project especially during those experimental disasters, the writing up period, and for the hours spent reading my thesis. I am also very grateful to Prof Roger patient's lab (University of Oxford) particularly Dr Feng Lui for being a great mentor for the confocal and *in-situ* work, it was a difficult but enjoyable month! I would like to extend my thanks to members of the Stringer lab for their support and helpful advice given during my project namely Andrew Hamilton and Helen Bischof. Also to my colleagues in the division Imogen Butcher and Kate Williamson for their moral support.

I am grateful to the zebrafish community at Manchester namely Dr Kelly Rooney for her useful advice throughout my project, Dr's Adam Hurlstone and Paul Walker for their help with transgenic fish work and use of equipment, and Dr Irene Ramirez for reagents and advice on the proliferation assay. The BSU staff for taking care of our fish, particularly Robert Hallworth for always being helpful and willing to set up 'weekend' fish.

My thanks also go to my advisers Prof's Paul Brenchley and John Gallagher for helpful comments and funding some of the confocal work carried out at the University of Manchester. The staff at confocal suite core facility for their helpful training and answering all my 'Intellectual' questions,

Lastly but by no means least I would like to thank my extended family, particularly my beloved parents for their belief, encouragement and their financial support over the last year despite the economic crisis! Also to my eight wonderful siblings (The Gorski tribe; Mehnaz, Ikhtlaq, Fara, Summernaz, Ashfaq, Amber, Sairah and Sameer) for sharing their 'scientific' anecdotes and imparting their wise words of wisdom.

## Chapter 1.0 Introduction

In all vertebrates the existence of a mature functional vasculature network is fundamental to their survival. The three major processes by which blood vessels are formed and remodelled are vasculogenesis, angiogenesis and arteriogenesis. The development of an elaborate vasculature network and circulatory pathway is regulated by cross talk between a number of signalling pathways including Wnt, Hh, FGF, BMP-4 and VEGF. The fine balance between stimulatory and inhibitory signals is critical to these physiological vasculature processes. However perturbation in the balance of pro-angiogenic versus anti-angiogenic factors contributes to a number of pathological vasculature disease states such as metastasising cancer, cardiovascular and neurological diseases. Although many growth factors have been targeted therapeutically not all have had their anticipated success.

Alternative strategies to discover novel molecules and signalling pathways are always of immense clinical interest. Over recent years the zebrafish has become a highly attractive model for studying vasculature development, the ease of genetic manipulation of the zebrafish genome has led to a number of vascular mutants that has given further novel insights into the molecular basis of vascular development. Critical to all vertebrates is the activity of VEGF, aside from its role in endothelial cell proliferation, migration, survival and vascular permeability, studies in zebrafish have revealed VEGF has an essential role in arterial-venous differentiation. VEGF is one of the major therapeutic targets in both pro and antiangiogenic strategies and continuous attempts to unravel novel targets, essential to VEGF signalling pathway have been successful but not translated well clinically.

In the last 10 years it has become increasingly evident that heparan sulphate proteoglycans (HSPGs) are indispensable to the activity of many signalling molecules including VEGF. The defects exhibited by HS mutants are testimony to their significance in regulating many developmental processes including vascular development. Heparan sulphate (HS) is linear polysaccharide synthesised by a concerted action of multiple enzymes that delineate a highly specific HS sequence. In particular enzymes regulating the sulphation pattern of HS i.e. 6-O endosulfatases are critical for HSPGs mediated interactions. Several *in-vitro* reports have provided direct evidence of sulfatases in modulating VEGF and FGF mediated including endothelial cell proliferation and migration. Consistent with these ideas the sulfs can contribute to pathological angiogenesis in several disease states. Although the *in-vivo* role of the sulfs in vascular development has not yet been investigated their ability to modulate many

signalling molecules critical to vascular development yields exciting possibilities of being potential therapeutic targets.

## **1.0 Overview of vascular development**

### **1.0.1 Vasculogenesis**

Important to the development of a functioning vertebrate vasculature network are the three processes vasculogenesis, angiogenesis and arteriogenesis. Vasculogenesis is the formation of new blood vessels and is triggered by specification of the angioblast from the haemangioblast. Signals from markers shared by the haemopoietic cell fate such as *flk-1*, *tie-2* are important in differentiation of endothelial cells (EC) from endothelial cell progenitors (EPC) <sup>1</sup>. One of the early stages in vascular development is the distinction between arteries and veins, although there is ambiguity in how early this specification event occurs, genetic studies in zebrafish have shown the important role of Sonic hedgehog (Shh), signalling pathway in arterial determination <sup>2</sup>. The migration and proliferation of EC from the angioblast to the site of blood vessel growth, is dependent on a vast number of signals from growth factors including vascular endothelial growth factor (VEGF), angiopoietin (Ang-1), and inhibitors of differentiation (Id) EC coalesce to form the initial vascular plexus <sup>1</sup>. Further remodelling requires the formation of arterial and venous boundaries that are established by the Eph-Ephrin system, where EphrinB2 is expressed on arterial cells and smooth muscle cells and EphrinB4 is expressed on venous <sup>3-5</sup>. Finally the primitive vascular plexus is stabilised by interactions of endothelial cells with smooth muscle cells (SMC) and pericytes. The extracellular matrix (ECM) molecules further strengthen the vessels connecting EC to surrounding tissue such as collagen I, collagen IV, laminin and elastin <sup>1</sup>. Initially vasculogenesis was thought to occur during early embryonic development, however circulating EPCs have often found in adult bone marrow. In cardiovascular diseases such as ischemia EPCs can contribute to vessel growth in diseases where EC can migrate from EPC's in adult bone marrow and migrate to the vasculature sites and differentiate into endothelial cells. EPCs have shown also to contribute to neovascularisation in the adult heart <sup>6</sup>

### **1.0.2 Arteriogenesis**

Once arteries and veins are established, existing arteries can be remodelled during development. The expansive growth of pre-existing vessels to form arterial networks is often termed as collateral growth and is an adaptive physiological response to increased blood flow

or to bypass occluded arteries in ischemic tissue <sup>7,8</sup>. Although mechanisms regulating the expansion of pre-existing vessels are still being uncovered, one of the major stimulators is thought to be shear stress. Shear stress can result from either an obstruction of blood flow in main artery resulting in blood to be redistributed through pre-existing arterioles or in response to inflammation, both increasing stress on residing ECs. As a result many growth factors are upregulated and certain growth factors carry shear stress elements in their promoter such as PDGF (platelet derived growth factor) and MCP-1 (monocyte chemoattractant protein). The upregulation of these factors activates EC and attracts and recruit monocytes. Growth factors such as MCP-1, TNF- $\alpha$  (tumour necrosis factor), PDGF (platelet derived growth factor), bFGF (basic fibroblast growth factor), aFGF (acidic fibroblast growth factor), and proteinases such as urokinase plasminogen activator (uPA) and matrix metalloproteinases (MMP's) enhance collateral growth by attracting monocytes to the endothelium partly through upregulation of PDGF (platelet derived growth factor) <sup>9,10</sup>. Monocytes invade areas of arterial collaterals where they release and stimulate the release of growth factors such as bFGF, VEGF and HGF (hepatocyte growth factor) and further enable SMC's to migrate and divide alongside vessels increasing the diameter of the vessels <sup>11</sup>. The function of arteriogenesis programme is to provide bulk blood flow to tissues that are ischemic. Interestingly this process unlike other vascular remodelling processes is not oxygen dependent as vessels can grow in non-hypoxic areas even in the absence of VEGF expression <sup>12,13</sup>.

### **1.0.3 Angiogenesis**

Angiogenesis is a vascular regeneration process forming new blood vessels from pre-existing vasculature. This occurs in embryonic development and in adulthood during wound healing, the female reproductive cycle and in the formation and growth of bone. Angiogenesis is a multistep process initiated by a release of growth factors from endothelial cells in response to metabolic stress such as hypoxia (oxidative stress), low pH or shear stress from inflammatory and tumour cells <sup>14</sup>. The binding of angiogenic growth factors to ECs initiates a cascade of events including controlled degradation of basement membrane, migration and proliferation of ECs into interstitial space, vascular tube formation and stabilisation of porous tubes by pericytes and smooth muscle cells (Fig. 1.0).

Angiogenesis is regulated by interaction between multiple growth factors and ECM to produce a fine network of sprouting capillaries to hypoxic areas. One of the unique properties of the angiogenesis process is that capillary tubes formed are driven by oxygen demand <sup>15</sup>.

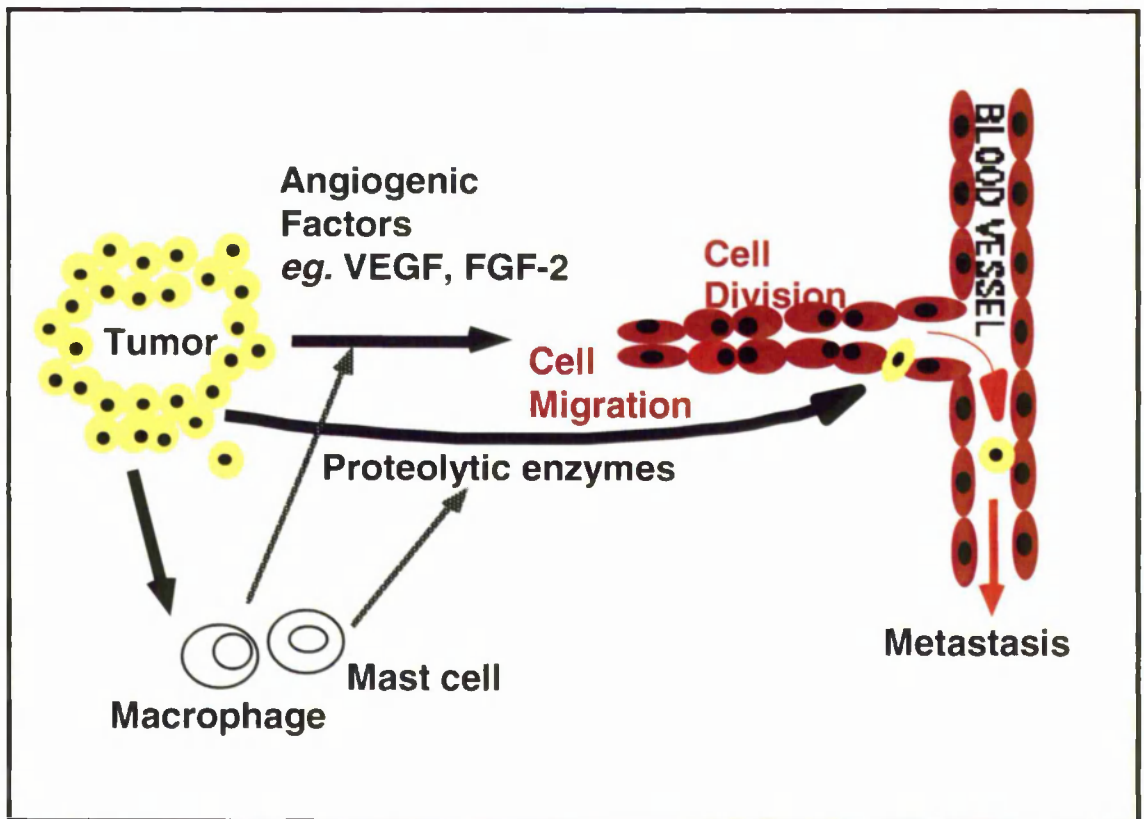


**Figure 1.0: An illustration of the angiogenic process**

Diagram shows the general mechanism of angiogenesis. Release of angiogenic factors from normal or diseased tissue (as in the case of tumours), activates endothelial cells so they can respond to mitogenic signals. Once the ECs become activated they generate matrix metalloproteinases (MMPs) that breakdown the ECM, thus allowing the migration and proliferation of the ECs from existing blood vessel to surrounding tissues. The projection of the sprouting endothelial cells is aided by adhesion molecules such as integrins, this allows the sprouting EC to roll up and form blood vessels. Simultaneously the tissue surrounding the tip of the new vessel is constantly being degraded by MMPs, allowing the extension of the blood vessel. The capillaries that develop within each tissue are unique and are driven by oxygen demand. Individual vessels connect to form loops that can then circulate blood. Finally, matured vessels are stabilized mainly by pericytes and SMCs <sup>1</sup>. Image provided by Sally Stringer.

However all three processes share an overlap in the growth factors and ECM protein and have been strategically exploited for therapeutic purposes.

## **1.1 Therapeutic vasculature targets**

A wide range of congenital and acquired human diseases are associated with pathological blood vessel formation. Incorrect artery and vein specification results in arterial venous malformations (AVM), this not only disrupts embryonic development but is one of the characteristic features of human syndromes such as hypotrichosis-lymphedema-telangiectasia (HLT) and hereditary hemorrhagic telangiectasia (HHT). Dilated capillaries and arterioles are also prevalent in these diseases<sup>16-18</sup>. Large AVM can lead to stroke if severe shunting occurs<sup>16</sup>. HHT type I and type II are caused by autosomal dominant mutations in the TGF- $\beta$  receptors ALK1<sup>19</sup> and mutations in the SOX18 gene (SRY-related HMG box) and SOX-7 gene are linked to HLT<sup>20</sup>. The molecular mechanism by which SOX proteins regulate arterial venous differentiation are still being uncovered, though it has been shown SOX proteins have redundant but essential functions and act downstream of Shh and VEGF<sup>21</sup>.

Over the last decade angiogenesis has received great interest because of its significant role in the pathogenesis of over 80 disease states and has subsequently been a target for therapies directed against malignancies, ischemia and inflammatory diseases. The regulation of blood vessel formation is governed by a balance of naturally occurring pro-angiogenic and anti-angiogenic factors surrounding the endothelium<sup>22</sup>. The induction of angiogenesis is proliferated by angiogenic growth factors including VEGF, PDGF, and TNF $\alpha$ . These work simultaneously with anti-angiogenic factors to fine tune the control of blood vessel growth in early development and in postnatal life. However when this tight regulation is perturbed, excessive or insufficient angiogenesis ensues. In the pathological disease states, tissues either have aberrant production of pro-angiogenic growth factors or conversely cannot produce adequate amounts of pro-angiogenic factors.<sup>23</sup>

### **1.1.1 Therapeutic targets of angiogenesis**

Angiogenesis is dependent upon complex interactions between a vast number of molecules including growth factors and their receptors, adhesion molecules and ECM proteins (Fig. 1.1). Critical to the angiogenic programme is a balance between pro and anti-angiogenic factors. The angiogenic factors can bind to heparan sulphate proteoglycan

<u>Stimulators</u>	<u>Inhibitors</u>
Vascular endothelial growth factor (VEGF)	Angiostatin
Fibroblast growth factor (FGF)	Endostatin
Hepatocyte growth factor (HGF)	Vasostatin
Platelet derived endothelial growth factor (PDGF)	Canstatin
Transforming growth factor (TGF)	Tumastatin
Angiogenin	Soluble VEGF receptor
Proliferin	Matrix metalloproteinase inhibitors
Interleukin-8	16-KDa prolactin fragment
Angiopoietin	Interleukin-12
Leptin	Arrestin
Granulocyte colony-stimulating factor	Platelet factor-4 (PF4)
Folistatin	Restin
Tumour necrosis factor- $\alpha$	Maspin
Pleitrophin	Interleukin-18

**Figure 1.1: A partial list of pro-angiogenic and anti-angiogenic factors.** Growth factors, chemokines and proteases active during vascular development. Angiogenic factors highlighted in red have the ability to bind heparin or heparan sulphate (adapted from <sup>293</sup>).

(HSPGs section 1.3) that are present on the endothelial cell surface and in the ECM, however only some of the growth factors targeted clinically will be discussed.

Growth factors can act directly by stimulating endothelial cells to proliferate and migrate or indirectly by stimulating the release of direct acting factors from endothelial cells, pericytes and inflammatory cells. One of the major triggers for the induction of growth factor activity is tissue hypoxia (oxidative stress) activating hypoxia inducible transcription factors (HIF- $\alpha$ ). Hypoxia inducible factor (HIF-1) stimulates cells to produce VEGF through binding to specific elements in the promoter region of VEGF. A VEGF gradient is formed that stimulates the growth of new blood vessels towards VEGF producing cells. In addition hypoxia can also stabilise VEGF mRNA<sup>24</sup>.

VEGF-A is a critical regulator of both vasculogenesis and angiogenesis with high specificity towards endothelial cells hence the name. Other members of the family include VEGF-B, VEGF-C, VEGF-D, VEGF-E and PlGF. The importance of VEGF-A as a regulator of EC proliferation, differentiation and survival has come from gene-targeted knockouts in mice<sup>25</sup>. Mutant mice lacking single allele of VEGF-A gene result in embryonic lethality by day E10 and E11 as a result of defects from gross vascular abnormalities in the cardiovascular system<sup>26,27</sup>. Thus VEGF-A is one of the most upregulated growth factors in physiological conditions and is expressed early in development in vertebrates where expression coincides temporally and spatially with blood vessel formation at numerous embryonic sites<sup>28-30</sup>. VEGF-A is produced by numerous cell lines including smooth muscle cells, T cells, macrophages and tumour cells<sup>31</sup>. Although VEGF-A is absolutely necessary for vasculogenesis and angiogenesis it is not sufficient, PDGF, FGF, angiopoietins (Ang-1), tyrosine kinase with immunoglobulin and epidermal growth factor homology domains (Tie) also aggregate in the areas active for angiogenesis, carrying out their function partly through upregulation of VEGF-A<sup>32</sup>.

The fibroblast growth factors (FGF) are one of the earliest characterised angiogenic growth factor, belonging to a family of 23 members. FGFs mediate cell signalling through four tyrosine kinase receptors FGFR-1, FGFR-2, FGFR-3 and FGFR-4. FGF-1 and FGF-2, also known as aFGF and bFGF respectively, have been the most extensively characterised in angiogenesis<sup>33</sup>. Although their *in-vivo* analysis has been hindered due to embryonic death of FGFR-1 and FGFR-2 null mice, mice expressing the dominant negative FGFR-1 display immature extraembryonic vasculature characterised by defective branching and reduced

endothelial migration and proliferation. This defects are consistent in FGFR-2 null mice<sup>34,35</sup> showing the ultimate necessity of FGF signalling. Interestingly FGF-1 and FGF-2 null mice do not show a striking morphological phenotype in contrast to their receptors, implicit of compensatory roles of FGF family in the vasculature. Both aFGF and bFGF induce endothelial cell proliferation, migration and a release of proteolytic enzymes during ECM degradation<sup>36,37</sup>. Critical to their activity is the role of their co-receptors HSPG's<sup>38</sup>. HSPG's exist in the extracellular matrix and in addition to inducing FGF signalling, they can act as storage depot for growth factors that can be liberated by the action of several HS enzymes such as heparanases (section 1.3).

As angiogenesis proceeds the new vasculature continues to proliferate and capillaries extend in a filopodial manner in response to VEGF regulation<sup>39</sup>. However the activity of growth factors on endothelial cells alone is not sufficient for formation of a mature functional vasculature network. Establishment of a functional vasculature network requires a surplus of pericytes and SMCs. The association of mural cells with vessels further regulates EC proliferation, survival, migration and differentiation<sup>40</sup>. PDGF-B, PDGFR- $\beta$ , Tie-2 and Ang-1 molecules are critical to vessel stabilisation and maintenance<sup>1</sup>. PDGF-B gene is expressed on megakaryocytes and EC's and functions by recruiting mural cells thus its receptor can be found on pericytes and SMC's. The significant role of PDGF is evident from PDGF-BB and PDGF-R $\beta$  null mice that die in *utero* from a 'leaky' vasculature network. PDGF-null embryos display cardiovascular defects, fragile dilated vessels and haemorrhages. Haemorrhages are signatory of a loss of microvascular pericytes however vessels maintain their permeability through increased VEGF expression in response to hypoxia promoting hematologic abnormalities<sup>41</sup>. Other members of the PDGF family also promote angiogenesis but the exact nature of their roles is less understood<sup>10</sup>. Certain studies have shown PDGF to have synergistic effects with VEGF in some tissues and this has been one of the key combinations of interest clinically<sup>1,11</sup>.

Also critical to vessel integrity is the cell signalling from angiopoietins. Primarily there are four angiopoietins with only Ang-1 and Ang-2 characterised as having a role in vascular maturation with the latter thought to function through antagonising Ang-1<sup>42</sup>. Their action is primarily mediated by Tie-2 receptor expressed exclusively on endothelial cells. Although Tie-1 is expressed also on EC's the ligands for Tie-1 have not been identified. Ang-1 appears to modulate EC survival, migration and tube formation through Tie-2 signalling. During sprouting angiogenesis vessels initially dilate in response to VEGF and Ang-1-Tie-2 signalling has a role in tightening vessels<sup>43</sup> through affecting molecules such as VE-cadherin

and platelet endothelial cell adhesion molecule (PECAM) and mainly functions by recruiting pericytes and SMC's to incorporate into the vasculature wall. Even though a vascular plexus can be formed in the absence of Ang-1 or Tie-2, their respective null mice die during embryogenesis due to vascular malformations contributing to cardiovascular defects <sup>44-46</sup>. VEGF signalling in conjunction with Ang-1 and Ve-cad is critical to survival of quiescent endothelial cells in normal adults <sup>47</sup>. However in certain tumours Ang-1 has shown to have anti-angiogenic properties <sup>48</sup>. It is thought upregulated levels of Ang-1 can interfere with the loosening of vessels inhibiting further sprouting <sup>1</sup>. On the other hand Ang-2 can stimulate growth of immature vessels in tumours possibly through synergising with VEGF, since VEGF and Ang-2 are both upregulated in hypoxic conditions. Furthermore Ang-2 and VEGF can induce angiogenesis in the heart <sup>48</sup>. Ang-2 is thought to act by antagonising the functions of Ang-1, thus resulting in destabilisation of vessel integrity. This allows EC's to detach from pericytes allowing further EC migration and sprouting in the presence of VEGF <sup>49,50</sup>. Consistent with the role of Ang-2 as an antagonist, mice overexpressing Ang-2 display a phenotype similar to Ang-1 and Tie-2 deficient mice <sup>42</sup>.

### **1.1.2 Pro angiogenic strategies**

Over the past decade angiogenic therapy has aimed at administering effectively pro and antiangiogenic agents to stimulate or inhibit blood vessel growth in different pathological disease states. Although certain strategies have shown efficacy in animal models the pre-clinical trials have not had the anticipated success.

Stimulating angiogenesis in ischemic diseases has been at the forefront of pro-angiogenic therapy. Strategies have focused on delivering individual pro-angiogenic growth factors such as VEGF, aFGF FGF by direct protein application or via gene therapy. Both protein and genes delivered intramuscularly or intravascularly in preclinical trials in animal models induced with myocardial and chronic ischemia, showed improvements in coronary blood flow and increased capillary density in infarcted myocardium. Delivery of VEGF<sub>165</sub> and VEGF<sub>121</sub> and FGF-5 in replication deficient adenoviral vectors in animals showed marked improvement in myocardial function <sup>51-53</sup>. However translation of these studies clinically have had mixed results. Several phase I trials for treatment of myocardial ischemia showed marked improvement in angina symptoms and myocardial perfusion in the first month via administration of bFGF, however after 3 months there was no evidence of myocardial perfusion despite the angiograms revealing capillary formation <sup>54</sup>. A separate study injecting naked plasmid encoding VEGF165 showed encouraging results in phase I trials but results

from phase II were disappointing as there was no difference after 3 months between the control and treated groups <sup>55</sup>. Although administration of single growth factors has shown some success in animal models attempts to stimulate angiogenesis in a directed and effective manner is proving to be quite challenging. Alternative strategies have aimed at stimulating arteriogenesis over angiogenesis in a bid to cope and deliver larger volumes of blood to ischemic tissue, by injecting a factor that is capable of producing a multitude of growth factors <sup>56</sup>. Studies administering combined angiogenic factors including VEGF and bFGF or angiotensin and VEGF, or factors that have the potential to initiate release of multiple angiogenic factors such as HIF- $\alpha$  and MCP-1 have shown to be effective in animal models with limb ischemia <sup>57-59</sup>. Prolonged activation with minimum side effects is often a problem in administering many pro-angiogenic factors as there are certain problems associated with the risks of overexpressing growth factors such as increased risk of hemangiomas that are often observed when overexpressing VEGF <sup>60</sup>.

On the other hand alternative approaches have utilised EPCs, these can enter circulation in response to vascular injury or in ischemia tissue. Recent studies have shown bone marrow and peripheral derived precursor cells to stimulate angiogenesis and incorporate into the neovasculature in ischemic hindlimb models <sup>61,62</sup>. Further proteins important in EPC mobilisation such as SDF-1 (stromal derived factor) have also been injected in ischemia hindlimb models resulting in increased blood perfusion to the ischemic limb and increased capillary network <sup>63</sup>. Several studies of EPC injections in pre-clinical models have shown promising outcomes, however with all potential therapeutic agents there are undesirable side effects such as uncontrolled EC growth possibly potentiating tumour growth <sup>64</sup>.

### **1.1.3 Antiangiogenic therapies**

Anti-angiogenic strategies have been at the forefront of cancer research since Judah Folkman postulated the dependency of tumours on angiogenesis to grow and metastasise <sup>22</sup>. In neoplastic diseases tumours cannot grow without having appropriate blood supply. Tumours can stimulate angiogenesis by incorporating into the host endothelium and secreting a variety of growth factors such as VEGF, bFGF <sup>65</sup>. Although tumour cells can form functional blood vessels, VEGF induced tumours often have immature and leaky vasculature. Tumour induced VEGF can promote mobilisation of EPC's to integrate into the tumour vasculature affecting tumour vasculogenesis. The majority of anti-angiogenic strategies have aimed at inhibiting different stages of angiogenesis. Over 50 anti-angiogenic agents have entered clinical trials,

ranging from regulators of endothelial growth and survival (cyclin dependent kinase and protein kinase B (Akt), to cell surface integrins and adhesion molecules<sup>66</sup>. Whilst the efficacy of these targets is currently under evaluation in clinical trials, the most promising results have come from targeting the growth factors and their receptor tyrosine kinases. Drugs such as Bevacizumab (VEGF inhibitor) are proving to be successful in phase I and phase II clinical trials for certain cancers. Bevacizumab (Avastin) was effective in phase III trials of colorectal cancer and showed slight progress in treatment of metastatic renal cancer delaying the onset of malignancy<sup>67</sup>. On the other hand trying to inhibit FGF induced tumours using suramin has had relatively little success. Despite showing encouraging results in animal models of glioblastoma, high doses of suramin showed complications associated with neuropathy and hypercoagulation possibly as result of interfering with other heparin binding molecules<sup>68,69</sup>. In phase II trials suramin compounds showed significant toxicity to patients compromising its role in future trials<sup>70</sup>. Alternative strategies have looked at inhibiting the activity of multiple growth factors one example is SU6668 a tyrosine kinase inhibitor that blocks signalling through VEGF-R2, FGF-R, and PDGF-R and has made small advances in phase I trials<sup>71,72</sup>. Whilst there is encouraging results from certain pre-clinical studies this type of antiangiogenic drug has not yet significantly improved survival rates.

A number of clinical trials involving both pro and antiangiogenic therapies have been instigated, most have not achieved their anticipated success. Problems range from choosing a viable target to sustaining prolonged effects of a drug without introducing significant complications, while this remains a major challenge other rational approaches need to be sought. This has prompted a renewed interest in improving our understanding of regulation of key angiogenic factors including VEGF and diverting attention back to *in vivo* models that are true representatives of the complexity of the vasculature. Unfortunately most *in vivo* models do not permit detail visualisation and functional analysis of cellular processes. For instance knockout of vascular growth factors in mammal results in embryonic lethality making functional analysis very difficult. In the last few years however *Danio rerio* (zebrafish) has become recognised as an important model for vertebrate vascular formation both in development and in adult tissues<sup>73</sup>.

## 1.2 Zebrafish as a model organism

Zebrafish *Danio rerio* are small tropical freshwater fish that can be cheaply housed and maintained in the laboratory environment. Over recent years zebrafish has lent itself as a popular model to study areas including vascular development, infection, immunity and drug discovery<sup>73</sup>. Its small size, rapid development, high fecundity and optical transparency are some of the attractive features that make it an ideal developmental model. Embryos are externally fertilised so they can be readily manipulated for experimentation. Embryonic development is rapid, mostly occurring within 6 days of post fertilisation (pf). In the first 3-4 days embryos can survive in the absence of a functional vasculature, as their small size enables them to survive by passive oxygen diffusion (Fig. 1.2). This allows the analysis of any genes that affect cardiovascular development. However one of the most significant features of the fish is transparency, allowing real time analysis of blood flow and vessel development at the cellular level, further augmenting its *in vivo* accessibility.

### 1.2.1 Zebrafish vascular development

One of the intrinsic advantages is the high degree of anatomical and functional conservation of vascular development and patterning between fish and other vertebrate species. Several zebrafish vascular models have been created that express green fluorescent protein (GFP) under the control of an endothelial promoter such as *fli-1* (friend leukaemia integration factor) or *flk-1* (fetal liver kinase)<sup>74,75</sup>. The transgenic zebrafish strains expressing eGFP (enhanced green fluorescent protein) in endothelial cells have been fundamental to our understanding of vasculature development both in zebrafish embryo and adult tissue. Through a combination of endothelial specific transgenic lines and microangiography the formation of the vasculature plan proceeds via two stereotypical processes vasculogenesis and angiogenesis.

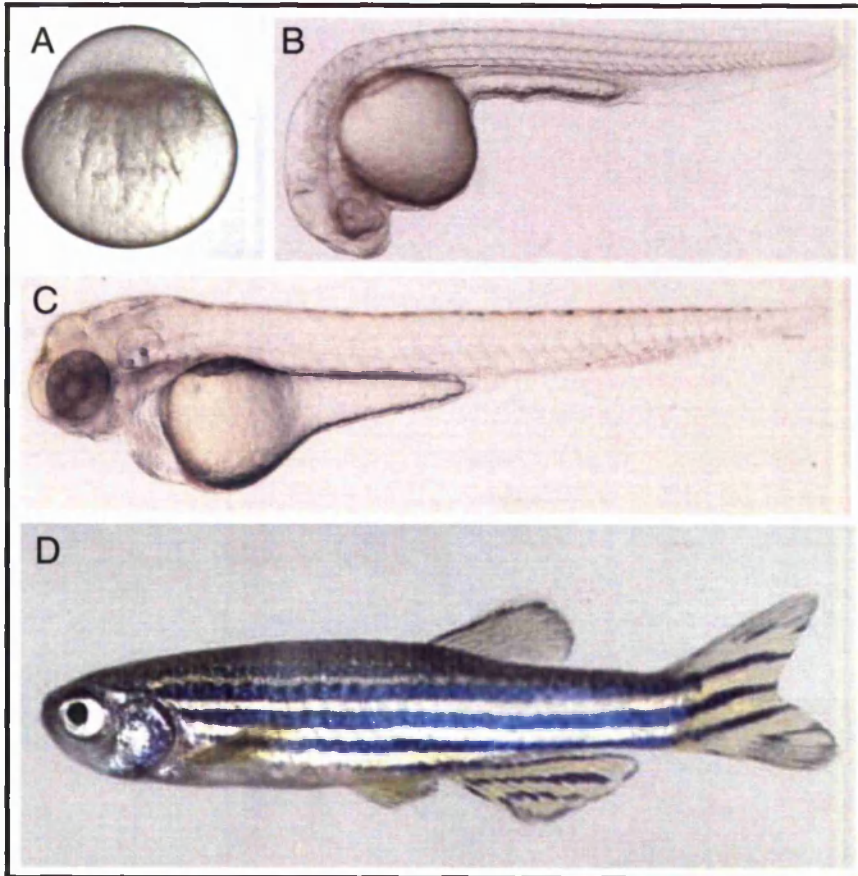


**Figure 1.2: Zebrafish embryos during larval and adult stages:** The zebrafish egg is laid and fertilised outside of the mother and divides every 15min so that embryo is fully formed by 24hpf (A) 2 cell stage embryo (B) embryos have a heartbeat at 24hpf , vascular development is studied between the embryonic stages of 12 somite-3dpf (C) 60hpf embryos, optical transparency is a key feature of zebrafish embryos allowing blood flow to be visualised externally (N.B embryos undergone PTU treatment) (D) Adult fish can grow up to 6cm in length and are usually competent to breed from 3 months to 2 years

### 1.2.1.1 Endothelial cell specification and migration

The earliest step in vascular development is the specification of endothelial cells known as the angioblast from the common progenitor cell termed the haemangioblast. Existence of such a cell is a testimony to the zebrafish *cloche* mutant as both the endothelial and haematopoietic lineages are affected<sup>76</sup> thus further showing conservation of the vasculogenesis programme in vertebrates. The haemangioblast transdifferentiates to give rise to both the haematopoietic cells marked by the expression of transcription factors such as runt related transcription factor (*runx3*) GATA binding protein 1,2 (*gata-1*, *gata-2*) and transcription factor *c-myb*<sup>77,78</sup>. Similar to mammals the endothelial lineage in zebrafish is marked by the regulated expression of friend leukaemia integration factor (*fli-1*), *flk-1*, growth differentiation factor 5 (*gdf5*) and endothelium-specific receptor tyrosine kinase receptor (*tie1*, *tie2*)<sup>79,80</sup>. At the eight somite stage (12hpf) haemangioblast can be first detected in the lateral plate mesoderm<sup>74</sup> (Fig. 1.3).

Angioblasts begin to migrate round 15hpf from the lateral plate mesoderm to the ventral midline at the origin where the new blood vessels will form<sup>81,82</sup> (Fig. 1.4A-B). During the early stage these progenitors are also thought to be specified as arterial or venous endothelial cells<sup>83</sup>. The first wave of angioblast migration coincides with the migration of arterial endothelial cells, this is followed by a second wave of migration of venous cells to their respective position in the vascular cord<sup>74</sup>. Signalling molecules such as Shh and VEGF emanating respectively from the notochord and somites are not only important in haemangioblast differentiation but play a crucial role in arterial and venous differentiation of endothelial cells at this stage during vascular development<sup>2</sup>.

### 1.2.1.2 Vascular lumenisation and initiation of circulation

Angioblasts appear to subsequently coalesce at the ventral midline to form a primitive cord. Cell-cell junctions between angioblasts first appear at 17hpf indicated by zona occluding 1 (ZO-1 pan endothelial),  $\beta$ -catenin and claudin 5<sup>74</sup>. Concurrently differentiation of the angioblast also begins into arterial and venous population of cells. This is indicated by expression of *ephrinB2a* a marker of differentiated arterial endothelial cells<sup>83,84</sup> in the dorsal most aspect of the vascular cord<sup>74</sup> and *flt-4* a marker of differentiated venous endothelial cells<sup>80</sup> expressed in the most ventrally located region. Although expression of arterial-venous markers is detected at 17hpf the specification event is thought to exist prior to migration<sup>74,83</sup>. The vascular cord starts to lumenise to form the dorsal aorta at 18hpf and the increase in the

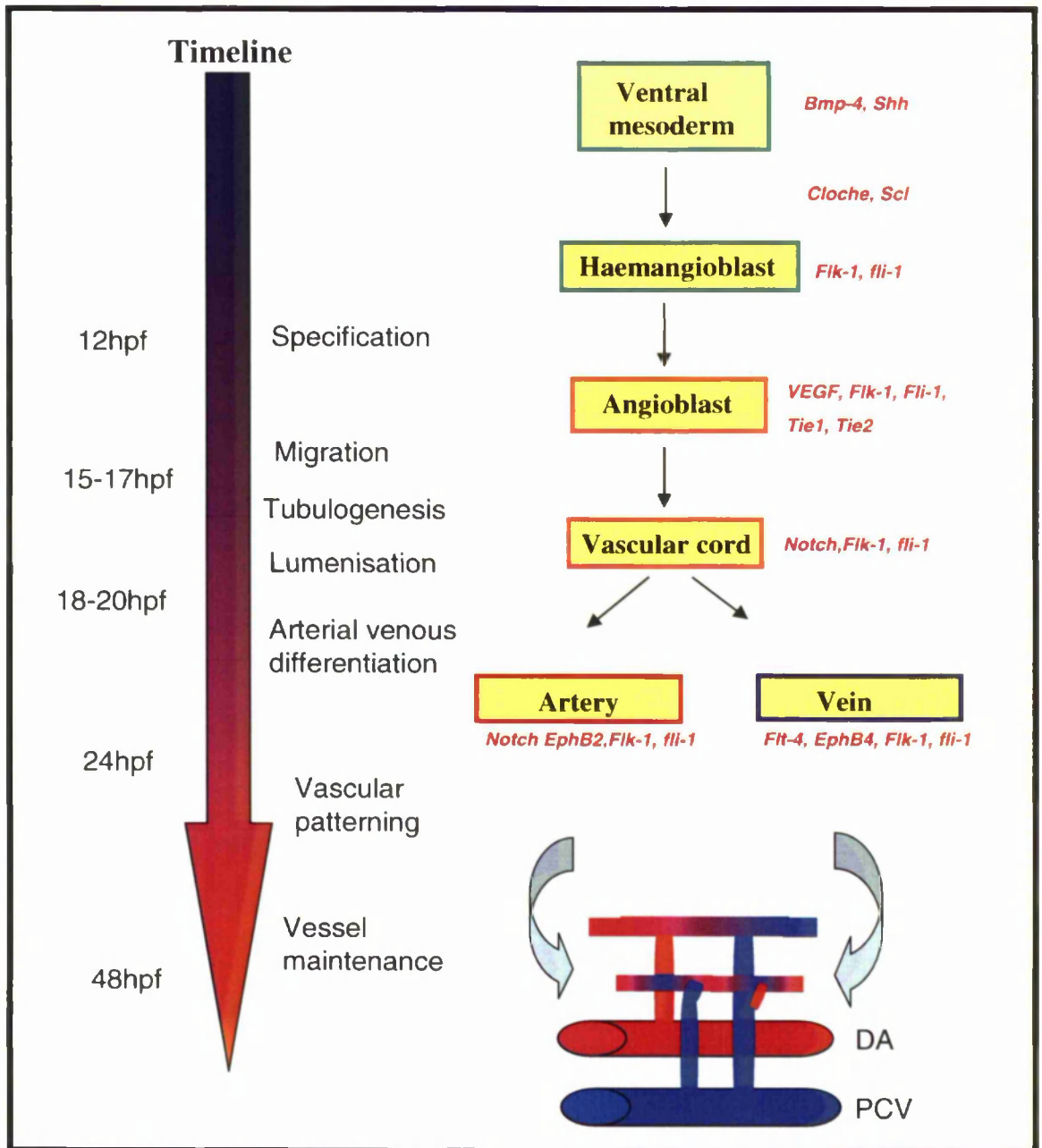


**Figure 1.3: Signalling molecules required for the formation of embryonic vasculature development.** Vascular development is initiated from the specification of the angioblast, occurring around 12hpf, and angioblast migrate to the lateral plate mesoderm whereby they differentiate and proliferate into arterial and venous endothelial cells. Subsequently cells form a vascular cord and lumenise forming the major axial vessels that have established arterial and venous identities. Bottom right hand corner is an illustration of sprouting intersegmental arteries (red) and veins from their respective axial vessel to connect and form the dorsal longitudinal axial vessels (DLAV). Signalling molecules highlighted in red signifies their involvement at particular stages, references to the signalling pathways can be found in the main text (adapted from <sup>74,87,98</sup>)

lumen size coincides with the change in shape of endothelial cells from cuboidal to an elongated form. By 24hpf the two defined axial vessels the dorsal aorta (DA) and posterior cardinal vein (PCV) are formed <sup>74,83</sup> (Fig. 1.4C) However the vessels are not patent at this stage.

Blood circulation commences around 26hpf (Fig. 1.5A). Initial circulation begins through a simple loop and blood exits the heart through the bulbous arteriosus into the ventral aorta where it flows rostrally through the aortic arches and into the left and right lateral dorsal aorta (LDA) and caudally into the single DA running down the trunk.

The DA continues into the tail (the most caudal part to the anal pore is known as the caudal artery) and joins the caudal vein (CV). The CV is a plexus of vessels and remains like this for a couple of days. Circulation from this CV plexus continues into the trunk becoming a single distinct posterior cardinal vein (PCV) (Fig. 1.5A). The PCV then splits into a pair of vessels in the anterior of the trunk emptying into the ducts of cuvier or future common cardinal vein (CCV), which fan out over the yolk cell coming together to the sinus venosus of the heart. A second circulatory loop comes online indicative of the patent cranial vasculature formed also by this stage. Blood exiting the aortic arches now flows bi-directionally into the primitive internal carotid arteries (PICA) each PICA divides into two branches. The Caudal division joins the brain midline, the cranial portion however goes interior into the optic capsule emptying into the primordial midbrain channel (PMBC). The PMBC continues rostrally to the anterior cerebral veins (ACV) and caudally into the primordial hindbrain channel (PHBC) <sup>85</sup>(Fig. 1.5B).

### **1.2.1.3 Functional secondary vessels formed by 60hpf**

As the primary vasculature is formed by vasculogenesis, the later forming intersegmental arteries (ISA), intersegmental veins (ISV) and parachordal vessels (PAV) are believed to form by angiogenesis <sup>86</sup>. By 20hpf ISA begin to emerge from the dorsal aorta sprouting bilaterally, and grow dorsally following each vertical myotomal boundary between somites. As the ISAs reach the dorsal lateral roof they divide into two major branches that turn caudally and rostrally elongating to fuse together and form the bilateral dorsal longitudinal anastomotic vessels (DLAV) (Fig.1.4D). Secondary sprouts then begin to emerge exclusively from the PCV, sprouting dorsally towards the nearest primary vessel with only some forming connections and linking the ISV to the primary vasculature. Only primary vessels not connected to the secondary vessels retain the arterial fate appearing as late as 2.5dpf.

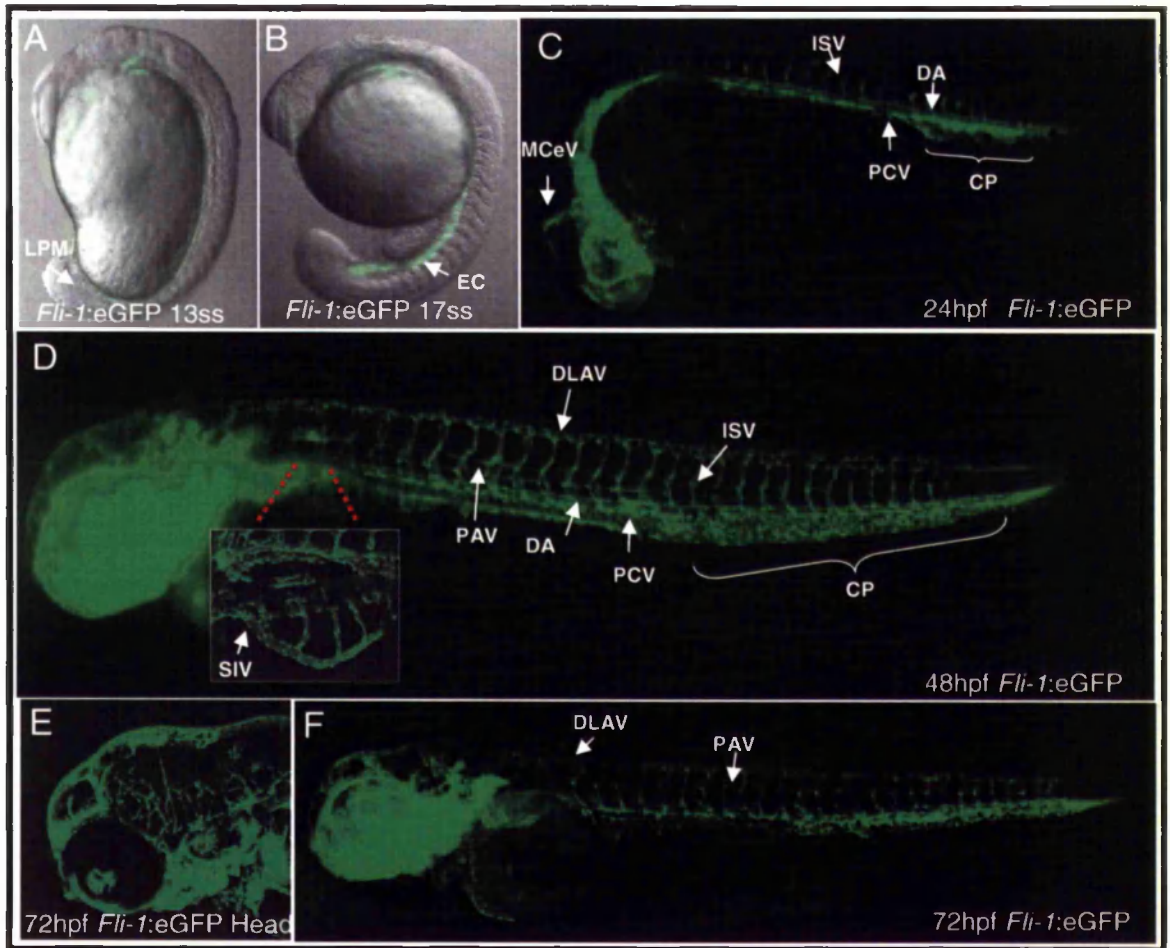


**Figure 1.4: Vascular development in *Fli1*:GFP zebrafish embryo.** Early stages of vascular development, white arrow denotes the migration of endothelial cells from the lateral plate mesoderm to the ventral midline (A). By 17hpf a cord of endothelial cells can be observed from tail to the anterior region of head, however the vascular lumen has not yet formed (B). At 24hpf the major axial vessels in the trunk namely DA and PCV are formed, and in the head cranial vessels are also formed though the cerebral vessels are not yet connected to the trunk vasculature. Angiogenesis also begins in the trunk and tail with intersegmental vessels sprouting from the DA and PCV and vessels branching from the CV to form the caudal plexus (C). At 48hpf ISV vessels are completed in trunk and tail and initiation of SIV and PAV begins (D). Cranial vasculature formed by 72hpf (E). By 72hpf all secondary vessels such as SIV and PAV are formed in the trunk of the embryo (F). CP, caudal plexus; DA, dorsal aorta; EC, endothelial cells; ISV, intersegmental vessels; LPM, lateral plate mesoderm; MCEV, mesencephalic vein; PAV, parachordal vessels; PCV, posterior cardinal vein; SIV, subintestinal vessels; SS, somite stage.

The parachordal vessels emerge from ISV at the level of the horizontal myoseptum on either side of the notochord. These are formed by angiogenic growth and usually sprout from the PCV. There is not an exact fixed sequence of which ISV will become artery or vein. The final arterial or venous identity of the ISV however is thought in part to be influenced by blood flow<sup>87</sup>. The basic pattern of trunk and tail intersegmental vessels is established by 2.5dpf and is relatively unchanged from here on in. Additional subsets of vessels believed to form via angiogenesis are the subintestinal vessels (SIVs), these begin to sprout as early as 2.5dpf from the anterior mesenteric artery (AMA) and eventually provide blood flow to the digestive system. By 3dpf the separation between the DA and PCV continues to increase with caudal vein plexus beginning to condense into a single more ventral channel (Fig. 1.4F). Another subset of parachordal vessels begins to form lateral to the notochord and appear later in the tail, these will eventually go on to form the lymphatic system<sup>88</sup>. A short profusion of vessels however begin to appear between the DA and PCV but largely disappear by 4.5dpf. The exact nature of these vessels is not yet understood. Blood circulation continues in the major axial vessels, caudal vein plexus and is established in all the ISV by 2.5dpf, while the SIV become functional at 3.5dpf<sup>87</sup> (Fig. 1.5C, D).

Following the establishment of the primary cranial vasculature at 1dpf, the nature of the 'secondary' cranial vasculature is not well understood. At 2dpf most newly formed cranial vessels penetrate into the brain substance, with many taking over from the earlier formed vessels and form new connections to supply blood flow to the developing brain. Certain cranial vessels are believed to form in the head via angiogenesis i.e basilar artery (BA) and central arteries (CtA)<sup>85</sup>. The BA is mainly derived from PHBC and single CtA extend dorsally from the BA and then drain into the PHBC. More rostrally to the single CtA are three pairs of the central arteries that extend from the basal communicating artery (BCA); anterior mesencephalic arteries (AMCtA) irrigate the forebrain, middle mesencephalic arteries (MMCtA) irrigate the midbrain and the cerebellar central arteries (CCtA) extend from the PHS, providing arterial blood flow to the hindbrain. The vessels made up of the BCA and primary head sinus (PHS) are thought to resemble the human cerebrum circle of Willis<sup>85</sup>. Although there continues to be an elaboration of small calibre vessels throughout the head post 3dpf, the overall wiring pattern of the major head vessels is unchanged after 2-2.5dpf (Fig. 1.4E) and functional circulation is active in the cranial vessels formed by this stage.

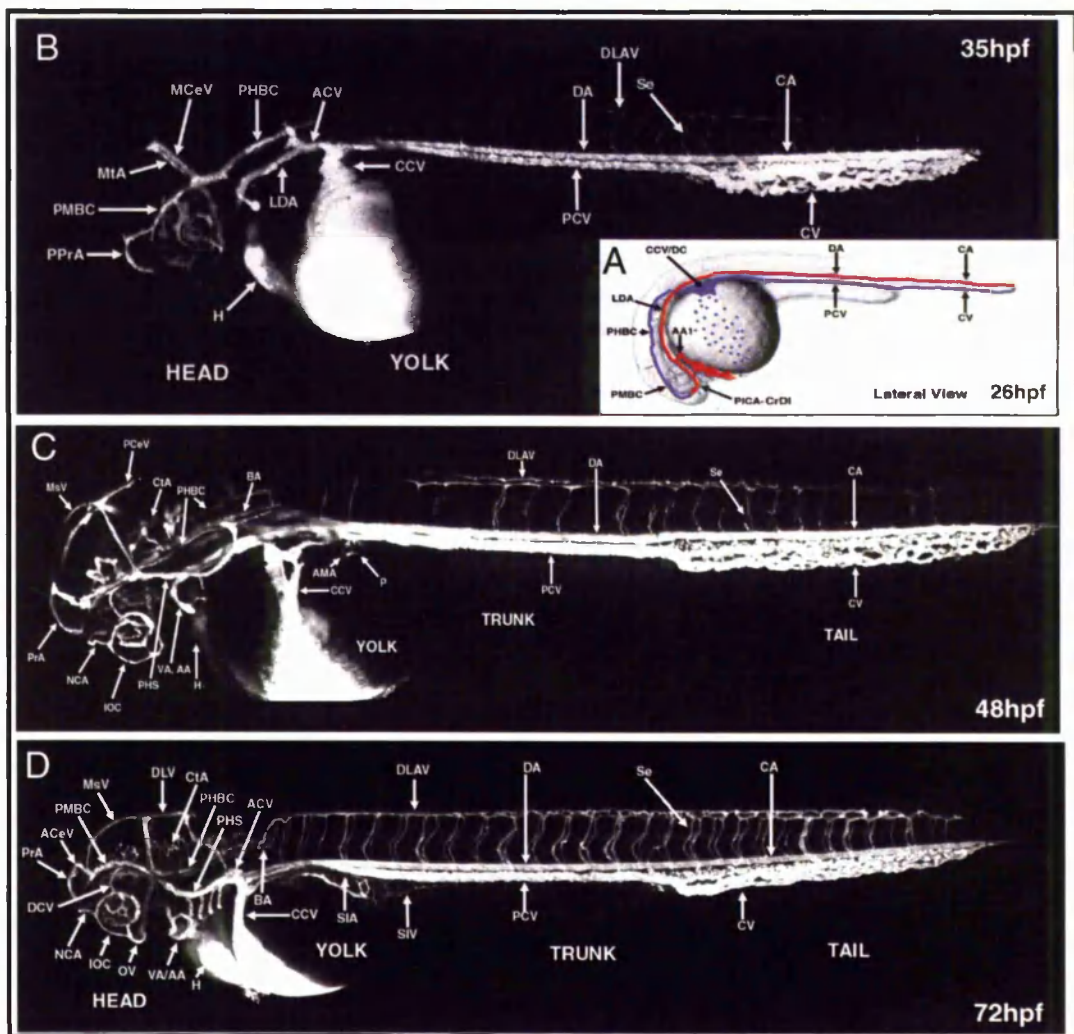


**Figure 1.5: Functional circulation during zebrafish embryonic development.** Blood circulation begins at 26hpf following a simple circulatory loop blood exits the heart through the bulbous arteriosus into the ventral aorta where its flows rostrally through the aortic arches and into the left and right lateral dorsal aorta (LDA), and caudally into the single DA running down the trunk. The DA continues into the tail and joins the CV. The CV is a plexus of vessels. Circulation from this CV plexus continues anterior into the trunk becoming a single distinct PCV. The PCV then splits into a pair of vessels in the anterior of the trunk, the PCV empties into the large sinus the ducts of cuvier or future common cardinal vein, which fan out over the yolk cell coming together to the sinus venosus of the heart (A). A second circulatory loop comes online, Blood exiting the aortic arches now flows bi-directionally into the primitive internal carotid arteries (PICA) each PICA divides into two branches. The Caudal division joins the brain midline however the cranial portion goes interior into the optic capsule, emptying into the primordial midbrain channel (PMBC). The PMBC continues rostrally to the anterior cerebral veins (ACV) and caudally into the primordial hindbrain channel (PHBC)(B). Blood now begins to circulate in developed ISVs and SIVs (C), patent connections are also made between the cerebral arteries and the DLAV through the BA linking the cranial vasculature to the trunk by 60hpf (D). (Micoangiograms of zebrafish vasculature adapted from <sup>87</sup>)

(Fig 1.5C,D). The functional circulation connecting the cranial vessels to the trunk vessels occurs later, despite the early connection of BA to the PHBC. At 2-2.5dpf the BA links the caudal ends of both PHBC to the paired DLAVs and eventually this connection will detach from the PHBC and blood flow will be solely from the BA at later stages <sup>85</sup>.

#### **1.2.1.4 Vessel maintenance**

The main axial vessels are established in the head and trunk by 2.5dpf, and the newly formed vasculature undergoes further remodelling to meet the requirements of the surrounding tissue. Like all vertebrates the integrity and maintenance of vessels is supported by the recruitment of mural cells i.e. SMCs and pericytes to the vascular endothelium. In zebrafish evidence for such cells also exists, like vertebrates SMCs and pericytes are derived from the lateral plate mesoderm and not transdifferentiated from endothelial cells <sup>89</sup>. Expression of SMC markers such as SMC $\alpha$ 22-a SMC $\alpha$ 22-b have been detected as early as 72hpf <sup>89,90</sup>. The conserved developmental origin of endothelial cells and SMCs indicates that zebrafish can be used to study the genetics of vascular associated human diseases.

#### **1.2.2 Zebrafish vascular mutants**

Large mutagenesis screen have identified a number of vascular mutants that have provided fundamental insights into vascular development enhancing our understanding of signalling molecules involved in early endothelial cell differentiation to vascular guidance. Screens performed using both forward and reverse genetic approaches with ENU (N-ethyl-N-nitrosourea) and TILLING (Targeted induced local lesions in genomes) have yielded novel mutations with vascular phenotypes such as *cloche*, *gridlock*, *plcgl*, and *out of bounds* <sup>91-94</sup>. This has been further augmented by vascular mutants generated by morphant technology and insertional mutagenesis using a gene trap approach <sup>95-97</sup>. The latest mutagenesis screen has identified 30 genes which are currently being characterised <sup>98</sup>. However from both forward and reverse genetic approaches certain vascular mutants have found to be highly reminiscent of human conditions such as hemangionomas arterio-venous malformation, and cerebral cavernous malformation, thus further lending its suitability as a model for human diseases.

### 1.2.2.1 Mutants affecting vasculogenesis

Mouse knockout models of signalling molecules or midline structures critical to vascular development causes embryonic lethality, hindering further characterisation of the molecular pathways and mechanisms of the genes involved. Compelling studies in zebrafish have given exciting new insights into vascular patterning and formation whilst unravelling new functional roles of previously well characterised signalling molecules. In zebrafish as in other species blood vessels development requires interactions between several signalling molecules, ligands, tyrosine kinase receptors and their downstream effectors. There is an increasing amount of data to suggest the signalling molecules involved in the assembly and maturation of the main axial vessels are produced by bordering tissues such as somites, endoderm, hypochord and notochord and this has been further substantiated in zebrafish mutants whilst unravelling novel mechanisms in the formation of axial vessels. Zebrafish mutants such as the *one eye pinhead (OEP)* that lack endoderm exhibits axial vessel defects with incomplete formation of the PCV whilst the DA is formed normally, thus suggesting the endoderm signals to the angioblast to form the axial vein<sup>79</sup>. Similarly the hypochord derived from endoderm origin is present only in zebrafish and xenopus and has shown to be important in contribution to the formation of axial vessels. Knockdown of genes expressed in hypochord such as *radar-1*, exhibit defects in vascular integrity and patterning in both DA and PCV<sup>99</sup>. In xenopus VEGF is shown to be secreted by the hypochord and is required for the development of the DA<sup>100</sup>, although this has not been proven in zebrafish, VEGF-C morphants lack endodermal derived tissue and exhibit defects in the axial vessels with the PCV more severely affected<sup>101</sup>, thus suggesting VEGF may also be derived from endodermal tissue or hypochord. On the other hand mutants in which notochord formation is inhibited such as *floating head (flh)* and *no tail (ntl)* mutants<sup>102,103</sup> display defects in the formation of the DA<sup>81</sup>. Although the PCV and cranial vessels development is largely unaffected in both mutants, the DA is not present suggesting signals emanating from the notochord are important in DA formation and patterning. While it could be thought other defects exhibited by these mutants i.e. the abberant somites maybe partly responsible for this, *ntl* mutants do not show fused somites like the *flh* mutants, thus indicating signals are derived from the notochord or other tissues dependent on notochord formation<sup>81</sup>.

Common to the endoderm, hypochord and notochord is the rich source of shh signal emanating from these tissue and structures. Shh is important in vascular development both in mice<sup>104,105</sup> and zebrafish<sup>79</sup>. The molecular mechanism by which Shh signal acts during

vascular development has come from zebrafish studies. *Sonic you* mutants lack the formation of the dorsal aorta as supported by the loss of expression of arterial markers such as *gridlock*, *notch* and *ephrinB2a*. Loss of notochord derived Shh results in the failure of DA formation in contrast to endoderm derived Shh which results in a failure of PCV formation thus planting a role of Shh in arterial and vein formation. Indeed Shh is shown to play a role in arterial venous differentiation in which *shh* sits at the top of signalling cascade, thus Shh mediate VEGF signalling in adjacent tissue which in turn mediates notch activation<sup>2,84</sup>. This is further complemented by studies in which mutants of the VEGF signalling pathway and notch mutant (*mindbomb*) revealed similar vascular defects such as loss of arterial identity, A-V shunts and haemorrhage<sup>84,91,106</sup>. Notch function is shown to be critical in positively contributing to a functional vasculature network both in mice and zebrafish<sup>84,107</sup>. Studies in zebrafish mutants show notch crosstalks with the VEGF pathway to positively and negatively regulate VEGF function. Notch activation by VEGFR-2 can positively activate arterial differentiation whilst notch can also inhibit VEGFR-3 signalling to regulate angiogenic sprouting<sup>84,108</sup>. The molecular mechanisms by which axial vessels are specified and formed has been further delineated in zebrafish mutants.

### 1.2.2.2 Mutants affecting angiogenesis

The development of both neural and vascular network is distinctly different, however it has long been proposed that nerve vessels and blood vessels share common guidance mechanisms<sup>109</sup> and this has been further substantiated in several zebrafish vascular mutants. Most studies have discovered novel roles of well characterised factors important in patterning the nervous system as also having a role in regulating the stereotypic patterning of vessels. One example is PlexinD which is a receptor of semaphorins and interacts with sem3A. One of the responses from this signalling complex is to repulse guidance of neural axons. Loss of plexinD (*out of bound mutant*) and sem3a result in similar vascular defects in ISV formation. In these mutants ISVs fail to branch correctly from the DA not following the chevron shape of the somites, resulting in incorrectly spaced and misguided ISV<sup>86,93</sup>. This suggests that vascular misguidance results from disruption of Sem3a-plexinD mediated repulsion. Another example of axonal guidance cues implicated in vessels patterning comes from *Unc5b* and its ligand *Netrin-1a*<sup>110</sup>. Although the ISVs sprout normally into the intersegmental space in the *netrin-1/unc5b* morphants, as they reach the horizontal myoseptum the ISVs deviate laterally rather than extending dorsally thus suggesting axonal guidance molecules also provide critical cues for navigating vessels<sup>111</sup>. A third family of proteins implicated in both neuronal and vascular

patterning is the ROBO (roundabout) family. ROBO receptor family bind slits protein and functions include repelling certain types of axons, stimulating of branching and elongation of axons through signalling via ROBO-1 and ROBO-2 <sup>112-114</sup>. More recently Robo-4 has shown to have a role in vascular guidance. *Robo-4* morphants display either missing ISVs or are arrested midway through their dorsal trajectory <sup>115</sup>. The exact mechanism by which *Robo-4* acts is unknown whether it mediates attractive or repulsive signals and if this indeed requires a genetic interaction with the slit protein. Although *in-vitro* roles have shown Slit-2 can repel endothelial cells <sup>116</sup>, a study by Suchting and colleagues having reported no interaction of Robo-4 with slit family members whereby Robo-4 functions to inhibit angiogenesis <sup>117</sup>. Nevertheless from the studies reviewed in zebrafish vascular mutants it is conceivable that zebrafish ISV patterning can be driven by specific neuronal guidance signalling molecules and opens up avenues for novel therapeutic targets. Intriguingly other anatomical studies of zebrafish mutants such as the *silent heart* show blood flow is important in refining the patterning of angiogenic vessels. Analysis of blood flow dynamics in *silent heart* mutants that lack a heart beat and circulatory flow do not affect sprouting of primary and secondary vessels <sup>118,119</sup> but play an important role at later stages in development refining the patterns of connections between these vessels and in assuming their final arterial or venous identity <sup>87</sup>.

### **1.2.3 Zebrafish as a therapeutic angiogenesis assay**

The rapid development of the angiogenic vessels i.e. ISVs and the subintestinal basket in conjunction with high resolution imaging of vascular transgenic zebrafish lines combines to form a high-throughput angiogenesis assay. Zebrafish have been utilised for large scale drug screens aimed at identifying inhibitors of angiogenesis. Anti-angiogenic compounds such as ZK222584 and SU5416 (VEGF inhibitors) have been added to Tg(*Flk1*:GFP) embryos at 13 somite stage and by confocal analysis and alkaline phosphatase assay has shown some compounds to exhibit anti-angiogenic activity, affecting later forming vessels such as ISVs and subintestinal basket <sup>120</sup>. In addition molecules have been isolated that can rescue the coarctation phenotype in *gridlock* mutants <sup>121</sup>. More recently however Bayliss and colleagues have characterised a new angiogenesis assay in the regenerating fin of the adult zebrafish. The striking similarities induced by VEGF inhibitors in adult zebrafish <sup>122</sup> provides unparalleled opportunities to study the zebrafish as model of tissue regeneration in vascular disease and opens up the applicability to testing hundreds of novel signalling molecules and identifying potential therapeutic targets.

Successful treatment of vasculature based diseases is still far from completion and as result novel strategies are currently being explored into molecules critical to growth factor activity. Over the past twenty years it has been well established that periceullar HSPGs are important in the endothelium and more important HS are important co-receptors for many growth factors and ECM proteins critical to vascular development.

### 1.3 Heparan Sulphate Proteoglycans (HSPG)

HSPGs are a family of cell surface and ECM macromolecules that consist of a protein core to which HS glycosaminoglycan chains are attached (section 1.4). These macromolecules can be classified into several families based on the structure of the protein cores and on the basis of their cellular location. The two major cell surface HSPGs are Syndecans and Glypicans both of which are cell surface proteins. The most abundant HSPGs in the extracellular matrix are the basement membrane Perlecan, Agrin and Collagen XVIII. The positioning of HSPGs at the cell surface is important, where they act as communicators between cells, as well as the ECM environment <sup>123</sup>( Fig. 1.6 )

#### 1.3.1 Glypicans

The glypican family of HSPGs are anchored to the cell surface via a covalent linkage by GPI (Glycosylphosphatidylinositol) and do not span the membrane. The GPI anchor confers great mobility but does not direct signal transduction, however the GPI can be cleaved by GPI specific phospholipase and releases glypican from the cell surface. The *in-vivo* functional role has not yet been determined, however soluble glypican can to bind to cell surface receptors and be endocytosed <sup>124</sup>. To date six glypicans have been identified in mammals, all glypicans are characterised by a large extracellular domain containing 14 numerous disulphide bridges that organize the protein into a compact globular structure, 2-3 GAG attachment sites are located in the C-terminus thus placing them in close contact to cell membrane (Fig. 1.6B). Although HS is only thought to attach to 'glycin', glypican 5 has shown to express CS indicating the support of CS attachment sites <sup>125</sup>. Each member of the family has overlapping and distinct developmental patterns of expression. Glypicans are predominantly expressed in the CNS (central nervous system), in kidney and to lesser extent in smooth and skeletal muscle. However only glypican-1 is found to be expressed on vascular EC/SMCs and is often upregulated in several metastasis cancer <sup>126</sup>.

The functional role of glypicans in developmental signalling and modulating morphogen gradients has come from experiments in cell culture systems and in animal models such as

*Drosophila* and zebrafish. Genetic studies of two glypicans *Dally* (*Dly*) and *Dally like protein* (*Dlp*) in *Drosophila* (akin to mammalian glypican 4&6) have shown an important role in modulating Wg (wnt) and Hh signalling. *Dly* and *Dlp* mutants exhibit similar defects in wing development and segmentation similar to that of *wg* *drosophila* mutants<sup>127-129</sup>. Further overexpression of *Dly* results in ectopic expression of *wg* in the tissue<sup>130</sup>. Analogous to this *knypek* (zebrafish glypican-4) mutant exhibits similar defects in convergent extension and gastrulation to *wnt-11* mutants, and dose dependent loss of *wnt-11* signalling further exacerbate the mutant phenotype<sup>131</sup>. *Dlp* is also a regulator of Hh signal transduction in contrast to *Dly*, *Dlp* regulates Hh signal in a positive manner, and mutations of heparin binding sites of *Dlp* attenuates Hh signalling, thus suggesting HS chains are equally important in contributing to modulating the signalling response. Conversely glypican-3 inhibits Hh signalling, but this does not require the HS chains. The core protein and GPI anchor are thought to be important in modulating Hh signalling<sup>132</sup>. A recent study shows that glypican-3 competes with patched (*ptc*) at the cell surface and induces endocytosis and degradation of the Shh-GPC-3 complex removing *Shh* from the cell surface and the GPI anchor regulates the cellular trafficking of *Dlp*<sup>133</sup>. This indicates the differences amongst glypican mediated Hh signalling can be attributed by the core protein and the HS chains. Interestingly mutations in mammalian glypican-3 have been linked to X-linked Simpson-Golabi-Behmel syndrome (SGBS), how the mutations causes the syndrome however is unknown, although the developmental abnormalities are similar to observed *ptc* mutants. While these reports suggest the core protein is important in mediating cellular responses, mutants of HS enzymes such *tout velu* (*ttv*) show HS chains are important in distribution of *Hh* and can attenuate *Hh* signalling<sup>134</sup>. In support of this *drosophila* mutant *sugarless* (*sgl*) *sulfateless* (*sfl*) (section 1.5.1) exhibit defects similar to *wg* mutants with further defects in the nervous system and midgut which are *wg* dependent, suggesting there is a cooperative role between HS chains and core protein<sup>127,135</sup>.

### 1.3.2 Syndecans

In vertebrates there are four family members syndecan-1, syndecan-2 (fibroglycan), syndecan-3 (N-syndecan) and syndecan-4 (amphiglycan). These are transmembrane proteoglycans comprised of short cytoplasmic domain, a single hydrophobic transmembrane, N-terminal signal peptide and an ectodomain<sup>136</sup> (Fig. 1.6A). The ectodomains contain 3-5 attachment sites for HS and CS chains although HS are mainly found. The cytoplasmic and

transmembrane domains are highly conserved as are the sites for GAG attachment, however sequences of the extracellular regional domain are fairly divergent between families members<sup>137</sup>. Syndecans can serve as links between ECM and cellular responses to form higher order complexes at the cell membrane<sup>138</sup>. The short cytoplasmic tail of syndecans can interact with multiple proteins, thus four amino acids in the C2 domain bind Type II PDZ domains such as syntenin, CASK/lin-2, synbindin and synectin<sup>139</sup>. The C1 domains portion is attachment site for the ERM protein such as Ezrin that is involved in organisation of the cytoskeleton and activating focal adhesion kinases<sup>140</sup>. Between the two cytoplasmic domains is a variable region that is distinct amongst syndecan family members conferring specificity and is partly responsible for syndecan activities *in-vitro*. Syndecan-3 and syndecan-4 serves as a binding site for syndemos<sup>141,142</sup>. Unlike glypicans, syndecans can transduce signals activating cell adhesion and motility. Although all syndecans do not possess a tyrosine kinase domain, they have been implicated in transducing signals. In particular syndecan-4 has shown to be capable of modulating FGF-2 signalling<sup>143</sup>, cross-talk with integrins and organise actin cytoskeleton. Distinct to other syndecans, syndecan-4 contains two PIP2 (phosphatidylinositol 4,5-bisphosphate) binding sites that is involved in syndecan-4 dimerisation and in conjunction with other PDZ containing protein can activate protein kinase C (PKC) allowing it to transduce signals similar to integrin linked kinases. Interestingly CASK proteins have been shown to enter the nucleus and directly regulate transcription in cultured neurons<sup>144</sup>. Along with their differences in structure the spatial and temporal expression patterns are distinct, with every mammalian cell expressing at least one or multiple syndecans. Syndecan 1&2 are predominantly expressed in epithelial and mesenchyme tissue with syndecan-2 also abundantly expressed in neuronal cells<sup>145</sup> and cells of bone and cartilage. Syndecan-3 expression is restricted to neuronal and skeletal tissue. Syndecan-4 is shown to be expressed in several different tissues but more specifically only Syndecan 1, 2 & 4 are expressed in vascular endothelial cells and smooth muscle cells. As a result syndecans can regulate the activity of many growth factors (TGF- $\beta$  FGF,HGF,VEGF) and morphogens (Wnt,Ihh), during development<sup>125 139</sup>.

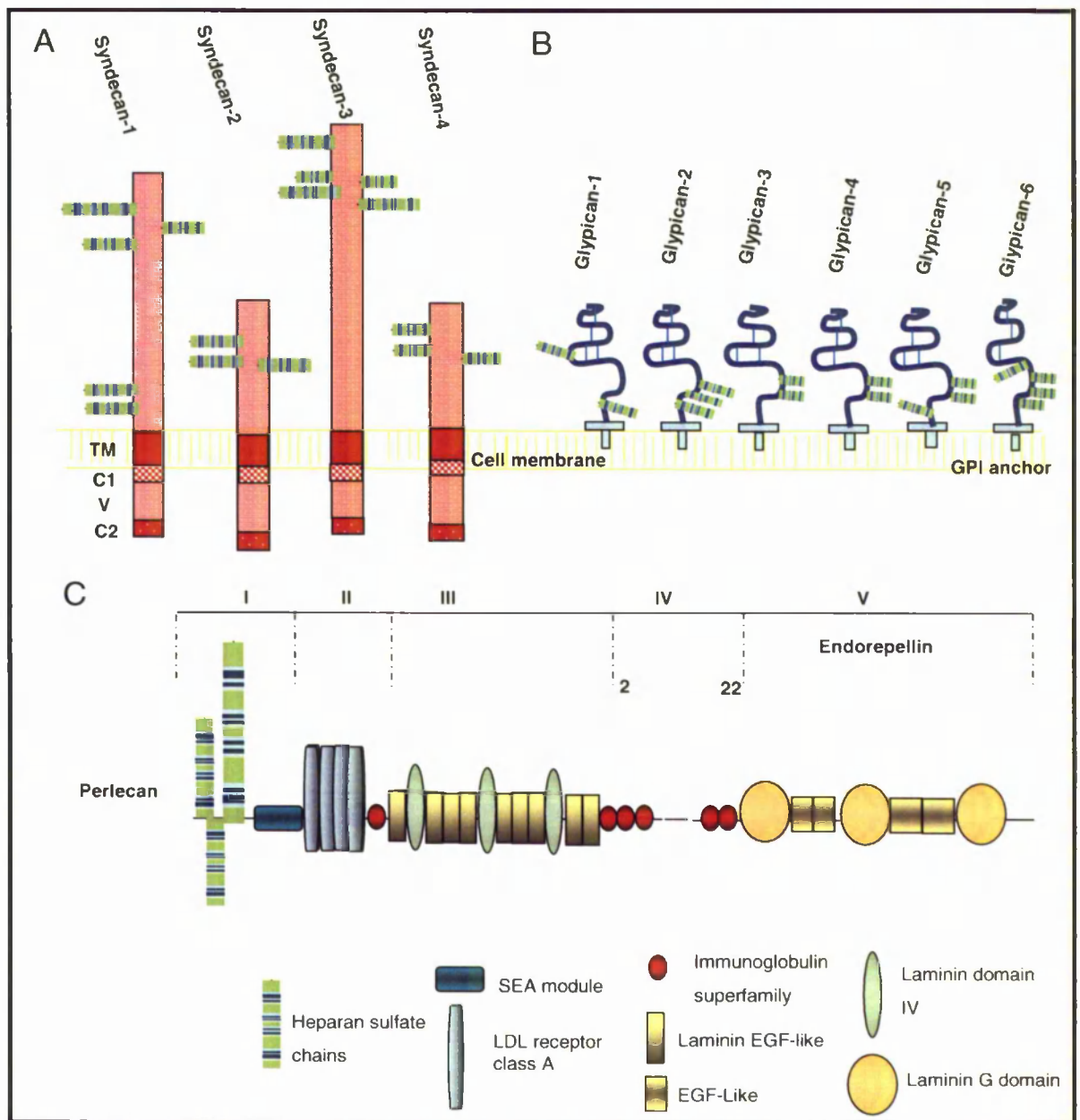


**Figure 1.6: Schematic representation of the structures of cell surface and extracellular matrix HSPGs.** (A) Members of syndecan family consist of three domain, extracellular domain, transmembrane (TM), cytoplasmic domain consisting of two conserved domain (C1 & C2), a variable region (V), HS chains and CS chains can be found to attach to extracellular domain of syndecans. (B) Members of glypican family are tethered to the cell surface via glycosylphosphatidylinositol (GPI) link, and contain a large extracellular domain including a cysteine-rich globular region attached exclusively to HS chains (C). Structural organisation of human perlecan, consists of five domains indicated by roman numerals, that can bind to other ECM proteins including laminin, endorepellin and different types of collagen. Perlecan like syndecan can accommodate HS and CS chains (adapted from <sup>139,174</sup>)

Syndecans play an important role in communication cellular responses during many different development processes such as cell patterning and cell signalling whereby the core-protein has shown to function non-cell autonomously. One example is the significant role of ectodermal derived syndecan-2 in left-right asymmetry through modulating TGF- $\beta$  signalling in the migrating mesoderm <sup>146</sup>. TGF- $\beta$  can directly interact with syndecan-2, and syndecan-2 morphants can be rescued by TGF- $\beta$ , however expression of mutated syndecan-2 cytoplasmic tail results in impaired response to TGF- $\beta$  <sup>147</sup>. However syndecan-1 cannot rescue syndecan-2 morphants suggesting *in-vivo* functional differences exist between family members <sup>146</sup>.

Syndecan-2 has also been shown to have a cell signalling role in angiogenesis, *syndecan-2* morphants in zebrafish show defects in ISV formation that is further abrogated with reduced levels of VEGF165 but not VEGF121 <sup>148</sup>. This suggests that syndecan may have a role in VEGF mediated angiogenesis, consistent with these ideas *in-vitro* knockdown of syndecan-2 in microvascular endothelial cells reduces cell adhesion and inhibits capillary like tube formation <sup>149,150</sup>. Although a direct interaction of syndecan-2 with VEGF has not been proven some of the structural changes accompanying the angiogenic responses such as cytoskeletal organisation and cell-adhesion maybe mediated through syndecan-2. However it is unlikely that the syndecan core protein mediates all cell signalling responses as certain studies show the core proteins of HSPGs are dispensable for VEGF signalling in endothelial cells <sup>151</sup>.

### 1.3.3 Perlecan, Agrin and Collagen XVIII

The final class of HSPG core protein reside in the basement membrane. Perlecan is a large macromolecule made up of five domains with a mass of 460kDa <sup>152</sup>. GAG attachment sites for HS and CS chains are located in the N-terminus and C-terminus respectively (Fig. 1.6C). It is secreted by multiple cell types including vascular EC & SMC but remains in close association where it interacts with other basement membrane proteins. Collagen XVIII can carry up to four HS chains and is abundant in kidneys and peripheral nervous system. Agrin is the most abundant GAG in basement membrane has a well characterised role in neurotransmission. Collectively agrin and perlecan constitute the negative charge barrier of basement membrane that controls membrane permeability <sup>153</sup>

Perlecan is a large macromolecule made up of five distinct domains. Each domain consists of repetitive structural motifs that share homology to proteins involved in lipid metabolism, internalisation of receptor for various ligands, cell signalling, neurite outgrowth and maintenance of basement membrane <sup>154-156</sup>. Domain I and domain IV contain attachment sites for glycosaminoglycan (GAG) chains including HS and CS. A characteristic feature of

perlecan is the structural heterogeneity that is further augmented by alternative splice variants of the protein, as a result perlecan can bind to a variety of proteins including growth factors (FGFs, PDGF, VEGF) ECM components (Fibrillin-1) and basement membrane proteins including laminin, nidogen and several types of collagen<sup>157</sup>. In humans perlecan has been linked to rare skeletal disorders, mutated perlecan-2 is strongly associated with the severe neonatal dyssegmental dysplasia Silverman Handmaker type (DDSH) and the Schwartz-Jampel syndrome (SJS)<sup>158,159</sup>. In these disorders truncated forms of perlecan domains are found and vary in the severity of phenotype, depending on the functional role of truncated perlecan.

Full length perlecan modulates many developmental processes including vasculogenesis, heart, chondrogenesis and the nervous system. The significance of perlecan in these processes is reflected by perlecan knockout mice that are embryonic lethal and die at E10-12 as a result of severe cartilage defects<sup>160</sup>, malformation cardiac outflow and abnormal coronary arteries<sup>161,162</sup>. One of the signalling pathways affected in these mice is the FGF signalling pathway. Perlecan has been shown to facilitate high affinity binding of FGF-2 to its receptors in HS deficient Chinese hamster ovary cells (CHO). Cell growth and vascular morphogenetic activity of FGF-2 have also been shown to be potentiated through its association with perlecan<sup>163</sup>. In human carcinoma cell lines perlecan is deposited along the basement membrane of newly formed tumour vessels and reduction in perlecan expression correlates with reduced tumour growth and angiogenesis. This is partly thought to be due to reduced activity of FGF-7<sup>164</sup>, since FGF-7 has shown to bind to domain III and IV of human perlecan<sup>165</sup>. Growth factors such as PDGF-BB have also been shown to bind to domain III and at low affinity for domains I and IV<sup>166</sup>.

#### **1.3.4 Role of HSPGs in the endothelium**

The expression of HSPGs on the multiple layers that constitute the formation of lumenised vessels such as the endothelial cells, pericytes, SMCs and ECM implies a fundamental role of the HSPGs during vascular development. This has been demonstrated in many cell culture and *in-vivo* experiments showing their role in pathological and physiological vascular processes. However this is not all potentiated by core proteins and like other developmental processes requires the co-operative role of the HS chains in modulating the cellular responses. Several glypican and syndecans can act as tumour suppressors in several carcinoma lines of hepatocellular, breast and pancreatic carcinomas. Their ability to reduce tumour growth is partly through inhibiting angiogenesis. In breast and pancreatic cancers glypican-1 is

overexpressed in contrast to other glypican family members and increases the mitogenic response to FGF, HGF and VEGF-A<sup>167,168</sup>. Inhibition of glypican-1 attenuates cell proliferation and migration of endothelial cells. As glypican-1 is exclusively expressed on endothelial cells it appears that cell autonomous effects of HS are significant in tumour angiogenesis<sup>167</sup>. It is thought glypicans control growth factor activity by serving as a chaperone, protecting VEGF from oxidising agents thereby controlling the release of VEGF to VEGFR-2<sup>169</sup>.

Syndecan-2 is often found upregulated in lung and colon cancers, while mainly syndecan-1 and 4 are increased in liver tumours<sup>170,171</sup>. Inhibition of syndecan-2 expression reduces proliferation of colon carcinoma cells and reduces tumour growth. This can be partly attributed to the binding of syndecans to growth factors such as FGF and VEGF. Syndecan-4 can bind to FGF and induce signalling in endothelial cells *in vitro*, while the cytoplasmic domain demonstrated an enhanced response to FGF2, removal of the syndecan-4 HS chain blocked FGF-2 signalling<sup>172</sup>, demonstrating both entities of the structure are required for controlled FGF mediated proliferation and migration of endothelial cells. Similarly syndecan-2 morphants exhibit defects in sprouting of angiogenic vessels that appears to be cooperative with VEGF activity<sup>148</sup>. The syndecan-2 core protein can mediate some of the angiogenic responses such as cell migration and capillary tube like formation,<sup>149,150,173</sup> likely through VEGF-VEGFR-2. A study by Jakobsson and colleagues have shown that the core protein is dispensable for VEGF mediated response in endothelial cells and HS chains can mediate VEGF signalling in a non-cell autonomous manner<sup>151</sup>. Similarly zebrafish perlecan morphants reveal defects in angiogenesis that can be rescued by VEGF overexpression, suggesting perlecan is acting on the VEGF pathway. Although direct interaction of VEGF with perlecan has not been proven, the perlecan HS chains are the main contributors to VEGF activity<sup>174</sup>. Perlecan can also regulate FGF angiogenic activities as mentioned previously through binding of specific FGF family members and FGF binding proteins. It is thought perlecan serves as co-receptor to deliver pro-angiogenic factors to their receptors either via core protein or HS chain. Perlecan acts as a reservoir for sequestering growth factors in ECM and releases them upon cellular stimuli, thus explaining the pro-angiogenic nature of perlecans during vascular development<sup>175</sup>. Conversely in human Kaposi sarcoma perlecan can act as a tumour inhibitor HSPG. This can be owed to the different binding partners of the perlecan domains. A C-terminal perlecan fragment named endorepellin has antiangiogenic activity<sup>176</sup>.

Interestingly additional pericellular HSPGs such as endostatin derived from collagen XVIII inhibit angiogenesis and tumour EC growth <sup>177</sup>. Endostatin, an 18kDa C-terminal peptide of collagen type XVIII, can modulate the activities of FGF2 and VEGF. Endostatin can inhibit FGF2 induced stimulation of endothelial cell growth but the anti-angiogenic activities of endostatin are found to be reduced by mutations in the heparin binding domain and not in the zinc binding region <sup>178,179</sup>. However in hepatocellular carcinomas and melanomas there are several conflicting reports as to whether HS binding domains are important, since mutating the zinc binding and heparin domain of human endostatin has a inhibitory role on endothelial cell migration in response to VEGF <sup>180</sup>, whereas mouse endostatin function was reduced via mutation of the heparin binding domain thus inhibiting FGF2 but not VEGF <sup>178</sup> signalling. This suggests not only are HS chains important but also confer specificity of endostatin activity on different growth factors. These discrepancies could also be attributed to the fact that endostatin can interact with HS chains of other HSPGs. Consistent with these idea glypican can act as a low affinity receptor for endostatin <sup>181</sup> or endostatin may interact with neighbouring HS chains of other ECM HSPGs such as perlecan.

HSPGs can serve as pro-angiogenic and anti-angiogenic role and this seems to be very much cellular context dependent. The binding of FGFs to different HSPGs may have different biological consequences. For instance syndecan inhibits FGF2 activity whereas perlecan promotes FGF proliferation and angiogenesis <sup>175</sup>. It is interesting that modifications of the HSPGs compositions can regulate the sensitivity of the cell to different FGFs. These studies point to the existence of an accurate and mutual control between growth factors and HSPGs in the endothelium during the angiogenesis process.

### **1.3.5 Degradation of HSPGs**

The mechanism of HS degradation is as important as synthesis in regulating development and is tightly regulated. HSPGs at the cell surface have a half life typically between 3-8hrs and are degraded either by endocytic pathway or shed into extracellular space by combined actions of enzymes sheddases and heparanases <sup>182</sup>.

#### **1.3.5.1 Endocytosis**

Endocytosis is the main route of metabolic turnover from the cell surface, most if not all are endocytosed. HSPGs are eventually degraded in lysosomes where exoglycosidases,

exosulfatases and N-acetyltransferase act in sequence to degrade the chains to individual sugars. After endocytosis HS can enter several distinct catabolic pathways, one specific to GPI anchored proteoglycans and the other for protein intercalated proteoglycans. GPI anchored proteoglycans are transferred to lysosomes where they undergo rapid and complete degradation in 25mins<sup>183</sup>. Once the HS proteoglycan is endocytosed degradation extends over a period of time. The cytoplasmic domain may interact with the cytoskeletal protein and this is thought to be involved in intracellular routing of the proteins. Once endocytosed HS fragments and core protein undergo stepwise degradation in the prelysosomal compartments. Firstly the core protein is extensively digested to liberate HS chains and the released HS chains are then rapidly cleaved by endoglycosidase activity to generate HS fragments. Although the proteolytic and endoglycosidic processes are closely coordinated they occur in separate compartments, such that proteolysis is required first in order for the HS chains to be liberated. After approximately 3hrs the HS fragments are rapidly and completely degraded to free sugars and sulfatases in a classic lysosomal compartment by endoglycosidases and exoglycosidases. The functional importance of HS oligos generated during intracellular processing is not clear. The remainder of the protein degraded in this way is shed into the extracellular space by enzymes such as sheddases. The regulated internalisation of GAG chains is as significant as synthesis, since defects in lysosomal enzymes responsible for membrane associated GAGs results in mucopolysaccharidoses (MPS). Accumulation of GAGs within cells is one of the characteristic features of Hunter syndrome as well as many other lysosomal storage diseases<sup>184</sup>.

#### **1.3.5.2 Sheddases and Heparanases**

Sheddases can convert membrane anchored molecules such as syndecans into soluble effectors that can produce agonistic or antagonistic functions. Therefore the activity of cell signalling molecules bound to syndecans at the cell surface can be modulated indirectly by this group of HSPG enzymes. Shedding accelerates the release of HS and sheddases may act by releasing growth factors from cell surface thereby disrupting gradient formation and signalling responses normally mediated by these growth factors<sup>185</sup>. The physiological role of shedding is not yet well understood, however syndecan shedding can be accelerated by cellular stress at the sites of injury or by plasmins, thus shed syndecans also have a role in recruiting chemokines<sup>186</sup>. In pathological conditions shed syndecan-1 can also promote tumour growth and progression<sup>187</sup> as well as promoting metastasis<sup>188</sup>. Interestingly shed

HSPGs remain biologically active and can regulate cell growth and metastasis, often being used as good indicators of disease severity and progression <sup>187,189</sup>. Recent insight into the mechanistic regulation of syndecan sheddases have shown shedding to be accelerated by heparanases <sup>190</sup>.

Heparanases (HPSE) also known as endo- $\beta$ -glucuronidases are a natural occurring group of HS specific enzymes that are responsible for degradation of HS chains (10-20 sugar units). There is evidence to suggest these fragments are more biologically active than native HS from which they are derived <sup>191</sup> and can promote growth factor activity <sup>192</sup>. Insight of HSPE function has largely come from tumourigenic studies whereby HSPE can indirectly promote angiogenesis by releasing HS bound growth factors such as VEGF and FGF2 that are residing in the ECM to enhance endothelial migration and proliferation <sup>155,175,193</sup>. HSPE can also enhance tumour growth and metastasis. In multiple myeloma HSPE appears to play a major role in regulating the tumour microenvironment since HSPE expression is increased in many myeloma cell lines. In addition to regulating the bioavailability of growth factors another route by which HSPE increase tumour growth is to upregulate the shedding of syndecans. In breast carcinoma cell lines HSPE can increase the levels of the soluble form of syndecan-1 further enhancing tumour growth and metastasis <sup>190</sup>. Consistent with these ideas HSPE can degrade HS chains of syndecan-1 and as a result syndecan-1 can mediate HSPE biological function <sup>194</sup>. However not all tumourogenesis requires the active form of HSPE, an inactive form of HSPE can promote cell adhesion, endothelial migration and invasion via indirect pro-angiogenic mechanisms <sup>195</sup>. The fact HSPE can regulate tumour progression in an inactive state suggests HSPE has another mode of regulating. Although exact mechanisms are not yet well understood a regulatory loop may exist between HSPE and sheddase to cooperatively regulate the tumour microenvironment <sup>196</sup>. Enzymatic degradation of HSPGs by heparanases and sheddases is likely to be involved in fundamental biological processes in normal development although it remains to be clarified. The nature of these enzymes further implies the significance of HS fragments as an indispensable tool for the activity of many growth factors and ECM molecules during vascular development without the necessity of the core protein.

## 1.4 Heparin/HS binding proteins

HS is a linear polysaccharide that belongs to a family of glycosaminoglycans, of which there are 6 members namely Chondroitin sulphate, Dermatan sulphate, Keratan sulphate, Hylauronic acid, Heparin and HS. Although HS was first identified through its closely related family member heparin, it is more widely distributed than heparin which is only found to be synthesised in connective tissue mast cells and O-2A progenitor cells <sup>197</sup>.

In addition to their distribution HS and heparin are also structurally distinct. Heparin/HS are made up of repeated disaccharide units of glucuronic acid (GlcA) and N-acetyl glucosamine (GlcNAc) residues that subsequently undergo deacetylation, epimerisation and sulphation at specific regions along the HS chain. The final sequence is composed of N, 2-O, 6-O and 3-O sulphate groups (Fig. 1.7). Whilst heparin is more highly sulphated and shows a small degree of diversity, HS is characterised by its alternating regions of low, partial and high sulphation content.

Evidence of the significance of the HS chains in modulating growth factors signalling comes from biochemical studies and structural studies modelling specific growth factor and HS interactions. Although there is a plethora of molecules critical to vascular development that bind to specific stretches of sulphated HS/heparin sequences (Table 1) such as TGF- $\alpha$  <sup>198</sup>, platelet factor 4 <sup>199</sup> HGF <sup>200</sup>, PDGF <sup>201,202</sup> VEGF <sup>203</sup> and FGF <sup>204,205</sup> only few examples will be discussed.

### 1.4.1 Fibroblast growth factors and receptors

Fibroblast family of growth factors (FGF) are amongst the most well characterised heparin/HS binding molecules. FGFs are involved in correct development and homeostasis of a wide range of cells and tissues. A wide variety of cells including neurons, epithelial cells,

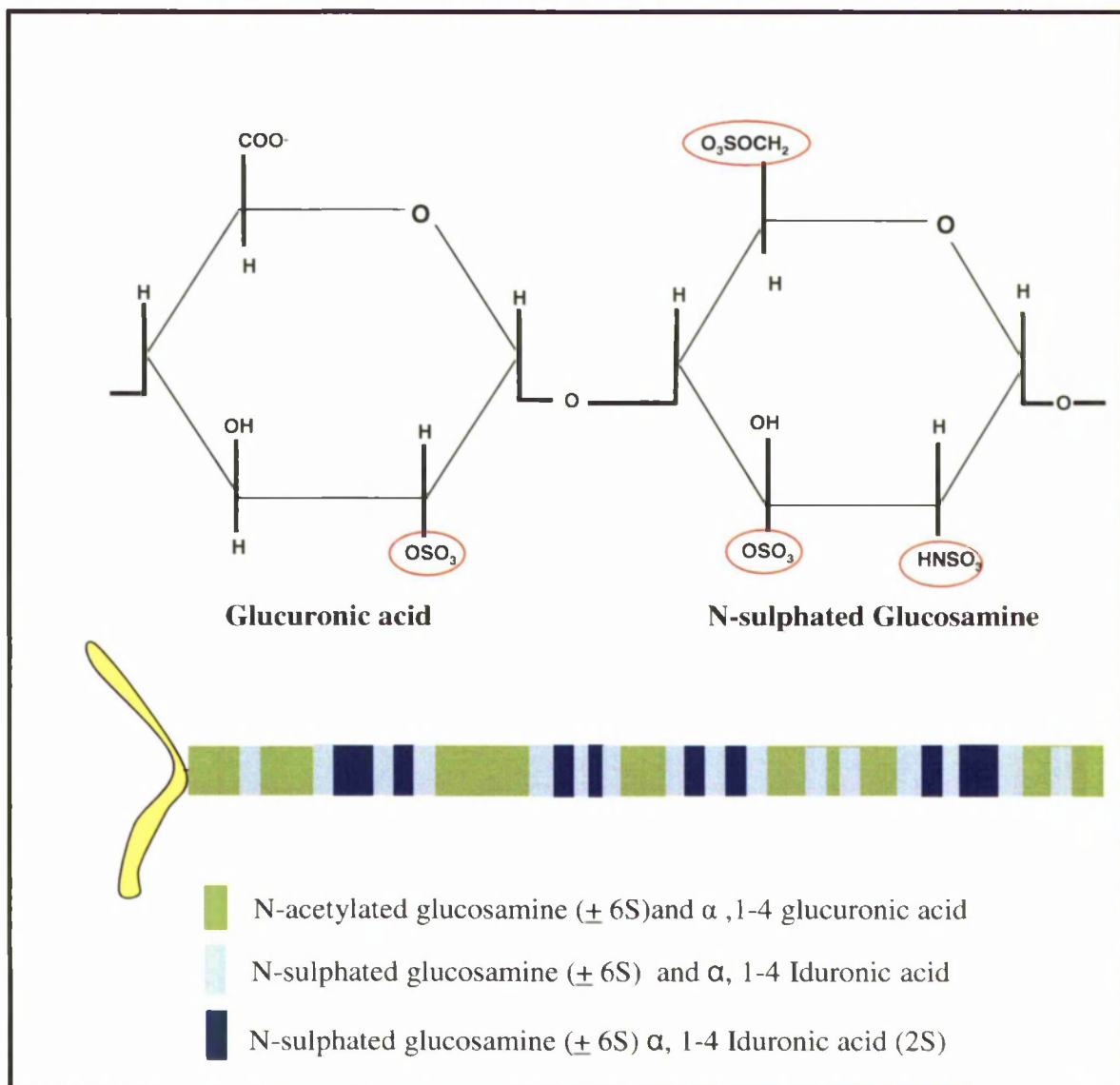


**Figure 1.7: Heparin/HS disaccharide structure of a HS chain.** HS chain is made of alternating units of glucuronic acid (GlcA) or iduronic acid (IdoA) and glucosamine residues (GlcN) that can be N-sulphated (NS) or N-acetylated (NAc). GlcNS can undergo further sulphation at C-3 and C-6 positions on GlcNS indicated by the red circle. GlcA and IdoA residues can undergo sulphation at C-2 position (indicated by red circle), however GlcA is rarely 2-O sulphated. HS chain is composed of regions of unmodified domain (green) interspersed with alternating regions of transition domain (light blue) and highly sulphated domains (blue).

fibroblasts and vascular smooth muscle cells express FGF1 and FGF2<sup>33</sup>. FGF2 can also be released by macrophages and by platelets in response to vessel inflammation and injury<sup>206</sup>. FGFs' signals are transmitted from the extracellular space into target cells via the cell surface protein receptors the FGFRs (FGF receptors). The high affinity receptors are the products of distinct genes namely FGFR1, FGFR2, FGFR3 and FGFR4. FGFR1-3 can be alternatively spliced to produce *a*, *b* and *c* isoforms. The *a* isoform is secreted and can function as a soluble receptor antagonist<sup>207</sup>, the *b*, and *c*, receptor variants display different ligand binding specificities and affinities<sup>208</sup>. FGFR2c can bind to FGF1 and FGF2 with equal affinity whereas FGFR2b binds FGF2 strongly than FGF1<sup>209</sup>. The FGFRs consist of an extracellular region of three Ig like domains (IgI, IgII, IgIII), a single transmembrane helix, and an intracellular tyrosine kinase domain. Following the binding of FGF to IgII and IgIII of the receptor tyrosine kinase domains the two receptors phosphorylate one another activating these domains to phosphorylate signalling targets thus FGF receptor dimerisation is crucial for efficient signal transduction<sup>210</sup>.

#### 1.4.1.1 FGFs and heparin/HS interactions

The FGFs and FGFR show high affinity for the polysulfated HS chain and its analogue heparin. In particular FGF1, FGF2, FGF4, FGF7 and FGF8 can bind heparin/HS modulating their biological activities *in-vitro* and *in-vivo*<sup>211</sup>. In addition to inducing FGF receptor dimerisation, HS sequesters FGF in the ECM and protects it from degradation<sup>175</sup>. Although FGFs have affinity for FGFRs in the absence of heparin, heparin increases the affinity of FGF for FGFR by one order of magnitude<sup>212,213</sup>. The presence of cell surface HS is required for a full range of signalling events associated with FGFR activation. It has been shown FGF-2, FGFR and heparin/HS can form a ternary complex in which HS increases the affinity of the growth factor for FGFR and HS chain serves as co-receptors. Evidence supporting the interactions of HS chains with FGFR reveals FGFRs possess heparin binding activity in IgII<sup>214, 215-217</sup>.

Two crystallographic models have been published for the FGF-FGFR-heparin complex that are predicted to form on different sites upon HS chains<sup>218</sup>. The assembly in which the two FGF-FGFR complexes are brought together to form the ternary complex is a topic of controversy since both models can exist in solution.

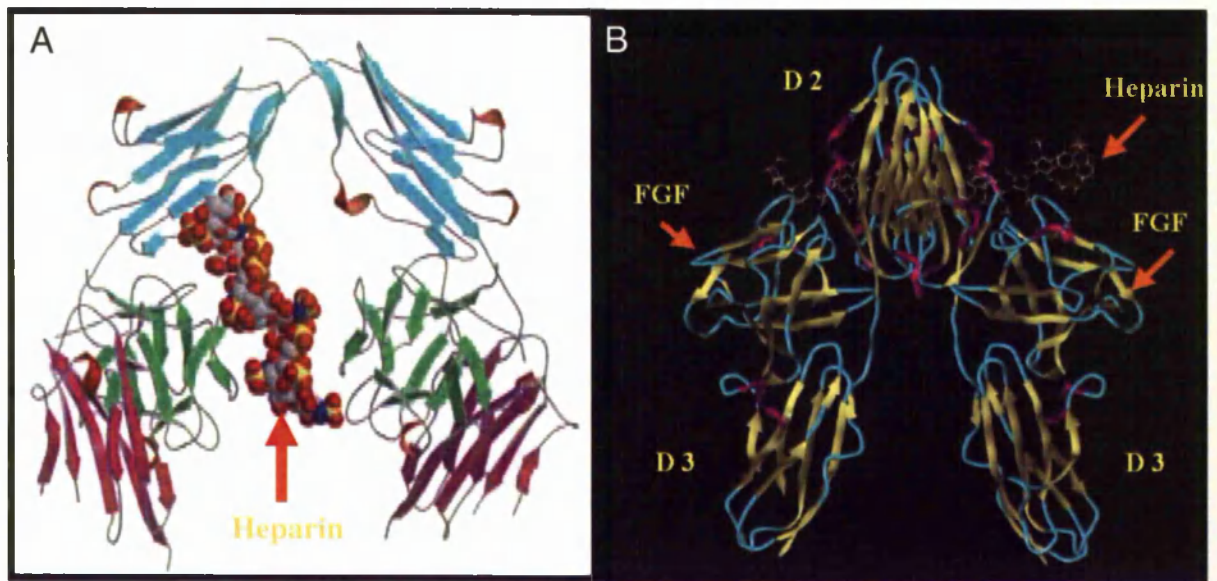


**Figure 1.8: Crystallographic FGF-FGFR-heparin models.** (A) The asymmetrical 2:2:1 complex published by Pelligrini and authors (2000). In the Pelligrini model heparin is the fundamental organising unit of the complex dimerising the two FGFs (cyan) in the absence of any protein-protein contact with FGFR (green-purple ribbons). (B) The symmetrical complex 2:2:2 published by Schlessinger and authors (2000). In the Schlessinger-Mohammadi model two heparin chains terminate at the centre of the structure, however interactions between FGFR (D2 & D3) and both members of the other FGF-FGFR complex (blue and yellow ribbons) are the main determinants of dimerisation, with heparin chains providing relief from electrostatic repulsion (Image taken from <sup>204,205</sup>).

The Pellegrini model shows heparin as the fundamental organising unit of the complex, dimerising the two FGFs in the absence of any protein-protein contact. This asymmetrical model is consistent with the crystallographic observations in a 2:2:1 FGF1-heparin complex<sup>205,219</sup> (Fig. 1.8A). In the alternative model by Schlessinger & Mohammadi the symmetrical 2:2:2 complex involves two saccharide structures that terminate at the centre of the structure. This model shows additional interactions between the FGFR and both members of the other FGF-FGFR complex as the main determinants of dimerisation with heparin contributing to the interaction and providing relief from electrostatic repulsion. This model also suggests that two molecules per heparin are also required per ternary complex<sup>204</sup> (Fig 1.8B). Recent experimental binding studies by Goodger and colleagues show the formation of either model is dependent on the sulphation and size of the heparin fragment<sup>220</sup>.

#### 1.4.1.2 HS structural requirements

The preparations of heparin derivatives and desulphated heparins have revealed the minimal sulphation requirements are different between the FGFs. *In vitro* studies have shown FGF1 to require a trisulphated disaccharide consisting of NS, 2S and 6S groups for binding and activity<sup>219,221-224</sup> with respect to the Schlessinger model this can only form at the highly sulphated region of two separate but proximal HS chains. Whereas FGF-2 requires disaccharides to be NS and 2S sulphated for maximum binding<sup>223,225</sup> and 6-O sulphate groups for activity<sup>222,226</sup>. Analysis of other FGFs shows similar heparin requirements as FGF1. Sequencing of heparin fragments has allowed more detailed studies of the specificity of FGFs and FGF-FGFR complexes showing in addition to sulphation the size of heparin/HS oligo is critical to this difference in FGF selectivity. Tetra and hexa saccharides absent in 2-O sulphation at the reducing end can still bind to FGF-2, but fail to dimerise FGF2 and the mitogenic potential is strongly reduced. However larger fragments such as octasaccharides, that are also independent of 2-O sulphation, can dimerise FGF2 and elicit a mitogenic response, thus the size and sulphation favours the formation of either symmetrical or asymmetrical ternary complex<sup>220</sup>. From *in-vivo* studies it appears the FGFR type plays a significant role in determining which heparins the FGF-FGFR bind since FGF-FGFRs show differences in the length and sulfation patterns of HS required to elicit the formation of FGFR dimers and biological activity. This exists even between pairs with a common FGF or FGFR and the FGF-FGFR complex has more specificity than either component alone in deciphering this specificity<sup>221,227</sup>. However recent finding by Kreuger and colleagues show that specific

sulphate groups can be bypassed by maintaining the overall sulphation density from either NS,2S,6S or 3S groups. This challenges the current criteria for HS selection, that specific sulphate groups are important in deciphering selectivity<sup>228</sup>. Although it appears selection of specific HS groups can be bypassed, these sulphates may be arranged spatially to dictate binding and the conformation the HS adopts could be more critical. As more NMR and mass spectrometry methods are available the conformation of HS is alluding to be an important factor in determining HS selectivity<sup>229</sup>. It can be concluded the biphasic role of HS to stimulate or inhibit FGF-2 signalling activities is strongly dependent on a combination of the chemical structure and length of the carbohydrate chain.

#### 1.4.2 VEGF-A and family of VEGFR

Vascular endothelial growth factor (VEGF) is another heparin/HS binding growth factor and has received much attention particularly as it is fairly specific to the vascular endothelium. VEGF-A is a homodimeric glycoprotein sharing greatest homology with PDGF family of growth factors. VEGF-A stimulated biological processes are mediated through their binding to three receptor tyrosine kinases VEGFR-1 (*flt-1*), VEGFR-2 (*flk-1/KDR*), VEGFR-3 (*flt-4*) and co-receptors such as neuropilins and HSPGs (Fig. 1.9). These are localised on the surface of various endothelial cell types<sup>230</sup>. VEGFR-1 and VEGFR-2 are expressed predominantly on vascular endothelial cells whereas VEGFR-3 expression becomes largely restricted to lymphatic endothelial cells and some fenestrated vascular endothelium<sup>231</sup>. Like VEGF, VEGFR-2 has shown to be expressed on other cell types such as tumour and neuronal cells and is responsive not only to VEGF-A but to short isoforms of VEGF-C & D<sup>232</sup>, whether they can induce a signalling response has not been determined. VEGFR-3 on the other hand is solely responsive to VEGF-C & D and is a regulator of lymphangiogenesis. However in zebrafish two copies of VEGF-A have been identified, *Vegf-a* is not required for the initial establishment of axial vessels but is important in the formation of angiogenic vessels. On the other hand in *Vegf-b* morphants, angiogenic formed ISVs are irregularly patterned and thinner showing *Vegf-a* and *Vegf-b* elicit distinct angiogenic response. Similarly in zebrafish three VEGF receptors can be identified *flk-1*, *flt-1* and *flt-4* with multiple copies of VEGFR-2<sup>233,234</sup>.

VEGFR-1 and VEGFR-2 are both upregulated by hypoxia and thus upon activation have been shown to fulfil different functional roles in angiogenesis. VEGFR-1 has stronger affinity for VEGF than VEGFR-2<sup>230,235</sup> but VEGFR-1 is weakly phosphorylated whereas VEGFR-2-VEGF-A binding causes dimerisation of the VEGFR and autophosphorylation of the tyrosine

residues. It is well known that VEGFR-2 mediates all angiogenic responses, as knockout of VEGFR-2 is embryonic lethal and mice die by E8.5 and E9.5. These mice exhibit defects in endothelial and haemopoietic differentiation<sup>236</sup>. Similar to VEGF-A mutants VEGFR-1 knockout mice are also embryonic lethal, and mice die as a result of disorganised network of blood vessels from excessive growth and branching of vessels that are non-functional<sup>237</sup>. VEGFR-2 mediates vascular endothelial cell like responses through the activation of phospholipase C- $\gamma$ 1 (PLC- $\gamma$ 1), phosphatidylinositol 3-Kinase (PI3-K) and the adapter molecule Shb<sup>238-240</sup>. Although VEGFR-1 can also interact with PI3K, phospholipase C, and Grb-2,<sup>241</sup> it's still not clear how signal transduction is induced. Surprisingly deletion of the tyrosine kinase domain of VEGFR-1 implicated in receptor dimerisation does not impair blood vessel formation in homozygous mice<sup>242</sup>. This suggests the signal transduction cascades induced by VEGFR-1 and 2 are somewhat different. VEGFR-1 has also been described by some as a negative regulator of VEGFR-2 signalling. A soluble form of *flt-1* can bind to VEGF thereby acting as a decoy receptor sequestering it from signalling through VEGFR-2<sup>243</sup>. VEGFR-2 is also capable of inducing different responses to different ligands for example VEGF-C can stimulate an angiogenic response through VEGFR-2 activation<sup>244</sup>, although VEGF-D can bind weakly to VEGFR-2 it does not induce a full angiogenic response, thus VEGF-D can stimulate EC migration but not proliferation. Although zebrafish *flk-1* morphants display less severe phenotype than murine *flk-1* knockout mice, one of the characteristic defects is arterial morphogenesis whereas vein development is unaffected, suggesting *flk-1* may cooperate with other receptors<sup>234</sup>. While the other *flk-1* homolog *Kdrb* appears to have a redundant role in arterial development expression of other VEGF receptors such as *flt-4* have shown to participate in arterial venous differentiation<sup>233</sup>. *Flt-4* morphants display defects in ISV formation and cranial central arteries<sup>101</sup>. Recent studies in zebrafish *flt-4* mutant have shown *flt-4* to be specifically important in mediating arterial morphogenesis and angiogenesis<sup>245,246</sup>. This suggests *flt-4* along with *flk-1* has a role in vasculogenesis as well as angiogenesis than previously anticipated from mouse studies<sup>247-250</sup>.

In both organisms there is growing evidence that suggests *flt-4* can modulate *flk-1* signalling by forming heterodimers with *flk-1*. In endothelial cell culture VEGFR-2-VEGFR-3 heterodimers display distinct phosphorylation patterns when compared to VEGFR-2 or VEGFR-3 homodimers<sup>251-253</sup>. Furthermore in zebrafish, *flt-4* morphants display defects in arterial formation like *flk-1* morphants, substantiating its cooperative role in arterial formation.

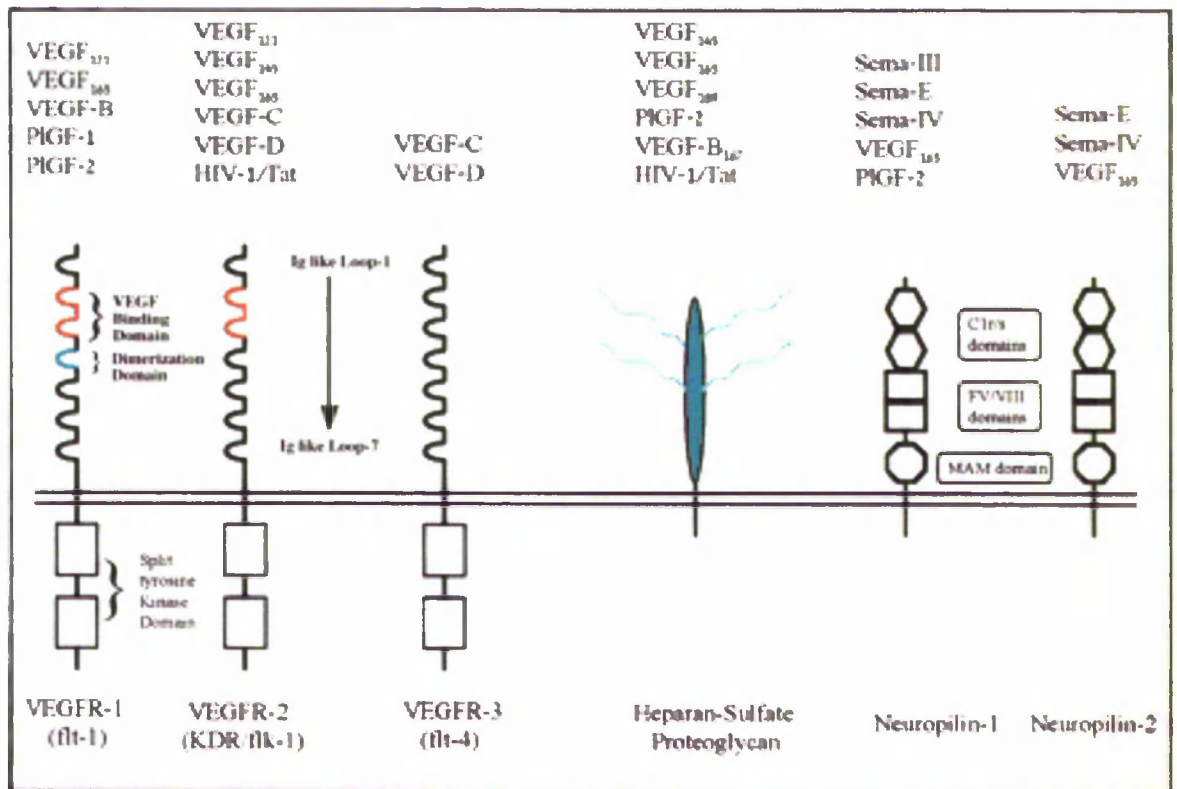


**Figure 1.9: Schematic representation of VEGF family of growth factors and VEGF receptors.** VEGFA isoforms mediate endothelial cell responses through binding to their high affinity receptors VEGFR-1 and VEGFR-2, other related growth factors PIGF and VEGF-B can also bind. Heparan sulphate proteoglycans (represented by a syndecan) and neuropilins acts co-receptors and bind to certain isoforms of VEGFA, however are unable to transduce a signal in the absence of tyrosine kinase receptors. Neuropilins are also receptors to the semaphorin family members involved in neuronal cell guidance and axonal growth (Image taken from <sup>244</sup>).

*Vegf-c* morphants display more severe defects compared to *flk-1* and *flt-4* morphants implying *Vegf-c* can activate both *flk-1* and *flt-4*<sup>101</sup> and signal through the formation of the heterodimers. VEGFR-3 (*flt-4*) is also essential for lymphatic development, in mice and zebrafish<sup>254</sup>. The exact role of *flt-4* in the zebrafish lymphatic system<sup>88</sup> has not yet been proven. It is conceivable that such cooperativity between VEGF receptors may exist in the lymphatic system. However VEGF-A can also bind to co-receptors such as Neuropilins and HSPGs, that have shown to modulate VEGF signalling<sup>255,256</sup> but these tend to be isoform specific.

#### 1.4.2.1 Splice Variants of VEGF-A

One of the key events of VEGF-A regulation is the splicing event that yields different lengths of VEGF mRNA, this not only confers structural differences but results in the striking contrasting expression and properties of VEGF-A family. VEGF-A is encoded by a single gene mapped to chromosome 6. The coding region of the gene contains 9 exons<sup>257</sup>. Through a mechanism of alternative mRNA splicing, different VEGF isoforms are generated that vary in their amino acid length. To date seven isoforms of the human VEGF genes have been investigated VEGF121, 145, 165a, 165b, 183, 189 and 206 (Fig 1.10). VEGF165b was latest isoform to be identified by Bates and colleagues that is shown to be generated by the inclusion of the exon8 distal splice site resulting in an isoform that differs in the C-terminal by 6 amino acids<sup>258</sup>. The mechanism by which these isoforms levels are regulated is not yet well understood. The isoforms differ in the presence or absence of exon6a, 6b and 7a, all of which encode for motifs that bind to heparin/HS<sup>259</sup>. These isoforms are all glycosylated and can bind heparin with the exception of VEGF121. The presence of the heparin/HS binding domain encoded by exons 6&7 contributes to the differences observed amongst isoforms, in terms of structure, function and cellular location<sup>260</sup>.

All isoforms possess a signal peptide and are secreted, but only VEGF121, 145 and VEGF165a are rendered diffusible. VEGF121 is the most soluble isoform due to its lack of heparin binding domains, and consequently has reduced retention at the cell surface and ECM. In contrast VEGF189 and VEGF206 contain both exons in their genetic makeup and through binding to HSPGs are completely sequestered in the ECM. The ECM bound isoforms can be released slowly by exposure to heparin or heparanses or through proteolytic cleavage such as plasmin and urokinase (uPA) that allows a mitogenic response which is otherwise hindered due to their large protein structure<sup>261,262</sup>. Proteolytic cleavage of VEGF189 by uPA can yield fragments with equal mitogenic activity to that of VEGF165a,

however not all VEGF isoforms contain a uPA site and can be cleaved by plasmin. The VEGF110aa fragment generated by this manner has 50% reduced mitogenic activity akin to that of VEGF121<sup>262</sup>. VEGF165a on the other hand has intermediate properties with a significant proportion (50-70 %) of it remaining bound to the cell surface and ECM<sup>261</sup>. This retention in the ECM is contributed by its heparin/HS binding capability. The 15 amino acids within the 44 residues encoded by exon 7 confer the heparin binding domain. Although most VEGF producing cells appear to express all three isoforms VEGF189, VEGF165, and VEGF121, VEGF121 and VEGF165a are the most potent isoforms. This is equally true in zebrafish where the presence of both isoforms results in effective upregulation of *flk-1* and *tie-1* expression rather than either isoform alone<sup>263</sup>.

Mice isoforms of VEGF are shorter than human by one amino acid. Each isoform can form dimers capable of binding to receptor tyrosine kinases, but studies in mice have shown their ability to stimulate mitogenicity differs amongst each other<sup>263,264</sup>. Mouse equivalent VEGF121 and VEGF165 isoforms display different phenotypes during retinal vascular development. Mice expressing just the VEGF164 isoform exhibit a normal healthy phenotype. In contrast mice expressing solely VEGF120 exhibit severe defects in vascular growth and patterning, these mice die shortly after birth as a consequence of impaired myocardial angiogenesis. VEGF188 mice display normal venous growth but arterial development is impaired. This suggests that VEGF121 alone is insufficient for angiogenesis<sup>264</sup> and highlights the importance of the heparin/HS domains encoded by exon6 and 7 in generating a functional VEGF signalling response. Corresponding studies of the mice isoforms in embryonic hindbrain development show HS is important in vascular patterning by restricting the bioavailability of the different VEGF isoforms<sup>265</sup>. A heparin binding domain exists also in the VEGF165b isoform presumed to have an antiangiogenic role, although it is able to bind to VEGFR-2 with the same affinity as VEGF165a it is unable to induce a full mitogenic response. However it has been reported VEGF165b can induce a transient vascular permeability response through the activity of VEGFR-1<sup>266</sup>, thus VEGF165b is expressed in the same tissues as VEGF165a albeit at lower concentration and can act as a competitive inhibitor of VEGF165a thereby negatively regulating angiogenesis. Even though the heparin binding domain is conserved this implies HS is required more for spatial distribution and maximum binding efficiency as opposed to signalling. Nevertheless it could imply the C-terminal structure of the isoform plays an essential role in inducing a conformational change of the protein to its receptor. This suggests that the sequences encoded

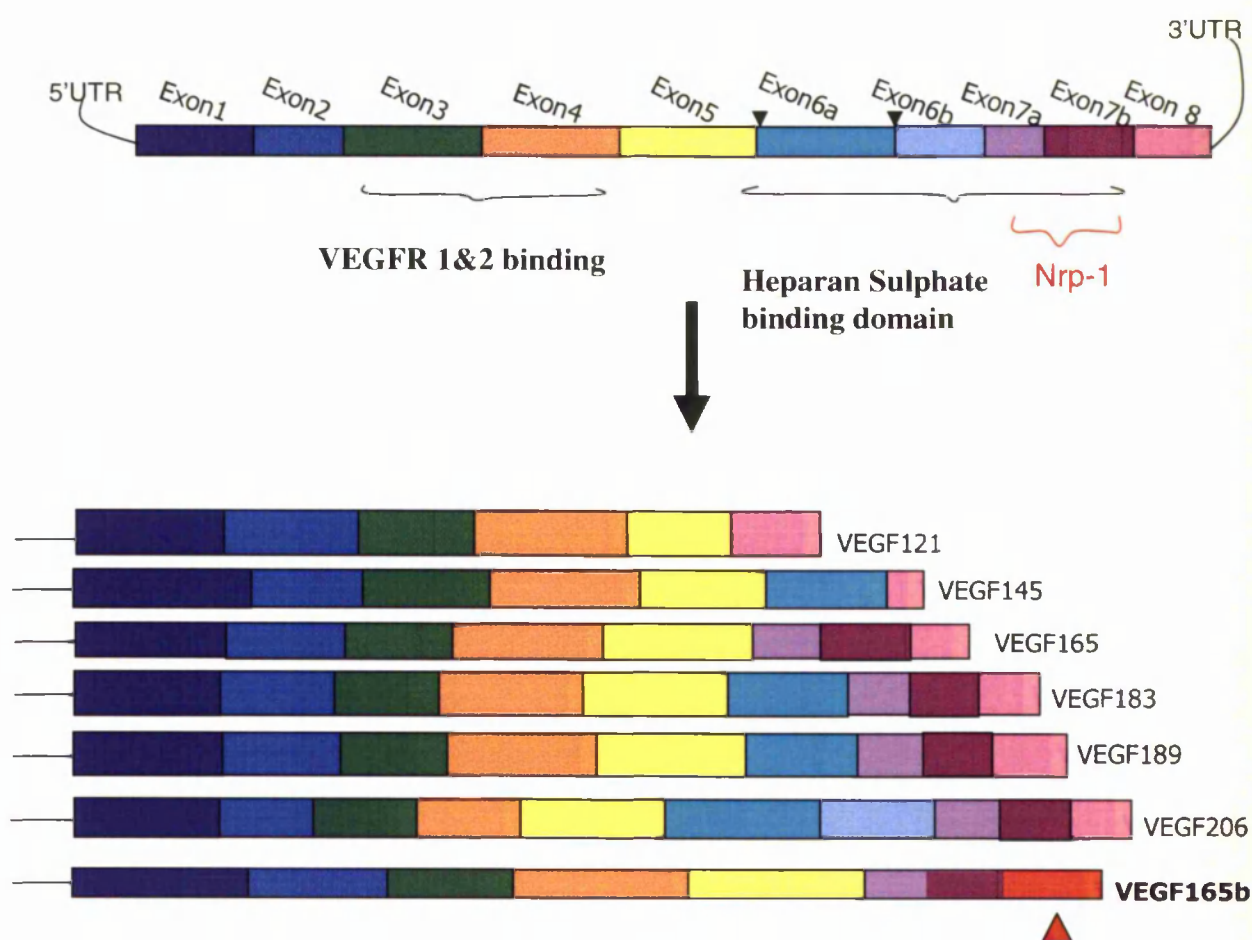


**Figure 1.10: Alternative splice variants of human VEGF-A gene.** The human VEGF gene through alternative splicing can produce seven isoforms, which differ in the presence and absence of the sequences encoded by exons 6 and 7. Sites of interaction with VEGFR1-2 exist between exons 2-5, Heparin binding domains exist in exons 6 and 7, and neuropilins bind to exon 7. Black arrowheads denote sites of cleavage by plasmin and uPA (urokinase type plasminogen activator). Domain sizes are shown at the end of the chain. Red arrow denotes the variation in VEGF165b isoform containing an exon short of six C-terminal residues (adapted from <sup>257</sup>).

By exon 6 and 7 confer different properties to VEGF isoforms, which are not only important in eliciting an angiogenic response but may have implications as to the additional functions of HS on VEGF mediated angiogenesis.

#### 1.4.2.2 Roles of VEGF165 in vascular development

A key feature of VEGF expression is the ability to induce multiple responses that are coordinated between endothelial cells for correct patterning, function and development of the vasculature. In addition to its well documented roles of inducing EC migration, differentiation and proliferation. VEGF is also required for the continued survival of EC due to its ability to inhibit apoptosis and capillary regression<sup>267</sup>. VEGF can also induce migration not only of EC but other cell types including angioblasts, haematopoietic precursors, monocytes and osteoblasts<sup>268,269</sup>. The ability of VEGF to exert a migratory role relies on its formation of chemotactic gradients to attract different cell types. VEGF upregulation can also enhance the expression of its cognate receptor (particularly found in tumour necrotic areas). Thus a unique response of VEGF-VEGFR signalling is the ultimate formation of the three dimensional vascular tube. VEGF also has strong permeability activity, hence its original name as vascular permeability factor VPF. This allows plasma proteins to leak into tissues forming a provisional ECM<sup>270</sup>. In addition to this permeabilizing role VEGF can mediate vasodilatation through inducing nitric oxide and consequently increase blood flow that precedes angiogenesis.

Studies in zebrafish have proven useful for dissecting vascular developmental pathways that elucidate the signalling pathway and mechanism by which VEGF regulates the processes mentioned above. One of the key processes yielded from the VEGF zebrafish mutants is its role in regulating arterial and venous differentiation of endothelial cells. While VEGF can induce multiple responses it is unlikely that these pathways are activated all at once. VEGF-A is shown to mediate distinct cellular outputs through distinct signalling VEGFR-2 and VEGFR-3 pathways<sup>108</sup>. Mutants of the VEGF signalling pathway such as phospholipase PLC- $\gamma$ 1 or *flk-1*(Kdra) genes affects arterial differentiation and development whilst vein development is unaffected<sup>91,106,234,271</sup>. Reduction of *flt-4* however affects only arterial morphogenesis, suggesting that *flk-1* and *flt-4* signal through distinct cellular pathways to regulate vascular development. The ability of VEGF to modulate response either through *flk-1* or *flt-4* has shown to require the activation of the Notch signalling pathway<sup>108</sup>.

### 1.4.2.3 Role of Heparin/HS in VEGF165 mediated angiogenesis

The ability of certain VEGF isoforms and their receptors to bind HS/heparin led to early suggestions that HS/heparin can modulate their activity. Indeed early studies show the profound effects of HS/heparin on VEGF and VEGFR. In HS depleted cells VEGF165 has reduced affinity for VEGFR-2 but this interaction is enhanced by addition of exogenous heparin<sup>272</sup>. However the VEGF165-VEGFR1 interaction in heparinase depleted cells is completely lost and addition of exogenous heparin only partially restores VEGF165 binding<sup>273</sup>. It is thought that VEGFR-1 and VEGF165 interaction requires cellular HSPGs and their role may be to present VEGF165 to its receptor<sup>273</sup>. However recent studies have shown that heparin not only enhances VEGF165-VEGFR-2 binding, but can amplify the signalling of VEGF165 (not VEGF121) through VEGFR-2 phosphorylation thus increasing VEGF dependent mitogenic activity and vascular tube formation<sup>274</sup>. The participation of heparin/HS in VEGF signalling can occur in a non-cell autonomous manner suggesting a novel mechanism of HS-VEGF mediated signalling<sup>151</sup>.

Besides modulating VEGF receptor activity, heparin/HS plays an important role in shaping the extracellular distribution of VEGF. The formation of the VEGF concentration gradient, requires essential guidance cues for vascular growth and branching<sup>265</sup>. Disruption of VEGF concentration results in restricted protrusive activity and migration of sprouting vessels in mice embryonic hindbrain<sup>275</sup>. In addition to localising VEGF, heparin interactions can also prolong their activity. Thus sequestration of VEGF in the ECM can protect it from enzymatic degradation<sup>261</sup> and natural inhibitors such as platelet factor-4 and  $\alpha$ 2-macroglobulin<sup>276</sup>. As mentioned previously ECM HSPGs bound to VEGF can release other HS bound growth factors such as FGF in the ECM, and can synergistically stimulate angiogenesis<sup>57</sup>. It has been determined that heparin/HS can restore the function of damaged VEGF. Thus in processes such as wound healing, oxidising agents can inactivate VEGF. However HSPG such as Glypican -1 can fulfil a role of a chaperone and restore VEGF binding ability to VEGFR-2<sup>169</sup>. In addition heparin/HS can also mediate the association of several different isoforms of VEGF to Neuropilin (Nrp) co-receptors. From both mice and zebrafish studies it has been shown NRP-1 is a mediator of VEGF dependent angiogenesis It has been speculated that NRP could initiate VEGF activity independent of VEGFR-2, as in tumours where NRP-1 is the only receptor present tumour angiogenesis increases<sup>256,277</sup>. Thus one study proposes NRP might associate with plexin transmembrane proteins through binding to semaphorins and consequently transduce signals through activation of small G-proteins and cytoskeleton<sup>278</sup>

mitigating some of the endothelial like responses. NRP-1 can also bind to heparin/HS, furthermore heparin/HS facilitates binding of VEGF165 to Nrp-1, where the role of NRP might be to serve as part of the multicomplex conformation to initiate VEGF downstream signalling<sup>279</sup>. In conclusion heparin/HS can affect VEGF bioavailability through affecting its diffusion, its half life and interaction with VEGFR.

#### **1.4.2.4 VEGF-VEGFR and HS/heparin interactions**

Although there is a vast knowledge on the wider roles played by heparin/HS in VEGF-mediated angiogenesis, the molecular mechanisms by which heparin/HS binds and regulates VEGFR is yet not clear, nevertheless sites for VEGFR/HS interaction have been modelled theoretically. VEGFR-1 is found to contain a heparin binding domain in fourth Ig loop which has been also been implicated in dimerisation<sup>280</sup>. VEGFR-2 can interact with heparin/HS and this is thought to be mediated through a hexapeptide sequence located between 6 and 7 Ig domains<sup>281</sup>. Although heparin binding domains in VEGF receptors have been identified no specific residues have been highlighted. Two identical heparin binding sites however have been found to exist on the VEGF165 dimer with both monomers binding to the same HS chain. Molecular modelling studies, with different length heparin molecules (5, 7 and 11 oligosaccharides in length), revealed interactions with the same basic residues Arg124, Arg145, Arg149, and Arg159<sup>203</sup>. In agreement with this, site directed mutagenesis studies also identified these as potential residues (Fig. 1.11). It appears that interactions between HS/heparin and the VEGF receptor contribute to allow maximal VEGF binding. However little is known about the action mechanism whether heparin/HS binds to VEGF or VEGFR-2 or both, simultaneously. Thus a model proposed by Ashikari and colleagues hypothesize, that in the presence of heparin a ternary complex is formed. This is thought to occur between VEGF, VEGFR2 and neuropilins through linking of a heparin molecule consistent with multiple HS binding sites on VEGF. However with the possible VEGF165-VEGF2 signalling also being regulated by HSPGs and neuropilins on neighbouring cells<sup>151</sup> adds a new level to the array of ternary complexes that could be formed and the number of heparin/HS molecules that maybe required. It is possible like FGF heparin may induce conformational changes in VEGF to bind and induce receptor dimerisation since the nature of VEGF molecule bound to heparin is such that it can interact at multiple sites.

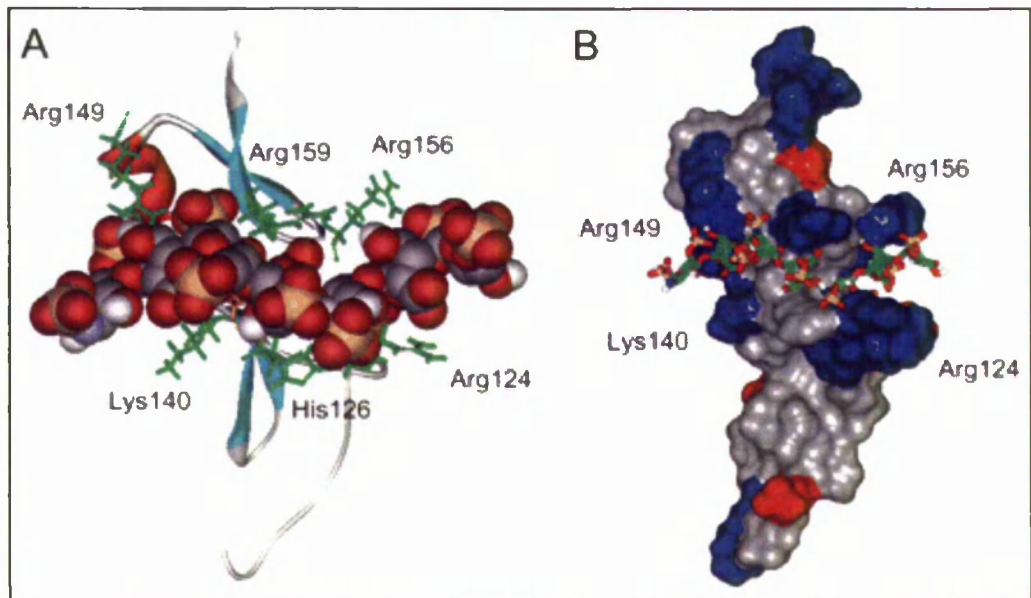


**Figure 1.11: Molecular modelling of a potential heptasaccharide docked with the VEGF165 heparin binding domain.** (A) Ribbon diagram of heptasaccharide docked in a region of the VEGF165 heparin binding domain. Molecular modelling depicts the most favourable intermolecular interaction energy calculated by Autodock. (B) Heptasaccharide is shown in a stick representation, the same complex showing the proximity and location of the heptasaccharide in relation to the VEGF165 monomer and potential amino acid residues involved in this interaction. (Image taken from <sup>283</sup>).

Similar to dissecting the HS requirements from FGF, binding studies of VEGF<sub>165</sub> and heparin/HS chains reveal that 2-O sulphation is not essential for binding to VEGF as in FGF and HGF, though 2-O sulphate groups are important for mitogenic activity of VEGF<sup>203,282</sup>. Heptasaccharides consisting of NS and 6S sulphate groups have also shown to be important for binding, particularly 6-O sulphate groups. Robinson and colleagues showed the minimal length of HS chain that can bind to VEGF is 22 saccharides in length and the fragments generated by HS specific enzymes K5 lyase i.e. N-acetylated and sulphated domains, bind stronger to VEGF monomer than the smaller sulphated domains alone. It can be deduced that alternating regions of HS sulphation are critical for spacing of the s-domains linking the two heparin binding sites allowing the binding of multiple sulphated domains to VEGF dimer<sup>283</sup>.

### 1.4.3 Heparin/HS oligonucleotides as a therapeutic tool

On the basis that size and sulphation patterns of heparin/HS can promote or attenuate angiogenic activity of several angiogenic molecules such as VEGF, HGF, PDGF and FGF-1 (Fig. 1.1) has led to several heparin like anionic molecules and heparin derivatives being tested as possible candidate drugs<sup>284</sup>.

Traditionally heparin has been used for over half a century as an anticoagulant, and plays a major role in determining the anticoagulative properties of the vessel surface, by binding to thrombin and protease inhibitors such as antithrombin III via a pentasaccharide sequence<sup>285</sup>. Heparin can also bind to platelet factor 4 (PF4) neutralising the activity of heparin like molecules such as antithrombin III therefore behaving as a procoagulant. PF4 is also chemoattractant for neutrophils, fibroblasts and monocytes and has a role in wound healing and repair<sup>286</sup>. PF4 is an important component of the anticoagulant effects of heparin<sup>287</sup>. As a result low molecular weight heparins (LMWH) are often used to prevent deep vein thrombosis (DVT) in patients with cancer. LMWH are shown to reduce the risk of bleeding complications<sup>288</sup>. Several *in-vitro* studies have shown LMWH to hinder the binding of growth factors to their receptors. *In-vitro* heparin fragments of less than 18 saccharides in length can reduce the activity of VEGF, and fragments of less than 10 saccharides also inhibit the activity of FGF. Soluble heparins compete with HS for the binding of growth factors<sup>289</sup>. Smaller molecular weight heparin fractions have also been shown to inhibit VEGF and bFGF mediated angiogenesis in contrast to unfractionated heparins *in-vivo*. As a result several oligosaccharides for example pentosan polysulfate have entered clinical trials but

unfortunately have long term complications such as hypercoagulation.<sup>290,291</sup> Certain treatments with LMWH or heparin has had no effect on tumour associated angiogenesis in colon cancer metastasis of rat liver<sup>292</sup>. Some LMWH such as Dalteparin however have been shown to improve survival of cancer patients<sup>293</sup>.

Both animal and *in-vitro* experiments have shown that heparins/HS chains can interfere with the angiogenic process and that these effects are not exclusively related to anticoagulant function of heparin but its ability to bind growth factors and ECM molecules involved in the angiogenic process. However it is still a matter of debate whether heparins and anticoagulant agents interfere with cancer progression and alter the prognosis of patients with malignancies. Although the effects of heparins on angiogenic growth factors have been discussed here, heparins can also modulate angiogenesis through their anticoagulant function. Thus activity of proteolytic enzymes binding to ECM components and pericytes implies the complexity in designing efficacious heparin/HS therapeutic agent. However it appears LMWH can improve survival rates in some human malignancies but more extensive trials are needed to confirm this hypothesis. The suitability of heparin oligos entering clinical trials is somewhat a topic of controversy and thus alternating strategies to exploit HS is continuously of immense clinical interest. One alternative approach to exploit heparin/HS chains has been to genetically modify HS chemical chain structure by generating knockout models and transgenic mutants of HS biosynthesis enzymes to assess their potential as anti or pro-angiogenic therapeutic targets.

## 1.5 Heparin/HS Biosynthesis

Heparan sulphate is complex and diverse polysaccharide chain that is abundant in many mammalian cells. The negatively charged polymer has a typical chain length between 50-200 disaccharides in length. HS sequence is not directly encoded by genes but is synthesised by the concerted action of multiple enzymes and the relative concentrations of these enzymes determine the overall HS structural organisation and consequently have shown to regulate the functional activity.

The HS chain is made up of repeated disaccharide units of glucuronic acid (GlcA) and N-acetyl glucosamine (GlcNAc). The precursor chain undergoes a series of biochemical reactions that partially modify its structure. This includes N-deacetylation and N sulphation of GlcNAc residues, C5 epimerisation of GlcA into IdoA, 2-O sulphation of both GlcA and

IdoA, 3-O sulphation and 6-O sulphation of glucosamine residues and a final post HS chain modification occurs at cell surface removing 6-O sulphate groups from sulphated glucosamine residues. This occurs non-uniformly throughout the chain forming regions of unmodified domains (GlcA-GlcNAc) interspersed with alternating partially modified sulphated domains (IdoA-GlcNS6S/GlcA-GlcNS6S) and highly sulphated domains (S domains). Many aspects of HS are also shared by heparin but contain a higher degree of polymerisation<sup>294</sup>. The domain structure of HS is easily distinguishable from heparin as it consists mainly of domains of IdoA-2S-GlcNS6S. A key feature of HS is the structural heterogeneity generated by non-uniform HS modifications that occur throughout the chain, thus reflecting the dynamic expression and regulation of the biosynthetic enzymes<sup>295</sup>. Most of the enzymes have been purified, cloned and characterised. The molecular mechanisms of HS synthesis enzymes and their significance in HS regulated processes have been derived from experimental studies in cell culture and animal models (Fig 1.12). Characterisation of these enzymes has revealed several isoforms with difference in specificity and expression pattern. Genetic and biochemical knockdown of these enzymes have not only revealed how important HS structure is but minor alterations in sulphation patterns have drastic consequences on many cell-signalling pathways, implying that HS synthesis is under strict regulation and distinct structural patterns of HS are critical for specificity.

### 1.5.1 HS Chain initiation

HS chain synthesis initiates in the Golgi. After the core protein has been synthesised in the rough endoplasmic reticulum it is translocated to the golgi for addition of GAG chains. The linkage to the protein core occurs via a common tetrasaccharide linkage region GlcA $\beta$ 1, 3 Gal $\beta$ 1, 3- Gal $\beta$ 1,4- Xyl $\beta$ 1,4, the xylose residues are transferred to specific serine residues on the protein core through the action of xylotransferases and the remaining residues are added by galactosyltransferases and glucuronosyltransferases respectively. It is the addition of the fifth residue that determines the type of GAG chain that is attached. Addition of  $\alpha$ -GlcNAc by N-acetyl glucosamine transferase, commits the chain to HS or heparin synthesis; where as the addition of  $\beta$ -GalNAc commits the chain to CS and DS<sup>296</sup>. It is thought that the HS selection is dependent on the protein sequence which surrounds the xylosylation site on the protein core. The downstream positioning of the acidic sequences Glu-Asp-Leu-Gly favour HS synthesis<sup>296</sup>. Thus addition of HS is

HS Biosynthesis Enzyme	Phenotype/ signalling molecule involved
<i>EXT-1, EXT-2</i>	Embryos fail to gastrulate, embryonic lethal, central nervous system, Ihh signalling
<i>NDST-1</i>	Neonatal lethal, pulmonary atelectasis, cyanosis, cranial haemorrhage, Hh, PDGF
<i>NDST-2</i>	Mast cells deficiency
<i>C5 epimerase</i>	Neonatal lethal renal agenesis lung defects
<i>HS2ST</i>	Neonatal lethal, renal agenesis, FGF
<i>HS6ST-1</i>	Embryonic lethal, angiogenesis defects
<i>HS6ST-2</i>	Embryonic mice survive and fertile
<i>HS3ST</i>	Normal coagulation
<i>Sulf1</i>	Reduced body mass and growth, skeletal, muscle innervation and neurological defects, GDNF
<i>Sulf2</i>	Reduced body mass and growth, skeletal, lung, muscle innervation and neurological defects, GDNF
<i>Dackel and Boxer (Ext2, Ext3)</i>	Axon sorting FGF4, FGF10
<i>Glce (C5 epimerase)</i>	Gastrulation defects, Bmp-4
<i>zfHS6ST-1</i>	Muscle differentiation, Wnt
<i>zfHS6ST-2</i>	Angiogenesis, VEGF
<i>Sugarless (HS copolymerase)</i>	Abnormal segmentation Wnt, Hh,
<i>Sulfateless (NDST)</i>	Abnormal segmentation Hh, TGF- $\beta$
<i>dHS2ST</i>	Branching morphogenesis and tracheal development FGF
<i>dsHS6ST</i>	Branching morphogenesis and tracheal development FGF
<i>dsHS3ST</i>	Tracheal and nerve development, Notch

**Figure 1.12: A partial list of mutants defective for HS biosynthesis enzyme in different species:** purple box highlight HS mutants in mice, light blue highlight zebrafish and yellow highlights *drosophila* HS mutants. The phenotypes of these mutants are listed and were possible signalling molecules contributing to these defect are mentioned. The table represents the wide variety of developmental processes influenced by HS biosynthesis, in particular the enzymes responsible for constituting different HS binding epitopes (adapted from <sup>295</sup>). References can be obtained from the main text (section 1.5).

favoured more if there is a Ser-Gly repeated motif Ser-Gly-Ser-Gly<sup>297</sup> flanked by a cluster of acidic residues at the N-terminus and hydrophobic residues at the C-terminus. The addition of the first GlcNAc residue initiates the polymerisation step thus alternating GlcA and GlcNAc are added stepwise to the non-reducing end of the forming HS chain. This is carried out through the action of glycosyltransferases which are encoded by a family of tumour suppressor genes EXT (Exotosin)

Vertebrate exotosin genes include EXT-1 and EXT-2. The importance of these enzymes in HS synthesis has been shown in Ext-1 knockout mice. Ext-1 deficient mice fail to gastrulate and exhibit bone growth deficiencies, as a result mice die at birth<sup>298</sup>. Analysis of the mutant brain in Ext-1 mice shows its important role in CNS assembly<sup>299</sup>. Even in hypomorphic Ext-1 mutant mice where HS loss is minimal, deformities were directly observed in chondrocyte differentiation linked to expansion of Indian hedgehog (Ihh) distribution and signalling. Similar Hh signalling was impaired in *drosophila* Ext mutants *tout-velu* (Ext-1), *sister of tout-velu* (Ext-2), and *brother of tout-velu* (Ext-3) in which Ihh was impaired, suggesting HS is important in Hh distribution<sup>300</sup> in addition to the core protein. Mutations in the EXT family has been associated with hereditary multiple exotoses a bone disorder characterised by benign bone tumours<sup>301</sup> although the underlying pathways affected is not yet well understood it is thought this is possibly caused by prolonged activation of Ihh signalling. However mutations of the EXT genes are less severe in the zebrafish, this could be attributed to multiple copies of the genes that exist, thus Ext-1 has three different isoforms with overlapping and distinct expression patterns<sup>302</sup>. Ext-2 (*dackel*), Extl-3 (*boxer*) and double mutants deficient for both Ext-2, Extl-3, genes, have an overall reduction of HS and exhibit defects in pectoral fin, branchial arch development and axonal guidance particularly in the optic tract<sup>303-305</sup>. The latter defects are thought to result as defect in Slit-Robo signalling however in single mutants this pathway is not affected suggesting that in the double mutants a certain degree of HS can function in these morphants<sup>305</sup>. Branchial arch defects have been linked to attenuation of FGF-10 signalling, thus administration of FGF-4 protein can activate target gene expression in both *dackel* and *boxer* mutants showing differential specificity of HSPGs in regulating the activities of different FGF ligands in vertebrates<sup>303</sup>. This implicates the different developmental pathways that Ext-1 can affect and may also be the signalling pathways affected in EXT-2 linked human diseases human that could be applied therapeutically.

### 1.5.2 Chain Modification

The next step in synthesis is a series of modifications that take place on the sugar residues. Firstly the polymer is partially N-deacetylated and then N-Sulphated through the action of a bifunctional enzyme N-deacetylase-N-sulfotransferase (NDST) (Fig. 1.13). To date four NDST have cloned and have not only found to be encoded by four different genes (NDST-1,2,3& 4) but differ mildly in functional activities and expression thus NDST-1 &2 only show signs of similar activities<sup>306</sup>. The enzyme typically modifies 40-50% of GlcNAc to GlcNSO<sub>3</sub> leaving some substrates unmodified<sup>294</sup>. The basic N-sulphation pattern of HS is very much dependent on the isoforms present and different combinations of the isoform may account for the differences in HS observed in different tissues. NDST-1 and NDST-2 are the most widely expressed in all embryonic and adult tissues with NDST-2 expression being particularly abundant in mast cells<sup>307,308</sup>. NDST3 &4 are expressed during embryonic development and then restricted to the adult brain. NDST-3 and NDST-4 have opposite levels of deacetylation and sulphation activities with the latter enzyme displaying weak deacetylation and high sulfation<sup>309</sup>. This led to the proposal NDST-3 and NDST-4 act mainly on partially modified N-glucosamine residues by NDST-1/NDST-2 suggesting differences in substrate specificities exist. Likewise these enzymes exhibit different properties with NDST-1 having higher sulphation and low acetylation activity in contrast to NDST-2

The difference in levels and distribution of the isoforms are consistent with the differences in phenotype observed in the NDST-1 and NDST-2 deficient mice. NDST-1 is widely distributed whereas NDST-2 expression is mainly confined to heparin producing mast cells. NDST-1 deficient mice die shortly after birth due to defects in lung development, accompanied by a reduction in N & O sulphation and epimerisation of HS<sup>310</sup>. In contrast NDST-2 deficient mice show a less severe phenotype thus mice are able to synthesise HS but not heparin and as a consequence exhibit severe defects in mast cell differentiation<sup>311</sup>. Different isoforms have different substrate preferences suggesting NDST-2 can also act on partially modified substrates<sup>312</sup> to form highly sulphated heparin but more importantly multiple isoforms contribute to the formation of HS chains.

NDST-1 deficient mice display cerebral hypoplasia and craniofacial defects that are consistent with impaired Shh and FGF activity<sup>313</sup>. Analogous studies in *Drosophila* NDST isoforms such as *sugarless* and *sulfateless* show severe defects in their morphology as a result of altered Wg, FGF, and Hh signalling pathways due to altered morphogen distribution and

aberrant activation of the receptor-ligand complex <sup>113</sup>. These pathways could be responsible for defects observed in NDST-1 mice. However N-sulfation is not only important but spacing of the N-sulphated domains has shown to be critical in PDGF-BB binding and activation. *In-vitro* binding experiments show increasing the length of heparin disaccharides decreases PDGF affinity for heparin and the interval between the sulphated domains is critically important in dictating the binding to PDGF. Smooth muscle and pericyte recruitment is hindered in NDST-1 mutants and PDGF mutants lacking the HS binding domain. This implies the strict regulation of NDST enzymes in generating specific sequences is a cell requirement and N-sulphated HS is important in PDGF mediated pericyte recruitment during vascular development <sup>201</sup>. It can be concluded that N-sulphation pattern is very much dependent on the type of isoform present, and implies this type of sulphation is important in modulating many HS bound proteins.

### 1.5.3 Epimerisation and 2-O Sulphation

Epimerisation is the following modification step that acts after the NDST enzymes, epimerizing certain glucuronic (GlcA) units to iduronic acid (IdoA). A single C5 epimerase acts on GlcA that are situated between GlcNSO<sub>3</sub> residues or GlcN to be sulphated <sup>151</sup>. Studies of the enzyme in isolation have found the reaction to be completely reversible <sup>314</sup>, however the action of 2-O sulphotransferases (HS2ST) on the C2 of uronic acid locks the epimerized configuration. In support of this, HS2ST favours IdoA residues thus sulphating them at faster rates under conditions when both substrates GlcA and IdoA are present <sup>315</sup>. This is further augmented by a lack of 2-O sulphation observed in C5 epimerase deficient mast cells although 6-O sulphation is not affected <sup>316</sup>. C5 epimerase (Hsepi) deficient mice fail to epimerise GlcA to IdoA distorting the heparin O-sulphation pattern. Hsepi knockout mice are embryonic lethal <sup>317</sup>, implying 2-O sulphation is a critical HS epitope. Loss and gain of function experiments in zebrafish show C5 epimerase morphants exhibit defects in dorsal ventral patterning that are associated with changes in expression of BMP and its inhibitors suggesting HS is important in regulating BMP distribution <sup>318</sup>. Administration of human C5 epimerase mRNA rescues enzymatic activity, thus preventing the development of severe

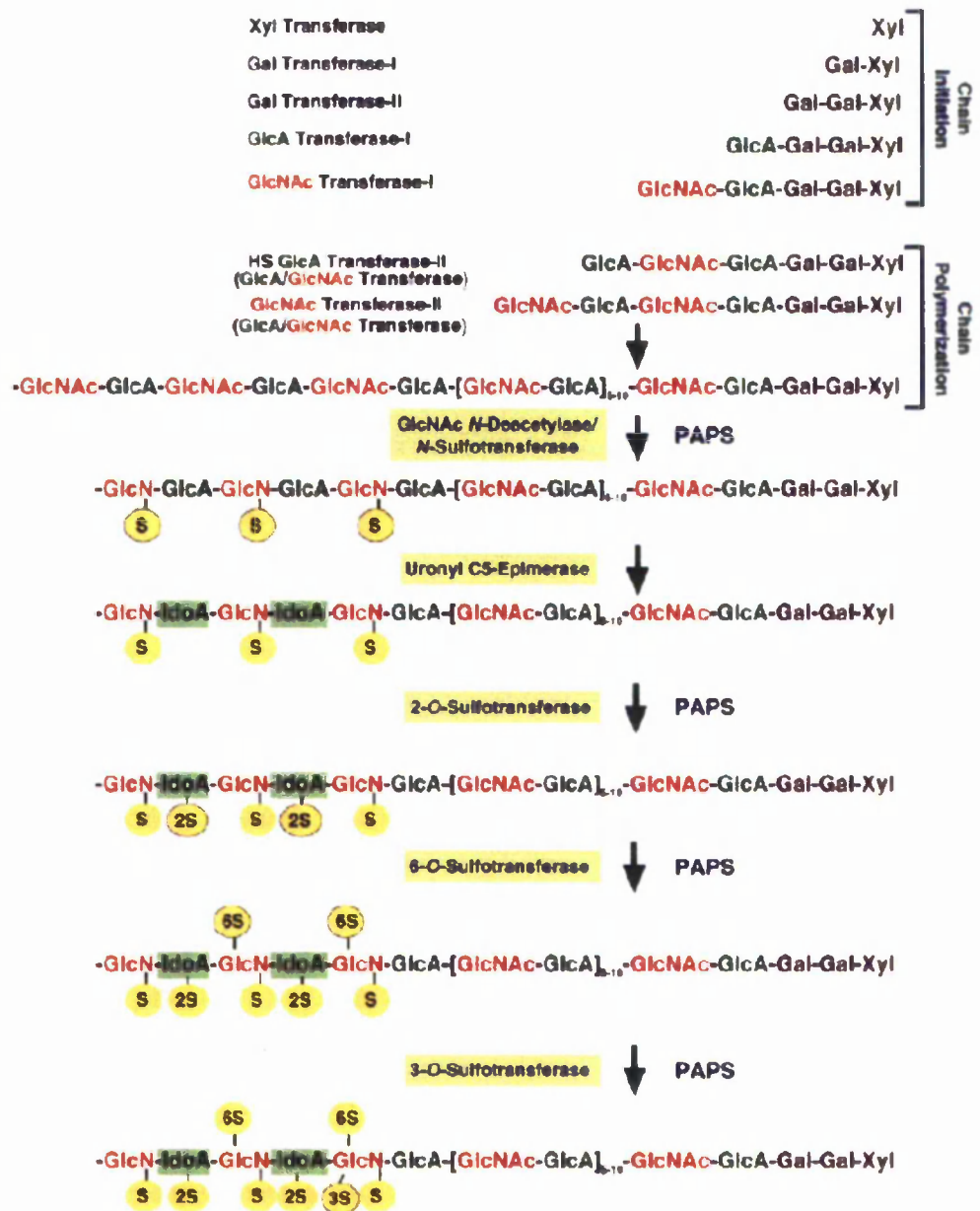


**Figure 1.13: A schematic representation of the enzymes involved in the biosynthesis of Heparin/Heparan sulphate.** HS is synthesised as a linear polymer between 50-200 units of alternating GlcA (glucuronic acid) and GlcNAc (N-acetylglucosamine) unit. This precursor is partially modified through a series of reactions, including N-deacetylation and N-sulfation through the action of NDST enzymes. The GlcNS modification is a necessary prerequisite for all other modifications. The chain undergoes C5 epimerisation of GlcA into IdoA (Iduronic acid) followed by sulphation at 2-O positions of GlcA and IdoA units, and sulphation at 3-O and 6-O positions of glucosamine. 6-O sulphation can occur on N-acetylated glucosamine as well as N-sulphated glucosamine (Image taken from <sup>294</sup>)

phenotypes this suggests enzyme specificity is fairly conserved within vertebrates and this pathway may possibly be targeted in Hspei KO mice.

HS2ST have been found to catalyse the 2-O-Sulphation of the Glc-A residues but only in regions neighboured by GlcNSO<sub>3</sub><sup>319</sup> and the longer the length of the N-Sulphated domains the greater the degree of 2-O sulphation<sup>320</sup>. This is found to be true in heparin but in HS not all IdoA residues is 2-O sulphated highlighting the remarkable complexity and diversity of the different structures produced.

The significance of 2-O sulphation can be demonstrated in the HS2ST deficient mice. Gene trap HS2ST mice exhibit multiple defects, for example kidney defects and abnormalities in the central nervous system<sup>321</sup>. The signalling pathways contributing to these defects are difficult due to embryonic lethality of these mice. However several *in-vitro* experiments have shown 2-O sulphate groups critical for binding to several ligands such as FGF-2. Biochemical analysis of mutant forms of HS show an expected loss of 2-O sulphation with a concomitant increase in N and 6-O sulphation. Importantly 2-O sulphate groups have been shown to be critical for HS binding to FGF-2 (section 1.4.1.2). Strikingly cells deficient in HS2ST show normal response to FGF-2 signalling<sup>322</sup> suggesting the loss of 2-O sulphation can be compensated possibly by the addition of other sulphate groups. This is further supported by *Drosophila* HS2ST mutants in which compensatory levels of 6-O sulphation can maintain FGF-2 signalling essential for tracheal development<sup>323</sup>.

The activity of both NDSTs and HS2STs leads to the generation of sulphated domains and at each stage only a fraction of potential substrates are modified thus leading to a complex diversity of HS sequences. Generation of functionally specific HS sequences *in vivo* has shown to depend on the specificity of the next set of enzymes 6-O sulphotransferases (HS6ST) and 3-O sulphotransferases (HS3ST).

#### 1.5.4 6-O sulphation

HS6STs transfer sulphate to C6 position of GlcNSO<sub>3</sub> or any GlcNAc residue as long as it is adjacent to GlcNSO<sub>3</sub> or IdoA (with or without 2-O sulphation) residue<sup>324</sup>. As a result 6-O sulphation is restricted within the sulphation and partially sulphated domains of HS chains. The spacing of the 6-O sulphated groups may be of functional significance as observed with the N-sulphated domains, contributing to the affinity of HS for different ligands. HS6ST consists of at least 3 isoforms, HS6ST-1, 2, & 3 which are encoded for separately. Although isoforms contain only 50% homology, they have similar substrate specificity with minor differences in target preference<sup>325</sup>. HS6ST-1 show relatively higher affinity towards target

sequences lacking 2-O sulphate e.g. the GlcA-GlcNS disaccharide unit. However all three can also catalyse 6-O sulphation of GlcNS3S<sup>326</sup> suggesting flexibility in the order of reactions.

*In vivo* and *in-vitro* studies have implicated the importance of the 6-O sulphate groups in HS mediated signalling. Although HS6ST-2 mice do not show an overt phenotype, HS6ST-1 mice are embryonic lethal and die due to vascular defects in the placenta consistent with role of 6-O sulphate groups in HS binding growth factors such as FGF and VEGF165 (section 1.4.2.3). Embryonic fibroblasts derived from double knockout HS6ST mice display reduced FGF-4 and FGF-2 signalling, whilst FGF2 binding affinity to residual HS is unaffected, however FGF-1 signalling is reduced in a dose dependent manner. This illustrates the differential requirements of FGF's for HS in eliciting a signalling response<sup>327</sup>.

To date four HS6ST genes have been identified in zebrafish which exhibit overlapping and distinct spatial expression patterns<sup>328</sup>. Knockdown of HS6ST-2 in zebrafish results in morphants with defects in the caudal plexus, showing HS6ST-2 is important in branching morphogenesis. The severity of phenotype further increases with knockdown of VEGF activity suggesting HS6ST and VEGF interact *in vivo*<sup>329</sup>. In a separate study by Bink and colleagues HS6ST appeared to be important in Wnt mediated muscle differentiation<sup>330</sup>, as these morphant exhibit severely curved bodies marked by a loss of chevron shaped somites. The different phenotypes observed imply strict levels of 6-O sulphation are important in zebrafish embryonic development and that HS6ST isoforms exhibit distinct *in-vivo* activities. This difference in isoform expression also exists in mouse brain thus the three HS6ST isoforms are differentially expressed in the developing cerebellum<sup>331</sup>. The complex expression patterns suggest that the structure of HS is altered spatiotemporally for regulating various biological activities. Consistent with zebrafish HS6ST-2 morphant, HS6ST *Drosophila* mutants also display defects in branching morphogenesis this however is associated with a loss of FGF-2 signalling<sup>323</sup>. It is clear that 6-O sulphation levels are important in modulating many developmental pathways and does not solely rely on sulphation attributed by N-sulfotransferases and 2-O sulphotransferases.

### 1.5.5 3-O sulphation

HS3STs are the final sulphotransferases to act on HS chain, transferring sulphate to C3 position of the GlcNSO<sub>3</sub>, or GlcNSO<sub>3</sub> (6-OS). These enzymes tend to modify only a few sugars per chain. At least seven members of the HS3STs have been identified HS3ST-1, 2, 3A, 3B, 4 & 5 each with differing substrate specificity<sup>332,333</sup>. HS3ST-1 does not act on HS

chain if 2-O sulphation of uronic acid (IdoA or GlcA) is adjacent to target GlcNSO<sub>3</sub> (6-OS), where as other isoforms utilise this recognition site for their activity<sup>334</sup>. Generally most of the isoform excluding HS3ST-1 do not require GlcNSO<sub>3</sub> to be 6-O sulphated<sup>135</sup>. Initially thought as the last step during biosynthesis of HS this shows that HS3STs could act prior to HS6ST, depending on the expression patterns of the isoforms in the cell. Although 3-O sulphation is the rarest modification between the 2-O and 6-O sulfotransferases it is absolutely essential in anticoagulation and viral infection. One of the well characterised heparin binding proteins is antithrombin. Many studies have shown the significance of 3-O sulphated HS in antithrombin binding, thus 3OST-1 can modify a specific precursor to create the antithrombin binding HS sequence<sup>335</sup>. Thus mice deficient in the HS3ST mice do not show a procoagulant phenotype even though there is a reduction in the levels of HS binding antithrombin form<sup>336</sup>. This suggests HS3STs may have other biological roles that can be compensated by other HS3STs. HS3ST-3 has shown to produce binding sites on the cell surface for the gD envelope protein of herpes simplex virus 1 which enables viral entry<sup>337</sup>. However in contrast to other isoforms HS3ST-5 has a broader substrate specificity, it can generate two types of 3S structure such as UA-GlcNS3S and UA-GlcNS-IdoUA2S-GlcNS(3S)6S, that can create both an antithrombin binding site to exhibit anticoagulant activity and a binding site for herpes simplex virus<sup>338</sup>. The range of signalling molecules affected by HS3ST is extended to notch family of proteins. In *Drosophila* HS3ST mutants have a role in notch intracellular trafficking and stability of notch protein<sup>339</sup>.

The differentially expressed sulfotransferases create different patterns of sulphation on HS that varies from cell to cell. However this pattern of modification is not just limited within the cell but 'remodelling' of the sulfation pattern occurs extracellularly completing the steps of HS synthesis. This activity belongs to a group of enzymes known as the 6-O endosulfatases that were first identified by Dhoot and colleagues 2001<sup>350</sup>, in a large genetic screen of genes responsive to Hh signalling. Quail sulf1 (Qsulf1) was found to regulate *wnt* signalling in somite formation through desulfation of HSPGs. Since their discovery experimental data on the sulfs has soared, shedding the significance of these enzymes in regulation of HS both in physiological and pathological processes and labelling it as one of the important determinants of overall HS function.

## 1.6 6-O endosulfatases (Sulfs)

### 1.6.1 Sulf structure and activity

Most of the early insights into sulfs came from quail, since then orthologues of Qsulf1 have been found in human, mice rat, *Xenopus*, *Drosophila* and *C.elegans* with vertebrates having two sulf enzymes compared to one in invertebrates. Cloning of the Qsulf1 and Qsulf2 enzyme revealed its distinction from other family member known as the lysosomal sulfatases (arylsulfatase). These evolutionary conserved proteins function intracellularly in removing terminal sulfate groups in the degradation of HS chains in the lysosome<sup>340-342</sup>. Extracellular sulfatase on the other hand acts on intrachain sulfgroups and is responsible for removing 6-O sulphate groups. Vertebrate sulfs characterised to date are comprised of four domains, N-signal peptide sequence for secretion, enzymatic domain, hydrophilic domain and C-terminal domain. Unique to all sulfatases both aryl and endosulfatases are the posttranslational modifications events i.e. generation of the C $\alpha$ -formylglycine in the catalytic site at which sulfate is directly bound and N-linked glycosylation that occurs through out the protein on certain asparagines residues<sup>340,343</sup>. N-linked glycosylation is required for Qsulf1 activity, although this has not been demonstrated in human sulfs. The distinguishing feature of the sulfs is the presence of the large hydrophilic domain (HD) residing between the N-terminal and C-terminal domain. This structure of sulfs has been studied extensively and recent studies with Qsulf1 and HSULF-2 have delineated specific roles of distinct regions of this hydrophilic domain. Initially from Ai and colleagues the HD was shown to be essential for anchoring the sulfs to cell surface and important in binding to various GAGs<sup>344</sup>. However two independent studies carrying out similar mutant binding studies revealed HD has more roles than previously anticipated. In all three studies directed deletion of regions of the C-terminal region of HD domain were used to locate a 14 amino acid basic peptide essential to sulf activity, and important in reducing affinity of HSULF-2 binding to heparin/HS<sup>344-346</sup>. Although sulfs can potentially bind to CS whether these chains can compete with HS chains for sulf activity *in-vivo* is unknown. However the binding of Heparin/HS chains is not restricted to the C-terminal region of the HD domain, but Frese and colleagues showed multiple sites maybe required for a stable interaction, since mutations at either end of the HD domain resulted in loss of HS binding<sup>345</sup>. In both quail and human sulfs the HD consists of furin type proteinase cleavage sites within the inner region, this is responsible for the disulfide linked subunits of catalytic N-terminal 75kDa unit and the C-terminal 50kDa unit. Although the uncleavable form retains enzymatic activity the HSULF-1/2 HD mutants failed to

potentiate wnt signalling when overexpressed. In this model they proposed the middle of HD is dispensable for GAG binding, but the inner region might be of structural importance to regulate HS affinity or to allow interactions with different GAG chains simultaneously. However the specificity to bind to HS chain is not derived from the HD domain but the catalytic site. Although the N-terminal 75kDa subunit is necessary for enzymatic activity this subunit is not sufficient for activity when expressed alone and cannot modify 4-MUS (4-methylumbelliferyl sulfate) and HS, showing the significance C-terminal role in the sulfatase family<sup>345,346</sup>.

*In vitro* studies showed both sulf-1 and sulf-2 to have identical substrate specificity, removing 6-O sulphate groups from highly sulphated domains of the HS chain i.e. UA (2S)-GlcNS(6S)<sup>344,347,348</sup>. However *in-vivo* studies in sulf knockout mice show there are distinct differences in their substrate specificity and this activity is not solely restricted to the transition domains, sulf-1 and sulf-2 can modify 6-O sulphation patterns on mono (UA-GlcNAc6S) and di-sulphated disaccharides (UA-GlcNS6S) however sulf-1 shows stronger specificity towards the 6-O sulphate groups in the tri-sulfated disaccharide<sup>349</sup>.

### 1.6.2 Molecular mechanism of sulfs

The literature reviewed so far showed 6-O sulphation to be important in generating specificity amongst HS binding proteins, the ability of sulfs to further control 6-O sulphation suggests this class of enzymes exert the final control in modulating many HS binding proteins. Several *in vitro* and *in vivo* studies have shown sulfs to modulate a wide variety of heparin/HS mediated signalling pathways, specific examples include FGF, BMP, VEGF, Hh and Wnt signalling pathways. Qsulf is shown to modulate wnt signalling during myogenic differentiation<sup>350</sup>, although there is evidence to suggest HSPGs can interact with wnt from studies in *Drosophila* HS mutants and that 6-O sulphated HS is important in this interaction. One of the mechanisms by which HS mediates wnt signalling has come from studies with Qsulf1, thus overexpression of Qsulf1 disrupts HS binding to wnt, allowing wnt to freely dissociate from HS to bind to its receptor frizzled and mediate a signalling response. This implies sulf acts in a positive manner to regulate wnt signalling. On the other hand, enforced Qsulf1 expression attenuates FGF-FGFR signalling in similar experimental conditions<sup>351</sup> consistent with the role of 6-O sulphate groups being important in FGF activity (section 1.4.1.2). In agreement with this ectopic sulf1 expression in *xenopus* embryos can inhibit FGF signalling<sup>352</sup>. In this mode of signalling removal of 6-O sulphate groups weakens FGF binding affinity for HS thus lowering the mitogenic response (Fig. 1.14). Bone morphogenetic

proteins (BMPs) are another group of molecules that can be regulated by HSPGs<sup>353</sup> although the exact structural requirements of HS sulphate groups for BMPs have not yet been fully characterised. 6-O sulphate groups are shown to be important from studies with Qsulf and Xsulf1. Heparin/HS can mediate BMP signalling, however there are conflicting reports in the exact mechanism by which the sulfs are involved. One *in-vitro* report by Viviano and colleagues show sulfs to have a positive role in BMP signalling since 6-O sulphate groups of HS are important in the binding of noggin a BMP inhibitor, and therefore disruption of this interaction by sulfatases releases noggin from the cell surface allowing BMP to induce a signalling response<sup>354</sup>. However a recent report of sulf-1 activity in *Xenopus* embryos shows sulf has an inhibitory role on BMP signalling. Embryos lacking sulf1 activity showed increased BMP expression, whereas ectopic sulf expression inhibits BMP signalling by interfering with BMP binding to its receptor<sup>352</sup>. It appears that the requirements of HS can intercept signalling at many different levels and implies the threshold of sulfation needed for noggin binding to HS may be a lot higher than to BMP-4. It appears the activity of sulf enzymes is very dose dependent and sulf activity is tightly regulated in order to efficiently mediate a correct cellular response.

As mentioned previously HSPGs and in particular HS enzymes such as Ext-1, NDST are important in morphogen distribution, while sulfs are important modulators of 6-O sulphation their role in Hh signalling adds to the significance of 6-O sulphation being a key contributor to HS mediated Hh distribution. In chick embryos overexpression of Qsulf1 modulates the switch of neural progenitors towards an oligodendroglial fate specification through enhancing the long range signalling of Hh protein. In regions of *sulf1* expression, strong levels of *shh* also accumulate with concomitant increase in *ptc* signalling<sup>355</sup>. The ability of sulf enzymes to modulate the heparin/HSPG interactions of a number of growth factors and chemokines has further been substantiated in the ELISA assay (enzyme linked immunoabsorbent assay) as treatment of heparin with sulfatase abolishes binding to FGF, VEGF and SDF-1<sup>356</sup>. It can be concluded sulfs can act as a positive or negative regulators of signalling molecules in different cellular contexts.

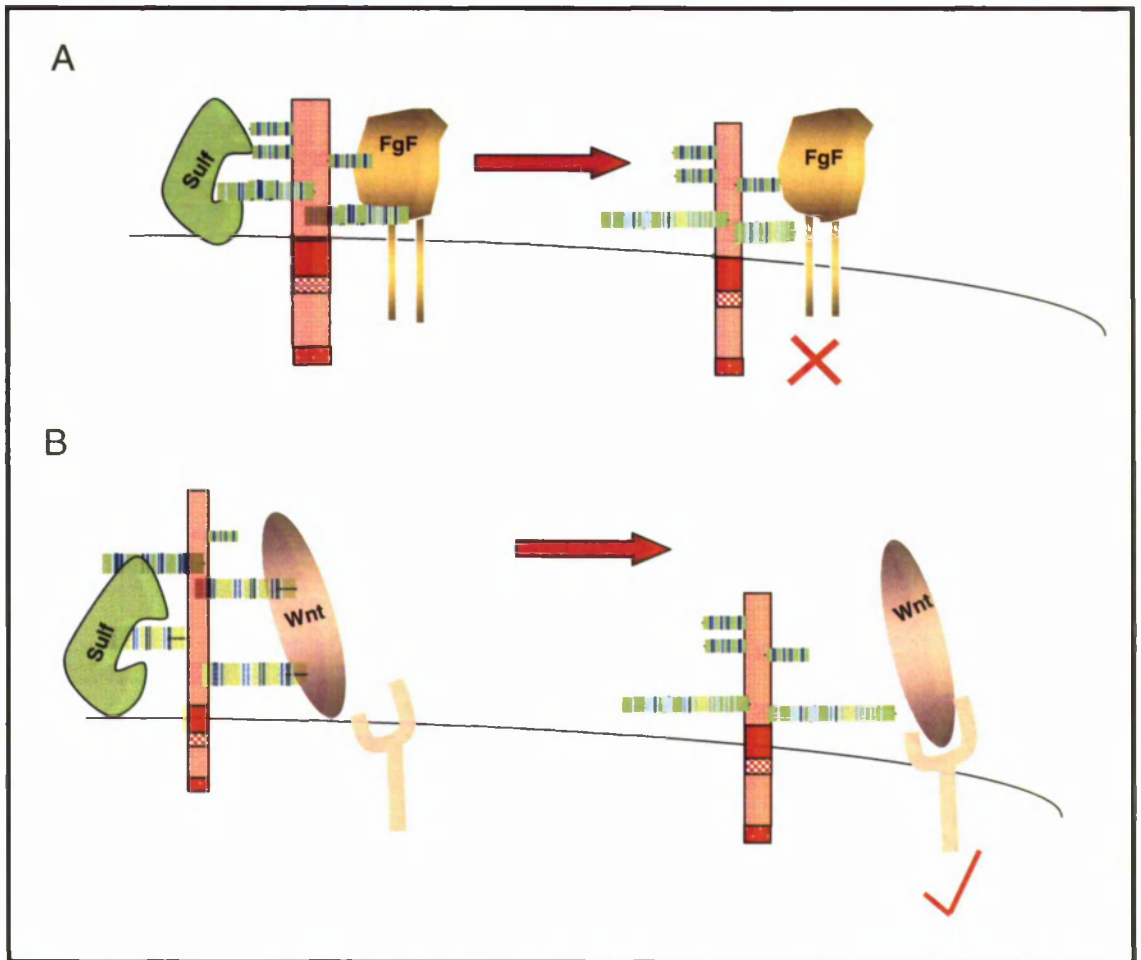


**Figure 1.14: A schematic representation of the role of sulfs in modulating HS binding proteins.** HS chains are translocated to the cell surface where the sulfation patterns are further remodelled by 6-O endosulfatases. FGF-FGFR and Wnts can bind to heparin/HS and 6-O sulphate groups are critical to this interaction. (A) Ectopic sulf expression removes 6-O sulphate groups essential for FGF-FGFR binding and reduces FGF signalling. (B) 6-O sulphated HS binds to *wnt*, however in the presence of sulfs removal of 6-O sulphate groups disrupts this interaction allowing *wnt* to move freely to bind to receptor frizzled and transduce a signalling response (adapted from <sup>351</sup>).

### 1.6.3 Role of sulfs during development

The ability of sulfs to modulate many different signalling pathways implies sulfs have a significant role during development. Surprisingly single sulf knockout mice created from homozygous inbred genetic background do not show an overt phenotype apart from increased mortality, suggesting there is some level of compensation<sup>349,357,358</sup>. This is further supported by the identical substrate specificity exhibited by these enzymes *in-vitro* and *in-vivo*. Interestingly surviving sulf-2 KO mice showed reduced body weight and growth<sup>349,357-359</sup>. However in two of these studies a range of developmental abnormalities were also observed at low-penetrance in sulf-2 KO mice. Although these have not yet been characterised some mice display defects in lung development and growth and the viability of these mice were also severely compromised. The differences in phenotype and penetrance levels observed can be owed to the genetic background as generation of *sulf2*<sup>-/-</sup> mice on more inbred genetic backgrounds did not display overt phenotype<sup>349,359</sup>. Interestingly double sulf KO mice are significantly smaller and have significantly reduced body mass with 50% dying at birth and an 80% later in embryogenesis. This suggests sulfs have an important role during development.<sup>349,357</sup>

Further characterisations of the single and double sulf KO have shown mild but distinct abnormalities in skeletal growth. *Sulf1*<sup>-/-</sup> mice showed reduced bone length and dorsally split vertebrae, whilst sulf-2 deficient mice displayed premature vertebrae ossification. The penetrance of skeletal defects was more severe in double knockout mice characterised by the small skeletal structure displaying fusions of individual sternbrae<sup>357,358</sup>. This suggests sulfs have distinct and functionally redundant roles during skeletal development. Other reports have elucidated role of sulfatases in mediating redundant functions in GDNF (glial-cell-line derived neurite factor) mediated esophageal innervation. In contrast to single sulf mice double sulf mutants display impaired muscle innervation and regeneration that is dependent on GDNF signalling<sup>360</sup>. Further studies by Kalus and colleagues show distinct roles for both sulfs in formation of hippocampal and cerebellar neurons suggesting an important role of sulfs in the developing nervous system. Thus neurological abnormalities may explain the high embryonic lethality associated in the single and double KO mice<sup>361</sup>. Consistent with these studies xsulf morphants show defects in growth and particularly have malformed brain vesicle that could be associated with neurological deficits. This is complemented by the expression patterns of *xsulf1/2* in the developing nervous system<sup>362</sup>. All the studies of sulf deficient mice

clearly imply redundant and essential role of sulfs in early embryonic and neonatal development

#### **1.6.4 Sulfs in pathological diseases**

Sulfs are frequently misexpressed during several pathological diseases mainly of cancerous nature examples include ovarian, breast, pancreatic, renal, and hepatocellular carcinoma. The findings from several recent studies are beginning to shed light on the role of sulfs as pro and antiangiogenic agent in tumour growth and metastasis highlighting their potential to be exploited as future therapeutic targets.

HSULF-1 is frequently downregulated in tumour cell lines derived from ovarian, breast and hepatocellular carcinomas<sup>363-367</sup>. Reexpression of sulf-1 in these tumour cell lines, decreases sulfation of cell surface HSPGs and abrogates signalling of FGF-2 and HGF. The loss in sulf-1 expression in these cancers may result from hypermethylation of its regulatory sequences since in hepatocellular carcinoma there is a loss of heterozygosity at the sulf locus and treatment with DNA methylase inhibitor restores sulf expression<sup>365</sup>. Similarly enforced expression of HSULF-1 in ovarian cell lines and squamous cell carcinoma diminishes FGF-2 and HB-EGF mediated cell proliferation, signalling, and enhances drug induced apoptosis<sup>363,366</sup>. In these cells expression of HSULF-1 inhibits HGF signalling thereby blocking invasion and growth normally stimulated by this growth factor. The ability of sulf-1 to reduce activities promoted by HGF is likely to be due to the reduced formation of complexes HS can make with growth factors such as FGF-2, HGF and VEGF. In support of this a recent study by Narita and colleagues showed forced expression of Hsulf-1 in xenografts derived from breast carcinoma cell lines reduces the formation of ternary complex formed between HS expressed on endothelial cells, FGF-2 and its receptor tyrosine kinase<sup>368</sup>. This may provide a plausible explanation of reduced endothelial proliferation and migration observed in the breast carcinoma cell lines and reduced tumour growth in xenografts. However this may not only involve the affect of one growth factor, since inhibition of HSULF-1 in xenograft derived endothelial cell lines can result in increased proliferation mediated by VEGF165a but not VEGF121<sup>368</sup>. Consistent with these observations removal of HS sulfation groups by chlorate treatment attenuated VEGF165a mediated signalling. The effects of sulf1 on angiogenic growth can also be mediated through their action on vascular smooth muscle cells. Qsulf1 is shown to mediate cell proliferation, migration, and adhesive properties of vascular smooth muscle cells<sup>369</sup>. This implies HSULF1 can mediate the signalling of growth factors in several

angiogenesis processes that may contribute to the severity of pathological diseases and lends itself an additional functional role as a tumour suppressor.

Interestingly HSULF-2 shows a lot of similarity to HSULF-1 in terms of expression patterns and substrate specificity, however contrary to the expression of HSULF-1, HSULF-2 is found to be constantly upregulated in many cancers such as breast, pancreatic and hepatocellular carcinomas (HCC). HSULF-2 expression is increased in almost all HCC cell lines. In comparison to HSULF-1 expression, forced *sulf2* expression activates MAPK and Akt pathways promoting HCC cell growth *in vitro* and *in-vivo*. This is thought to occur by promotion of FGF signalling through upregulation of glypican-3. Targeting of HSULF-2 by short hairpin RNA abrogates HCC cell proliferation and migration further supporting the role of HSULF-2 as promoter of tumorigenic growth. In this instance glypicans may act as anchorages of tumour dependent growth as glypicans are also overexpressed in many metastasising cancers and are crucial to the mitogenic and angiogenic potential of cancer cells<sup>167</sup>. In pancreatic adenocarcinomas wnt signalling is found to be activated aside from other growth factors. Thus exposure of these cells to inactive form of HSULF-2 inhibits both wnt signalling and cell growth leading to the hypothesis that HSULF-2 promotes wnt signalling in cell growth and tumourigenicity<sup>370</sup>. This is consistent with the findings that Qsulf promotes wnt signalling by releasing from its receptor<sup>351</sup>. However this is not the complete story, since in some tumour lines HSULF-2 is also shown to be an inhibitor of myeloma tumour growth<sup>371</sup>. This implies that there maybe additional mechanism by which the sulfs function, thereby giving them dual functions, whereby HSULF-1 is thought to have a tumour suppressor role an oncogenic role has been attributed to *sulf2*<sup>372</sup>, moreover HSULF-1 can regulate tumour growth partly by angiogenesis. The ability of HSULF-2 to regulate tumour growth partly by angiogenesis is conceivable, as consistent with *in-vitro* studies the addition of exogenous HSULF-2 to chick chorioallantoic membrane (CAM) increases vessel growth<sup>373</sup>. However this strikingly contrasts with the functions of exogenous Qsulf1 as an inhibitor of vessel growth in CAM assay<sup>351</sup>. Although this maybe a species dependent functional difference the mechanism is likely to be similar. Their role in modulating growth factor signalling is either one of two mechanisms proposed by several studies. Firstly, they can act at the cell surface to modify HS 6-O sulphation thus refining HS interaction with growth factors in a positive or negative manner depending on the nature of HS-protein in context. Secondly sulfs may be capable of modifying sulphation patterns of ECM bound HS-ligands and act by regulating their bio-availability since full length HSULF enzymes are often found secreted in conditioned media. Interestingly the role ascribed to sulfs seems to share a similar mechanism

to that of heparanases and with the well documented role of heparanases in tumour growth and metastasis (section 1.3.5.2), one needs to be careful when interpreting such activities in different carcinoma lines, since combined effects of heparanases and HSULF1 has been shown to account for large changes in tumour growth in ovarian cancer<sup>374</sup>.

The role of sulfs from several *in-vitro* based studies in physiological conditions, is equally apparent in pathological conditions and further implies there are differences amongst the two sulf family members that is also a reflection on their *in-vivo* roles during normal development. In combination of the *in-vitro* and *in-vivo* experiments in physiological and pathological conditions, the ability of sulfs to modulate many different signalling pathways and confer detrimental defects in spite of the presence of other key HS enzymes is a testament to their position as key editors of the sulphation patterns of the HS chain.

#### **1.6.5. 6-O sulphation – a specific code governed by the sulfatases**

HS is produced by many cell types with many different primary structures, this can be attributed to the functions and the differential regulation of the multiple HS biosynthetic enzymes. NDST enzymes act first to produce the substrates for subsequent sulfation, however mutants deficient for HS biosynthesis enzymes show that mutant HS can still be further modified with increased sulfation at various positions, for example HS2ST mutants show increased 6-O sulphation and N-sulphation suggesting that the N and O-sulphation order is not directly sequential<sup>322</sup>. Similarly in HS6ST mutant's 3-O sulphation is increased irrespective of the lack of 6-O sulphation. In sulf1/2 double mutant's an increase is observed in 2-O sulphation however the lack of correlation with the HS6ST isoforms provides further impetus that sulfs are the major regulators of sulphation<sup>349</sup>. This suggests there is flexibility in the order of reactions than previously anticipated<sup>323</sup>. In the cell lines derived from sulf or HS6ST KO mice FGF signalling is severely compromised, for example in HS6ST mutant mice FGF-2 signalling is severely disrupted likewise on the other side of the equilibrium in the double sulf mutants signalling of FGF-2 and FGF-4 is increased<sup>327,347</sup>. This suggests the critical balance of 6-O sulphation is essential for FGF signalling during normal development. However in *Drosophila* HS2ST and HS6ST mutants sulphation is compensated by sulphate groups at other positions and FGF-2 signalling is unaffected, whereas in HS2ST:HS6ST double mutants FGF-2 signalling is strongly disrupted. The compensatory increases in sulphation patterns suggests that the strict requirement of 6-O sulfation may be surpassed if

the overall levels of sulphation density is achieved thus challenging the current selective criteria; specific sulphation groups are essential for selectivity<sup>228,323</sup>. On the other hand HS specificity is instrumental to some proteins such as antithrombin that specifically requires 3-O sulphate groups in the pentasaccharide sequence. However the flexibility in the order of reactions seems to provide a plausible explanation for the type of HS structures observed in HS enzyme-deficient mutants and the ability to function normally in signalling pathways.

Over the last few years it been proposed that this type of flexibility can be achieved through the formation of a gagosome complex that incorporate specific family members depending on their abundance in the cell type, allowing them to act on multiple stages during HS biosynthesis. This model was proposed by Ledin and colleagues (2006) as an explanation to the lack of contribution of NDST-2 during development, except in the absence of NDST-1. NDST-1 would be part of a gagosome complex whereas NDST-2 would be 'Frozen out' and is only incorporated in the complex in the absence of NDST-1. This could be conceivable for HS6ST isoforms aswell, explaining the lack of contribution by the HS6ST-2 isoform during development as HS6ST-2 mice are viable and fertile where as HS6ST-1 mice are embryonic lethal. The idea of a gagosome complex is further strengthened by interactions of some of the enzymes *in vivo* i.e. C5 epimerase and HS2ST, similarly EXT-1 and EXT-2 interact to form an HS polymerase complex<sup>375,376</sup>.

Furthermore in double sulfs and sulf-2 KO mice the expression of other biosynthetic machinery is increased such as HS2STs, HS6STs isoforms and sulf-1, thus implying the sulf enzymes may control expression of other HS biosynthesis enzymes. A recent study shows sulfs can regulate their own expression through modulating HS binding protein signalling such as TGF- $\beta$ <sup>377</sup>. The ability of sulfs incorporated into this gagosome complex is conceivable as recent evidence suggests full length HSULFs are localised in the ER as well as at the cell surface implying sulfs as the major determinants of sulfation patterns both in and outside of the cell<sup>347</sup>.

## 1.7 Summary: Aims and Objectives

Since their discovery, publications on the sulf enzymes have soared, showing the 6-O endosulfatases to be the major regulators of 6-O sulphation and the overall determinants of HS function. Single sulf knockout mice show subtle defects in growth, skeletal tissue, muscle innervations and regeneration and development of the nervous system, furthermore double sulf knockout mice die shortly after birth, reinforcing the significant role of these enzymes during development. The on-going studies of sulfs in pathological diseases such as cancer conclude that sulfs are also promoters and inhibitors of angiogenesis. However their physiological role in vascular development is unknown. The creation of transgenic zebrafish vasculature lines has aided our understanding of mammalian vascular development and lends itself as a suitable model in which to investigate functions of genes in vascular development that cannot be addressed in other animal models. The aim of this project is to ultimately investigate the role of 6-O endosulfatases during zebrafish vascular development in attempt to further enhance our knowledge of the sulfs and if they can be exploited therapeutically in vascular based diseases.

- The initial aim is to characterise the 6-O endosulfatase transcripts in zebrafish. Conservation of the Sulf protein sequence in different species can then be analysed in addition to its spatial and temporal expression pattern in zebrafish using whole-mount *in situ* hybridisation (WISH) (chapter 3).
- Secondly to knockdown the *sulf1c* transcripts using antisense morpholinos in zebrafish and subsequently follow vascular development and circulatory defects exhibited in the resulting morphant larvae by confocal microscopy. To also further characterise the molecular cascades in which zebrafish *sulfs* are involved by WISH of different vascular markers (chapter 4, chapter 5, & chapter 6).
- Finally, the consequence of morpholino knockdown of *sulf2a* and *sulf2* in zebrafish will be analysed. The efficacy of the *sulf* morpholinos will be assessed as well as the overall morphology and vasculature (chapter 7). To address the specificity of the morpholinos HS disaccharide analysis will be performed on all morphants by using High performance liquid chromatography (HPLC).

## Chapter 2.0 Materials

All materials not listed were purchased from Sigma-Aldrich. All kits were used following the manufacturer's instructions unless otherwise stated. A more detailed description of the techniques used for a particular experiment can be found in the relevant results chapter.

### 2.0.1: Purification of Bacterial cultures

- **LB Medium**

  - 10g/l Bactotryptone

  - 5g/l yeast extract

  - 10g/l NaCl

  - adjusted to pH 7.0

  - Supplemented with 16g/l bactoagar for a solid medium

- **LB Agar plates**

  - 15g of Bacto Agar

  - made up to 1 litre of L.B

- **Antibiotics:** Ampicillin 100mg was weighed and dissolved in 1ml of dH<sub>2</sub>O and 50µg/ml used in the final working concentration

### 2.0.2: Cloning and Transformation

- Roche restriction enzymes
- T4 DNA ligase (Promega)
- TOP10 chemically competent *E.coli* cells purchased from Invitrogen
- pGEMT vector (Promega)
- Isce1 Vector (Hurlstone laboratory)
- Full length *Sulf1c* & *Sulf2b* cloned into pCS2+ vector obtained from Ken Kramer, *Flk*, *Fli-1*, *Ve-cad*, *Tie-2*, *VEGF*, plasmids obtained from Oxford and Sheffield labs.

### 2.0.3: PCR reactions

- Primers designed using Primer3 Software and ordered from MWG oligonucleotide.
- Taq polymerase (Roche)
- dNTPs , oligo dT, (Bioline)
- Reverse transcriptase (AMV) (Roche)

### 2.0.4: Agarose gel electrophoresis

- **TBE Buffer (10x)**  
54g Tris  
27.5g Boric acid  
20ml of 0.5M EDTA  
made up to 500ml dsH<sub>2</sub>O
- **TBE (1x)**  
50ml of TBE buffer (10x)  
made up to 500ml dsH<sub>2</sub>O
- **TAE (50X)**  
242g of Tris base  
57.1ml of glacial acetic acid  
100ml of 0.5M EDTA  
Made up to 1litre with dH<sub>2</sub>O
- **TAE (1X)**  
20mls of TAE (50x) made up to 1litre with dH<sub>2</sub>O
- **Ethidium Bromide 10mg/ml**  
Final working concentration used 0.5ug/ml
- **HyperladderI and IV-** 1kb and 10kb ladders obtained from Bioline

## 2.0.5: Zebrafish care and maintenance

- **Fish Stocks**

Wildtype fish AB and p53<sup>-/-</sup> homozygous transgenic line were housed in Biological safety unit facility at the university of Manchester (UMBSF)

Transgenic Lines tg(*flil*: GFP) and tg(*gata-1*:dsRed) originally described by <sup>75,378</sup> were obtained from Tim Chico University of Sheffield. Double transgenics were developed by paired matings tg(*flil*:GFP;*gata1*:dsRed) and raised in UMBSF.

Tg(*Flkl1*:GFP;*gata1*:dsRed) line originally described by <sup>379</sup> was obtained from Roger Patient lab, University of Oxford and raised in UMBSF.

- **1x Danieau Buffer**

58mM NaCl

0.7mM KCl

0.4mM MgSO<sub>4</sub>

0.6mM Ca (NO<sub>3</sub>)<sub>2</sub>

5.0mM HEPES pH 7.6

- **Embryo water**

1.5ml of concentrated salt stock (40g of instant Ocean salts dissolved in 1litre)

Made up to 1 litre with dH<sub>2</sub>O.

- **Glass microneedle pulling**

Thin walled glass capillaries (world precision instruments, 1.0mm diameter cat no: TW100F-4) were pulled using the following program; H=450, Pull=20, Vel=40, Time=80.

- **BT Fix**

2g of paraformaldehyde was added to 50mls of 1x PBS and dissolved by heating to 65°C, for ~1-2hrs.

- **Tricaine (MS222)**  
1g of Ethyl-amino-benzoate was added to 5ml of 1M Tris (pH9) and made up to 500ml dH<sub>2</sub>O.
- **Pronase (Fluka Biochemika)**  
Dissolve 100mg of pronase in 1ml of embryo water and store in aliquots at -20°C.
- **Phenylthiourea (PTU)**  
15g of PTU was weighed in fume cupboard and dissolved in 100mls DMSO. Aliquots were covered in foil and stored at 4°C. For experimentation used 1:10,000 dilution.

## 2.0.6: Whole mount in-situ hybridisation

- **10x PBS**  
80g NaCl  
2g KCl  
11.5g Na<sub>2</sub>HPO<sub>4</sub>  
2g KH<sub>2</sub>PO<sub>4</sub>  
Made up to 1 litre and pH adjusted to 7.4
- **1x PBST**  
50mls 10x PBS  
5mls 10% Tween 20  
made up 445mls with DEPC treated H<sub>2</sub>O
- **10x TBS**  
40g NaCl  
2g KCl  
30g Tris-HCl  
made up to 500ml with DEPC treated H<sub>2</sub>O
- **1x TBST**  
50mls 10x TBS

5mls 10% Tween 20  
made up to 445mls with DEPC treated H<sub>2</sub>O

- **20x SSC**

175.3g NaCl

88g Na citrate

Made up to 1 litre with dH<sub>2</sub>O and pH7.0

- **Hybridisation buffer**

50% formamide

5x SSC

50ug/ml heparin

5mM EDTA

0.5 mg/ml rRNA

1M citric acid

- **Solution 1**

50% formamide

5x SSC

1% SDS

made up to 25mls with DEPC treated H<sub>2</sub>O

- **Solution 2**

0.5M NaCl

10mM Tris HCl pH7.5

0.1% Tween 20

made up to 25mls with DEPC treated H<sub>2</sub>O

- **Solution 3**

50% formamide

2x SSC

Made up to 25mls with DEPC treated H<sub>2</sub>O

- **NTMT buffer**
  - 100mM NaCl
  - 100mM Tris HCl pH 9.5
  - 50 mM MgCl<sub>2</sub>
  - 0.1% Tween 20
  
- **Levamisole**
  - 200mM stock = 48.2mg/ml in DEPC treated H<sub>2</sub>O
  
- **Staining dye**
  - BM Purple diluted in 1:1 with NTMT buffer.
  
- **HILS**
  - 5mls of lamb serum
  - 45mls of 1x TBST
  
- **Antibody Solution**
  - 60μl levamisole
  - 1500μl recovered supernatant
  - 600μl HILS
  - 3840μl DEPC H<sub>2</sub>O

### 2.0.7: Proliferation assay

- **Primary antibody solution**
  - αPH3 rabbit Ab (Lowe lab) was diluted 1 in 500 in Ab solution made up of PBST, 0.1% tween20, and 10% Fetal calf serum (FCS)
  
- **Secondary antibody solution**
  - DaR donkey Ab (Lowe lab) was diluted 1 in 500 in Ab solution made up of PBST, 0.1% tween20, and 10% Fetal calf serum (FCS).

### 2.0.8: Apoptosis assay

- ApopTag Red *In Situ* Apoptosis Detection Kit purchased from Chemicon International

### 2.0.9: Imaging of the Zebrafish

- **3% Methylcellulose**  
3g of methylcellulose was added to 100ml of embryo water. Leave overnight on magnetic stirrer to dissolve. Aliquots were stored at -20°C for long term storage and 4°C for frequent use.
- **PolyD-lysine coated coverslip bottom dishes** purchased from BD Biocoat
- **Microscopes and software**  
Zeiss Stereolumar V12 images accumulated in axiovision software 4.6  
Zeiss Axioimager Z1 compound microscope images accumulated in axiovision software using panorama programme  
Leica TCS SP5 AOBS upright confocal

### 2.0.10: Heparan sulphate extraction

- **Protease Buffer**  
50mM Tris/HCL (pH8)  
1mM CaCl<sub>2</sub>,  
1% triton
- **Elution buffer**  
50mM NaCl  
1M NaCl pH6  
Made up to 500mls with dH2O

- **Loading Buffer**  
50mM sodium phosphate buffer  
0.15M NaCl pH6
- **Digestion buffer**  
0.1M sodium acetate pH7  
10mM Calcium acetate
- **Enzyme mix**  
200mIU/ml heparinase  
Heparitinase II  
Heparitinase

#### 2.0.11: HPLC Buffers/Solutions

- **Standards:** Unsaturated Heparan/Heparin disaccharide mixture (Seigaku) stock concentration 1nmol/ $\mu$ l
- **Buffer A:** 1litre of dH<sub>2</sub>O of pH3.5
- **Buffer B:** 1M NaCl (HPLC grade) pH3.5
- **Buffer C:** 0.5% 2-Cyanoacetamide
- **Buffer D:** 1M NaOH

## 2.1 Methods

**Note:** The Protocols described were carried out in accordance with COSHH safety guidelines. All micropipette tips and 1.5ml/0.6ml eppendorf tubes were autoclaved. Moisture was removed by storing in a Kiln at 100°C for 24hrs. A more detailed description of the techniques used for a particular experiment can be found in the relevant results chapter.

### 2.1.0: Expression and purification of plasmid DNA

#### 2.1.1: Overnight cultures

Using sterile techniques 5mls of LB was pipetted into 20ml universal bottle with the appropriate antibiotic added in ratio of 1:1000. A flamed wire loop was then used to scoop some cells either from a colony on an agar plate or from glycerol stocks. The loop was then inserted into the LB medium, and cap slightly fastened so air could escape. The culture was placed in incubator overnight at 37°C with shaking at 225rpm. For midi-preparation, cultures were grown for 8hours and 1ml of day culture was used to inoculate a flask of 100ml LB media containing 50µg/ml of the appropriate antibiotic.

#### 2.1.2: Mini/Midi purification of Plasmid DNA

Plasmid DNA was purified from 5ml/100ml overnight cultures using the QIAprep Spin Miniprep and Midiprep kit (QIAGEN) respectively. Purifications steps were carried out following the manufacturer's protocol. DNA was eluted from column in a final volume of 50µl. For midi preps of plasmids, DNA pellet was resuspended in a 100µl of distilled water (dH<sub>2</sub>O). The concentration of the DNA was determined by reading the optical density at 260nm using a ND1000 nanodrop machine.

#### 2.1.3: Purification of DNA from Agarose slice

For small size DNA fragments or linearised plasmid, DNA was purified from agarose gels. DNA bands from agarose gel were carefully sliced with a clean scalpel blade, being careful not to remove extra agarose, and ensuring minimal exposure to U.V light. For high quality DNA purification the QIAquick Gel Extraction Kit (QIAGEN) was used following the

manufacturer protocols or for high DNA yield, Gel kit from Amersham Biosciences was routinely used. Purified DNA was eluted from the column in a final volume ranging between 25-40 $\mu$ l, depending on the intensity of the band under U.V examination. A microlitre of each sample was run on 0.8-1% agarose gel electrophoresis to visualize integrity of DNA and subsequently concentration was measured using nanodrop machine.

#### **2.1.4: Purification of DNA from enzyme based reactions**

DNA was purified from several reaction mixes (e.g. PCR reactions, restriction digests) by following the protocol provided by the QIAquick PCR Purification Kit (QIAGEN) or GFX kit (Amersham Biosciences). Purified DNA was eluted with TE buffer from the column in a final volume of 30 $\mu$ l-40 $\mu$ l.

#### **2.1.5: Phenol/Chloroform Extraction**

This method was also used to remove any proteins from DNA samples. Equal volume of phenol was mixed with DNA sample. The mixture was then vortexed for a few seconds and centrifuged for 1min at 13000g (full speed). The aqueous phase (upper layer) containing the extracted DNA was transferred to a clean 1.5ml eppendorf tube. An equal volume of chloroform was added and same procedure repeated as above. The aqueous DNA was removed to a fresh 1.5ml tube. DNA was then ethanol precipitated.

#### **2.1.6: Ethanol Precipitation**

DNA volume was measured and a 1/10x volume of 3M sodium acetate (pH 5.5) was added along with 2.5x volume of ice-cold ethanol (100%). The sample was well mixed and placed on ice for 30mins or at -20 $^{\circ}$ C overnight. Sample was then micro centrifuged at full speed for 20mins at 4 $^{\circ}$ C. The supernatant was decanted carefully ensuring the pellet was not disturbed. Pellet DNA was washed with 100-200 $\mu$ l of ice cold 70% ethanol. The sample was subsequently centrifuged at full speed for 10 mins at 4 $^{\circ}$ C and the ethanol decanted. The DNA pellet was then air-dried for 10-15mins and stored as a pellet (for DNA sequencing reactions) or resuspended in a suitable volume of dsH<sub>2</sub>O.

### **2.2.0: Cloning and Transformation**

#### **2.2.1: Producing Agar plates**

Solid LBA (400ml) was heated in a microwave for 10 mins at medium settings. Melted agar was then cooled to 50 $^{\circ}$ C in a water bath. Antibiotic was added in a ratio of 1:1000. Using sterile techniques, approximately 20ml of agar was poured into a labeled Petri dish. Plates

were left for 1hr to sufficiently cool down. The plates were then dried in a laminar airflow cabinet for half an hour. The plates were then stored at 4°C until further use.

### **2.2.2: Restriction Digests**

Vector and insert DNA was digested using restriction enzymes (supplied from Roche) to produce the appropriate sticky or blunt ends. If both restriction enzymes required the same buffer solution, digests were performed simultaneously. The appropriate amounts of enzyme units were used per µg of DNA, along with appropriate amount of 10x buffer according to the manufacturer's specification. Digests were incubated at 37 °C for three hours for low DNA concentrations or overnight for highly concentrated DNA samples. DNA fragments were run on agarose gel electrophoresis and, purified from agarose gel (2.1.3) and stored at -20 °C until required.

### **2.2.3: Ligation**

Following purification of vector and insert from restriction endonuclease digestion or from QIAquick PCR purification kit (Qiagen) DNA insert of interest was ligated to the appropriate vector using T4 DNA ligase and 10x Ligase buffer supplied from Roche. A minimum of 100ng of vector DNA was always added, while appropriate amounts of insert DNA were added to give the required vector: insert ratios of 1:1, 1:3, 1:5. T4 DNA ligase was diluted to a final concentration 0.05units/µl with 10x ligase buffers and was adjusted with dsH<sub>2</sub>O to give a final volume of 20µl. Ligation control containing only linearised vector without ligase was also prepared. The reaction mixes were then incubated at 16°C overnight or 4°C.

### **2.2.4: PET TOPO<sup>®</sup> Cloning (Sub cloning)**

Blunt ended products were generated either by PCR or restriction digests. 10-20ng depending on the size of PCR product was used. Prepared pGEMT vector (promega) was briefly centrifuged. All reagents were added on ice, Insert was added to give the required vector: insert ratio of 5:1, 3:1 as suggested by the manufacturer. Final volume was made up to 20µl with 2 x rapid ligation buffer 3units/µl of ligase enzyme and the remaining with dH<sub>2</sub>O. The reaction mixes were then incubated for 1hr at room temperature and subsequently transformed

### **2.2.5: Transformation using CaCl<sub>2</sub> treated competent cells**

An appropriate volume of plasmid solution or 10µl of the ligation mix was mixed in 50µl aliquots of Dh5α competent cells (Invitrogen). Sample were mixed by flicking, and left on ice for 20mins (15 mins for TOPO reaction mixes). Cells were then heat shocked at 42°C for

30secs and immediately transferred on to ice. Cells were resuspended in 250µl of pre-warmed S.O.C medium and then incubated at 37°C for 1hr. 100µl aliquots of transformed cells were then streaked on to pre-warmed selective agar plates and incubated at 37°C overnight.

### **2.2.6: Analysis of *E.coli* Transformants**

Potential recombinants were analyzed by Colony PCR. 10-20 Colonies from each plate were removed using individual sterile toothpicks and transferred to a PCR tube containing 50µl of PCR mixture, with relevant primers chosen to positively identify the required DNA fragment. A drop of this suspension was then spotted on a fresh agar plate (divided into squares and numbered) containing the appropriate antibiotic. The plates were then incubated at 37°C overnight.

## **2.3: Polymerase Chain Reaction**

### **2.3.1 Primer design for PCR**

Forward and reverse primers were designed to selectively amplify the product of interest in PCR reactions. Where possible primers were designed to be 20 nucleotides in length, containing equal number of G: C to A: T nucleotide, with the most 3' nucleotide being a cytosine or guanine. All primers were designed to have an approximate annealing temperature ( $T_m$ ) of 55 °C unless otherwise stated. The approximate  $T_m$  was calculated using the following equation:  $T_m = (G + C) \times 4 + (A + T) \times 2$

Primer sequences and size of amplicon can be found in the Materials and Methods section of the appropriate Results chapter.

### **2.3.2: Standard PCR**

Stock primer concentrations of 100µM were diluted to a working concentration of 10µM. A general PCR reaction mix was made up 1ul of DNA or cDNA template, 2mM of dNTPS mix (containing dATP, dCTP, dGTP, dTTP), 1x PCR buffer, 1.5mM MgCl<sub>2</sub>, 10pmols of each primer, and 0.5units of Taq polymerase. The final volume of PCR reaction was made up to 25µl with nuclease free H<sub>2</sub>O. All volumes were scaled up for greater volume PCRs. The temperature and times of the PCR cycles used to amplify from the template were worked out depending on the  $T_m$  of the primers and the size of the amplification product. Two programmes routinely used are listed below. Negative controls using water as the substrate were performed for all reactions.

### ***Sulf* gene amplification- programme 1**

No of cycles	Temperature/ mins or secs	Stage
1	94°C - 5mins	Denaturation
34	94°C - 30 secs	Denaturation
	59°C - 30 secs	Annealing
	72°C - 1min	Primer extension
1	72°C - 7mins	Polymerase extension

### ***Beta actin* amplification programme 2**

No of cycles	Temperature/ mins or secs	Stage
1	95°C - 10mins	Denaturation
25	95°C - 15 secs	Denaturation
	54°C - 5 secs	Annealing
	72°C - 10 secs	Primer extension
1	72°C - 7mins	Polymerase extension

#### **2.3.3 Long range PCR**

For amplification of products larger than 3kb the Expand long range enzyme mix (Expand Long range dNTPack, Roche) was used instead of Taq DNA polymerase. Reagents were made up in similar concentrations to standard PCR, except 1.75 units of enzyme mix was used and PCR mix was made up with 3% DMSO in the final reaction. PCR programme was set up as follows;

No of cycles	Temperature/ min or secs	Stage
1	92°C - 2 min	Denaturation
10	92°C - 10 secs	Denaturation
	55°C - 15 secs	Annealing
	68°C - 5 min	Primer extension
24	92°C - 10 secs	Denaturation
	55°C - 15 secs	Annealing
	68°C - 5 min	Primer extension
1	68°C - 7 min	Final extension

#### 2.3.4: DNA sequencing

Unless otherwise stated the primers used to amplify a product of interest in a PCR analysis were also used as sequencing primers. Separate premixes were made up of 4pmol of forward or reverse primer, 10-20ng of purified DNA product or 300ng of plasmid bearing cDNA of interest and made up to a final volume of 10µl with sterile H<sub>2</sub>O. Premixes were sent to DNA sequencing facility in the University of Manchester (UMSF) and results analysed on a Chromas LITE software version 2.01.

### 2.4: Preparation and Running agarose gels

#### 2.4.1 Agarose gel electrophoresis

The DNA products of PCR and restriction digests were visualized by agarose gel electrophoresis. Agarose gels were used at 0.8-1.2% (w/v) agarose concentration in order to resolve DNA molecules ranging from 0.5 to 3kb in size. A gram of agarose was added to 100mls of 1x TBE and then heated in a microwave for 3-4 minutes in order to dissolve the agarose. Melted agarose was then cooled for 5-10mins and ethidium bromide was added to give a concentration of 0.5µg/ml. The solution was then poured into a gel tray with a comb positioned at one end (to form the wells). Once the gel was solidified, comb was removed and placed in a gel tank. The tank was then filled with 1xTBE buffer, ensuring the whole gel was

well covered. Samples to be analyzed were loaded in 1x gel loading dye and a 1 kb DNA ladder was used as a size standard. Electrophoresis was conducted at 110 volts for 45-50mins. Gels were visualized under U.V light and imaged using UVIPRO software. If necessary, products were excised from the gel and purified using a QIAquick gel extraction kit (Qiagen)

## **2.5: Zebrafish Care and experimental methods**

### **2.5.1: Zebrafish care and staging**

Embryos were collected and raised in 35mm Petri dish containing methylene blue water. Embryos were kept at 28.5°C throughout development and staged using standard morphological criteria<sup>380</sup>. Staging was carried out prior to any fixing of embryos.

### **2.5.2: Marbling and Collection of Zebrafish embryos**

A tray of marbles was placed in the bottom of the tank of adult female and male fish. Alternatively for timed injections fish were set up in breeding boxes in a ratio of 4:2 males to females. Following morning dividers were removed and subsequently embryos were collected.

### **2.5.3: Preparing microinjection plates- Agarose chambers**

A 1% hot agarose solution made up with embryo water was poured into a 35mm petri dish. After the gel solidified another 10mls of agarose was added to the dish. The plastic mould was set into the liquid agarose and forceps were used to eliminate any bubbles. After the agarose set a small amount of embryo water was added and the plate stored at 4°C until further use.

### **2.5.4: Preparing morpholinos and estimating the amount to inject**

Stock morpholinos purchased from Gene Tools, LLC ([www.gene-tools.com](http://www.gene-tools.com)) came as 10ng/nl concentration and were diluted to working solutions of 1ng/nl or 3ng/nl with dH<sub>2</sub>O or 1X Danieau buffer. A final working concentration of 0.1% w/v aqueous phenol red was also added as a tracer. All needles were calibrated to quantify volume to be injected. Morpholinos were heated at 65°C for 5mins as requested by manufacturer and centrifuged for 2mins to prevent precipitation and consequently reduced the likelihood of a blocked needle. A small

volume of 3µl of morpholino was pipetted into needle and placed in the needle holder. A small part from the tip of the needle was broken with forceps to allow flow of solution.

#### **2.5.5: Microinjecting Zebrafish embryos**

The Petri dish was warmed in microwave and then placed under the microscope. Embryos were then pipetted from a glass pipette and transferred onto the agarose troughs, usually 30 embryos were loaded per lane. Using fine forceps, embryos were lowered into the troughs and aligned in the same orientation. A minimum amount of embryo water was added to trough to prevent embryos drying out. Embryos were pressure injected using a pulled glass micropipette and a microinjector (Digitimer), through the chorion into the yolk. Solutions of morpholino antisense oligonucleotides were prepared and heated to 65°C prior to use. Embryos were then incubated at 28.5 °C in embryo media. From 24hpf until the time of fixation, the embryos were incubated in embryo media containing 1X PTU to prevent pigmentation and development was followed for 2-3 days.

#### **2.5.6: Dechorination of Zebrafish embryos**

Embryos post 24hpf were dechorinated manually using forceps. If more than 20 embryos, they were subjected to pronase treatment. 20+ embryos were placed in 1.5ml eppendorfs and 10µl of 100mg/ml of pronase was added to the dish, and was placed in the 28.5°C incubator for 5mins. After 5mins the embryos were pipetted into petri-dish containing embryo water several times to remove the weakened chorion.

#### **2.5.7: Microangiography**

Wildtype and morphant embryos at 48-50hpf stage were anaesthetised and used for microangiography. Red fluospheres® carboxylate modified microspheres 0.02µm (Invitrogen) were sonicated for 30secs and microcentrifuged for 2mins at high speed. Microspheres were diluted 1:1 with 2% BSA (Sigma) in dH<sub>2</sub>O, and centrifuged at maximum speed for 2min. Embryos were then lowered into 0.8% tricaine agarose bed, and then orientated under the microscope to face the dorsal view.

#### **2.5.8: DNA extraction from Zebrafish embryos**

Embryos were dosed with the anaesthetic tricaine (MS222, Sigma) then collected in a 1.5 ml eppendorf tube. For a sample size less than 20, 500µl of DNA extraction buffer was added, with 20µg/ml of Proteinase K and the sample incubated at 55 °C overnight. The following day the sample was centrifuged at 13,000 rpm for 1 minute and the excess tissue removed

before performing a second 10 minute centrifugation at 13,000 rpm. The supernatant was transferred to a clean 1.5 ml eppendorf tube and underwent a phenol/chloroform extraction. The upper aqueous layer was removed and transferred to a clean 1.5 ml eppendorf tube then an equal volume of 100% isopropanol was added. The sample was mixed by inverting the eppendorf tube several times until DNA precipitation was visible. A loop or pipette tip was then used to remove the DNA which was transferred to a clean 1.5 ml eppendorf tube containing 500 $\mu$ l of 70% ethanol. The sample was centrifuged for 10 minutes and the ethanol was removed. The DNA pellet was air dried for 10-20 minutes and resuspended in 100-500 $\mu$ l dH<sub>2</sub>O depending on the size of the DNA precipitate. One to two microlitres was used in the PCR reaction depending on the concentration of the purified DNA.

### **2.5.9 Total RNA extraction from zebrafish embryos**

Wildtype and morphant embryos were collected and rinsed in embryo water before being dechorinated. They were then sonicated briefly (30 sec 3 times at 4-5 watts) in 1ml of TRI Reagent (20 embryos) and left to stand at room temperature for 5mins. 200 $\mu$ l of chloroform was then added to each sample and was thoroughly mixed for 15secs. Sample was allowed to stand for 15mins at room temperature and was subsequently centrifuged at 12000xg for 15mins at 4°C. The aqueous phase was then transferred to a pre-labelled fresh tube containing 500 $\mu$ l of isopropanol and mixed thoroughly. Following the stand at room temperature for 20mins sample was then centrifuged at 12000xg for 10mins at 4°C. Supernatant was carefully removed ensuring the pellet was not disturbed. The pellet was then washed in 1ml of 75% of ethanol and vortexed. Sample was then left in freezer for 1hr or left overnight at -20°C. Following the wash, sample was centrifuged at 7500xg for 5mins at 4°C (or at 12 000xg for 10mins if pellet floated). Supernatant was removed and the RNA pellet left on the bench top to air dry. RNA pellet was then dissolved in RNase free distilled water or DEPC H<sub>2</sub>O. Samples were occasionally incubated for 2hrs at 37°C with DnaseI. The concentration of the RNA was determined by reading the optical density at 260 nm on a nanodrop ND1000 spectrophotometer. Samples were then stored at -80°C until further use. For high quality RNA, RNeasykit (Invitrogen) was used following the manufactures instructions. RNA was eluted with DEPC H<sub>2</sub>O in a final volume of 10 $\mu$ l.

#### **2.5.10: cDNA synthesis**

Approx 1 $\mu$ g of RNA was added to 200 $\mu$ l PCR tube, containing 1 $\mu$ l of oligonucleotide T primer and 10mM dNTP's, made it up to a final volume of 12 $\mu$ l with DEPC H<sub>2</sub>O. Sample was

then incubated in a 65°C heating block for 5mins and immediately chilled on ice whilst the following solutions were added; 4µl of AMV-RT buffer, 2µl of 0.1M DTT and 1µl RNase inhibitor. The reaction was equilibrated at 42°C before a 1µl of AMV-reverse transcriptase was added. Samples were then incubated at 42°C for an hour and then additional 10mins at 72°C to denature the enzyme. A 1µl of this reaction was quantified using nanodrop machine, and subsequently used in RT-PCR reactions.

### **2.5.11: mRNA synthesis**

Messenger RNA was generated from plasmids using the mMessage machine kit (Ambion). Approx 1µg of purified linearised plasmid was transferred to sterile eppendorf. Reaction was assembled at room temperature following the manufactures instructions. RNA was purified from the reaction using phenol:chloroform extraction and isopropanol precipitation. RNA pellets were resuspended in RNAase free H<sup>2</sup>O, quantified and stored at -20°C until further use.

## **2.6: Whole mount in situ hybridisation (WISH)**

### **2.6.1: Transcription of Dig-labelled riboprobes**

RNA labelling was carried out with DIG RNA labelling kit from Roche. Approx 1µg of purified linearised plasmid (containing gene sequence of interest) was made up to 13µl with RNase free water. This was then added to a mixture containing the following: 2µl of NTP labelling mixture, 2µl of transcription buffer, 1µl of RNase inhibitor and 2µl of T7, T3 or Sp6 RNA polymerase. The type of RNA polymerase used was determined by sequencing the plasmid for orientation of the gene of interest. Both antisense and sense probes were generated using different polymerases. Solution was mixed and spun briefly in centrifuge for 30secs. This was then followed by an incubation step for 2hrs at 37°C. Sample was then incubated with DNase I (2µl) for a further 15mins at 37°C, and reaction was stopped by adding 2µl of 0.2M EDTA (pH8.0). The riboprobe was precipitated with 50 µl of DEPC-H<sub>2</sub>O, 25 µl of 10mM ammonium acetate and 200 µl of 100% ethanol at -20°C overnight. After precipitation, the RNA was washed with 70% ethanol, air-dried and resuspended in 20µl of DEPC-H<sub>2</sub>O. Riboprobes were stored at -20 °C until further use.

### **2.6.2: Fixing Embryos**

Wildtype and morphant embryos still in chorion (less than 24hr) or dechorinated embryos were fixed in BT fix overnight at 4°C. For storage embryos were dehydrated for 5mins, through methanol series MEOH: 25% in PBST, 50%, 75% and finally 100% MEOH. All washes were carried out on orbital shaker at room temperature.

### **2.6.3: Hybridisation**

Embryos were rehydrated by washing them in a descending methanol/PBST series starting with 100% methanol, 75%, 50%, 25% MEOH in PBST. This was followed by two further washes with PBST. Embryos older than 24hrs were then treated with 10µg/ml of Proteinase K in PBST for 5-15mins. The timing varied, depending on the stage of embryo (as for older embryos time was extended to 15mins). Proteinase K treated embryos were then washed twice in freshly prepared 2mg/ml glycine. Embryos were further washed in PBST and refixed in BT for 20minutes at room temperature. Following another two washes in PBST, embryos were prehybridised in a minimal volume (1ml) of hybridisation mix at 65°C, for 1-3hrs. This was then replaced by prewarmed hybridisation buffer containing riboprobe (2µg/ml) and was left to hybridize overnight. All hybridisations were carried out in a shaking waterbath at 65°C and were left for 20-24hrs.

### **2.6.4: Post hybridisation washes and preabsorption of antibody**

Following day, hybridisation solution was removed as much as possible with minimal exposure to air. Embryos were washed twice with solution 1 for 30mins at 65°C, followed by a short wash of 10mins with a mixture (1:1) of solution 1 & 2 at the same temperature. Embryos were then washed twice with solution 2 for 30mins at 37°C, followed by two washes with solution 3 at 65°C. All washes were carried out in shaking waterbath. HILs solution containing freshly prepared 200mM levamisole was then added to embryos and left for 1hr-2hrs at room temperature. Whilst embryos were left in pre-block, antibody solution was prepared as follows; 1.5ml of TBST was added to 3mg of blocking reagent and heated to 70°C for 30mins. As this was cooled on ice 15µl of HILS and 3µl of Antibody (-coupled to alkaline phosphatase) was added to tube. Sample was left on ice for 1hr and then spun in microcentrifuge for 10mins at 12000xg. The remaining supernatant was then added to the antibody solution. The blocking HILs solution was then removed from embryos and replaced with antibody solution. Samples were left shaking overnight at 4°C. Note: all volumes of solutions used were scaled up for samples greater than six.

### **2.6.5: Removal of Antibody**

Embryos were washed three times for 5mins with freshly prepared TBST/2mM levamisole. This was then followed by five extended washes for 1hr each with TBST/2mM levamisole. Samples were stored overnight at 4°C.

### **2.6.6: Staining and Detection**

Following day embryos were washed three times for 10mins with freshly prepared NTMT/2mM levamisole at room temperature. The colour reaction was then performed by incubation in BM Purple AP substrate (Roche). This reaction was performed in the dark with rotation at room temperature and monitored at regular intervals. When satisfactory signals were developed the colour reaction was terminated by washing three times in TBST. To clear the embryos were washed in 50% formamide and 50% TBST. For storage purposes and reduction of background signal embryos were passed into a series of ascending glycerol /PBST solutions. Firstly through 20% glycerol, 40%, and then finally stored in 80% glycerol. Images were taken using a Zeiss Axioimager Z1 compound microscope, using a plan aprochomat 10x/0.45 objective.

### **2.7: Proliferation assay**

Wildtype embryos and morphant embryos were fixed in 4% PFA at the stage of interest and left overnight at 4°C or longer. Following day embryos underwent a descending series of methanol washes;

3 x 5'mins 100% MeOH

1 x 5'mins 75% MeOH/25% PBST

1 X 5 mins 50% MeOH/50% PBST

1 X 5mins 25% MeOH/75% PBST

Final 3 x 5mins washes were done in 100% PBST.

PBST was decanted from the tubes and embryos incubated with 200µl of primary antibody solution per tube at 4°C. On Day 2, primary antibody solution was removed and embryos were washed 6 times for 20mins in PBST. PBST was replaced with 200µl of secondary antibody solution per tube and incubated overnight at 4°C. Day 3 secondary antibody solution was removed and embryos were washed 3 times at 30mins each with PBST. Embryos were stored in PBST at 4°C until imaging.

## **2.8: Apoptosis Assay**

Wildtype and morphant embryos were fixed in 4% PFA overnight or for 3hrs at room temp in glass bijous. Embryos were washed for 10mins in PBST three times followed by 1 hour incubation at room temperature in 10µg/ml of Proteinase. For older embryos i.e. >72hpf incubation was increased to two hours. Embryos were washed twice with PBST for 5min and then re-fixed in 4% PFA for 20mins at room temperature. Washes with PBST were repeated three times for 5mins each. Embryos were stored for 7min at -20°C in acetone: ethanol (1:2) and then repeatedly washed again with PBST for 5min each. A volume of 100µl of equilibration buffer (provided from kit) was added to embryos and incubated for an hour, followed by 90mins incubation at 37°C in 16µl TdT (terminal deoxynucleotidyl transferase) enzyme and 30µl reaction buffer per sample. Embryos were then incubated for 3 hours with 300µl of stop buffer at 37°C and then repeatedly washed with PBST for 5min. A pre-mixed aliquot containing 68µl of blocking solution and 62µl of anti-Dig Rhodamine was applied to each sample and left overnight at 4°C on a shaker. Following day samples were washed four times in PBST for 30mins each and then re-fixed at room temperature in 4% PFA. This was followed by a series of short 5min washes in PBST four times and 10min in 25%-75% stocks of glycerol. Embryos were subsequently stored at -20°C until imaging.

## **2.9 Imaging of the vasculature**

### **2.9.1: Mounting of embryos**

For short term imaging and lower magnifications anesthetized embryos were mounted in 3% methylcellulose on depression slides. Embryos were transferred using pipettes and lowered into the methylcellulose at the bottom of the depression 'well'. Orientation was adjusted with fine forceps. For short movies and higher magnification, embryos were transferred into 0.8% LMP agarose covering the glass coverslip of the micropetri-dish. The agarose was allowed to be sufficiently cooled before adding embryos to the medium. Once the embryos were set in the different mediums, 300µl of tricane water (0.003%) was pipetted over embryo to keep media moist aswell as maintaining anesthetized embryos.

### **2.9.2 Confocal imaging**

Images were collected on a Leica TCS SP5 AOBS upright confocal using a *10x/ 0.50 Plan Fluotar* objective and 1x confocal zoom. The confocal settings were as follows, pinhole 1 airy unit, scan speed 1000Hz unidirectional, format *512 x512*. Images were collected using the

following detection mirror settings; GFP 494-530nm; Texas red 602-665nm; Cy5 640-690nm using the 488nm (100%), 594nm (100%) and 633nm (100%) laser lines respectively. When it was not possible to eliminate cross-talk between channels, the images were collected sequentially. When acquiring 3D optical stacks the confocal software was used to determine the optimal number of Z sections. Z stacks were taken every 1.5 $\mu$ m, with each frame averaged three times. Laser power was adjusted during stack collection with higher power for deep image planes and lower power for shallower planes. Only the maximum intensity projections of these 3D stacks are shown in the results. For short movie (1min) scan speed setting was 1400Hz phase, bidirectional format 512x122. Images were then processed and analyzed using ImageJ (<http://rsb.info.nih.gov/ij>).

### **2.9.3 Widefield imaging**

Images were collected on Zeiss stereolumar fluorescent stereomicroscope 1.5x objectives and different zoom levels. Images were captured using an axiocam through axiovision software 4.6. Specific band pass filter sets for GFP and Texas red were used to prevent bleed through from one channel to the next.

## **2.10: Heparan sulphate (HS) extraction and purification**

### **2.10.1: Degradation of embryos**

Wild type and morphant embryos (ranging from 48-55hpf) were dechorinated by pronase treatment and then rinsed in dH<sub>2</sub>O. Embryos were placed in eppendorfs and lyophilised for 15mins until all the water had evaporated. The remaining pellet was resuspended in 500 $\mu$ l of protease buffer and sonicated for 30secs at 4-5 watts with probe sonicator. This step was repeated three times. Protease was added to the following tubes to give a final concentration of 0.8mg/ml. Samples were left in the shaking waterbath at 55°C.

### **2.10.2: Separation and partial purification of HS**

All samples were heated to 95°C for 5mins to inactivate protease. To ensure all DNA RNA, protein were degraded 1 $\mu$ l of MgCl<sub>2</sub> and 0.5 $\mu$ l of benzonase was added and incubated for 2hrs at 37°C. Benzonase was heat inactivated for 2mins at 96°C. A volume of 12 $\mu$ l of 4M NaCl was added and sample was spun in microcentrifuge for 10mins at maximum speed and insoluble material removed. Supernatant was retained and loaded on to equilibrated Vivapure Mini D spin filter (Diethylaminoethyl-DEAE) (Sartorius AG, Germany). In order to

equilibrate the DEAE spin filters 400µl of elution buffer was added and filter spun for 1min at 500xg, followed by wash with 400µl of loading buffer. All eluates at this stage were discarded. This was then followed by loading of the supernatant and was centrifuged for 1min at 500g. Eluate was reloaded on the same filter and centrifuged again. This step was repeated and eluate was discarded at this stage, 400µl of loading buffer was then re-applied to the spin filter and spun for 1min at 500xg, and eluate discarded. An equal volume of elution buffer was added and spun for 1min at 500xg and the eluate was stored.

### **2.10.3: Desalting and digestion of HS**

Eluate was loaded on to an Ultrafree MC (Biomax -5) filter and spun at maximum speed for 4-5mins until retentate (liquid through the filter) was  $\leq 30\mu\text{l}$ . Retentate was washed with 50µl of dH<sub>2</sub>O and spun each time. This was repeated at least four times. Retentate was then removed to a new tube and filter membrane was rinsed with 50µl of dH<sub>2</sub>O four times and these washes were pooled together with retentate giving a final volume of 230µl of GAG mixture.

Samples were then loaded on PD10 gel filtration column. Prior to loading PD10 columns were washed four times (the length of the column) with dH<sub>2</sub>O to remove any salt. Samples were then eluted with 0.5ml fractions of water, storing only fractions 7 & 8. After collection of 1ml samples (fractions 7 & 8) samples were placed in speed vac and left for 3hours to dry. Pellet was resuspended in 5µl of distilled water, and prepared for digestion with Heparinases. Five microlitres of digestion buffer and 5µl of enzyme mix (consisting of equal quantities of 0.33mlU/ml heparinase, heparinitase II and heparitinase I) was added to tubes. Tubes were placed in shaking incubator overnight at 37°C. Following the digestion step, 12µl of dH<sub>2</sub>O was added to the digest mix to give a final volume of 23µl, of which 20µl was used to load onto the HPLC.

### **2.11: SAX High performance liquid chromatography (HPLC)**

All wash buffers and solutions used were sterile filtered prior to use on Agilent 1100 series high performance liquid chromatogram (HPLC). Tubing was consistently washed with isopropanol prior to running each sample.

#### **2.11.1: Loading HS standards and samples**

ProPac PA1 analytical column (Dionex USA) was equilibrated with Buffer A and B for 5mins until a stable baseline was achieved. Samples of a final volume of 20µl were syringed into a

20µl injection loop. Following sample loading the loop contents were washed on to column with 1ml of dH<sub>2</sub>O, pH3.5. Disaccharides were eluted at a flow rate of 1ml/min with a linear gradient of 1M NaCl over 45mins. Separated disaccharides were fluorescently labelled by mixing with equal portions of Buffer C and Buffer D that were dispensed at a flow rate of 0.45ml/min and reacted at 122°C in a post column reactor (CRX400 Pickering laboratories USA). The eluant was monitored on line by fluorescence excitation at 346nm and 410nm emission. Following each run of samples column was washed for 10mins in 100% Buffer B and then 15mins in 100% Buffer A. Peaks were eluted at different time points and identified by reference to HS standards of known concentration (0.16nmol). Results were displayed as chromatogram and peaks quantified using ChemStation software.

## Chapter 3.0 Paper one

Running Title: Expression patterns of Heparan sulphate modifying enzymes 'Sulfatases' during Zebrafish development

**Authors:** Bushra Gorski<sup>1</sup>, Simon Whelan<sup>1\*</sup>, Sally Stringer<sup>1</sup>

Submitting to Developmental dynamics

<sup>1</sup> School of Clinical and Laboratory Sciences, 46 Grafton Street, University of Manchester

<sup>1\*</sup> Faculty of Life Sciences, Michael Smith building, University of Manchester

### **Author Contributions:**

Bushra Gorsj: Planned and performed all the WISH experiments and analysis, carried out the bioinformatics analysis, and wrote the manuscript

Simon Whelan: created the percentage identities score and assisted with the Bioinformatics interpretation.

Sally Stringer: Devised the project, supervised BG, critically read the manuscript and made helpful comments

### **Acknowledgments**

We like to acknowledge BHF and University of Manchester medical school studentship for funding S.S and B.G. We would like to thank Xingbin Ai (Boston Biomedical research, Massachusetts) and Ken Kramer (NIH, Bethesda) for providing the zebrafish sulf constructs for *in-situ* probes.

## Abstract

Sulfatases are heparan sulphate proteoglycan modifying enzymes that edit the final sulfation pattern by removal of 6-O sulphate groups from the heparan sulphate chain. To date two sulf genes have been identified in mammals and recent *in vivo* and *in vitro* experimental studies reveal the significance of sulf function in regulating many signalling pathways important during embryonic development. Here we report the three orthologs that have been identified in zebrafish namely *sulf1c*, *sulf2a* and *sulf2*. All predicted proteins contain the conserved motifs that characterise other vertebrate sulfs. Zebrafish have two copies of the *sulf2* gene in contrast to mammals, consistent with partial duplication in the teleost lineage. Our expression analysis by WISH reveals the sulfs are expressed in a restricted spatial and temporal manner. *Sulf1c* and *sulf2a* are broadly expressed in CNS and non-neuronal tissue including heart, somite boundaries, olfactory system and otic vesicle. Whereas *sulf2* expression is almost entirely restricted to the CNS, only *sulf1c* and *sulf2* are provided maternally. The three sulfs have overlapping but distinct expression patterns reflecting divergent regulation during development and implying possible functional divergence after duplication

## Introduction

Heparan sulphate (HS) is dynamic molecule residing on every cell and in the extracellular matrix in the form of proteoglycans such as syndecans, glypicans and perlecan. The HSPG families consist primarily of 2 or more HS chains that are attached to the protein core (Gallagher et al., 1990). HS chains are highly heterogeneous in nature both structurally and functionally. This diversification can be attributed to the complex expression patterns and substrate specificity of the different biosynthetic enzymes.

HS is synthesised in the golgi, as an alternating polymer of N-acetyl glucosamine and glucuronic acid, then the glycosaminoglycan chain (GAG) undergoes deacetylation, N-sulfation, epimerisation and O-sulfation. This is carried out by the action of highly specific biosynthetic enzymes acting co-operatively to form multiple domains of HS. HS chains differ in chain length as well as domain composition. There are three types of domains occurring naturally in HS. The 'S-domain', characterised by regions of high sulphation, is often flanked on either side by partially sulfated 'transition domains' and this whole sulphated area is spaced by low or non-sulfated domains of N-acetylated glucosamine and glucuronic acid. The

spacing of the sulphated domains and the sulphation pattern is critical for fulfilling the role of HS as a co-receptor in many cell signalling pathways (Gorsi and Stringer, 2007)

The O-sulphation pattern is dictated primarily by the action of multiple sulfotransferases (OSTs) acting within the cell namely the 2-OSTs, 6-OSTs and 3-OSTs, adding sulphate groups to their respective positions on the HS chain. However, the final level of control on the sulphation pattern is exerted extracellularly by a group of enzymes known as the 6-O endosulfatases (sulfs), removing sulphate groups from the HS chain.

Sulfs are regarded as the final editors of the HS synthesis programme and were first identified in quail, subsequently orthologs have been found in human, mice, zebrafish, rat, chick and fruit fly. Initially it was thought that sulf activity was restricted to the highly sulphated domains of HS (Ai et al., 2003). However, sulfs are capable of modifying the transition and low sulphated domains (Lamanna et al., 2006; Ai et al., 2007). The significance of this post-modification step in HS synthesis is instrumental in fine tuning the HS-protein interactions as evident from genetic and biochemical studies where altering the level of sulphation has shown to affect signalling in both physiological and pathological conditions.

Dynamic changes in HS sulfation attributed to sulfs have been shown to modulate a number of signalling molecules including Shh, Wnt, Bmp-4, GDNF, FGF and VEGF. This has been implicated in several developmental models, where sulfs can control wnt dependent myogenesis by allowing wnt to freely associate with its receptor (Dhoot et al., 2001); regulate oligodendroglial specification by enhancing the diffusion gradient of shh (Danesin et al., 2006); mediate mesoderm induction and angiogenesis by mediating FGF/HS/FGFR complex (Ai et al., 2003); regulating GDNF mediated muscle innervation and regeneration (Ai et al., 2007) and is also a regulator of Bmp-4 signalling through inhibiting the interaction with its cognate receptor (Freeman et al., 2008). Thus, sulf enzymes can regulate HS dependent signalling in both a positive or negative manner. This ultimately depends on the requirement of the 6-O sulphation to the HS binding protein. For example, specific sulphate groups (6S) have been shown to be dispensable for FGF2-HS binding but critical for FGF/FGFR2 signalling (Ishihara et al., 1995), and therefore removal of the 6-O-sulfate group disrupt FGF signalling (Wang et al., 2004). Similarly VEGF binding and activity requires moderately 6-O sulphated HS (Ashikari- Hada et al., 2005; Robinson et al., 2005) and treatment of heparin with HSULF-2 abolishes its binding to VEGF (Uchimura et al., 2006). Although the exact nature of the structural HS requirement have not been decoded for bmp-4 activity it is implicit strict levels of 6-O sulphation are critical to BMP regulation, since *in-vitro* studies show Qsulfl can also dissociate the interaction of BMP with its inhibitor noggin conversely,

allowing BMP to freely associate with its receptor and promote signalling (Viviano et al., 2004).

The biphasic nature of sulfs is equally apparent in pathological conditions where upregulation of sulfs in different cancer cell lines have opposite roles in tumour growth *via* similar signalling cascades. In pancreatic tumours, HSULF-2 increases tumour growth mediated by wnt signalling (Nawroth et al., 2007) consistent with a pro-angiogenic role of HSULF-2 in CAM assay (Morimoto-Tomita et al., 2005). It is possible therefore that tumour growth in cancer cells overexpressing *sulf2* is potentiated by tumor angiogenesis. In hepatocellular and breast carcinomas, however enforced HSULF-1 expression inhibits tumour growth/angiogenesis partially by inhibiting FGF, HGF and VEGF stimulation of tumour cell growth and metastasis (Lai et al., 2004). This is consistent with *in vitro* studies showing low FGF /HS/FGFR2 signal complex in these conditions (Lai et al., 2006; Narita et al., 2006). Clearly in pathological conditions sulfatases can have both a pro or anti-angiogenic role depending on the importance of 6-O sulphation in the context of the perturbed signalling environment. This indicates the level of complexity in HSPG regulation by sulf enzymes alone at many different levels and reflects the many developmental processes it can influence. While many studies have shown sulfs to affect signalling molecules and their target pathways, sulf single knockout mice show no striking phenotype in overall development, with mild defects reported in bone formation, lung and esophageal innervation (Lum et al., 2006; Ai et al., 2007; Ratzka et al., 2008). However, double knockout mice exhibit reduced body mass and die shortly after birth suggesting functional redundancy amongst the sulf family (Lamanna et al., 2006; Holst et al., 2007). This is consistent with the reported overlapping expression profiles of sulf enzymes during mice embryonic development (Lum et al., 2006; Ratzka et al., 2008). However the distinct subtleties in the phenotypes of single sulf knockout mice and the severe phenotype in the xenopus *sulf1* deficient embryo reflect the dynamic regulation of sulf enzymes in a spatial and temporal manner. Here, we identify three sulf homologs in the zebrafish by phylogenetic analysis and describe the expression patterns of three sulfatases *sulf1c*, *sulf2a* and *sulf2*. Their expression patterns partially overlap in both neuronal and non-neuronal tissue, while *sulf2* is specifically expressed in the CNS, *sulf1c* and *sulf2a* are expressed more broadly. This implies that many developmental processes can be regulated by the sulf enzymes during zebrafish development.

## Results

### Sulfatase family

Sulfatase enzymes hydrolyse sulfatase esters on a variety of molecules including GAGs. Although there are two types of sulfatases, namely arylsulfatases and endosulfatases the mechanistic and structural features are largely conserved *via* the unique posttranslational modification event generating a formylglycine that is critical to the catalytic activity of the sulfs (von Figura et al., 1998; Dierks et al., 1999). The feature that distinguishes the sulfs, is the central hydrophilic domain which contains residues essential for heparan binding, docking to the cell surface and activity (Ai et al., 2006; Frese et al., 2009; Tang and Rosen, 2009). Further glycosylation of 10-11 asparagines residues prevalent throughout the full length sulf protein have also been shown to contribute to heparin binding and catalytic activity (Ambasta et al., 2007). All previously identified endosulfatase are composed of four distinct regions; a short N-terminal signal peptide, a highly conserved enzymatic domain, a hydrophilic domain and c-terminal domain.

Using the cloned sequence of human sulf endosulfatase, we mined genomic databases for sulf orthologs in several species. From the databases we found the number of copies of sulf increased in vertebrates with zebrafish having 3 copies of the endosulfatase genes respectively. In the zebrafish three extracellular sulfatases can be readily identified as *sulf1c*, (acc no: ENSDARG00000038428) *sulf2* (acc no: ENSDARG00000018423) and *sulf2a* (acc no: ENSDARG00000013838 ).

ClustalW alignment showed there is considerable conservation with the active site regions of these enzymes (Fig. 1). Although the signal peptide is less well conserved, each sulf enzyme consists of a conserved sulfatase domain of 372 amino acids which has been assigned based on comparison with PFAM database of protein domain families (Bateman et al., 2002). Within the amino terminal domain of the putative sulfatase domain are double cysteine residues that are modified postranslationally to N-formylglycine and form part of the catalytic site of these enzymes (Dierks et al., 1999) (Fig. 2C). In addition the 10 to 11 potential N-linked glycosylation sites are well conserved in these enzymes. Although the hydrophilic domains and c-terminal domains are present in all three enzymes, these are less well conserved in *sulf2* and *sulf2a* in comparison to their mammalian homologs. The phylogenetic tree however groups all three zebrafish sulf proteins in the sulf family with high bootstrap support. (Fig. 2B)

The predicted amino acid sequences show a high homology to known SULF proteins of other species. *Sulf1c* and *sulf2a* show 73% and 74% amino acid identity to mammalian *sulf1* and *sulf2* protein respectively, whereas zebrafish *sulf2* shows only 68% identity to respective mammalian *sulf2* ortholog. However the least homology is between zebrafish *sulf* family members with *sulf1c* showing 65% and 59% homology to zebrafish *sulf2a* and *sulf2* respectively (Fig 2A).

To test whether the zebrafish *sulfs* are true orthologs of human *sulfs* we inspected the synteny near the human and mouse gene. Zebrafish *sulf1c* had immediate neighbours that also map close to their respective orthologs in human and mice. However from the mapping of the *sulf2* & *sulf2a* there appears to be a lack of synteny at this gene location, suggestive of a likely duplication event early in the teleost radiation (Taylor et al., 2001).

Together with the combination of sequence similarity in characterised domains and conserved synteny these findings indicate that *zfsulf1c* is orthologous to other *sulf1* genes and *sulf2a* and *sulf2* are orthologous to other *sulf2* genes.

### **Developmental expression patterns**

The expressions pattern of the three zebrafish *sulf* genes, *sulf1c*, *sulf2a* and *sulf2* were analysed both spatially and temporally. From RT-PCR data we found all three *sulfs* to be expressed throughout development except *sulf2a* was not expressed maternally (Fig. 3.0).

To analyse their expression during embryonic development we performed whole mount *in-situ* hybridisation (WISH) with riboprobes for the respective genes. As controls we performed WISH with sense probes of each *sulf* gene and markers staining specifically for muscle and vasculature (Supplementary data). The expression patterns of *sulf1c*, *sulf2* and *sulf2a* were analysed by WISH from early somitogenesis to 48hpf and the results are summarised in Table 1. It must be noted Table 1 is not a complete list of all structures showing expression but gives a representative example of differential expression. All three *sulf* family members show strong expression in the brain however in some cases expression is often restricted to specific regions of the neurocranium.

### **Expression of *sulf1c***

The *sulf1c* message is maternally provided and is weakly expressed during early cleavage stages to the sphere stage. *Sulf1c* is also ubiquitously expressed during gastrulation (data not shown). During early somitogenesis *sulf1c* expression is restricted in the ectoderm and

mesodermal tissue. The dorsal view of the 5 somite stage reveals stronger expression in the somite boundaries than in the somites of the presomitic mesoderm layer (Fig. 4A,D). In the mid-somitogenesis stage (17 somite stage) *sulflc* expression is detected in the ventral midline, specifically known as the floorplate of the spinal cord and is strongly detected in the hindbrain floorplate (Fig. 4M). The dorsal midbrain and hindbrain are also positive for *sulflc* transcripts (Fig. 4J). Expression is also observed in the posterior most somites, somite boundaries, axial vessels and tail bud (Fig. 4G). During late somitogenesis *sulflc* expression is maintained in head but has now expanded to include most of the hindbrain and ventral midbrain, expression also begins now in the forebrain and in the developing eye lens. The developing branchial arches and the pronephric ducts show pronounced *sulflc* message and the expression is maintained in the somite boundaries (Fig. 5A, D)

At 24hpf, *sulflc* is expressed broadly in the forebrain, mid brain and hindbrain. This broad expression is not uniform and is strongest in the eye, dorsal telencephalon, and cerebellar primordia and extends caudally to the mid-hindbrain boundary (Fig. 5G,J). Although hindbrain floorplate continues to strongly express *sulflc* the floorplate express low levels with weaker expression in the rest of the spinal cord. It is also continued to be expressed in the branchial arches, pronephric ducts and somite boundaries. Weak expression in the axial vessels also evident at this stage, though stronger expression is now observed in the developing caudal plexus (Fig. 5K,L). *Sulflc* is also beginning to be expressed at low levels in the olfactory bulb (thought to reside in the cells of the dorsal telencephalon, Wilson et al 1990). At 36hpf *sulflc* expression appears strong in the eye lens, and in the forebrain relative to 24hpf; expression is not only restricted to the dorsal telencephalon but expressed in the ventral telencephalon and the dorsal diencephalon. Expression is also detected in the tegmentum in the midbrain, and in the bilateral cell clusters in the hindbrain (Fig. 5S).

At 48hpf, expression in the head becomes more restricted, thus reduced expression continues in the hindbrain floor plate and is now also reduced in the dorsal telencephalon. However strong expression is maintained in the ventral telencephalon and dorsal diencephalon and spreads from diencephalon caudally to the optic tectum and tegmentum in the midbrain (Fig. 6G). Expression is also maintained in the eye lens but now also beginning in the choroid plexus. Non-neuronal structures are also positive for *sulflc* at this stage particularly in the anterior and medial cranial vessels such as primary head sinus (PHS) and primordial hindbrain channels (PHBC). The pectoral finbuds and heart also begin to express *sulflc* and in the pharyngeal derived mesoderm. Expression continues in the axial vessels with noticeable presence of the *sulflc* transcript also now in the hypochord, the caudal fin folds are also

positive for *sulf1c* (Fig. 6A). At the 60hpf stage expression is maintained in the distinct regions of the head but appears more stronger particularly in the forebrain, midbrain structures, (Fig. 6J) choroid plexus, otic vesicle and finbuds (Fig. 6M). Strong expression is beginning in the first pharyngeal arch and continues in the heart and axial vessels (Fig. 6D,M).

### **Expression of *sulf2a***

*Sulf2a* message can be detected strongly during early somitogenesis where it's expressed in the presomitic mesoderm and somite boundaries (Fig. 4B,E). At 17 somite stage *sulf2a* is expressed in the floor plate with strongest expression in the ventral hindbrain floorplate (Fig. 4N). Broad expression is observed in the head, however unlike *sulf1c*, expression is stronger in the ventral region of the midbrain and hindbrain with weak expression in the developing eye (Fig. 4K). The ventral somite boundaries contain the strongest *sulf2a* expression in the trunk compared to weak expression apparent in the posterior and medial somites (Fig. 4H). No expression is observed in the tail bud. During late somitogenesis (25 somites) *sulf2a* continues to be expressed in these structures with little expression also now in the tail bud (Fig. 5B,E). Like *sulf1c*, *sulf2a* is broadly expressed throughout the nervous system at 24hpf, however strongest expression is observed in the ventral telencephalon and dorsal diencephalon and expression extends ventrocaudally into the tegmentum in the midbrain and anterior-rostrally to the cerebellar primordium (Fig. 5M). Similar to *sulf1c*, there are continued low levels of expression in the floorplate with strongest expression in the anterior floorplate and in the spinal cord neurons (Fig. 5H). It is also expressed at low levels in the rest of the spinal cord. Unlike *sulf1c* no expression is observed in the caudal plexus, however *sulf2a* expression is expressed in other non-neuronal structures including the branchial arches and the pronephric ducts (Fig. 5N,O). At 36hpf *sulf2a* continues to be expressed in the dorsal diencephalon and is now much stronger in the dorsal telencephalon relative to the ventral regions at 24hpf, and is detected weakly in the tegmentum opposite to *sulf1c* expression. *Sulf2a* continues to be detected in the floorplate and in the bilateral cell clusters in the hindbrain. Expression is also beginning in the otic vesicle (Fig. 5T)

At 48hpf expression becomes restricted to specific regions in the head, with reduced expression in the spinal cord and dorsal telencephalon (Fig. 6B). In contrast to *sulf1c*, strong expression is centred in the ventral diencephalon, from this structure *sulf2a* expression extends upwards and outwards rostrally into the optic tectum in the midbrain and can now

also be detected in the choroid plexus. Expression is maintained in the otic vesicle and is now also beginning in the cranial vessels in the PHBC and PHS (Fig. 6H).

At 60hpf expression is maintained in the head structures with little or no expression in the trunk (Fig. 6E). However expression is much weaker in the dorsal diencephalon and optic tectum relative to 48hpf (Fig. 6N). Like *sulf1c* strong *sulf2a* expression is maintained in the otic vesicle and the choroid plexus and strong expression begins in the heart and the first pharyngeal arch.

### **Expression of *sulf2***

Similar to *sulf1c*, the *sulf2* transcript is present maternally and ubiquitously expressed during early cleavage stages and gastrulation (data not shown). Expression is continued through somitogenesis, at the early somite stage expression is observed in the somite boundaries similar to the other two sulfs (Fig. 4C,F). During mid somitogenesis, expression becomes restricted in distinct regions of the head and trunk; the presumptive forebrain, the tegmentum in the midbrain region, hindbrain floorplate and in the dorsal and ventral regions of the spinal cord (Fig. 4I,O). In the hindbrain strong expression is also observed most caudal to the mid-hindbrain boundary, in the approximate region of rhombomere 1-4. In contrast to the other two sulfs, *sulf2* is also observed in the hypochord (Fig. 4I,L) and not detected in the eye, somites or somite boundaries and axial vessels at this stage. During late somitogenesis *sulf2* is expanded to include most of the hindbrain and ventral mid-forebrain. Expression is beginning to be observed in the optic recess and dorsal telencephalon (Fig. 5C). It continues to be strongly expressed in the spinal cord and can also now be detected weakly in the notochord and hypochord (Fig. 5F). At 24hpf, *sulf2* expression in the spinal cord, forebrain, midbrain and hindbrain is continued. This expression is not uniform however and is strongest in the bilateral clusters of cells in the dorsal telencephalon and in a rostral-caudal stripe in the ventral diencephalon (Fig. 5I). In contrast to the other two sulfs, the cerebellar primordia is weak for *sulf2* expression but *sulf2* transcripts are more strongly detected in rhombomeres 1,2, 4 and 6. Expression is also detected in spinal cord neurons (Fig. 5P,Q). In the tail, expression is restricted to the spinal cord and in the hypochord (Fig. 5R). At 36hpf strong expression is maintained in these regions in the head (Fig. 5U) with strong expression also observed now in the dorsal diencephalon and in ventral telencephalon. Expression continues in the tegmentum and is also beginning in the optic tectum in the midbrain, rhombomeres and in the spinal cord. By 48hpf expression *sulf2* continues to be weakly expressed in the spinal

cord with stronger expression apparent in the anterior spinal cord. Similar to *sulf2a* expression *sulf2* transcripts are in distinct regions of the head (Fig. 6C). It is also now more strongly expressed in the ventral diencephalon, optic tectum, and the choroid plexus. Expression is weaker in the otic vesicle compared to the other sulfs and very little expression is detected in the anterior-medial cranial vasculature. The pectoral finbuds also begin to show weak *sulf2* expression (Fig. 6I). During the pec-fin stage, (60hpf) *sulf2* message is detected ubiquitously in the head (Fig. 6O). Strong expression is observed in the ventral diencephalon and in region approximate to the pharyngeal arches, ventral and dorsal telencephalon and choroid plexus (Fig. 6O). Unlike *sulf1c* and *sulf2a*, the *sulf2* transcripts are not detected in the eye and in the otic vesicle. *Sulf2* continues to be expressed in other non-neuronal tissues particular the heart, pectoral fin buds, and the caudal fin folds. By this time *sulf2* expression has also diminished to low levels in the trunk, and no longer expressed in the posterior spinal cord, but strongly in the pronephric ducts and axial vessels (Fig. 6F).

## Discussion

### Three Sulfatase genes in zebrafish

Since the discovery of a novel sulfatase in the quail embryo as a HS specific 6-O endosulfatase, information regarding their role and activity has been further substantiated by reported *in vitro* and *in vivo* functional roles and expression patterns of sulf homologs in humans, rat, mice, quail, chick and frog. In this paper we report the phylogenetic analysis and *in-situ* expression of *sulf1c*, *sulf2a* and *sulf2* in zebrafish.

Many mammalian genes have two zebrafish orthologs due a duplication of the teleost genomes that is presumed to have occurred during evolution (Taylor et al., 2001). Therefore the discovery of two *sulf2* genes is not surprising. *Sulf1c* is likely to be a species ortholog of HSULF-1 based on nucleotide and amino acid sequence comparisons and on conserved synteny between the human, mice and zebrafish genomes. *Sulf2* and *sulf2a* also appear to be true orthologs of vertebrate *sulf2* gene and have conserved structural motifs and amino acid sequence despite no conserved synteny with human and mice genome. Duplicated genes are retained in evolution likely by partitioning the functions and expression of the original gene (Lynch and Conery, 2000; Lynch and Force, 2000). To validate this one might expect the zebrafish *sulf2a* or *sulf2* mutant phenotype to equal the phenotype of the mammalian *sulf2* mutant. However no known zebrafish *sulf2* mutants exist to date and *sulf2* knockout mice are virtually normal apart from the reduced size and body mass. Alternatively gene expression patterns can be used to infer function. That is the combined expression of *sulf2a* and *sulf2* might be expected to mirror the expression pattern of mammalian *sulf2*.

### Comparison of HS sulfatases expression from various species

Sulfs have an essential role in modulating the HS sulphation patterns and are major regulators of 6-O sulphation in the cell, since double *sulf* knockout mice die after birth (Lamanna et al., 2006; Lamanna et al., 2008). Therefore it is not surprising we found most structures to have at least one family member expressed during early embryonic development. However there were several structures including the CNS, pectoral finbuds and pronephric ducts that expressed multiple family members. Although it's difficult to correlate different developmental stages amongst species, zebrafish sulfs are expressed in similar structural pattern to other vertebrate sulfs. Like mouse *sulfs*, strong expression is conserved in many structures including the spinal cord, floor plate, choroid plexus, forebrain, midbrain,

hindbrain, pectoral fin buds, heart, somites, blood vessels. In particular the expression pattern of the spinal cord is highly similar to that of rat, mouse and xenopus. *Msulfl* is detected in the floor plate of the spinal cord whereas *msulf2* has more broad expression, detected in the dorsal and ventral regions of spinal cord. Similarly only *zfsulf2* is detected in the caudal notochord and somites, whilst *sulf1c* is the major source of sulf in the eye, olfactory epithelium like the mammalian sulf homologs (Nagamine et al., 2005; Lum et al., 2006; Winterbottom and Pownall, 2009). All three sulfs are expressed in the choroid plexus similar to rodents. Although we detected very weak *sulf2* expression in the notochord during early development, expression of *sulf1* and *sulf2a* was absent, consistent with only *msulf2* only expressed in the notochord. Interestingly this contrasts with *Qsulf1* that is abundantly expressed in the notochord, suggesting a species specific difference.

However there are some discrepancies that exist between expression of the sulf genes in zebrafish and rodents. Firstly both mouse sulfs are expressed in limb buds analogous to finbuds in zebrafish, however only *sulf1c* and *sulf2* were detected in the pectoral finbuds whilst *sulf2a* was absent, despite *sulf2a* showing higher sequence similarity than its *sulf2* paralog, to mammalian sulf2. Here *sulf1c* and *sulf2* transcripts are abundantly expressed but very little *sulf2a*, which might have become dispensable during evolution due to the continued expression of the other two sulfs. Likewise *sulf2a* shows restricted and weaker expression in the posterior spinal cord compared to mammalian *sulf2* and is not detected in the notochord. We also detected strong *sulf2a* expression in the otic vesicle, in contrast to *msulf2*. More recently it has been shown that *msulfs* are abundantly expressed in cartilage and bone (Ratzka et al., 2008). Although these structures come on line post 2.5dpf we were able to detect sulf expression at 60hpf in the pharyngeal arches and pectoral finbuds that eventually will form the jaw skeleton and the girdle cartilages (Kimmel et al., 1995). Lastly we observed unique expression of the three sulfs in the cranial vasculature albeit *sulf2* weakly and also *sulf1c* and *sulf2* in the axial vessels. Although some *msulf1* has been reported in the vasculature, *msulf2* is expressed in mesenchymal tissue surrounding the axial vessels (Lum et al., 2006; Holst et al., 2007) similar to our *sulf2a* profile.

Overall the *sulf1c*, *sulf2a* and *sulf2* expression patterns are similar to their respective homologs. The remarkable similarities in expression of the zebrafish *sulf1c* to the mammalian sulf1 further supports that *sulf1c* is indeed a sulf ortholog and likely to function in a similar manner to vertebrate *sulf1*. However the differences in expression could suggest novel functional roles during development. Despite *sulf2a* and *sulf2* showing discrete differences to mammalian *sulf2*, combined expression patterns mirror the *msulf2* expression profile. From

these findings we speculate the diversification of the *sulf2* gene might provide another example of subfunctionalisation model (Lynch and Force, 2000), in which presence of both genes is necessary to emulate the original gene expression pattern and possibly function. Interestingly this has also been hypothesised with the *Ext1* genes in zebrafish (Siekmann and Brand, 2005) suggestive of a possible recurring theme in HS enzymes.

### **Expression profile of HS enzymes in zebrafish**

The clearly defined expression patterns of sulfatases bear strong resemblance to the previously published expression patterns of other HS biosynthesis enzymes such as *Ext1* C5 epimerase, 2OSTs, 6OSTs, and 3OSTs (Siekmann and Brand, 2005; Cadwallader and Yost, 2006b; Cadwallader and Yost, 2006a; Cadwallader and Yost, 2007) suggesting that sulf substrates are synthesised locally. Most structures examined have at least one member with low levels or ubiquitous expression and at least one member with specific expression. For example *sulf1c* and *sulf2a* are more ubiquitously expressed in the hindbrain whereas *sulf2* expression is restricted in the rhombomeres in the hindbrain. The coordinated expression of at least one member might be necessary for generation of specific HS structures *in vivo*. Comparing the *sulf* expression profile to that of 2OST, 6OSTs and 3OSTs we found structures that were devoid of 6OST or 2OST expression yet expressed other HS enzymes including 3OSTs and sulfatases. While the latter could be owed to the possible activity on neighbouring cells, the presence of 3OSTs in cells forming the major sulfate groups on HS further lending support to the role flexibility in the HS biosynthesis (Ledin et al., 2006).

In addition it appears that the expression patterns are highly regulated to generate HS specific sulphation patterns. One example of this is in the rhombomeres, thus FGF signalling plays a significant role in patterning the hindbrain (Maves et al., 2002), and given that 6-O sulphation is critical to FGF activity we founds our *sulf2* expression patterns to be complementary to that of 6OSTs in this region. Although all 6OSTs are expressed in the hindbrain 6OST1a is strongly expressed in the anterior spinal cord and later in approximately in the rhombomere 3 region, whilst no *sulf2* expression is detected in rhombomere 3 but only in adjacent rhombomeres, thus suggesting a fine balanced level of 6-O sulphation in the patterning of the HS. Conversely we found both *sulf1c* and *sulf2a* expression to be concentrated more in somite boundaries than somites, whilst 2OST and 6OST1b appears to be strongly expressed in the somites and 6OST-2 strongly in the somite boundaries. This implies the importance of generating specific 6-O sulfated HS species during muscle development. From our results we found sulfs to be strongly expressed in the pronephric ducts and heart yet no 2OST, or any

6OST expression was reported in these structures. Interestingly this observation could be linked to recent *in-vitro* data in which transcription of 2OSTs and 6OSTs is increased in cell lines derived from double sulf knockout mice, suggesting sulfs as possible regulators of the transcription of other HS biosynthetic enzymes. This is further supported by the intracellular localisation of full length protein in the endoplasmic reticulum(ER) Thus beyond the scope of their function as extracellular 6-O sulfatases, sulfs may have more significant role in being the majors regulators of all types of sulfation in and outside of the cell (Lamanna et al., 2008), could this imply a dual function of the sulfs enzymes?

### **Zebrafish sulfatase structure and expression patterns: Novel functional implications?**

All three zebrafish sulfatases contain the predicted motifs conserved in vertebrate sulfs. In general the vertebrate *sulf2* are structurally different from *sulf1* particularly in the hydrophilic domain (HD). This is also evident in zebrafish sulfs, whereby *sulf2a* and *sulf2* like their mammalian counterpart have conserved sequence regions not evident in *sulf1c*. Studies on human and quail sulf HD signifies its important role in heparin binding, anchorage to cell surface and enzymatic activity. In particular the predicted 14 basic amino acid sequence residing in the HD domain marginally contributes to these functional roles (Ai et al., 2006; Frese et al., 2009; Tang and Rosen, 2009). Although these sequences are fairly conserved in the zebrafish sulfs, the additional stretch of sequences in the C-terminal region of HD of *sulf2* and *sulf2a* may confer different function, such that it may alter heparin binding affinity, or its localisation to the cell surface. Recently it has been shown that human SULF2 can modify sulfation of the ECM and shed HSPGs consistent with reports of active full length enzyme found in the conditioned medium (Lamanna et al., 2008) thus suggesting sulfs are more mobile than previously anticipated. It would be interesting to address the HD function of zebrafish sulfs to observe whether this activity is conserved in all vertebrates and if sulfs can modify 6-O sulphation on neighbouring cells.

The expression patterns of the sulfs in the brain and spinal cord neurons are consistent with the role of HS in axonal guidance. Thus many HS deficient animals or 6-O sulphated deficient HS show defects in axonal guidance and sorting (Inatani et al., 2003; Bulow and Hobert, 2004; Lee et al., 2004). Similarly sulf have a role in neurite sprouting in embryonic esophagus (Ai et al., 2007). We found sulfs to be strongly expressed in the neural tube throughout early development, thus suggesting sulfs have a role in patterning and maintenance of neural tube. One of the key molecules involved in ventral neural tube patterning is Shh expressed both in the notochord and floorplate in vertebrates (Odenthal et al., 1996). Thus *in vitro* studies have

shown *Qsulfl* regulating the range of *shh* signalling in oligodendrial specification (Danesin et al., 2006). Given their co-expression it's likely that sulfs maybe having a similar role in shaping the *shh* gradient in neural tube and notochord and therefore modulating *shh* mediated processes. Early vascular patterning is also modulated by *shh* signalling, thus arterial venous identification proceeds via the Shh-VEGF-notch signalling cascade (Lawson et al., 2002). Given the close proximity of *sulflc* expression in relation to the expression of HS regulated proteins suggests a possible role of *sulflc* intercepting in this cascade (B.Gorsi *et al* unpublished observations). Ubiquitous expression during gastrulation suggests a possibility sulfs may have a role in convergent extension. Finally *sulflc* and *sulf2* are expressed in the early developing pectoral finbuds suggests sulfs can regulate the morphogenesis or patterning of the finbuds.

### **Summary**

Taken together our results reveal the existence of the least three different members of the sulf family in zebrafish, with two copies of the sulf 2 genes most likely to have arisen from a gene duplication event during the teleost lineage. Their expression throughout embryogenesis comprises partially overlapping and mutually exclusive domains suggesting possible functional redundancy in certain tissues. In addition, the expression patterns show a spatial shift over time; at somitogenesis stages transcripts are ubiquitously expressed in head and trunk however over later stages the brain, pronephric ducts, axial vessels and fin buds express sulf genes.

The similarities between the sulf predicted proteins indicate that they are likely to have similar molecular properties. However, differences in expression suggest that although their coding regions are largely similar their promoters and enhancers may have diverged more substantially, leading to possibly novel functions. Future functional tests of three genes will determine if their functions have diverged and to what extent they regulate other developmental processes. Given the expression of the sulfs in a number of structures shown here during development reflects on their roles in modulating many HSPGs interactions during normal processes.

## **Experimental procedures**

### **Zebrafish care and husbandry**

Fish were maintained and bred under standard conditions in accordance with the University of Manchester Biological safety facility (BSF). AB strains were housed at BSF and embryos were staged according to (Kimmel et al., 1995), as equivalent hour's postfertilisation at 28.5°C

### **Bioinformatics analysis**

All amino acid sequences were placed in Clustalw alignment tool. Evolutionary distances were inputted into NJplot to construct phylogenetic tree

### **Whole mount *in Situ* Hybridisation**

Embryos were fixed in 4% PFA overnight or for 3hrs at 4°C, then were dehydrated through a methanol series and stored at -20°C until use. Plasmids and constructs used to generate probes were a kind gift from Ken Kramer and Xingbin Ai. Whole mount *in-situ*s were performed using standard methods Jowett and Lettice, 1994. *Sulf1c*, *Sulf2* probe *Sulf2a* plasmid was generated by digesting plasmids with *Sall*, *Age1* and *PstI* (Roche technologies) and transcribing with T7 polymerase (Roche) respectively. Approximately 200ng/ml of probe was used. Sense probes were used to confirm the specificity of antisense probes.

All samples were mounted in 80% glycerol and viewed by using normaski optics on a LSM5 Zeiss compound microscope. Digital images were captured by using Zeiss colour camera. All images were processed in adobe photoshop CS2

## References

- Ai X, Do AT, Kusche-Gullberg M, Lindahl U, Lu K, Emerson CP, Jr. 2006. Substrate specificity and domain functions of extracellular heparan sulfate 6-O-endosulfatases, QSulf1 and QSulf2. *J Biol Chem* 281:4969-4976.
- Ai X, Do AT, Lozynska O, Kusche-Gullberg M, Lindahl U, Emerson CP, Jr. 2003. QSulf1 remodels the 6-O sulfation states of cell surface heparan sulfate proteoglycans to promote Wnt signaling. *J Cell Biol* 162:341-351.
- Ai X, Kitazawa T, Do AT, Kusche-Gullberg M, Labosky PA, Emerson CP, Jr. 2007. SULF1 and SULF2 regulate heparan sulfate-mediated GDNF signaling for esophageal innervation. *Development* 134:3327-3338.
- Ambasta RK, Ai X, Emerson CP, Jr. 2007. Quail Sulf1 function requires asparagine-linked glycosylation. *J Biol Chem* 282:34492-34499.
- Ashikari- Hada S, Habuchi H, Kariya Y, Kimata K. 2005. Heparin regulates vascular endothelial growth factor(165)-dependent mitogenic activity, tube formation, and its receptor phosphorylation of human endothelial cells - Comparison of the effects of heparin and modified heparins. *Journal Of Biological Chemistry* 280:31508.
- Bateman A, Birney E, Cerruti L, Durbin R, Eddy SR, Griffiths-Jones S, Howe KL, Marshall M, Sonnhammer EL. 2002. The Pfam protein families database. *Nucleic Acids Res* 30:276-280.
- Bulow HE, Hobert O. 2004. Differential sulfations and epimerization define heparan sulfate specificity in nervous system development. *Neuron* 41:723-736.
- Cadwallader AB, Yost HJ. 2006a. Combinatorial expression patterns of heparan sulfate sulfotransferases in zebrafish: I. The 3-O-sulfotransferase family. *Dev Dyn* 235:3423-3431.
- Cadwallader AB, Yost HJ. 2006b. Combinatorial expression patterns of heparan sulfate sulfotransferases in zebrafish: II. The 6-O-sulfotransferase family. *Dev Dyn* 235:3432-3437.
- Cadwallader AB, Yost HJ. 2007. Combinatorial expression patterns of heparan sulfate sulfotransferases in zebrafish: III. 2-O-sulfotransferase and C5-epimerases. *Dev Dyn* 236:581-586.
- Danesin C, Agius E, Escalas N, Ai X, Emerson C, Cochard P, Soula C. 2006. Ventral neural progenitors switch toward an oligodendroglial fate in response to increased Sonic hedgehog (Shh) activity: involvement of Sulfatase 1 in modulating Shh signaling in the ventral spinal cord. *J Neurosci* 26:5037-5048.
- Dhoot GK, Gustafsson MK, Ai X, Sun W, Standiford DM, Emerson CP, Jr. 2001. Regulation of Wnt signaling and embryo patterning by an extracellular sulfatase. *Science* 293:1663-1666.
- Dierks T, Lecca MR, Schlotterhose P, Schmidt B, von Figura K. 1999. Sequence determinants directing conversion of cysteine to formylglycine in eukaryotic sulfatases. *Embo J* 18:2084-2091.
- Freeman SD, Moore WM, Guiral EC, Holme AD, Turnbull JE, Pownall ME. 2008. Extracellular regulation of developmental cell signaling by XtSulf1. *Dev Biol* 320:436-445.
- Frese MA, Milz F, Dick M, Lamanna WC, Dierks T. 2009. Characterization of the human sulfatase sulf1 and its high-affinity heparin/heparan sulfate interaction domain. *J Biol Chem*.
- Gallagher JT, Turnbull JE, Lyon M. 1990. Heparan sulphate proteoglycans. *Biochem Soc Trans* 18:207-209.

- Gorsi B, Stringer SE. 2007. Tinkering with heparan sulfate sulfation to steer development. *Trends Cell Biol* 17:173-177.
- Holst CR, Bou-Reslan H, Gore BB, Wong K, Grant D, Chalasani S, Carano RA, Frantz GD, Tessier-Lavigne M, Bolon B, French DM, Ashkenazi A. 2007. Secreted sulfatases Sulf1 and Sulf2 have overlapping yet essential roles in mouse neonatal survival. *PLoS One* 2:e575.
- Inatani M, Irie F, Plump AS, Tessier-Lavigne M, Yamaguchi Y. 2003. Mammalian brain morphogenesis and midline axon guidance require heparan sulfate. *Science* 302:1044-1046.
- Ishihara M, Takano R, Kanda T, Hayashi K, Hara S, Kikuchi H, Yoshida K. 1995. Importance of 6-O-sulfate groups of glucosamine residues in heparin for activation of FGF-1 and FGF-2. *J Biochem* 118:1255-1260.
- Jowett T, Lettice L. 1994. Whole-mount in situ hybridizations on zebrafish embryos using a mixture of digoxigenin- and fluorescein-labelled probes. *Trends Genet* 10:73-74.
- Kimmel CB, Ballard WW, Kimmel SR, Ullmann B, Schilling TF. 1995. Stages of embryonic development of the zebrafish. *Dev Dyn* 203:253-310.
- Lai JP, Chien J, Strome SE, Staub J, Montoya DP, Greene EL, Smith DI, Roberts LR, Shridhar V. 2004. HSulf-1 modulates HGF-mediated tumor cell invasion and signaling in head and neck squamous carcinoma. *Oncogene* 23:1439-1447.
- Lai JP, Yu C, Moser CD, Aderca I, Han T, Garvey TD, Murphy LM, Garrity-Park MM, Shridhar V, Adjei AA, Roberts LR. 2006. SULF1 inhibits tumor growth and potentiates the effects of histone deacetylase inhibitors in hepatocellular carcinoma. *Gastroenterology* 130:2130-2144.
- Lamanna WC, Baldwin RJ, Padva M, Kalus I, Ten Dam G, van Kuppevelt TH, Gallagher JT, von Figura K, Dierks T, Merry CL. 2006. Heparan sulfate 6-O-endosulfatases: discrete in vivo activities and functional co-operativity. *Biochem J* 400:63-73.
- Lamanna WC, Frese MA, Balleininger M, Dierks T. 2008. Sulf loss influences N-, 2-O-, and 6-O-sulfation of multiple heparan sulfate proteoglycans and modulates fibroblast growth factor signaling. *J Biol Chem* 283:27724-27735.
- Lawson ND, Vogel AM, Weinstein BM. 2002. sonic hedgehog and vascular endothelial growth factor act upstream of the Notch pathway during arterial endothelial differentiation. *Dev Cell* 3:127-136.
- Ledin J, Ringvall M, Thuvesson M, Eriksson I, Wilen M, Kusche-Gullberg M, Forsberg E, Kjellen L. 2006. Enzymatically active N-deacetylase/N-sulfotransferase-2 is present in liver but does not contribute to heparan sulfate N-sulfation. *J Biol Chem*.
- Lee JS, von der Hardt S, Rusch MA, Stringer SE, Stickney HL, Talbot WS, Geisler R, Nusslein-Volhard C, Selleck SB, Chien CB, Roehl H. 2004. Axon sorting in the optic tract requires HSPG synthesis by ext2 (dackel) and extl3 (boxer). *Neuron* 44:947-960.
- Lum DH, Tan J, Rosen SD, Werb Z. 2006. Gene trap disruption of the mouse heparan sulfate 6-O-endosulfatase, Sulf2. *Mol Cell Biol*.
- Lynch M, Conery JS. 2000. The evolutionary fate and consequences of duplicate genes. *Science* 290:1151-1155.
- Lynch M, Force A. 2000. The probability of duplicate gene preservation by subfunctionalization. *Genetics* 154:459-473.
- Maves L, Jackman W, Kimmel CB. 2002. FGF3 and FGF8 mediate a rhombomere 4 signaling activity in the zebrafish hindbrain. *Development* 129:3825-3837.
- Morimoto-Tomita M, Uchimura K, Bistrup A, Lum DH, Egeblad M, Boudreau N, Werb Z, Rosen SD. 2005. Sulf-2, a proangiogenic heparan sulfate endosulfatase, is upregulated in breast cancer. *Neoplasia* 7:1001-1010.

- Nagamine S, Koike S, Keino-Masu K, Masu M. 2005. Expression of a heparan sulfate remodeling enzyme, heparan sulfate 6-O-endosulfatase sulfatase FP2, in the rat nervous system. *Brain Res Dev Brain Res* 159:135-143.
- Narita K, Staub J, Chien J, Meyer K, Bauer M, Friedl A, Ramakrishnan S, Shridhar V. 2006. HSulf-1 inhibits angiogenesis and tumorigenesis in vivo. *Cancer Res* 66:6025-6032.
- Nawroth R, van Zante A, Cervantes S, McManus M, Hebrok M, Rosen SD. 2007. Extracellular sulfatases, elements of the Wnt signaling pathway, positively regulate growth and tumorigenicity of human pancreatic cancer cells. *PLoS One* 2:e392.
- Odenthal J, Haffter P, Vogelsang E, Brand M, van Eeden FJ, Furutani-Seiki M, Granato M, Hammerschmidt M, Heisenberg CP, Jiang YJ, Kane DA, Kelsh RN, Mullins MC, Warga RM, Allende ML, Weinberg ES, Nusslein-Volhard C. 1996. Mutations affecting the formation of the notochord in the zebrafish, *Danio rerio*. *Development* 123:103-115.
- Ratzka A, Kalus I, Moser M, Dierks T, Mundlos S, Vortkamp A. 2008. Redundant function of the heparan sulfate 6-O-endosulfatases Sulf1 and Sulf2 during skeletal development. *Dev Dyn* 237:339-353.
- Robinson CJ, Mulloy B, Gallagher JT, Stringer SE. 2005. VEGF165 binding sites within heparan sulfate encompass two highly sulfated domains and can be liberated by K5 lyase. *J Biol Chem*.
- Siekman AF, Brand M. 2005. Distinct tissue-specificity of three zebrafish ext1 genes encoding proteoglycan modifying enzymes and their relationship to somitic Sonic hedgehog signaling. *Dev Dyn* 232:498-505.
- Tang R, Rosen SD. 2009. Functional consequences of the subdomain organization of the sulfs. *J Biol Chem*.
- Taylor JS, Van de Peer Y, Braasch I, Meyer A. 2001. Comparative genomics provides evidence for an ancient genome duplication event in fish. *Philos Trans R Soc Lond B Biol Sci* 356:1661-1679.
- Uchimura K, Morimoto-Tomita M, Bistrup A, Li J, Lyon M, Gallagher J, Werb Z, Rosen SD. 2006. HSulf-2, an extracellular endoglucosamine-6-sulfatase, selectively mobilizes heparin-bound growth factors and chemokines: effects on VEGF, FGF-1, and SDF-1. *BMC Biochem* 7:2.
- Viviano BL, Paine-Saunders S, Gasiunas N, Gallagher J, Saunders S. 2004. Domain-specific modification of heparan sulfate by Qsulf1 modulates the binding of the bone morphogenetic protein antagonist Noggin. *J Biol Chem* 279:5604-5611.
- von Figura K, Schmidt B, Selmer T, Dierks T. 1998. A novel protein modification generating an aldehyde group in sulfatases: its role in catalysis and disease. *Bioessays* 20:505-510.
- Wang S, Ai X, Freeman SD, Pownall ME, Lu Q, Kessler DS, Emerson CP, Jr. 2004. QSulf1, a heparan sulfate 6-O-endosulfatase, inhibits fibroblast growth factor signaling in mesoderm induction and angiogenesis. *Proc Natl Acad Sci U S A* 101:4833-4838.
- Winterbottom EF, Pownall ME. 2009. Complementary expression of HSPG 6-O-endosulfatases and 6-O-sulfotransferase in the hindbrain of *Xenopus laevis*. *Gene Expr Patterns* 9:166-172.

## Figures

zfSulf2a	MAAHGLAARLLPLLLLTMLVAHASIFLSNRRLKPFDRDRRNIRPNILILITDDQDIEL	60
zfSulf2	MAVGWRPATLLLVFILTFCISLDGSTYLSGQRQRSLDRDRRNVRPNMILILITDDQDIEL	60
zfSulf1c	-NMQLVSLANMVLAAPLVCFG---FTTRGGLRGEVQDRRNIRPNILIMITDDQIVEL	56
<hr style="border: 1px solid red;"/>		
zfSulf2a	GSMQVMNKTRRIMEQGGTHFSNAFVITTPMCCPSRSSMLTGKYAHNHNTYTNNEHCSSPSW	120
zfSulf2	GSMQAMNKTKRIMMQGGTHFSNAFATTMCCPSRSTILTGYVHNHNTYTNNEHCSSPSW	120
zfSulf1c	GSIQVMNKTRKLINEGGTSTFNAFVITTPMCCPSRSSMLTGKYVHNHNTYTNNEHCSSPSW	116
<hr style="border: 1px solid red;"/>		
zfSulf2a	QAQHEIRTEFGVYLNNITGYRTAFFFGKYLNEYNGTYIPPGWKEWVAMVKNSRFYNYTLIRNG	180
zfSulf2	QAHEIEHTFAVHLNNSGYRTAFFFGKYLNEYNGSYVPPGWREWVALVKNSRFYNYTLIRNG	180
zfSulf1c	QAQHEIRSFAYVYLNNITGYRTAFFFGKYLNEYNGSYLPPGWREWGLIKNSRFYNYTVIRNG	176
<hr style="border: 1px solid red;"/>		
zfSulf2a	VREKHGFEYPKDYLTLLITNDSINYFRMSKKIYPIHPFVIMVISHAAPHCPEDAAPQYIIA	240
zfSulf2	IREKHGTOYPKDYLTLLITNDSINYFRMSKKIYPIHPFVMMVLISHAAPHCPEDAAPQYISSA	240
zfSulf1c	NKEKHGADYAKDYFTLLITNDSINYFRMSKKIYPIHPFVMMVISHAAPHCPEDAAPQYSEL	236
<hr style="border: 1px solid red;"/>		
zfSulf2a	FPNASQHITPSYNYAPNPKHWIMRYTGPMKFIHMEFTNMQRKRLQTLISVDDSVKQVY	300
zfSulf2	FPNASQHITPSYNYHAPNPKHWIMRYTGPMKFVIMQFTNMQRRLQTLISVDDSVKQVY	300
zfSulf1c	FPNASQHITPSYNYAPNPKHWIMQYTGPMKFIHMEFTNYLHKRLQTLISVDDSVKQVY	296
<hr style="border: 1px solid red;"/>		
zfSulf2a	NMVDITGELDNTYVYIYTAHGHYHIGDFGLVKGKSMFYEDDIRVPEFYVRCPNVEAGINPH	360
zfSulf2	NMVEITGELDNTYIYMSDHGHYHIGDFGLVKGKSMFYEDDIRIPEFYVRCPNVEAGINPH	360
zfSulf1c	NALVDITGELDNTYIYIYTAHGHYHIGDFGLVKGKSMFYEDDIRVPEFVRCPNVEAGARNPH	356
<hr style="border: 1px solid red;"/>		
zfSulf2a	IYVNIIDLAPTIIDIAAMDVTPMDGRSTLFLDTDRMMNRFQLNKKGKQVWRDPSFLVERGK	420
zfSulf2	IYVNIIDLAPTIIDIAAMDVTPMDGKSLKLEIETERPVRNFHSYKAKIWRDPSFLVERGK	420
zfSulf1c	VYVNIIDLAPTIIDIAAMDVTPMDGKSLKLEIETKGNRFKPNRKKPKVWRDPSFLVERGK	416
<hr style="border: 1px solid red;"/>		
zfSulf2a	IIRHVLNDGKDM-AEEFNYPKPYQRVLDLQRAEYJTPCEQIQOKWQVEQDATSKLRLSK	479
zfSulf2	IIRHVL-LADGK---EVLQNSLPKYQRVRLDQRAEYJTPCEQIPGOKWQVEQDGTGMPRLYK	476
zfSulf1c	IIRKEDSASSLNTQHSLSLPKYKVKVEVQQAQEFJTPCEQIPGOKWHVEEVSGKWRLOK	476
<hr style="border: 1px solid red;"/>		
zfSulf2a	CKMSSLSAVQKPSVSSINSQLYLQSIISTPDVSLNSEPQEQNCQPKSYRLSTYSK---SK	536
zfSulf2	CKMAGLFAAPR--ALGLMAANRGOILAAPHGS-----DYLDCEP---AAPLKR---KR	521
zfSulf1c	CKGSLKE-----GSKKRTSLR---RSYDNRE-----KIDHCGERPYLAKAABRAHRO	523
<hr style="border: 1px solid red;"/>		
zfSulf2a	LFSKMKKSLKSFNRNFAPALSMTGGDLIAVLDNEHRNLSL-----RLSTADED	588
zfSulf2	ALTKKLNKKSVPNRNWARVSPYHLDSNVYITLDEKGYRPLNINTSLMLGRKQAVYQON	581
zfSulf1c	FGSSNPRYRPRFVHTRPASLSVEFEGEITDVLQADDTELEPRPISKRYHEPEPGFD	583
<hr style="border: 1px solid red;"/>		
zfSulf2a	EEF-----SAAEPTTISQSNLSVPESSIKVTHSRCSILANETVKQDVGLYKSLQAWFQK	643
zfSulf2	EEY-----SMGPTEDN-FNSLTPPAALKVYI-RCSILMNDTVKQDGGLYKSLQAWFQK	634
zfSulf1c	SDFGLESDDSESSEMQSDDTNAVGYPNLSKVTH-KCFILINDTVRCEREIYQSSRAWFQK	642
<hr style="border: 1px solid red;"/>		
zfSulf2a	LHIDIEETLOTKIKNIREVRGHLKARPEQDCKNYKYKSKYKSLRKYKTFGHGFDSL	703
zfSulf2	LHIEIEETLOTKIKNIREVKGHLKEVRPKQECNENMYQYSSR-ALFLLRSAQTHSVNR	693
zfSulf1c	NEVDIEEIQLODKMKKIREVRGHLKRRRPEQDCSKSYFSKEREQKNPERLKNRNDHL	702
<hr style="border: 1px solid red;"/>		
zfSulf2a	CVCRKGQ-EKIKKAWMLEQKPRKKLRKLLKRLRNNITCSMPGLTCFTHDNQHWQAPFW	762
zfSulf2	MTS-----KIKKQWLMKEQKRRKKLRKLLKRLRNNITCSMPGLTCFTHDNQHWQAPFW	747
zfSulf1c	HPFKEAMQEVLSKAQLYNEIRRRKKERKVRKPKQKGGDCSLPGLTCFTHNNDHWQAPFW	762
<hr style="border: 1px solid red;"/>		
zfSulf2a	TLGPFCACTSANNNYWCMTINETHNLFCEFATGFLEYFDINTDPYQIMVANNILDRY	822
zfSulf2	TLGPFCACTSANNNYWCMTINETHNLFCEFATGFLEYFDINTDPYQIMNGVSHLDRD	807
zfSulf1c	NLEGFCACTSSNNNYWCLRTVNETHNLTFCFATGFLEYFDLNSDFYQITNAMYIWEKD	822
<hr style="border: 1px solid red;"/>		
zfSulf2a	VLNQIVQLMELGCKGHKQCN-IRTRSLDM-GKERSYDEYR-----	864
zfSulf2	AVNHMQQLMKLRSCKGHKECNQPDIDISLVTGKERNITLYDYRPLHRRKRPKVKKASSK	867
zfSulf1c	ILSQILSOLMEMRSCQGHKQCN-IRPRSSDA-GSKDGGSYDQHR-----	864

**Figure 1.0: Clustalw alignment of zebrafish sulf proteins.** Residues identical in all three proteins are indicated with white lettering on a black background. Residues that are similar in two of the three proteins are highlighted in black lettering on grey background, with similar residues highlighted in bold. Conserved sulfs domains highlighted by the different coloured lines are assigned on based on comparison of protein family of alignments. Sulfs contain four structural domains, including the N-terminal signal peptide (yellow line), the enzymatic domain (red underline), hydrophilic domain (blue underline) and the C terminus (green underline).



**Figure 2.0: Phylogenetic analysis of predicted zebrafish sulf proteins based on Clustalw alignment**

**A:** Percentage identities between sulf proteins. Zebrafish sulfatases are the most divergent species from human and mouse sulfatase. *Zfsulf1c* and *sulf2a* are more closely related to their human orthologues than *zfsulf2*.

**B:** Phylogenetic tree of predicted sulf proteins. Scale represents the number of amino acids, 0.1 = 100aa

**C:** Alignment of the portion of the enzymatic domain, red dotted box highlights the catalytic site of sulf proteins. The critical cysteine residue (highlighted in yellow box) that is converted to formylglycine is required for catalytic activity is conserved across species. Two of the 11 N-linked asparagines required for glycosylation are found to be conserved (purple box). *Zfsulf2* contains two alternate residues in replacement of the valine and serine residues in the catalytic domain of the *sulf*.

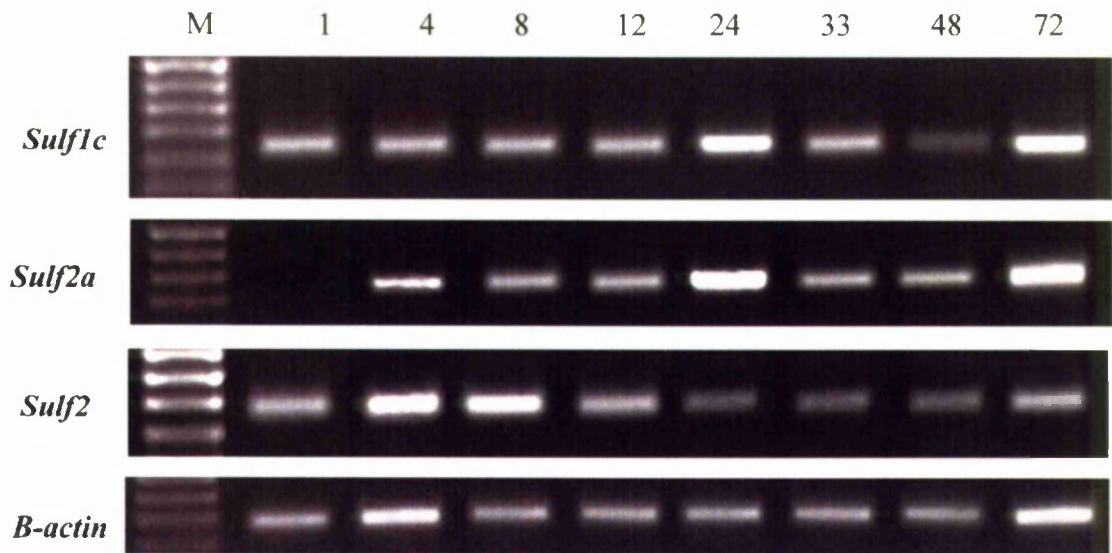


**Figure 3.0: RT-PCR of *sulf* transcripts during zebrafish development.**

*Sulf1c*, *Sulf2a* and *Sulf2* primers were designed to amplify 512bp, 498bp, and 687bp respectively with inclusion of the ATG start site. *β-actin* primers designed to amplify 298bp. The resulting PCR products were electrophoresed on a 1% agarose gel. The intensity of 300bp DNA fragment using *β-actin* specific primers amplified was used to evaluate the relative amount of cDNA used in each PCR. Marker lane represents 1kb ladder.

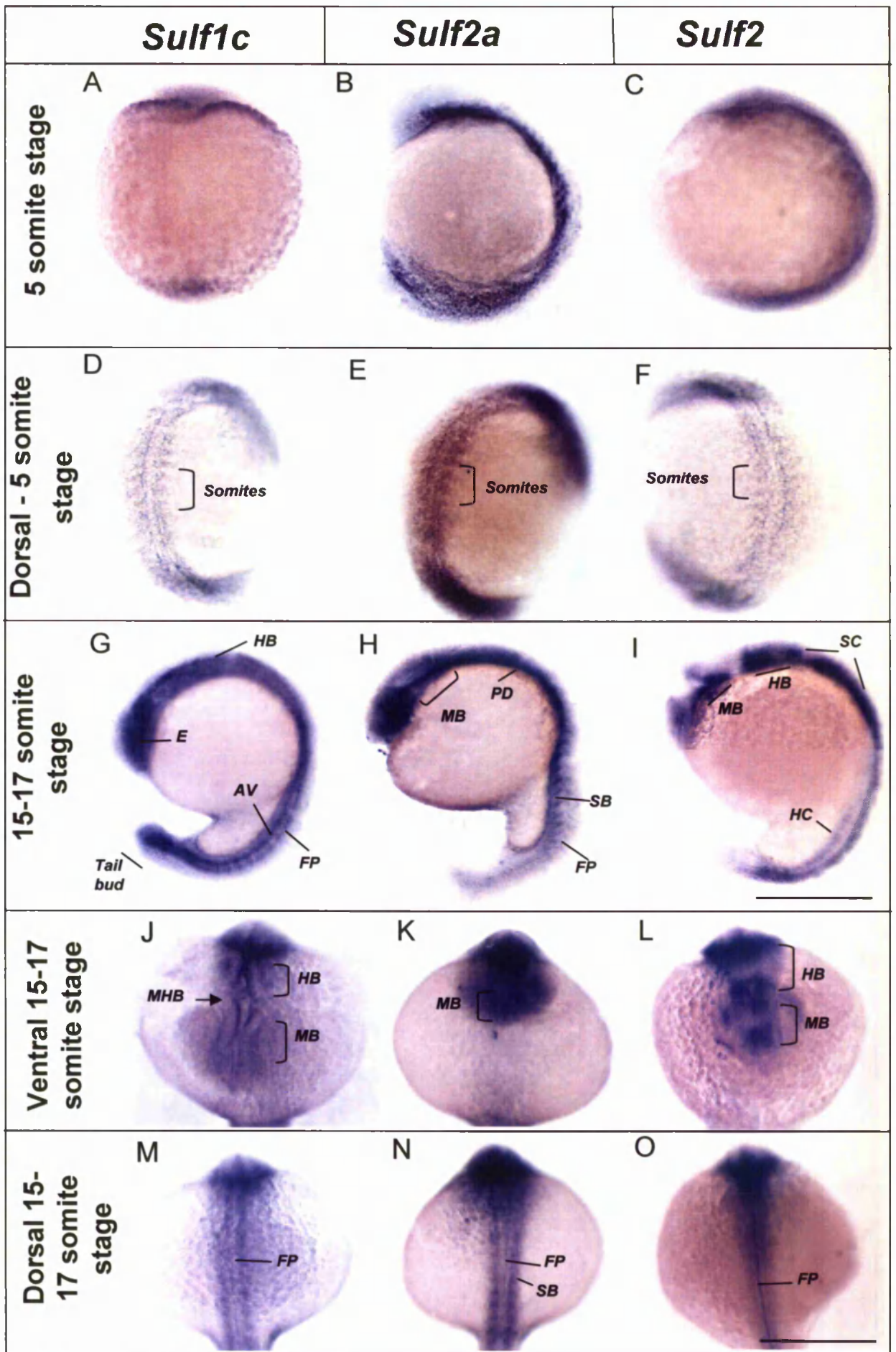


**Figure 4.0: Expression of Heparan sulphate (HS) sulfatase genes during early zebrafish development.** Expression of *sulf1c* at 5 somite stage, lateral view (A) and dorsal view (D) and 15-17 somite stage, lateral view (G) and ventral (J) dorsal view (M). Expression of *sulf2a* at 5 somite stage, lateral view (B) and dorsal view (E) and 15-17 somite stage, lateral view (H) and ventral (K) dorsal view (N), Expression of *sulf2* at 5 somite stage, lateral view (C) and dorsal view (F) and 15-17 somite stage, lateral view (I) and ventral (L) dorsal view (O). AV, axial vessels; E, eye; FP, floorplate; HB, hindbrain; HC, hypochord; MB, midbrain; PD, pronephric ducts; SB, somite boundaries. SC, spinal cord. Scale bar is 200 $\mu$ m.

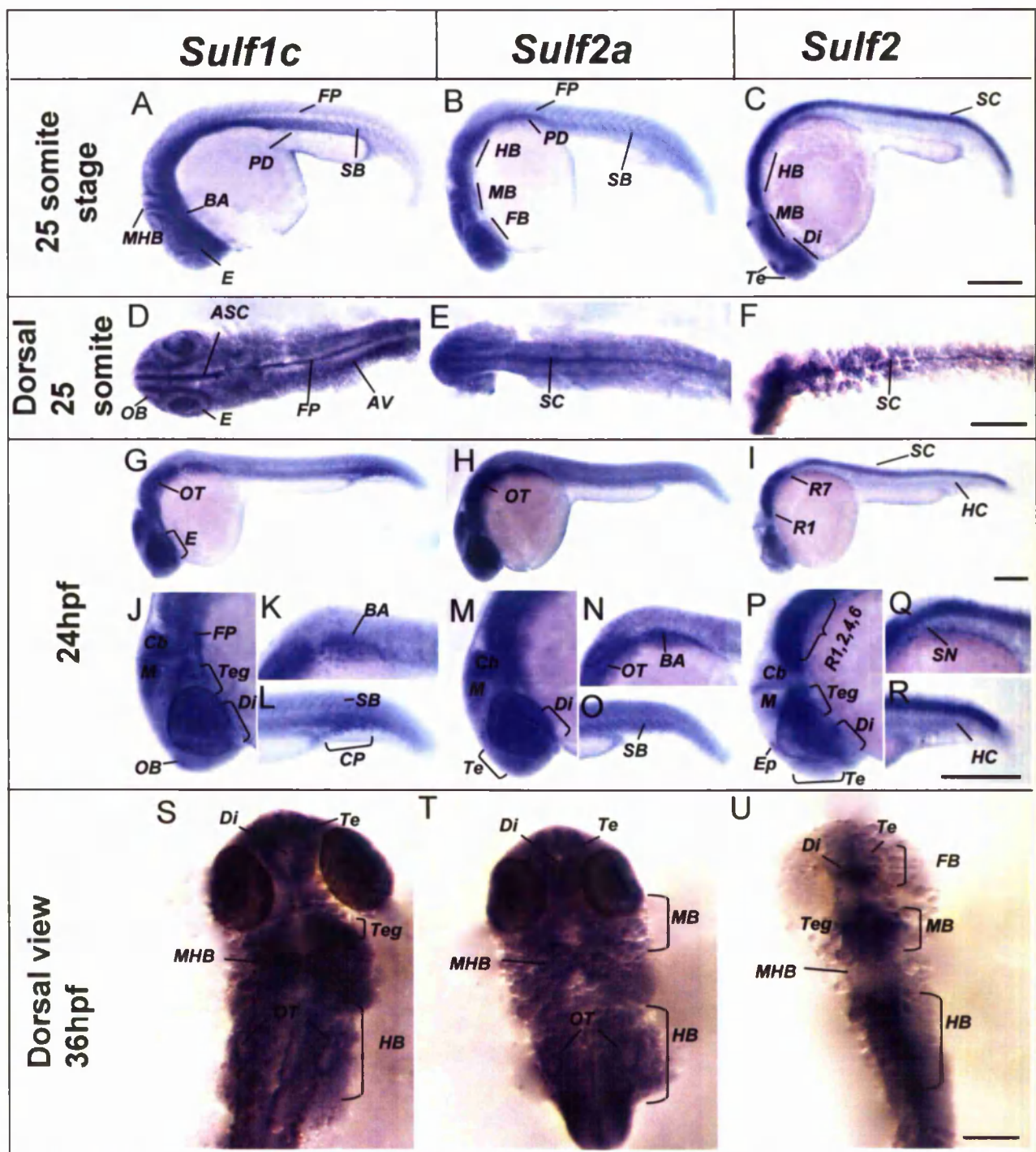


**Figure 5.0: Expression of sulfatases during segmentation and pharyngula period.** Expression of *sulf1c* at 25 somite stage, lateral and (A) dorsal view (D), lateral view at 24hpf (G), close up of head, anterior trunk, and tail (J,K,L) and 36hpf dorsal view (S). Expression of *sulf2a* at 25 somite stage, lateral and (B) dorsal view (E), lateral view at 24hpf (H) close up of head, anterior trunk, and tail (M,N,O) and 36hpf dorsal view (T). Expression of *sulf2* at 25 somite stage, lateral and (C) dorsal view (F), lateral view at 24hpf (I) close up of head, anterior trunk, and tail (P,Q,R) and 36hpf dorsal view (U). ASC, anterior spinal cord; AV, axial vessels; BA, branchial arches; Cb, cerebellum; CP; caudal plexus; Di, diencephalon; E, eye; Ep, epiphysis; FB, forebrain; FP, floorplate; HB, hindbrain; HC, hypochord; M, mesencephalon; MHB, mid-hindbrain; OB, olfactory bulb; OT, otic vesicle; PD, pronephric ducts; R, rhombomeres; SB, somite boundaries; SN; spinal cord neurons; Te, telencephalon; Teg, tegmentum. Scale bar 200 $\mu$ m.

	Sulf1c				Sulf2a				Sulf2			
	5/17 som	24hpf	48hpf	60hpf	5/17 som	24hpf	48hpf	60hpf	5/17 som	24hpf	48hpf	60hpf
Olfactory system	-/±	+	+	+	-/-	-	-	-	-/-	-	-	-
Eye												
Eye lens	NA/±	++	++	++	NA/±	±	+	-	NA/-	-	±	±
Optic vein	NA	NA	±	+	NA	-	+	+	NA	-	±	±
Otic vesicle	NA	+	++	++	NA	+	++	++	NA	-	±	±
Forebrain												
Telencephalon	NA	++	±	+	NA	++	±	±	NA	+	+	+
Diencephalon	NA	+	+	++	NA	++	+	+	NA	++	+	++
Midbrain												
Tegmentum	-/-	++	-	++	-/+	++	±	-	NA	++	++	±
Hindbrain												
Cerebellum	NA	++	+	±	NA	++	+	±	NA	++	±	±
Hindbrain floorplate	±/++	++	±	±	NA	++	++	++	NA	++	++	++
Choroid plexus	NA	NA	+	++	NA	NA	++	++	NA	NA	++	++
Broad expression	+/+	++	+	+	+/+	++	+	+	+/+	++	+	+
Spinal cord												
Floor plate	+/+	++	+	+	+/+	+	+	+	+/+	+	+	±
Roof plate	-/-	-	-	-	-/-	-	-	-	+/+	+	+	+
Broad expression	+/+	-	-	-	+/+	-	-	-	+/+	+	-	-
Cranial vasculature												
PHBC	NA	-	++	+	NA	-	+	±	NA	-	+	±
PMBC	NA	-	+	+	NA	-	±	±	NA	-	±	±
MCeV	NA	++	+	+	NA	++	±	±	NA	++	±	±
Others	NA	-	+	+	NA	-	±	±	NA	-	±	-
Trunk vasculature												
Intersegmental vessels	NA	-	-	-	NA	-	-	-	NA	-	-	-
Axial vessels	-/++	+	+	+	-/-	±	±	-	NA/-	-	-	+
Notochord	-/-	-	-	-	-/-	-	-	-	-/-	±	-	-
Hypochord	-/-	±	-	-	-/-	±	-	-	-/-	±	-	-
Somites	±/±	±	-	-	±/±	±	-	-	±	±	-	-
Heart	NA	+	++	+	NA	±	+	++	NA	++	±	-
Pronephric ducts	-/++	++	+	++	-/±	++	±	-	-/-	±	±	+
Branchial arches	NA	++	±	±	NA	++	±	-	NA	+	-	-
Pectoral finbud	NA	NA	+	++	NA	NA	-	-	NA	NA	±	++
Tail bud	+/++	++	-	-	+/±	+	-	-	+/±	±	-	-

**Table 1: Summary of zebrafish sulfatase developmental expression; 5 and 17 somite stage, 24, 48 and 60hpf, hours post fertilisation; -, no expression; ± weak expression; + moderate expression; ++ strong expression; NA structure does not exist at this stage.**

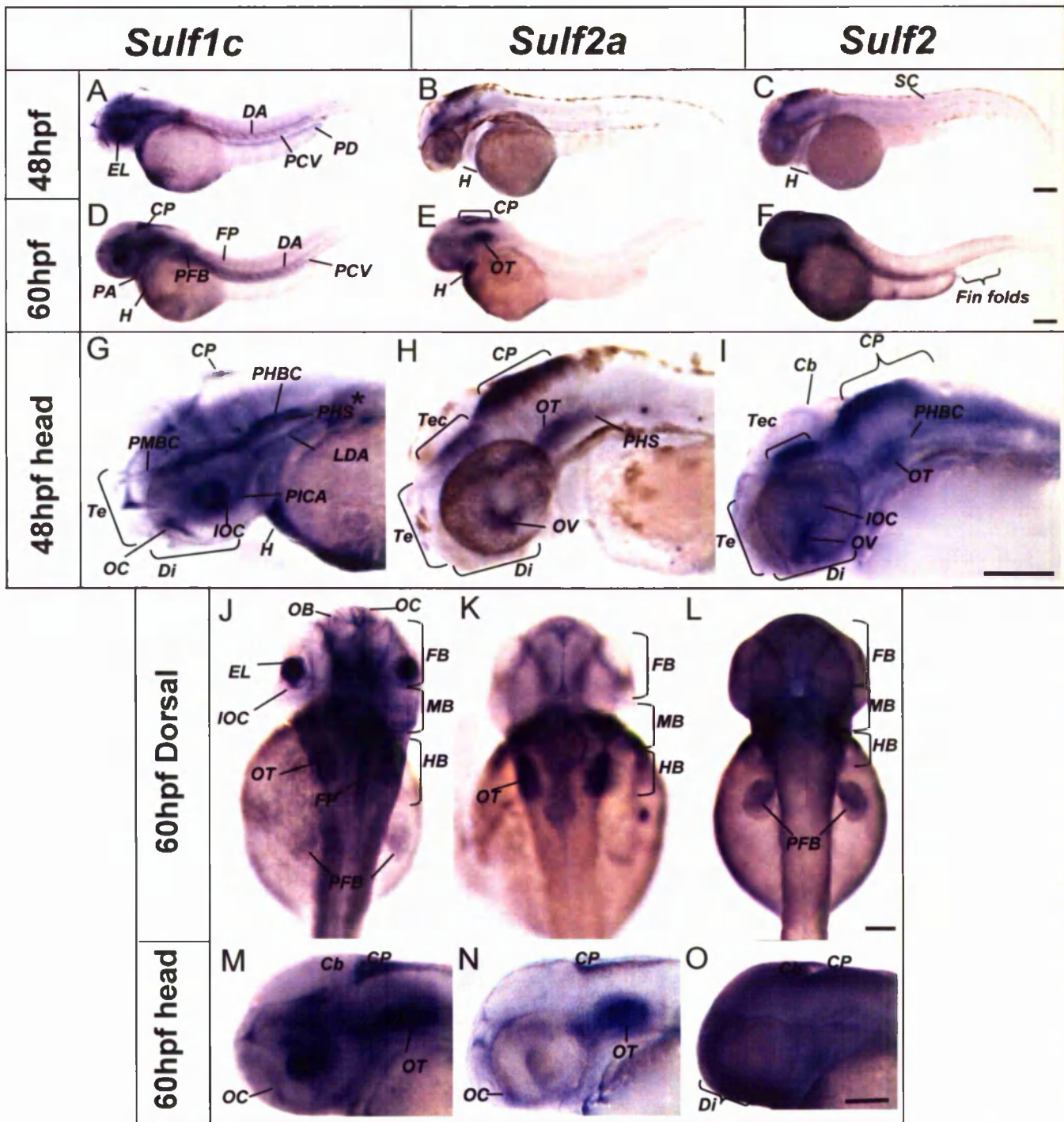


**Figure 6.0: Expression of sulfatases during the long-pec and pec fin stage.** Expression of *sulf1c* at 48hpf whole shot, arrow denotes caudal fin folds (A) and lateral view of head (G), whole shot of embryo at 60hpf (D), lateral head (M) and dorsal view (J). Expression of *sulf2a* at 48hpf whole shot (B) and lateral view of head (H), whole shot of embryo at 60hpf (E), lateral head (N) and dorsal view (K). Expression of *sulf2* at 48hpf whole shot (C) and lateral view of head (I), whole shot of embryo at 60hpf (F), lateral head (O) and dorsal view (L). Cb, cerebellum; CP, choroid plexus; DA, dorsal aorta; Di, diencephalon; E, eye; EL, eye lens; FB, forebrain; FP, floorplate; H, heart; HB, hindbrain; IOC, inner optic circle; LDA, lateral dorsal aorta; MB, midbrain; OB, olfactory bulb; OC, oral cavity; OT, otic vesicle; PA, pharyngeal arch; PCV, posterior cardinal vein; PD, pronephric ducts; PFB, pectoral finbuds; PHBC, primordial hindbrain channel; PHS, primary head sinus; SB, somite boundaries; SC, spinal cord; Te, telencephalon; Teg, tegmentum. Scale bar 200 $\mu$ m

## Supplementary Figures

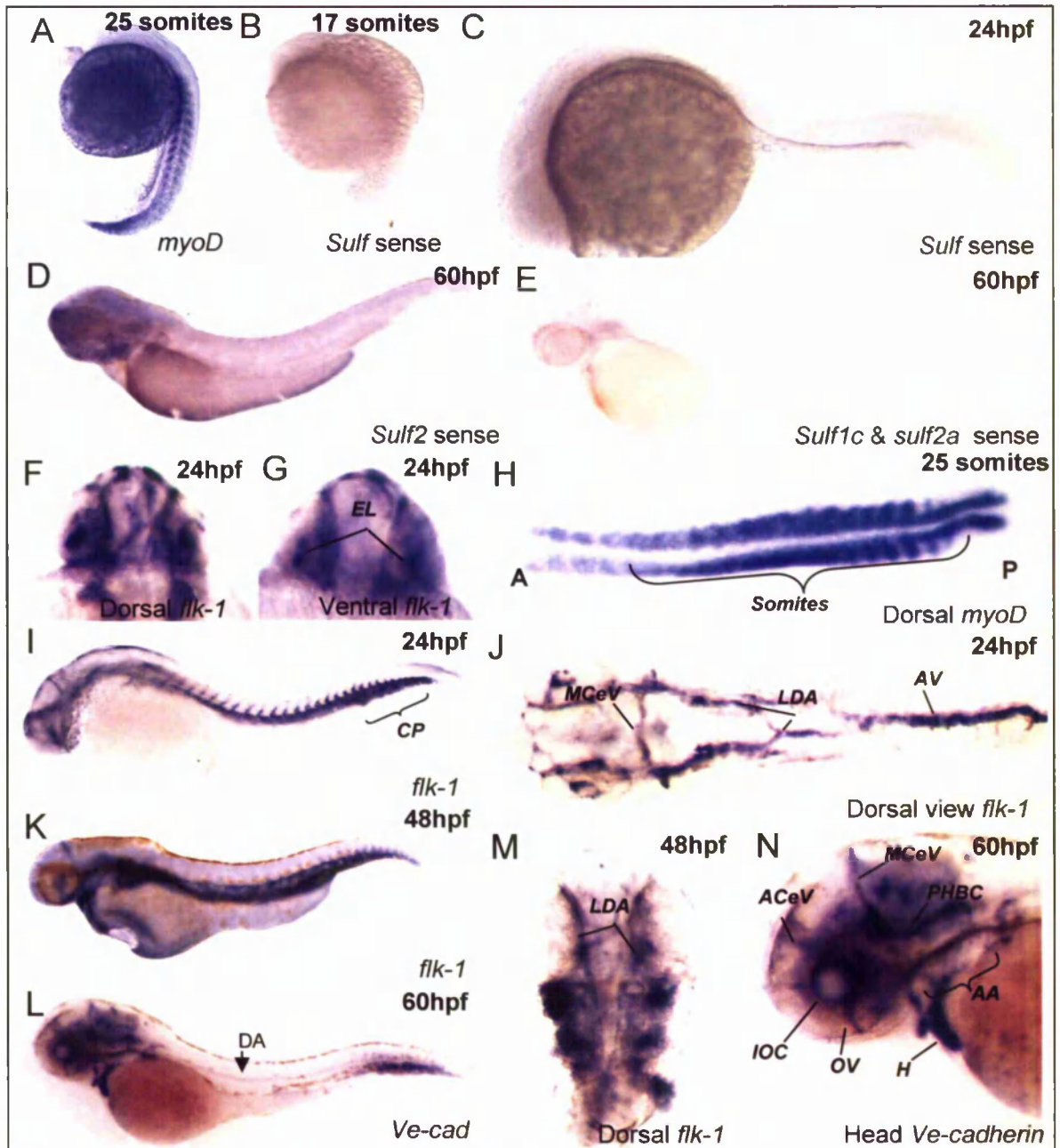


**Figure S1: Expression of sulfatase sense probes and endothelial and muscle markers during zebrafish development.** Representative images of sulf sense probes at 17 somite stage (B), 24hpf (C) and 48hpf (D,E). Markers used as positive control for all WISH experiments, *myoD* expression at 17 somite stage (A) dorsal view of somite staining (H). Expression pan-endothelial marker *flk-1* at 24hpf lateral view of whole embryos (I) and dorsal view of flat mount of (J), dorsal (F) and ventral view (G) of head at 24hpf. Lateral view of *flk-1* expression at 48hpf (K) and dorsal view (M). Lateral view of embryo expressing *ve-cad* at 60hpf (L) and close up of the head of embryo (N). AA, aortic arches; ACeV, anterior cerebral vein; AV, axial vessels; CP; caudal plexus; E, eye; EL, eye lens; H, heart; IOC, inner optic circle; LDA, lateral dorsal aortae; MCEV middle cerebral vein; OV, optic vein; PHBC, primordial hindbrain channel; PICA, primitive internal cartoid artery; PrA, prosencephalic artery.

# Chapter 4.0 Morpholino Knockdown of *Sulf1c* in zebrafish

## 4.1 Introduction

The aim of this research is to investigate the role of HS modification enzymes known as the 6-O endosulfatases during zebrafish vascular development. The results from chapter three indicate that *zfsulf1c* is a homolog of the human, mice and quail *sulf1* showing a strong degree of conservation in the enzymatic domain bearing the catalytic site, and in its spatial expression pattern. *Zfsulf1c* is strongly expressed in the developing central nervous system, pronephric ducts, somite boundaries and in the cranial and trunk vasculature.

Studies reviewed on *sulf1* function in chapter one highlight the compelling role of sulfatases in modulating many cell signalling molecules such as Bmp-4, Hh, FGF, Wnt and VEGF, all of which are critical to the development of a functioning vasculature network<sup>2,27,33,381,382</sup>. Several loss and gain experiments have demonstrated *sulf1* as a positive or negative regulator of angiogenesis. For example overexpression of human or quail *sulf1*, acts as a potent inhibitor of FGF2 mediated angiogenesis by a marked reduction in vessel density in the CAM assay and in xenografts derived from breast carcinoma lines<sup>351,367,368</sup>, whilst a loss of HSULF-1 increases FGF2 and VEGF<sub>165</sub> mediated proliferation of endothelial cells<sup>368</sup>. In both cases *sulf1* is thought to affect growth factor-HS-receptor complex formation implicating a role of *sulf1* in mediating cellular behaviour of endothelial cells of more than one signalling pathway.

Conversely a change in HS 6-O sulphation induced by the loss of sulfotransferases further strengthens the importance of achieving a fine level of 6-O sulphation during vascular development. Mice deficient in the HS6ST1 enzyme are embryonic lethal with surviving embryos displaying reduced vascular branching in the placenta region and this was found to coincide with low levels of *VEGF* expression<sup>383</sup>. Likewise partial loss of HS6ST in zebrafish results in defects in vessel branching in the tail of HS6ST morphants and the penetrance of this defect increases synergistically with lowered levels of *VEGF* expression<sup>329</sup> implying diverse functional roles of 6-O sulphated HS in mediating *VEGF* directly and indirectly. It is

evident that altering the equilibrium of 6-O sulphation both *in vitro* and *in vivo* can have important consequences on the vasculature.

Despite the significant affects of perturbing the 6-O sulphation levels through *sulf1* regulation no vasculature abnormalities have yet been reported in *sulf1*<sup>-/-</sup> mice<sup>349</sup>. Interestingly though an increased number of *sulf1*<sup>-/-</sup> embryos do not survive in the first few months, therefore it is possible that the increased neonatal lethality phenotype observed may result from vascular complications in the placenta similar to phenotype of the HS6ST1 knockout mice.

One of the aims of this research is to determine if zebrafish *sulf1c* can affect the structural modifications of HS *in vivo* i.e. capable of modifying the 6-O sulfation pattern of HS thus showing conservation of enzyme function. HS disaccharide composition will be analysed in *sulf1c* morphants by SAX-HPLC. Secondly, to determine if *sulf1c* has a functional role in vasculature development. To test this morpholinos targeting the *sulf1c* gene were designed and injected into a zebrafish vasculature transgenic line. As described previously the zebrafish serves as an invaluable model to study vasculature development. In particular the generation of *tg(fli1:GFP)* and *tg(gata:dsRed)*<sup>75,378</sup> expressing green fluorescent protein (GFP) and red protein in endothelial and erythroid cells respectively, make this an ideal system to delineate the formation of a functioning vasculature. Tracking GFP positive endothelial cells by high resolution confocal imaging during early development has revealed anatomically the vasculature plan proceeds in a similar manner analogous to that of mammals allowing comparisons to be made across species<sup>85</sup> (see section 1.3). To date no undesirable effects have been noted in this transgenic line and it is now used as a common tool in which to study developmental vasculogenesis and angiogenesis.

One of the routine technologies to study gene function in zebrafish embryonic development and indeed in other organisms has come from the use of antisense morpholinos. Morpholino (MO) antisense technology is used to modify gene expression by 'knockdown' of the gene of interest. This technique potentially allows a quick insight into their role in early development without a genetic loss of function mutation<sup>384</sup>. Morpholinos are chemically modified oligonucleotides synthesised 25 nucleotides in length, similar to DNA and RNA oligonucleotides apart from the ribose ring is replaced with morpholine ring and consists of neutral phosphordiamidate backbone. This altered structure confers advantages over conventional oligonucleotides<sup>385,386</sup>. MO's undergo Watson-Crick base pairing but do not activate RnaseH when bound to RNA and are resistant to many degradative enzymes conferring high stability. To date MO are not known to be subject to any endogenous

enzymatic degradation<sup>96</sup>. In addition their neutral charge minimises interactions with other components of the cell likely to reduce their overall non specificity/toxicity. Unlike nucleic acids MO's do not generate an interferon mediated inflammatory response and bind specifically to complementary nucleotide sequences with high affinity<sup>387</sup>. These short oligonucleotides can be designed to block translation by binding to the start of the initiation codon<sup>388</sup> thereby blocking translation of mRNA into protein or to block splicing by binding across an exon-intron boundary, causing a removal of exon to generate an out of frame mature RNA<sup>389</sup>, thus both methods can effectively reduce or knockdown gene/protein of interest. One of the advantages of using the splice blocking morpholino is RT-PCR can be used to confirm the effectiveness of the splice blocking morpholino (SBMO), PCR products of the truncated version of mRNA can be detected on electrophoresis gel. Studies by Draper and colleagues were the first to demonstrate the removal of exon from targeting exon-intron splice junction produced a phenotype identical to that of a loss of function mutation<sup>384,389</sup>. The general efficacy of morpholinos has also been shown in screening studies whereby knockdown of particular genes phenocopied with their genetic mutant counterparts<sup>390,391</sup>.

Given the expression profile of *sulf1c* discussed in previous chapter and the known role of sulfatases to modulate many HS binding proteins it was hypothesised that the *sulf1c* can actively affect HS structure similar to mammalian sulfs. It is predicted *sulf1c* can positively or negatively affect vasculature development depending on the sulfation requirements of the co-localised HS binding protein.

In this chapter the optimisation of the different morpholino sequences and doses are tested and the overall morphology of the *sulf1c* phenotypes is discussed. The fluorescent analysis of vasculature and blood circulatory defects of the *sulf1c* morphants are presented in the next chapter.

## **4.2 Materials and methods**

### **4.2.1 Morpholino oligonucleotide**

Region of target sequence within the *sulf1c* gene was sent to Gene Tools and designed by their criteria i.e. with GC content of about 50% and little or no secondary structure. The translational blocking morpholinos were designed to be complementary to 25 nucleotides at the translation initiation site (ATGMO). Splice blocking morpholino was designed complementary to the splice acceptor site of exon4 (SBMO) (Fig. 4.0). The standard negative

translational blocking morpholinos were designed to be complementary to 25 nucleotides at the translation initiation site (ATGMO). Splice blocking morpholino was designed complementary to the splice acceptor site of exon4 (SBMO) (Fig. 4.0). The standard negative control MO for all experiments used was 5 pair base mismatch morpholino resembling *sulf1c*-5'UTR morpholino recommended by Gene Tools.

BLAST ([www.ncbi.nlm.nih.gov/blast/Blast.cgi](http://www.ncbi.nlm.nih.gov/blast/Blast.cgi))<sup>392</sup> was used to check the MO sequence was specific to zebrafish *sulf1c*.

<b>Sulf1c MO</b>	<b>MO Sequence</b>	<b>5'UTR and cDNA sequence Intron3-exon4 sequence</b>
<b>S1c- 5'ATGMO</b>	<b>CACCAGCTGCATCATGGGACTGCCA</b>	gattacctgtgaggattccaaccttctga ttcgcgttcgcagtccc <b>ATGATGC</b> <b>AGCTGGTGAGCCTGGCT</b> TGGATGATG
<b>S1c-SBMO</b>	GTAGTCCTGGTAGTGGTAGAATAAT	catatttattat <b>taccactaccagGACTACTTT</b> ACTGATC
<b>Control Mo 1</b>	<b>CACgAGgTGgATCAtcGGACTcCGA</b>	
<b>Control Mo 2</b>	GTAcTCgTGGTAgTGGTtGAATAAtAT	

\* Note: Lower case in MO sequence signifies mismatch base pairs; Lower case in cDNA sequence signifies 5'UTR sequence and upper case signifies first exon, and Lower case in SBMO target sequence signifies intron 3 and upper case exon 4 sequence

From morpholino stock solution of 10ng/nl, working concentrations of morpholino were made up at 1ng/nl for the lower doses and 3ng/nl to 5ng/nl for the higher doses. Microinjection needles were calibrated to inject similar size volumes and injected at 1 cell stage (Fig. 4.1).

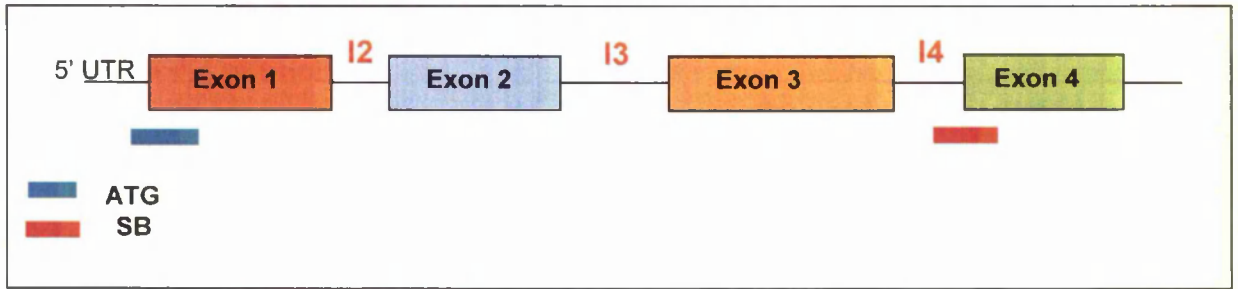


**Figure 4.0:** A schematic representation of the *sulf1c* pre-mRNA showing the targeting sites of three *sulf1c* antisense morpholinos: The approximate position of ATG (turquoise box) and splice blocking (SB) sulf morpholinos is indicated on the pre-mRNA (diagram not to scale). The translational blocking morpholinos were designed as follows; The ATG morpholino is designed 9bp in the 5'UTR and runs 14bp downstream of ATG site. SB morpholino target 19bp of intron3 with remaining 6bp targeting within exon4.



**Figure 4.1:** Picture showing the approximate microinjection target area in yolk of zebrafish embryo at 1 cell stage. Embryos were injected between 1 cell and four cell stage for morpholino injections, plasmids were injected at 1 cell stage. The site of injection is depicted by the red line. Scale bar 250µm, adapted from Kimmel *et al* 1995.

#### 4.2.2 PCR amplification of morpholino target sites

Genomic DNA was extracted from two day old embryos from *tg(fli1:GFP;gata-1:dsRed)*, *tg(flk:GFP;gata:dsRed)*, *p53<sup>-/-</sup>* zebrafish strains. PCR primers were designed outside of the region targeting the morpholino site. Products of the expected size were gel extracted and sent to UMSF to be sequenced. Primers to identify *sulf1c* translational and splice blocking morpholino sites were as follows;

S1c-5'ATG: *Fwd*:5'TGTCTTCCAGGAGCAGTGTG3'

*Rev*: 5'GAGCTTGCCATGAAGGTGAC-3'.

S1c-SB: *Fwd*:5'CCAGGTAAAGTGTAGCTATGGCAAA-3';

*Rev*: 5'GGACGTCCGCAAATAGTTGA-3.

#### 4.2.3 Preparation and HS Disaccharide analysis of *sulf1c* morphants

In order to test the specificity of the *sulf1c*-ATG morpholino, HS disaccharide composition of the injected embryos was analysed by strong anion exchange chromatography (SAX-HPLC). This technique allows separation of disaccharides based on overall charge density, and the resulting disaccharides are labelled by post-column fluorescent derivatisation, allowing a quantitative profile of the different sulphated disaccharide components.

Embryos were injected with S1c-ATGMO and development followed until 2dpf. *Sulf1c* morphant embryos were segregated for HS extraction. The number of embryos used per extraction often varied depending on the survival rate of the injected embryos. Total glycosaminoglycans (GAG) were isolated and HS purified by methods previously described (section 2.10). Partially purified HS was digested overnight with a mixture of digestion enzymes of equal quantities, HepI, II, and III (0.33 mIU).

Each of the heparinases has a distinct cleavage site within the HS chain. Heparinase I cleaves selectively within the S domains as is dependent on the 2-O sulphated IdoA residue, recognising GlcNS( $\pm$ 6S)-IdoA(2S)<sup>393</sup>. As IdoA (2S) units are fairly low in abundance in HS the amount of cleavage sites per chain are limited.

Complete degradation of the enzymes require a further combination of HepII and HepIII. HepII also known as heparitinase II has very broad specificity cleaving glycosidic linkages of the GlcNR( $\pm$ 6S)-GlcA/IdoA( $\pm$ 2S) (where R represents either GlcNac or GlcNS) and can therefore reduce heparin down almost entirely to disaccharides<sup>394</sup>. HepIII also known as heparitinase selectively cleaves linkages of the type GlcNac/GlcNS( $\pm$ 6S)-GlcA/IdoA but will

not cleave glycosidic bonds of to 2-O sulphated IdoA. As HepIII cleave mainly within the transition domains and non-sulphated domains the combination of these three heparinases completely depolymerise HS chains to disaccharides (Fig. 4.2).

The resulting disaccharides were separated on strong anion exchange column and labelled by post column fluorescent derivatisation. Specific HS disaccharide peaks from wildtype, CMO and ATGMO injected samples were identified by comparison to elution times of known standard HS peaks (unsaturated disaccharides). The area was measured under each peak by drawing a baseline across the width of all the peaks. Each area was then divided by the area of equivalent standard HS peak and multiplied by the number of nmoles of known concentration (0.016nmol) to give the number of total nmoles of each disaccharide. Then the amount of this disaccharide as a % of total HS was calculated.

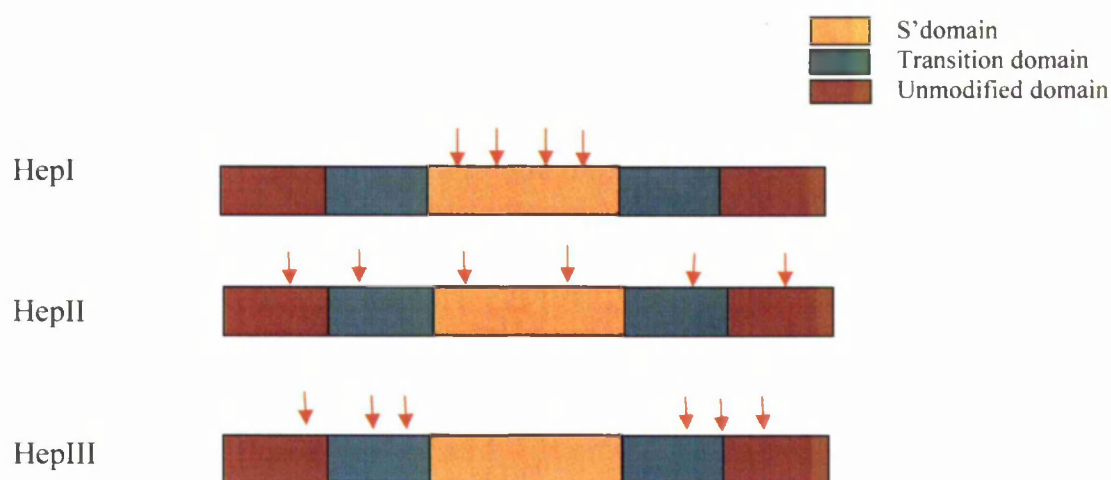


**Figure 4.2: A schematic representation of cleavage sites of three heparan sulphate degrading enzymes.** HEPI specifically cleaves linkages of the type GlcNS( $\pm$ 6S)-IdoA(2S) therefore activity is restricted within the s domains. HepII has broader specificity cleaving linkages of the type GlcNR( $\pm$ 6S)-GlcA/IdoA( $\pm$ 2S) (where R represents either GlcNac or GlcNS) and therefore acts on the whole chain length. HepIII specifically cleaves at GlcNac/GlcNS( $\pm$ 6S)-GlcA/IdoA restricting its activity with the transition and non-sulphated domains.

#### 4.2.4 Analysing the affect of S1c-SBMO on *sulf1c* transcript

To confirm if the S1c-SBMO was having an affect on the *sulf1c* transcript RT-PCR was performed on cDNA of *sulf1c* morphants at both 1dpf and 2dpf. Embryos were injected with the S1c-SBMO at different doses and RNA extracted at the appropriate time point. One

microgram of RNA was synthesised into cDNA and 1µl of this used in the PCR reaction. Negative control was carried out by substituting cDNA with Dnase free water. Forward and reverse primers were designed in exon2 and exon5 respectively to allow amplification of wildtype *sulf1c* transcript (713bp). This primer design also allowed for amplification of an aberrant *sulf1c* transcript excluding exon4 (523bp). To control for possible 5kb intron3 inclusion in the final transcript primers were designed either end of intron3 boundaries; in the 3' region of exon3 and 5' region of Intron3 to amplify a product of 800bp and Intron3-exon4 to amplify 546bp product. Primers were also designed for to amplify  $\beta$ -actin gene (298bp) from all samples. This was used as a positive control to ensure all cDNA samples were of the same approximate concentration and quality. RT-PCR reactions to analyse  *$\beta$ -actin* underwent 25 cycles to ensure the reactions were not saturated. The SBMO RT-PCR reactions underwent 34 cycles and the products were run on 1.2% agarose gel and bands excised from the gel to be sequenced. Primers used for the RT-PCR were also used to sequence the purified amplicons. Primer sequences and annealing temperatures used for RT-PCR were as follows;

Gene amplified	Annealing temperature used for PCR	Primer sequences
S1c Exon2- Exon5	53°C	Fwd: 5'ATGAACAAAACCCGCAAGAT-3' Rev: 5'CAGAGTCGTCCACAGACATGA-3'
S1c Exon3- Intron3	55°C	Fwd: 5'TCTGTGCGAACGGGAATAAG-3' Rev: 5'AGAGGGGCGTGGTTAAGAAT-3'
S1c Intron3- Exon4	52°C	Fwd: 5'CCAGGTAAAGTGTAGCTATGGCAAA-3' Rev: 5'GGACGTCCGCAAATAGTTGA-3'
$\beta$ -actin	54°C	Fwd: 5'CCTCCGGTCGTACCACTGGTAT-3 Rev: 5'CAACGGAAGGTCTCATTGCCGATCGTG-3'

## 4.3 Results

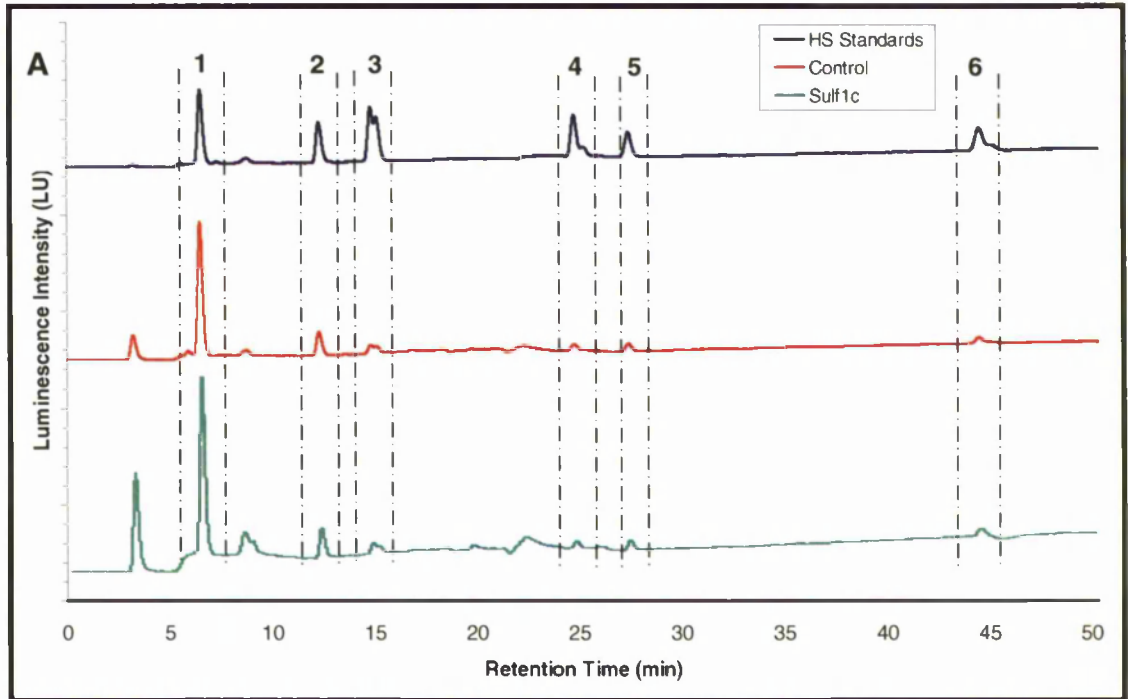
### 4.3.1 Analysis of HS disaccharide content

To determine the efficacy of the S1c-ATGMO the HS disaccharide composition of the *sulflc* morphants was analysed to assess whether *sulflc* could affect the structure of HS *in vivo*. It was hypothesised that if knockdown of *sulflc* was effective changes in the 6-O sulfated disaccharides would be expected. *Tg(Flil:GFP; gata1:dsRed)* embryos were injected with 5ng of S1c-ATGMO and only reproducible and consistent 48hpf *sulflc* phenotypes were selected for GAG extraction (section 2.10). Partially purified HS was digested with HepI, II & III and disaccharide content analysed on HPLC.

HS disaccharide composition was determined by using previous methods described in section 4.2.3. The HS profile of non-injected wildtype embryos was compared to CMO and ATGMO injected samples (Fig. 4.3A). The data presented is the average percentage of disaccharide expression amalgamated from five experiments (Fig. 4.3B). The six most abundant disaccharides (labelled 1-6) including the three 6-O sulfated disaccharides  $\Delta$ UA-GlcNAc6S,  $\Delta$ UA-GlcNS6S, and  $\Delta$ UA2S-GlcNS6S were present in wildtype, CMO and S1c-ATGMO injected samples. In the HS profile of S1c-ATGMO morphants there appeared to be a small decrease in the monosulfated 6-O sulfated disaccharide peaks  $\Delta$ UA-GlcNAc6S (8%) compared to wildtype. An increase was observed in the di-sulfated  $\Delta$ UA-GlcNS6S and tri-sulfated  $\Delta$ UA2S-GlcNS6S disaccharide compared to CMO and non-injected samples, though a statistically significant moderate increase (~26%) was observed in the latter peak with a concomitant significant decrease in the  $\Delta$ UA2S-GlcNS peak. The S1c-ATGMO injected samples were repeated from five separate samples with similar outcomes. On analysis of the overall change in levels of specific sulphation in the *sulflc* morphants compared to wildtype (Fig 4.4C) there appeared to an increase in the total 6S (20%) and NS (0.9%) groups with a decrease in the 2S groups (4%). From these results it was concluded that S1c-ATGMO can increase 6-O sulphation specifically albeit not completely.

### 4.3.2 Analysis of S1c-ATGMO injected embryos

From the HPLC data it was evident S1c-ATGMO can specifically affect HS disaccharide content *in vivo*. In particular analysis of the *sulflc* morphants revealed a significant increase in 6-O sulphation consistent with the substrate specificity of quail and mice sulfi<sup>344,349,360</sup>.



**B**

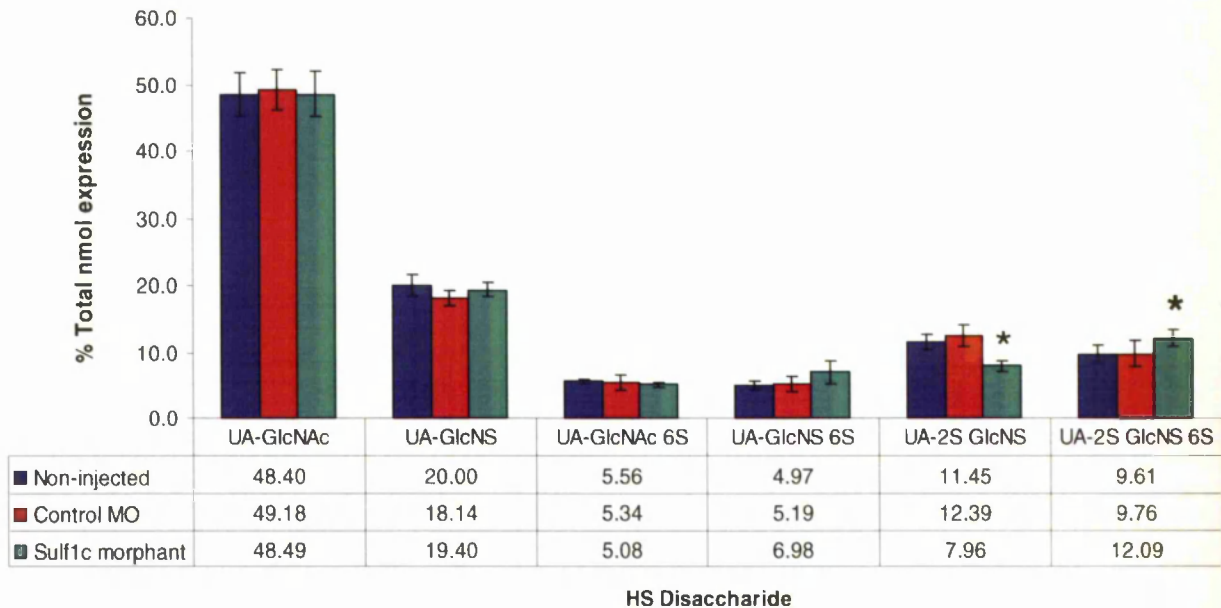
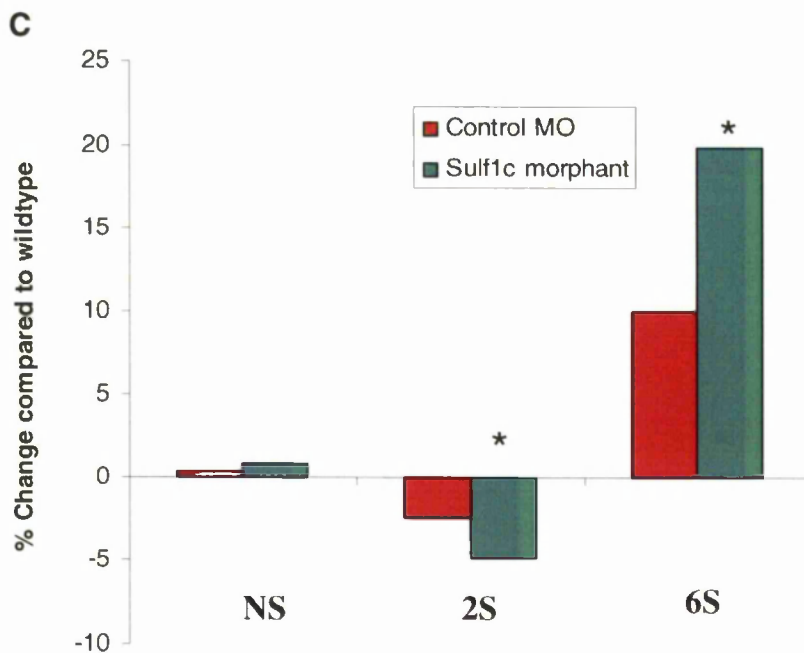


**Figure 4.3: Heparan sulphate profiling of *sulf1c* ATGMO morphant embryos. A:** Representative chromatograms of HS standards (blue), non-injected and CMO injected embryos (red) and 5ng of *sulf1c* morphants (green). Six disaccharides were identified by comparison to the elution times of known HS standard peaks; peak 1:  $\Delta$ 4,5 unsaturated hexuronate-*N*-acetyl glucosamine ( $\Delta$ UA-GlcNAc); peak 2:  $\Delta$ UA-*N*-sulfated glucosamine, ( $\Delta$ UA-GlcNS); peak 3:  $\Delta$ UA-6-*O*-sulfated GlcNAc( $\Delta$ UA-GlcNAc6S); peak 4:  $\Delta$ UA-6-*O*-sulfated GlcNS, ( $\Delta$ UA-GlcNS6S); peak 5:  $\Delta$ UA2-*O*-sulfated GlcNS ( $\Delta$ UA2S-GlcNS); peak 6:  $\Delta$ UA2S-GlcNS6S.

**B:** Graphical depiction of disaccharide analysis of HS extracted from 48hpf non-injected, CMO injected embryos and 5ng of S1c-SBMO injected embryos, represented as a total percent of heparan sulfate. The six most abundant disaccharides are indicated on the x axis. S1c-morphants display a 26% increase in the tri-sulfated disaccharide compared to control. Average calculated from multiple individual experiments (n), non-injected n=5, control injected n=3, (50-60 embryos per sample) S1c-ATGMO injected n=5, (50-55 embryos per sample) **C:** Percentage change in overall HS sulphation composition in *sulf1c* morphants compared to wildtype. A moderate increase (20%) in total 6S sulphate groups of *sulf1c* morphants confirms specificity of the S1c-ATGMO. Asterix(\*) indicates significant changes from wildtype, statistical tests performed using paired t-test  $p < 0.05$ .



To investigate the role of the *sulf1c* (S1c) activity during zebrafish vascular development, injections with S1c-ATGMO were performed in multiple batches of *tg(fli:GFP;gata:dsRed)* embryos. Data was amalgamated and is represented as a chart (Fig. 4.4). Embryos injected with different doses of ATGMO were assessed alongside every control morpholino (CMO) injected and non injected sample. The data for the non-injected controls was combined as these samples were devoid of morphants characteristics. As a CMO, a 5bp missense targeting the ATG start site was designed. All injections were performed with CMO alongside to ensure that injection of a particular concentration of the non-sequence specific morpholino did not give a phenotype that could be mistaken for a morphant phenotype. Preliminary experiments at doses ranging from 0.5ng to 2ng were performed on embryos but as this revealed no morphant phenotype higher doses were used for future experiments for both control and ATGMO. To give an indication of the affects of morpholino on the survival rate embryos were scored for mortality at 24hpf.

Although on average 20% of the non-injected samples died in the first 24hpf, the mortality rate seen in the MO-injected samples was generally higher than their non-injected counterparts. Increasing the MO dose tended to decrease the survival rate in CMO injected embryos but not S1c-ATGMO injected suggesting death was independent of MO concentration injected. All surviving healthy embryos were analysed at 2dpf and scored by their overall morphological defects. The majority of embryos in the CMO injected and non-injected, and a subset of S1c-ATGMO injected, displayed overall body shape similar to that of wildtype embryos at the same stage.

One of the common caveats of using any antisense technology either MO or RNA is that a wide range of phenotypes maybe observed that are off-target affects. It was expected that a percentage of embryos may display a range of phenotypes not specific to gene knockdown of interest. Abnormal phenotypes can result from mistargeting affects of MO<sup>96</sup> or unhealthy embryos can also give rise to abnormal development. Consistent with these ideas a small percentage of phenotypes observed in non- injected and CMO injected embryos also appeared to be occasionally present in the ATGMO injected embryos. These abnormalities were variable and different to the defects exhibited by the S1c-ATGMO injected embryos described below. Although the non-specific abnormalities varied they were often extreme and usually included a combination of small head, eyes, curved body, pericardial oedema, shortened body axis, twisted tail (Fig. 4.5,D,F,E). The penetrance of the non specific mutants increased with increasing dose of CMO and ATGMO. However the occurrence of non-

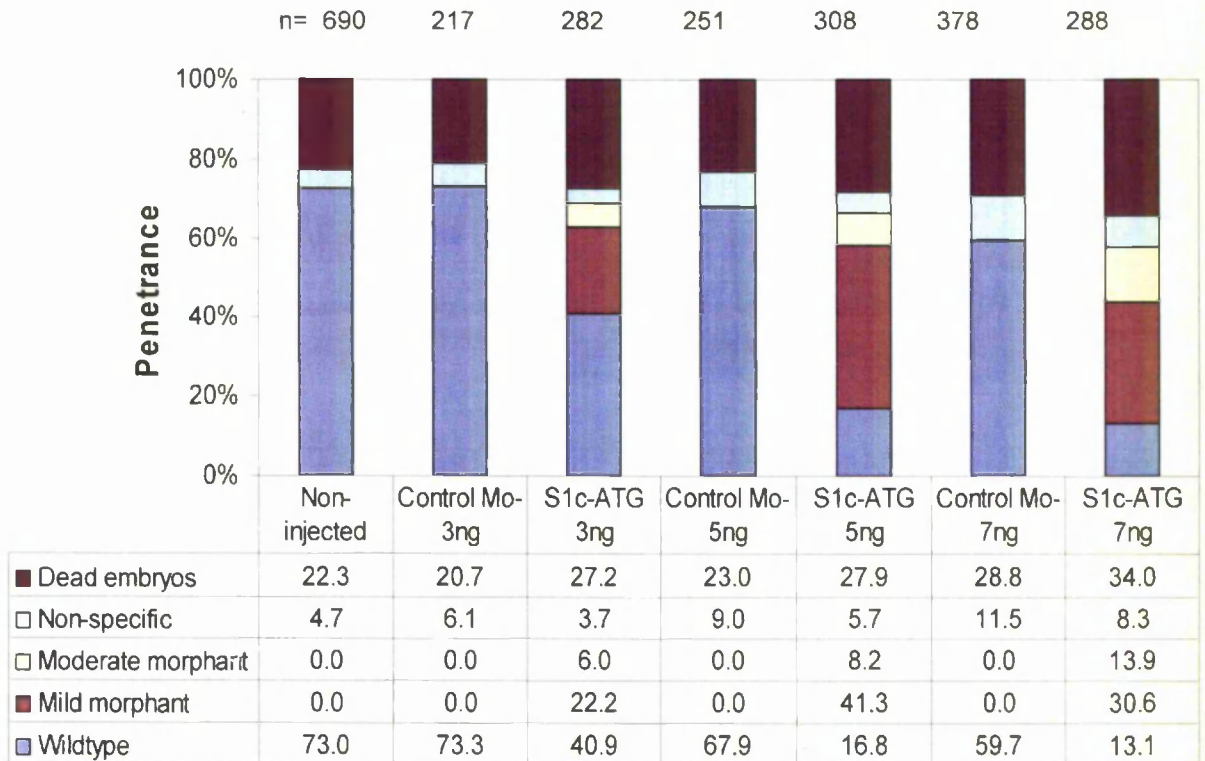


**Figure 4.4: Chart showing the analysis of *flil:gata* embryos injected with different doses of S1c-ATG Morpholino (MO).** Data shown in chart is combined from four experiments and the average penetrance of each category represented as a percentage. The data from non-injected controls was further combined and is represented as one bar in chart. Embryos were analysed at 24hpf for mortality rate (Dead) and scored. Surviving embryos were analysed at 48hpf and categorised into the following categories; wildtype, non-specific, mild and moderate morphant. Mortality was generally lower in ATGMO injected embryos, with the increase in dose range having a minimal effect. All non injected and control MO injected contained a small subset of embryos that were non-specific which were relatively lower in S1c-ATGMO injected embryos. Majority of control injected and non injected embryos showed morphology similar to that of wildtype embryos of the same stage. The percentage of wildtype embryos decreased with increasing dose of S1c-ATGMO. Although an increase in the percentage of *sulflc* morphants was not observed at the highest dose injected, a dose dependent increase was observed at the lower concentrations with 28.2 % and 49.5% penetrance at 3 and 5ng respectively.

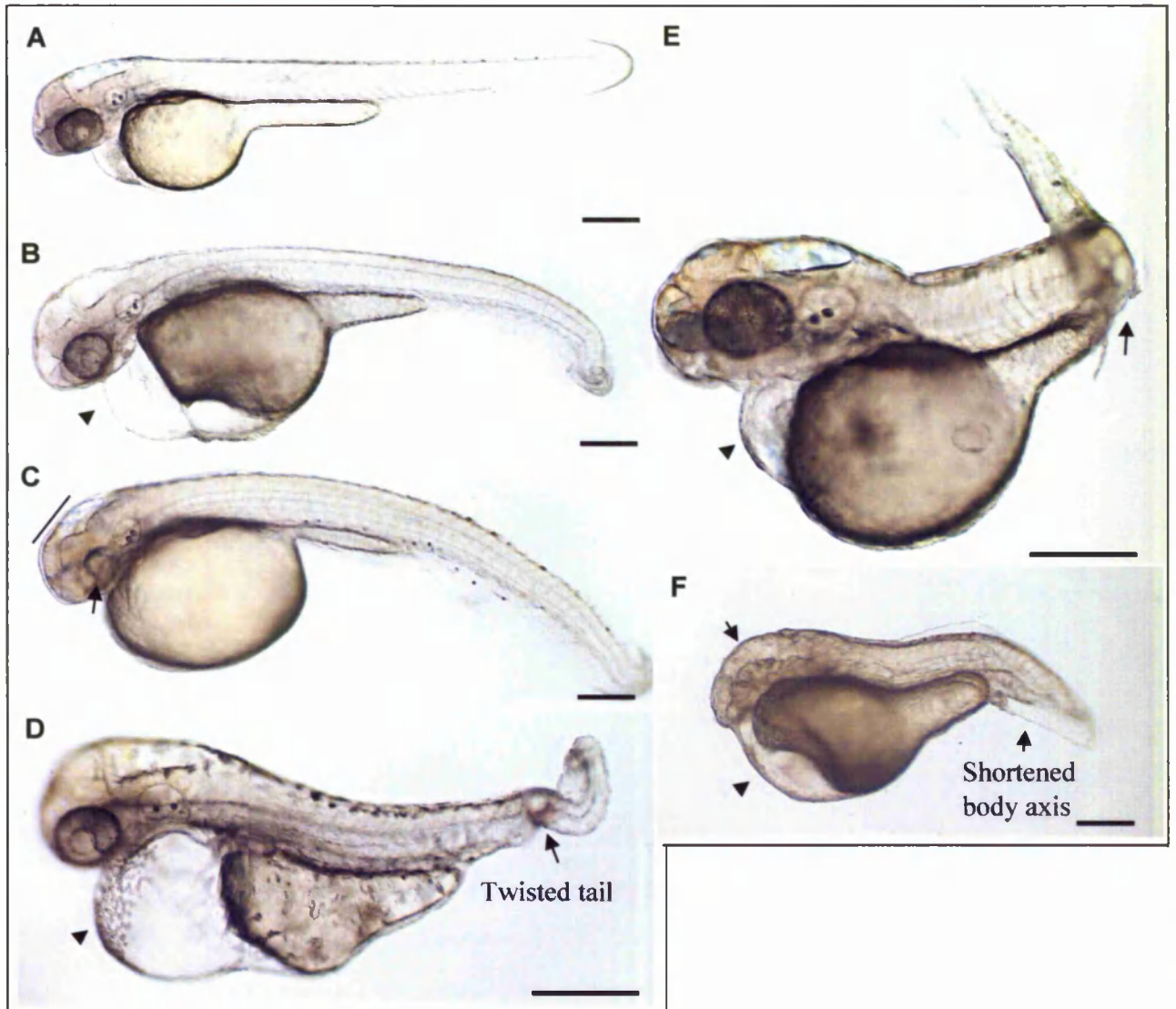


**Figure 4.5: Brightfield Images of 48hpf embryos classed as non-specific phenotypes :** A small percentage of mutated embryos were often observed in samples of non-injected, CMO-injected (A) and Slc-MO injected embryos (B-F). Typical examples of phenotypes are shown at 48hpf, Non-specific mutants often displayed small eyes and head (B,C) indicated by black arrow and blackline, black arrowhead represents pericardial oedema (B), and occasionally combined with deformed twisted or inverted tails (D,E) depicted by the black arrow. Some mutants displayed severely shortened or curved body axis (B,C) with loss of anterior structures (F) represented by black arrow. Morphological defects exhibited by these non-specific mutants were variable and different to those classed as *sulflc* morphants and were therefore excluded from the morphant phenotype analyses. Scale bar is 200µm.

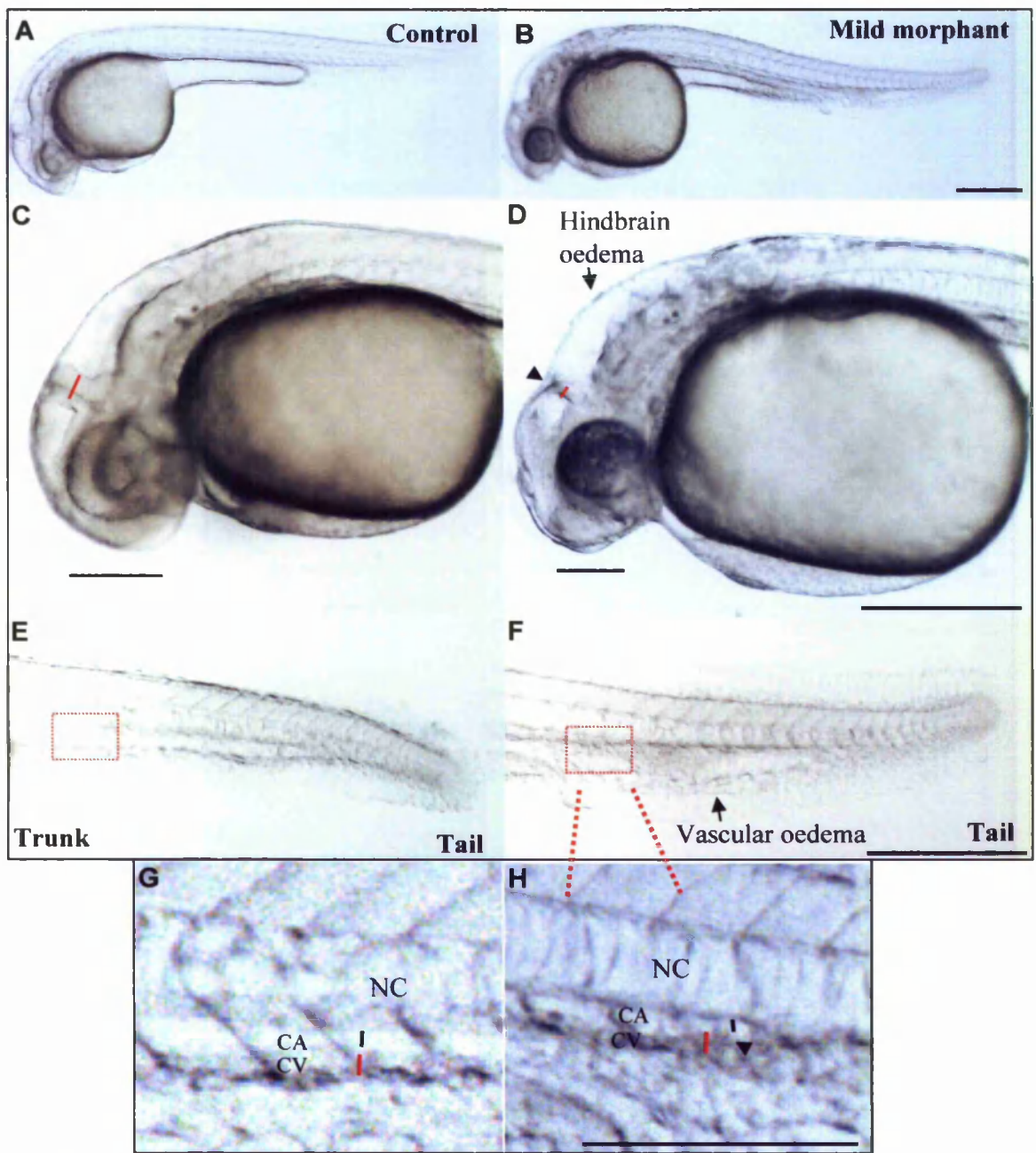


**Figure 4.6: Defects exhibited by the mild class of *sulflc* morphant at 28hpf.** Embryos were injected with CMO and S1c-ATGMO and compared at 28hpf. Brightfield image of control and *sulflc* mild morphant. Whole shot of the control injected embryo (A) and *sulflc* mild morphant (B). Higher magnification of the head of morphant (D) revealed depressed mid-hindbrain boundary and narrowing of the width of the mid-hindbrain boundary (marked by the width of the red line), with oedema in the hindbrain ventricle. Mild morphants also exhibited smaller head and eyes compared to control injected (C). In the mid region of the tail, vascular oedema was present in the tail of the *sulflc* morphants (F) indicated by black arrow. Blood can be observed pooling in a localised region of the tail (indicated by the red arrowhead) compared to continuous blood flow in the control (E). Close up of the tail (highlighted by the red box) revealed strong dysmorphogenesis of the caudal artery (CA) and caudal vein, in the mild morphant (H) compared to control (G). The boundary delineating the CA and CV can not be clearly distinguished with fusion of the two boundaries indicated by the black arrowhead. The lumens of the CA and CV are indicated by the black line and red line respectively, thus evident in these morphants was the narrowing of the CA. CA, caudal artery; CV, caudal vein; NC, notochord. Scale bar is 200 $\mu$ m.

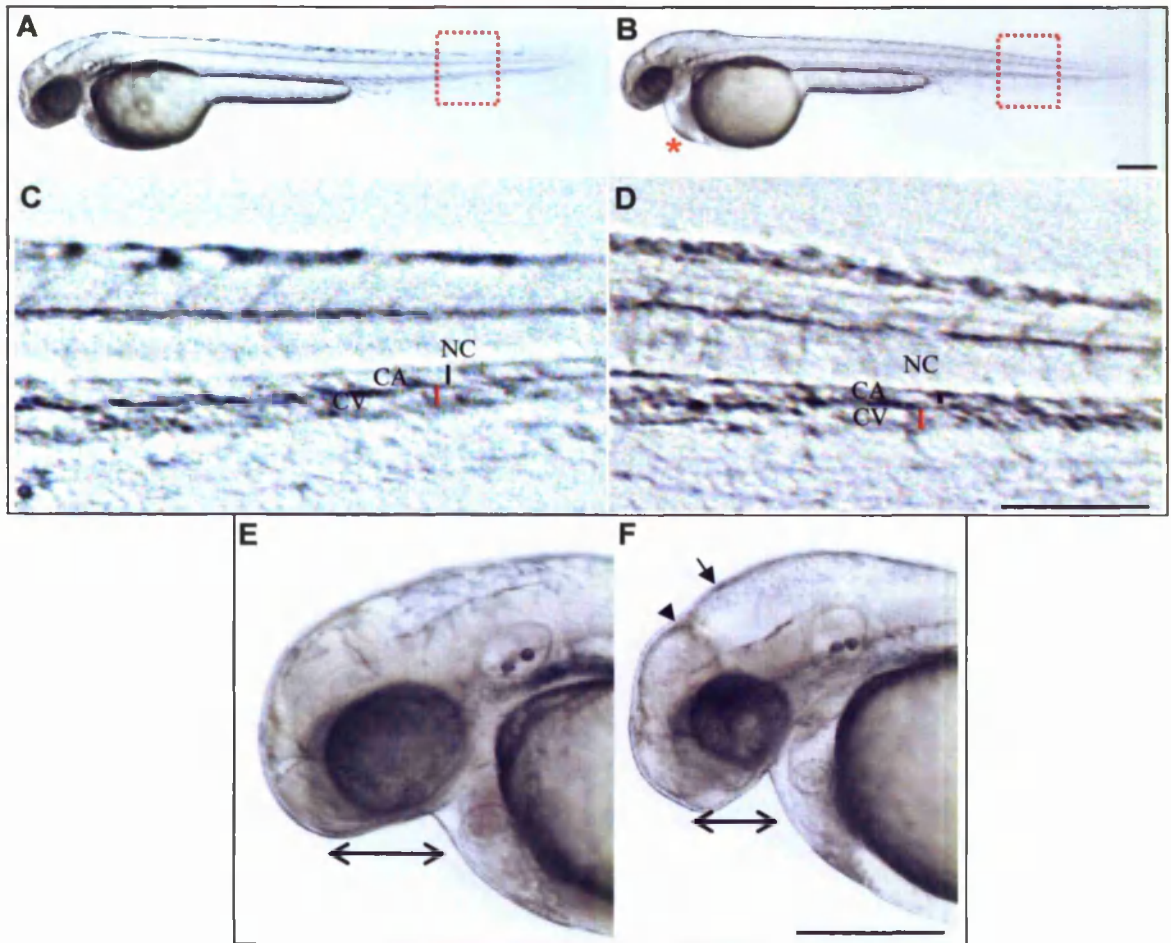


**Figure 4.7: Defects exhibited by mild class *sulflc* morphant at 48hpf.** Embryos were injected with CMO and S1c-ATGMO and compared at 48hpf. Brightfield image of control and *sulflc* mild morphant. Whole shot of the control injected embryo (A) and *sulflc* mild morphant displaying pericardial oedema (B) indicated by red asterisk. Vascular oedema is reduced in the tail of the morphants (B,D) while the abnormal size of the CA is still present, indicated by the reduced size of the lumen (black line) compared to control (C). Higher magnification of the head of 48hpf morphant (F) revealed the depressed mid-hindbrain boundary (black arrowhead) and mild swelling of the hindbrain ventricle (black arrow). The small head and eyes were also prevalent in these morphants shown by the reduced doubleheaded arrow, at this stage. CA, caudal artery; CV, caudal vein; NC, notochord. Scale bar is 200 $\mu$ m.

specific mutants were greater in the CMO injected samples. This is because developmental abnormalities observed in these samples appeared to be sequence specific and were also classed as non-specific (Fig. 4.5B,E).

### 4.3.3 *Sulflc* morphants display vascular related morphological defects

A significant proportion of *sulflc* phenotypes were identified in injected embryos that displayed specific and reproducible affects (referred to as *sulflc* morphants from here in). The morphants were categorised on the basis of their vascular morphology. However detailed vascular and circulatory defects are discussed in the next chapter, only the overall morphology will be discussed here. Mild morphants also referred to as the 'characteristic phenotype' in the following chapter were separated on the basis of vascular defects in the trunk and head. The moderate morphants were separated on the basis of exhibiting similar features of the characteristic phenotype but at a greater severity. Phenotypic traits were initially characterised at 1-2dpf and the morphology of these morphants was followed until 3.5dpf.

Although injection at 3ng of S1c-ATGMO resulted in a small percentage of *sulflc* morphants (mild & moderate) (28.2%), a significant increase was observed in the penetrance of *sulflc* morphants at 5ng (49.5%). Although a dose dependent increase in the moderate phenotype was observed at a higher dose of 7ng an increase in the overall penetrance of *sulflc* morphants was not observed (Fig. 4.4). The overall body shape of the mild class morphants appeared phenotypically normal at 1dpf however mild alterations were observed in the head and tail (Fig. 4.6B,D). Mild morphants displayed generally smaller head and eyes than their wildtype counterpart. In addition to this the morphological features of the head were also altered, thus depression at the mid-hindbrain boundary was evident from the narrowing of the mid-hindbrain boundary (Fig. 4.6D), likely to be a result of apoptosis of brain cells. In contrast to the reduced size of the head, the hindbrain ventricle of the morphants had an inflated and oedemic appearance compared to wildtype. Likewise vascular oedema was observed in the ventral mesoderm proximal to the intermediate cell mass (ICM) (Fig. 4.6F). Despite the mild oedema observed in the head and tail blood circulation initiated in the main axial vessels as normal. However on close inspection of continuation of the main axial vessels in the tail i.e. caudal artery (CA) and caudal vein (CV), the morphants exhibited a narrower CA compared to wildtype siblings and disorganisation of the CA-CV boundaries was also prominent feature in the caudal end of tail (Fig. 4.6H marked by black arrowhead). At 2dpf (48hpf) the mild oedema in the visibly reduced head size and small eyes phenotype was

persistent, however the vascular oedema in the tail was visibly reduced, with blood flow short circuiting at the most posterior site of the vascular oedema. Under brightfield microscopy the absence of circulation in the caudal region of the tail was evident as a result of the interruption in the blood flow further upstream of CA. In wildtype embryos a clear demarcation of the boundary is formed between the two vessels. While the CA-CV boundaries of the morphants appeared defined the CA was narrower than the CV and evident at these sites were aberrant connections between the CA and CV resulting in premature return of the venous blood flow thus resulting in no circulation in the most caudal end of tail (Fig. 4.7B,D). In contrast blood circulation in the head of the morphants was present in all major cerebral vessels such as MCeV, PMBC and the PHBC.

At 3dpf the overall morphology of morphant remained unchanged from 2dpf (data shown in next chapter), although blood circulation in the head and eyes appeared robust, some morphants showed signs of haemorrhage with blood leaking into the extravascular tissue in the mid-hindbrain region. Blood circulation was normal in the anterior region of the trunk, with blood flowing down the major axial vessels, and being returned to the heart through recycling from the ISVs and posterior cardinal vein. Despite the blood short circuiting in the caudal end of the trunk, some blood circulation reached to the end of the tail through re-routing through the ISVs. Pericardial oedema was occasionally present in the mild morphants although the severity of cardiac oedema varied between morphants. At 4dpf the morphology of the morphants was identical to 3dpf, with no sufficient rescue of the observed defects. These morphant larvae were also unable to swim normally.

The overall body shape of the moderate morphants was mildly curved in contrast to the mild characteristic phenotype (Fig. 4.8). Although no obvious defects in the somites or notochord were present the moderate class morphants displayed strong curvature in the tail. Also evident at 1dpf in these morphants was the morphological phenotypes observed with the mild morphant such as smaller head and eyes, depressed mid-hindbrain boundary and hindbrain oedema. In addition the vascular oedema in the tail of the morphants was also prevalent phenotype showing expansion of the ventral mesoderm tissue proximal to the ICM (Fig 4.8B) Despite the delay in the blood circulation initiation, blood appeared to be circulate slowly in all major vessels formed in the head and tail. On 2dpf the head morphology was persistent, but the oedema in the tail appeared to be reduced. However the premature connection between the CA and CV was also evident in these morphants resulting in little or no blood flow to the end of the tail. Despite the morphological alterations in the head the circulation appeared to

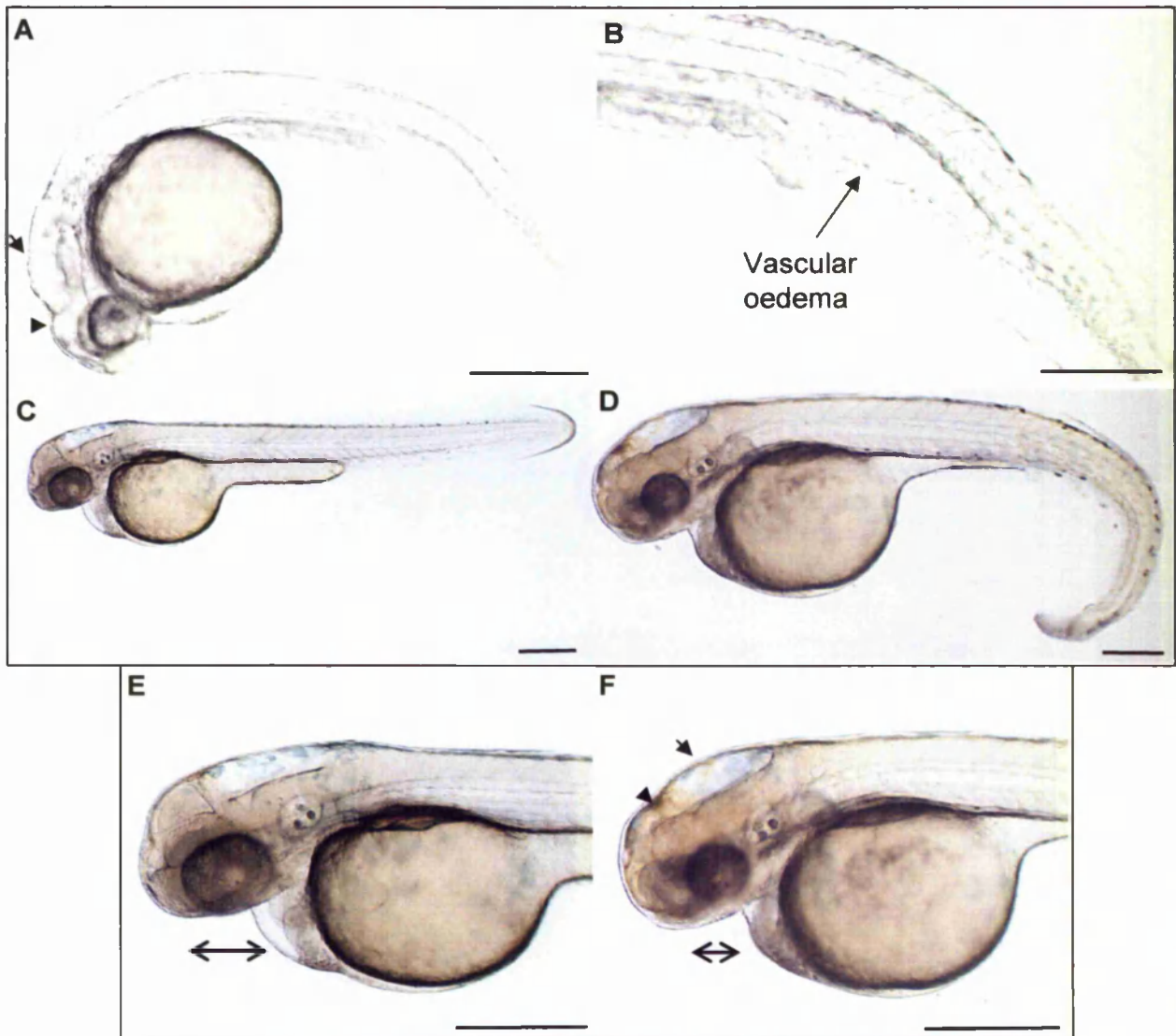


**Figure 4.8: Defects exhibited by the moderate class of the *sulflc* morphant at 1dpf and 2dpf.** Embryos were injected with CMO and S1c-ATGMO and compared at 28hpf and 48hpf. Brightfield image of control and *sulflc* mild morphant. Whole shot of the *sulflc* moderate morphant 28hpf (A), The moderate class of embryos displayed smaller head and eyes with a depressed mid-hindbrain boundary (black arrowhead) and mild swelling of the hindbrain ventricle (black arrow). Evident in this class of morphants was the mild curvature in the tail of the morphants concomitant with vascular oedema in the region of the intermediate cell mass (B). At 48hpf, the curved tail of the morphants (D) was clearly distinguishable from the control injected embryos (C). Also prevalent in these morphants was the morphological alterations observed at 1dpf, with morphants displaying smaller head and eyes (F) compared to control (E) indicated by the size of the black doubleheaded arrow. Depressed hindbrain (black arrowhead) and mild swelling was observed in the hindbrain (black arrow). Scale bar is 200 $\mu$ m.

be normal in the major cerebral vessels such as mesencephalic vein (MCeV) and primordial hindbrain channel (PHBC). At 3dpf overall morphology of morphant remained unchanged from 2dpf, similar to mild morphants little blood flow eventually reached the end of the tail as evident by the pooling of red blood cells in the posterior region of the CA, however this did not result from continuous blood flow from the DA but most likely from functioning ISVs. Also these morphants were unable to swim effectively.

#### 4.3.4 S1c-SBMO affects splicing of *sulflc* transcript

Results from injections with the S1c-ATGMO revealed that the morpholino can specifically modify the 6-O sulphation of and that the phenotype of *sulflc* morphant appears to be specific to *sulflc* morpholino. In order to further test the specificity of the morpholino, it is recommended using a non-overlapping morpholino to confirm phenotype (Gene Tools). It was therefore decided to design another morpholino in order to assess whether the phenotype of *sulflc* morphant could be phenocopied by targeting a different region of the *sulflc* transcript. Splice blocking morpholino (SBMO) are designed to cause abnormal splicing of the pre-mRNA of interest causing either the removal of an exon into the processed mRNA or an inclusion of an intron if the SBMO is targeting the first or last exon-intron boundary.

To determine the efficacy of the S1c-SBMO, primers were designed to detect aberrant splicing of the *sulflc* mRNA induced by the SBMO (Fig. 4.9). Embryos were injected with S1c-SBMO at different doses and RNA extracted from *sulflc* morphants at 24hpf, cDNA was synthesised and RT-PCR performed on these samples.

In all samples, including the non-injected and control MO-injected samples the presumed WT band of approximately 713bp was seen. Although the intensity of the wildtype band appeared severely reduced in the morpholino injected samples, as the dose increased, the expected shorter product of approximately 523bp in size was not detected in these samples (4.10A). While most SBMO acting at the splice acceptor site tend to induce the exclusion of an exon, it has also been noted that blocking at this site can rarely allow the inclusion of an intron followed by the exon (to be deleted)<sup>389</sup>. To address the possibility if the whole or partial 5kb intron insert maybe included in the final *sulflc* transcript, primers were designed at the 5' and 3' end of the Exon-Intron boundary (Fig. 4.9). The first product size would be 800bp thus confirming the 5'end of the intron was inserted. The second set of primers was used to detect the 3' end of the intron3-exon4 boundary producing a product of approximately 546bp. As intronic sequences are known to be highly polymorphic in nature, it

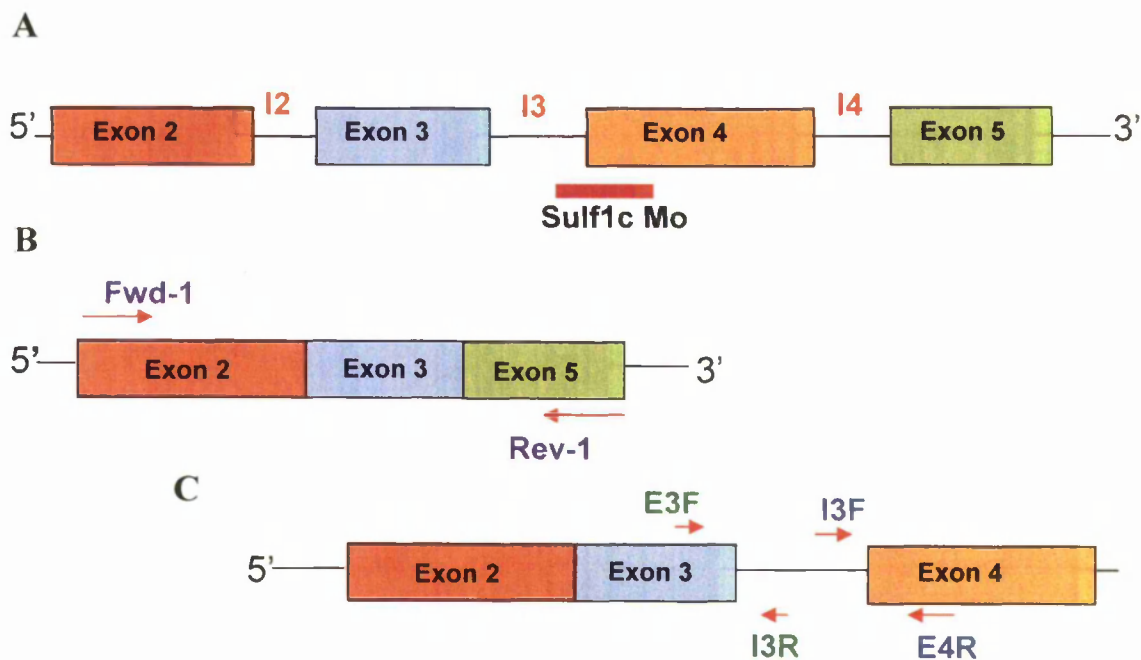


**Figure 4.9:** A schematic representation of the possible outcomes of *sulf1c* mRNA transcript by targeting with S1c-SBMO and the position of the primers used in RT-PCR analysis. **A:** SBMO was designed to bind to a splice acceptor site positioned at the Intron3-exon4 boundary (denoted by the red bar). Two of the predicted outcomes are indicated **B:** One possibility being the exclusion of exon4 from transcript, so the forward and reverse primers were designed to amplify from exon2 to exon5 detecting the removal of exon4. **C:** The second possibility is inclusion of the 5kb intron3. Two sets of primers were designed to detect the exon3-intron3 and intron3-exon4 boundaries. The direction of primers are indicated by the red arrows. Diagram not drawn to scale.

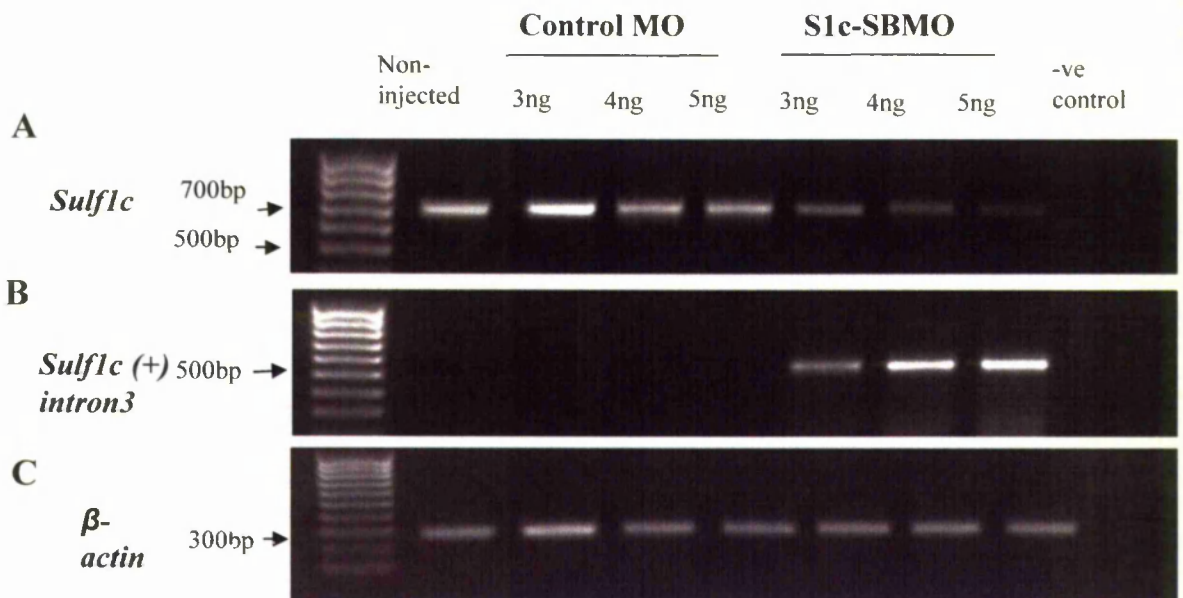
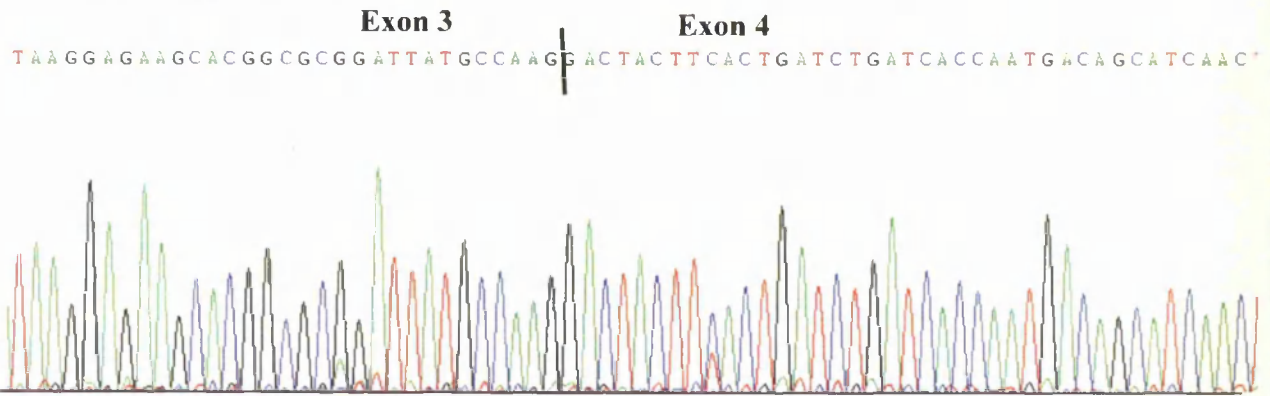


**Figure 4.10: RT-PCR analysis at 24hpf to determine the affect of S1c-SBMO on the *sulf1c* pre-mRNA.** *Fli1:gata* embryos were injected with 3, 4, 5ng of the CMO and equivalent doses of SBMO. RNA was extracted and cDNA synthesised from non-injected, CMO-injected and S1c-SBMO injected embryos at 24 hpf. **A:** The S1c-SBMO RT-PCR was performed and the products separated on a 1.2 % gel. Non injected , CMO-injected samples and S1c-SBMO produced a single band of approximately 713bp. As the concentration of SBMO increased from 3ng-4ng, the intensity of the band decreased. **B:** A separate PCR was carried out with second set of primers to detect presence for inclusion of intronic DNA in the final *sulf1c* transcript described in fig4.10 .RT-PCR was performed using same cDNA from all non injected and morpholino injected samples. No band was detected in control samples and non injected. A 546bp product containing a portion of the intron3-exon4 was observed in S1c-SBMO injected samples. The intensity of band was stronger between 3 and 4ng . **C:**  $\beta$ -actin RT-PCR was performed as a positive control. Following 25 cycles of the RT-PCR the 298bp  $\beta$ -actin band was of similar intensity in all reactions containing cDNA. The negative controls (-ve) in which sterile water was used as a substrate did not produce an RT-PCR product. The size standard is a 1 kb ladder with 300, 500 and 700bp bands indicated.

**A** Wildtype *sulf1c* transcript



**B** Intronic *sulf1c* transcript

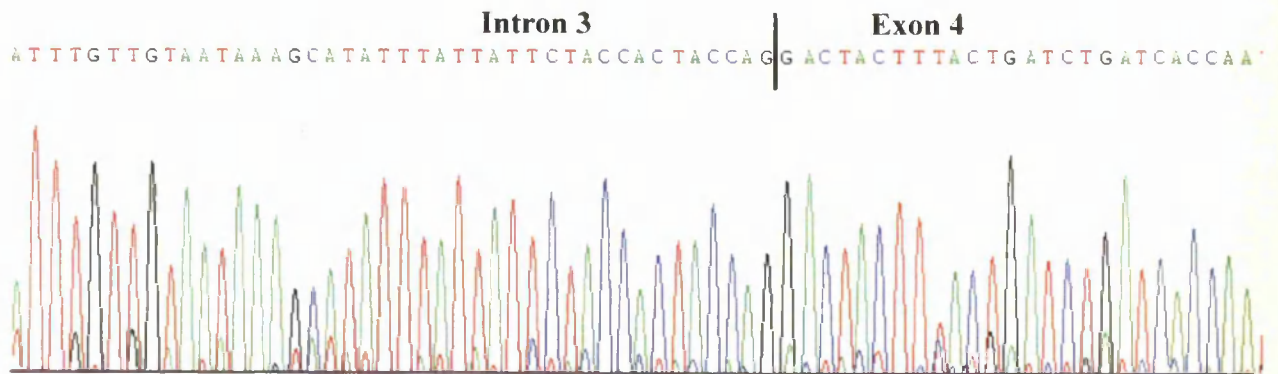


**Figure 4.11: Sequence chromatograms of the intron and exon boundaries of the *sulf1c* transcript.** RT-PCR products shown in Fig 4.10 were sequenced. **A:** A region of the 713bp wildtype *sulf1c* sequence, vertical black line represent the exon3/4 boundary. **B:** A region of the 546bp intron3-exon4 sequence included in the *sulf1c* transcript, vertical black line represents the intron and exon boundary.

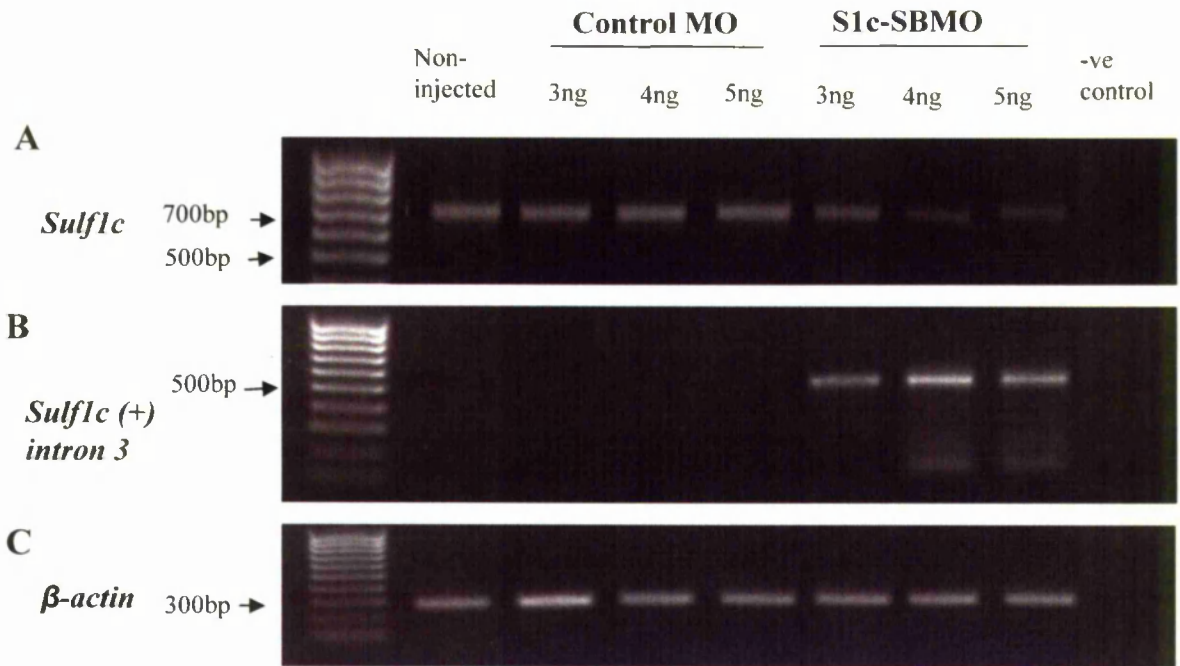


**Figure 4.12: RT-PCR analysis to determine the affect of S1c-SBMO on the *sulf1c* pre-mRNA at later stage during development.** *Fli1:gata* embryos were injected with 3, 4, 5ng of the CMO and equivalent doses of SBMO. RNA was extracted and cDNA synthesised from non-injected, CMO-injected and S1c-SBMO injected embryos at 48hpf. **A:** The S1c-SBMO RT-was performed and the products separated on a 1.2 % gel. Non injected, CMO-injected samples and S1c-SBMO produced a single band of 713bp. As the concentration of SBMO increased from 3ng-4ng, the intensity of the band decreased. **B:** A separate PCR was carried out with second set of primers to detect presence for any intronic DNA described in Fig 4.9. RT-PCR was performed using same cDNA from all non injected and morpholino injected samples. No band was detected in control samples and non injected. A 546bp product was observed in S1c-SBMO injected samples. The intensity of band was stronger with increasing dose. **C:**  $\beta$ -actin RT-PCR was performed as a positive control. Following 25 cycles of the RT-PCR the 298bp  $\beta$ -actin band was of similar intensity in all reactions containing cDNA. The negative controls (-ve) in which sterile water was used as a substrate did not produce an RT-PCR product. The size standard is a 1 kb ladder with 300, 500 and 700bp bands indicated.

was decided to initially test the primer pairs on *flil:gata* genomic DNA to optimise PCR conditions. The PCR amplification of the first product of 800bp was unsuccessful as a very weak band was observed and attempts to sequence the amplicon was unsuccessful (data not shown). However attempts with the second set of primers using genomic DNA in PCR revealed the amplification of the expected product of 546bp. This set of primers was used in all cDNA samples and RT-PCR performed. In this additional PCR reaction, bands of the correct size were visualised in all SBMO injected samples. Sequencing of these amplicons confirmed the band of ~713bp was *sulflc* transcript and the short product ~523bp included a portion of the intronic region and exon4 in the final *sulflc* transcript (Fig. 4.11). The intensity of the short product increased with the respective decrease in the wildtype band from 3 to 5ng, suggesting this product is in excess of the wildtype transcript. As no difference was detected in the intensity of the wildtype transcript in the CMO this further confirmed knockdown of the native *sulflc* expression by the S1c-SBMO. The negative controls in which cDNA was replaced with sterile water did not produce an RT-PCR product.

Although MOs are a commonly used method to knockdown a gene of interest during zebrafish embryogenesis, their action is transient as they are diluted as the embryo grows. Although the SBMO was shown to interfere with splicing of the *sulflc* pre-mRNA in zebrafish at 24hpf, *sulflc* has been shown to be expressed at relatively late stages of embryonic development. It was therefore important to determine the efficacy of the SBMO at stages later than 24hpf. *Flil:gata* embryos were injected with similar doses as previously mentioned and RNA extracted at a later time point 48hpf (Fig. 4.12). The decrease in the wildtype *sulflc* band compared to the control and non-injected samples showed knockdown of *sulflc* was persistent until at least 2dpf of the SBMO injected samples. Although the efficacy of the SBMO decreases over time, considerable knockdown of the *sulflc* transcript is achieved until at least 48hpf.

#### **4.3.5 S1c-SBMO morphants exhibit morphological and vascular defects similar to S1c-ATG morphants**

From the RT-PCR data it can be concluded that S1c-SBMO can effectively knockdown levels of the *sulflc* transcript and the detection of a portion of the intron in the final transcript could possibly result in aberrant transcript.

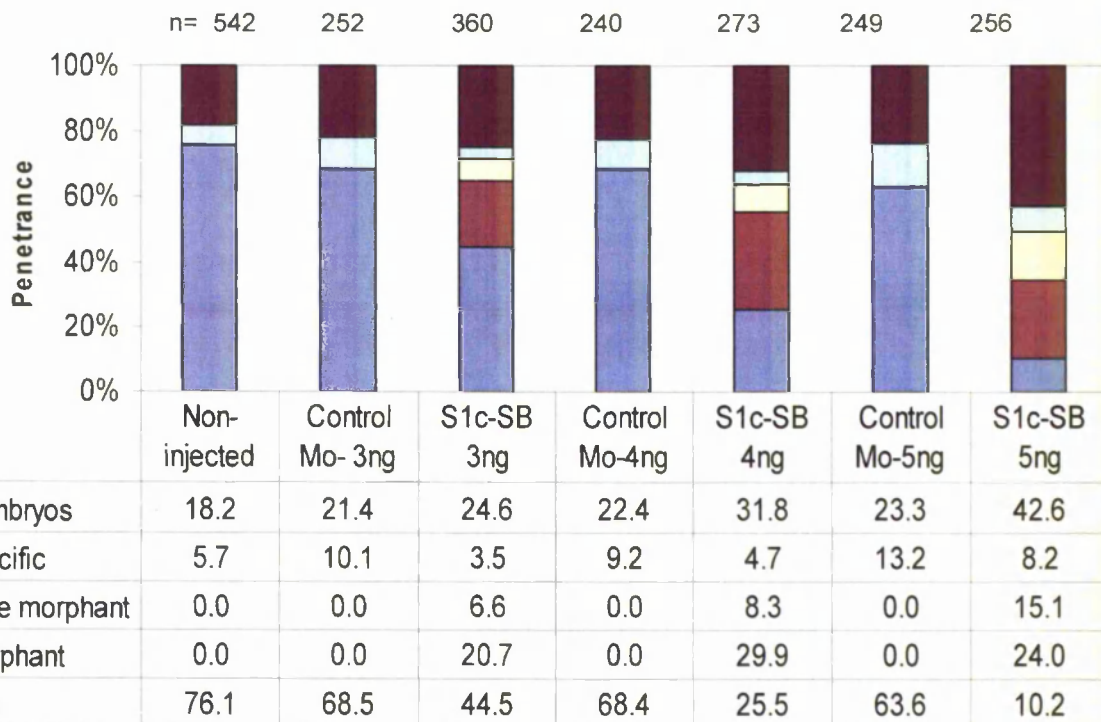


**Figure 4.13: Chart showing the analysis of *flil:gata* embryos injected with different doses of S1c-SBMO.** Data shown in chart is combined from three experiments and the average penetrance of each category represented as a percentage. Tg(*flil*:GFP;*gata*:dsRed) embryos were injected with 3ng, 4ng and 5ng of SBMO and compared to control injected and non-injected embryos. Embryos were scored at 24hpf for mortality rate and surviving embryos were analysed at 2dpf. These embryos were categorised into four different classes depending on their overall morphology into wildtype, non-specific, mild and moderate morphant. Mortality was higher in S1c-SBMO and CMO injected embryos compared to the non-injected at 24hpf, and this increased with higher concentrations of the morpholino. In particular a 23% increase in mortality was observed in embryos injected with 5ng of SBMO. Majority of non-injected and control injected embryos exhibited an overall body shape identical to wildtype embryos. A small subset of embryos classified as non-specific were prevalent in all morpholino and non-injected embryos, this increased with increasing doses of SBMO. Although a low penetrance of *sulf1c* morphants (27.3%) was observed at 3ng, an increase in penetrance was observed at 4 and 5ng with 38% and 39% of embryos exhibiting *sulf1c* morphant phenotype.

Preliminary injections were carried out with a similar dose range to S1c-ATGMO, however injections at the higher doses of morpholino ( $\geq 7$ ng) resulted in nearly 60-100% death with 2ng showing no morphant phenotype (data not shown). Further injections were carried out between concentrations 3-5ng. As with ATGMO injections data from three separate S1c-SBMO experiments was amalgamated and the average penetrance of the different class of phenotypes were represented in the chart (Fig. 4.13). The survival rate of non injected embryos, CMO were compared alongside the S1c-SBMO injected embryos. Although the non-injected and CMO-injected samples showed a similar survival rate in the first 24hpf, an increase in mortality was observed in all SBMO injected samples with the greatest mortality observed at 5ng of SBMO. The mortality induced by the SBMO was not only limited to the first 24hpf. A small percentage of embryos displaying signs of neural toxicity died at 2dpf and those were also included. Likewise the survival rate decreased with increasing dose of SBMO. A subset of embryos were prevalent in the non-injected, CMO and SBMO injected samples that displayed non-penetrant developmental abnormalities (Fig. 4.5F). These were classed as non-specific as many displayed characteristic off-target effects such as loss of anterior head structure and shortened body axis<sup>96,395</sup>. Although a greater percentage of non-specific mutants were found in the CMO the penetrance of the non-specific phenotypes increased with increasing dose of both CMO and SBMO.

A wide spectrum of SBMO injected embryos displayed reproducible phenotypes that were previously classed as mild and moderate morphants in the ATG-MO injected samples (Fig. 4.14). Although overall penetrance of the *sulf1c* morphant phenotype was significantly lower than the ATGMO injected samples, the total percentage of morphants increased with increasing dose. A higher penetrance of the *sulf1c* moderate morphant was observed at 5ng of SBMO compared to the highest dose (7ng) of S1c-ATGMO used. SBMO mild morphants exhibited characteristics similar to that of ATGMO morphants. At 1dpf morphants exhibited a smaller head and eyes, with mild oedema in the hindbrain. Vascular oedema was observed in the same region of the tail proximal to the ICM. At 2dpf the morphological phenotype in the head was evident (Fig. 4.14D,F) along with the abnormal phenotype in the tail, thus short circuiting of blood circulation in the main axial vessels was present at the region of the vascular oedema site. The SBMO moderate morphant exhibited similar characteristics to S1c-ATGMO at 1dpf (Fig. 4.14G) and 2dpf (data not shown). Although the head and tail morphological defects were present in these embryos the overall body shape appeared moderately curved compared to the moderate morphant observed with the S1c-ATGMO,

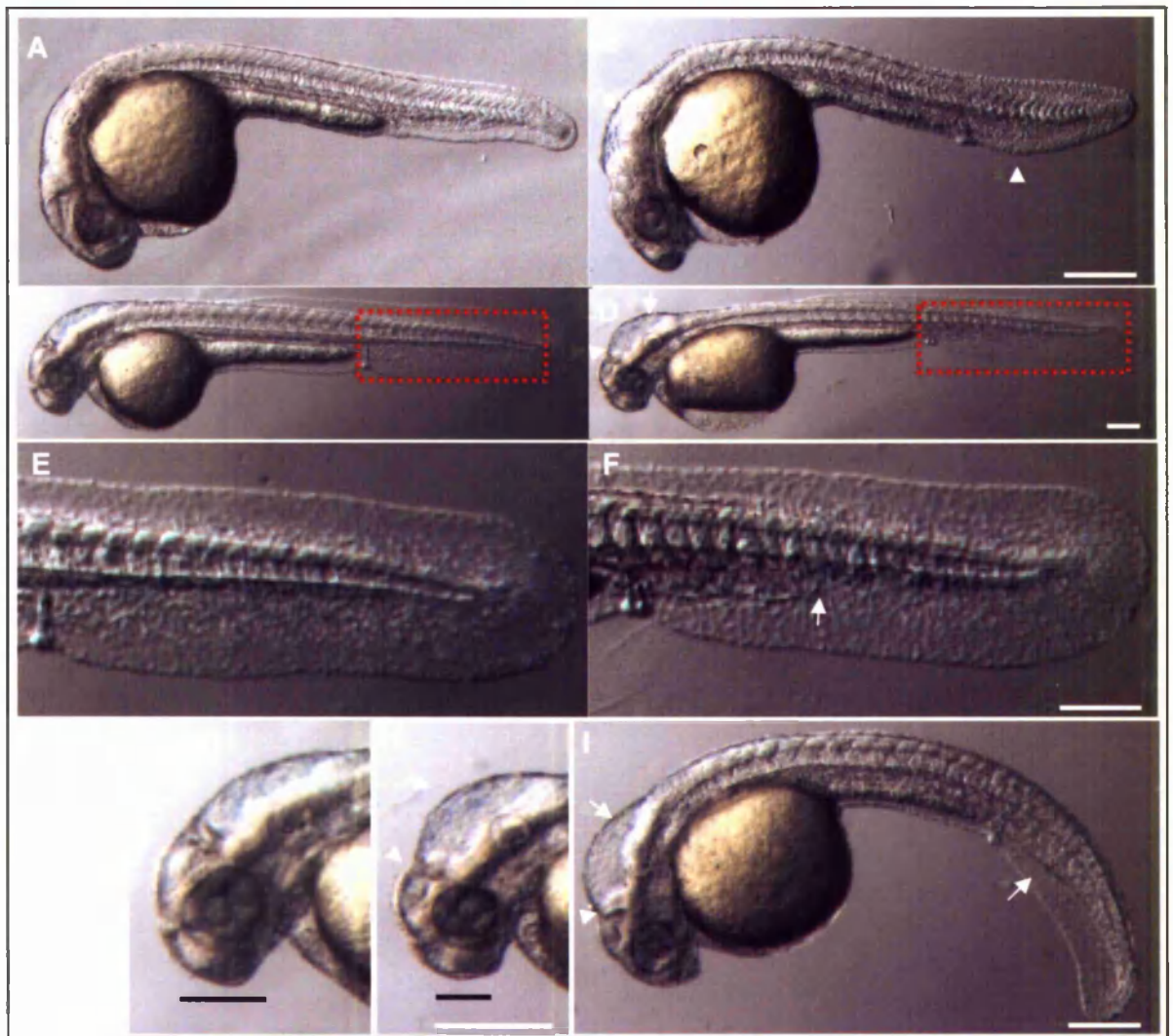


**Figure 4.14: Defects exhibited by the mild and moderate class of the S1c-SBMO injected embryos.** *Tg(fli1:GFP;gata:dsRed)* embryos were injected with CMO and S1c-SBMO and segregated into mild and morphant phenotypes based on the criteria mentioned previously. Brightfield images of control and *sulflc* mild morphant at 26hpf (A,B) and 48hpf (C,D). Mild morphant exhibit small head and eyes with depression in the mid-hindbrain boundary and mild oedema in the hindbrain ventricle (white arrow). Also evident at 26hpf is the expansion of the ventral mesoderm tissue in the tail of the morphants (white arrowhead). At 48hpf the morphological defects in the head (D,H) of the *sulflc* morphant are obvious. Morphants (D,H) display smaller head and eyes compared to control (C,G) (represented by the length of black line) with the vascular defect in the tail also present. Abnormal CA and CV connection is formed in the *sulflc* morphant resulting in premature return of venous blood flow (F, white arrow). An example of the moderate morphant at 26hpf shows similar phenotypic traits to mild morphant with identical morphological defects in the head including hindbrain oedema and depressed mid-hindbrain boundary (white arrow). The overall body shape of the moderate morphant is mildly curved with oedema in the tail also present (corresponding white arrow). Scale bar is 200 $\mu$ m.

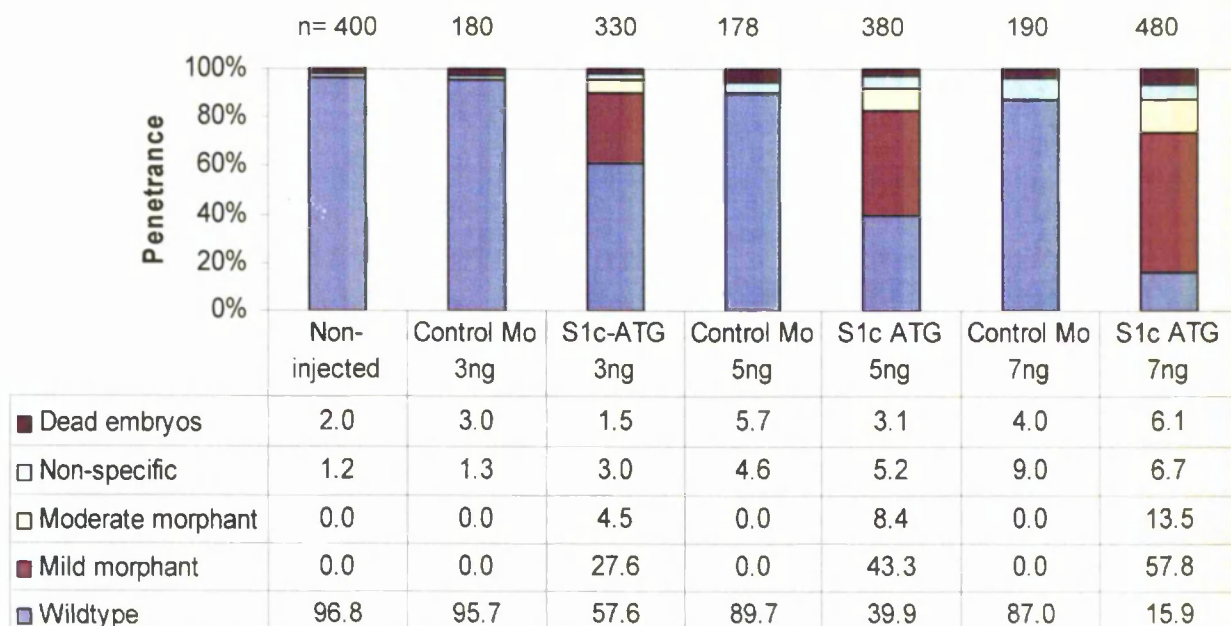


**Figure 4.15: Chart showing the analysis of *flk1:gata* embryos injected with S1c-ATGMO.** Data shown is combined from multiple experiments (n), ATGMO, n=3; CMO, n=2, and the average penetrance of each class is shown as a percentage. Embryos were injected at 1-4 cell stage with 3, 5 and 7ng of S1c-ATGMO and compared to control injected and non injected. Embryos were scored at 24hpf for mortality and the surviving embryos analysed at 2dpf. Mortality was comparable between non injected and all morpholino injected samples. The majority of embryos in non-injected, control injected and a subset of embryos in ATGMO injected samples displayed normal morphology. A small subset of embryos classified as non specific were prevalent in all samples although moderately higher in morpholino injected samples. Injections with S1c-ATGMO at 3ng in *flk1:gata* embryos resulted in a small percentage (32.1%) of the total number of embryos displaying the mild and moderate phenotypes. However the penetrance of the *sulflc* morphants significantly increased with increasing dose, with 5ng and 7ng ATGMO injected embryos resulting in 51.7% and 71.3% of *sulflc* morphants.

suggesting a muscle defect. Interestingly close analysis of the trunk of the morphants revealed no somite or notochord defects.

#### **4.3.6 Characteristic phenotype of *sulflc* morphant has a higher penetrance in *flk:GFP;gata:dsRed* line**

The results so far suggest both morpholinos give reproducible and consistent phenotypes albeit at different concentrations. To further confirm the *sulflc* morphant phenotypes and obtain detailed analysis of the cranial vasculature, it was recommended to use an alternative vasculature transgenic line namely the *flkl:GFP;gata:dsRed* transgenic line. Flk (friendly leukaemia integrated kinase) is a VEGF receptor expressed on endothelial cells. All injections carried out in the *tg(flkl:GFP;gata:dsRed)* were performed in Roger Patient's lab (Weatherall institute, Oxford) Circulatory and vascular defects in the characteristic phenotype were recorded and results are presented in the next chapter. Identical range of concentrations of the S1c-ATGMO were used in the *tg(flkl:GFP;gata:dsRed)*, and the results displayed in the chart (Fig. 4.15)

Mortality was generally higher in morpholino injected embryos compared to control. However in comparison to the injections in the *fli1:gata* transgenic line the mortality in general was lower at all concentrations injected. Although injections at 3ng only gave 32% penetrance of the *sulflc* morphants, injections at higher doses of 5ng and 7ng gave 52% and 71% penetrance of *sulflc* morphants respectively (Fig. 4.15). This showed a striking contrast to the penetrance levels of the same morpholino in *fli1:gata* line particularly at the high concentration (Fig. 4.16). Although the trunk circulatory defects were present in the morphants, interestingly small differences in the overall morphology were apparent. At 1dpf mild morphants exhibited small head and eyes compared to control, however no defects were observed in mid-hindbrain boundary and hindbrain oedema was absent in these morphant. Similarly at 2dpf and 3dpf in the mild morphants the small head and eyes was evident despite the absence of hindbrain oedema. Moderate morphants also lacked the hindbrain oedema phenotype whilst retaining the small head and eye characteristic traits. While S1c-ATGMO gave reproducible and similar phenotypes in both the *fli1* and *flkl* transgenic lines, the significant difference in the

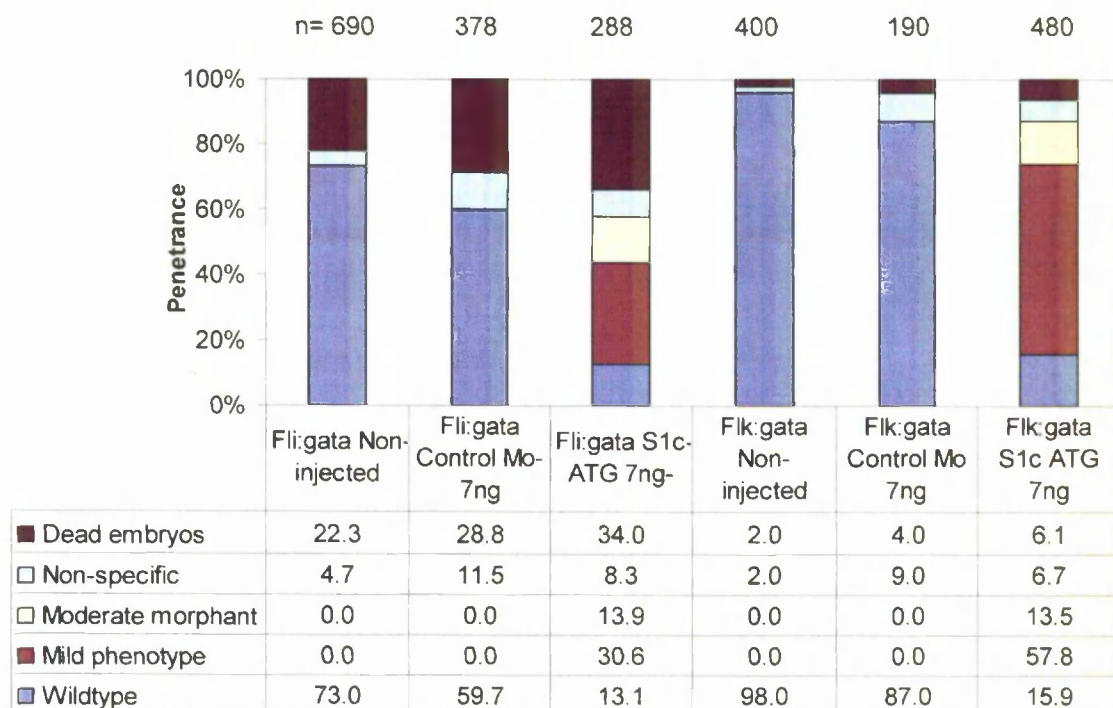


**Figure 4.16: Comparison of the S1c-ATGMO injected samples in *fli1:gata* and *flk1:gata* embryos.** Data shown is results pooled from four experiments of *fli1:gata* injected embryos and three of the *flk1:gata* injected embryos. Average penetrance is represented as a percentage. Embryos were injected with 7ng of S1c-ATGMO in both endothelial transgenic lines. All embryos were scored for mortality at 24hpf and surviving embryos analysed at the 2dpf. Mortality was generally higher in morpholino injected *fli1:gata* embryo compared to non injected, whilst mortality was comparable in *flk1:gata* non injected, CMO and S1c-ATGMO injected embryos. A higher percentage of non-specific embryos was present at in *fli1:gata* non-injected and morpholino injected samples compared to *flk1:gata* injected embryos. Whilst the percentage of wildtype embryos decreased with increasing the dose of ATGMO in both strains, a significantly higher percentage of *sulf1c* morphants was present in the *flk1:gata* (71.3%) strain compared to *fli1:gata* (44.5%) at 7ng of ATGMO.

penetrance and the mild morphological changes in the *sulflc* morphants could not go unnoticed.

#### **4.3.7 Analysis of the *sulflc* MO sites**

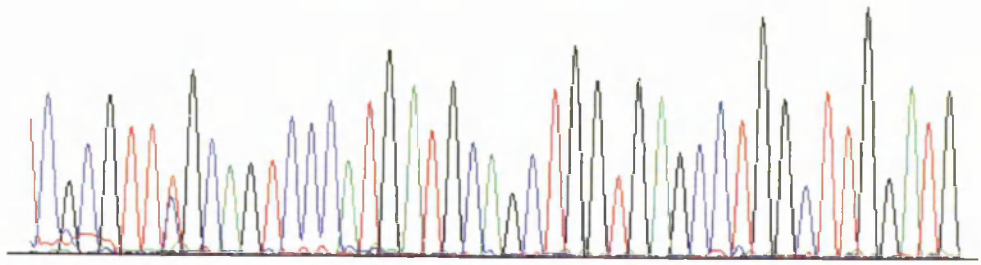
Unlike inbred mouse colonies it is not possible to maintain zebrafish lines on a 100% inbred background, probably as a result of differing husbandry conditions (Pers comm. Dr.K.Rooney). Whilst establishing the zebrafish *sulflc* sequence, it was noted that the zebrafish tg(*fli1*:GFP;*gata*:dsRed) strain housed at the University of Manchester Biological Services Facility (UMBSF) carried a number of silent polymorphisms within *sulflc* (data not shown). Strain differences have been noted whereby gene knockdown or knockout can give rise to different mutant phenotypes (personal comm. Gene tools). It was therefore important to ensure the MO target sites in the zebrafish strains used in these studies were identical to the synthesised MOs. PCR and sequencing were used to verify the SBMO and ATGMO target sequences in the strain housed at the UMBSF. The ATGMO target sequence in the tg(*fli1*:GFP;*gata*:dsRed) strain contained a polymorphism at position 24 of the antisense MO thus corresponding to a nucleotide position within exon one (Fig. 4.17A) The sequence chromatogram showed that the two alleles of *sulflc* are present within the population the sequence of one is identical to the synthesised ATGMO sequence while the other allele contained a thymine (T) instead of a cytosine (C) and therefore is different to the synthesised ATGMO. The SBMO was identical to the synthesised MO and ATGMO target site in the tg(*flkl*:GFP;*gata*:dsRed) (Fig. 4.17B,C).

#### **4.3.8 Injection of *sulflc* mRNA partially rescues morphological and circulatory phenotype**

From the results presented so far it is evident two independent morpholinos targeting the knockdown of *sulflc* transcript can specifically induce consistent and reproducible phenotypes, but most importantly exhibit the same phenotypic traits in the *fli1*:GFP;*gata*:dsRed embryos. Despite the difference in concentration of the MO's required to reach a high penetrance of the *sulflc* morphant, the tail and head defects observed in the *sulflc* morphants appear to be specific to the *sulflc* knockdown. To confer additional confidence in the knockdown of gene function of 'interest' is to co-inject mRNA of the full

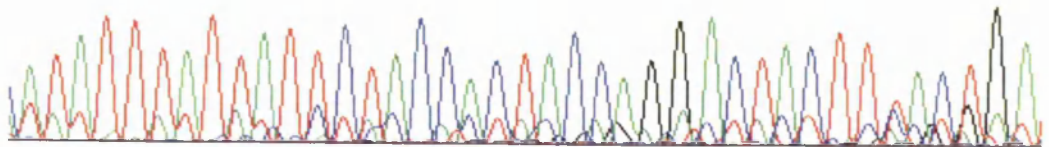
**A** *Sulflc*-ATGMO site: tg(*fli1*:GFP;*gata*:dsRed)

CGCGT TTSCAGTCCCA TG ATGCA GCTGGTGAGCCTGGC TTGGATG



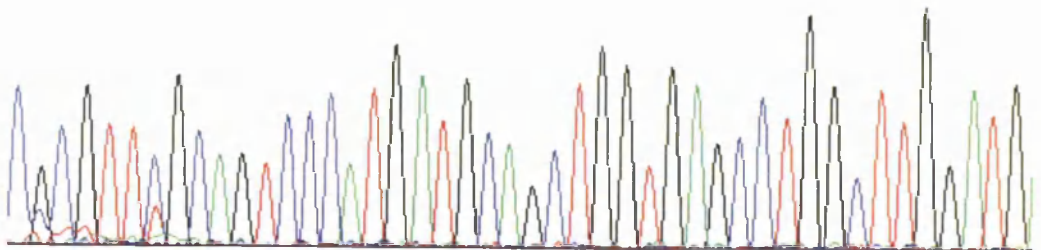
**B** *Sulflc*-SBMO site: tg(*fli1*:GFP;*gata*:dsRed)

ATA TTTTATTTATTTCTACCAC TACCAG GACTACTTTACTG A



**C** *Sulflc*-ATGMO site: tg(*flkl*:GFP;*gata*:dsRed)

CGCGTTCGCA GTCCCA TG ATGCA GCTGGTGAGCCTGGC TTGGATG



**D** *Sulflc*-ATGMO site: tg(*p53*<sup>-/-</sup>)

CGCGT TTGCA GTCCCA TG ATGCA GCTGGTGAGCCTGGC TTGGATG

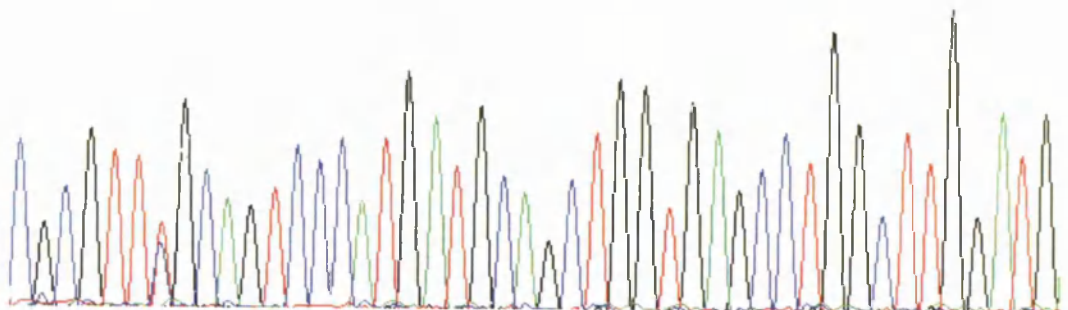


**Figure 4.17: Sequence chromatograms of the *sulf1c* morpholino target sites in the different transgenic lines.** The sequence chromatograms show the sense strand with the morpholino target sites underlined in a black line. **A,C,D:** S1c-ATGMO target sequence in the *tg(Flil:GFP;gata:dsRed)*, *tg(flkl:GFP;gatal:dsRed)* and *tg(p53<sup>-/-</sup>)* respectively. Both the *tg(Flil:GFP;gata:dsRed)* and the *tg(p53<sup>-/-</sup>)* strains carry a polymorphism circled at position 24 of the antisense MO corresponding to a nucleotide position in the first exon. The S1c-ATGMO target sequence in the *tg(flkl:GFP;gatal:dsRed)* is identical to the synthesised ATGMO sequence. **B:** S1c-SBMO target sequence in *tg(Flil:GFP;gata:dsRed)* is identical to the synthesised SBMO sequence, the vertical line represents the intron-exon boundary

length gene alongside the morpholino and to observe whether defects in morphants can be rescued. *Sulflc* mRNA was synthesised from full length *sulflc* cDNA by using mMessage T7 kit (Ambion).

Since *sulflc* is expressed ubiquitously during development, both maternally and zygotically it was predicted that injection of exogenous *sulflc* mRNA may result in an 'overexpression' phenotype. Therefore preliminary experiments were performed with injecting *sulflc* mRNA alone in order to titrate down to a dose that would produce minimal 'overexpression' phenotypes. A range of concentrations were injected. At the highest dose of 500pg, 45% of embryos exhibited mild and severe forms of cyclopia with the severe form exhibiting curved body axis and distorted notochord (Appendix I). Similarly injections at slightly lower doses of 200pg and 250pg also showed majority (35-40%) of embryos displaying the cyclopia phenotype in contrast to control GFP mRNA injected embryos, with only a small subset displaying overall body shape similar to that of wildtype embryos at the similar stage. However injections at a lower dose of 50pg and 100pg of *sulflc* mRNA resulted in majority of embryos with wildtype like characteristics. There was a small percentage (~10%) of embryos present both in control and *sulflc* mRNA injected that displayed developmental abnormalities and these were classed as non-specific as they were occasionally present in the non-injected. Since the background levels remained constant at this dose, the concentration was chosen for subsequent rescue experiments. Although S1c-ATGMO gave higher penetrance of the characteristic phenotype than SBMO it was decided to co-inject SBMO with S1c-mRNA to reduce the likelihood of possible binding of the two constructs. The fact that the SBMO can potentially bind to 6bp of the exon sequence of the mRNA seems unlikely to interfere with the activity of the morpholino as it has been reported that binding of >17 nucleotides would result in affect of morpholino (pers comm Gene tools). Control injections with GFP mRNA were carried out alongside to ensure specificity of the *sulflc* mRNA in the proceeding rescue experiments.

Transgenic (*fli1:GFP:gata:dsRed*) embryos were co-injected with increasing concentrations of *sulflc* mRNA and 4ng of S1c-SBMO, resulting phenotypes were analysed at 48hpf and compared to control GFP injected (Fig. 4.18). Control injections with GFP mRNA were carried out alongside to ensure specificity of the *sulflc* mRNA in the proceeding rescue experiments. Non-injected and injected embryos displaying developmental abnormalities not associated with the phenotypes of *sulflc* morphants were classed as non-specific.

Percentage frequencies (%)	4ng S1c-SBMO	50pg GFP mRNA + 4ng-S1c-SBMO	100pg GFP mRNA + 4ng S1c-SBMO	150pg GFP mRNA + 4ng S1c-SBMO	50pg S1c mRNA + 4ng S1c-SBMO	100pg S1c mRNA + 4ng S1c-SBMO	150pg S1c mRNA + 4ng S1c-SBMO
Wildtype	21.7 (±2.6)	24.1 (±2.7)	22.4 (±0.7)	20.6 (±0.9)	32.5 * (±1.0)	30.5 (±2.1)	24.4 (±2.2)
Mild morphant	30.3 (±3.4)	28.9 (±2.1)	29.2 (±2.9)	28.6 (±1.9)	16.0 * (±1.9)	17.2 (±2.5)	10.1 (±1.1)
Moderate morphant	10.5 (±1.4)	8.1 (±2.2)	9.6 (±0.8)	8.6 (±1.6)	8.4 ~ (±0.5)	8.2 (±0.3)	6.3 (±1.6)
'Overexpression' phenotype	0.0	0.0	0.0	0.0	* 3.1 (± 2.5)	4.1 (±2.7)	14.0 (±3.1)
Non-specific	5.3 (±0.8)	6.0 (±0.8)	8.1 (±0.4)	8.5 (±2.2)	5.3 (±1.5)	7.8 (±0.1)	10.3 (±2.6)
Dead	32.1 (±1.4)	32.9 (±2.0)	30.7 (±3.4)	33.7 (±2.1)	34.7 (±0.1)	32.1 (±0.4)	34.9 (±1.4)
<b>Total No of embryos</b>	<b>171</b>	<b>200</b>	<b>197</b>	<b>206</b>	<b>136</b>	<b>243</b>	<b>134</b>

**Figure 4.18: Frequencies (%) of the morphological defects of the *sulflc* morphants and partial rescue of the mild morphant.** Data shown is combined from three experiments (n), microinjections performed with 4ng of SBMO alone (n=6) were amalgamated and a representative of all experiments *Fli1:gata* embryos were co-injected with 4ng SBMO and 50,100,150pg of *sulflc* mRNA and compared to control injected (GFP mRNA). The percentages for the combined injections were averaged from two experiments and the accompanying standard error in brackets. All embryos were scored for mortality at 24hpf. Two day old embryos were segregated based on their overall morphology and the phenotypes scored. There was very little difference in mortality between SBMO and SBMO injected with mRNA. The percentage of wildtype embryos was comparable between SBMO alone and control injected while a significant increase (~50%) of wildtype embryos was observed in embryos co-injected with 50pg of *sulflc* mRNA. Concomitantly, the percentage of embryos possessing the mild phenotype significantly reduced with increasing concentration of the *sulflc* mRNA whilst the percentage of moderate morphants was not significantly affected in comparison to control injected. Statistical test performed using one way annova \* p<0.05, ~ statistically not significant p>0.05.

Although the mortality was comparable in SBMO alone and control GFP mRNA co-injected samples, mortality was higher in the *sulflc* mRNA co-injected samples. As the concentration of the *sulflc* mRNA increased the penetrance of the mild morphant significantly decreased compared to the control injected. A moderate decrease of 44% was observed at 50pg of *sulflc* mRNA with a relatively mild increase in the percentage (35%) of wildtype embryos. Although the highest decrease in the mild morphant was observed with increasing doses of mRNA i.e. 100pg and 150pg this was not accompanied with a respective increase in wildtype embryos but showed an increase (~50%) in embryos with the cyclopia 'overexpression' phenotype compared to control-injected. However the penetrance of the moderate morphant phenotype did not appear to significantly decrease with increasing concentrations of *sulflc* mRNA. Even at 50pg of *sulflc* mRNA, where a significant decrease was observed in the mild phenotype compared to control injected no appreciable difference was observed in the moderate morphant.

Despite the significantly mild rescue of the morphology of the mild phenotype at 50pg and 100pg of mRNA, the high percentage of *sulflc* characteristic and moderate morphant phenotypes persistent in these co-injected samples was fairly evident in comparison to the control injected. Those embryos that had retained the characteristic morphology of the *sulflc* morphants were subjected to further analysis. Although the overall morphology of these embryos could not be rescued the axial and cranial circulatory phenotype was scored and results are represented as a bar graph (Fig 4.19 and Fig 4.20).

Interestingly 51% and 38% of mild and moderate morphant co-injected with 50pg of mRNA had normal axial circulation compared to control injected whilst a significantly greater percentage of morphants had normal circulation at 100pg of mRNA. Simultaneously the cranial circulation of the morphants was analysed at each concentration, while a significant 34% and 30% of mild and moderate morphants possessed a normal cranial circulation compared to control injected. There was greater percentage of morphants exhibiting normal cranial circulation at 100pg of mRNA. Although significant levels of axial and cranial circulatory defects were rescued with the lowest dose of *sulflc* mRNA, greater rescue was achieved in the axial circulation in comparison to cranial circulation in the *sulflc* morphants.

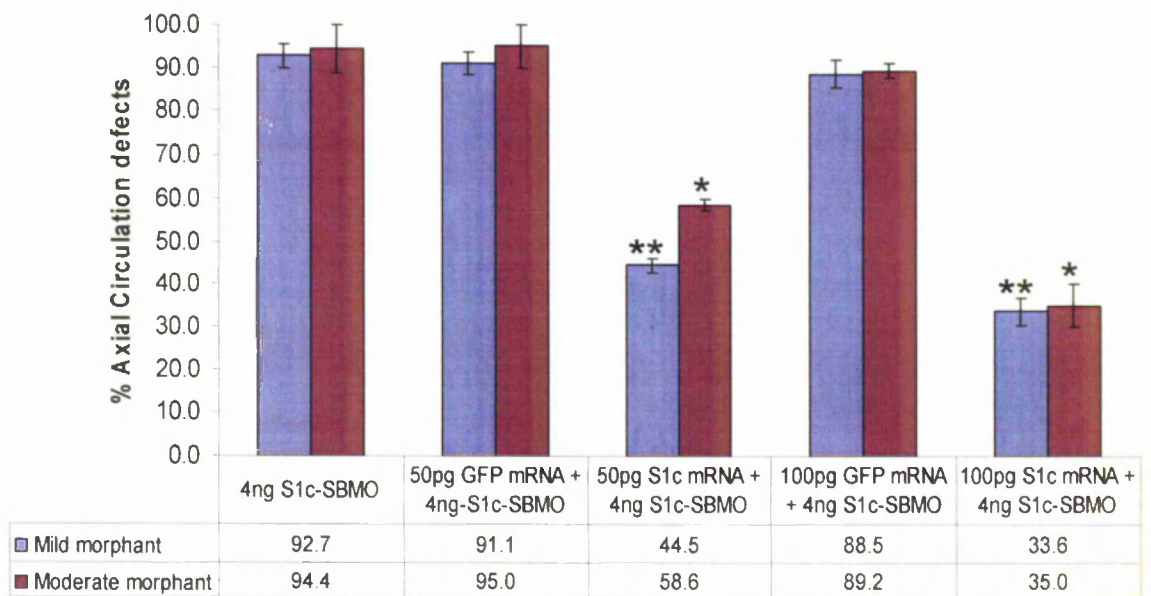


**Figure 4.19: Graphical depiction of the percentage of axial circulatory defects of the *sulflc* morphants and partial rescue of the axial circulation in *sulflc* morphants.** *Fli1:gata* embryos were co-injected with 4ng SBMO and 50, 100pg of *sulflc* mRNA and compared to control injected GFP mRNA. The percentages of axial circulatory defects in the embryos possessing the mild and moderate phenotype were averaged from two experiments. Co-injections of SBMO with 50pg of *sulflc* mRNA resulted in 51% and 38% rescue of axial circulation in mild and moderate morphants compared to control injected. Injections with 100pg of *sulflc* mRNA resulted in a greater percentage of mild (62%) and moderate morphants (57%) with normal axial circulation compared to control injected. Statistical test was performed using one way ANOVA \*\* $p < 0.001$ , \* $p < 0.01$ .

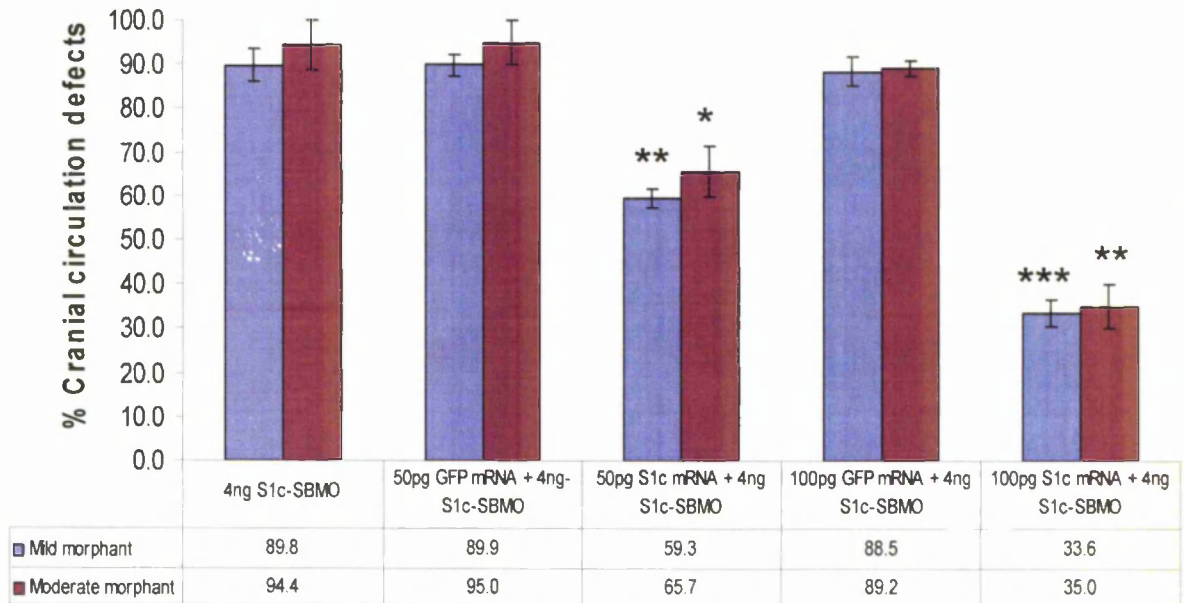


**Figure 4.20: Graphical depiction of cranial circulatory defects of the *sulflc* morphants and partial rescue of the cranial circulation in *sulflc* morphants.** *Fli1:gata* embryos were co-injected with 4ng SBMO and 50, 100pg of *sulflc* mRNA and compared to control injected GFP mRNA. The percentages of cranial circulatory defects in embryos possessing the mild and moderate phenotype were averaged from two experiments. Co-injections of SBMO with 50pg of *sulflc* mRNA resulted in 36% and 20% rescue of defective cranial circulation in mild and moderate phenotypes compared to control injected. A higher percentage of rescue of the defective cranial circulation was observed with co-injection of 100pg of *sulflc* mRNA in mild (62%) and moderate morphants (60%), with 55% and 54% of mild and moderate morphants respectively, displaying normal cranial circulation. Statistical test was performed using one way ANOVA \*\*\* $p < 0.001$ , \*\* $p < 0.01$ , \* $p < 0.05$

#### 4.3.9 *Sulflc* morphants reproducible in *p53*<sup>-/-</sup> fish

Results from the rescue experiment suggest injection of low doses of *sulflc* mRNA can partially rescue the mild morphant phenotype. Although an increase in the percentage of wildtype embryos was observed, a significantly greater percentage of injected embryos displayed normal circulation. A subset of co-injected embryos retained the mild and moderate phenotypic traits described in 4.3.2 and 4.3.4 even though in 40-50% morphants had normal axial and cranial circulation. This suggests that some of the characteristic defects evident in the *sulflc* morphants may not be specific to *sulflc* knockdown alone. It has been noted that 15-20% of morpholinos used in gene-knockdown experiments in zebrafish show off targeting affects that include small head and eyes<sup>96</sup>. The latest studies by Robu and colleagues (2007) showed that this off targeting affect results in activation of *p53* dependent cell death pathway. These embryos display neural death at 1dpf, by later stages these affected embryos result in smaller head and eyes with evident depression in the mid-hindbrain boundary. Since the *sulflc* morphants exhibited these characteristic traits, the possibility of off-targeting induced by the SBMO or ATGMO could not be excluded. A good tool for this purpose has been the generation of the *p53*<sup>-/-</sup> zebrafish. The *p53* knockdown by itself does not induce any significant defects, as *p53* is not required for normal development in mammals or fish<sup>396,397</sup>. Importantly it has also been shown that reduced levels of *p53* do not affect the development of the embryos or specific morphant phenotypes<sup>395</sup>.

The *sulflc* ATGMO site was sequenced from the *p53*<sup>-/-</sup> strain this was found to contain a polymorphism in exact position of ATGMO target sequence in the tg(*fli1*:GFP;*gata*:dsRed) Embryos of *p53*<sup>-/-</sup> genetic background were injected with the 5ng of the S1c-ATGMO respectively. This dose was chosen as previous results in the tg(*fli1*:GFP;*gata*:dsRed) embryos showed this to be the optimum in producing a high penetrance of the *sulflc* morphants whilst inducing minimal mortality. Data was amalgamated from the three experiments and average penetrance recorded (Appendix II).

The mortality was comparable between the non-injected, CMO and ATGMO injected embryos. A small subset of embryos were present in all injected samples that displayed developmental abnormalities, that had also been observed in the tg(*fli1*:GFP;*gata*:dsRed) S1c-ATGMO injected embryos, these too were classified as non-specific. However they varied in their overall phenotype with some seemingly possessing normal size head and eyes but retaining other morphological defects such as curved tail (data not shown). Interestingly not all the phenotypes categorised as non-specific were present in the non-injected or injected

samples, suggesting certain non-specific phenotypes were a results of non-specific activation of *p53*. This is consistent with the reduction of the non-specific phenotypes and increase in the percentage of wildtype embryos observed in comparison to the S1c-ATGMO tg(*fli1*:GFP;*gata*:dsRed) injected embryos.

Encouragingly the reproducible circulatory defects of the mild morphants were prevalent in the *p53*<sup>-/-</sup> fish possessing identical defects to SBMO/ATGMO tg(*fli1*:GFP;*gata*:dsRed) injected embryos (Appendix III). The overall morphology of both mild and moderate was relatively unchanged. Despite the presence of the small head and eyes phenotype in the *sulflc* morphants there were no signs of narrow mid-hindbrain boundary and hindbrain oedema in the mild and moderate phenotypes. Although further experiments could be done, the data form these preliminary experiments suggest that those characteristic traits maybe specifically up-regulated by *p53* and therefore non-specific to the *sulflc* knockdown.

## 4.4 Discussion

### 4.4.1 Slc-ATGMO can modify 6-O sulphation levels of the tri-sulfated disaccharide

As a role of *sulflc* in zebrafish has not yet been described and a zebrafish mutant for this gene is currently not available, it was decided to use a reverse genetics approach by using MO knockdown to investigate the role of *sulflc* in vascular development. Morpholino antisense oligonucleotides were used that selectively block translation of mRNA. They have been proven to be effective and specific translational inhibitors in zebrafish<sup>398</sup>. To test the specificity of the injected morpholinos SAX-HPLC was utilised, to analyse the HS disaccharide content of the *sulflc* morphant and compare it to wildtype embryos. Disaccharide analysis of embryos injected with HS6STs<sup>329,330</sup> or *sulflc* mRNA<sup>352</sup> revealed significant changes in 6-O sulphation demonstrating the sensitivity of the methods used to detect changes in 6-O sulphation (Fig. 4.3). In our study the HS sulfation profile of the *sulflc* injected embryos was assessed using methods previously described by Chen and colleagues (2005). The total level of HS extracted from control and *sulflc* morphants was comparable to previous results of 48hpf total HS extracted from HS6ST morphants<sup>329,330</sup> confirming the injection of *sulflc* morpholinos did not introduce any aberrant changes in the overall content of HS. Significant changes were observed in the tri-sulfated and the respective di-sulfated (UA2S-GlcNS) disaccharides with an overall increase in total 6S groups by 20%, this suggests that *sulflc* is predominantly acting on the 6-O sulphate groups in a fashion most similar to murine and quail *sulf1*<sup>344,349,360</sup>. Although we observed a general increase in disulfated disaccharide (UA-GlcNS6S) similar to mouse *sulf1*<sup>349,360</sup> these changes were not statistically significant. While more experiments could be done, this data indicates that the tri-sulfated disaccharide is more susceptible to *zfsulflc* action than other disaccharides consistent with previous *in vitro* reports<sup>344,354</sup>.

A specific but partial affect on 6-O sulphation levels was observed in the *sulflc* morphants, however it was difficult to assess whether the morpholino injection abolished *sulflc* protein levels completely. Unfortunately due to a lack of antibody to *sulflc* we were not able to investigate this further. However the moderate increase could be possibly be due to one of three reasons; zebrafish possesses more than one *sulf* gene coding for the *sulf* enzymes that may have identical substrate specificity compared to the *sulflc* a situation found in human, mice and quail<sup>344,348,349,360</sup>. There could be partial compensation by the expression of the

other sulf enzymes, a scenario found in *sulf2* knockout mice in which decreased levels of *sulf2* are overridden by *sulf1c* overexpression. Alternatively sulf1c activity maybe partially recovered by 48hpf of development similarly to what is found for other proteins in transient knockdown studies<sup>386</sup>. In support of this, RT-PCR analysis of the SBMO S1c morphants at 48hpf showed weak levels of wildtype *sulf1c* transcript. The limited effects of the morpholinos on HS maybe attributed to the low doses that were used to avoid non-specific toxicity. If time permitted it would have been interesting to look at the disaccharide profile of the morphants injected with 7ng of S1c-ATGMO.

Nevertheless zebrafish *sulf1c* can act on similar tri-sulfated disaccharide species as in mice indicating conservation of function. Although these disaccharides maybe present within a different oligosaccharide sequence, since the disaccharide profiling does not give information concerning the structural context of any given disaccharide.

#### **4.4.2 S1c-SBMO reduces the expression of the *sulf1c* wildtype transcript**

SBMO are designed to interfere with splicing of the pre-mRNA transcript thereby producing an aberrant transcript. SBMOs targeted to the splice junction of the first or last exon usually cause inclusion of the intron into the mRNA while those targeted to internal splice junctions usually induce exclusion of an exon<sup>384</sup>. The *sulf1c* SBMO was designed to bind to the splice acceptor site of exon 4 (from a total of 19 exons) and it was therefore predicted that this MO would produce an aberrant *sulf1c* transcript that did not include exon 4. However the results presented in this chapter indicate that this was not the case for the SBMO used in these studies. Although the expression of the wildtype *sulf1c* transcript was reduced the predicted aberrant product was not detected, instead a short product was amplified that suggested that exon 4 was included in the final transcript along with a portion of intron 3 sequence. The nature and prevalence of the shorter product was not investigated further and it is therefore possible that both the amplified wildtype transcript and the shorter product are present within the full length *sulf1c* transcript. The shorter product increased with increasing dose of morpholino thus suggesting this product was more abundant than the wildtype transcript and this persists into the later stages of development. Preliminary attempts to amplify across exon3-exon4 were unsuccessful and therefore it remains to be determined if the full length of Intron3 was included. However in most cases it has been reported targeting a splice acceptor site as opposed to splice donor site results in exclusion of the preceding intron (Pers comm, Gene tools). If this is the case then there are two possible outcomes. Firstly the predicted intron containing *sulf1c* transcript would produce a shift in the reading frame resulting in the

introduction of a premature stop codon at the beginning of the intron3 sequence. Translation of the shorter open reading frame is predicted to produce a 193 amino acid protein (Appendix IV) compared to the 873 amino acid protein of the wildtype transcript which contains a portion of the *Sulf1c* enzymatic domain but would lack the remaining enzymatic domain and most importantly the hydrophilic domain, also important for sulf activity<sup>344</sup>.

Secondly aberrant mRNA transcripts formed this way can be consequently degraded through a surveillance mechanism known as non-sense mediated mRNA decay (NMD)<sup>399</sup>. If an aberrant mRNA with a premature stop codon is generated, the exon junction-complex will not be removed from the transcript, thus activating NMD and subsequent degradation of the aberrant mRNA<sup>400</sup>. To date, authors have shown that premature stop codons underlying loss-of-function alleles result in loss of transcript expression<sup>401-404</sup>. Although not definitively proven in the case of *sulf1c*, we predict the remaining 3' region of the *sulf1c* transcript would not be translated if the intron3 was included and therefore would retain its exon-junction complexes and be targeted for degradation. WISH analysis to detect *sulf1c* transcript in the *sulf1c* morphants could be used to test this hypothesis. Furthermore, if the truncated *sulf1c* protein is not targeted for degradation it is probable that this abnormal protein will not have an effect on the developing embryo as it does not contain most of the predicted functional domains. Expression of the *sulf1c* protein should be compared between controls and *sulf1c* morphants. However, an antibody to detect the zebrafish *sulf1c* protein is not currently available and therefore protein analysis is limited.

#### **4.4.3 S1c-ATGMO and SBMO show consistent phenotypes**

The results from the HPLC and RT-PCR show that morpholinos are specific to *sulf1c* and that the knockdown of *sulf1c* with ATGMO and SBMO give reproducible phenotypes albeit at different concentrations and penetrance levels. Although it is difficult to predict the efficacy of a morpholino, differences between the efficacious concentration of the ATGMO and SBMO were not overlooked. It is possible the SBMO may have relatively easy access to its target site whereby the ATGMO may need a higher dose to induce *sulf1c* knockdown as the MO site maybe buried within the complex secondary structure of pre-mRNA. However the ATGMO gave a higher percentage of morphants with a more consistent phenotype. The lower penetrance in the SBMO maybe contributed by maternal *sulf1c* mRNA that is not targeted by the SBMO. This however is unlikely to explain the entire story as higher concentrations of SBMO resulted in significantly high mortality. The reduced number of morphants observed in

these analyses maybe down to the largely unexpected amount of death induced by SBMO in the first 24hpf. As discussed previously it is difficult to predict the off-target effects of a morpholino. The high lethality associated with the SBMO in combination with exclusion of many morphants displaying presumed non-specific and off-target defects resulted in a small number of SB morphants available for analysis compared to ATGMO. Although increased mortality was seen in the ATGMO-injected embryos compared to the non-injected controls this was similar to the CMO injections of the same concentration suggesting that death is largely independent of ATGMO sequence, unlike the S1c-SBMO.

A number of possibilities may explain these observations. Firstly, as discussed the SBMO may be highly efficient at knocking-down *sulflc* and a minimum level of *sulflc* may be needed for the embryo to survive, similarly *sulfl* knockout mice show increased mortality in the first few months<sup>349</sup>. Secondly, as discussed previously MOs can induce off-targeting effects which can manifest as a variety of outcomes<sup>395</sup>. It is possible that although the SBMO is capable of knocking down *sulflc*, it also induces MO off-targeting effects which lead to decreased survival and/or non-specific defects. In support of the latter hypothesis, the *sulflc*-SB morphants exhibited a high percentage of non-specific phenotypes.

The variability in the death rate at 24hpf was a limitation to the study as it was difficult to judge mortality induced by a particular MO injection as true function of *sulflc* knockdown, since high mortality rate (18-26%) was seen in the control injected and non-injected. Female zebrafish of breeding age can lay hundreds of embryos every week which are fertilised by a male outside of the mother. A proportion of these embryos die possibly due to developmental defects. Various possibilities could account for this variability such as the general health of the adult fish and their eggs. In support of this the mortality rate of non-injected and ATGMO-injected at UMBSF was significantly higher than the *tg(flkl:GFP;gata:dsRed)* observed at the University of Oxford and subsequent attempts to breed from the adult *flkl:gata* fish at UMBSF have proven to be very difficult. However this is unlikely to be restricted to aquarium conditions and animal husbandry as the AB (wildtype) injected embryos derived from the UMBSF showed a higher survival rate up to 24hpf compared to the *tg(flil:GFP;gata:dsRed)* embryos, in the same aquarium (data not shown). Although it is not known why the *tg(flil:GFP;gata:dsRed)* embryos show decreased survival in the first 24 hours following fertilisation, it is possible that the adult strain is less healthy or more inbred than other strains, thus yielding a higher percentage of abnormal or unhealthy embryos. Nevertheless similar *sulflc* morphant phenotypes were achieved in the AB and *tg(flkl:GFP;gata:dsRed)* (also on an AB background) at the University of Oxford using both

MOs utilised in this study (data not shown). It is therefore concluded that the problems associated with the zebrafish at the UMBSF was an unfortunate hindrance but did not affect the morphant phenotype.

#### 4.4.4 The ATGMO specifically knocks-down *sulflc*

The ATGMO was shown to effectively knockdown *sulflc* expression in the *tg(fli1:GFP;gata:dsRed)* strain. To test the reproducibility of the ATGMO, injections were performed in the *tg(flk1:GFP;gata:dsRed)*. Both strains were maintained on an AB background so it was therefore not surprising that an almost identical *sulflc* morphant phenotype was achieved in both strains. The results of the ATGMO HPLC in combination with the highly specific and reproducible phenotype induced by the ATGMO suggest that this MO is specific for *sulflc*. However the percentage of the *sulflc* morphants were greater in the *tg(flk1:gata)* line even at the higher doses. As discussed previously the animal husbandry and general health of the strain may have contributed to the relatively moderate penetrance of morphants in the *tg(fli1:gata)* line. Interestingly sequencing of the ATGMO sites revealed a heterozygous polymorphism within the *tg(fli1:gata)* but not the *tg(flk1:gata)*. The nature and prevalence of this sequence variant was not investigated further and it is therefore possible that heterozygous (C:T) as well as homozygous (C:C or T:T) variants of this polymorphism are carried within the *tg(fli1:gata)* population. This was found to be the case for the *p53<sup>-/-</sup>* zebrafish which are also maintained on an AB background at UMBSF (Fig 4.3). Thus, the ATGMO may be less efficient at knocking-down *sulflc* in embryos carrying the homozygous mis-match thymine nucleotide; these ATGMO-injected embryos may be seen as wild-type or with a less mild morphant phenotype. This may explain why a small percentage of S1c-ATGMO exhibited defective axial circulation but normal cranial circulation (data shown in next chapter)

Although the *tg(flk1:gata)* strain is also on an AB background the SBMO target site in this strain was identical to the synthesised ATGMO possibly explaining the greater number of *sulflc* morphants seen in this strain compared to their counterparts. Despite this caveat, the results show that a clear, specific and reproducible morphant phenotype can be achieved with the ATGMO in the *tg(fli1:gata)* strain. As a greater number of *sulflc* morphants were generated in the *tg(flk1:gata)*, it is hypothesised that the polymorphism in the strain reduces the efficacy of the ATGMO and is therefore evidence to its specificity for *sulflc*. If time and zebrafish stocks had permitted, *tg(fli1:gata)* adult zebrafish could be separated on the basis of

their genotype and injections performed in the offspring of adult zebrafish whose ATGMO target sequence is identical to the synthesised MO to see if this increases the number of morphants. It would be of interest to confirm the specificity of the ATGMO by injecting *tg(fli1:gata)* carrying homozygous cytosine alleles and homozygous thymine alleles.

#### **4.4.5 The characteristic features of *sulflc* morphants can be partially rescued**

To test the specificity of the *sulflc* morpholinos and obtain further validation of the *sulflc* morphant phenotypes it is recommended to co-inject MO with an RNA/DNA construct of *sulflc* to rescue the *sulflc* morphant. For example, if this does not reproduce the morphant phenotype then it is hypothesised that the MO is specific for the *sulflc* transcript. Initial experiments were performed with injecting *sulflc* mRNA alone to titrate to a dose where no ‘ectopic’ phenotype was observed. Interestingly in all the doses injected we observed a range of mutants displaying severe developmental defects. Mutants often exhibited gastrulation defects associated with convergent extension, poorly developed forebrain and notochord and somite defects. However characteristic in all these mutants was the cyclopia phenotype (Appendix I). This ‘overexpression’ phenotype was also consistent with the findings of Dr Ken Kramer (NIH, Bethesda). However this ‘overexpression’ phenotype bears some though not complete resemblance with ectopic sulf phenotype of *xenopus* embryos<sup>352</sup>. Although *xenopus* embryos display poorly developed forebrain and shortened body axis increasing the concentrations of the *sulflc* mRNA did not induce the cyclopia phenotype. This could be attributed to possibly the differential localisation of the *sulflc* mRNA expressing cells, since injection of *sulflc* mRNA in *xenopus* in the ventral two blastomeres produces a phenotype that strikingly contrasts with the phenotypes observed from injecting in the presumptive mesoderm layer, thus the latter displaying bearing similar characteristic traits with our ‘ectopic’ *sulflc* phenotype.

In zebrafish the cyclopia phenotype is associated with two classes of mutants; in the first class of mutants *cyclops* and *one-eyed pinhead*, large parts of the ventral CNS do not form, this is followed by a reduction in the optic stalk and fusion of the retinae in developing eye at the ventral-mid forebrain<sup>405-407</sup>. In these mutants cyclopia is correlated with low levels of Hh<sup>408,409</sup>. In the second class of mutants such as *silberblick*, *tribolite* and *knypek* (also *knypek* and *tribolite* double mutants) the formation of the ventral CNS is disturbed resulting in

malformed ventral midline, this is followed by incomplete separation of the eyes. In these mutants partial/full cyclopia significantly correlates with reduced levels of *wnt-11* signalling<sup>131,405,410,411</sup>. This would imply that ectopic *sulf1c* expression negatively regulates *wnt* or *shh* signalling. Our results contrast with previous *in-vitro* and *in-vivo* reports show that overexpression of Qsulf1 has a positive role in Wnt and Shh signalling<sup>350,352,355</sup>. Although our 'overexpression' phenotype has not been definitively proven, the striking similarities may represent an unidentified signalling mechanism involved in cyclopia, modulated by zebrafish *sulf1c*. While the nature of 'overexpression' phenotype was not investigated further it would be interesting to further confirm the specificity of this phenotype by injecting zebrafish sulf1c protein versus sulf1c mutant protein and assess the HS disaccharide content of these embryos. Experiments designed to test the signalling pathways affected by ectopic *sulf1c* expression would further corroborate the conserved function of zebrafish *sulf1c* protein

Co-injections of SBMO with the lowest concentration of *sulf1c* mRNA resulted in partial rescue of the mild morphant phenotype as a significant percentage of embryos displayed wildtype morphology. Despite increasing the concentration of the *sulf1c* mRNA a greater rescue of the moderate morphant phenotype was not observed. Interestingly we observed a greater rescue in the axial and cranial circulatory defects exhibited by the *sulf1c* morphants, suggesting this was specific to loss of *sulf1c* activity. Although there was a high percentage of morphant displaying the morphological defects in the head this decreased with increasing dose of mRNA, and instead of observing a concomitant increase in the wildtype embryos we observed an increase in the cyclopia phenotype. It was difficult to judge if these head morphological defects were specific to *sulf1c* activity. However partial rescue was obtained in the mild morphants suggesting precise levels of *sulf1c* activity are required for normal development of the zebrafish embryo and this is under strict regulation both spatially and temporally. In support of this we observed a higher percentage of morphants exhibiting normal axial circulation compared to cranial circulation. As the cranial circulatory defect appears later in development, the lower percentage of rescue maybe a reflection on the spatial expression and short half life of *sulf1c* mRNA.

Although more rescue experiments could be done to further confirm specificity it must be noted a higher percentage of rescue is difficult to achieve particularly as *in-situ* data show the *sulf1c* is ubiquitously expressed both spatially and temporally and therefore a small amount is likely to induce an overexpression phenotype. Considering sulf1 orthologs are highly conserved it may be possible to use synthesised *sulf1* RNA from another species to rescue the

morphant phenotype if there were sufficient base mismatches in the ATGMO target region. Unfortunately such an experiment was not possible in the time frame given for this project.

While we could significantly rescue the circulatory defects of *sulflc* morphant it was undetermined whether the morphological defects in the head could be rescued such as the small head, eyes, narrow mid-hindbrain boundary and hindbrain oedema. These phenotypes are characteristic off-target effects thought to be mediated partially or completely by non-specific upregulation of p53 induced cell death. Off-target effects cannot be predicted and are sequence specific. The authors suggest that the specificity of a particular MO can be tested by either co-injection of a p53 MO to knockdown *p53* expression or MO injection into *p53*<sup>-/-</sup> embryos. Importantly, reduced *p53* levels do not affect embryonic development or specific morphant phenotypes<sup>395</sup>.

Preliminary evidence showed that injection of the ATGMO (5ng) into *p53*<sup>-/-</sup> embryos<sup>396</sup> reproduced almost identical *sulflc* mild morphants observed in the *tg(fli1:gata)* and *tg(flkl:gata)*. Although the small head was evident other morphological defects such as the hindbrain oedema and narrow mid-hindbrain boundary were not detected. Collectively the data imply that the ATGMO is specific for *sulflc* and does cause a mild up-regulation of p53. Interestingly the *p53 sulflc* mild morphants bear greater resemblance to the *tg(flkl:gata)* mild morphants. This contrasts with the head morphological defect possibly being mediated by p53, as it would be expected to observe these defects also in the *tg(flkl:gata)* fish. This suggests one of two possibilities; the observed head defects are specific to *sulflc* knockdown or this maybe a strain specific off-target effect. It has been noted that strain specific phenotypes have arisen from silent polymorphisms (Pers comm. Dr Rooney). Interestingly the majority of these p53-moderate morphants still exhibited features that are assumed to be caused by mis-targeting such as a ventrally curved body axis. Considering non-specific up-regulation of p53 signalling by certain MOs was only recently described<sup>395</sup> it is possible that other, as yet unidentified, signalling pathways are also non-specifically upregulated leading to mis-targeting anomalies.

#### **4.4.6 *Sulflc* morphant phenotype in comparison to other species**

The results presented in this chapter indicate that the MOs designed to target the *sulflc* pre-mRNA can knockdown the wild-type *sulflc* transcript in zebrafish. The results of the HS

disaccharide analysis and RT-PCR in combination with the highly specific and reproducible phenotype induced by the MOs suggest that they are specific for *sulflc*.

*Sulflc* morphants are overtly normal with modest reduction in the overall head and eyes and strong dysmorphogenesis in the DA. Although there is ambiguity over the specificity of the hindbrain oedema and narrow mid-hindbrain boundary in these morphants the possibility that this phenotype is *sulflc* specific cannot be ruled out. This may allude to more strain specificity affect than MO specificity. In agreement with the *sulfl<sup>-/-</sup>* mice, that are normal viable and fertile we found *sulflc* morphants were also viable despite the mild morphological abnormalities However the lack of early vascular phenotype may not have been observed due to the later expression of these genes in amniotes<sup>357,412</sup> as compared to zebrafish *sulflc* that has both maternal and zygotic expression.

However the *sulflc* morphants do bear some resemblance morphologically with knockdown of *sulfl* in *xenopus* embryos. Consistent with our observations *xenopus* morphants displayed defects in the anterior head structure; particularly the size of the forebrain and eyes is reduced. The more severe *xenopus* morphants display no eye lens, reduced retina formation, shortened body axis with poorly differentiated somites and loss of floor plate. However we did not observe these latter defects even in the moderate morphant. A small percentage of *sulflc* injected embryos displayed similar characteristics such as the severe dorsalisation of anterior posterior body axis, however we classed these as non-specific mutants as they were infrequently present in S1c-MO and control injected samples. Further injections at the higher concentration were unsuccessful due to the toxicity of the of the S1c morpholinos. The mild differences between *sulflc* morphants and the *xenopus* morphants maybe down to several possibilities; one *sulfl* in *xenopus* is differentially expressed to zebrafish *sulflc* in a temporal and spatial manner for example we detected strongest expression in the vasculature and somite boundaries in contrast to *xenopus* expression at the equivalent tailbud stage. Secondly the efficacy of the MO, the authors were able to efficiently knockdown *xsulfl* with SBMO while we detected low levels of endogenous *sulflc* mRNA after knockdown suggesting this may contribute to the lack of severe phenotype. Alternatively targeting to different regions of the *sulflc* mRNA may imply that the removal of the exon containing cysteine residues results in a more severe phenotype, unfortunately we were unable to target this exon from either end of the intron, due to the high percentage of non-specific targets identified via blast and therefore targeted a second region of the enzymatic domain. However it has also been noted differences in defects can occur in a species dependent manner, observations have been made with HS6STs, for example mice deficient HS6ST show defects in normal axon branching<sup>413</sup>

whilst *c.elegans* lacking HS6STs exhibit axon navigation defects at the optic chiasm<sup>414</sup>. Equally the lack of severe phenotype maybe owed to the genetic redundancy between other genes encoding for the sulfatases. This has been shown to be the cases in mice *sulf1* or *sulf2* knockouts that display mild phenotypes although double knockout mice display gross reduction in bodyweight and die shortly after birth<sup>349,357,360</sup> implying that these enzymes have overlapping functions *in vivo*. Although *xenopus sulf1* and *sulf2* display overlapping expression in the hindbrain and neural tube<sup>362</sup> the function of *xsulf2* has not been proposed. In this chapter we have shown that expression of the *sulf1c* transcript in zebrafish can be knocked down and can consequently affect HS structure *in vivo*. The reproducibility of our phenotype by both MO and consistency amongst different transgenic lines further strengthens the specificity of the phenotype and the fact that we observed similar phenotypes in embryos classed as non-specific mutants, suggests a greater likelihood that our ATGMO and SBMO are targeting the same genetic pathway i.e. the *sulf1c* gene. The phenotypes observed in *xenopus* embryos in combination with our studies, implies *sulf1* has many development roles consistent with the diverse nature of HS to participate in many different signalling pathways.

## Chapter 5.0 Paper two

Running Title: A novel role of zebrafish *sulflc* in arterial venous identity

**Authors:** Bushra Gorski<sup>1</sup>, Xing Ma<sup>2</sup>, Tim Chico<sup>2</sup>, Ken Kramer<sup>3</sup>, Feng Liu<sup>4</sup> Roger Patient<sup>4</sup>, Sally Stringer<sup>1</sup>

### Submitting to Blood

- 1 Division of Cardiovascular Science, University of Manchester
- 2 Developmental and Biomedical genetics, University of Sheffield
- 3 NIH, Bethesda Maryland
- 4 Weatherall institute of molecular medicine, University of Oxford

### **Author Contributions:**

Bushra Gorski: Planned the experiments, carried out data analysis and wrote the complete manuscript.

Xing Ma and Tim Chico: Originally identified the defect and carried out preliminary work and provided the *flkl:GFP* and *gata:dsRed* transgenic lines.

Ken Kramer: Identified the zebrafish *sulflc* homologue and generated the full length *sulflc* construct for rescue experiments and *in-situ*.

Feng Lui: Provided the vascular probes for the In-situ work and carried out some of the confocal imaging.

Roger Patient: Provided the *flkl:GFP;gata:dsRed* transgenic line and most of the confocal and in-situ analysis was carried out in Patient lab.

Sally Stringer: Initially designed and planned the project. Also critically read and made helpful suggestions in preparation of the manuscript.

**Acknowledgments:** We acknowledge University of Manchester Medical School strategic studentship and BHF for funding, B.G and S.S. We also like to thank Diabetes UK, the BSU staff at the University of Manchester for taking care of the aquarium. Also staff at the confocal microscope core facility in Faculty life sciences, University of Manchester.

## Abstract

In the last 5 years it has become clear that pericellular HSPGs are essential for ligand receptor complexes and gradient stabilisation of key vascular growth factors including FGF, and VEGF. In particular the 6-O sulphate groups on Heparan sulphate (HS) chains are critical to modulating these interactions. The VEGF signalling pathway is essential for many aspects of blood vessel formation including arterial differentiation. Our study has focused on elucidating the role of the *sulf1c* enzyme that acts to fine tune HS interactions by removing 6-O-sulphation from HS during vascular development.

Our results show *sulf1c* transcript to be spatially and temporally expressed in the endothelium of the head and tail during vasculogenesis and angiogenesis. Loss of *sulf1c* results in defects in initial vascular patterning and maturation. Confocal imaging of the *sulf1c* morphants at 26hpf revealed strong dysmorphogenesis in the caudal aorta and cranial central arteries thus leading to vascular occlusion of the distal aorta and lack of circulation. Expression of arterial markers downstream of VEGF signalling such as *notch*, *delta* and *ephrinB2* are severely reduced at 24hpf with a concomitant increase in expression of the *flt4* venous marker in the dorsal aorta. Furthermore the structural changes detected by HPLC analysis, show a significant increase in the tri-sulphated disaccharide. Collectively this data implies a novel *in-vivo* role of *sulf1c* in arterial venous identity and arterial vessel maturation.

## Introduction

The development, survival and function of all organs is critically dependent on the blood supply being channelled through a vast network of correctly patterned blood vessels. The formation of blood vessels occurs by two distinct processes; vasculogenesis is the *de novo* formation of vessels from angioblast; angioblasts migrate from lateral plate mesoderm to ventral midline where they differentiate into endothelial cells that form mature vascular tubes. In angiogenesis new vessels sprout from pre-existing vessels and are further remodelled to form a mature blood vessels<sup>1</sup>. The formation of a mature functional vascular network relies on a plethora of growth factors and their receptors, such as vascular endothelial growth factor (VEGF), angiopoietins, and ephrins. Most notable to these processes is VEGF as its activity is critical to the function and maintenance of the vascular endothelium<sup>2</sup>. Aside it's well characterised role for many aspects of blood vessels formation including proliferation, migration and as a vascular permeability factor of endothelial cells. Recent experimental

evidence in zebrafish has shown VEGF to have a role in arterial venous differentiation through a pathway controlled by sonic hedgehog (*Shh*). Loss of *shh* leads to downregulation of VEGF, which attenuates *notch* signalling. While VEGF overexpression can rescue arterial differentiation in embryos lacking *shh* activity but cannot rescue arterial expression in embryos deficient for *notch* function. Notch activates the expression of arterial markers such as ephrinB2<sup>3</sup>. Importantly this molecular distinction between arteries and veins is one of the early events of vascular development that leads to the expression of specific arterious and venous markers such *ephB2a* and *ephB4* respectively<sup>4</sup>. Genetic loss of arterial venous specification leads to the expression arteriovenous malformations and consequently circulatory defects. In humans this is thought to be responsible for congenital hereditary arteriopathies such as HTT (hereditary hemorrhagic telangiectasia) characterised by anomalous fusion between arteries and veins<sup>5,6</sup>. Identification of other regulators will enhance our understanding of blood vessel formation and could provide the basis for therapeutic targets.

Several studies have demonstrated the absolute requirement of heparan sulphate proteoglycans (HSPGs) in regulating VEGF<sub>165</sub> receptor signalling complex both in *vitro* and in *vivo*<sup>7,8</sup>. Structurally HSPGs are composed of HS attached to core protein at the cell surface and in the extracellular matrix. Regulation of biological process by HSPGs is achieved mainly through the distinct sulphation patterns created by the sulfotransferases and sulfatases. Previous *in vivo* studies in zebrafish have shown loss of 6-O sulphation in HS6ST2 morphants display defects in angiogenesis showing reduced branching in the caudal plexus and the penetrance of these morphants increases synergistically with low levels of VEGF suggesting a correct level of 6-O sulphation is critical in VEGF mediated angiogenesis<sup>9</sup>.

Sulfatases are extracellular enzymes that act at the final modification step of HS biosynthesis removing 6-O sulphate groups from the HS chain thus providing the final level of control in ligand–receptor signalling<sup>10</sup>. Sulfatases can positively or negatively regulate growth factor signalling pathways depending on the significance of 6-O sulphated HS epitopes to the HS binding ligand/receptor. For example ectopic *sulf1* expression can inhibits VEGF and FGF mediated angiogenesis<sup>11,12</sup>, interestingly desulfated HS can also enhance Hh signalling<sup>13</sup>. Conversely loss of *sulf1* function can promote VEGF and FGF mediated angiogenesis<sup>11</sup>. This highlights the level of complexity that is added by *sulf1* in HS mediated physiological processes. However the physiological role of *sulf1* during vascular development is relatively unknown.

Over recent years the zebrafish has emerged as valuable tool for studying both physiological and pathological vascular development<sup>14</sup>. In addition to its optical transparency, the ability of embryos to survive in the absence of a functional vasculature network has made it particularly amenable to vascular studies. The striking degree of conservation of cell signalling pathways in developing vasculature has allowed us to address the role of HS modifying enzymes sulfatases (sulfs) in blood vessel formation.

Three sulfs have been identified in zebrafish showing homology to mammalian sulf family, however *sulf1c* only displays expression in the trunk vasculature. Here we report the characterisation and functional analysis of a unique role of *sulf1c* gene during vascular development in zebrafish. *Sulf1c* is strongly expressed in the developing vasculature of the head and tail during mid-somitogenesis and this broad pattern of expression continues to be expressed during angiogenesis. Embryos lacking *sulf1c* expression show defects in axial vessel patterning and maturation characterised by arterial malformations and lack of blood circulation. In association with these morphological defects, loss of *sulf1c* causes downregulation of arterial markers such as *notch5*, *deltaC*, *ephrinB2* with concomitant overexpression of the venous marker *flt-4* (*Vegf* receptor 3) in the caudal artery. We also observed downregulation of *vegf* and *ang-1* in the cranial vasculature. We propose a role of the HS modifying enzyme *sulf1c* in arterial venous identity.

## Methods

### Zebrafish stocks

Transgenic fish (Tg) were housed in the BSF at University of Manchester, Tg(*fli1*:GFP)<sup>15</sup>, Tg(*flkl*:GFP)<sup>16</sup>. Tg(*gata1*:dsRed)<sup>17</sup>. Double transgenic Tg (*flkl*:GFP;*gata1*:dsRed) were developed by paired matings. Both *fli-1* and *flk-1* promoters are expressed in the endothelial lineage and *gata-1* expressed in the erythrocyte lineage Embryos were raised under standard conditions at 28°C and staged as described in <sup>18</sup>. For in situ hybridisation and morphant analysis, embryo media was supplemented with 0.003% 1-phenyl-2-thiourea after 24hpf to prevent melanin formation <sup>19</sup>.

### Isolating zebrafish *Sulf1c* cDNA

*Sulf1c* was identified by a blast search of the human *sulf1* gene against the *Danio rerio* genome on *Ensembl*. Three extracellular *sulf* homologs were found of comparable homology to human sulfatase; namely *sulf1c* on chromosome 24, *sulf2* on chr 11 and *sulf2a* on chr 23. The full length fragment was cloned into the pCS2+ vector The deduced amino acid sequence of *sulf1c* (Acc nu:NM\_0010023846) was aligned with *Mus musculus* and *Homo sapiens* sulf1 using Clustalw alignment software 2.0. Real time polymerase chain reaction (RT-PCR) analysis was performed using the following primer set for *sulf1c* (*forward*: 5'TGTCTTCCAGGAGCAGTGTG3'; *reverse*: 5'GAGCTTGCCATGAAGGTGAC-3'). PCR primers were designed to amplify the 700bp from the translation initiation site of the zebrafish orthologue. Structural features of the zebrafish *sulf1c* protein were predicted using *Pfam* <sup>20</sup>.

### Confirmation of knockdown *sulf1c*-SB morpholino

RNA was extracted from zebrafish embryos at several different time points. Wildtype and morphant embryos (20-30 per group) were sonicated in trizol and cleaned up using RNeasy kit (Invitrogen). RNA was purified following manufacturers instructions. cDNA synthesis was carried out in a total volume of 20µl using 1µg of purified RNA, 20U of AMV reverse transcriptase. PCR was performed in a total volume of 50µl, 1.5mM MgCl<sub>2</sub>, and 10pmol of primers. Primer sequences used to detect wildtype *sulf1c* transcript were same as mentioned above. Primers used to detect Intronic region of *sulf1c* transcript were as follows

*Intron3 forward*: 5'CCAGGTAAAGTGTAGCTATGGCAA-3';

*Exon4reverse*: 5'GGACGTCCGCAAATAGTTGA-3.

Housekeeping gene  $\beta$ -actin (*forward*: 5'-CCTCCGTCGTA CCACTGGTA T-3'

*reverse*: 5'-CAACGGAAGGTCTCAT TGCCGATCGTG-3'.

Experiment were repeated in triplicates.

### **Whole-mount in situ hybridisation**

For generation of *sulflc* in-situ probe, primers were designed to isolate 5'UTR region of *sulflc* gene, region of non-homology between the remaining two sulfs homologs. cDNA was amplified using the following set of primers (*foward*: 5'CCCACGATACAGACCTCGTT-3'; *reverse*: 5'GAGCTTTGCTGTCCACTTCC-3'). The PCR fragment of 511bp was TA cloned into pGEMT vector (Promega, Madison) and the orientation confirmed by sequencing the PCR product. Whole mount RNA in-situ was carried out as previously described in Jowett and Lettice 1994<sup>21</sup>. Dioxygenin labelled RNA probes were transcribed from linear cDNA constructs, *Vegf*, *notch5*, *deltaC*, *ephrinB2*, and *flt-4*. Staining was monitored under a dissecting microscope and embryos mounted in 80% glycerol for imaging. Brightfield images were taken using Leica stereo microscope at 80x magnification. For higher magnification (x100) images were took using Zeiss Axioimager Z1 compound microscope, using a plan aprochomat 10x/0.45 objective.

### **Morpholino mediated knockdown of *sulflc* and rescue experiment.**

Antisense morpholinos (Gene tools, Corvallis OR)

S1c-ATG (5'-CACCAGCTGCATCATGGGACTGCGA-3') and

S1c-SB (5'-GTAGTCCTGGTAGTGGTAGAATAAT-3') were directed against the 5-ATG start codon and the predicted splice acceptor site at the end of exon 3 respectively. Mismatch

S1c-MO (5'CACgAGgTGgATCATcGGACTcCGA-3') was used as a control for all experiments. Embryos were routinely injected into 1-4cell stage embryos at a concentration of 4-5ng with 0.01% of phenol red. For rescue experiment embryos, *sulflc* full length construct was cloned into pCS2+ and linearized with *Apal*. SP6 RNA polymerase was used for in vitro synthesis of capped mRNA (Ambion, Austin, TX). Embryos were co-injected with 5ng of *sulflc* MO and 50pg of *sulflc* mRNA.

### **Microangiography**

Red fluorescent carboxylate modified microspheres 0.02µm (Invitrogen) were sonicated for 30secs and microcentrifuged for 2min at high speed. Microspheres were diluted 1:1 with 2% BSA (Sigma) in dH<sub>2</sub>O, and centrifuged at maximum speed for 2min. Embryos were then lowered into 0.8% tricaine agarose bed, and then orientated under the microscope with dorsal

side facing up. Microspheres were microinjected into the sinus venosus/cardinal vein of zebrafish embryos at 50hpf as described in <sup>22</sup>.

### **Microscopy**

Embryos were mounted on depression slides using 3% methylcellulose or for long term imaging embedded in low melting point agarose coated dishes. All live images of blood flow were photographed using a Zeiss Stereolumar V12 images accumulated in axiovision software version 4.6. Lateral and dorsal images of the trunk and cranial vasculature were taken using a Zeiss LSM 510 META confocal laser microscope and all z-stacks of vasculature were generated using Zeiss LSM software.

### **Extraction and SAX-HPLC analysis of HS disaccharides**

HS was extracted from wildtype and morphants as described by Chen *et al* 2005 <sup>9</sup>. Purified HS samples were treated with a mixture of recombinant heparinases I, II and III/ (0.33mIU each, Seikagaku America, USA) in 0.1M sodium acetate buffer, pH 7.0, containing 10mM calcium acetate. The mixture was incubated at 37°C overnight and then made up to 20µl with water to load onto the HPLC. Disaccharide composition was analysed by strong anion exchange and labelled with post-column fluorescent derivatisation. A Pro-Pac PA1 SAX column (Dionex) was equilibrated in dH<sub>2</sub>O pH3.5 and disaccharides were eluted with a linear gradient of sodium chloride (0–1 M over 70 min). Peaks were identified and calibrated by reference to standards of known concentration (0.16nmoles) separated under the same run conditions. The area of each peak was determined using ChemStation software (Agilent technologies).

## Results.

### Identification and cloning of zebrafish *sulflc* gene

Genomic database mining identified three homologs of the extracellular sulfs in zebrafish, one homolog to *HSULF-1*, '*sulflc*' and two homologs to *HSULF-2*, '*sulf2*' and '*sulf2a*'. This paper focuses on the unique role of *sulflc* in the vasculature. Based on the mapping of neighbour genes zebrafish *sulflc* is syntenic with the human chromosomal location 8q13.2 i.e. the region harbouring the *sulflc* gene. The full length of the transcript is 4.6kb (Ensembl Accession number ENSDART00000027022) and was cloned from RNA isolated from zebrafish at 24hpf.

The predicted amino acid sequence reveals (Ensembl analysis zebrafish assembly version 7.0, sanger institute Cambridge UK) 73% identity to human and murine *sulf1*, with nearly perfect conservation of the sulfatase domain. The cDNA encodes a putative 874 amino acid protein organised into three conserved domains, N-terminal, hydrophilic and C-terminal (Figure S1). The N-terminal retains the enzymatic sulfatase domain, featuring the conserved cysteine residue site that undergoes posttranslational modification to form N-formylglycine critical for the hydrolytic cleavage of the sulphate group from the substrate<sup>23,24</sup>. In addition all the asparagine linked glycosylation sites in the enzymatic and C terminal shown to be important in heparin binding are also conserved<sup>25</sup>.

### Spatial and temporal expression of *sulflc*

*Sulflc* transcripts were present in fertilized embryos at developmental stages prior to the onset of zygotic transcription, indicating that these messages are maternally derived (Figure 1A). From RT-PCR consistent levels of expression can be observed during gastrulation and somitogenesis with expression downregulated at 48hpf.

To investigate the potential role of *sulflc* during vascular development, we examined the expression profile of *sulflc* in more detail. By whole mount in-situ (Figure. 1B) we detected *sulflc* expression from 50% epiboly stage to 48hpf. At the onset of gastrulation *sulflc* transcripts appear diffused throughout the blastoderm and can be detected along the entire dorsal axis. During early and mid somitogenesis stages (10-22hpf) strong *sulflc* expression can be detected in the eye, presumptive midbrain-hindbrain structures, dorsal floorplate of spinal cord, axial vessels and in the somite boundaries. By 24hpf strong expression is maintained in these regions with strong expression in the heart, branchial arch and caudal plexus. Interestingly at this time point blood circulation is being initiated, and the caudal

plexus is actively formed by angiogenesis as evident with expression of the *flk1* (VEGFR) marker at 24hpf. At 48hpf expression is restricted to the head with strong expression in the anterior neurocranium, otic vesicle and in the cranial vasculature including the primordial hindbrain channel (PHBC). Expression is maintained in the main axial vessels and pronephric ducts.

### **Morpholino knockdown of *sulflc* message**

To assess the functional role of *sulflc* (S1c) in zebrafish vascular development, we designed two independent antisense morpholinos, one to target the ATG start codon to inhibit protein translation and the second designed to target the predicted splice acceptor site at the Intron3-Exon4 boundary, to inhibit correct splicing of the *sulflc* pre-mRNA. Tg(*flk*:GFP;*gata*:dsRed) transgenic zebrafish embryos in which GFP and dsRed expression is driven by the promoters of the pan-endothelial and erythroid markers *flk-1* and *gata-1* respectively, were injected at the 1-4 cell stage with 5ng of S1c-ATGMO and the development of vasculature morphology directly observed in live embryos.

Brightfield analysis of the S1c-injected embryos at 1dpf revealed reproducible and consistent morphological abnormalities (Figure 2A-I). At 5ng of S1c-ATGMO, 63% of *sulflc* morphants exhibited a “characteristic phenotype” with mild reduction in the size of the head and eyes and an expansion of the ventral mesoderm tissue in the tail, in comparison to control MO injected samples. By 2dpf, the morphological appearance of the head appeared relatively unchanged with majority of morphants displaying pericardial oedema and defects in the trunk circulatory pattern became more apparent. At the caudal end of the trunk, morphants displayed no blood circulation and in the most extreme cases blood cells could be observed leaking from the trunk vasculature, moving dorsally and pooling in the extravascular tissue of the tail caudal plexus (Figure 2D,F,H). Although the head morphology appeared overtly normal 50% of morphants displayed haemorrhage at 3dpf (Figure 2G) with weak circulation beginning in the most caudal end of the tail. Due to the mild circulatory defects and enlarged pericardial oedema we measured the heart rate and observed no significant changes (T.Chico unpublished observations). A subset of *sulflc* morphants were categorised as moderate and displayed similarly consistent circulatory defects, however these morphants displayed an overall ventrally curved body axis (Figure S2). Since it was difficult to assess if the vascular and circulatory defects in this class of morphants was a primary affect of the morpholino, these morphants were excluded from further analysis and results from here on in refer to the characteristic phenotype as the *sulflc* morphant.

The specificity of the characteristic phenotype was further confirmed by another set of morpholinos. The advantage of using a splice blocking morpholino is that its effectiveness can be confirmed by RT-PCR (Figure 2J-M). The *sulf1c* morphant was reproduced with this morpholino albeit a lower dose and penetrance levels. Conventionally this splice blocking morpholino acts to eliminate exon4 from the *sulf1c* message a region of the enzymatic domain of *sulf1c*, thus causing a shift in the open reading frame and introducing a premature stop codon resulting in a predicted non functional shorter *sulf1c* transcript. From RT-PCR analysis we found the *sulf1c* wildtype activity to be reduced until at least 48hpf (Figure 2M) at the optimum dose injected but were unable to detect the predicted shorter aberrant *sulf1c* transcript. At MO targeting certain splice junctions it has been reported inclusion of the whole or partial intron<sup>26</sup>. We designed new primers to test this alternative hypothesis and found a shorter transcript containing a stretch intron3 and exon4 in the final *sulf1c* mRNA that increased with increasing dose of SBMO. To eliminate the possibility of short product being amplified from genomic DNA, primers were tested in equivalent RNA extracted samples and no band of similar size was observed (data not shown). Entering the sequence of the possible inclusion of the whole intron into the open reading frame finder (NCBI) revealed introduction of several stop codons in the intron3 region suggesting the likely formation of an aberrant *sulf1c* transcript.

Published research estimates 15-20% of morpholinos exhibit off-target effects, and that these non-specific effects are mediated through the activation of the apoptotic p53-dependent pathway. Affected embryos display neural death at 24hpf and develop with characteristically small head and eyes<sup>27,28</sup>. Since *sulf1c* morphants displayed small head and eyes we tested the specificity of ATGMO in homozygous p53<sup>-/-</sup> fish<sup>29</sup>. Encouragingly the defects in 'characteristic phenotype' were reproducible in the p53<sup>-/-</sup> fish suggesting the effects do not cause non-specific upregulation of p53 (data not shown).

### **An increase in 6-O sulphation of *sulf1c* morphants**

To further confirm the specificity of the *sulf1c* phenotype we determined if the S1c-ATGMO could affect the structural modifications of HS *in vivo*. Previous reports show sulfatase act at the cell surface and can remove 6-O sulphate groups from tri-sulfated, di- and mono sulfated disaccharides<sup>30,31</sup>.

HS extracted from 48hpf wildtype and *sulf1c* morphants was digested into disaccharides and separated by HPLC. Peaks were assigned by comparison to known standards. Specificity of the morpholino was assessed by determining the sulfation profile of the disaccharide

components of the wildtype versus S1c-ATGMO injected samples. Six disaccharides were present including the three sulphated disaccharides (Figure 3.0A). A general increase was observed in both the di and tri-sulphated disaccharides  $\Delta$ UA-GlcNS6S,  $\Delta$ UA2S-GlcNS6S respectively in the 48hpf *sulflc* morphant embryos compared to control though only the increase in the tri-sulphated disaccharides UA(2S)-GlcNS(6S) was statistically significant ( $P < 0.05$ ) with a concomitant decrease in the di-sulfated UA(2S)-GlcNS (Figure 3.0B). This is consistent with HS disaccharides desulfated by mice and quail *sulfl*<sup>30-32</sup>. Analysis of heparan sulphate composition was performed in duplicate with similar outcomes. There was no change in HS derived disaccharides from control MO injected samples indicating the changes observed were not a result of stress due to injection. These results suggest zebrafish *sulflc* can desulfate similar HS disaccharide species implying conservation of function. However the moderate changes in 6-O sulphation imply there are other sulfatase genes in the zebrafish that can compensate for the remaining sulfatase function.

### **Circulatory defects of *sulflc* characteristic phenotype**

Also evident in the *sulflc* characteristic phenotype were the circulation problems appearing as early as 29hpf in the tail and at 48hpf in the head of the morphants. The range and penetrance of circulatory phenotypes caused by both ATG and SB morpholinos were examined. These defects ranged from aberrant circulation in the head and tail to a more subtle phenotype in which circulation is reduced in localised regions of the head and tail.

*Sulflc* morphants were segregated at 26hpf (1dpf) on the basis of the embryos displaying the “characteristic phenotype” and analysed at four different time points to determine the precise onset of the circulatory defect. Since morphological defects were observed in head and tail of *sulflc* morphants we recorded both axial and cranial circulation. At 26hpf axial circulation appeared normal in wildtype and *sulflc* morphant embryos with blood flowing in a simple circulatory loop down the dorsal aorta (DA) and returning to the heart via the posterior cardinal vein. At 35hpf circulation proceeds normal in wildtype, blood flows down the DA and CA and is returned to the heart by posterior cardinal vein (PCV). However in both S1c-ATGMO and S1c-SBMO the *sulflc* morphant displayed arterious venous (A-V) shunt in which blood passes caudally down the DA and returned to the heart via the vestigial rostral A-V connection formed at 26hpf. This short circuit results in absent/reduced blood flow in the caudal artery (CA) and caudal plexus (Figure S3). By 48hpf some of the intersegmental vessels (ISVs) in the control embryos are lumenised and gradually begin to possess weak

morphants there is some weak circulation in the ISV's and despite the presence of the A-V shunt blood flow can now reach end of the tail through patent circulatory route provided by the functioning ISV. By 3dpf all ISV possess blood flow and the caudal vein plexus begins to slowly condense down into a single more ventral channel to return blood flow to the heart<sup>22,33</sup>. This proceeds as normal in the wildtype embryos (Figure 4C). Although most of the ISVs possess blood circulation in the *sulflc* morphant the CV remains as a plexus of vessels with A-V shunt preventing blood flow to the most caudal end of the artery as a result blood flow is continuously shunted through dorsally connected ISV's to bypass the obstruction, providing blood to caudal region of tail (Figure 4D). The number of *sulflc* morphants exhibiting the circulatory defect was quantified. Consistently 94% and 95% of the S1c-SB and S1c-ATG *sulflc* morphants displayed A-V shunt (Figure 4I).

Another characteristic feature of the *sulflc* morphants was the reduced head size and the prevalence of haemorrhage at 3dpf, (Figure 2F,G) this prompted our directions towards recording the route of cranial circulation of the morphants. The perfusion of cranial circulation begins a few hours later than trunk circulation<sup>22</sup>. At this early stage heart beat is weak and blood circulation of the *sulflc* morphants is indistinguishable from wildtype (Figure S3). At 35hpf the heartbeat quickens and strengthens and the number of circulating blood cells increases in the control embryos, whilst *sulflc* morphants exhibit weak cranial circulation. By 2-3dpf in wildtype embryos, blood continues to caudally through the lateral dorsal aortae (LDA) and rostrally through the internal carotid arteries (ICA). Each ICA divides into two branches at the base of the eye; the cranial and caudal division. The cranial division continues rostrally whereas the caudal division loops dorsally and caudally to connect to the equivalent branch via the basal communicating artery (BCA). Blood flows caudally to posterior connecting segments into the medially located basilar artery (BA) running dorsal to the hindbrain and blood flow is channelled to the primordial hindbrain channels (PHBC) via the cerebellar central arteries (CCtA) penetrating the hindbrain (Figure 4A,C,G). Three pair of CtA extend from the BCA to the forebrain, midbrain and hindbrain namely the anterior and posterior mesencephalic central arteries (MMcTA, PMcTA) to irrigate the forebrain and midbrain respectively, with CCtA providing arterial feed to the hindbrain<sup>22</sup>. Eventually these vessels all drain into the PMBC (primordial midbrain channel) -PHBC junction carrying venous blood flow. In 86% and 93% of S1c-SB and ATGMO morphants respectively, strong circulation was observed in the main arterial cranial route such as LDA, BCA, BA and PHBC, however we detected little or no circulation in the anterior, posterior mesencephalic central arteries and CCtA penetrating the forebrain, midbrain and hindbrain

respectively (Figure 4B denoted by red arrows). Although by 3dpf, circulation was present in mid-forebrain central arteries, very weak circulation was detected in the CCtA. Furthermore it was noted that 35-51% of S1c-SB and S1c-ATGMO morphants with weak cranial circulation in the hindbrain, further developed haemorrhage in the head (Figure 4J & S5 .C).

To confirm the specificity of the morpholino we co-injected *Sulf1c*-SB morpholino with carefully optimised doses of full length mRNA to rescue the circulatory defects present in *sulf1c* morphants. In three independent experiments analysis of the morphants at 3dpf showed a moderate rescue of the phenotype with 77% of embryos retaining normal axial and cranial circulation (one way ANOVA  $p < 0.05$ ) (Figure 4K). The circulatory defects in the morphants implied a defective vasculature, prompting us to closely examine the vasculature of the *sulf1c* morphants.

### ***Sulf1c* morphants display defects in vascular patterning and integrity**

Most vessels after 24hpf form via angiogenesis such as the ISVs, caudal plexus and a subset of secondary cranial vessels<sup>22</sup>. To determine whether the circulatory defects in *sulf1c* morphants stemmed from defects in vascular patterning prior to circulation we used confocal microscopy to analyse the vasculature of transgenic fish. Early observations at 12ss stage in *sulf1c* morphants showed *flk*<sup>+</sup> positive labelled endothelial cells migrating from the lateral plate mesoderm into the ventral midline, suggestive of correct endothelial cell specification and differentiation from haemangioblast (Data not shown). Close inspection at 26hpf of the developing DA in the wildtype revealed fully lumenised axial vessels with clear initiation of angiogenesis in the caudal plexus and in the trunk, evident by the sprouting of ISVs. In contrast the *sulf1c* morphants showed striking defects in the developing vasculature caudal to the region of A-V shunt (Figure 5A& B). At the site of A-V shunt a mass of rounded shaped endothelial cells appeared to accumulate at the caudal end of the DA thus forming a narrow caudal artery (CA). By 2dpf the morphants revealed strong dysmorphogenesis of the caudal artery (Figure 5D,F). On closer inspection demarcations between the artery and vein are poorly defined in the morphant compared to wildtype embryos that display clearly distinguishable CA and CV boundaries (Figure 5D, H). The poor segregation of axial vessels and lack of lumenisation result in the arteriovenous shunt in the *sulf1c* morphant. In addition the caudal vein plexus caudally proximal to the A-V shunt of the *sulf1c* morphants appeared disorganised. In comparison to the wildtype the increasing mass of rounded endothelial cells do not organise into a branched vascular plexus (Figure 5E and F red arrowheads). This branching defect of the caudal plexus remained relatively unchanged in *sulf1c* morphants at

3dpf. This data implies the blood pooling in the extravascular tissue is likely to be due to the immature formation of the caudal plexus.

Analysis of the head vasculature was also carried out, we followed cranial vessel patterning of embryo until 3dpf. At 1dpf when the cranial circulation is weak in the *sulflc* morphants, the lateral and dorsal images of the cranial vasculature show normal cranial vascular patterning of the primary vessels such as PHBC, BA and MCEV in *sulflc* morphants (Figure S4). However analysis of the endothelial structures on 2dpf revealed striking differences in vessel patterning of a subset of cranial vessels. Although the pattern of the primary vasculogenic vessels such as the PHBC, BA and MCEV appear fully lumenised (Figure 5I,K) confocal analysis revealed very few patent CCTA. The reduced number of CCTA formed thin endothelial cord like tubes either failing to connect to the basilar artery or CCTA that do form the connection are not patent (Figure 5J,L,N). We also observed some existing CtA connections absent by 3dpf (Figure 5N). Such defects are likely to be responsible for weak circulation and the consequent haemorrhage that ensues in these areas of the head. Furthermore this data suggests that impaired central artery lumenisation is the proximal vascular defects in the head of the *sulflc* morphants and is likely to be responsible for the vessel patency.

The vascular defects present in the head and tail of the *sulflc* morphants allude to impaired vascular lumenisation. To confirm the integrity of the functional vasculature (i.e. vessel leakiness and lumen patency) microangiography was conducted in *tg(fli1:GFP)* wildtype and *sulflc* morphants by injecting red fluorescent microspheres into the sinus venosus. Functional circulation was observed in wildtype, whilst in *sulflc* morphants circulation did not progress into the most caudal region of the tail, with circulation of microspheres being blocked at the level of A-V shunt (Figure 5K,L). Simultaneously the fluorescent microsphere could be observed 'leaking' into mesodermal tissue surrounding the cranial vasculature of the hindbrain. This was consistent with previous circulatory defects noted in the *tg(fli & flk1:GFP; gata:dsRed) sulflc* morphants.

### ***Sulflc* morphants lack arterial expression**

In order to elucidate the cellular basis of the caudal artery defect we next analysed the expression of several different markers of endothelial lineage in control and *sulflc* morphants by whole mount in-situ hybridisation (WISH) at 24hpf. No differences in the expression pattern of the pan-endothelial markers *tie-2* and *vegfr* receptor 2 *flk-1* was detected in *sulflc* morphants (Figure 6A) This implies there is no significant defect in angioblast differentiation, proliferation and migration or coalescence of these cells at the midline and that the DA, PCV

and ISV development is correctly initiated with primary vascular tubes present at their proper location. This was consistent with our confocal observations of the vasculature.

To test whether *sulflc* plays role in endothelial cell specification into arterial and venous cells, *sulflc* morphants were analysed for expression of arterial markers such as *notch5*, *delta4*, and *ephrB2*. When compared to wildtype embryos the *sulflc* morphants showed a specific loss of all arterial marker expression in the presumed region of the A-V shunt of the CA, whilst neural expression remained unaffected (Figure 6C-N). To determine consequently the effects on venous cell fate we analysed the expression of the *vegf* receptor 3 (*flt-4*) marker in the *sulflc* morphants. These experiments showed a clear ectopic expression of *flt-4* in the CA in addition to its normal restricted expression in the caudal vein (Figure 6O-R). Thus expression of venous marker is expanded at the expense of a loss of arterial expression. The expression of all arterial venous markers in the head was unaffected compared to the control. Consistent with the morphological defects this data demonstrates a possible role for *sulflc* in specifying arterial-venous identity.

#### ***Sulflc* morphants affects *Vegf* and *Ang-1* expression in head**

Expression of the pan-endothelial marker (*flk-1*) in the head of the *sulflc* morphants appeared to show no differences in expression to wildtype embryos at 24hpf thus suggesting primary cranial vessels are correctly initiated and are present at their correct location consistent with the confocal analysis of the morphants. To test the cellular basis of defect in the central arteries we analysed the expression of pan-endothelial and vascular patterning markers, prior to the onset of the secondary cranial vessel formation. Whole mount in-situ was performed with *ang-1*, *tie2*, *ve-cad* and *vegf* in *sulflc* morphants. Although no difference was observed in *tie-2* *ve-cad* expression in the head of the *sulflc* morphants, weak *vegf* and *ang-1* expression was evident in the mid-forebrain of the morphants compared to wildtype (Figure 7A-L). We further tested *vegf* expression at 28hpf in *sulflc* morphants and found *vegf* to be reduced in the mid-forebrain regions in comparison to control injected (Figure S7). While *in vitro* studies have shown *vegf-1* can upregulate *ang-1* in retinal pigment epithelial cells<sup>34</sup>, this has not been proven in zebrafish, but however suggests *sulflc* could be possibly acting upstream of *vegf* pathway and is consistent with unaltered levels of *vegf* expression in the tail of *sulflc* morphants.

## Discussion

Enormous structural diversity is created by deacetylation, sulphation and epimerisation of HSPGs by HS enzymes, thus providing a platform for HS to bind to a wide range of proteins including morphogens, growth factors that are critical for the proper development and patterning of a functional circulatory system. A specific 6-O sulphation pattern of HS created by HS6STs and sulfatases are essential for vessel formation both *in vitro* and *in-vivo*. This is evident as HS6ST1<sup>-/-</sup> mice die at birth<sup>35</sup> partly due to vascular complications and zebrafish HS6ST morphants display defects in angiogenesis<sup>9</sup>. In this report we propose a novel functional role of the zebrafish *sulflc* orthologue in vasculogenesis and angiogenesis.

In zebrafish *sulflc* is expressed in early through to late-somitogenesis stages, strongest expression can be found in the anterior central nervous system, pronephric ducts, somite boundaries and in the endothelium of the cranial and tail vasculature. In agreement with this, knockdown of *sulflc* results in mild morphological defects in the head and tail of the morphants displaying smaller head and eyes with strong dysmorphogenesis of the axial vessels compared to wildtype. The fact that we did not observe a stronger and earlier vascular phenotype even though *sulflc* is ubiquitously expressed in early stages of development suggests there maybe functional compensation by other sulf enzymes identified in the zebrafish genome sequence. Consistent with these ideas we found only a small increase specifically in HS 6-O sulphation of these morphants. In support of compensatory function mice *sulfl* have functionally redundant roles in skeletal development<sup>36</sup>.

On analysis of the circulatory defects we found a greater number of S1c-ATG morphants displaying A-V shunt and impaired cranial circulation compared to S1c-SB morphant, although the penetrance of A-V shunt was greater in both sets of morphants by 3dpf. The low penetrance in SB-morphants could be attributed to the contribution of maternal *sulflc* mRNA to the gene pool, nevertheless these defects are specific to *sulflc* function as we were able to achieve partial rescue of the circulatory defects.

The lack of circulation in the localised regions of the head and tail are likely to be due to the vascular defects present in the *sulflc* morphant. In the head we observed a subset of immaturely formed secondary cranial vessels (CtA) this was further confirmed by microangiography. To eliminate the possibility that these later appearing vascular defects are a result of changes in rate of blood flow as opposed to genetic defects in the vasculature we measured the heart rate of the morphants and found no significant difference compared to

secondary affect to immature vasculature. The remaining amount of sulfic protein maybe sufficient for other regions of head vessel development. In the tail, we found strong dysmorphogenesis of the caudal artery and A-V shunt, likely to be the cause of lack of circulation in the tail. Similar vascular morphogenetic defects have been described in many other mutants or morphants, of which many have impaired Shh, VEGF or Notch signalling. Particularly in mutants of the VEGF pathway and Notch (mindbomb mutant) display arterious-venous malformations leading to circulatory defects in the cranial vessels, DA And ISVs<sup>37-42</sup>.

In zebrafish arterial identity is controlled by a signalling cascade whereby Shh secreted by the notochord/hypochord induces the expression of VEGF in the somites which in turn signals presumptive arterial cells to upregulate *Notch3* expression. *Notch3* expression is detected as early as 17hpf coinciding with the first wave of arterial angioblast migration to form the DA. During the second wave of angioblast migration to generate the venous vessel, *notch3* acts to downregulate *Flt4* expression in the dorsal aorta and activates *EphrinB2a* to allow DA cells to acquire fully arterial characteristics at 24hpf. In the fully matured vasculature *ephrinB2a* expression is restricted to the DA while *flt-4* is exclusively expressed in PCV<sup>40</sup>. To test if *sulfic* was acting on this pathway we assayed for expression of arterial venous markers. We found the caudal artery is non-functional as a consequence of lack of proper arterial-venous identity. The morphants failed to fully express specific arterial markers *ephrinB2a*, *Notch*, *Delta* in the caudal region of tail while exhibiting normal neural expression suggesting *sulfic* is required for initiation of arterial expression in the DA. As the expression of *tie-2* was unaffected, this further confirmed that there was a loss of expression of arterial markers rather than a loss of endothelial cells. However the of concomitant increase in *flt-4* expression in the CA corresponding to the region loss arterial expression, at a time where its expression should normally downregulated to allow the artery to fully acquire arterial characteristics, suggests that *sulfic* may act to repress venous fate, thus leading to an increase in the vein fate at the expense of the artery. The *sulfic* morphant bears strong resemblance with the *VEGFR2*, *PLC-γ1* (phospholipase C gamma-1) downstream effectors of VEGF and the *mindbomb* mutant<sup>37,38,40</sup>. In all cases only arterial development and differentiation is affected with characteristic loss of arterial expression markers such as *notch* and *ephrinB2a*. Thus consistent with the notion that notch signalling in arterial endothelial cell differentiation is modulated in part by *vegf* signalling output<sup>3</sup>. From *in vitro* based studies 6-O sulphated HS mediated by sulfatases have shown to have a significant role in modulating VEGF activity<sup>11</sup> in particular the 6-0 sulphates group are critical requirement of HS to bind to VEGF<sup>43</sup>. We propose angioblast

specification and differentiation proceeds normal in *sulflc* morphants however during early arterial endothelial differentiation (17-18hpf) an increase in 6-O sulphation in the somite boundaries sequester the bioavailability of somitic VEGF in regions of the caudal artery. In support of this HS binding has shown to be essential to spatially restrict VEGF to regulate vascular branching<sup>44</sup>. However the concurrent increase of 6-O sulphation, co-existing where *sulflc* is expressed during early development i.e. the endothelium at 24hpf suggests some of this arterial identity is restored hence the localised region of loss of arterial expression in the tail. Since we also observed decreased *vegf* expression in the head of the morphants, with concomitant decrease of *ang-1*, the reduced expression pattern of *VEGF* persisted at a later timepoint. It is possible that mild changes in the VEGF gradient in the head of the *sulflc* morphants may create an environment that does not allow complete formation and maturation of later developing vessels i.e. CtA. Further studies will be required to investigate this hypothesis.

Surprisingly we did not detect changes in *VEGF* expression in the tail region of *sulflc* morphants, a possibility is that changes in HS profile by *sulflc* may affect the signalling activity of other HS binding proteins that in turn can mediate VEGF signalling not expression. One possible candidate is *Shh* that acts further upstream of VEGF in the arterial venous cascade, thus *Qsulfl* has shown to regulate *Shh* distribution<sup>13</sup>. Hypothetically loss of *sulflc* may restrict the distribution of Hh in regions where it is normally expressed. Further studies will be necessary to investigate these hypotheses and to identify such a factor. However this study provides the first *in-vivo* evidence of HS modifying gene *sulfl* having a role in arterial venous identity and is necessary for vascular patterning and integrity of arteries. We conclude that subtle changes in sulfate moieties of HS brought about by morpholino mediated knockdown of *sulflc* have specifically localised defects in agreement with the nature of HS enzymes under strict developmental regulation. These results further strengthen the notion that a fine balance of 6-O sulfation pattern provided by *sulfs* is critical to control HS mediated physiological processes. Our findings that *sulflc* affects arterial venous identity and maturation could make it a potential candidate for HTT.

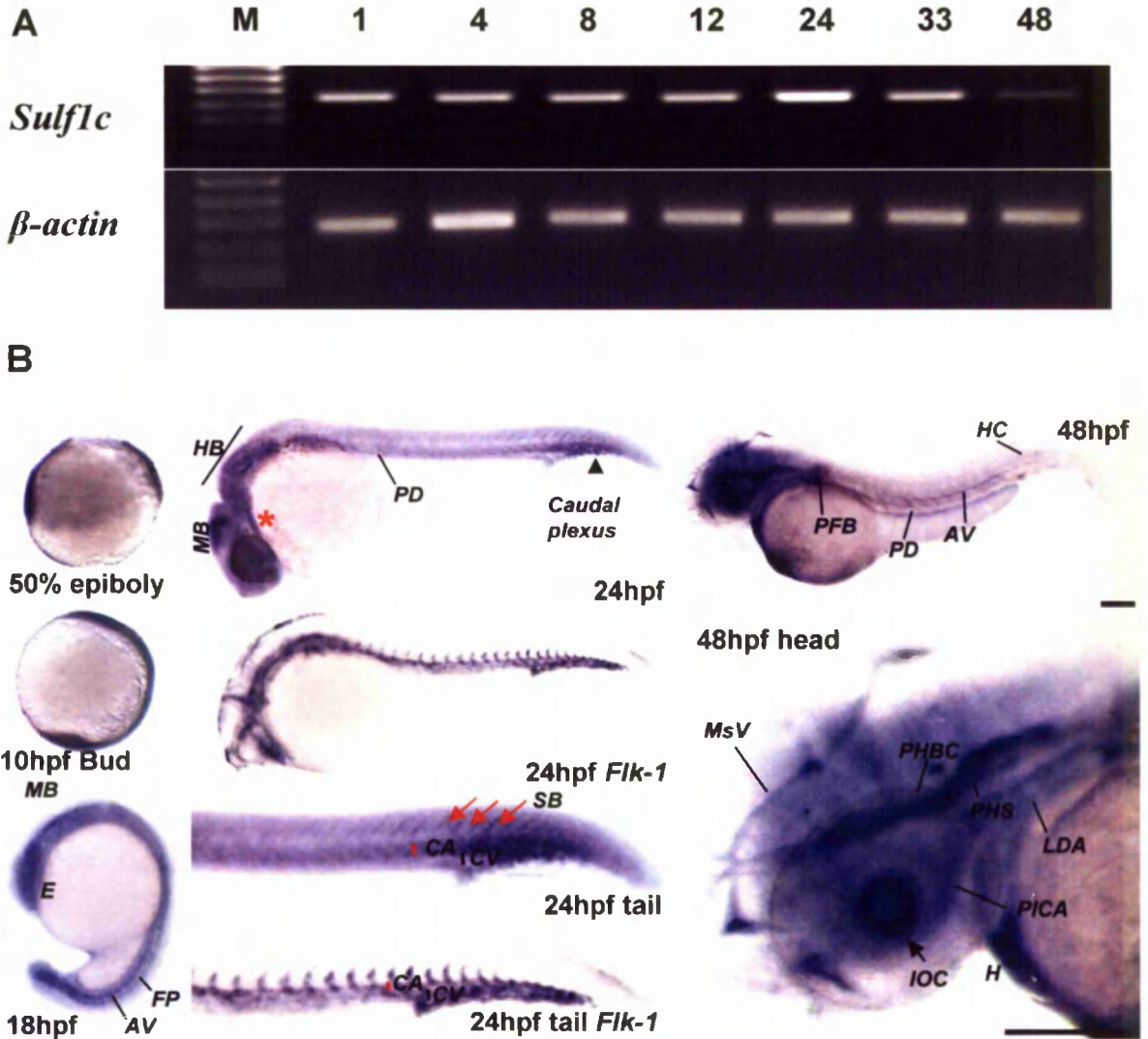
## References

1. Carmeliet P. Angiogenesis in health and disease. *Nat Med.* 2003;9:653-660.
2. Carmeliet P, Ferreira V, Breier G, et al. Abnormal blood vessel development and lethality in embryos lacking a single VEGF allele. *Nature.* 1996;380:435-439.
3. Lawson ND, Vogel AM, Weinstein BM. sonic hedgehog and vascular endothelial growth factor act upstream of the Notch pathway during arterial endothelial differentiation. *Dev Cell.* 2002;3:127-136.
4. Adams RH, Wilkinson GA, Weiss C, et al. Roles of ephrinB ligands and EphB receptors in cardiovascular development: demarcation of arterial/venous domains, vascular morphogenesis, and sprouting angiogenesis. *Genes Dev.* 1999;13:295-306.
5. Irrthum A, Devriendt K, Chitayat D, et al. Mutations in the transcription factor gene SOX18 underlie recessive and dominant forms of hypotrichosis-lymphedema-telangiectasia. *Am J Hum Genet.* 2003;72:1470-1478.
6. Hirashima M, Suda T. Differentiation of arterial and venous endothelial cells and vascular morphogenesis. *Endothelium.* 2006;13:137-145.
7. Ashikari-Hada S, Habuchi H, Kariya Y, Kimata K. Heparin regulates vascular endothelial growth factor(165)-dependent mitogenic activity, tube formation, and its receptor phosphorylation of human endothelial cells - Comparison of the effects of heparin and modified heparins. *Journal Of Biological Chemistry.* 2005;280:31508.
8. Jakobsson L, Kreuger J, Holmborn K, et al. Heparan sulfate in trans potentiates VEGFR-mediated angiogenesis. *Dev Cell.* 2006;10:625-634.
9. Chen E, Stringer SE, Rusch MA, Selleck SB, Ekker SC. A unique role for 6-O sulfation modification in zebrafish vascular development. *Dev Biol.* 2005;284:364-376.
10. Gorski B, Stringer SE. Tinkering with heparan sulfate sulfation to steer development. *Trends Cell Biol.* 2007;17:173-177.
11. Narita K, Staub J, Chien J, et al. HSulf-1 inhibits angiogenesis and tumorigenesis in vivo. *Cancer Res.* 2006;66:6025-6032.
12. Wang S, Ai X, Freeman SD, et al. QSulf1, a heparan sulfate 6-O-endosulfatase, inhibits fibroblast growth factor signaling in mesoderm induction and angiogenesis. *Proc Natl Acad Sci U S A.* 2004;101:4833-4838.
13. Danesin C, Agius E, Escalas N, et al. Ventral neural progenitors switch toward an oligodendroglial fate in response to increased Sonic hedgehog (Shh) activity: involvement of Sulfatase 1 in modulating Shh signaling in the ventral spinal cord. *J Neurosci.* 2006;26:5037-5048.
14. Vogel AM, Weinstein BM. Studying vascular development in the zebrafish. *Trends Cardiovasc Med.* 2000;10:352-360.
15. Lawson ND, Weinstein BM. In vivo imaging of embryonic vascular development using transgenic zebrafish. *Dev Biol.* 2002;248:307-318.
16. Jin SW, Beis D, Mitchell T, Chen JN, Stainier DY. Cellular and molecular analyses of vascular tube and lumen formation in zebrafish. *Development.* 2005;132:5199-5209.
17. Traver D, Paw BH, Poss KD, Penberthy WT, Lin S, Zon LI. Transplantation and in vivo imaging of multilineage engraftment in zebrafish bloodless mutants. *Nat Immunol.* 2003;4:1238-1246.
18. Kimmel CB, Ballard WW, Kimmel SR, Ullmann B, Schilling TF. Stages of embryonic development of the zebrafish. *Dev Dyn.* 1995;203:253-310.
19. Westerfield M, Doerry E, Kirkpatrick AE, Driever W, Douglas SA. An on-line database for zebrafish development and genetics research. *Semin Cell Dev Biol.* 1997;8:477-488.

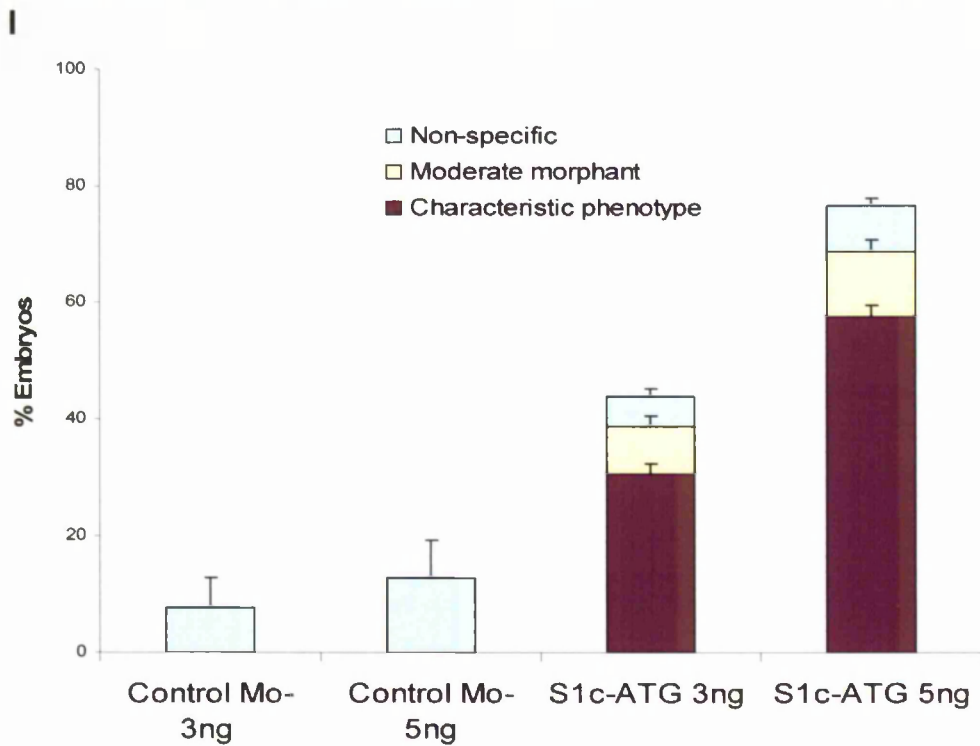
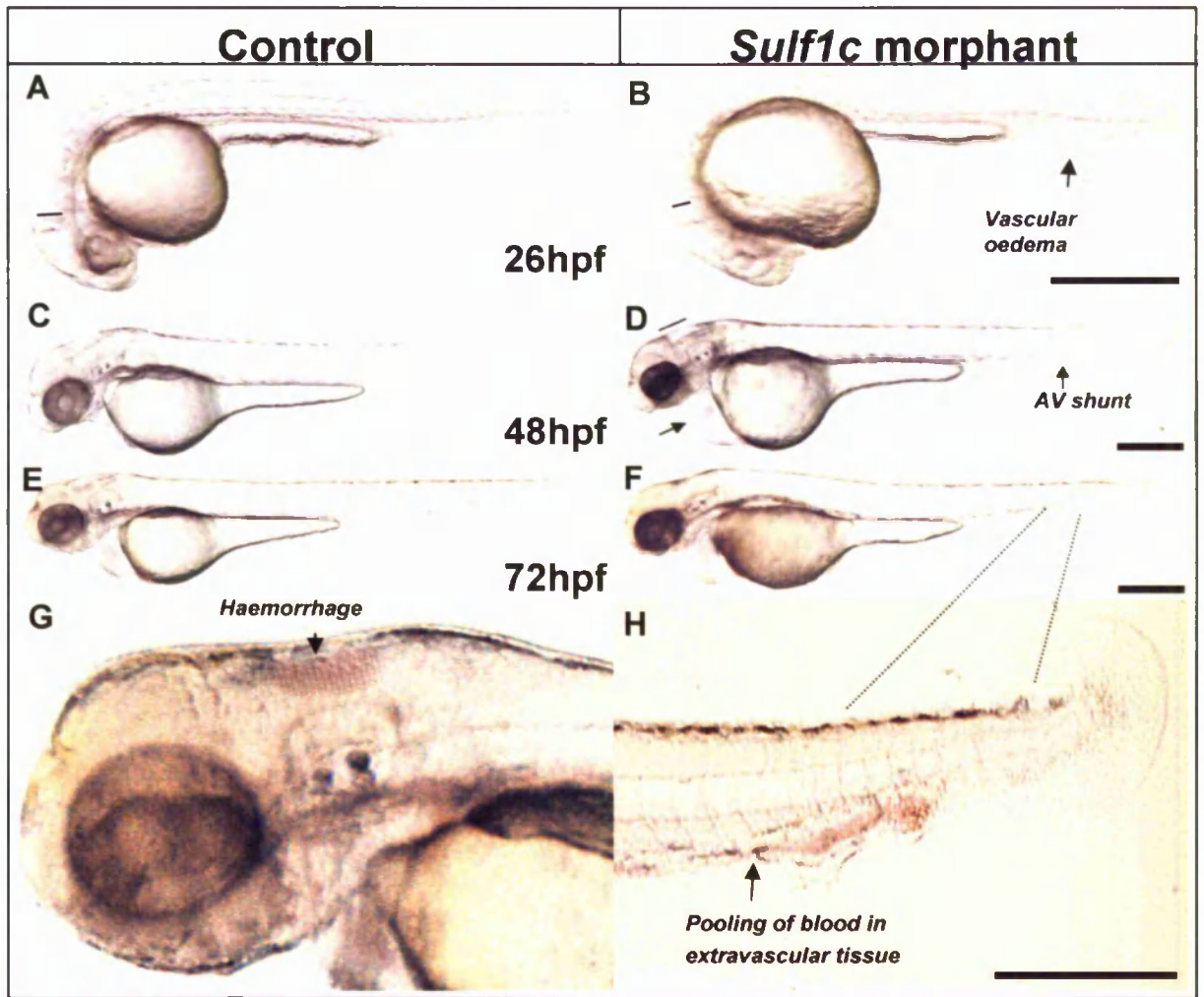
20. Bateman A, Birney E, Durbin R, Eddy SR, Howe KL, Sonnhammer EL. The Pfam protein families database. *Nucleic Acids Res.* 2000;28:263-266.
21. Jowett T, Lettice L. Whole-mount in situ hybridizations on zebrafish embryos using a mixture of digoxigenin- and fluorescein-labelled probes. *Trends Genet.* 1994;10:73-74.
22. Isogai S, Horiguchi M, Weinstein BM. The vascular anatomy of the developing zebrafish: an atlas of embryonic and early larval development. *Dev Biol.* 2001;230:278-301.
23. Dierks T, Lecca MR, Schlotterhose P, Schmidt B, von Figura K. Sequence determinants directing conversion of cysteine to formylglycine in eukaryotic sulfatases. *Embo J.* 1999;18:2084-2091.
24. von Figura K, Schmidt B, Selmer T, Dierks T. A novel protein modification generating an aldehyde group in sulfatases: its role in catalysis and disease. *Bioessays.* 1998;20:505-510.
25. Ambasta RK, Ai X, Emerson CP, Jr. Quail Sulf1 function requires asparagine-linked glycosylation. *J Biol Chem.* 2007;282:34492-34499.
26. Morcos PA. Achieving targeted and quantifiable alteration of mRNA splicing with Morpholino oligos. *Biochem Biophys Res Commun.* 2007;358:521-527.
27. Ekker SC, Larson JD. Morphant technology in model developmental systems. *Genesis.* 2001;30:89-93.
28. Robu ME, Larson JD, Nasevicius A, et al. p53 activation by knockdown technologies. *PLoS Genet.* 2007;3:e78.
29. Berghmans T, Mascaux C, Martin B, Ninane V, Sculier JP. Prognostic role of p53 in stage III non-small cell lung cancer. *Anticancer Res.* 2005;25:2385-2389.
30. Ai X, Kitazawa T, Do AT, Kusche-Gullberg M, Labosky PA, Emerson CP, Jr. SULF1 and SULF2 regulate heparan sulfate-mediated GDNF signaling for esophageal innervation. *Development.* 2007;134:3327-3338.
31. Lamanna WC, Baldwin RJ, Padva M, et al. Heparan sulfate 6-O-endosulfatases: discrete in vivo activities and functional co-operativity. *Biochem J.* 2006;400:63-73.
32. Ai X, Do AT, Kusche-Gullberg M, Lindahl U, Lu K, Emerson CP, Jr. Substrate specificity and domain functions of extracellular heparan sulfate 6-O-endosulfatases, QSulf1 and QSulf2. *J Biol Chem.* 2006;281:4969-4976.
33. Huang CC, Lawson ND, Weinstein BM, Johnson SL. *reg6* is required for branching morphogenesis during blood vessel regeneration in zebrafish caudal fins. *Dev Biol.* 2003;264:263-274.
34. Hangai M, Murata T, Miyawaki N, et al. Angiopoietin-1 upregulation by vascular endothelial growth factor in human retinal pigment epithelial cells. *Invest Ophthalmol Vis Sci.* 2001;42:1617-1625.
35. Habuchi H, Nagai N, Sugaya N, Atsumi F, Stevens RL, Kimata K. Mice deficient in heparan sulfate 6-O-sulfotransferase-1 exhibit defective heparan sulfate biosynthesis, abnormal placentation, and late embryonic lethality. *J Biol Chem.* 2007;282:15578-15588.
36. Ratzka A, Kalus I, Moser M, Dierks T, Mundlos S, Vortkamp A. Redundant function of the heparan sulfate 6-O-endosulfatases Sulf1 and Sulf2 during skeletal development. *Dev Dyn.* 2008;237:339-353.
37. Covassin LD, Siekmann AF, Kacergis MC, et al. A genetic screen for vascular mutants in zebrafish reveals dynamic roles for Vegf/Plcg1 signaling during artery development. *Dev Biol.* 2009;329:212-226.
38. Covassin LD, Villefranc JA, Kacergis MC, Weinstein BM, Lawson ND. Distinct genetic interactions between multiple Vegf receptors are required for development of different blood vessel types in zebrafish. *Proc Natl Acad Sci U S A.* 2006;103:6554-6559.

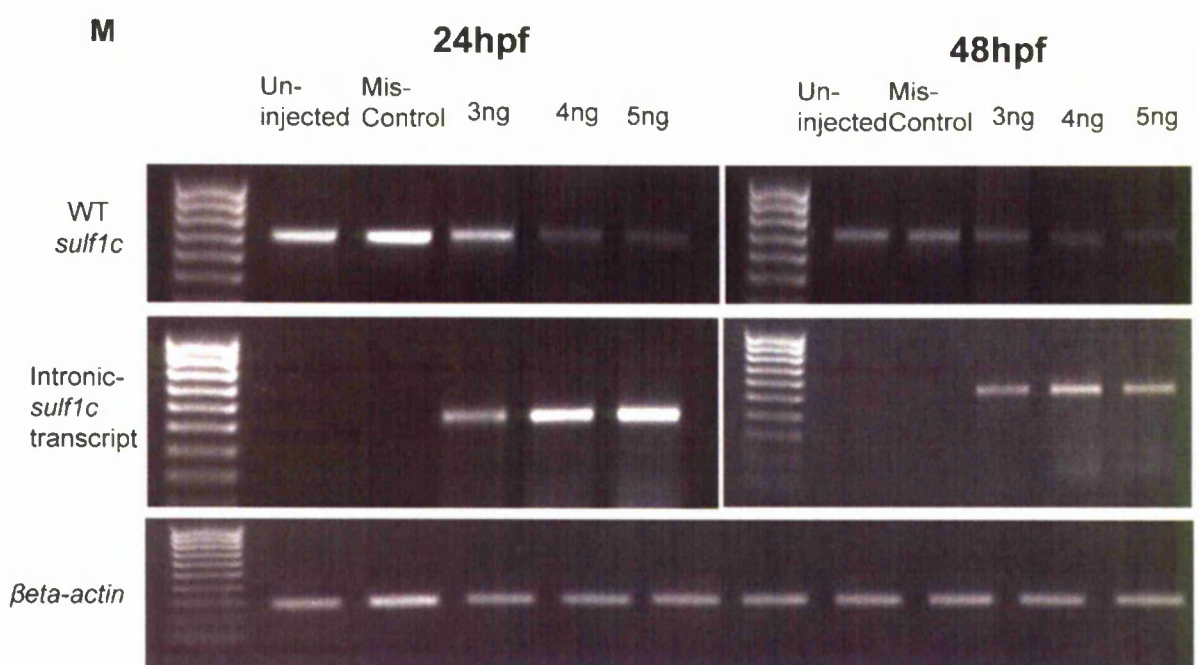
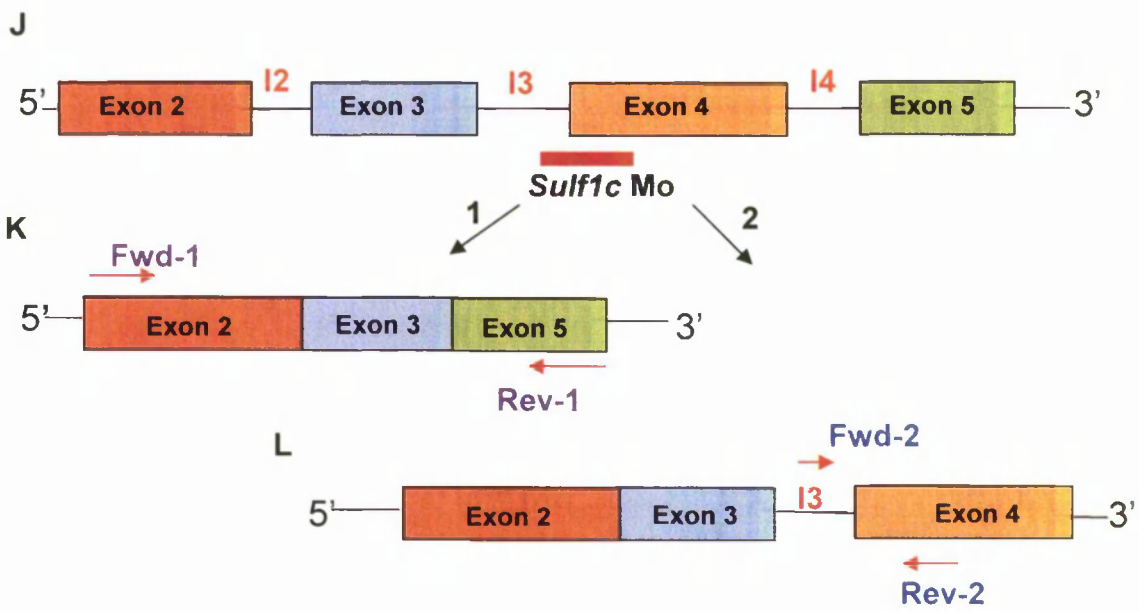
39. Lawson ND, Mugford JW, Diamond BA, Weinstein BM. phospholipase C gamma-1 is required downstream of vascular endothelial growth factor during arterial development. *Genes Dev.* 2003;17:1346-1351.
40. Lawson ND, Scheer N, Pham VN, et al. Notch signaling is required for arterial-venous differentiation during embryonic vascular development. *Development.* 2001;128:3675-3683.
41. Nasevicius A, Larson J, Ekker SC. Distinct requirements for zebrafish angiogenesis revealed by a VEGF-A morphant. *Yeast.* 2000;17:294-301.
42. Ober EA, Olofsson B, Makinen T, et al. Vegfc is required for vascular development and endoderm morphogenesis in zebrafish. *EMBO Rep.* 2004;5:78-84.
43. Robinson CJ, Mulloy B, Gallagher JT, Stringer SE. VEGF165 binding sites within heparan sulfate encompass two highly sulfated domains and can be liberated by K5 lyase. *J Biol Chem.* 2005.
44. Ruhrberg C, Gerhardt H, Golding M, et al. Spatially restricted patterning cues provided by heparin-binding VEGF-A control blood vessel branching morphogenesis. *Genes Dev.* 2002;16:2684-2698.

## Figures



**Figure 1.0: Spatial and temporal expression pattern of *sulf1c* during zebrafish embryonic development:** RT-PCR of *sulf1c* transcript and housekeeping gene  $\beta$ -actin during zebrafish embryonic development (A), *sulf1c* primers were designed to amplify a 512bp product including the ATG start site, and  $\beta$ -actin primers designed to amplify 298bp. WISH analysis of *sulf1c* transcripts at different developmental stages (B). Embryos are anterior to left and lateral to the top. At 50% epiboly and Bud stage *sulf1c* is expressed ubiquitously throughout the entire dorsal axis. At 17 somite stage (18hpf) strong expression is detected in the developing eye, midbrain and hindbrain roofplate. This continues into the posterior roofplate and expression is also observed in the axial vessels and somite boundaries. At 24hpf *sulf1c* expression is strongly maintained in the head, particularly in the midbrain (black arrow) anterior spinal cord (black arrowhead), somite boundaries (red arrows) and in the developing vasculature of trunk and tail (black arrowhead), analogous to *flk-1* expression. At 48hpf expression is in eye lens, cranial vasculature and axial vessels. CA; caudal artery; CV, caudal vein; E, eye; FP, floorplate; H, heart; HB, hindbrain; HC, hypochord; IOC, inner optic circle; LDA, lateral dorsal aortae; MHB, mid-hindbrain boundary; MsV, mesencephalic vein; PHBC, primordial hindbrain channel; PHS, primary head sinus. SB, somite boundaries. Scale bar is 500 $\mu$ m.

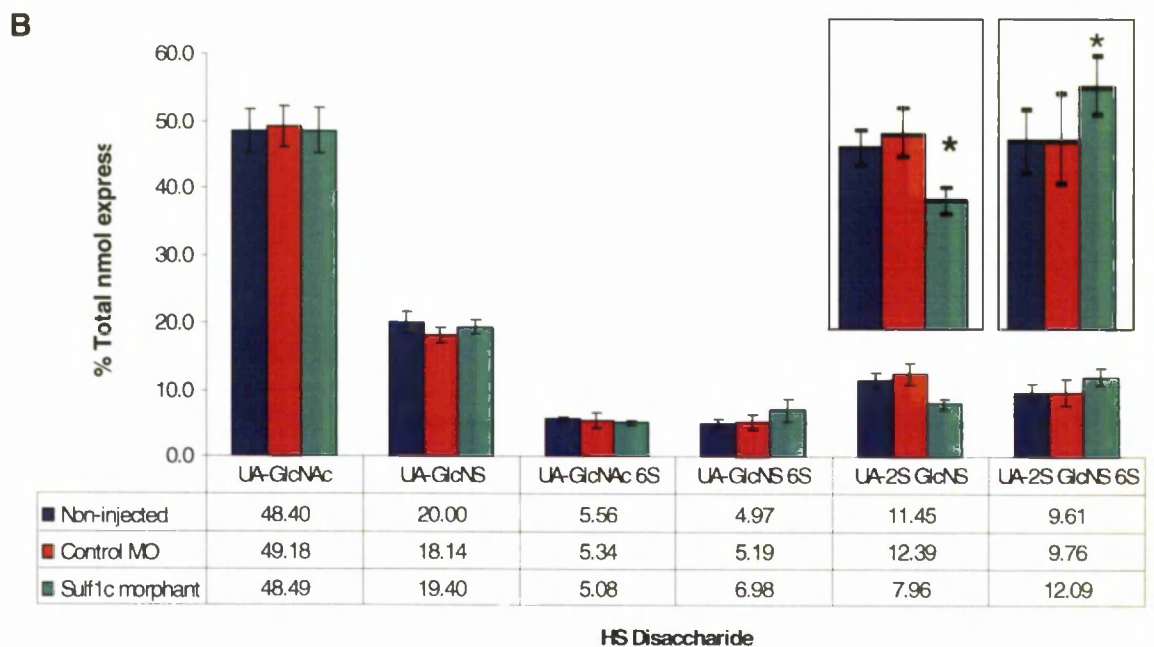
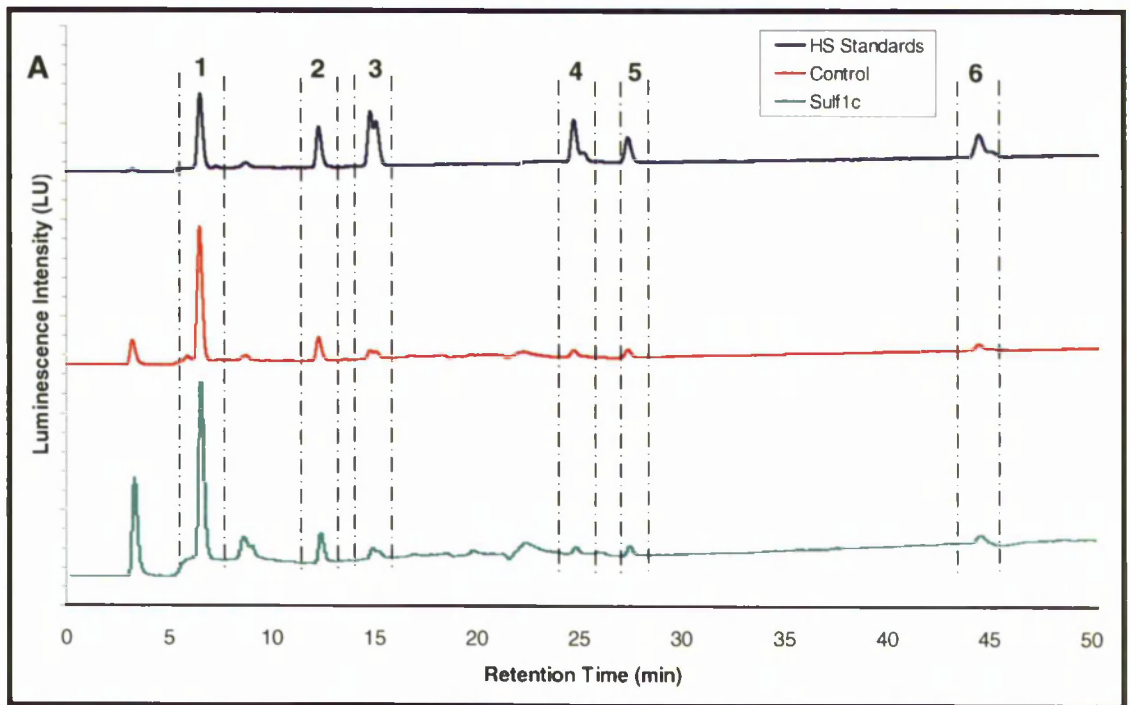




**Figure 2.0: *Sulflc* morphants display a 'characteristic phenotype':** Tg(*flk1*:GFP;*gata*:dsRed) embryos were injected with control mismatch MO and S1c-ATGMO. A-F: Brightfield images of control injected embryos and the 'characteristic phenotype' of the *sulflc* morphant Morphological appearance (lateral view) of 26hpf control (A) and *sulflc* morphant (B). *sulflc* morphants are characteristic of small head, mild depression in hindbrain (indicated by length of black line) and vascular oedema in the tail (Black arrow). Head of 60hpf control embryo (C) and *sulflc* morphant (D), morphants display pericardial oedema and pooling of blood in caudal region of tail (black arrows), depression in the hindbrain is also persistent (black line). 72hpf control (E) and *sulflc* morphant (F). A subset of morphants also displayed haemorrhage (black arrow) at 72hpf (G). Close up of tail of morphant (H) shows pooling of blood in the extravascular tissue (black arrow). Scale bar of images A-H ;500µm.

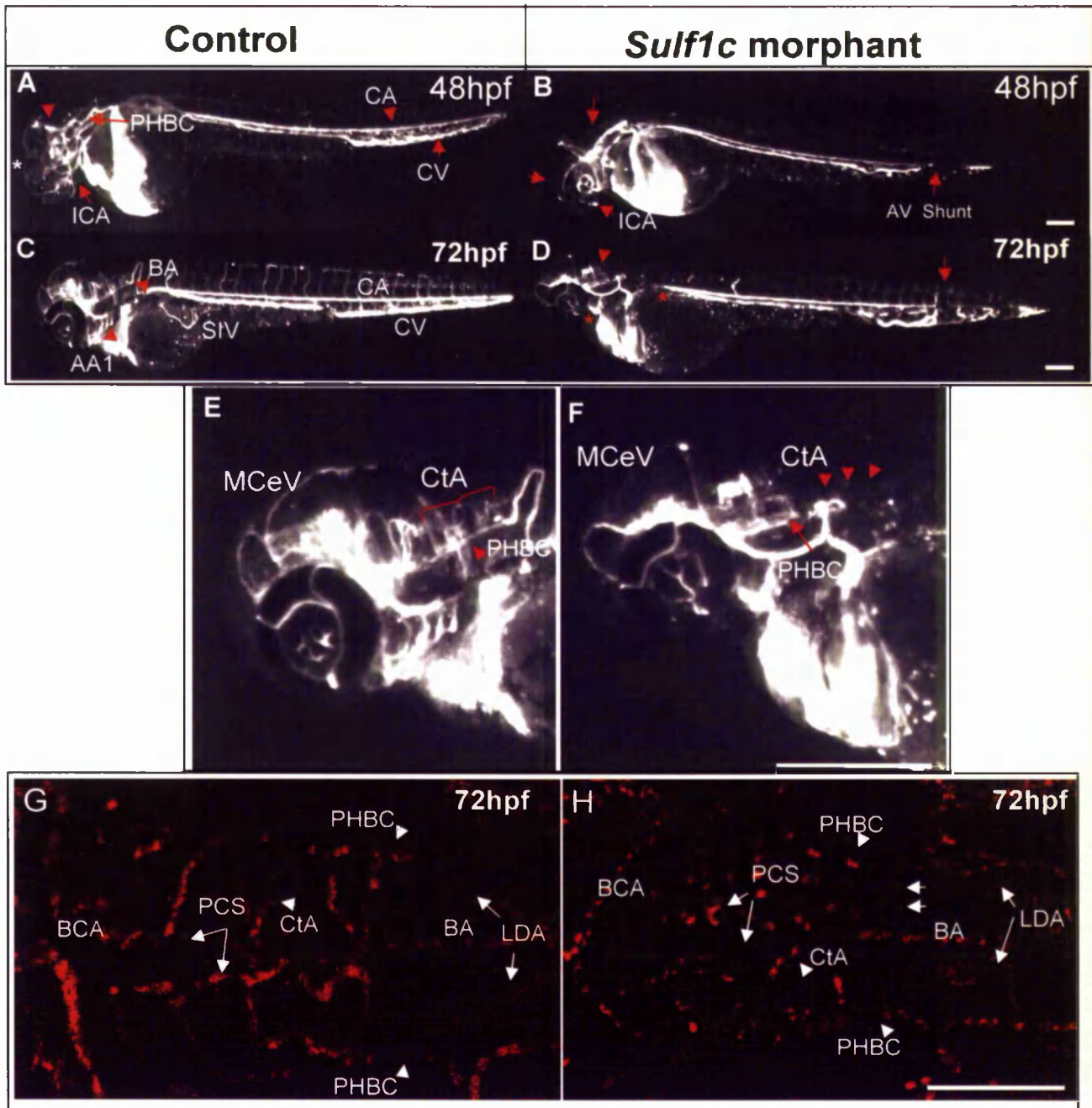
Graphical representation of the average percentage of embryos displaying the characteristic phenotype (I), n is number of experiments (n=4, 70-80 embryo per experiment), error bars indicate standard error.

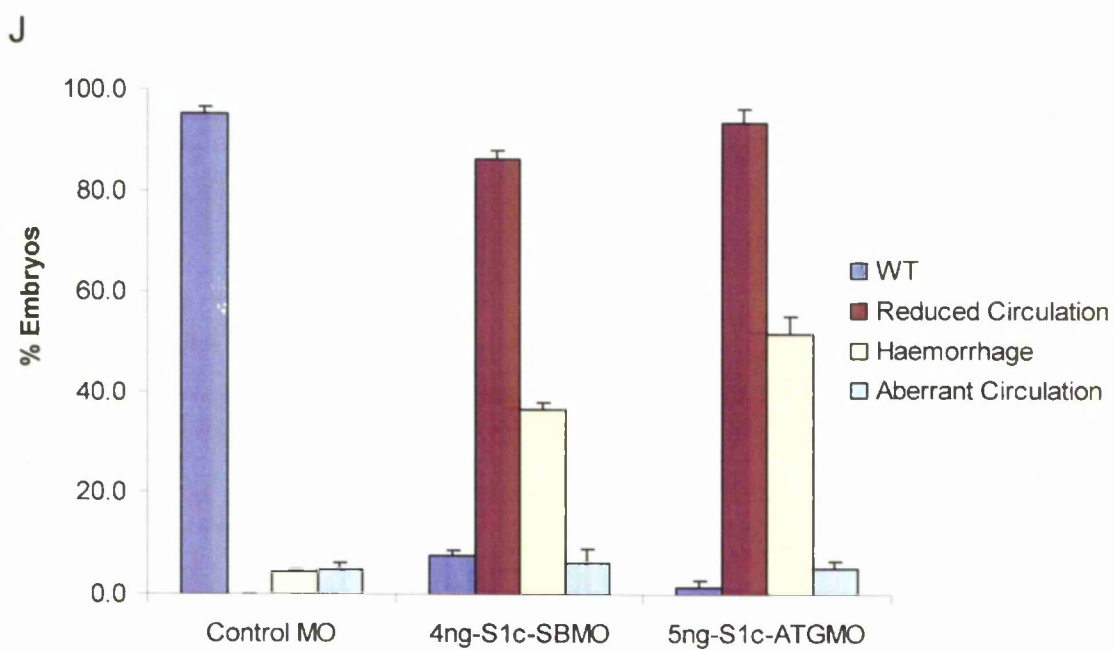
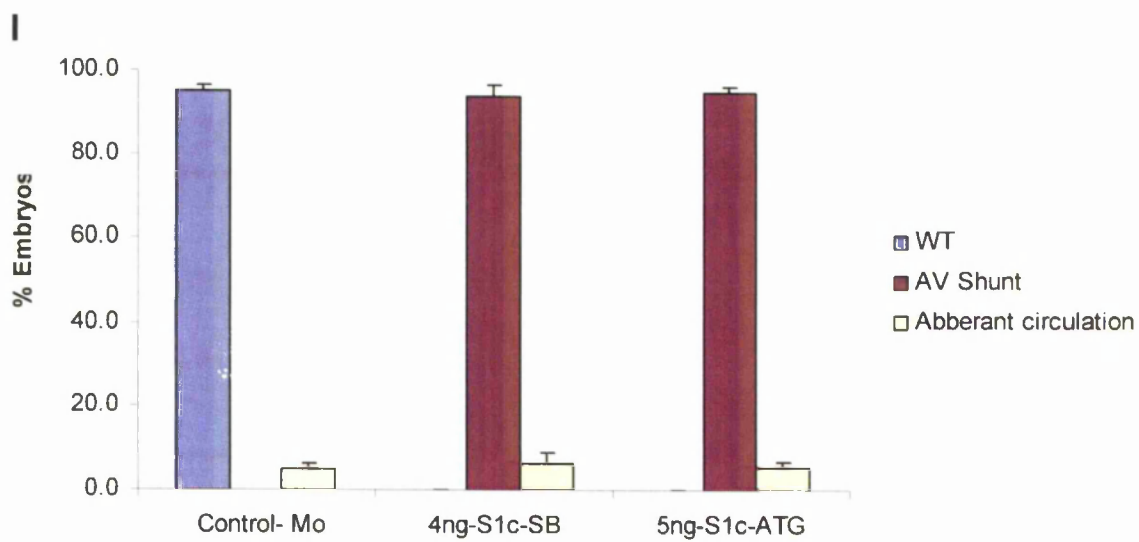
A schematic representation of the intron3-exon4 boundary targeted by *sulflc* splice blocking morpholino (diagram is not to scale) (J). One of the predicted aberrant spliced product that would be observed upon targeting of this splice site depicting the removal of exon4 (K). Forward and reverse primers were designed in exon2 and exon5 respectively, producing a product of 523bp if exon 4 was excluded. Second predicted aberrant transcript that could be observed on blocking splicing at this site (L). Fwd primer was designed in latter region of intron3 whilst reverse primer was in exon4 producing a band of 546bp. This transcript was detected in all *sulflc* morphants. RT-PCR of S1c-SBMO injected embryos confirming knockdown of *sulflc* expression (M) left to right shows increasing concentration of S1c-SBMO reduces the intensity of the wildtype *sulflc* transcript (713bp) and an increase in the intensity of the aberrant *sulflc* transcript. Moderate levels of knockdown of *sulflc* expression was effective to 48hpf. (298bp).

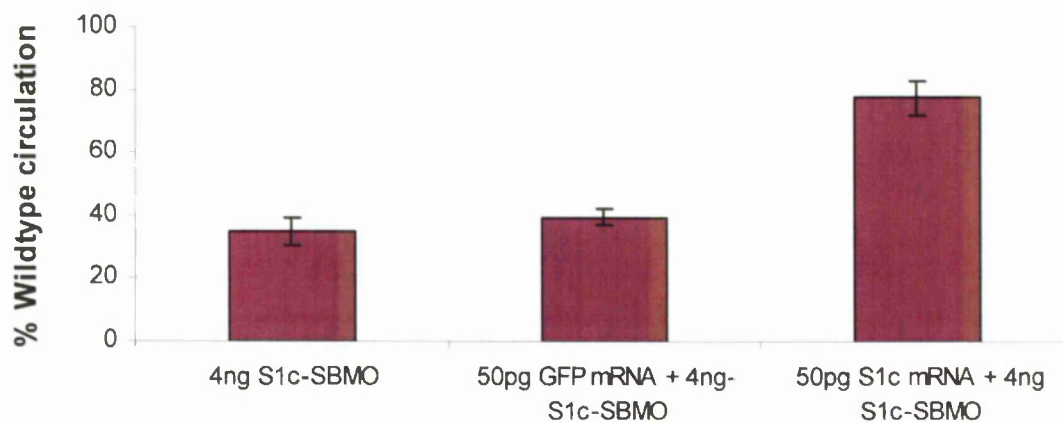


**Figure 3.0: *Sulf1c* knockdown increases 6-O sulphation of tri-sulphated disaccharide;**  
**A :** A representative chromatogram of the wildtype (control) and 5ng of *sulf1c* injected embryos. Six disaccharides were identified by comparison to the elution times of known HS standard peaks; peak 1:  $\Delta$ 4,5 unsaturated hexuronate-*N*-acetyl glucosamine ( $\Delta$ UA-GlcNAc); peak 2:  $\Delta$ UA-*N*-sulfated glucosamine, ( $\Delta$ UA-GlcNS); peak 3:  $\Delta$ UA-6-*O*-sulfated GlcNAc( $\Delta$ UA-GlcNAc6S); peak 4:  $\Delta$ UA-6-*O*-sulfated GlcNS, ( $\Delta$ UA-GlcNS6S); peak 5:  $\Delta$ UA2-*O*-sulfated GlcNS ( $\Delta$ UA2S-GlcNS); peak 6:  $\Delta$ UA2S-GlcNS6S.

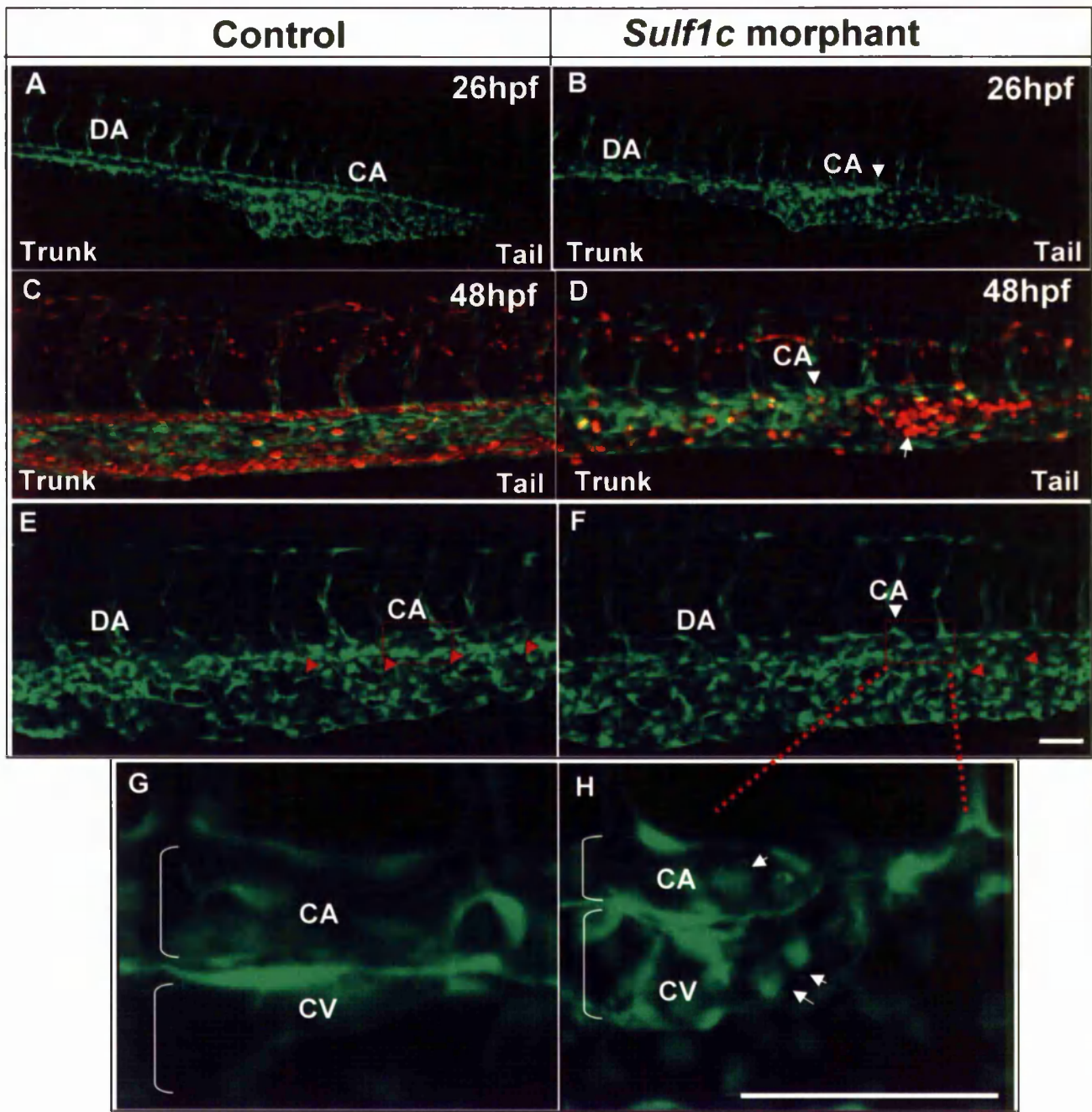
**B:** Disaccharide analysis of HS extracted from 48hpf wildtype and control MO injected, and *sulflc* morphant embryos. The six most abundant disaccharides are indicated on the *x* axis. Asterix (\*) denotes significant changes in disulphated and trisulfated disaccharide compared to control injected embryos. Boxed region highlight the decrease and increase in disulphated UA-2SGlcNS and trisulfated disaccharide UA-2SGlcNS(6S) respectively. Standard deviation calculated from 5 individual experiments (n=5) 40-60 embryos per experiment (T-test  $p < 0.05$ ).



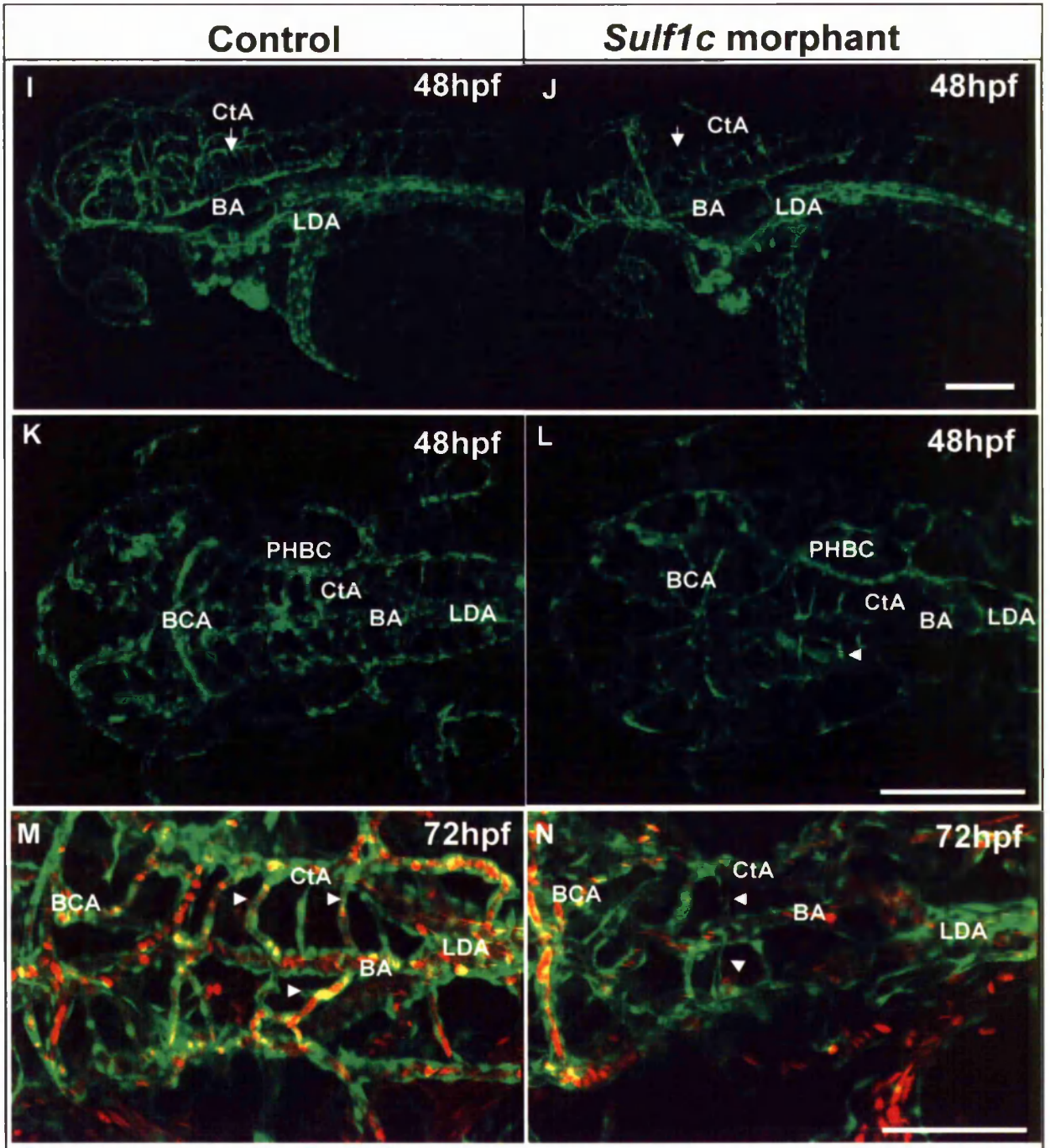


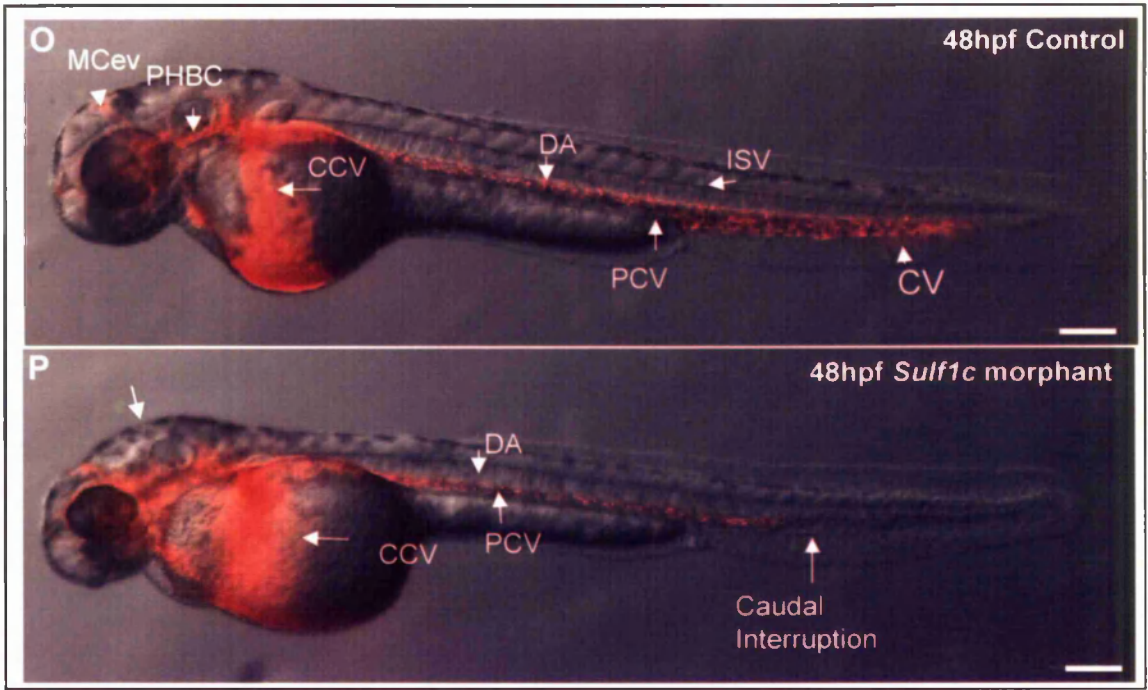
**k**

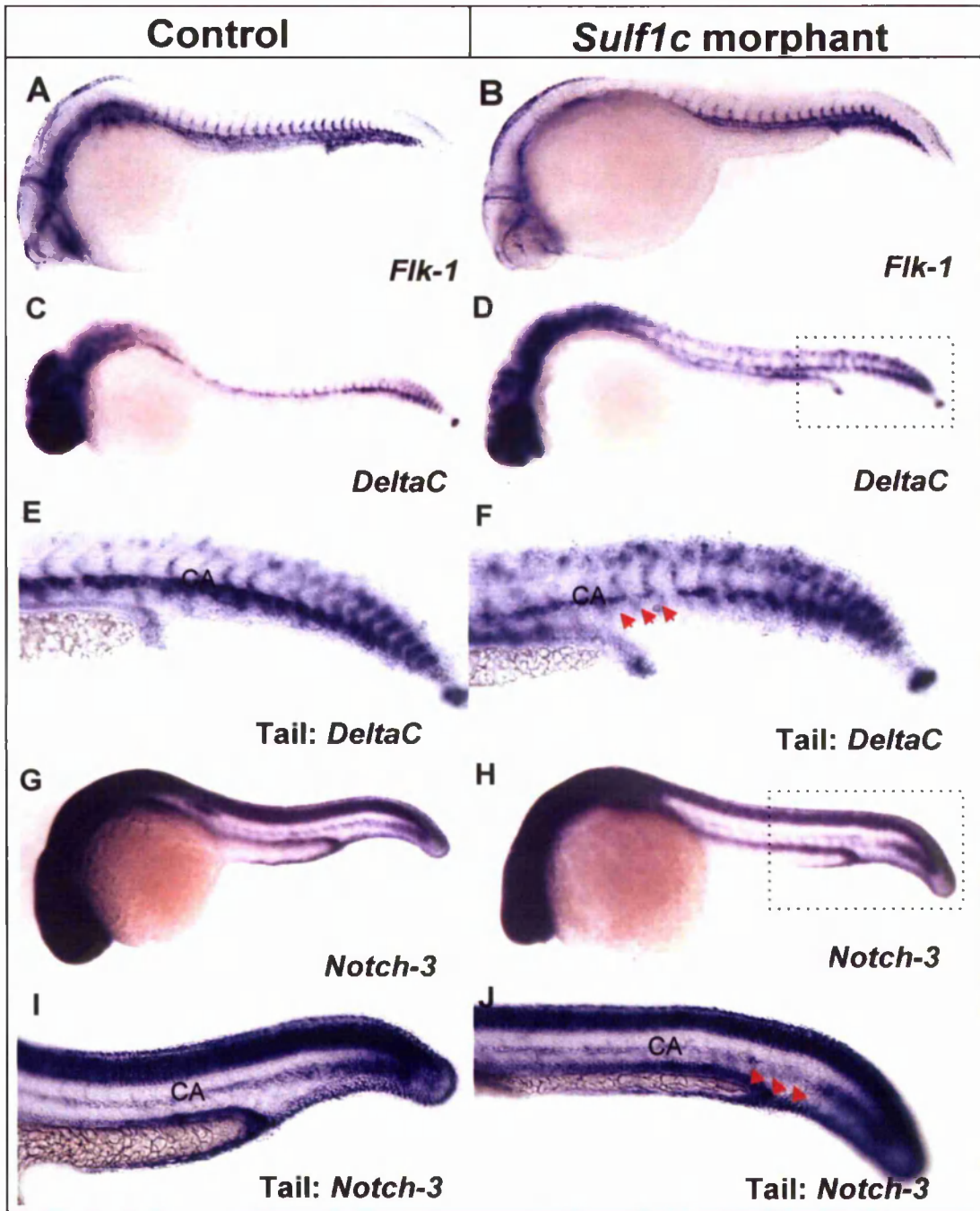
**Figure 4.0: *Sulflc* morphants exhibit circulatory defects that can be rescued by *sulflc* mRNA:** One to four cell stage *tg(fli1:GFP;gata:dsRed)* embryos were injected with 4ng and 5ng of S1c-SB and ATGMO respectively. **A-F;** Fluorescent digital stereoisimages of live blood flow in 48hpf control embryos and *sulflc* morphants. Images are representative of both MO. 48hpf control (A) strong blood flow in the mesencephalic vein (red arrowhead) and in the mid-forebrain region (white asterix). *Sulflc* morphant (B) display weak circulation in the cranial vessels spanning the forebrain-midbrain (red arrowheads) and also interruption of blood flow forming an artery-vein shunt in the tail (denoted by red arrow). 72hpf control embryo (C) strong blood circulation is present in all primary and secondary vessels including subintestinal basket. In contrast *sulflc* morphant (D) display weak circulation in the hindbrain (red arrowhead). Blood flow is rerouted at the level of A-V shunt via the ISVs (red arrow). Also notable in morphants is weak or no blood flow in pharyngeal arches and the subintestinal basket (red asterix). Close up of the lateral images of cranial circulation in control embryos (E). *Sulflc* morphants display weak circulation in central arteries penetrating hindbrain (F). Confocal images of the dorsal view of cranial circulation in the control (G) Circulation absent in left and right central arteries of morphant (H) (double white arrows). Scale bars 200 $\mu$ m (A-D) and 100 $\mu$ m (E-H). Graphical representation of number of 72hpf *sulflc* morphants with defects in axial circulation (I), 93 % and 94% of S1c-SB and S1c-ATG morphants display A-V shunts respectively. A small subset of the morphants also display aberrant circulation (Figure S3, E). Quantification of *sulflc* morphants showing defects in cranial circulation (J), 87% and 90% of S1c-SB and S1c-ATG morphants display weak circulation (N=4, 70-80 embryos per experiment). Rescue experiment (K) displaying the total percentage of embryos with normal axial and cranial circulation after injection of 50pg *sulflc* mRNA with S1c-SBMO. *Sulflc* morphants were partially rescued in comparison to GFP mRNA injected controls. (N=3, 65-70 embryos per experiment) Error bars indicate standard error, one way *Anova*  $p < 0.05$ . BA, basilar artery; BCA, basilar communicating artery; CCV, common cardinal vein; CtA, central arteries; DA, Dorsal aorta; ICA, internal cartoid artery; ISV, intersegmental vessels; LDA, lateral dorsal aorta; MCeV, mesencephalic vein; PCV, posterior cardinal vein; PHBC, primordial hindbrain channel; SIV, subintestinal basket.



**Figure 5.0: *Sulflc* knockdown results in impaired vascular lumenisation at the site of circulatory defect.** Confocal microscopic analysis of the vasculature in *tg(flk1:GFP;gata:dsRed)* control injected embryos and *sulflc* morphants. **A-H:** lateral views of trunk. Developing vasculature of tail in 26hpf control embryo (A). Tail of 26hpf *sulflc* morphant (B) white arrow denotes the site of caudal defect. 48hpf control embryo (C) blood circulates normal in the trunk via the dorsal aorta (DA) and reaches to the tail through the caudal artery (CA). In the tail of *sulflc* morphant (D), white arrowhead denotes the site of A-V shunt, CA appears to be blocked leading to accumulation of blood pooling (white arrow) out of tissue caudal plexus. Caudal plexus of control embryos (E), red arrowheads denote correct lumenised plexus and branching of vessels. While the caudal plexus of *sulflc* morphant (F), denote a less branched network of vessels (red arrowheads) proximal ventral to the site of A-V shunt. Red box highlights the region of vascular defect in relation to the tail caudal plexus. Higher magnification of the vascular defect at the site of A-V shunt in 48hpf control (G) and *sulflc* (H) morphant. Correct lumenisation of CA can be observed in control embryos. In contrast caudal artery appears narrower and disorganised, white arrows denote rounded endothelial cells. Lateral images of the cranial vasculature in 48hpf control (I) and *sulflc* morphant (J). *Sulflc* morphants display reduced number of central arteries (white arrow). Dorsal view of cranial vasculature in control (K) and *sulflc* morphant (L). The *sulflc* morphant display incorrectly patterned central arteries that are not lumenised (white arrowhead). compared to control, Higher magnification of blood circulation in the central arteries in control embryos (M) white arrowhead denote correct lumenisation of vessels with blood flowing in all vessels. In *sulflc* morphants (N) blood flow is restricted to the basilar artery (BA) and absent in most of the CtA, (white arrowheads). Microangiography of 48hpf *fli1:GFP* control (O) and *sulflc* morphants (P). Fluorescent microspheres unable to circulate fully in the head and tail, blood flow is interrupted in the trunk, (white arrow indicates the site of caudal interruption). white arrowhead denotes pooled fluorescent microspheres indicative of a leaky cranial vasculature. BA, basilar artery; BCA, basilar communicating artery; CCV, common cardinal vein; CtA, central arteries; DA, Dorsal aorta; ISV, intersegmental vessels; LDA, lateral dorsal aorta; MCEV, mesencephalic vein; PCV, posterior cardinal vein; PHBC, primordial hindbrain channel. Scale bar 50µm.







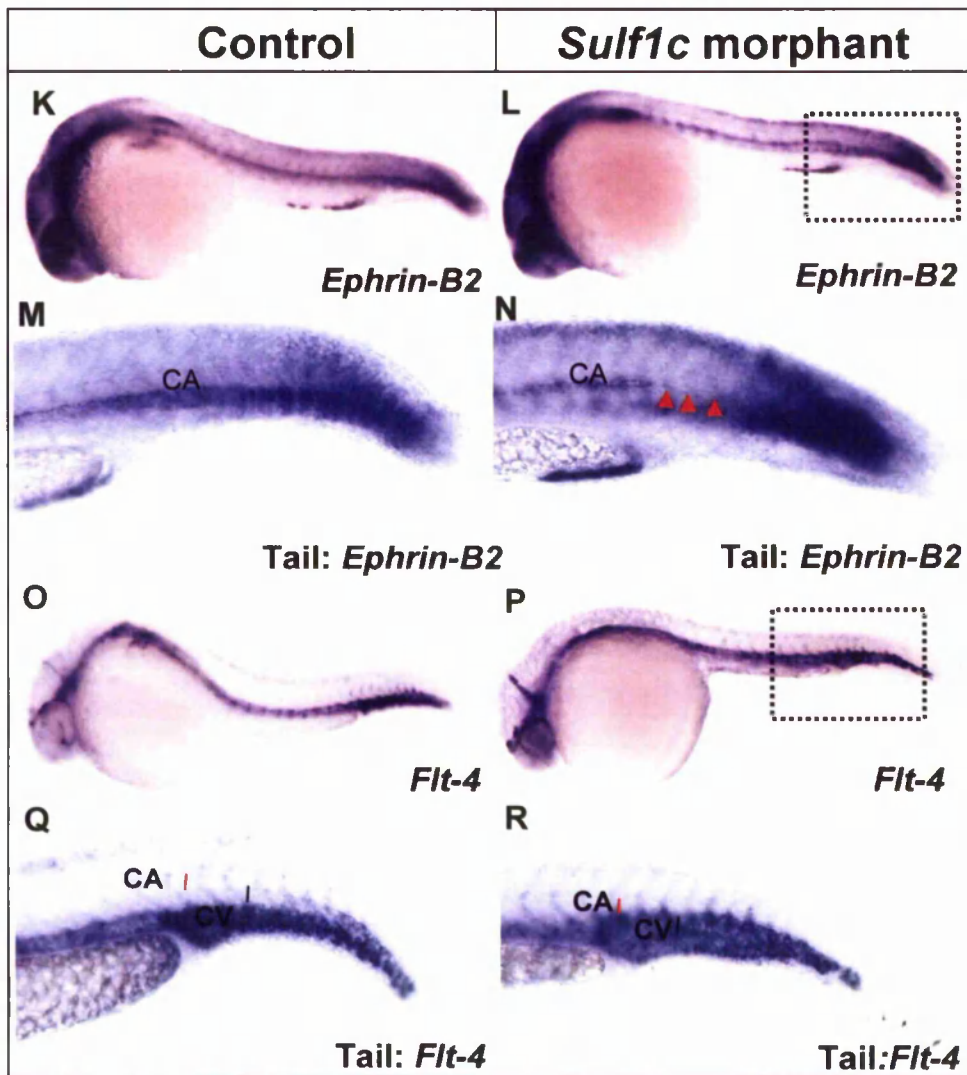


**Figure 6.0: *Sulf1c* knockdown affects arterial gene expression**

Control injected embryos and *sulf1c* morphants were analysed at 24hpf for the expression of the indicated arterial and venous markers by WISH (A-R). Lateral views of the whole embryo and higher magnification of the tail are shown. Expression of the pan-endothelial marker *flk-1* (A-B) is unaffected in *sulf1c* morphants. *Sulf1c* morphants display lack of expression of arterial markers such as *DeltaC* indicated by red arrowheads (panel C-F; 16 out of 21 embryos examined) *notch5* shown by red arrowheads (panel G-J; 18 out of 24 embryos examined) and *ephrinB2a* (panel K-N; 11 out of 15 embryos examined). *Sulf1c* morphants were also characterised by the expansion of the venous marker *flt-4* (panel O-R; 19 out of 24 embryos examined). Arterial and venous markers were normally expressed in all the control embryos examined (ranging from 10-15 embryos per experiment). CA; caudal artery; CV; caudal vein.

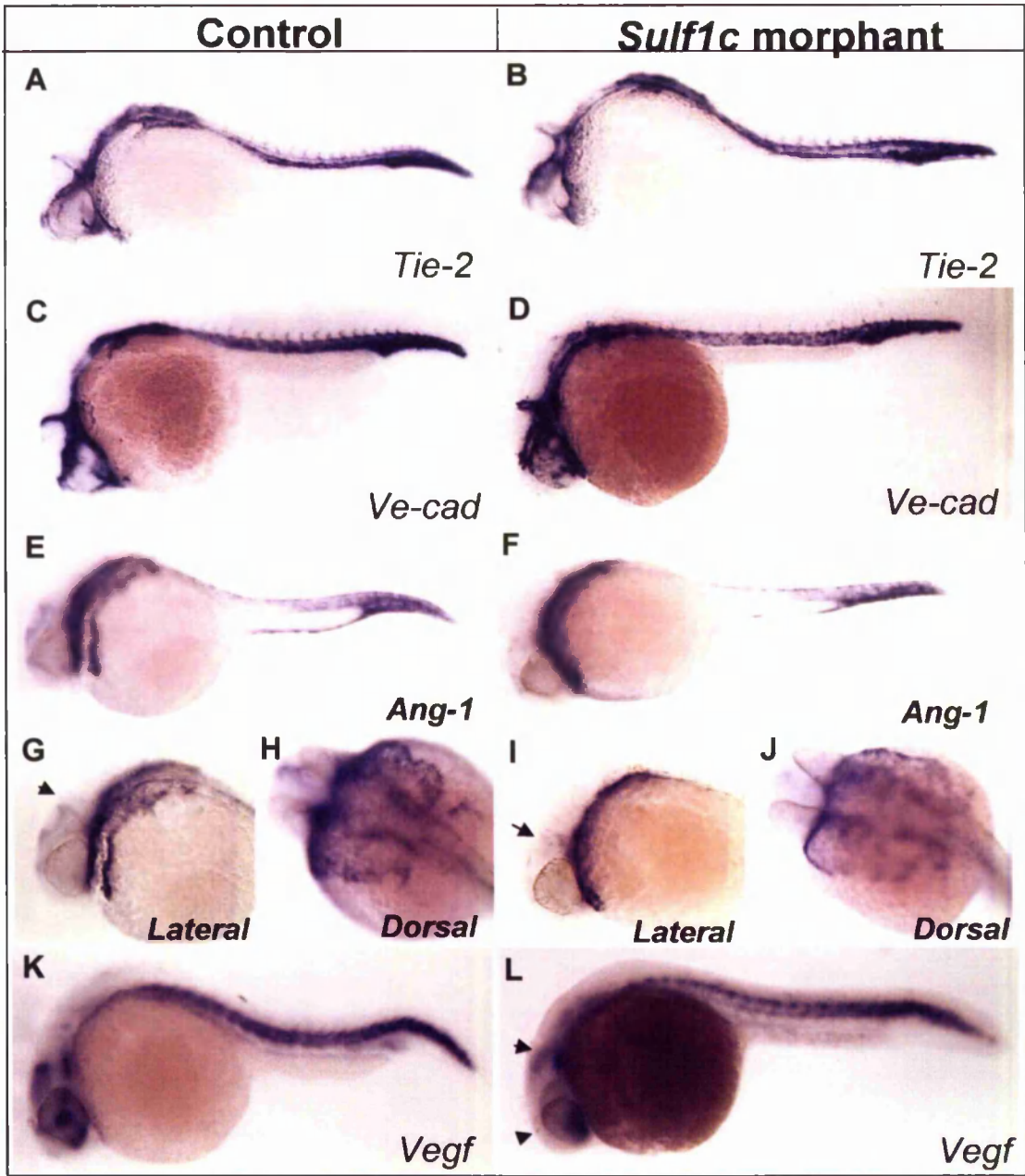


**Figure 7.0:** *Sulf1c* morphants display loss of expression in *ang-1* and *vegf* in the head. Control injected embryos and 24hpf *sulf1c* morphants were analysed by WISH. No difference was detected in the expression of *tie-2* (A,B), *ve-cad* (C,D) in the head of the *sulf1c* morphants. Evident in the developing mid-hindbrain is the loss of *ang-1* expression in the head of the morphants (F,I,J), reduction of *vegf* expression (K-L) also observed in mid-hindbrain ((black arrow) and forebrain (black arrow head)

Supplementary figures

A

	zfsulf1	xsulf1	qsulf1	msulf1	hsulf1
Hsulf1	73.9	77.8	87.2	94.1	
Msulf1	73.5	76.9	86.7		
Qsulf1	73.8	81.0			
xsulf1	69.7				
zfsulf1					

**Figure S1: Percentage identities and Clustalw alignment of vertebrate sulf1 proteins.** A: Percentage identities between vertebrate sulf1 proteins. Zebrafish sulf1 is the most divergent species from human and mouse sulfatase. B: Clustalw alignment of vertebrate sulf proteins. Residues identical in all four proteins are indicated on pink background. Conserved sulfs domains highlighted by the different coloured lines are assigned on based on comparison of protein family of alignments. Sulfs contain four structural domains, including the N-terminal signal peptide (yellow line), the enzymatic domain (red underline), hydrophilic domain (blue underline) and the C terminus (green underline).

B

HSulf1 MKYSCCALVLAVLGTTELLGSLCSTVRSRFRGRIOQERKNIRPNIIILVLTDDQDVELGSL 60  
 Msulf1 MKYSLWALLLAVLGTQLLGSLSCTVRSRFRGRIOQERKNIRPNIIILVLTDDQDVELGSL 60  
 AvSulf1 MKTSWFALFLAVLSTELLTSHSSTLKSRLFRGRVQOERKNIRPNIIILVLTDDQDVELGSL 60  
 ZfSulf1c -MMQLVSLAWMMVLAAPLVCFGFTTRGQGLRGRVQGDRRNIRPNIIILIMTDDQDVELGSL 59

HSulf1 QVMNKTRKIMEHGGATFINAFVTTMCCPSRSSMLTGKYVHNHNVYTNNENCSSPSWQAM 120  
 Msulf1 QVMNKTRKIMEQGGATFINAFVTTMCCPSRSSMLTGKYVHNHNVYTNNENCSSPSWQAM 120  
 AvSulf1 QVMNKTRRIMENGASFINAFVTTMCCPSRSSMLTGKYVHNHNIYTNNENCSSPSWQAT 120  
 ZfSulf1c QVMNKTRKIMEDGGTSFINAFVTTMCCPSRSSMLTGKYVHNHNTYTNNENCSSPSWQAQ 119

HSulf1 HEPRTFAVYLNNTGYRTAFFGKYLNEYNGSYIPGWREWGLIKNSRFYNYTVCRNGIKE 180  
 Msulf1 HEPRTFAVYLNNTGYRTAFFGKYLNEYNGSYIPGWREWGLIKNSRFYNYTVCRNGIKE 180  
 AvSulf1 HEPRTFAVYLNNTGYRTAFFGKYLNEYNGSYIPGWREWGLVKNRSRFYNYTISRNGNKE 180  
 ZfSulf1c HEPRSFVYLNNTGYRTAFFGKYLNEYNGSYIPGWREWVGLIKNSRFYNYTVCRNGNKE 179

HSulf1 KHGFDYAKDYFTDLITNESINYFKMSKRMYPHRPMMVISHAAPHGPEDESAPQFSKLYPN 240  
 Msulf1 KHGFDYAKDYFTDLITNESINYFKMSKRMYPHRIMMVISHAAPHGPEDESAPQFSKLYPN 240  
 AvSulf1 KHGFDYAKDYFTDLITNESINYFRMSKRIYPHRPMMVISHAAPHGPEDESAPQFSSELYPN 240  
 ZfSulf1c KHGADYAKDYFTDLITNDSINYFRTSKRMFPHRPMMVISHAAPHGPEDESAPQYSELPFN 239

HSulf1 ASQHITPSYNYAPNMDKHWIMQYTGPMPLPIHMEFTNI LQRKRLQTLMSVDDSVRLYNML 300  
 Msulf1 ASQHITPSYNYAPNMDKHWIMQYTGPMPLPIHMEFTNVLQRKRLQTLMSVDDSVRLYNML 300  
 AvSulf1 ASQHITPSYNYAPNMDKHWIMQYTGPMPLPIHMEFTNVLQRKRLQTLMSVDDSMERLYQML 300  
 ZfSulf1c ASQHITPSYNYAPNMDKHWIMQYTGPMKPIHMEFTNYLHRKRLQTLMSVDDSVKQVYNAL 299

HSulf1 VETGELENTYIIYTADHGYHIGQFGLVKGKSMYPDFDIRVPPFFIRGPSVEPGSIVPQIVL 360  
 Msulf1 VESGELDNTYIIYTADHGYHIGQFGLVKGKSMYPDFDIRVPPFFIRGPSIEPGSIVPQIVL 360  
 AvSulf1 AEMGELENTYIIYTADHGYHIGQFGLVKGKSMYPDFDIRVPPFFIRGPSVEPGSVVPQIVL 360  
 ZfSulf1c VDTGELDNTYIIYTADHGYHIGQFGLVKGKSMYPDFDIRVPPFFVRGPNVEPGARNNHVVL 359

HSulf1 NIDLAPTILDIAGLDTPPDVGKSVLKLDDPEKPGNRFRFTNKKAKIWRDFTLVERGKFLR 420  
 Msulf1 NIDLAPTILDIAGLDSPPDVGKSVLKLDDLEKPGNRFRFTNKKAKIWRDFTLVERGKFLR 420  
 AvSulf1 NIDLAPTILDIAGLDTPPDMDGKSVLKLDDLERPGNRFRFTNKKTKIWRDFTLVERGKFLR 420  
 ZfSulf1c NIDLAPTILDIAGLDTPPDMDGKSILKLLQEKTGNRFKPNRKPVWRDFTLVERGKILR 419

HSulf1 KKEE--SSKNIQOSNHLPKYERVKELCQQARYQTACEQPGQKWQCIEDTSGKLRIRHKCKG 478  
 Msulf1 KKEE--SGKNIQOSNHLPKYERVKELCQQARYQTACEQPGQNWQCIEDTSGKLRIRHKCKG 478  
 AvSulf1 KKEE--ANKNTQOSNQLPKYERVKELCQQARYQTACEQPGQKWQCTEDASGKLRIRHKCKV 478  
 ZfSulf1c KKEDSASSLNTQHSNSLPKYKVKVEVCQQAQEFQTPCEQPGQKWHCVEEVSGKWRLOKCKG 479

HSulf1 PSDLLTVRQSTRNLYARGFHDKDKECSCRESGYRASRSQRKSQRQFLRNQGTPKYKPRFV 538  
 Msulf1 PSDLLTVRQARNLYSRGLHDKDKECHCRDSGYRSSRSQRKNQRQFLRNKGTPKYKPRFV 538  
 AvSulf1 SSDILAIRKRTRS IHSRGYSGKDKDCNCGDTFERNRSTQRKNQRQFLRNPSAQYKPRFV 538  
 ZfSulf1c -SLKEGSKKRTRSLRSRSYDNREKDCCHGERPYKAAKAARRAHRQFGQS-SNPRYRPRFV 537

HSulf1 HTRQTRSLSVFEGEIIYDINLEEEEEELQVLQPRNIAKRHDEGHKGP-RDLQASSGGRGR 597  
 Msulf1 HTRQTRSLSVFEGEIIYDINLEEEE-LQVLPPRSIAKRHDEGHQGF-IGHQAAAGDIRNE 596  
 AvSulf1 HTRQTRSLSVFEGEIIYDINLEEEE-LQVLKTRSTIKRHAEND---KKAETDGAPGDT 594  
 ZfSulf1c HTRPARSLSVFEGEIIYDVLQADD-KTLEPRPISKRHYEPEPGFSDSDFLESDDGSEE 596

HSulf1 MLADSSNAVGPPTTVRVTHKCFILPNDSIH CERELYQSARAWKDHKAYIDKEIEALQDKI 657  
 Msulf1 MLADSSNAVGLPATVTVTHKCFILPNDTIH CERELYQSARAWKDHKAYIDKEIEVLQDKI 656  
 AvSulf1 MVADGTDVIGQPSSVRVTHKCFILPNDTIR CERELYQSARAWKDHKAYIDKEIEALQDKI 654  
 ZfSulf1c MQSDTNAVGYPNLSLVTHKCFILINDTVR CERELYQSSRAWKDHKNFVDHEIEQLQDKM 656

HSulf1 KNLREVRGHLKRRKPEECSCSKQSYNKEKGVK-KQEKLS---HLHPFKEAA-QEVD SK 712  
 Msulf1 KNLREVRGHLKRRKPEECGCGDQSYNKEKGVK-RQEKLS---HLHPFKEAAQEVD SK 712  
 AvSulf1 KNLREVRGHLKRRKPEECDCQSYNKEKGVK-TQEKIKS---HLHPFKEAA-QEVD SK 709  
 ZfSulf1c KKLREVRGHLKRRRPEECDCSKSYFSKEREQKNKPERLKNRNDHLHPFKEAM-QEVD SK 715

HSulf1 LQLFKENRRRKKERKEKRRQRKGEESLPLGLTCFTHDNHWHQTAFFWNLGSFCACTSSN 772  
 Msulf1 LQLFKEH-RRRKKERKEKRRQRKGEESLPLGLTCFTHDNHWHQTAFFWNLGSFCACTSSN 771  
 AvSulf1 LQLFKEN-RRRKKERKGGKRRQKGGDECSLPLGLTCFTHDNHWHQTAFFWNLGSFCACTSSN 768  
 ZfSulf1c AQLYNEI-RRRKKERKVRKRQKGGDDCSLPLGLTCFTHDNHWHQTAFFWNLGGFCACTSSN 774

HSulf1 NNTYWCLRTVNEHNFLECFEATGFLEYFDMNTDPYQLTNTVHTVERGILNQLHVQLMEL 832  
 Msulf1 NNTYWCLRTVNEHNFLECFEATGFLEYFDMNTDPYQLTNTVHTVERSILNQLHIQLMEL 831  
 AvSulf1 NNTYWCLRTVNDTHNFLECFEATGFLEFFDMNTDPYQLTNTVHTVERGILNQLHVQLMEL 828  
 ZfSulf1c NNTYWCLRTVNEHNTLFCFEATGFLEYFDLNSDPYQLTNAVYTVVEKDILSQLHSOLMEM 834

HSulf1 RSCQGYKQCNP RPKNLDVGNKDGGSYDLHRGQ-LWDGWEG 871  
 Msulf1 RSCQGYKQCNP RPKSLDIGAKEGNYDPHRGQ-LWDGWEG 870  
 AvSulf1 RSCQGYKQCNP RPKGLLETGNKDGGSYDPHRGQ-LWDGWEG 867  
 ZfSulf1c RSCQGHKQCNP RPSSDAGSKDGGSYDQHRTOPTWDVHKG 874

## Supplementary figures

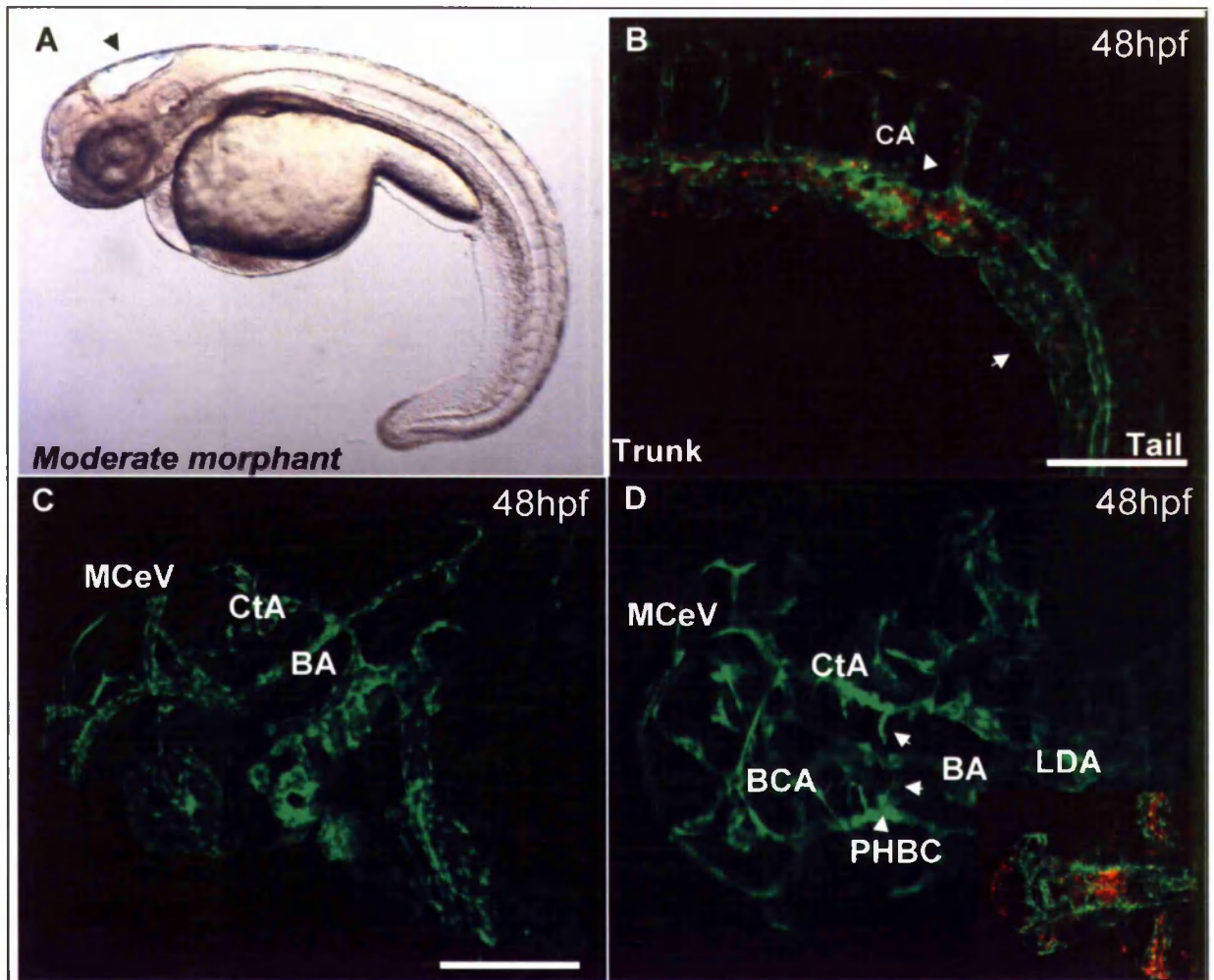


**Figure S2: Vascular and circulatory defects in *sulf1c* moderate morphant phenotype**  
 A: Brightfield image of 48hpf severe *sulf1c* morphant, displaying curved spine and mild hindbrain oedema (indicated by black arrow). B: Confocal analysis of tail in severe morphant, embryos display interruption of blood flow in caudal artery in similar position to that of characteristic *sulf1c* morphants, white arrow shows weak circulation in tail region. C: lateral view of the severe morphant displaying defects in cranial vasculature, severe reduction in the number of central arteries (CtA). Dorsal view of cranial vasculature (D) reveals immature formation of CtA, white arrowheads point to CtA not forming correct connections to basilar artery (BA). Inset :Example of haemorrhage in the *sulf1c* characteristic and moderate morphant phenotype. Reduced blood flow in the cranial vessels with haemorrhage present in region of vascular defect. BA, basilar artery; BCA, basilar communicating artery; CCV, common cardinal vein; CtA, central arteries; DA, Dorsal aorta; ISV, intersegmental vessels; LDA, lateral dorsal aorta; MCeV, mesencephalic vein; PCV, posterior cardinal vein; PHBC, primordial hindbrain channel. Scale bar 100µm

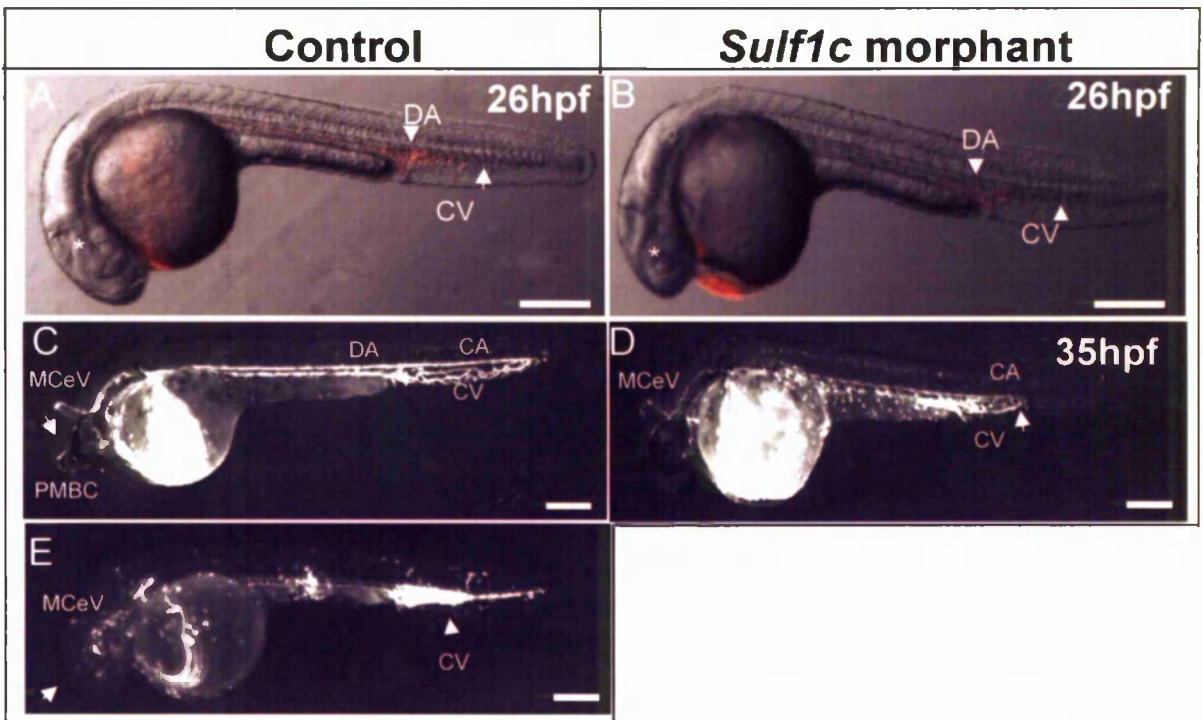


**Figure S3: Circulatory flow exhibited by *sulf1c* characteristic morphant at 1dpf.** Transgenic (*fli1:GFP;gata:dsRed*) embryos were injected with 5ng of S1c-ATGMO or 4ng of S1c-SBMO, and fluorescent digital stereoislices taken are representative of the blood circulation. Lateral view of 26hpf control injected embryo (A) blood circulation initiating in the trunk with very weak circulation (marked by white asterisk) in the head. Circulation of *sulf1c* characteristic morphant (B) is similar to that of control. 35hpf control (C) injected embryo. *Sulf1c* characteristic morphant display weak circulation in head of *sulf1c* morphant embryos, white arrow points to premature A-V connection formed in the tail as a result of the vascular occlusion in caudal artery. *Sulf1c* characteristic morphant displaying aberrant circulation (E) blood pooled in the tail indicated by red arrowhead and lack of circulation in the head marked by white arrow. DA, dorsal aorta; CA, caudal artery; CV, caudal vein; MCEV, mesencephalic vein; PMBC, primordial midbrain channel. Scale bar 200 $\mu$ m

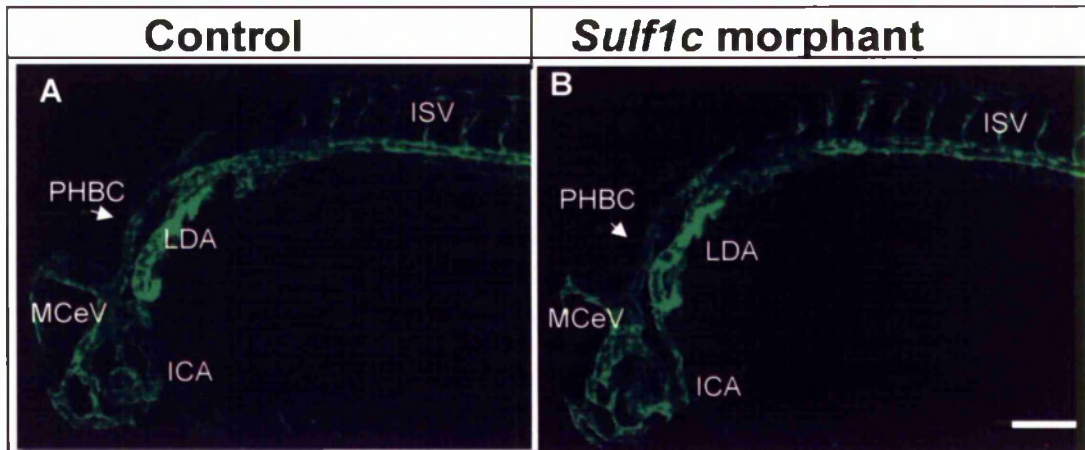


**Figure S4: *Sulf1c* characteristic phenotype exhibit wildtype like properties in the cranial vasculature at 26hpf.** *Tg(flk1:GFP;gata:dsRed)* embryos were injected with 5ng of control MO and *S1c*-ATGMO and confocal images taken of the anterior region of embryo including cranial vasculature and anterior trunk. Lateral images of head of control embryo (A) and the *sulf1c* characteristic morphant (B). The primary cranial vessels are lumenised Vessels a. PHBC primordial hindbrain channel; MCEV, mesencephalic vein; LDA, lateral dorsal aorta; ICA, internal carotid artery; ISV, intersegmental vessels. Scale bar: 100 $\mu$ m

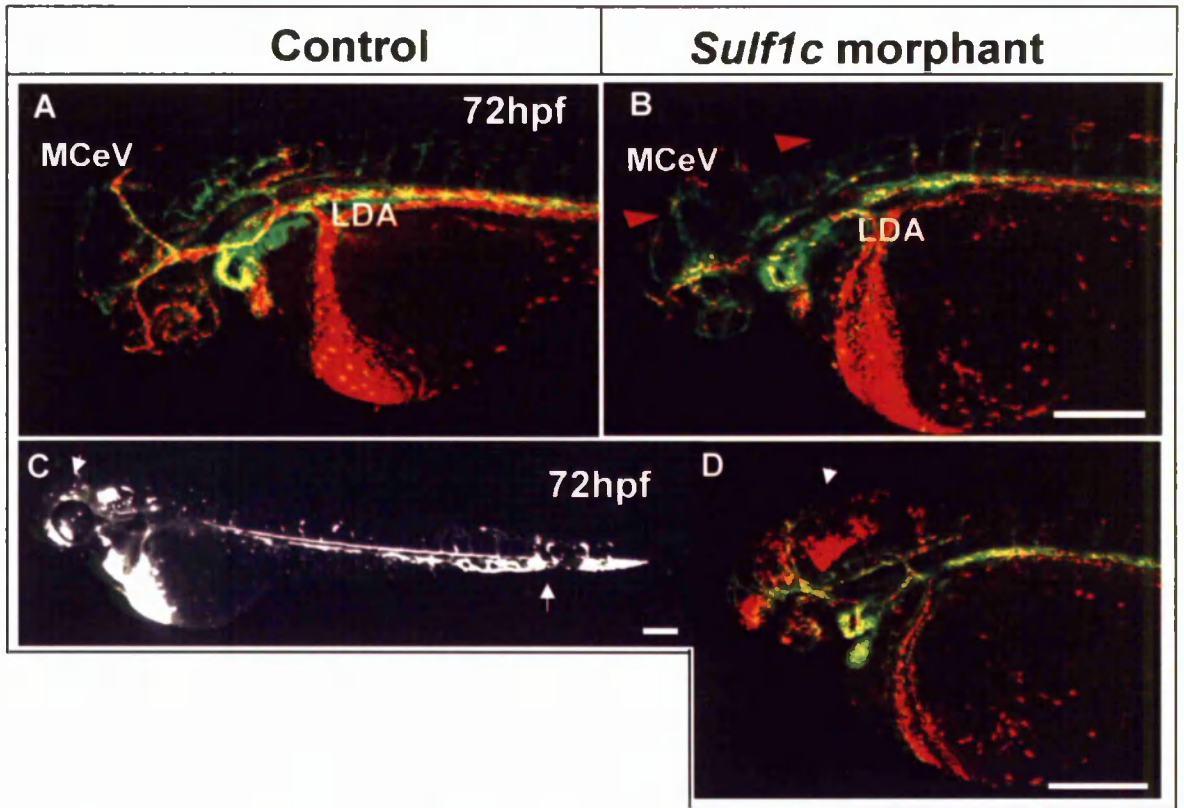


**Figure S5: *Sulf1c* morphants display reduced blood flow in the hindbrain and further develop haemorrhage at 3dpf.** Tg(*Flk1*:GFP;*gata*:dsRed) embryos were microinjected with 5ng of S1c-ATGMO. Circulation is normal in the head of control embryo (A). Circulation is reduced in the midbrain and hindbrain of *sulf1c* morphant (B) denoted by red arrow. *Sulf1c* characteristic morphant display haemorrhage (D) lateral view of whole embryo (C) exhibiting reduced circulation in the head and A-V shunt (white arrow). LDA, lateral dorsal aorta; MCEV, mesencephalic vein. Scale bar 200 $\mu$ m.

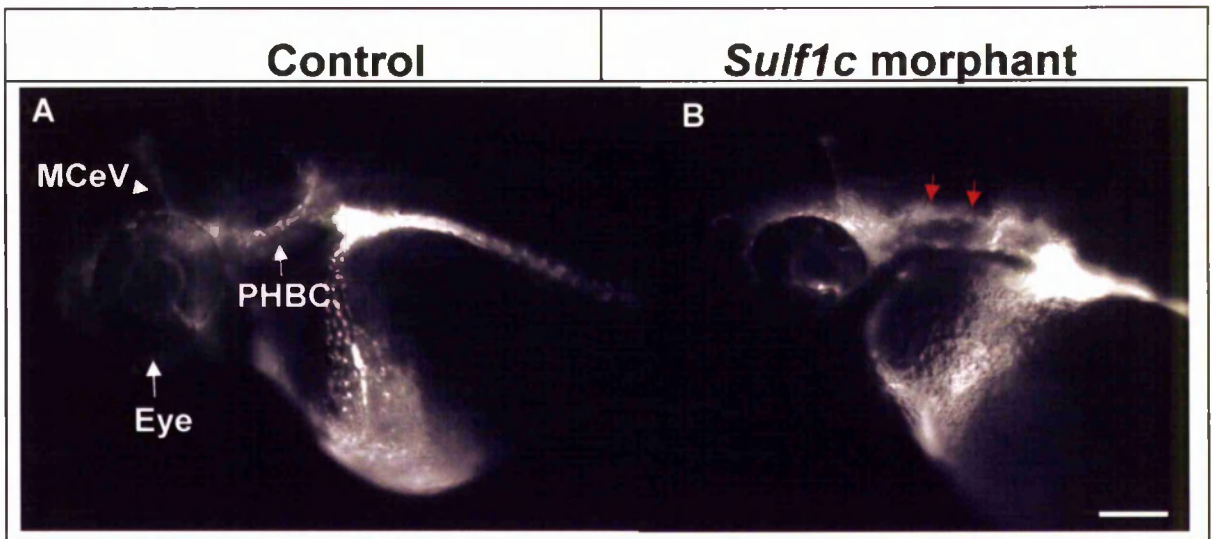


**Figure S6: Microangiography confirms leaky cranial vasculature in the head *sulf1c* characteristic morphant:** *Tg(fli1:GFP)* control embryo and *sulf1c* morphants were injected at 60hpf with fluorescent microspheres into sinus-venous cardinal vein and lateral views of the head taken on fluorescent stereomicroscope. Microangiography of control embryo (A) displaying normal anterior circulation in the cranial vasculature. Microangiography of *sulf1c* morphant (B) display leakiness of fluorescent microspheres in hindbrain. Red arrows denote perfusing out of vessels. MCEV, mesencephalic vein; PHBC, primordial hindbrain channel. Scale bar 200 $\mu$ m.

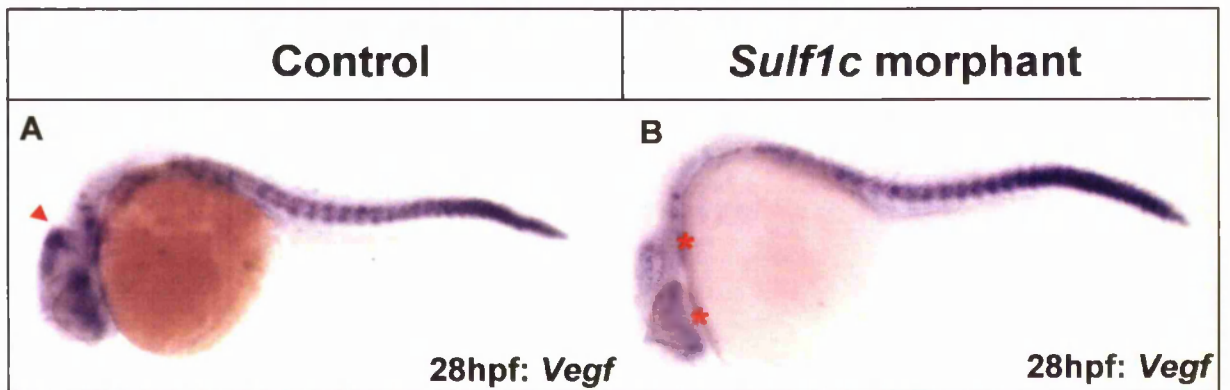


**Figure S7: *Sulf1c* knockdown affects *vegf* expression in the head;** Control injected embryos and *sulf1c* morphants were analysed for *vegf* expression by WISH (A-F). 28hpf control embryo (A) strong *vegf* expression in the developing mid-hindbrain denoted by red arrowhead. *Sulf1c* morphant (B) embryos show reduced *vegf* expression in the head indicated by red asterix. Scale bar 200 $\mu$ m.

# Chapter 6.0 Continuing the characterisation of *sulflc* morphant

## 6.1 Introduction

The data presented on *sulflc* so far imply a unique role of zebrafish *sulflc* in arterial differentiation and in vascular maintenance. Loss of *sulflc* activity results in arterial venous shunts in caudal plexus and immature and leaky cerebral vasculature in regions coinciding with its temporal and spatial expression patterns during embryonic development. Analysis of arterial markers in the tail vasculature by whole mount in situ implies a loss of arterial markers in the caudal artery with concomitant upregulation of the venous marker. Arterial differentiation in zebrafish is shown to proceed *via* a signalling cascade mediated by *Hh-VEGF-notch*<sup>2</sup>, components of all which have the ability to bind or be regulated by HSPGs. It was hypothesised that *sulflc* modulation of HS can disrupt the signalling of HS regulated proteins at different stages. It was speculated the loss of *sulflc* activity was having a direct affect on VEGF activity. VEGF regulates many stages of vascular development including migration, differentiation and proliferation of endothelial cells. From our confocal analysis of the vascular region surrounding the A-V shunt there appeared to be an unprecedented increase in the number of endothelial cells (visualised by the *flil*-eGFP transgene) at the site of defect (Fig 6.0B, D, F, H), this led us to hypothesise whether an ‘overproliferation’ of endothelial cells was resulting in a block in the caudal artery as opposed to the loss in arterial identity thus preventing further blood circulation in the tail. To test this alternative possibility we measured the number of proliferative endothelial cells in the tail of the *sulflc* morphant at several timepoints. In support of our hypothesis several *in vitro* experiments have shown that loss of HSULF1 or extracellular domain of human D14 protein (notch ligand) increases *VEGF* mediated proliferation of endothelial cells<sup>368,415</sup> this suggests that changes in cell proliferation may contribute to the vascular phenotype and morphogenesis.

Results from chapter five indicated that loss of *VEGF* expression was evident in the developing mid-forebrain of *sulflc* morphants and possibly an affect on VEGF activity is responsible for the loss of arterial differentiation. As these result pointed towards the involvement of VEGF and coincided with one of the ultimate aims of testing the role of 6-O sulphation in VEGF mediated angiogenesis, we attempted to create a robust VEGF assay to further test these hypotheses in the zebrafish with a future aim of co-injecting the *sulflc*

morpholino and assessing the affects on ectopic vessel formation.

## **6.2 Materials and methods**

### **6.2.1 Proliferation assay**

Transgenic *fli*:GFP embryos were injected with 5ng S1c -ATG morpholino and control morpholino. ATG morpholino was used for all subsequent experiments as it gave a higher penetrance of the characteristic *sulf1c* morphant. *Sulf1c* morphants displaying the characteristic phenotype were segregated and fixed in 4% paraformaldehyde, at different time points. Approximately 20-40 embryos were used for each experiment. Embryos then underwent the proliferation assay (described section 2.8). For imaging all embryos were mounted laterally in 0.8% agarose on depression slides. Images were collected on a Leica TCS SP5 AOBS upright confocal using a 20x/ 0.50 Plan Fluotar objective and 1x confocal zoom. The confocal settings were as follows, pinhole 1 airy unit, scan speed 1400Hz unidirectional, format 512 x512. Images were collected using the following detection setting; GFP: 494-530nm; Cy5: 640-690nm using the 488nm (100%), and 633nm (100%) laser lines respectively. Z stacks were taken every 1.5µm through the depth of whole tail, the frame was averaged at least three times to reduce background. Images shown are maximum projections. Samples were then scored blind. To quantify the number of proliferative cells in the caudal plexus region, a template was drawn around the caudal plexus of GFP images and pasted on to the equivalent anti-PH3 antibody stained samples. Images were imported into Adobe Photoshop and Cy5 positive cells were labelled with red dot. Each dot was automatically recorded on and tallied up at the end. This was repeated for each image and number of proliferative cells in the tail region was recorded (Fig 6.1).

### **6.2.2 VEGF165 assay**

A fish expression vector FRM containing the human *VEGF165* cDNA under the control of the carp  $\beta$ -actin promoter, was provided by Jon Larson (Minnesota). *VEGF* plasmid was transformed and a colony grown up 5ml LB broth containing 100µg/ml of the appropriate antibiotic. One millilitre of this was used to inoculate 100ml LB broth and incubated

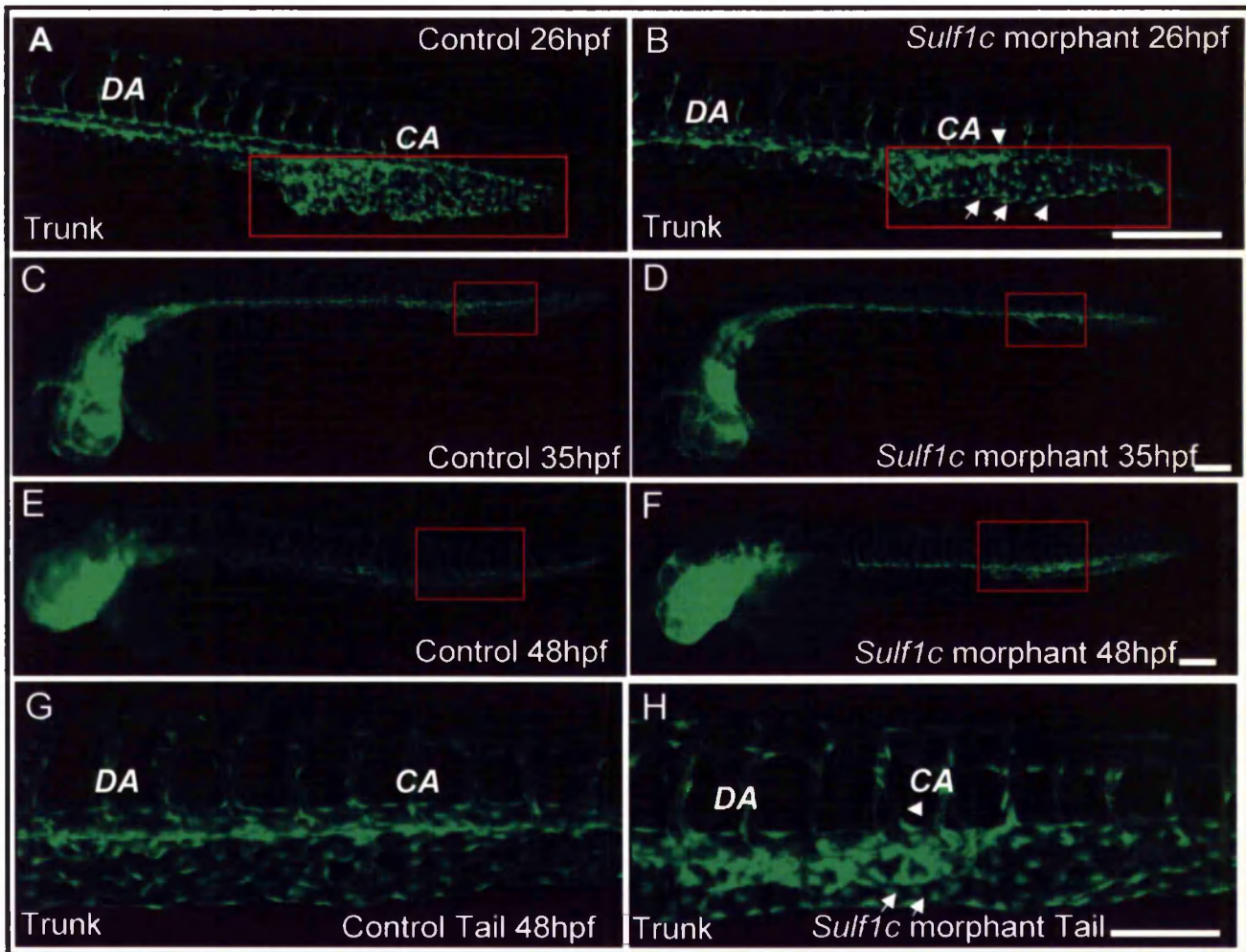


**Figure 6.0: Tail vascular defects in *sulf1c* characteristic morphant** Embryos were injected with 5ng of control morpholino and *S1c*-ATGMO and vasculature analysed at different timepoints *Fli:GFP* images of control injected embryos and *sulf1c* mild morphant. Confocal images of the tail region in control (A) and *sulf1c* morphant (B), red rectangular box highlights the region measured. Arrowhead points to the region of caudal defect and the white arrows denote mass of rounded endothelial cells not organised into a vascular plexus compared to control injected. Fluorescent stereoisimages of 35hpf control (C) and *sulf1c* morphant (D) 48hpf control (E) and *sulf1c* morphant (F). Confocal images of a close up of the 48hpf tail region in control (G) and *sulf1c* morphant (H) White arrowhead points to caudal artery block and white arrows denote the increased number of endothelial cells. Scale bar is 200 $\mu$ m.

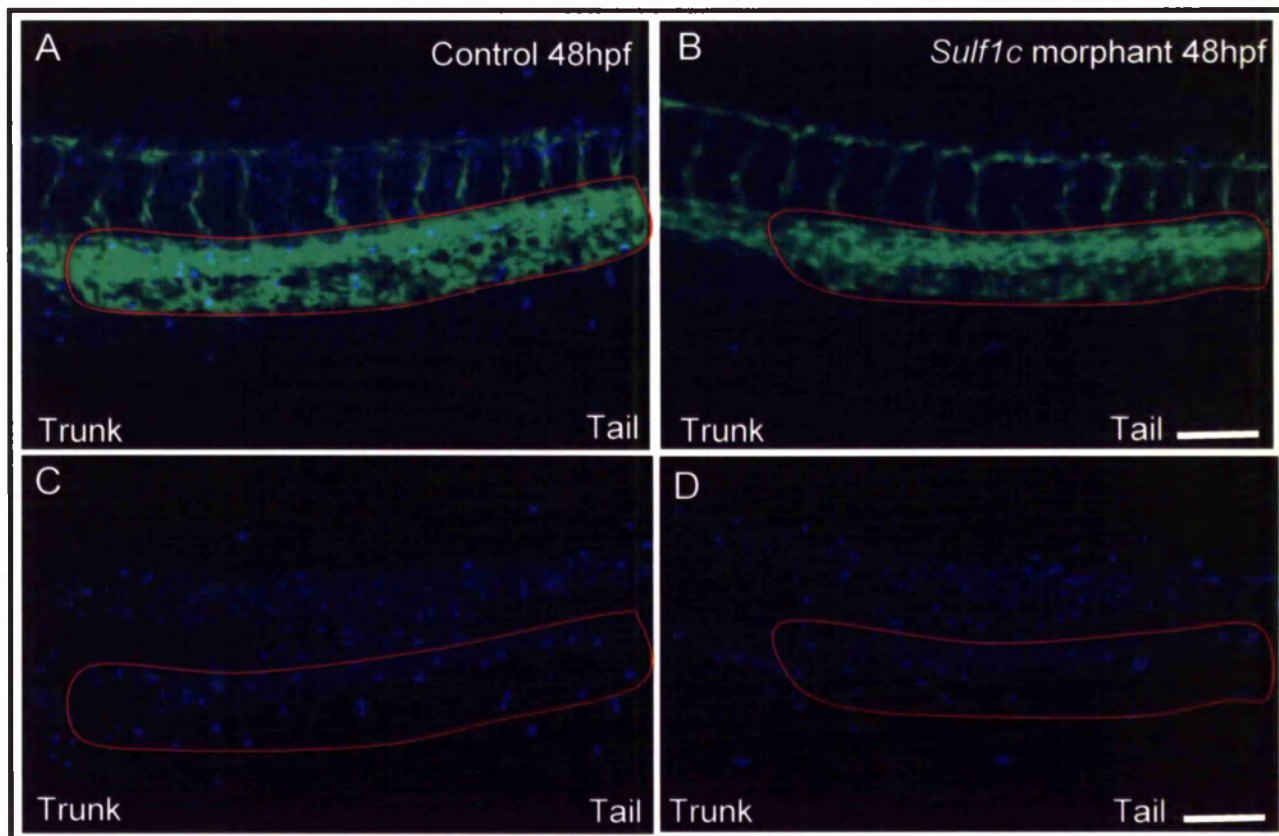


**Figure 6.1: Anti-phosphohistone H3 (pH3) antibody staining of proliferative cells in tail of 48hpf control injected embryos and *sulf1c* morphant.** Whole mount immunohistochemistry of embryos was carried out with anti-pH3. Embryos were mounted in 1% LMP agarose and z stacks took every 1.5µm through the depth of the whole tail. Overlay of *flil*:GFP endothelial cells and Cy5 positive cells in the tail of control injected embryos (A). Overlay of *flil*:GFP endothelial cells and Cy5 positive cells in the tail of *sulf1c* mild morphant. Region of caudal plexus measured is outlined by the red shape (B). Cy5 positive cells in the tail of control injected embryo (C). Cy5 positive cells in the tail of the *sulf1c* mild morphant (D). Red shape highlights the region of tail of proliferative cells included in the quantification. Scale bar 200µm

overnight at 37°C. Plasmid was purified using Qiagen midi-prep kit. 300ng of plasmid along with 2pmol of T7 promoter primer was sent to the sequencing facility to confirm the orientation of the *VEGF165* insert. *VEGF165* plasmid was diluted with sterile dH<sub>2</sub>O to working concentrations of 0.5pg/nl and 4pg/nl with 0.01 % of phenol red.

### 6.2.3 Creating I-SceI hsp70:*VEGF165* construct

The pCS2<sup>+</sup> vector encoding *VEGF165* gene was provided by Helen Bischof. Approximately 7µg of plasmid was digested with 4µl of *BamHI* in a final volume of 50µl to excise the *VEGF* gene. A ~546bp product was run on 1% agarose gel and purified using the gel extraction kit (Qiagen). pCS2<sup>+</sup> vector encoding the heat shock promoter (HSP70) flanked by the *I-SceI* restriction sites was provided by the Hurlstone laboratory. Approximately 7µg of *I-SceI* HSP70 plasmid was linearised with 4µl of *Sall* in a total volume of 50µl. Plasmid was purified using gel extraction kit. Purified products were eluted in a volume of 41.5µl and was subsequently used in blunting reaction made up of the following components; 5µl of T4 DNA polymerase, 10x DNA polymerase buffer, 10mM dNTPs, 0.5µl of BSA, and the remaining made up with dH<sub>2</sub>O in a final volume of 60µl. Reaction was incubated at 12°C for 15mins. Products were purified from nucleotide mix using GFX clean up kit (Amersham Biosciences). Purified products were eluted in a final volume of 40µl and subsequently set up in overnight digest at 37°C with *XbaI*. Products were cleaned up using GFX kit. Purified HSP70 vector was subsequently CIP'd by calf intestine phosphatase enzyme (CIP) in reaction made up to 50µl with 10x NEB buffer (Promega). Samples were incubated for 1hr at 37°C. Product was purified as mentioned previously. Both *VEGF* product and HSP70 plasmid were quantified and set up in a ligation reaction and transformed as described in section 2.2.0. Colonies were screened by PCR using the following primer set HSP70 *fwd primer*: 5'-GTGCGCGCTCTGCTGTATTT-3'; *VEGF rev primer* 5'-GCAGTAGCTGCGCTGATAGA-3' to amplify a product of 1.2kb.

Positive bands of the correct size visualised on 1% agarose gel, were grown up and purified. 300nanograms of the plasmid were sent to UMSF to be sequenced. Both the 5' HSP70 *fwd primer* and SP6 promoter primer downstream of the *VEGF165* gene were used to confirm the orientation of insert.

#### 6.2.4 Microinjection of *I-SceI* construct

Solutions were prepared fresh on the day of injection and assembled on ice. The *I-SceI* construct containing the HSP70: *VEGF* gene was diluted to a working concentration of 100ng/ $\mu$ l. 2 $\mu$ l of this was added to a mix consisting of 10x *I-SceI* buffer, 0.1 $\mu$ l of phenol red, 8.4 $\mu$ l of DEPC H<sub>2</sub>O. A second *I-SceI* construct containing a fluorescent reporter cassette namely KTR4: cherry was also added to the mix to give a final concentration of 20ng/ $\mu$ l. Finally the *I-SceI* meganuclease (5000 U/ $\mu$ l) was added last to the mix to make up a total volume of 15 $\mu$ l of solution. The sample was mixed briefly by pipetting up and down the tube. The sample was kept on ice during the duration of injections. Three microlitres of the solution was backfilled into the needle and microinjection proceeded as described in section 2.5.5. Unlike morpholinos, plasmid DNA was microinjected at the one cell stage to allow optimum chance of efficient integration

## 6.3 Results

### 6.3.1 *Sulflc* morphants display an decrease in cell proliferation in the tail plexus at 26hpf

During vascular development endothelial cells differentiate, proliferate and migrate to form the primary vascular plexus. GFP positive endothelial cells can be visualised migrating from the lateral plate mesoderm in vascular specific transgenic lines to the ventral midline to the origin of the site where blood vessels will form. A second wave of proliferation of endothelial cells occurs during angiogenesis in which endothelial cells sprout from pre-existing vessels proliferating and migrating to form an organised vasculature plexus in the tail, this is further remodelled at 3dpf into single tube. Angiogenic development is not only limited to the tail but some of the later cranial vessels and intersomitic vessels in the trunk appearing between 24hpf and 60hpf are also formed via this process. Analysis of the *sulflc* morphants tail revealed a block in the caudal aorta and ventrally proximal to this region appeared an increased number of endothelial cells compared to the control at 26hpf and 48hpf. To determine whether the A-V shunt in the caudal artery was a result of increased cell proliferation, the number of proliferative cells in the caudal plexus of the *sulflc* morphant was counted. As a measure of proliferation, immunohistochemistry was carried out on whole embryos, using antibody specific for phosphorylated histone H3. Phosphorylation of histone H3 requires active Cdk1 (cyclin dependent kinase) and is an initial event accompanying chromosome condensation, Anti-PH3 specifically labels chromosomes from prophase to anaphase and thus a useful marker for entry into mitosis. The secondary antibody is conjugated with Cy5 fluorophore to detect the presence of the proliferating cells.

Non-injected, CMO and S1c-ATGMO injected samples were incubated with anti-PH3, followed with staining of secondary antibody to identify positive proliferating cells. As a negative control, wildtype and S1c-ATGMO injected embryos were incubated with only secondary antibody to identify background staining (Fig 6.2G). Parameters on the confocal microscope were set identical to the images taken of the negative control samples to eradicate the background noise. Fluorescent images of the vasculature and proliferating cells were acquired with the GFP and Cy5 lasers respectively. Images were taken sequentially and overlaid to ascertain the area of the caudal plexus encompassing the proliferating cells. The number of proliferating cells was counted and represented as a graph in Fig 6.3. Fluorescent images of CMO injected tails are compared alongside the tail of *sulflc* morphants during different timepoints (Fig 6.2 A-F). Anti-pH3 stained embryos were compared alongside each

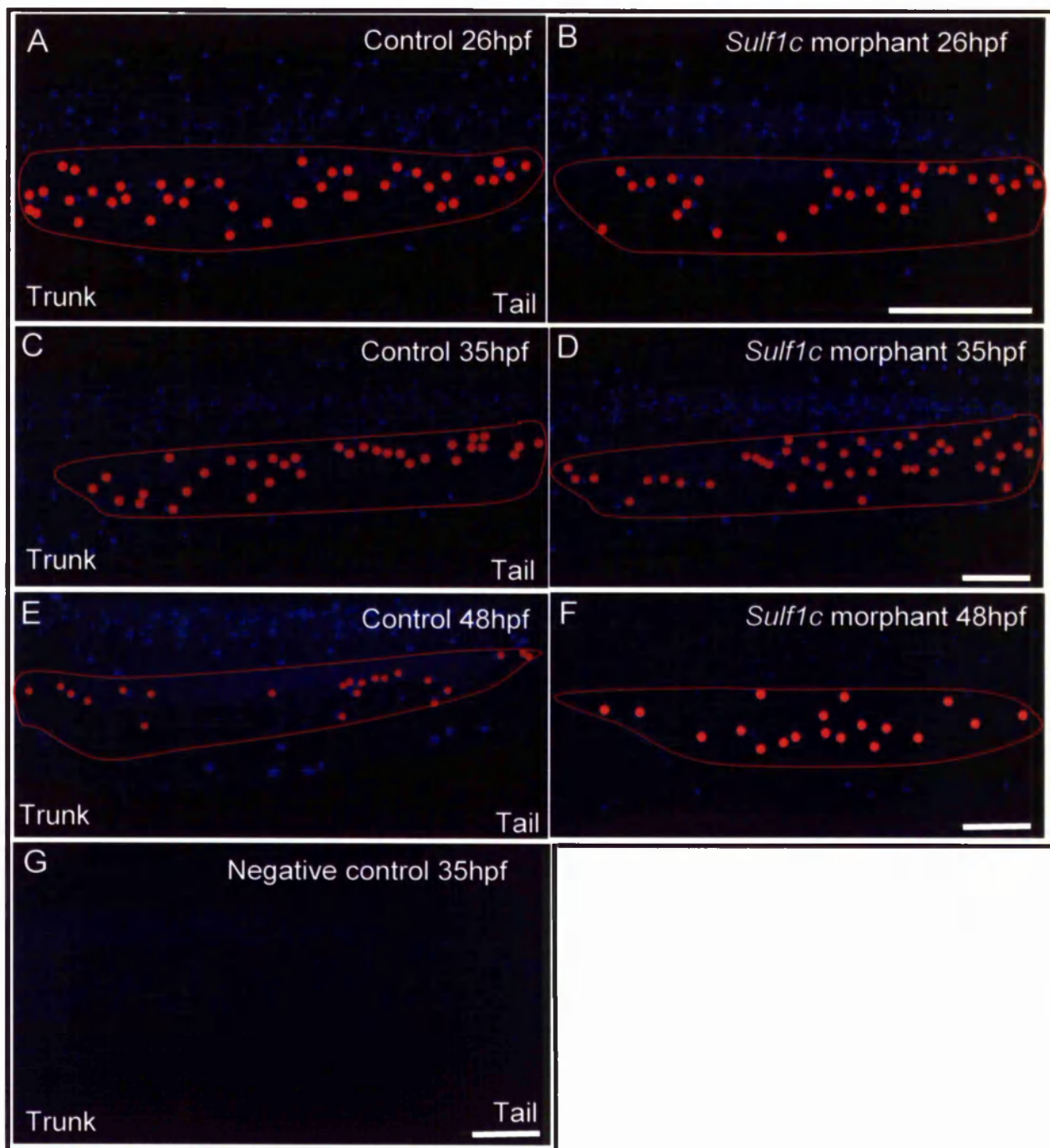


**Figure 6.2: Region of proliferative cells quantified in control injected and *sulf1c* characteristic morphant.** Fluorescent GFP images were taken sequentially with Cy5 images and the z-series stacked together, only maximum intensity projections are shown in these images. Area of the caudal plexus was obtained from *flil*:GFP images by drawing freestyle around the region of interest. This was copied on to equivalent Cy5 stained image and cells within that region marked by red dot and counted. Representative samples at the different timepoints are shown in images (A-F). Tail of 26hpf control injected embryo (A) and *sulf1c* mild morphant (B) 35hpf control (C) and *sulf1c* mild morphant (D), 48hpf control injected embryo (E) and *sulf1c* mild morphant (F). Representative image of negative control (G), cy5 stained cells were measured to be  $<15\mu\text{m}$  and this was set as the upper threshold for the background. Scale bar  $200\mu\text{m}$ .

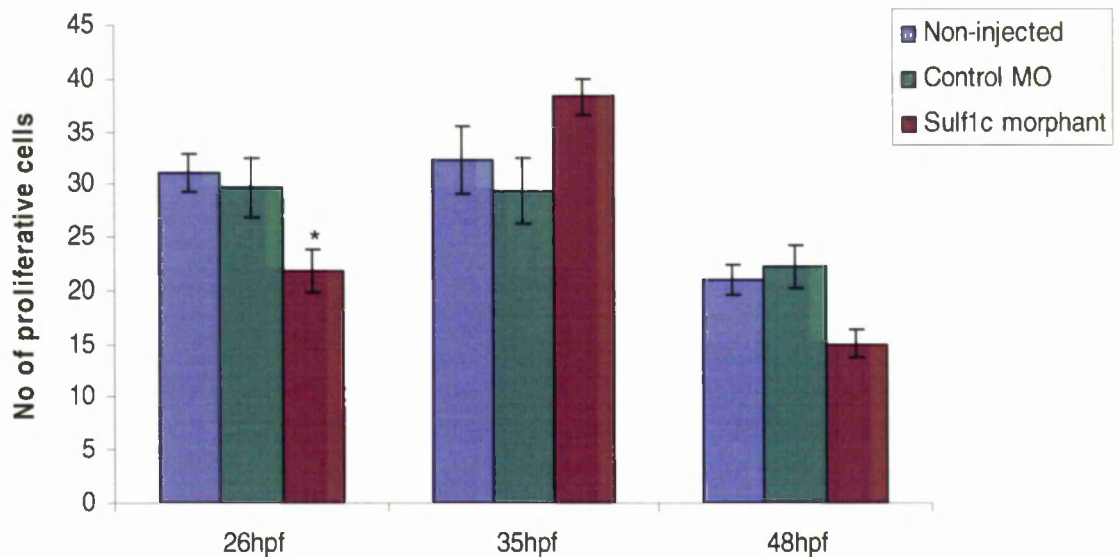


**Figure 6.3: Quantification of the number of proliferating cells in the caudal plexus of control injected and *sulf1c* characteristic morphant.** *Fli1*:GFP embryos were injected with 5ng of Slc-ATGMO and characteristic morphants fixed at different timepoints for the proliferation assay. The data is the average number of proliferative cells and SE is the standard deviation from the number of proliferative cells in each embryo. The proliferative cells were quantified from 30-35 morphants and averaged over the sample size and compared to non-injected and control injected at 26hpf. The number of proliferative cells in the *sulf1c* morphant at 26hpf was significantly lower than wildtype embryos. Asterix (\*) denotes statistical significance,  $p < 0.05$ . At 35hpf and 48hpf, forty embryos were used per experiment. While a 75% increase in proliferation was observed in the *sulf1c* morphants at 35hpf compared to 26hpf a small (~20%) increase was observed compared to control samples at the same stage. Conversely a general decrease was observed at 48hpf in all samples from 35hpf. A ~28% decrease was observed in the number of proliferative cells in the *sulf1c* morphants compared to control and non-injected. Statistical t test at 35hpf:  $p > 0.05$ ; 48hpf:  $p = 0.05$ .  $n = 1$  where  $n$  is the number of experiments

other at 26hpf the timepoint at which the block in the caudal artery was present in the *sulflc* morphants. From confocal observations there appeared to be an increase in the number of endothelial cells (Fig 6.0B) however quantification of the number of proliferative cells revealed a significant decrease (26%) in the *sulflc* morphants compared to CMO and non-injected embryos. Although at 35hpf the total number of proliferative cells in the control samples was similar to 26hpf controls, a 75% increase was observed in the *sulflc* morphants. Interestingly by this time point the blood circulation is active and the short circuiting of the blood flow is evident in the morphants. By 48hpf a general decrease was observed in the total number of proliferative cells in CMO and *sulflc* morphants compared to 35hpf. This decrease (28%) was mild in the *sulflc* morphants compared to the controls but a greater increase (61%) was observed in the *sulflc* morphants from 35hpf to 48hpf. This is consistent with the idea that angiogenic network of vessels in the tail are formed by this point and therefore the number of proliferative endothelial cells is likely to be reduced.

#### 6.3.1.2 Discussion

The block in the caudal aorta of the *sulflc* morphants as discussed previously possibly lies with the loss of arterial identity of endothelial cells in a localised region of caudal artery. To test the alternative possibility that the block in the caudal artery was due to overproliferation of endothelial cells, we measured the number of proliferative cells in the whole caudal plexus region. Proliferation was measured over three timepoints between non-injected, CMO and ATGMO injected. Although the method was an approximation of proliferating 'endothelial' cells it yielded interesting results. From our confocal observations there appeared to be a greater number of disorganised endothelial cells in the *sulflc* morphants compared to wildtype. However from our experiments we found a significant decrease in the number of proliferating endothelial cells in *sulflc* morphants at 26hpf compared to the control injected samples. While a general increase in proliferation was observed at 35hpf in the control injected and *sulflc* morphants, the difference between the control and *sulflc* morphants was not significant, suggesting the number of proliferating cells contributing to the caudal plexus is not different. Similarly a reduction in the total number of proliferative cells was observed at 48hpf in all samples though a greater reduction was observed in the *sulflc* morphants. This is in agreement with caudal plexus formed by this point and is therefore likely these endothelial cells may have reached the quiescent stage.

Although visually there appeared to be more GFP endothelial cells in the caudal plexus this was not due an increase in proliferation. To determine whether the decrease in proliferation at the observed timepoints coincided with increased apoptosis preliminary experiments were performed with the tunel assay (section 2.8). At the different timepoints no difference was revealed in the number of apoptosed cells compared to control injected (Appendix V). Although more repeats could be done the preliminary data indicates that the true changes in proliferation is unlikely to be a natural response to increased apoptosis but perhaps specifically regulated in response to defect in cell signalling molecules such as VEGF.

It can be concluded the apparent increase in GFP labelled endothelial cells were not due to an increase in proliferation or a decrease in apoptosis. However the low level of proliferation of endothelial cell measured in this region support the hypothesis that there may be a low level of VEGF activity here. Low levels of VEGF activity have also been shown to lead to a loss of arterial marker expression<sup>2,416</sup>. It can be therefore be concluded that the block in the caudal aorta is likely to stem from a loss of arterial identity.

## Limitations

Although the anti-pH3 is routinely used to detect proliferative cells, the number of proliferative cells counted was a crude approximation of the number of proliferating endothelial cells as opposed to other cell types. It was noted that at all the time points some cy5 stained cells were not co-localised with GFP, despite their presence in the measured caudal vasculature region. It is likely 90% of the cells present in this region are endothelial cells<sup>85</sup>. However the possibility other proliferating cells may also be present cannot be excluded. Determination of cell number in the PCV and CV can be hampered by the transient presence of variable numbers of haemopoietic cells which seed and differentiate in both the PCV and CV<sup>417</sup>, this may largely account for the non-co localised cy5 cells at the later stages in these regions.

From our confocal observations there generally appeared to be a greater number of disorganised endothelial cells in *sulf1c* morphants compared to control however this did not equate to increased number of proliferative cells as initially anticipated. As the number of endothelial cells was not quantified it is difficult to interpret this result. Unfortunately in the *fli1:GFP* line it is very difficult to differentiate between one or two endothelial cells

particularly at regions where cells have matured and form part of the functioning vasculature. However a common tool now employed to account for endothelial cell number has been generation of the *fli1*: nGFP transgenic line<sup>418</sup> in which the *fli1* promoter drives GFP expression in the nuclei of endothelial cells aiding the monitoring of each endothelial cell visually. If time permitted it would have been desirable to count the number of proliferating cells in this transgenic line, as a total percentage of proliferated endothelial cells present. This would allow specifically to co-localising the number of proliferating cells approximate to the region of defect and present an accurate measure of the number of proliferating endothelial cells.

### 6.3.2 Creating a VEGF assay

VEGF is required for new blood vessel formation, angiogenic sprouting and plays an important role in modulating vascular permeability in both embryonic and adult stages<sup>258</sup>. In zebrafish VEGF has shown to play an important role in angiogenesis and cell signalling role in arterial endothelial differentiation<sup>2,390</sup>. So far *in vitro* studies have shown addition of exogenous *VEGF* to endothelial cells lines or CAM can induce vessel like structures or ectopic branches. Similarly in zebrafish, addition of VEGF protein/plasmid has shown to induce subtle ectopic branches in the angiogenic formed subintestinal basket<sup>329,419</sup>. While these methods show overexpressing *VEGF* can mediate early phases of angiogenesis, we aimed to induce a robust network of ectopic vessels in the trunk of the *fli1*:GFP embryo that could be quantifiable and used in future co-injection experiments with morpholino.

To create an ectopic *VEGF* assay *in vivo*, *fli1*:GFP embryos were injected with several different doses of FRM:*VEGF* plasmid to optimise the concentration of ectopic vessel formation. However embryos were first co-injected with  $\beta$ -actin:GFP initially at the one cell stage to test the efficiency of the  $\beta$ -actin promoter (Fig. 6.4)

### 6.3.3 Ectopic *VEGF* results in outgrowth of vessels

Injections were performed in *Fli1*: GFP embryos and vasculature analysed at 2dpf. As preliminary experiments at lower concentrations than 2pg displayed vascular morphology similar to that of wildtype embryos in, all subsequent injections were carried out at higher doses, ranging from 2pg-10pg. Injections were repeated with each dose at least once and the data from both sets amalgamated and penetrance represented as average percentage.

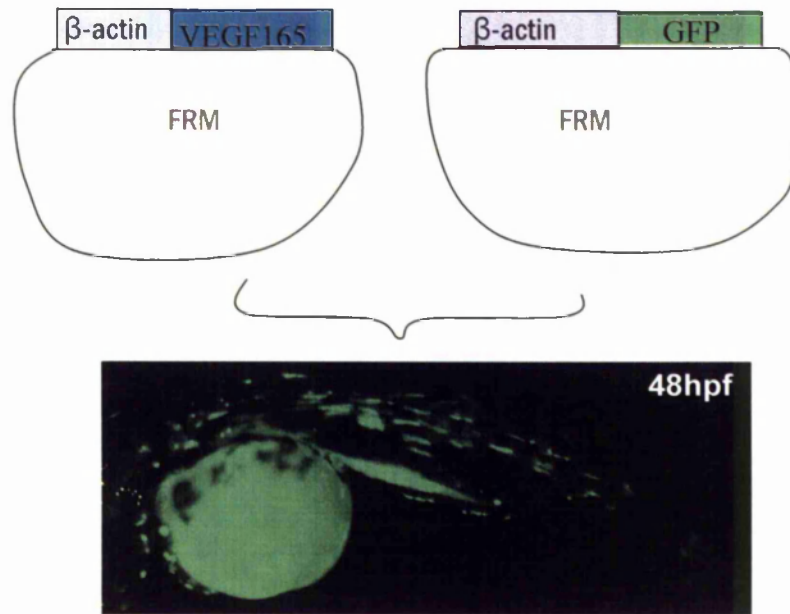


**Figure 6.4:** A schematic diagram of the Frm constructs co-injected at one cell stage and the phenotype at 48hpf. Human VEGF165 and GFP was cloned under  $\beta$ -actin promoter in FRM construct (provided by Jon Larson Minnesota). The *AB* wildtype embryos were microinjected with the two constructs. An example of 48hpf embryo expressing GFP mainly in the muscle, this was an indicator that  $\beta$ -actin promoter was functioning and it was assumed that *VEGF* was also being *co*-expressed.

Non-injected controls were compared alongside the control and FRM:VEGF injected each time, and the data from each experiment was combined and represented as one bar in the chart, as they were devoid of ectopic phenotype. Control injections were performed with empty FRM vector only to ensure injections at a particular concentration did not induce a phenotype that could be mistaken for an ectopic *VEGF* mediated phenotype. To give a clear indication as to the mortality induced by increasing the doses of *VEGF* plasmid, mortality was scored at 24hpf.

Although approximately 25% of death was observed in non-injected controls this was not significantly different to control and FRM: *VEGF* injected. Mortality rate in the control FRM and FRM:*VEGF* injected was generally equivalent or lower than in the non-injected samples. Increasing plasmid concentration did not increase the mortality in both control and FRM:*VEGF* plasmid injected. The survival rate of embryos in both control and FRM:*VEGF* injected was similar at the same plasmid concentration. All surviving embryos were analysed at 48hpf to fully assess the extent of any ectopic vessels. Majority of embryos in non injected, control FRM injected and a small subset in the FRM: *VEGF* injected showed vasculature formation identical to the wildtype at the same stage. The percentage of wildtype embryos decreased with increasing concentration of *VEGF* plasmid. A small percentage of embryos were present that showed overt developmental abnormalities these were classed as non-specific as they were occasionally present in non-injected or control injected samples. There were also low penetrance of embryos present in the *VEGF* injected samples that displayed severe defects in the overall morphology such as pericardial oedema and inverted tails these were also classed in 'non-specific' category as the severity of the phenotype would compromise future co-injections with the morpholino.

A wide spectrum of phenotypes were found in the FRM:*VEGF* injected embryos that were reproducible and appeared specific to *VEGF* plasmid. These embryos were grouped as mild, moderate and severe depending on the vascular morphology of the intersegmental vessels (ISVs) and axial vessel i.e. PCV, DA, CA, CV. Since there appeared to be multiple affects on the vasculature in one embryo varying from one extreme to another, these were defined as ectopic sites. Endothelial cells sprouting dorsally/ventrally from three or less ISVs, or clumped as a mass of cells at their stalk were referred to as an ectopic site. Mild class phenotype was separated on the basis of having one to few ectopic sites distributed in a mosaic pattern in the trunk vasculature without affecting the overall morphology of embryo. Moderate class phenotype was separated on the basis of having severe ectopic *VEGF* site with

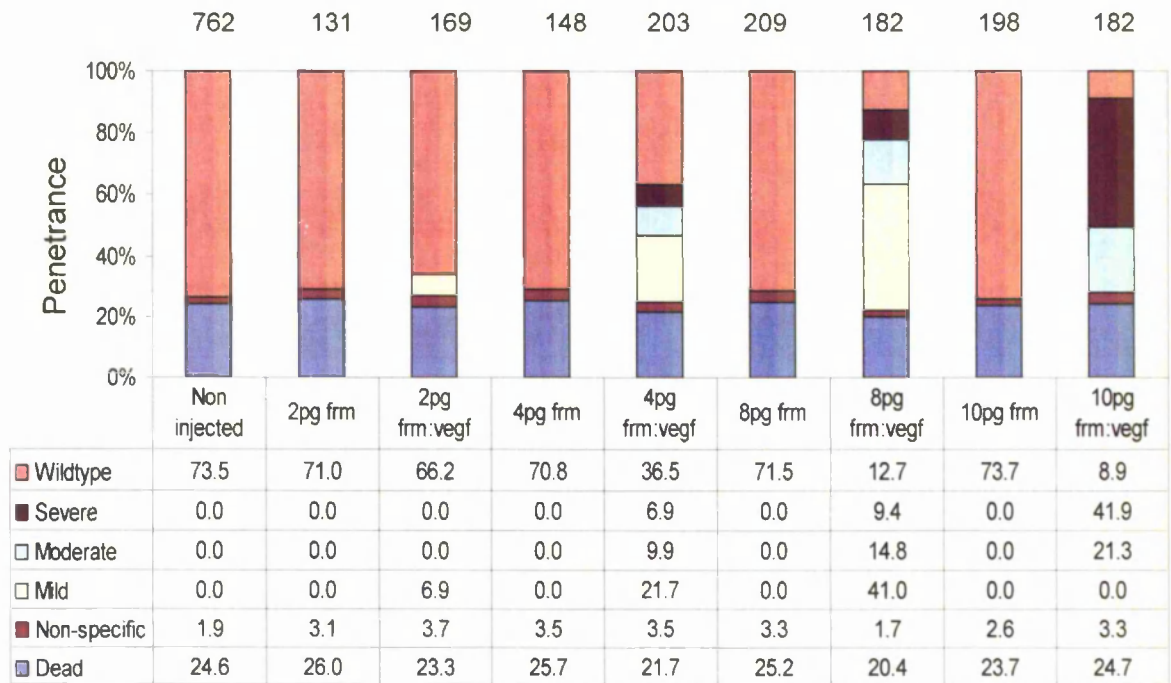


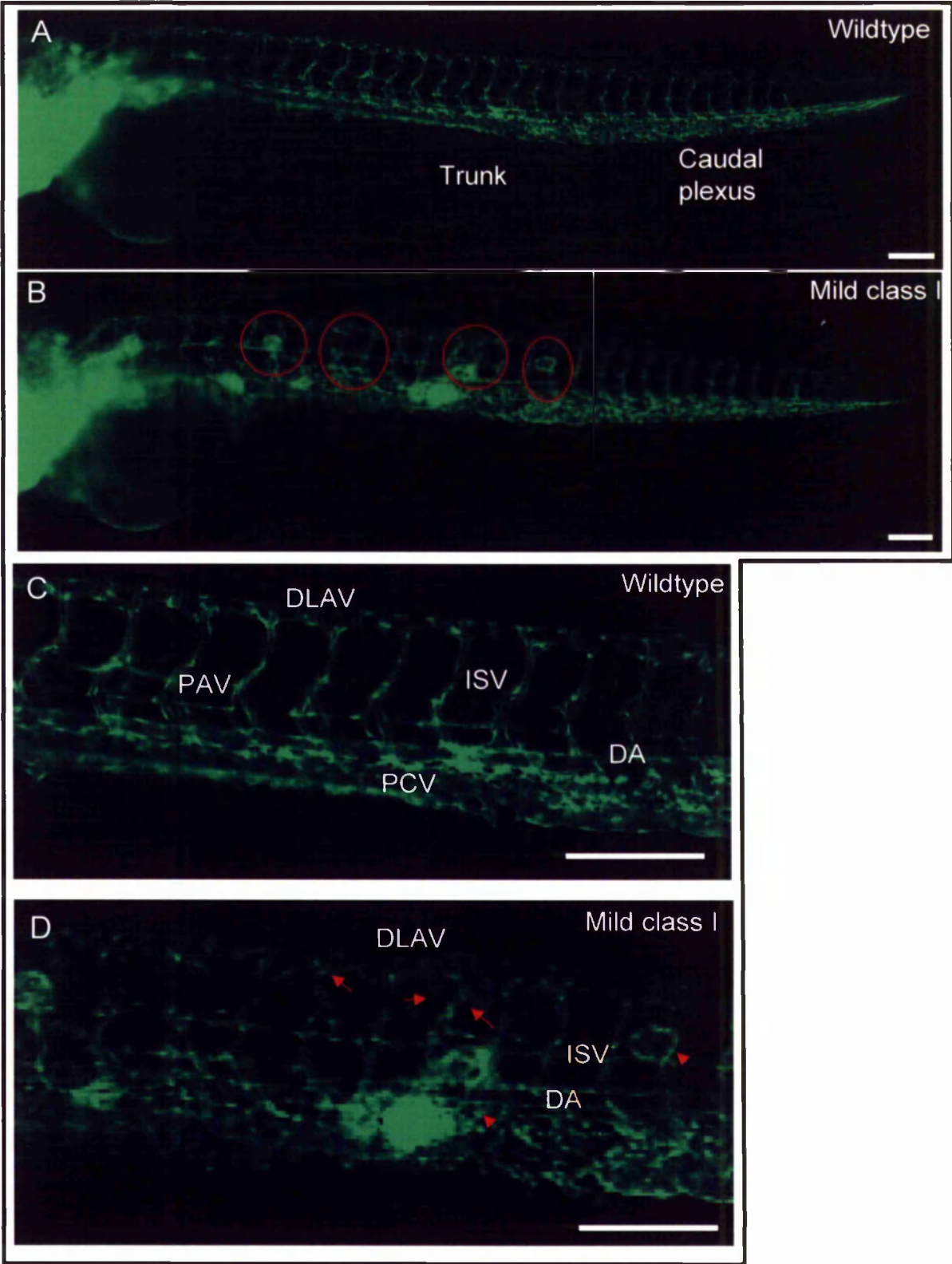
**Figure 6.5: Chart showing the analysis of *flil:GFP* embryos injected with *Frm:VEGF* plasmid.** Data shown is combined from two experiments and percentage penetrance represented as an average. All embryos were scored at 24hpf for mortality rate (Dead) and surviving embryos were analysed at 3dpf and categorised into different classes. These were scored as wildtype, non-specific and the embryos displaying phenotypes of *VEGF* overexpression were further characterised into mild, moderate and severe phenotypes based on the vascular morphology of the ISVs and axial vessels. *Frm-VEGF* plasmid was injected at a range of concentrations 2-10pg and compared against control injected *Frm*-vector only and non-injected. The mortality in control injected and *Frm:VEGF* plasmid injected was comparable. Majority of embryos in the control injected and non-injected and a subset in *frm:VEGF* injected displayed vascular morphology identical to that of the wildtype embryos. A small subset of non-specific embryos existed in all non-injected and injected embryos that were prevalent in all doses injected. Injection of the *frm:VEGF* plasmid at 2pg produced a small percentage of embryos displaying only mild ectopic *VEGF* phenotype, Injections at the higher dose of 4pg and 8pg of *frm:VEGF* produced 38% and 65% of embryos displaying ectopic *VEGF* phenotypes represented by all three classes.

mild dilation of the axial vessel. Severe class of embryos were separated on the basis of fused ISVs, and severe dilation of the posterior cardinal vein.

Fluorescent images were taken at 3dpf and are represented in Figures 6.6-6.8. The mild and moderate class of embryos were further categorised based on the number of ectopic sites present the data was collated and represented as an average percentage (Fig. 6.9). It must be mentioned that although the head appeared morphologically normal in all classes apart from the severe, the cranial vasculature was difficult to image for ectopic vessels due to the strong GFP expression in the neurocranium and as a result was excluded from analysis.

The mild class of embryos appeared morphologically normal at 3dpf with no alterations in the head or morphological defects in the tissue. However fluorescent images of the vasculature revealed regions of bright GFP, (Fig. 6.6B,F) indicative of a dense number of endothelial cells in the trunk. These were represented as a clump of endothelial cells amassed in a ball shape at the stalk of the ISVs, (Fig. 6.6 B,D) or occasionally ventral to the parachordal vessels (Fig 6.6 B,D,E,G red arrow). In a total of 70% of embryos exhibiting the mild class I and II phenotypes a mass of endothelial cells were located medially between the DA and PCV forming an aberrant connection (Fig. 6.6 D,H). In 29% of embryos there was a mixture of both ectopic sites (Fig. 6.6B). All embryos in mild class I and III also displayed ectopic branches sprouting laterally from the ISV's midline (Fig. 6B). Sprouting of ectopic branches appeared to be located in the most anterior ISV's and restricted to the most upper dorsal region of the ISV's, with endothelial cells migrating prematurely from horizontal myoseptum and anastomosing with adjacent ectopic branches to form the DLAV (Fig 6.6 D,F,H). The frequency and location of these ectopic sites varied greatly from embryo to embryo.

The majority of embryos in the moderate class showed normal overall body shape to that of control and non-injected samples, though a small percentage had mildly inverted tails (Fig 6.7 A,B). In this class of embryos the ectopic sites appeared more severe than in the mild class. In both moderate classes ISV's were dilated and unilaterally or bilaterally fused with the adjacent ISV (Fig 6.7 C&D red arrows). In a few of the ectopic sites the merging of ISV's amassed to what appeared similar to a ball of endothelial cells not organised into branches. The ectopic sites appeared non uniformly throughout the trunk of the embryo either situated in the medial trunk or in the most caudal region of the tail plexus. In the moderate class I the most posterior ISVs were mildly dilated but not fused together. Other common features included mild dilation of the posterior cardinal vein, or ectopic branched sites.



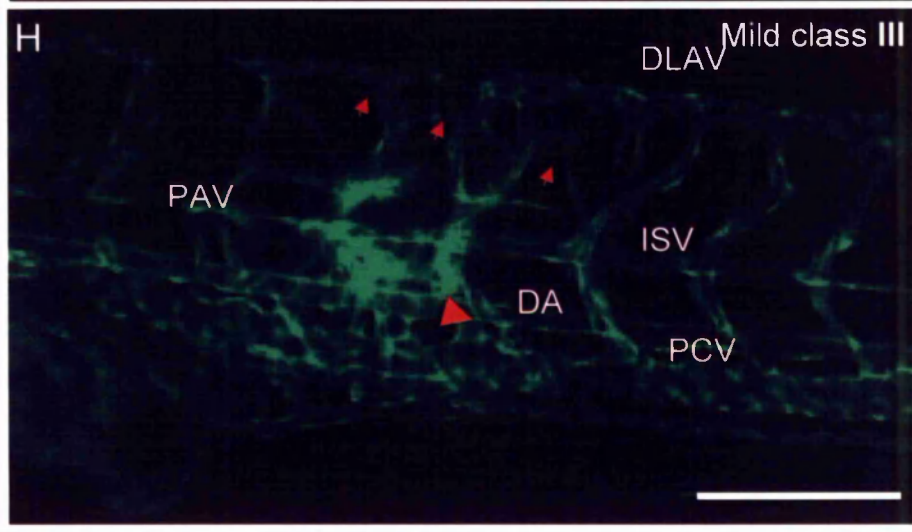
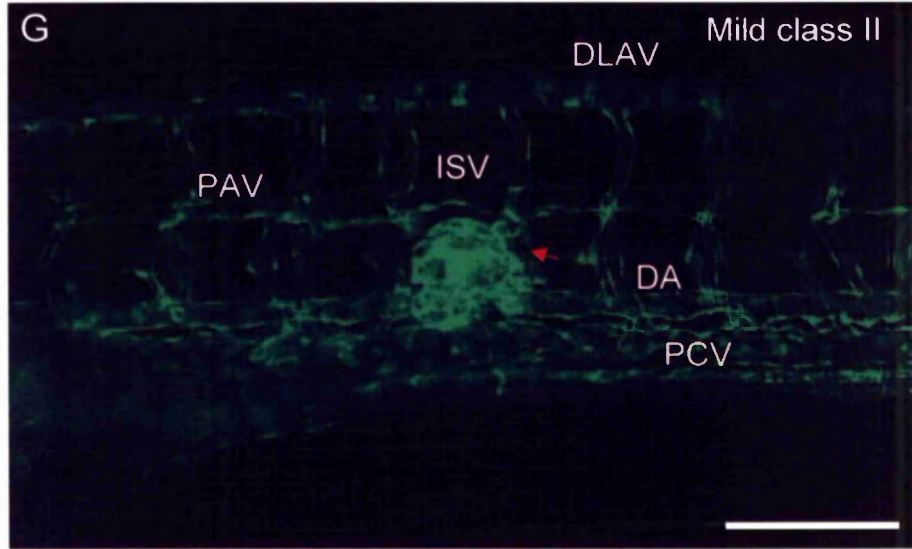
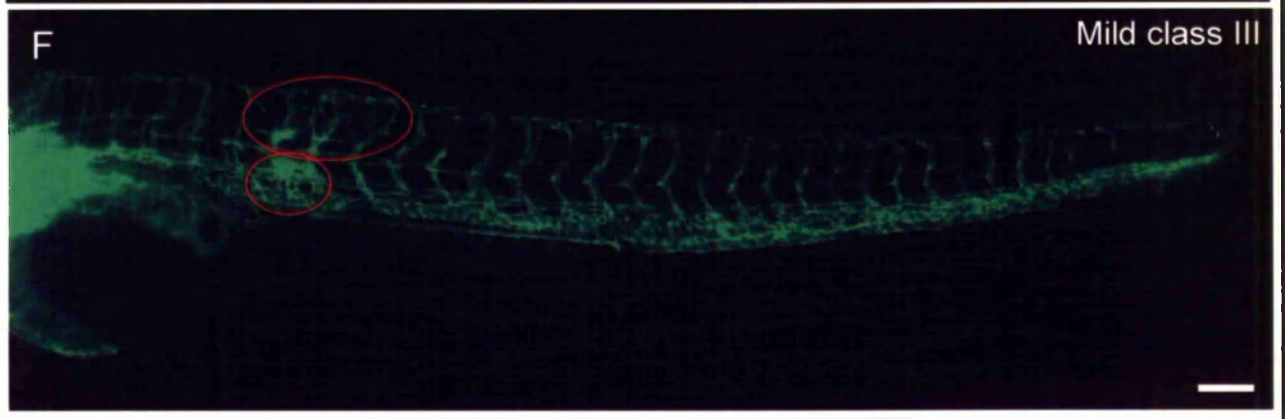
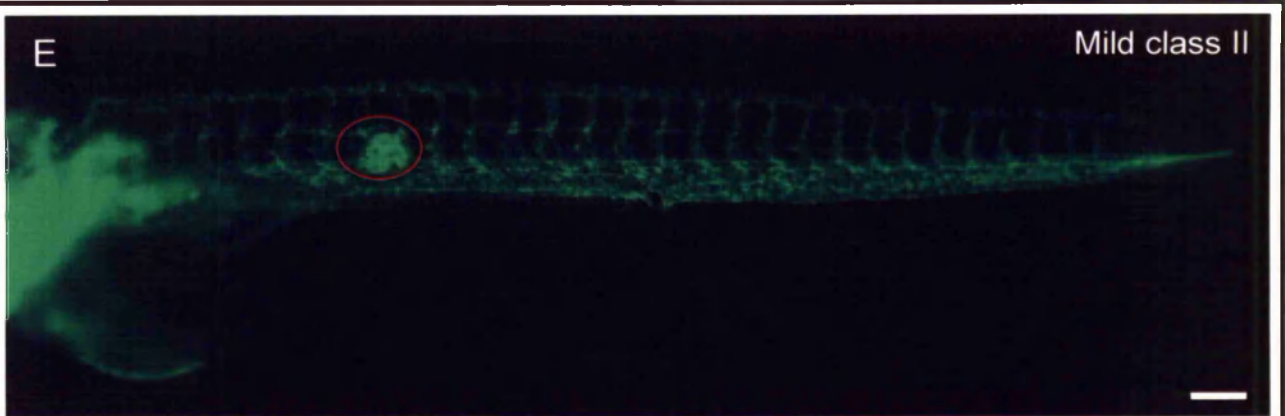


**Figure 6.6: Vascular phenotypes observed in mild class of 3dpf embryos injected with frm: *VEGF* plasmid.** *Fli1*:GFP embryos were injected with Frm:*VEGF* plasmid at the one cell stage and vascular development analysed at 3dpf by comparison to control injected Frm embryos. Lateral images of the whole trunk (A,B,E,F) and close up images (C,D,G,H) of a region of the ectopic site were taken on the zeiss stereomicroscope. Control injected embryos showed normal overall morphology and vascular development typical of 3dpf embryo. Mild class of embryos showed similar overall morphology while analysis of trunk vasculature revealed different levels of severity of ectopic *VEGF* sites. Control embryo show normal vascular formation and patterning (A,C). An example of one of the mild class embryos (B), red circle denotes the sites designated as ectopic sites in the trunk. Close up of the ectopic site (D) red arrows denote the dense sprouting vessels connecting the intersegmental vessels and DLAV. Red arrowhead points to a dense accumulation of endothelial cells not organised into a network of vessels. A second example of mild class embryo (E,G) featuring only one ectopic site highlighted by the red circle, appears as ball of endothelial cells. Third example of mild class embryo (F,H) showing ectopic vessels sprouting from the most anterior ISV's and forming connections with DLAV indicated by red arrows, red arrowhead depicts a mass of endothelial cells. DA:dorsal aorta; PCV: posterior cardinal vein; ISV: intersegmental vessels; DLAV: dorsal lateral anastomotic vessels, PAV: parachordal vessels. Scale bar is 200µm.

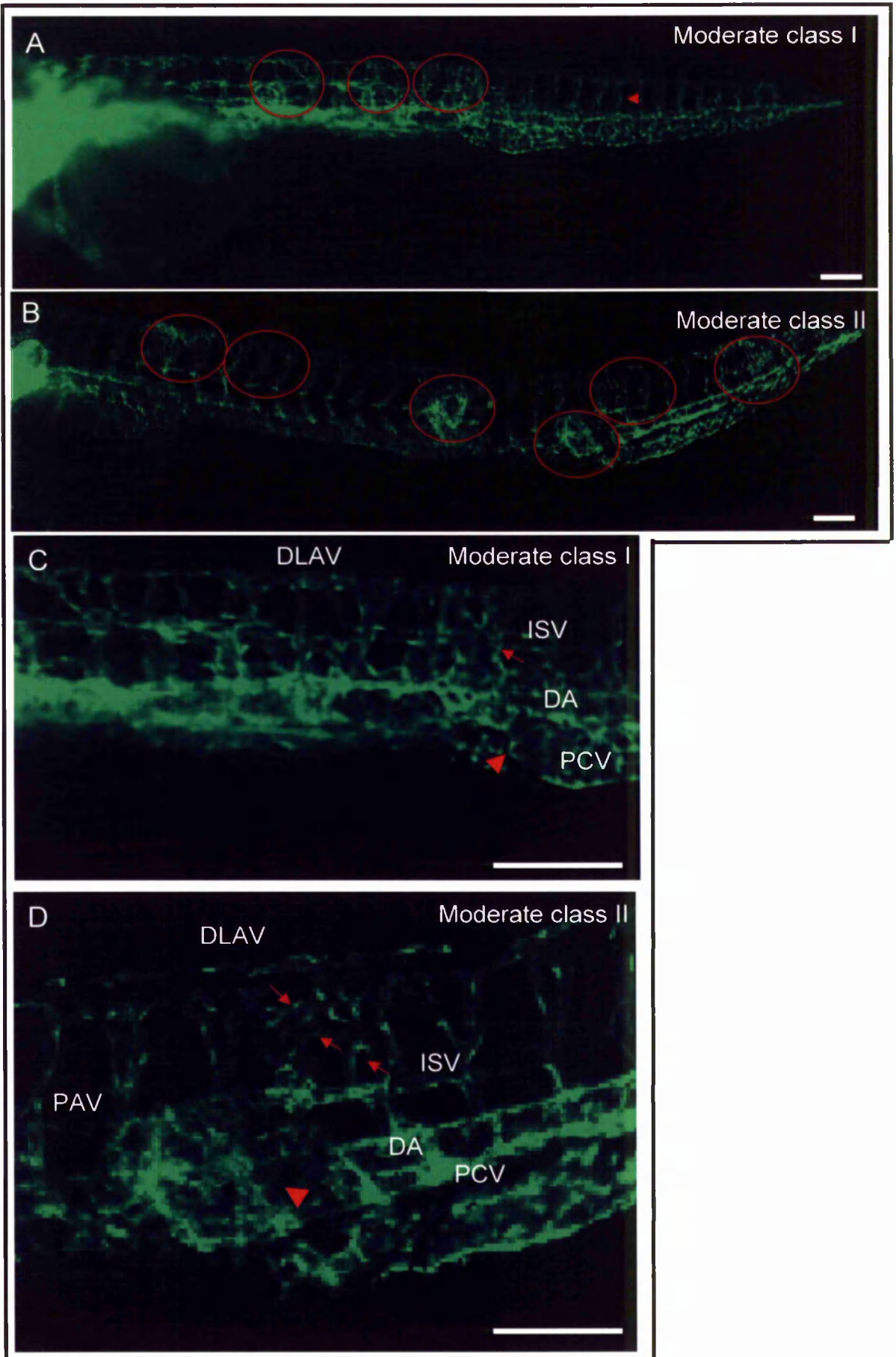


**Figure 6.7: Vascular phenotypes observed in moderate class of 3dpf embryos injected with frm: VEGF plasmid.** *Fli1*:GFP embryos were injected with Frm:*VEGF* plasmid at the one cell stage and vascular development analysed at 3dpf by comparison to control injected Frm embryos. Lateral images of the whole trunk (A,B) and close up images of a region of the trunk were taken on the zeiss stereomicroscope (C,D). Control injected embryos showed normal overall morphology and vascular development typical of 3dpf embryo. An example of moderate class I phenotype displaying (A) three ectopic sites distributed non-uniformly in the trunk, highlighted in red circles. Red arrowhead denotes posterior ISV incorrectly patterned, not following the chevron shape of the somites. Close up of ectopic site reveals (C) dilated ISV's fused together and mild dilation of posterior cardinal vein indicated by red arrow and arrowhead respectively. Second example of moderate class phenotype displaying four ectopic sites (B), close up of the ectopic site in the tail (D). exhibits fusion of ISV and red arrowhead denotes a mass of endothelial cells /migrating from ISV's forming ectopic site ventral to the PCV. DA:dorsal aorta; PCV: posterior cardinal vein; ISV: intersegmental vessels; DLAV: dorsal lateral anastamotic vessels, PAV: parachordal vessels. Scale bar is 200 $\mu$ m.

In the most severe class of embryos the overall body shape was moderately affected compared to the mild and moderate class of embryos (Fig 6.8A,B). There was strong dysmorphogenesis of the PCV, with poor demarcations between the artery and vein (brightfield image not shown). In severe class I the fusion of ISVs was clearly evident in two of the ectopic sites. The most prominent feature of this class was the aberrant separation of the DLAV accompanied with severe dilation of the posterior cardinal vein. In contrast to the control injected embryos in which the DLAV that normally “zipper” together in a caudal to rostral progression, in both examples of the severe class embryos the separation of the DLAV appeared as a result of ectopic vessels branched from either DLAV or fused dilated ISVs (Fig 6.8C,D). In addition all severe class II embryos the ISVs fail to sprout from the dilated PCV, where as ISV sprouting from the DA were unaffected. However not all medial and caudal ISV migrated laterally to their future positions to form DLAV (Fig 6.8D). As a result most of ISV’s appear to be incorrectly patterned not following the chevron shape of the somites.

#### **6.3.4 Number of Ectopic *VEGF* sites in mild and moderate class embryos display high variation**

The presence of ectopic vegf sites in the mild and moderate class of embryos did not affect the overall morphology of the embryo. In contrast the severe class embryos, displayed defects in the overall morphology. Embryos displayed pericardial oedema and vascular oedema in the tail with 20% of embryo also displaying a curved body axis. As the phenotypes of this class would severely compromise the health of the embryo for future co-injection experiments, these embryos were excluded from further analysis. Injections were repeated at 8pg to determine if the frequencies of different mild and moderate classes were consistent and whether the ectopic feature could be used as a valid measure of *VEGF* overexpression. To test this, the frequency of different types of mild and moderate class (featuring the different number of ectopic sites) was recorded from three additional experiments and calculated as a percentage of the total number of mild and moderate embryos.

From the chart (Fig. 6.9) it can be deduced that all classes were present at fairly moderate penetrance levels. Although the similar number of ectopic sites were present in each class as described above the frequency of the mild class and moderate class varied significantly in each experiment with similar penetrance levels between mild class I and mild class III

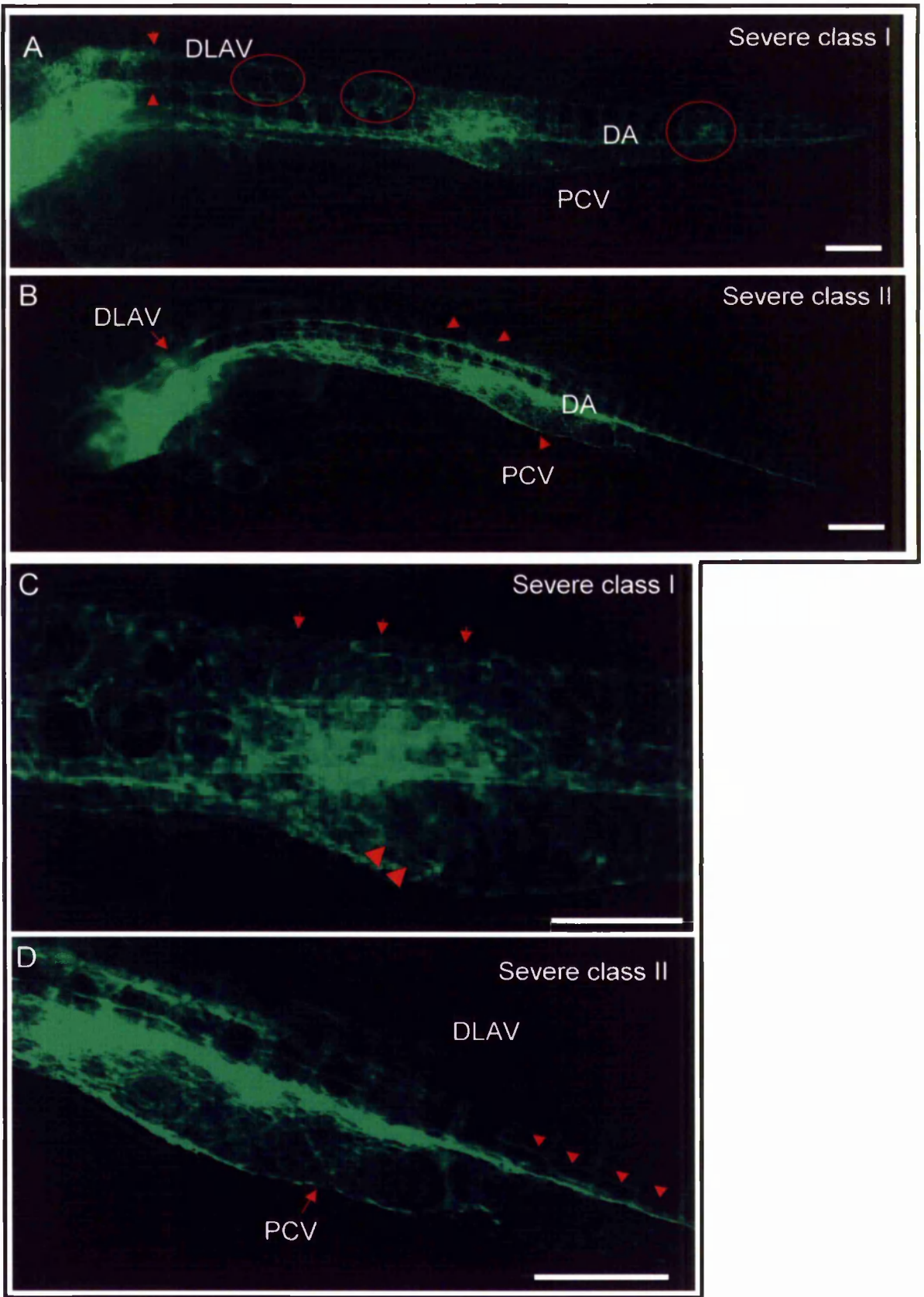


**Figure 6.8: Vascular phenotypes observed in severe class of 3dpf embryos injected with frm: *VEGF* plasmid.** *Fli1*:GFP embryos were injected with Frm:*VEGF* plasmid at the one cell stage and vascular development analysed at 3dpf by comparison to control injected frm embryos. Lateral images of the whole trunk (A,B) and close up images of a region of the trunk were taken on the zeiss stereomicroscope (C,D). Control injected embryos showed normal overall morphology and vascular development typical of 3dpf embryo. Embryos in this class showed severe defects in overall morphology i.e. pericardial oedema and vascular oedema in the tail. An example of severe class I phenotype (A), ectopic sites are highlighted by the red circle. Interruption of the paired DLAV is shown as result of ectopic vessels spouting from one or the other DLAV, gap is marked by red arrows. Close up one of the ectopic *VEGF* region (C) can be shown in severe fusion of intersegmental vessels and dilation of posterior cardinal vein are indicated by red arrows and arrowhead respectively. Severe class II phenotype embryos (B) display similar characteristics. The dilation of posterior cardinal vein with concomitant loss of sprouting ISVs from the PCV was also a prevalent feature. Close up of the severe phenotype (D) shows the irregular shaped ISV's. DA: dorsal aorta; PCV: posterior cardinal vein; ISV: intersegmental vessels; DLAV: dorsal lateral anastamotic vessels, PAV: parachordal vessels. Scale bar is 200 $\mu$ m.

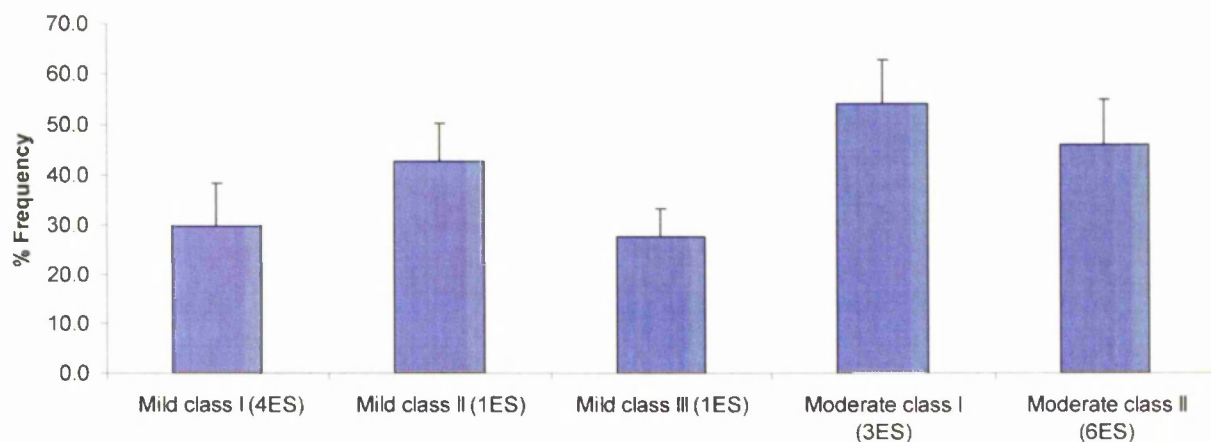


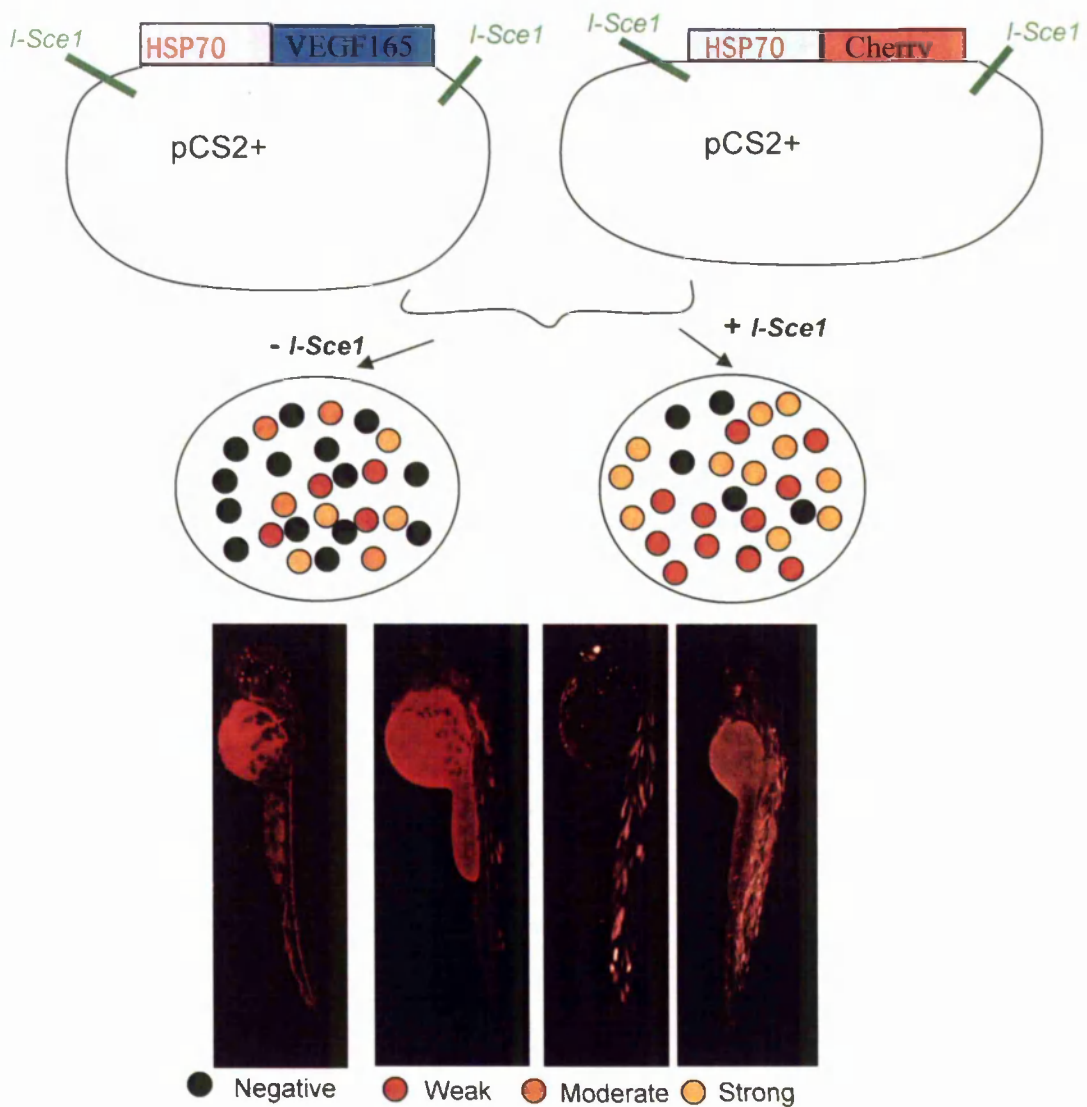
**Figure 6.9: Frequencies (%) of mild and moderate phenotype class following ectopic *VEGF* expression.** *Fli1*:GFP embryos were injected with 8pg of FRM;*VEGF* plasmid and mild and moderate phenotypes segregated for analysis. Data is combined from three experiments where the number of total embryos in mild and moderate class is 110 and 46 respectively. Frequencies of each class were calculated as a percentage of the equivalent class total. The injected embryos were categorised based on the characteristics of the ectopic sites (ES), and the severity of accompanying ectopic vascular phenotypes. Standard error is the standard deviation of three experiments.

(Fig. 6.9). This made it difficult to choose an adequate representative of ectopic *VEGF* phenotype for quantification since each class displayed a different number of ectopic sites. Therefore if an increase or decrease was observed in the number of ectopic sites it would be difficult to determine if this was a true effect of the S1c morpholino or fell into a different category of phenotype. Whilst a reliable measure of the ectopic *VEGF* assay was not achieved, future injections with the FRM:*VEGF* plasmid were not co-injected with *sulf1c* morpholino and other strategies were sought.

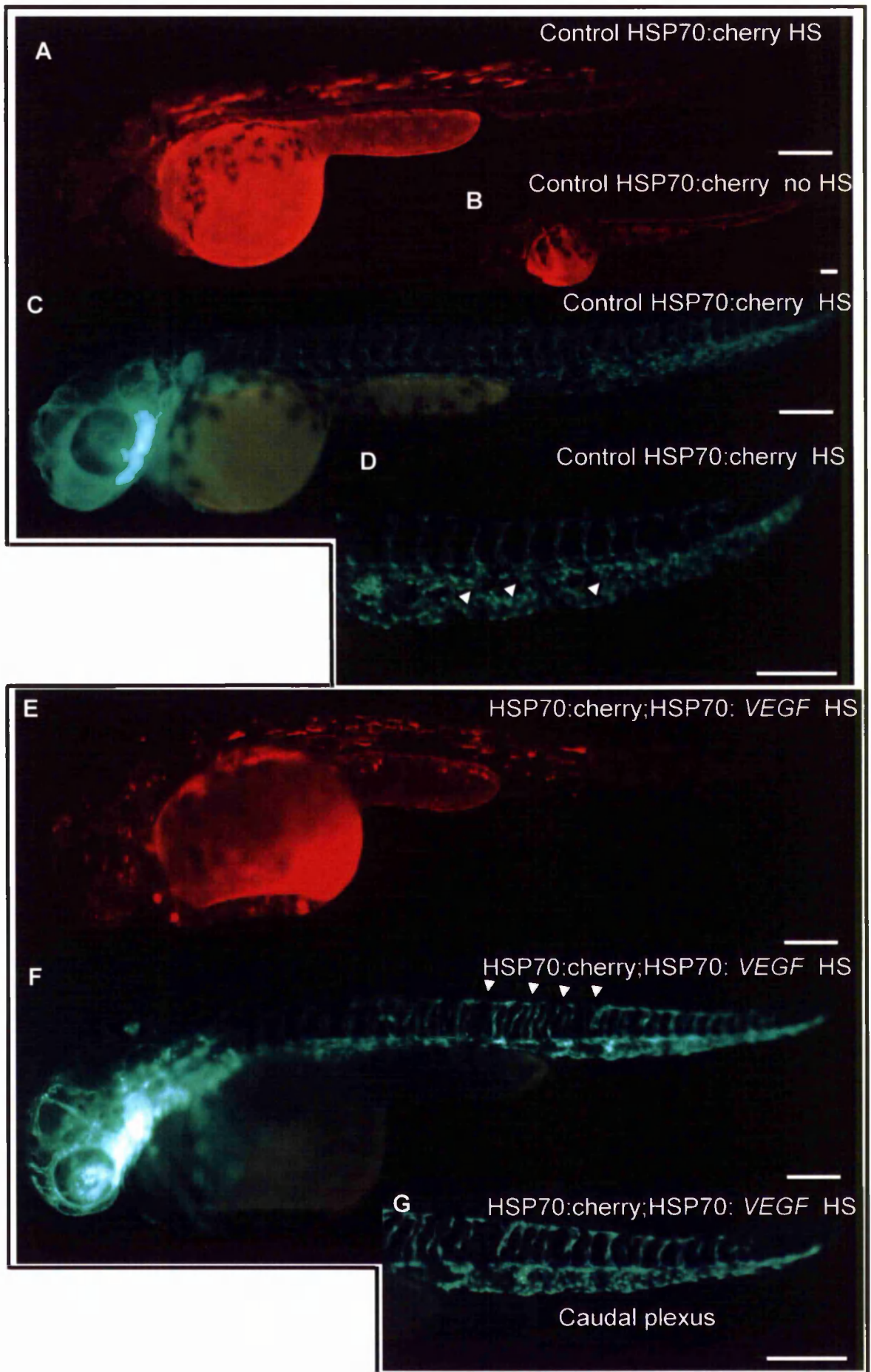
To generate a consistent and stable level of *VEGF* overexpression, it was decided to create a transgenic line that would allow temporal and spatial control over ectopic *VEGF* expression. While transgenic lines have been created with microinjecting Frm plasmid the germline transmission is fairly low and particularly  $\beta$ -actin promoter is restricted to muscle at later stage during development thus hindering ubiquitous expression. As zebrafish transgenesis techniques have become refined over the years, the ability to create transgenic lines with high transgenesis efficiency has relied on the use of systems like the *I-SceI* meganuclease approach. This was first utilised in medaka<sup>420</sup> and since has been shown to work in many organisms including zebrafish<sup>421</sup>. The *I-SceI* meganuclease is intron encoded endonuclease that cleaves 18bp recognition sites flanked on either side of gene of interest, thus the recognition sequence is found only once in  $7 \times 10^{10}$  bp of random sequence and given the size of the zebrafish genome it is likely the site is not present<sup>421</sup>. Co-injection of transgene and meganuclease enzyme is known to increase transgenesis efficiency up to 30.5%<sup>420</sup> as well as the distribution (76%) of the co-injected plasmid in F0 animals (Fig 6.10). We utilised this system in attempt to create a transgenic line that would allow us to produce a consistent level of *VEGF* overexpression. Since *VEGF* expression is derived from both maternal and zygotic gene pool during zebrafish development, we utilised a system that allows for temporal control of *VEGF* by placing it under the control of zebrafish heat shock promoter (HSP70). This was to eliminate early effects of *VEGF* activation

### **6.3.5 Testing the HSP70: *VEGF* construct in *flil*:GFP; *gata*:ds-Red line**

Human *VEGF* cDNA was isolated from pCS2<sup>+</sup>, and cloned into *I-SceI* vector downstream of HSP70 promoter. HSP70: *VEGF* construct was sequenced to verify the correct orientation of the *VEGF* gene. Preliminary experiments were aimed at optimising the timepoint (hpf) and



**Figure 6.10: A schematic representation of the functional consequences of the *I-SceI* meganuclease.** *I-SceI* is an endonuclease that cuts at 18bp recognition sequences flanking both sides of gene of interest (represented by green line). Linearisation of DNA by *I-SceI* greatly facilitates transient expression as well as increasing transgenesis frequency. Injection without *I-SceI* results in lower penetrance of embryos with cherry expression and consequently low transgenesis frequency. Co-injections with *I-SceI* leads to increased number of embryos with cherry expression (coloured dots indicate different levels of cherry expression). *I-SceI* it is thought to increase transgenesis frequency by reducing concatemerisation, through cleaving generated concatemers from endogenous ligase/replicase activity thus providing more recombinogenic ends that facilitate highly efficient integration, adapted from (Thermes *et al* 2002). Fluorescent ds-Red images of *flil:gata* embryos co-injected with both constructs, HSP70: heat shock promoter.



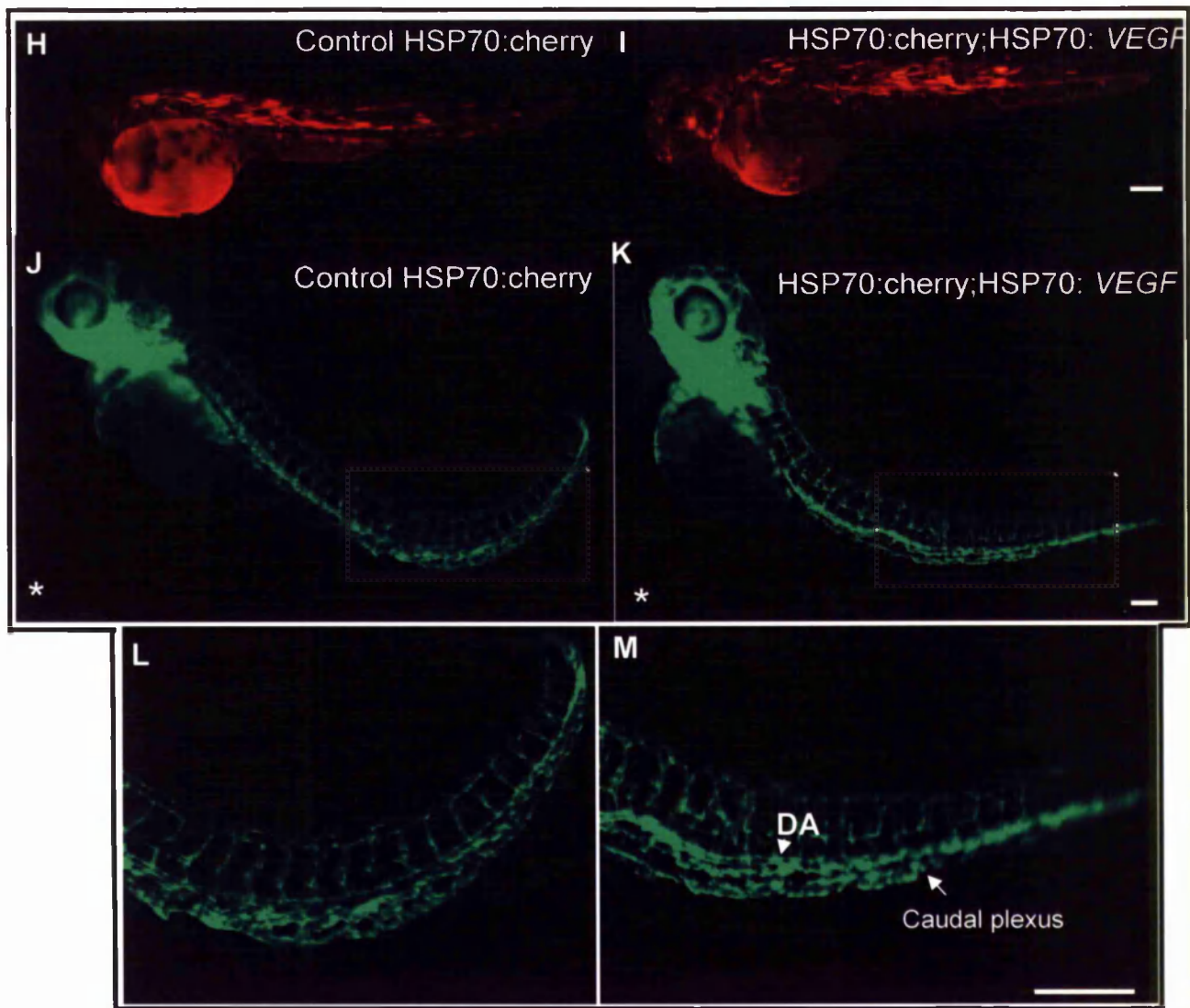


**Figure 6.11: *Tg(fli1:GFP;gata:dsRed)* embryos co-injected with HSP70:cherry and HSP70:VEGF display mild phenotypes characteristic of ectopic VEGF.** Embryos were injected either with HSP70:cherry alone or co-injected with HSP70:VEGF and then heat shocked at 18hpf for 2hrs, and phenotypes analysed at 35hpf. A: Control HSP70:cherry injected with heat shock (HS) treatment inset HSP70:cherry injected no heat shock. This confirmed HSP70 promoter was functioning. C-D: A representative image of the whole vasculature of the heat and non-heat treated HSP70:cherry injected embryo. A close up of the tail (D) shows a branched lumenised caudal plexus (indicated by white arrowheads). HSP70:VEGF co-injected embryo display moderate levels of cherry expression (E). Fluorescent image of the whole vasculature (F) shows embryos display mild dilation of the PCV with reduced branching evident in the plexus (indicated by white arrowheads) and irregular patterned ISVs (G). Co-Injected embryos were also heat treated intermittently at 1dpf and 2dpf (H-M). Control HSP70:cherry injected 35hpf embryo, showed moderate levels of cherry expression (H) and vasculature morphology analysed at 72hpf (J,L) appeared identical to that of heat treated non-injected embryos. HSP70:VEGF co-injected embryos displayed comparable levels of cherry expression in the trunk at 35hpf (I), analysis of the vasculature at 72hpf (K,M) revealed mild dilation of DA, and CV with irregular branching of the ISVs. Scale bar 200 $\mu$ m \* Note embryos did not display any overt morphological abnormalities, apart from mild curvature of the tail, however the vasculature images were taken in the tilted position to encapture the whole vasculature in the same focal plane.

duration of heat shock. One cell stage embryos were microinjected with *I-SceI* mix containing HSP70:*VEGF* and HSP70:*cherry* or HSP70:*cherry* alone. A batch of 18hpf embryos from these injected samples were incubated at 37°C for 2 hours and compared to non-heat treated injected embryos. Embryos were placed back in the 28°C incubator and left to develop overnight and scored using a leica stereomicroscope with a GFP and texas red filter equipped with Leica DFC420C digital camera for imaging (Leica microsystems). Under the same exposure of fluorescent light, the heat-shocked embryos were compared to non heat-shock injected embryos to observe corresponding levels of cherry expression to ascertain if the HSP70 promoter was working. Although mild mortality was observed in the heat treated samples it was evident the levels of cherry expression were stronger compared to injected embryos that received no heat shock treatment (Fig. 6.11B). It can be assumed that cherry expression is driven by heat shock promoter and likewise any gene downstream of the heat shock promoter is likely to be expressed.

### **6.3.6 Analysis of the HSP70: *VEGF* injected samples reveal mild *VEGF* overexpression phenotype**

As vasculogenesis initiates at eight somite stage with initial specification and migration of endothelial cells, we tried a wide range of time points before and after to attain an ectopic *VEGF* phenotype in F0 embryos. Tg(*fli1*:GFP; *gata*:ds-Red) embryos were co-injected with the two constructs mentioned and compared to the resulting phenotypes of the HSP70 cherry alone Preliminary experiments revealed heat-shock treatment for short periods of 30mins to a 1hr at two somite stage and eight somite (10hpf-12hpf) resulted in high mortality with surviving embryos displaying severe developmental abnormalities. Following experiments were heat shocked at later stages during development. HSP70:*VEGF* injected embryos at 17 somite stage (18hpf) were heat shock treated for the same amount of time. Surviving embryos were placed in 28°C incubator and were then assayed for cherry expression the following day. There was slight mortality of embryos both in control injected and HSP70:*VEGF* injected however the survival rate was greater in both control and co-injected embryos compared to the previous attempts. Majority of embryos appeared morphologically normal. Interestingly in 40% of HSP70:*VEGF* injected displayed normal overall morphology while the analysis of the vasculature showed a mild phenotype previously observed with FRM-*VEGF* plasmid. These embryos displayed dilated posterior cardinal vein and irregular patterned intersegmental vessels (Fig. 6.11F,G). To test if a stronger ectopic *VEGF* phenotype could be observed such

as ectopic branches, embryos were heat shocked intermittently. A separate batch of co-injected embryos were heat shocked initially at 18hpf for 2hpf and then for 30mins at 35hpf and 48hpf. Embryos were analysed at 3dpf for ectopic VEGF features. Although strong expression of the HSP70-cherry construct was observed in the control and HSP70:VEGF dilation of the axial vessels and caudal plexus was only observed in HSP70:VEGF injected embryos (Fig. 6.11 H-K). Ectopic branches were not evident, though majority of ISVs appeared to be irregularly patterned.

Due to time frame of the project it was not possible to optimise the duration of heat shock and analyse different timepoints to recapitulate the ectopic VEGF phenotypes observed with the Frm-VEGF plasmid. It was decided to raise the embryos into adulthood and genotype positive founders for experimentation with the F1 generation.

Embryos were co-injected with two *I-SceI* constructs, HSP70: VEGF and one containing cherry under the expression of keratinocyte promoter (KTR4 cherry). KTR4 was used as a marker for screening purposes, The quality of cherry expression within the F0 generation allowed to reflect on the quality of the injection and served as an efficient and reliable selection of potential founder fish that may also be positive for the HSP70: VEGF plasmid, thus mosaic expression of the cherry was also good indicator of distribution. Embryos showing strong mosaic cherry expression throughout the trunk were grown up to adulthood and genotyped. To date thirty out of sixty adult fish were outcrossed to wildtype and the F1 generation genotyped. DNA was extracted at 3dpf and screened by PCR using the same primer set mentioned previously. However no positive founders have yet been identified

## 6.4 Discussion

VEGF can be transiently overexpressed in the developing embryo by microinjecting mRNA or plasmid. While both methods are effective short term, plasmid is more stable compared to mRNA and is known to persist in embryo until at least 4dpf. To date injections with VEGF plasmid or protein has shown to increase branching of subintestinal vessels<sup>329,419</sup>. One of the aims of the project was to create a VEGF assay to test the role of 6-O sulphation on VEGF mediated angiogenesis. The subintestinal basket is one of the common assay for ectopic angiogenesis. Subintestinal vessel (SIV) formation initiates at 60hpf and is fully formed by 3dpf. Aside the SIV, the trunk is another area active for angiogenesis, the first wave of angiogenesis occurs at 24hpf with the bilateral sprouting of ISV from dorsal aorta and posterior cardinal vein, simultaneously dorsal branching occurs from caudal vein to form a

plexus of vessels. Vessels in the trunk are fully formed by 48hpf. We wanted to develop a robust VEGF assay that would allow us to quantify ectopic vessels in the trunk as early as 48hpf for future co-injections with morpholinos. Our primary concern of quantifying ectopic vessels in the SIV basket was that the morpholino would be diluted by 60hpf and endogenous levels of *sulf1c* mRNA expressed at 72hpf (results from chapter 3) therefore the loss of *sulf1c* on mediated angiogenesis may not be observed.

#### **6.4.1 Microinjection of VEGF plasmid induces phenotypes that are hallmarks of VEGF activity**

VEGF promotes new blood vessel formation and angiogenic sprouting by mediating a variety of biological effects on endothelial cells. These effects include differentiation, proliferation, migration, survival and vascular permeability of endothelial cells<sup>234,258</sup>. This occurs through the action of receptor tyrosine kinases that activate a multitude of downstream cell signalling pathways, however it is improbable that all the pathways are simultaneously activated within an endothelial cell. The precise cellular response to VEGF must be tightly regulated in endothelial cells for normal blood vessel development. We injected VEGF plasmid in zebrafish embryo and induced a wide range of vasculature phenotypes that were specific to VEGF activity. Although the severity of the affect varied between embryos the phenotypes were reproducible and were not prevalent in the non-injected and control injected. In support of these observations, injections performed with mutated VEGF by a member of the Stringer lab further confirmed the specificity of VEGF plasmid with embryos not displaying ectopic phenotype. The mild category of ectopic VEGF phenotypes displayed increased endothelial cell proliferation through the formation of extended branches from ISV or a cluster of endothelial cells throughout the trunk of the embryo. The more severe phenotypes displayed dilated main axial vessels and ISVs. This is consistent with the response of patent vasculature to constitutive activation of *Akt* or exogenous VEGF (a downstream VEGF target) that display an increase in vascular permeability<sup>422,423</sup>. While the varying location of the VEGF ectopic sites in the trunk can be attributed to the natural mosaicism of microinjecting plasmids, the combined high variation in the frequencies of the different classes led to difficulties in assigning a measure of ectopic VEGF and as a result further experiments were abandoned.

The lack of temporal control over *VEGF* activity due to short term instability and transient expression of the *VEGF* plasmid, led us to generating transgenic line that would produce stable and consistent levels of *VEGF* expression. The ease of creating transgenic zebrafish has been aided by the use of unique and compatible vectors in fish that improve integration efficiency into the genome. Encouragingly injections of the *I-SceI* HSP70:*VEGF* construct revealed similar phenotypes to the *Frm:VEGF* plasmid confirming the specificity of *VEGF*. Although the severe form of the ectopic *VEGF* phenotype i.e. increased vascular permeability was prevalent in these embryos, ectopic branches were not observed, this is because high concentration of HSP70:*VEGF* construct were used as advised by protocol<sup>424</sup> to be an effective concentration for increasing transgenesis efficiency. Although the mild phenotypes were absent in these injected embryos it was not a concern as it is hypothesised that the germline transmission in the F0 generation is likely to vary in each embryo and therefore the progeny of the adults would produce different ectopic *VEGF* phenotypes. Unfortunately due to the time frame of the project we were unable to find any positive founders and are currently screening the progeny of potential HSP70:*VEGF* adult fish.

## Limitations

Although we were able to induce transient ectopic *VEGF* phenotypes in the mild form of ectopic branches and the severe form resulting in vascular dysfunction, one of the limitations to this research was not being able to produce a consistent and highly reproducible ectopic *VEGF* phenotype in the trunk that could be assayed routinely. Though injecting plasmid always results in mosaic expression accounting for the different ectopic features observed within one embryo, the variations in the *VEGF* mediated response were not anticipated for example severe dilation even at the lower concentrations of plasmid. Thus hindering a suitable measure of ectopic *VEGF* quantification.

However future work will focus on raising positive founders of the potential HSP70:*VEGF* adult fish and selecting independent lines of ectopic *VEGF* expression. The aim is to develop a transgenic line that we can quantify ectopic vessels both in the trunk and in the subintestinal basket. Once the ectopic phenotype has been established it would be interesting to inject *sulfl* protein or *sulflc* MO into the transgenic line and assess the effects on the ectopic vascular effects induced by *VEGF*. Secondly it would be interesting to test the specificity by assaying the expression of a downstream target of *VEGF* signalling pathway such as *flk1*, *flt4*, *notch*,

and *dlt4*. Unfortunately due the time frame of the project we were not able to test for such targets to further confirm the specificity of the *VEGF* constructs used.

# Chapter 7.0 Morpholino mediated knockdown of *sulf2a* and *sulf2*

## 7.1 Introduction

In mammals the *sulf2* enzyme is a single gene product whereas in zebrafish two genes have been identified *sulf2a* and *sulf2* that are likely to have arisen from gene duplication. Zebrafish *sulf2a* shows greater sequence homology to mammalian *sulf2* than its family member *zfsulf2*. The results from chapter 3 indicate that transcripts of *sulf2* gene are detected during the early cell division stage (1hpf) suggesting a maternal contribution to the zygotic pool however *sulf2a* is detected as early as 4hpf. The spatial expression patterns of *sulf2* and *sulf2a*, show overlapping and distinct regions of expression throughout the early developmental stages. *Sulf2* expression is expressed broadly throughout the central nervous system while in contrast *sulf2a* expression is fairly restricted. Strong expression is detected in the somite boundaries, developing brain and the roofplate of spinal cord. Moreover *sulf2a* shows strong overlap with *sulf1c* expression pattern. To date analysis of *sulf2* knockout mice reveal a reduction in their overall size and body mass with no major abnormalities despite an increase in mortality. However characterisation of these mice exhibit minor defects in the skeletal tissue, lung development and other neurological abnormalities<sup>349,357-359,361</sup>. This clearly emphasises a functional significance of the *sulf2* enzyme during embryonic and adult stages. The signalling pathways affected in the *sulf2*<sup>-/-</sup> embryos have not yet been characterised, however there is wealth of *in vitro* data showing *sulf2* is important in modulating the activity of many HS binding proteins through altering the 6-O sulphation patterns of HS. Such activities have been demonstrated in ELISA (Enzyme linked immunoabsorbant assay) binding assays where treatment of heparin with recombinant HSULF2 protein disrupts the interaction with various growth factors such as FGF and VEGF either in the pre-binding or bound state to heparin<sup>356</sup>. Consistent with these ideas addition of exogenous HSULF2 protein to chick chorioallantoic membrane (CAM) increases the number of vessel branches thus evidence of a proangiogenic role of HSULF2. It is possible that *sulf2* acts to modulate the bioavailability of growth factors at the cell surface<sup>373</sup>. The ability of *sulf2* to modulate the activity of HS binding growth factors critical to vascular development, suggests a possible role of the enzyme in embryonic vascular development. Despite the fact that vascular abnormalities have not yet been reported in the *sulf2*<sup>-/-</sup> knockout mice it's suffice to note that the viability of these mice is severely affected as shown in the three independent separate studies<sup>349,357,359</sup> with one report alluding to possible causes in the cardiovascular and/or placenta function thus consistent with

mice *sulf2* being the major source of sulf expression in the embryonic heart and placenta <sup>359</sup>. In the absence of *sulf2* signalling through one or more growth factor pathways is altered, compromising the survival of these mice.

One of the aims of this research was to determine if zebrafish homologs *sulf2a* and *sulf2* can affect the structural modifications of HS *in vivo* i.e. are capable of modifying the 6-O sulfation pattern of HS thus showing conservation of enzyme function. Secondly, to determine whether *sulf2a* and *sulf2* have functionally non-redundant roles in vascular development. To test this antisense morpholinos targeting the *sulf2* and *sulf2a* pre-mRNA transcript will be injected into *flil*:GFP embryos with a view of knocking down their activity. Morpholino technology has proven to specifically affect the overall 6-O sulfation patterns of HS disaccharides as studies by Bink *et al* (2004) <sup>329</sup> and Chen *et al* (2005) <sup>330</sup> in zebrafish clearly demonstrated the reduction of 6-O sulphated disaccharides through blocking the translation of the 6-O sulfotransferases mRNA transcripts.

As discussed previously in chapter 4, *flil*:GFP transgenic zebrafish are a highly attractive model for real time *in vivo* imaging of vasculogenesis and angiogenesis. The two vascular processes can be easily distinguished in the trunk. A clear example of angiogenesis during zebrafish development is the formation of primary intersegmental vessels (ISV's) which sprout from the dorsal aorta, grow dorsally along the vertical myoseptum and then branch and interconnect to form the dorsal longitudinal anastomotic vessel <sup>86,87</sup>. For this reason the zebrafish trunk vasculature should provide an invaluable model to study the vascular phenotypic consequences of the loss of *sulf2a* and *sulf2* function.

In combination with results from chapter 3 and the proposed roles of vertebrate *sulf2* function, it is hypothesised zebrafish *sulf2a* and *sulf2* are conserved 6-O endosulfatases that can actively modulate HS structure and function, at sites that correlate with its expression. As the sulfation status is clearly essential for the activities of many growth factors including VEGF, FGF and PDGF, *sulf2a* or *sulf2* can regulate the activities of these growth factors in a positive or negative manner depending on the role of 6-O sulphation in the signalling complex. Since the protein conservation between the *sulf2a* and *sulf2* is greater than *sulf1c*, and there is overlap amongst the three sulf expression patterns. It is predicted that some functional redundancy between *sulf2a* and *sulf2* may occur at the early stages during vascular development.

## 7.2 Materials and methods

### 7.2.1 Morpholino oligonucleotides

The region of target sequence within the *sulf2a* (S2a) and *sulf2* (S2) gene was sent to Gene Tools and designed by their criteria i.e. with GC content of about 50% and little or no secondary structure. The translational blocking morpholinos were designed to be complementary to 25 nucleotides sequences in the 5' untranslated region (5'UTR- MO) and at the translation initiation site (ATG-MO). Splice blocking morpholino was designed to be complementary to splice acceptor site of exon4 (SB- MO). The standard control MO for all experiments used was 5 pair base mismatch morpholino resembling *sulf2a* and *sulf2* 5'UTR morpholino recommended by Gene Tools. BLAST ([www.ncbi.nlm.nih.gov/blast/Blast.cgi](http://www.ncbi.nlm.nih.gov/blast/Blast.cgi))<sup>392</sup> was used to check the MO sequence was specific to zebrafish *sulf2a* and *sulf2*.

Sulf2a MO	MO Sequence	5'UTR and cDNA sequence Intron3-exon4
S2a-5'UTR	CATCACCACCACTAAAACCTGTGACC	Ggtgtagtgtgtgagcgcgagagcccgtcgc gggtcacagtttttagtggtggttgAT
S2a-5'ATG	GTCGAGCCGCAAGTCCATGTGCCGC	GGCGGCACATGGACTTGC GGCTC GACTCTTGCCACTGCTGCTGCTGGCC ATGTTGGCAGTAGCTCATGC
S2a-SB	GTAGTCCTACAGGAGGCACAGAGAT	attagatctctgtgctctctgtag
Control Mo	GTCcAGgCGCAiGTCCAaGTGgCGC	GACTACCTGACAGATCTCATAA

Sulf2 MO	MO Sequence	5'UTR and cDNA sequence Intron3-exon4
S2-5'UTR	CTAGTAAGGTCGCAGTTTTTTGTCA	atggcagtcacgcgaggacacatcccctctatctga agggtgacaaaaactgcgacctactagtaagtgtg
S2-5'ATG	FACTGCCATGACCTTAACCAGTGCT	ggaggtggagcactggttaaggtcATGGCAG TAGGGTGGAGACCGGCCACCCT TCTCCTAGTCTTCATCCTGACGT
S2-SB	CAAAGAATGCTGAAACAGAAAGCCA	tctgataataatggettctgtttteag
Control Mo	TACaGCCAaGAgCTTAiCCAGaGCT	CATTCTTTGGGAAGTATCTGA

\* Note: Lower case in MO sequence signifies mismatch base pairs; Lower case in cDNA sequence signifies 5'UTR sequence and upper case signifies first exon, and Lower case in SBMO target sequence signifies intron 3 and upper case exon 4 sequence

### 7.2.2 Amplifying the morpholino target sites of *sulf2a* and *sulf2*

Genomic DNA was extracted from two day old embryos from *flil*: GFP zebrafish strain. PCR primers were designed outside of the region targeting the morpholino site. Products of the

expected size were gel extracted and sent to UMSF to be sequenced. Primers to confirm the presence of the *sulf2a* and *sulf2* splice blocking morpholino sites were as follows (Fig. 7.0).

### 7.2.3 RT-PCR analysis of *sulf2a* and *sulf2* morphants

To confirm if the S2 and S2a SBMO were having an affect on the *sulf2* transcript RT-PCR was performed on cDNA of *sulf* morphants at 1dpf. Embryos were injected with the SBMO at different doses and RNA extracted at 24hpf. One microgram of RNA was synthesised into cDNA and 1 $\mu$ l of this used in the PCR reaction. A negative control was carried out substituting cDNA with Dnase free water. For *sulf2a* transcript primers were designed in the exon3 and exon6 to amplify a wildtype *sulf2a* transcript (650bp). This primer design also allowed for amplification of a predicted aberrant *sulf2a* transcript excluding exon4 (480bp) (Fig. 7.1A,C)

Forward and reverse primers were designed in exon3 and exon5 to allow amplification of wildtype *sulf2* transcript (562bp). This primer design also allowed for amplification of a predicted aberrant *sulf2* transcript excluding exon4 (410bp) (Fig. 7.1B, C)

Primers were also designed to amplify  $\beta$ -actin gene (298bp) from all samples. This was used as a positive control to ensure all cDNA samples were of the same approximate concentration and quality. RT-PCR reactions to analyse  $\beta$ -actin underwent 25 cycles at 54 $^{\circ}$ C annealing temp to ensure the reactions were not saturated. The SBMO RT-PCR reactions underwent 34 cycles and the products were run on 1.2% agarose gel and bands excised from the gel to be sequenced. Primers used for the RT-PCR were also used to sequence the purified amplicons. Primer sequences used for RT-PCR were as follows;

Gene amplified	Annealing temperature	Primer sequences
S2- 5'UTR/ATG	55 $^{\circ}$ C	Fwd: 5'TGGAGCACTGGTTAAGGTCA -3' Rev: 5' CTCCAGCCAGGAGGAACATA-3'
S2- SB Intron3-Exon4	52 $^{\circ}$ C	Fwd: 5' GAAACATGAAGGATTTGTGTGG- Rev: 5' GATCAATAAATGCGGGCTTG-3'
S2a-5'UTR/ATG	55 $^{\circ}$ C	Fwd: 5'CCAGAGGGTGAAGTTGGTGT-3' Rev: 5'TGCGGAAGTAATTGATGCTT-3'
S2a Intron3-Exon4	52 $^{\circ}$ C	Fwd: 5'TCATTCTACCTGTTCTGGCTCA-3' Rev: 5'ACTTTGACCTCCTTTGTGAAGC-3'

### 7.2.4 Preparation and HS Disaccharide analysis of *sulf2a* and *sulf2* morphants

In order to test the specificity of the morpholino and hence characterise *sulf2* and *sulf2a* function, heparan sulphate disaccharide composition of the injected embryos were analysed by strong anion exchange chromatography (SAX-HPLC). HS extraction and analysis was carried out as previously described (section 4.2.3)

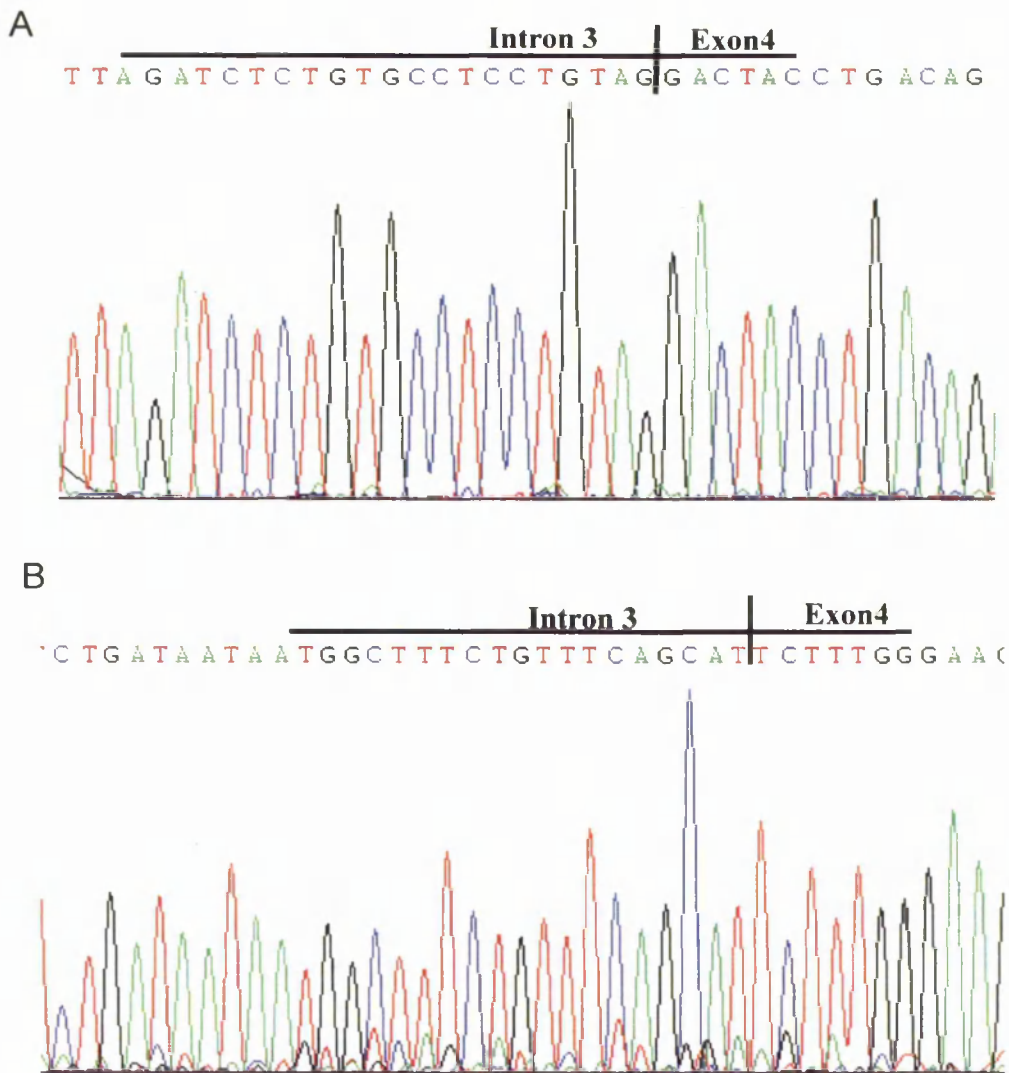


**Figure 7.0: Sequence chromatograms showing the *sulf2a* and *sulf2* SBMO target site** Genomic DNA was extracted from 24hpf *fli1*:GFP embryos and morpholino target sites amplified. PCR product 501bp of *sulf2a* (A) and 551bp of *sulf2* (B) were sequenced. Horizontal black line highlights the morpholino target site and the small vertical black line highlights the Intron3-Exon4 boundary.

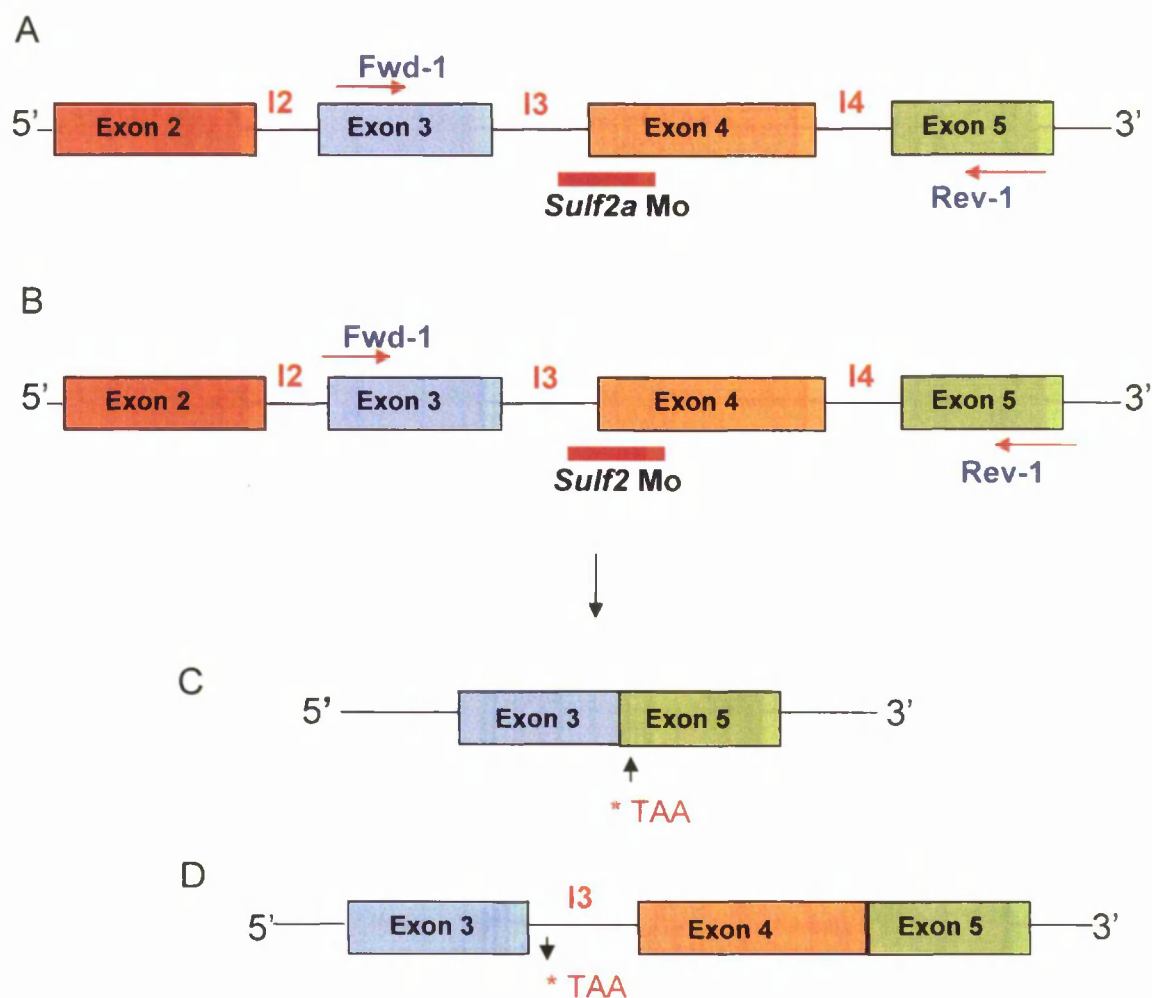


**Figure 7.1:** A schematic representation of the possible outcomes of *sulf2a* and *sulf2* mRNA transcript by targeting of the *sulf2a* & *sulf2* -SBMO. **A:** S2a-SBMO was designed to bind to a splice acceptor site positioned at the Intron3-exon4 boundary (denoted by the red bar) of the *sulf2a* gene. **B:** S2-SBMO was designed to bind to a splice acceptor site positioned at the Intron3-exon4 boundary of the *sulf2* gene (denoted by the red bar). Possible outcomes of the final transcript **C:** One possibility being the exclusion of exon4 from transcript, the forward and reverse primers were designed to amplify from exon3 to exon5 detecting the removal of exon4. **D:** Second possibility is inclusion of the 2.5kb or 2.8kb intron3 in the *sulf2* and *sulf2a* transcript respectively. The position of primers are indicated by the red arrows for both genes. Generation of either transcript for both *sulf* genes is predicted to introduce a stop codon (highlighted by position of TAA) Diagram not drawn to scale.

## 7.3 Results

### 7.3.1 *Sulf2a* and *sulf2* SBMO reduces the level of their respective transcript

To determine an embryonic functional role of the *sulf2a* (S2a) and *sulf2* (S2), two independent splice blocking morpholino (SBMO) were designed to effectively inhibit the splicing of their pre-mRNA transcript. SBMO act by intercepting conventional splicing of the pre-mRNA either at an exon-intron boundary or intron-exon boundary. This can result in exclusion of an exon or inclusion of intron in the final mRNA product (Fig 7.1C,D) with the latter product less frequently encountered. As mentioned previously the advantage of using the SBMO's is that the efficacy can be determined by RT-PCR. An RT-PCR reaction was designed to check the efficacy of the morpholino level and if the aberrant spliced product of the *sulf2a* and *sulf2* mRNA induced by SBMO could be detected. *Fli1*: GFP embryos were injected with a range of SBMO concentrations 3, 5 and 8ng of S2-SBMO, RNA was extracted at 24hpf cDNA was synthesised and RT-PCR performed.

In an experiment performed with S2a-SBMO a range of doses from 3, 5, and 8ng of S2a-SB were injected in *fli1*: GFP, and RNA extracted from 24hpf old embryos, cDNA was synthesised and RT-PCR performed. In all samples including the non-injected and control injected, the wildtype transcript of 650bp was observed. This appeared to decrease with increasing concentrations of the SBMO. However an expected shorter aberrant product (450bp) of the *sulf2a* transcript was not observed in any of the samples. Sequencing of the larger band revealed the appropriate region of the *sulf2a* transcript amplified (Fig. 7.2A,B)

Identical RT-PCR was set up with the S2-SBMO, in all samples including the non-injected and control injected the wildtype transcript of 562bp was seen (Fig. 7.3A). The intensity of the band decreased with increasing dose of the SBMO with very little difference between the last two concentrations. An additional band was also observed at 350bp only in the SBMO injected samples. This appeared slightly smaller than the expected size. To exclude the possibility that this maybe a non-specific product, PCR was repeated at slightly higher temperature of 55°C to allow for more stringent annealing conditions, however the bands were still present in the SBMO injected samples. Sequencing of both the large and small bands was performed, this revealed that the larger band corresponded to the expected region of the *sulf2* transcript (Fig. 7.3B), whilst the sequence chromatogram of the smaller band gave a noisy signal, indicative of a mixture of sequences (data not shown). The small sized band was cloned into pGEMT vector and sequenced. The sequence readout revealed non-specific amplification of zebrafish cDNA.

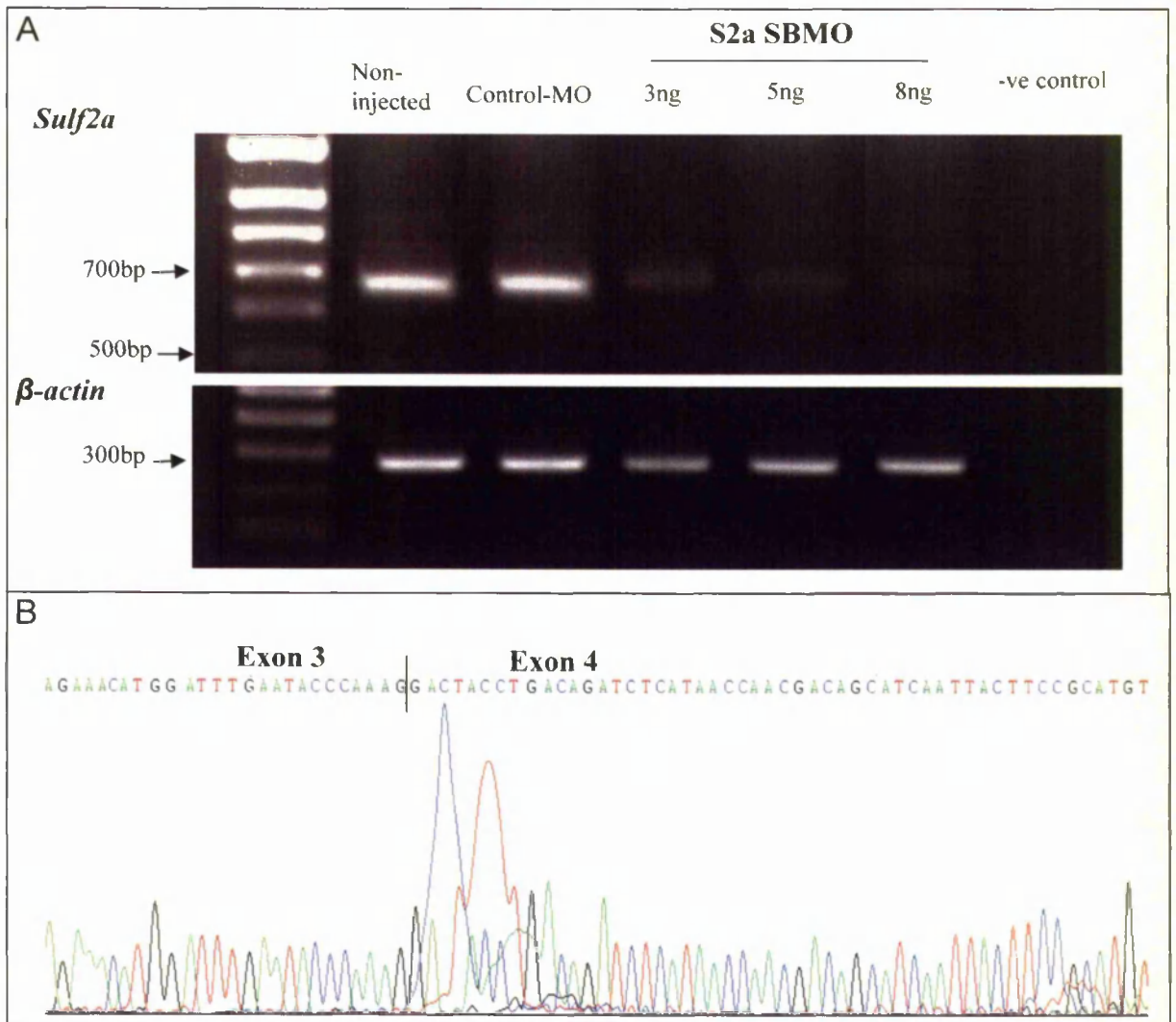


**Figure 7.2: RT-PCR analysis at 24hpf to determine the affect of S2a-SBMO on the *sulf2a* pre-mRNA.** *Fli1*:GFP embryos were injected with 3, 5, 8ng of the CMO and equivalent doses of SBMO. RNA was extracted and cDNA synthesised from non-injected, 8ng of CMO-injected and S2a-SBMO injected embryos at 24hpf. **A:** The S2a-SBMO RT-was performed and the products separated on a 1.2 % gel. Non injected and CMO-injected samples produced a single band of 650bp. Samples injected with the S2a-SBMO also produced a single band of approximately 650bp. As the concentration of SBMO increased from 3ng-5ng, the intensity of the band decreased. The intensity of the *sulf2a* band was weaker with increasing dose.  $\beta$ -actin RT-PCR was performed as a positive control. Following 25 cycles of the RT-PCR the 298bp  $\beta$ -actin band was of similar intensity in all reactions containing cDNA. The negative controls (-ve) in which sterile water was used as a substrate did not produce an RT-PCR product. The size standard is a 1 kb ladder with 300, 500 and 700bp bands indicated **B:** A partial sequence chromatogram of the wildtype *sulf2a* transcript. This confirmed the *sulf2a* transcript was present in all samples but at relatively low concentrations in the SBMO injected samples.

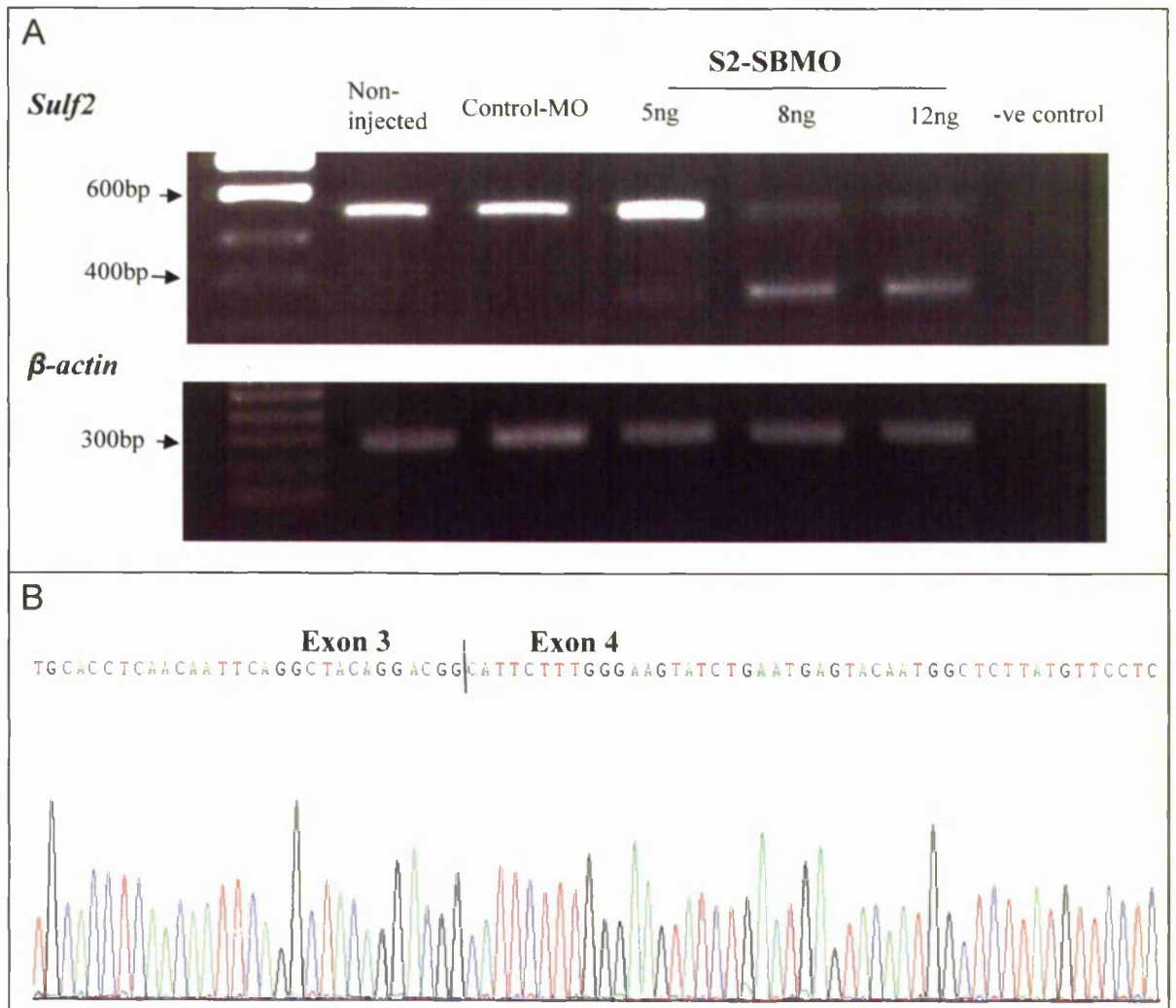


**Figure 7.3: RT-PCR analysis at 24hpf to determine the affect of S2-SBMO on the *sulf2* pre-mRNA.** *Fli1*:GFP embryos were injected with 5, 8, 12ng of the CMO and equivalent doses of SBMO. RNA was extracted and cDNA synthesised from non-injected, CMO-injected and S2-SBMO injected embryos at 24hpf. **A:** The S2-SBMO RT-PCR was performed and the products separated on a 1.2 % gel. Non injected and CMO-injected samples produced a single band of 562bp. Samples injected with the S2-SBMO also produced a single band of approximately 562bp and a small band of approximately 350bp. As the concentration of SBMO increased from 5ng-8ng, the intensity of the large band decreased and the small band increased. The intensity of the large band became weaker with increasing dose.  $\beta$ -actin RT-PCR was performed as a positive control. Following 25 cycles of the RT-PCR the 298bp  $\beta$ -actin band was of similar intensity in all reactions containing cDNA. The negative controls (-ve) in which sterile water was used as a substrate did not produce an RT-PCR product. The size standard is a 1 kb ladder with 300, 400 and 600bp bands indicated. **B:** A partial sequence chromatogram of the presumed *sulf2* band . This confirmed the *sulf2* transcript was present in all samples but at relatively low concentrations in the SBMO injected samples

$\beta$ -actin was used as positive control; amplification of the gene was tested in all cDNA samples used in the SBMO RT-PCR. The positive control showed they were all of similar quality and concentration. The negative controls in which cDNA was replaced with sterile water did not produce an RT-PCR product (Fig. 7.2 & 7.3)

### 7.3.2 HS Disaccharide analysis of *sulf2a* and *sulf2* SBMO injected embryos

From the RT-PCR data a significant level of reduction in the *sulf* transcripts was observed in SBMO injected samples. To determine the functional specificity of the zebrafish *sulf2* homologs the composition of HS sulphated disaccharides of the SBMO injected samples was analysed. *Fli1*:GFP embryos were microinjected with 5ng of S2a-SBMO, as this dose gave the least amount of dead embryos compared to higher dose, and a significant reduction in the level of wildtype *sulf2a* transcript was also observed at this dose. GAGs were extracted and partially purified HS was digested with HepI, II & III and disaccharide content of 48hpf wildtype embryos versus CMO and SBMO injected embryos analysed on HPLC. The six most abundant disaccharides (labelled 1-6 in Fig. 7.4A) including the three 6-O sulfated disaccharides  $\Delta$ UA-GlcNAc6S,  $\Delta$ UA-GlcNS6S,  $\Delta$ UA2S-GlcNS6S were present in wildtype, CMO and S2a-SBMO injected samples. There also appeared to be two additional peaks eluting before and after the first  $\Delta$ UA-GlcNAc peak, that were present in all three loaded samples. As these peaks were identified in the blank run (injected with milliQ dH<sub>2</sub>O) it is therefore likely that this can be attributed to background noise. In the HS profile of 48hpf S2a morphants, there appeared to be an increase in all the three 6-O sulfated disaccharides compared to wildtype, with a statistically significant increase in 6-O sulfation of the trisulfated disaccharide ( $\Delta$ UA2S-GlcNS6S) in the S2a morphants (Fig. 7.4B). Overall, knockdown of the *sulf2a* transcript appeared to show a decrease (0.5%) in NS and increase in the 6S groups (41%). There also appeared to be an unexpected increase (5%) in the 2-O sulphate groups. Analysis of the heparan sulfate composition was performed in triplicates for the morphants with similar outcome. From these results it can be concluded that *sulf2a*-SBMO injection can significantly increase 6-O sulphation of N-sulphated glucosamine residues in  $\Delta$ UA2S-GlcNS6S disaccharide with minimal affect on the mono and di-sulphated disaccharides.

The HS disaccharide content was analysed of S2-SB morphants by the same method. *Fli1*: GFP embryos were injected with 5ng of S2-SBMO and 48hpf S2-morphants were selected for GAG extraction. The six most abundant disaccharides (labelled 1-6 in Fig. 7.5A) including the three 6-O sulphated disaccharides  $\Delta$ UA-GlcNAc6S,  $\Delta$ UA-GlcNS6S,  $\Delta$ UA2S-GlcNS6S were present, however several additional small peaks were also observed in the standards, CMO and SBMO

injected samples that eluted at different time points to disaccharides. The signals were disregarded as they were present in blank run indicative of background noise (Fig. 7.5A). However one peak was persistent in all HS preps (excluding the standards) derived from CMO and SBMO injected that eluted relatively early than the six disaccharides. As this peak was not identified in the blank run it is possible the cyanoacetamide could be labelling a sugar chain from a glycosylated protein, previously observed in zebrafish HS preps (personal comm Dr Stringer). The areas of the six HS peaks were calibrated against corresponding area of the HS disaccharides standards of known concentration (0.016nmol) and expression levels of the disaccharide components expressed as a percentage (Fig 7.5A,B). The HS profile of S2-SB morphants was compared to control (wildtype embryos). In the HS profile of 48hpf S2-SBMO morphants there appeared to be a few trends in the sulphated disaccharides although none were statistically significant. A small increase (6%) in the tri-sulfated disaccharide  $\Delta$ UA2S-GlcNS6S, with a relatively comparable decrease in the disulfated disaccharide  $\Delta$ UA2S-GlcNS was observed. A mild decrease (16%) was observed in the  $\Delta$ UA-GlcNS6S. Whilst the highest increase (21%) was found of the monosulfated disaccharide  $\Delta$ UA-GlcNAc6S compared to control injected. On the whole there appeared to be a mild decrease (0.2%, 2%) in the overall N-sulfate groups (NS) and 2-O sulfate group (2S) respectively and a small increase (~4%) in the 6-O sulfate groups (6S). From these results it can be concluded that S2-SBMO does appear to have mild affect on the 6-O sulfation of trisulfated disaccharide but a greater affect on the mono and di-sulfated disaccharides.

### 7.3.3 Analysis of S2a-SBMO injected embryos

RT-PCR analysis showed that S2a-SBMO was capable of reducing the levels of *sulf2a* transcript in all concentrations injected, thereby reducing the level of *sulf2a* mRNA expression. Consistent with this data, HS disaccharide analysis of S2a morphants revealed a significant increase in the 6-O sulfation of N-sulfoglucosamine residues in the trisulfated disaccharide, compared to wildtype embryos. This confirmed the specificity of the morpholino and is in agreement with previous *in-vitro* reports of mammalian and quail *sulf2* specificity<sup>344,349,360</sup>. From the results in chapter 3, zebrafish *sulf2a* protein shares greater sequence homology with human and mice *sulf2*

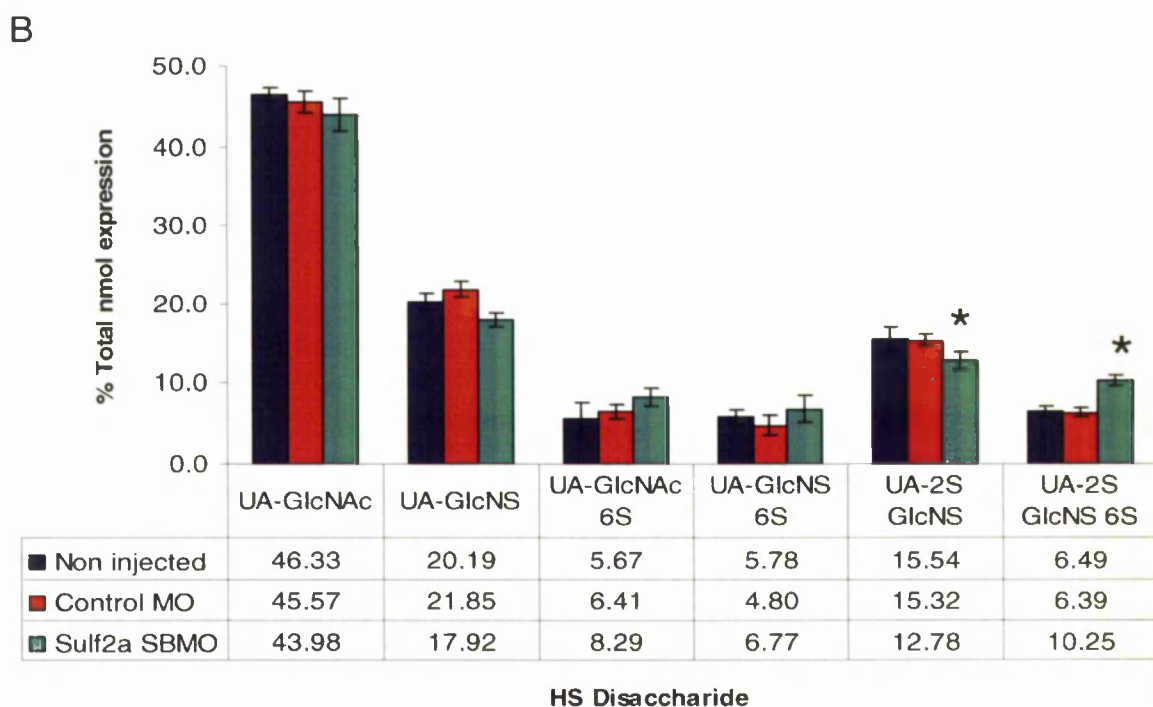
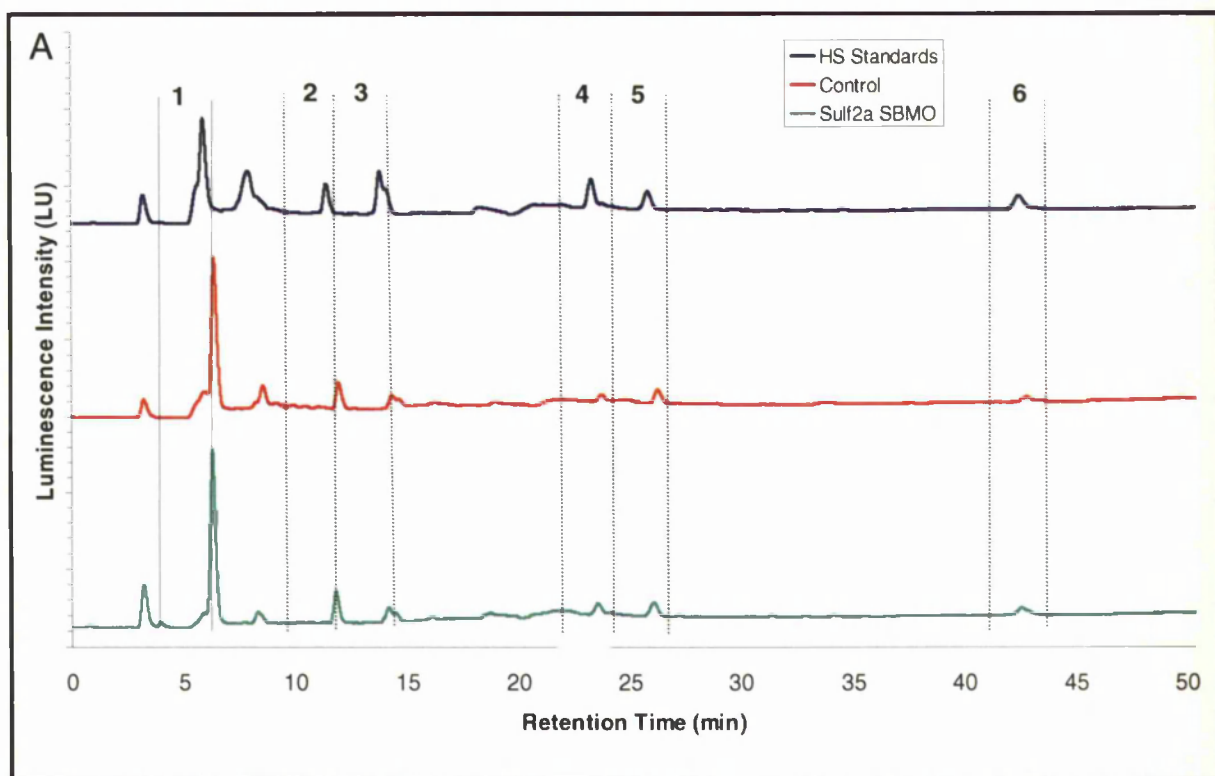


**Figure 7.4: Heparan sulphate profiling of *sulf2a* SBMO morphant embryos.** A: Representative chromatograms of HS standards (blue), non-injected and CMO injected embryos (red) and 5ng of *sulf2a* morphants (green). Six disaccharides were identified by comparison to the elution times of known HS standard peaks; peak 1:  $\Delta$ 4,5 unsaturated hexuronate-*N*-acetyl glucosamine ( $\Delta$ UA-GlcNAc); peak 2:  $\Delta$ UA-*N*-sulfated glucosamine, ( $\Delta$ UA-GlcNS); peak 3:  $\Delta$ UA-6-*O*-sulfated GlcNAc( $\Delta$ UA-GlcNAc6S); peak 4:  $\Delta$ UA-6-*O*-sulfated GlcNS, ( $\Delta$ UA-GlcNS6S); peak 5:  $\Delta$ UA2-*O*-sulfated GlcNS ( $\Delta$ UA2S-GlcNS); peak 6:  $\Delta$ UA2S-GlcNS6S. 283

**B:** Graphical depiction of disaccharide analysis of HS extracted from 48hpf non-injected, CMO injected embryos and 5ng of S2a-SBMO injected embryos, represented as a total percent of heparan sulfate. The six most abundant disaccharides are indicated on the x axis. S2a-Morphants display a 42% increase in the tri-sulfated disaccharide compared to control Asterix(\*) indicates significant changes from wildtype (t test  $P < 0.05$ ) Average calculated from two individual experiments control injected n=2, 50-60 embryos per sample, S2a-MO injected n=3, 50-55 embryos per sample.

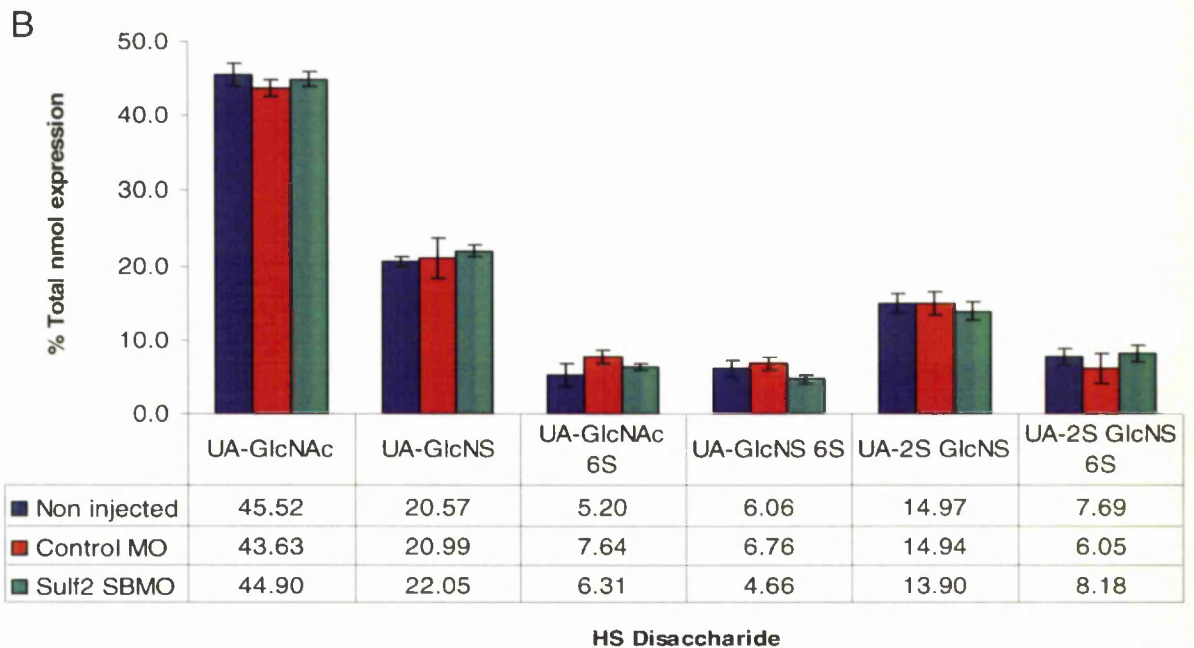
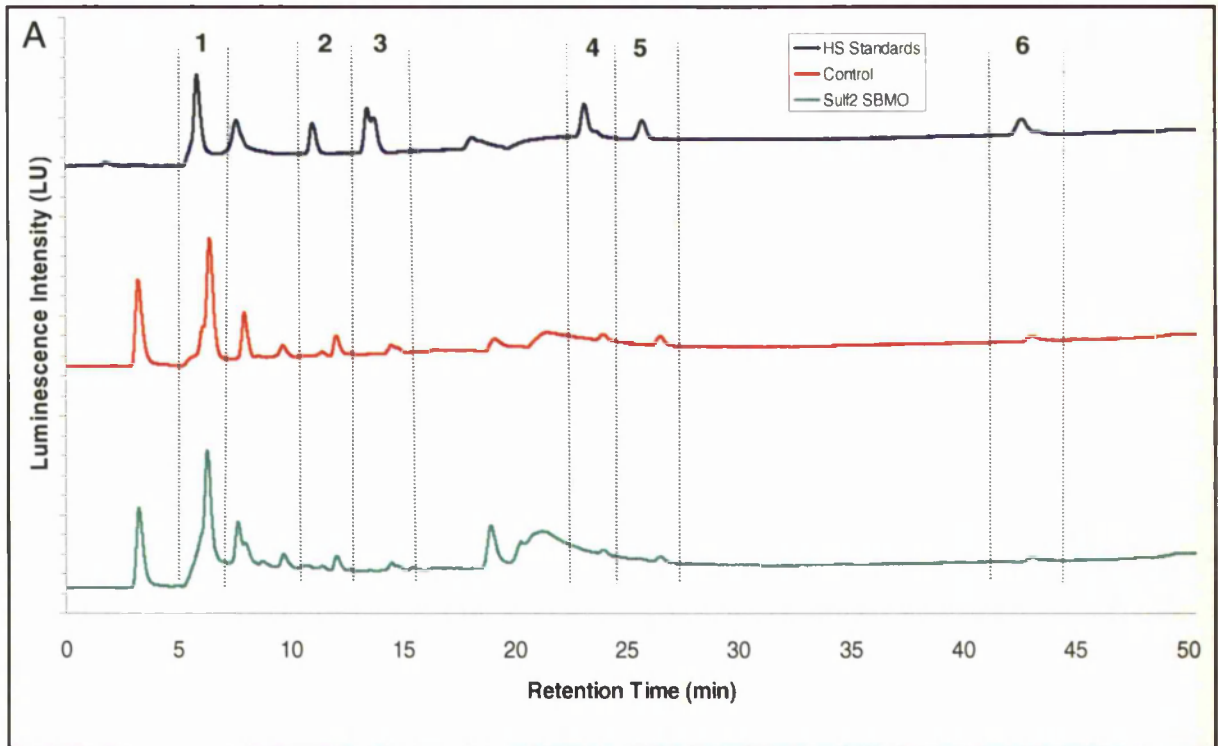


**Figure 7.5: Heparan sulphate profiling of *sulf2* SBMO morphant embryos. A:** Representative chromatograms of HS standards (blue), non-injected and CMO injected embryos (red) and 8ng of *sulf2* morphants (green). Six disaccharides were identified by comparison to the elution times of known HS standard peaks; peak 1:  $\Delta$ 4,5 unsaturated hexuronate-*N*-acetyl glucosamine ( $\Delta$ UA-GlcNAc); peak 2:  $\Delta$ UA-*N*-sulfated glucosamine, ( $\Delta$ UA-GlcNS); peak 3:  $\Delta$ UA-6-*O*-sulfated GlcNAc( $\Delta$ UA-GlcNAc6S); peak 4:  $\Delta$ UA-6-*O*-sulfated GlcNS, ( $\Delta$ UA-GlcNS6S); peak 5:  $\Delta$ UA2-*O*-sulfated GlcNS ( $\Delta$ UA2S-GlcNS); peak 6:  $\Delta$ UA2S-GlcNS6S.

**B:** Graphical depiction of disaccharide analysis of HS extracted from 48hpf non-injected , CMO injected embryos and 5ng of S2-SBMO morphants, represented as a total percent of heparan sulfate. The six most abundant disaccharides are indicated on the *x* axis. Average calculated from 3 individual experiments non-injected and CMO injected n=2, 40-50 embryos per sample, S2-MO injected n=3, 40-50 embryos per sample.

than zebrafish *sulf2*. A proangiogenic role has been ascribed to HSULF-2<sup>373</sup>. It was hypothesised knockdown of *sulf2a* in zebrafish would result in changes in vasculature coinciding with or surrounding the region of *sulf2a* expression. As the head vasculature is difficult to image in the *fli1*:GFP embryos due to background GFP expression in the pharyngeal arches and cartilage mesenchyme<sup>75</sup> only the trunk and tail vasculature was analysed in all the injected and non-injected embryos. Knockdown of the zebrafish *sulf2a* was achieved by injection of SBMO and the vasculature phenotype of the trunk in the resulting morphants analysed in the *fli1*: GFP fish.

Embryos were microinjected with different concentrations of *sulf2a* morpholino. As preliminary experiments performed at 2ng showed that embryos did not produce a morphant phenotype, however injections at a higher concentration of 10ng resulted in increased mortality and greater percentage of non-specific phenotypes (data not shown). Therefore all injections were carried out at concentrations ranging from 3-8ng. S2a-SBMO injections were carried out in different batches of *fli1*: GFP embryos and the data amalgamated and compared to the non-injected and control morpholino (CMO) injected embryos. Analysis of the non-injected controls was carried out alongside, but the data was combined into one chart as these samples were absent of morphants characteristics (Fig. 7.6). A CMO containing 5bp mismatch bases in the morpholino targeting the 5'UTR region of the *sulf2a* transcript was designed. Injections were performed with CMO alongside to ensure that a non-sequence specific morpholino did not produce abnormalities that could be mistaken for a morphant phenotype at a particular concentration. To give a clear indication of the affect of the SBMO on survival rate, embryos were scored for mortality in the first 24hpf and compared with non-injected and control injected samples.

Although death rate was higher in S2a-SBMO injected samples compared to the non-injected, the rate of mortality was significantly higher in the CMO injected samples of the same concentration. This is because a small percentage of severely abnormal embryos were also often present at 24hpf (data not shown). These embryos were discarded and classed as dead embryos as they usually died before 48hpf. Likewise the average survival rate decreased in SBMO and CMO injected samples with increasing concentration of the morpholino. All surviving embryos were analysed at 2-3dpf by their overall morphology and vasculature. The majority of CMO and S2a-SBMO injected embryos displayed a body shape and a developing vasculature identical to wildtype embryos at the same stage and this decreased with increasing morpholino concentration. A small percentage of low-penetrance phenotypes were present in non-injected and all MO injected samples so were categorised as non-specific.

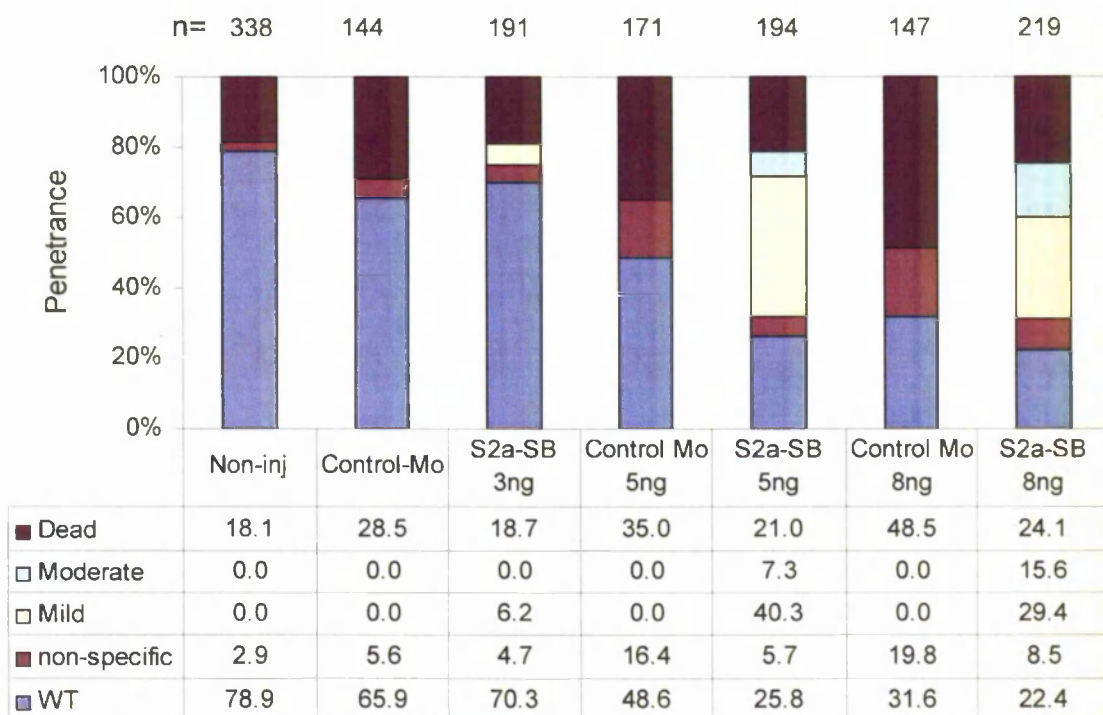


**Figure 7.6: Chart showing the analysis of the *fli1*:GFP embryos injected with different doses of *sulf2a* morpholino.** Data shown is combined from three experiments and average penetrance represented as a percentage. The data from non-injected controls were further combined and is represented as one bar in chart. Embryos were scored at 24hpf for mortality rate and surviving embryos were analysed at 2dpf. These embryos were categorised into four different classes depending on their overall morphology into wildtype, non-specific, or morphants. Morphants were categorised further into mild and severe class depending on the severity of the vasculature defect. Embryos were injected with 3,5 and 8ng S2-SBMO and compared to control MO injected and non-injected embryos. Mortality was generally higher in control MO or SBMO injected samples compared to control and this tended to increase at higher MO concentrations. The majority of control MO and a subset of S2-SBMO injected displayed overall body shape and vasculature identical to that of the non-injected embryos. A small percentage of non-specific phenotypes was seen in all samples and their prevalence tended to increase with increasing MO concentration. Injections of 3ng of the S2-SBMO resulted in a small percentage of embryos with mild phenotype. Injections of 5ng and 8ng of S2-SBMO resulted in 47 % and 45% of morphants respectively, represented by both classes.

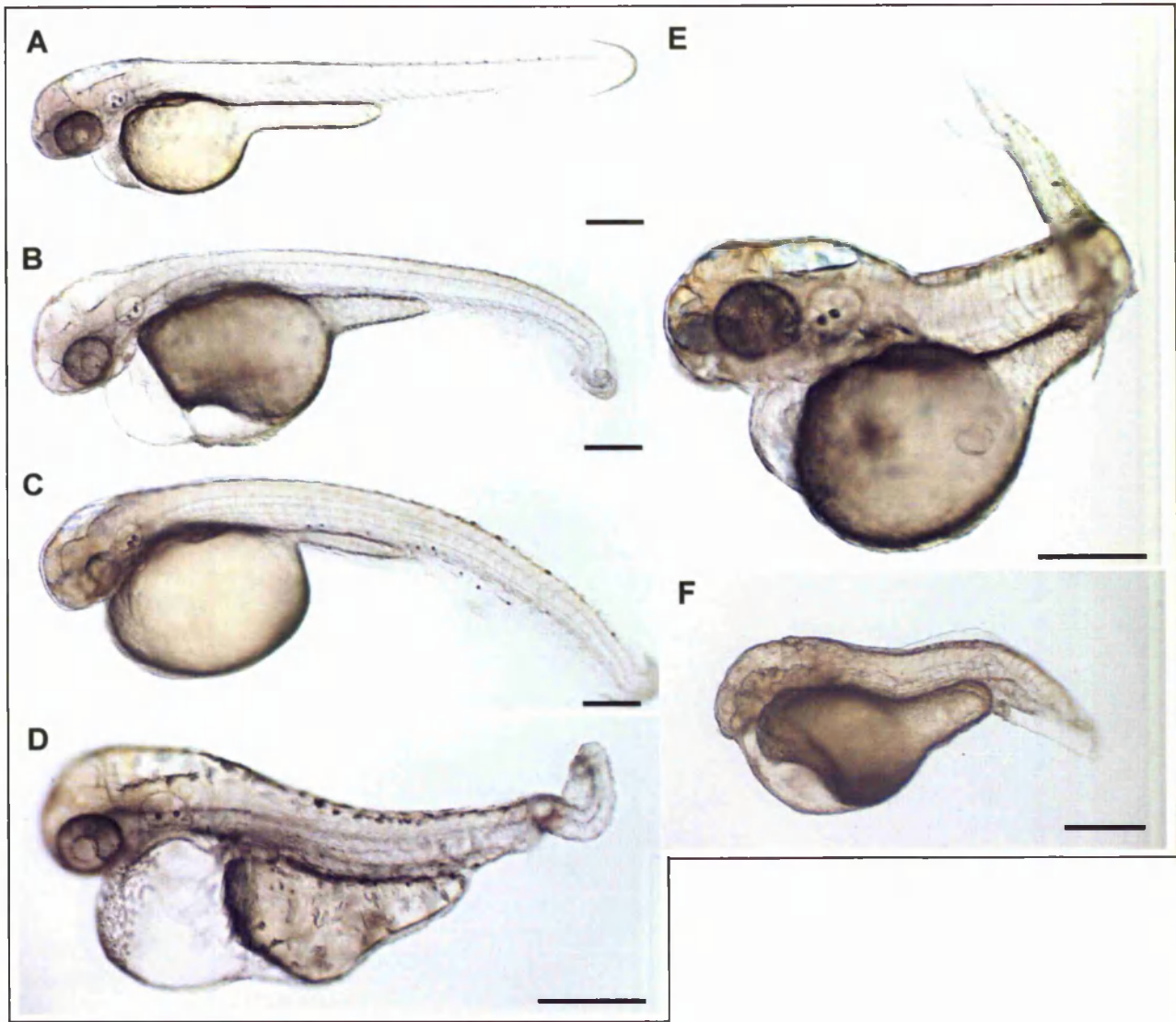


**Figure 7.7: Brightfield Images of non-specific phenotypes** : A small percentage of mutated embryos were often observed in samples of non-injected, CMO-injected and *sulf2* and *sulf2a* MO injected embryos . Wildtype embryo (A). Typical examples of 48hpf embryos classed as non-specific (B-F). Morphological defects exhibited by the non-specific mutants were variable and different to those classed as *sulf2/2a* morphants and were therefore excluded from the morphant phenotype analyses (see Fig 4.5 for further detailed description of morphants) Scale bar 200 $\mu$ m.

These non-specific embryos either displayed characteristic abnormalities as a result of MO mis-targeting<sup>395</sup> or displayed abnormalities different to the defects exhibited by the S2a-SBMO injected samples described below. These abnormalities often included a combination of oedema, small head and eyes, curved body or shortened body axis. As these defects were occasionally present in the non-injected and CMO injected samples they were classed as non-specific and excluded from analyses. Although the number of non-specific phenotypes increased in the CMO and SBMO injected samples, a greater percentage was identified in the CMO injected samples. This is because in proceeding analyses, a vast number of phenotypes that were present in the CMO injected samples were devoid in SBMO injected and non-injected samples and therefore were also classified as non-specific (Fig. 7.7B)

A number of embryos were identified in the S2a-SBMO-injected samples which displayed specific and reproducible phenotypes. These are referred to as S2a-morphants hereafter. The S2a morphants were categorised into mild and moderate phenotypes based on overall vasculature morphology. The mild class of morphants were separated based on trunk vessel defects, and the moderate class were separated on the basis of possessing vascular defects in the trunk and tail. Phenotypic traits were initially characterised at 1-2dpf, the morphology of these morphants was followed until 3.5dpf. Although injection at 3ng induced a very few embryos with morphant phenotype (10.9%), a significant percentage of surviving embryos injected with 5 and 8ng S2a-SBMO were classed as morphants.

The mild class of morphants appeared slightly shorter compared to the wildtype embryos of the same stage. Mild oedema was observed in the hindbrain whilst the size of the head and eyes appeared phenotypically normal. The trunk of this class of morphants also appeared to exhibit mild kinks in the notochord present largely in the mid and posterior regions of the trunk with latter distortion of the notochord resulting in a dorsally inverted tail (Fig. 7.8B). Proximal to the notochordal defects were rounded shaped somites in contrast to the normal chevron shape observed in the non-injected and control injected samples (Fig. 7.8D, black arrows). Despite the mild defects in the trunk, blood circulation appeared to be robust in main axial vessels and ISV's under viewing with the standard light microscope. Consistent with these observations analysis of the trunk vasculature revealed fully lumenised dorsal aorta and posterior cardinal vein with no major defects noted in the branching of the caudal plexus. ISV migration was initiated at

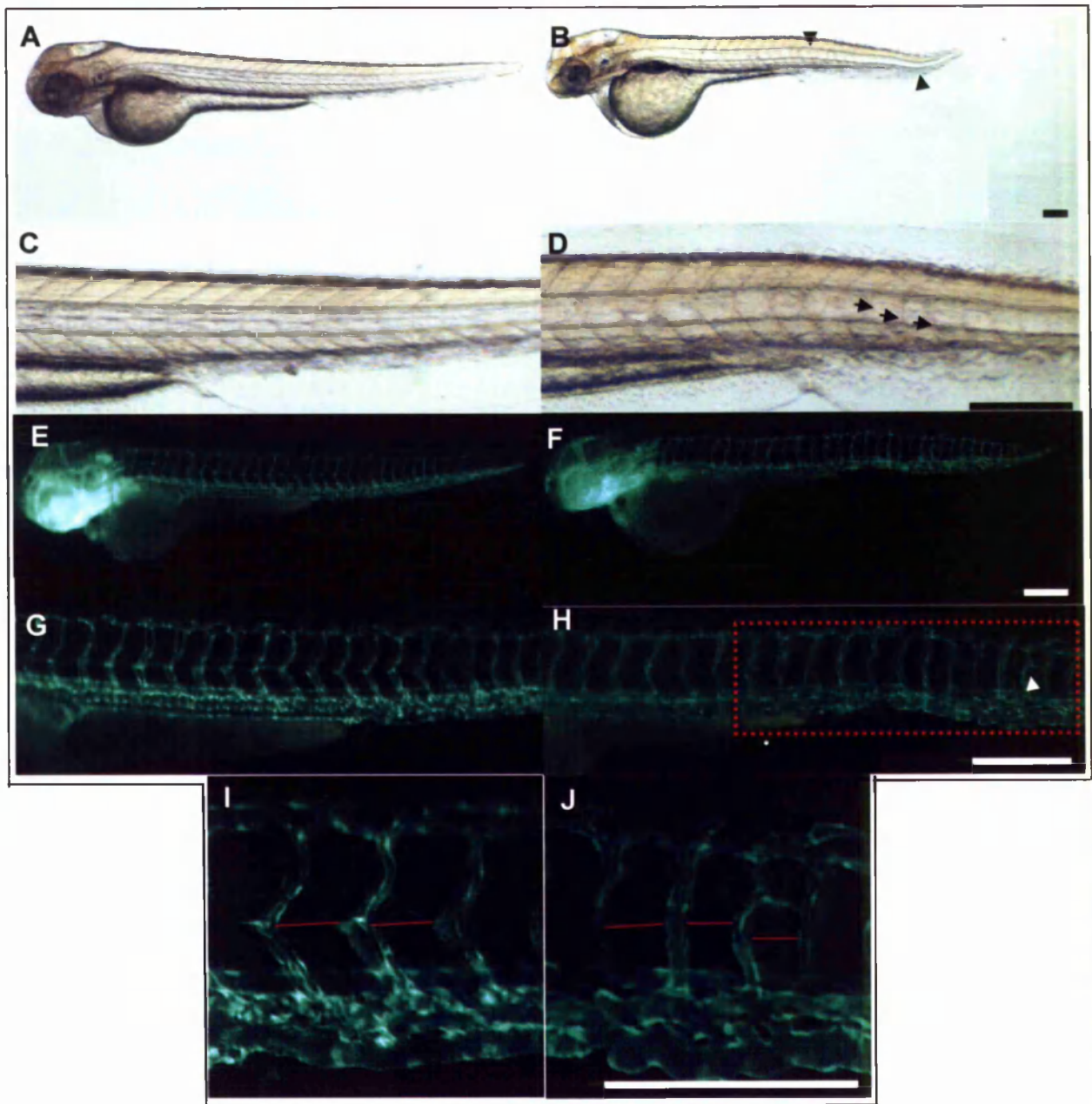


**Figure: 7.8: Morphological and vascular defects exhibited by the mild class *sulf2a* morphants** *Fli1*:GFP embryos were injected at 1-4 cell stage with S2a-SBMO and analysed at 2dpf. Brightfield (A-D) and fluorescent images (E-J) of 48hpf control injected and S2a mild morphants. Lateral views of the control injected embryo (A) S2a mild morphants (B). Mild defects were noted in the notochord (highlighted by the black arrowheads). Close up of the somite patterning and notochord in the control injected (C) and S2a morphant (D) revealed rounded somites in the mid region of the morphant trunk, particularly noticeable in regions adjacent to the trunk (black arrows). Fluorescent images of the vasculature of control injected (E) and S2a morphant (F). Close up of the mid region of the trunk vasculature in control injected (G) and S2a morphant injected (H). ISVs appear irregularly patterned (highlighted by red dotted box) branching with occasional ectopic branching between adjacent ISVs (white arrow). ISVs were also not evenly spaced (J) (indicated by the spacing of the red lines) between somite boundaries appearing a couple  $\mu\text{m}$  shorter compared to control injected (I). Scale bar is  $200\mu\text{m}$

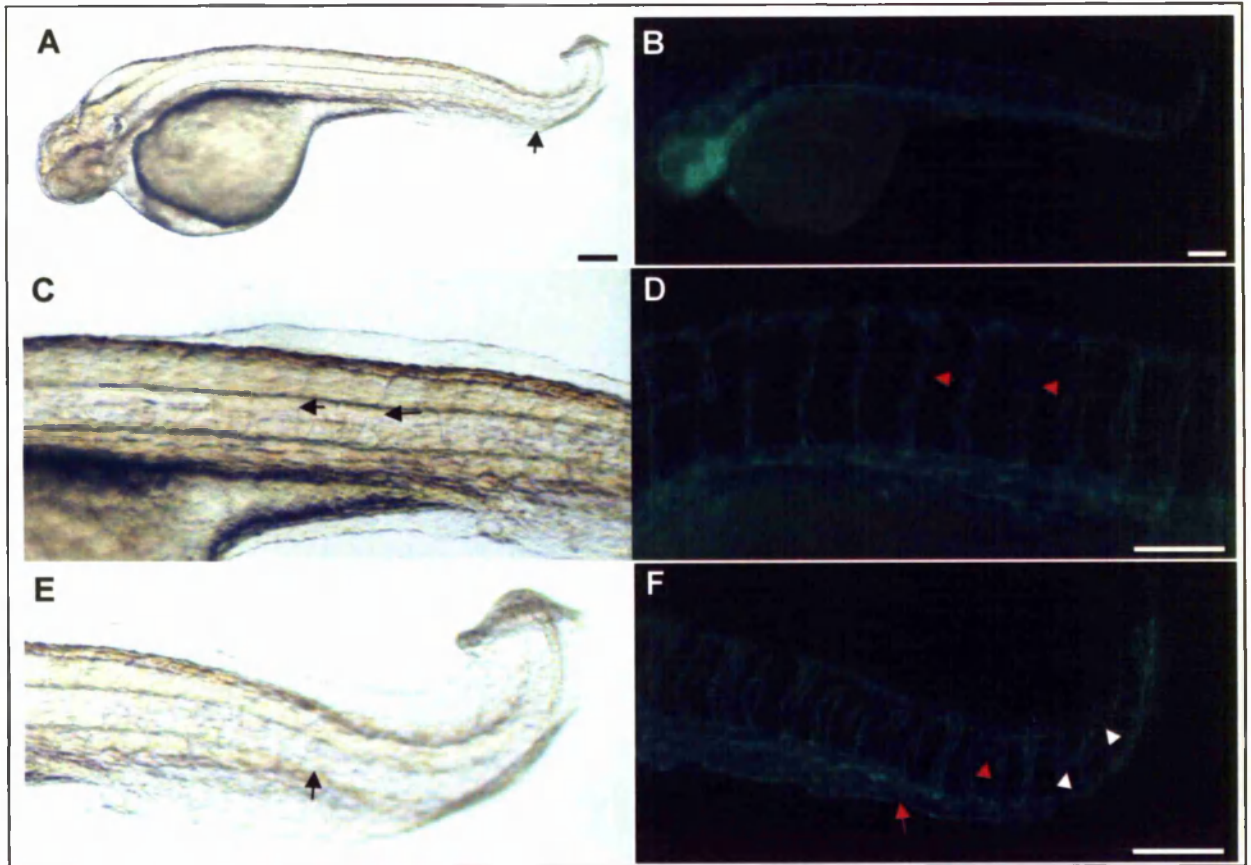


**Figure 7.9: Morphological and vascular defects exhibited by the moderate class *sulf2a* morphants** *Fli1*:GFP embryos were injected at the 1-4 cell stage with S2a-SBMO and analysed at 2dpf. Fluorescent images of 48hpf S2a moderate morphants were taken and compared to control injected embryos (Fig. 7.8A,C,F,H). Brightfield (A,C,E) and fluorescent images (B,D,F) of 48hpf S2a moderate morphants. Lateral views of the S2a moderate morphant (A) exhibiting small head and eyes and curled tail. Close up of the trunk (C) revealed clear loss of the chevron shape of the somites with morphants displaying rounded somites (black arrows), this persisted throughout the trunk of the embryo (E), including the region of the dorsally kinked notochord (black arrow). Fluorescent image of the vasculature of moderate morphant. All ISVs appear to be affected in their overall pattern (B). Close up of the ISVs in the anterior trunk (D) revealed narrower and less branched ISVs and were unevenly spaced. (red arrows). ISVs defects were also evident in the tail of morphants (F), some ISVs did not follow the stereotypic pattern forming aberrant connections with adjacent ISVs (white arrows). Evident in these embryos was also a reduced but dense caudal plexus (red arrow). Scale bar 200 $\mu$ m.

approximately the same time point as the wildtype counterparts (Fig. 7.8E,F). The growth and patterning of the ISVs appeared normal in the first four anterior trunk segments which displayed appropriate growth along intersegmental boundaries, and correct left right mirroring of vessels. However mild defects were apparent in the ISV of the mid and posterior regions of the trunk as the morphants displayed an irregularly spaced arrangement of intersegmental vessels compared to normal patterning of ISVs observed in wildtype embryos at the same stage (Fig. 7.8G,I). The ISVs appeared to sprout from the DA and PCV normally at 20hpf (data not shown) but do not extend rostrally and caudally to the intersegmental boundaries and as a result form elongated ISVs, similar to that of the *sulf2* mild morphants. Also *sulf2a* morphants exhibited occasional premature dorsal branching of ISV to adjacent vessels in contrast to branching at their most dorsal extent to form the DLAV (Fig. 7.8H,J). While these defective vessels did not appear to support blood flow, the anterior-mid ISV appeared to be functional. However this varied and occasionally in some morphants circulation was absent in all ISV's.

The overall body shape of the moderate class of morphants was also slightly shorter than wildtype of the same stage. The moderate class of embryos displayed those vascular defects associated with the mild phenotype but a greater percentage of mispatterned ISV's. While hindbrain oedema was persistent in this class of embryos the head and eyes appeared smaller than the wildtype embryos at the same stage (Fig. 7.9A). The overall body shape of the embryos was curved compared to the milder phenotype despite the defects in the notochord observed in the posterior end of the trunk being similar. This resulted in the caudal region of tail to curve dorsally (Fig. 7.9C,D). Interestingly the somite patterns appeared to be rounded throughout the whole length of the trunk as opposed to being restricted in the regions proximal to the site of the notochord defect only. Close inspection of the trunk revealed functional blood circulation in the main axial vessels, but this did not persist to the end of the tail, resulting in short circuiting of the blood flow.

On analysis of the vasculature, morphants displayed fully lumenised axial vessels, with interruption of the caudal aorta rostrally proximal to the curved tail consistent with the blood flow observations. The caudal plexus was generally smaller and appeared dilated (Fig. 7.9B). Nevertheless vessels were able to support blood flow. Although a initial delay in the migration of the vessels was observed at 33hpf all ISV did not reach the horizontal myoseptum in comparison to the wildtype (data not shown), most ISVs however eventually catch up and appeared to branch dorsally and connect with adjacent branches to form the DLAV. Evident in the embryos was the irregular shaped intersomitic vessels that were prevalent through out the trunk (Fig. 7.9D). While the few anterior ISVs appeared to support blood flow the mid-posterior ISVs did not appear to

support any blood flow consistent with the aberrant appearance of these vessels (data not shown), as the most posterior ISV appeared disorganised with a few not migrating to their most dorsal extent, instead forming premature dorsal extensions at the levels of the horizontal myoseptum (Fig. 7.9F).

#### 7.3.4 Analysis of S2-SBMO injected embryos

The results presented in chapter 3 indicate that *sulf2* is a fairly conserved protein sharing homology with mammalian *sulf2* in sequence and expression. The emerging theme from our HS disaccharide analysis is that zebrafish *sulf2* can remove 6-O sulfate groups from monosulfated and tri-sulfated disaccharide species consistent with *in-vivo* and *in-vitro* reports of mice, human and quail *sulf2*<sup>344,349,356</sup>. While *zfsulf2* shares strong similarities in sequence and expression patterns with *sulf2a* it is hypothesised that knockdown of zebrafish *sulf2* would result in S2-SBMO morphants exhibiting similar defects to *sulf2a* morphants during vascular development in regions where *sulf2* is the major source of sulf. Knockdown of the zebrafish *sulf2* was achieved by injection of SBMO and the vasculature phenotype of the trunk in the resulting morphants analysed in the *fli1*: GFP fish.

RT-PCR analysis showed that S2-SBMO was capable of reducing the levels of *sulf2* transcript thereby reducing the level of *sulf* mRNA expression during zebrafish development. The level of *sulf2* knockdown increased at the higher dose of 12ng compared to 5ng of S2-SBMO.

As preliminary experiments performed at 3ng did not produce a morphant phenotype, injections at a higher concentration of 15ng resulted in 100% death rate (data not shown). Therefore all injections were carried out at concentrations ranging from 5-12ng. S2-SBMO injections were carried out in different batches of *fli1*: GFP embryos and the data amalgamated and compared to the non-injected and control morpholino (CMO) injected embryos. Analysis of the non-injected controls was carried out alongside, but the data was combined into one chart as these samples were absent of morphants characteristics. As a CMO a 5bp missense morpholino targeting the 5'UTR of the *sulf2* transcript was designed. To give a clear indication of the affect of the SBMO on survival rate, embryos were scored for mortality in the first 24hpf and compared alongside non-injected and control injected samples. On average ~26% of the non-injected embryos were dead in the first 24hpf while in comparison the mortality rate was often higher in CMO and SBMO injected embryos. This tended to increase with increasing dose. The survival rate of the SBMO and CMO injected samples was similar at each MO concentration. All surviving embryos were analysed at 2-3dpf and scored for overall morphology and vasculature defects. The

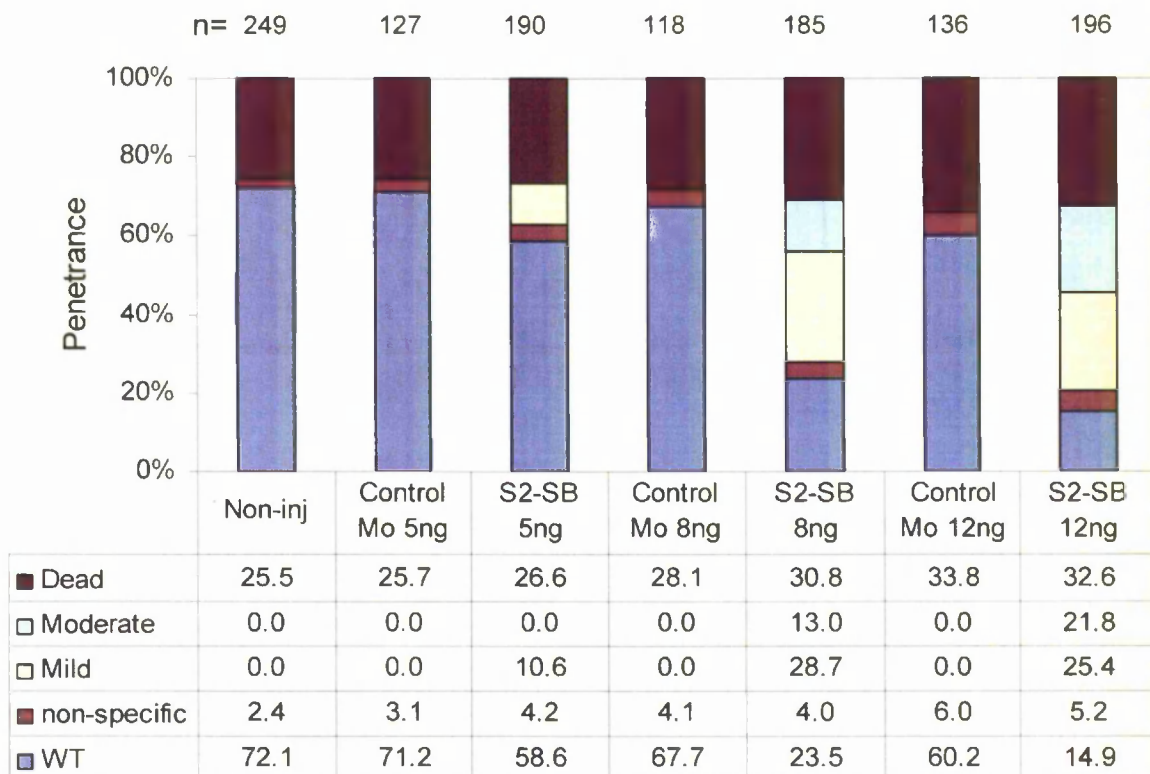


**Figure 7.10: Chart showing the analysis of the *flil*:GFP embryos injected with different doses of *sulf2* morpholino.** Data shown is combined from three experiments average penetrance represented as a percentage. The data from non-injected controls were further combined and is represented as one bar in chart. Embryos were scored at 24hpf for mortality rate and surviving embryos were analysed at 2dpf. These embryos were categorised into four different classes depending on their overall morphology into wildtype, non-specific or morphants. Morphants were categorised further into mild and severe class depending on the severity of the vasculature defect. Embryos were injected with 5,8 and 12ng S2-SBMO and compared to control MO injected and non-injected embryos. Mortality was generally higher in control MO or SBMO injected samples compared to control and this tended to increase at higher MO concentrations. Majority of control MO and a subset of S2-SBMO injected displayed overall body shape and vasculature identical to that of the non-injected embryos. A small percentage of non-specific phenotypes was seen in all samples and their prevalence increased with increasing MO concentration. Injections of 5ng of the S2-SBMO resulted in a small percentage of embryos with mild phenotype. Injections of 8ng and 12ng of S2-SBMO resulted in 41 % and 47% of morphants respectively, represented by both classes.

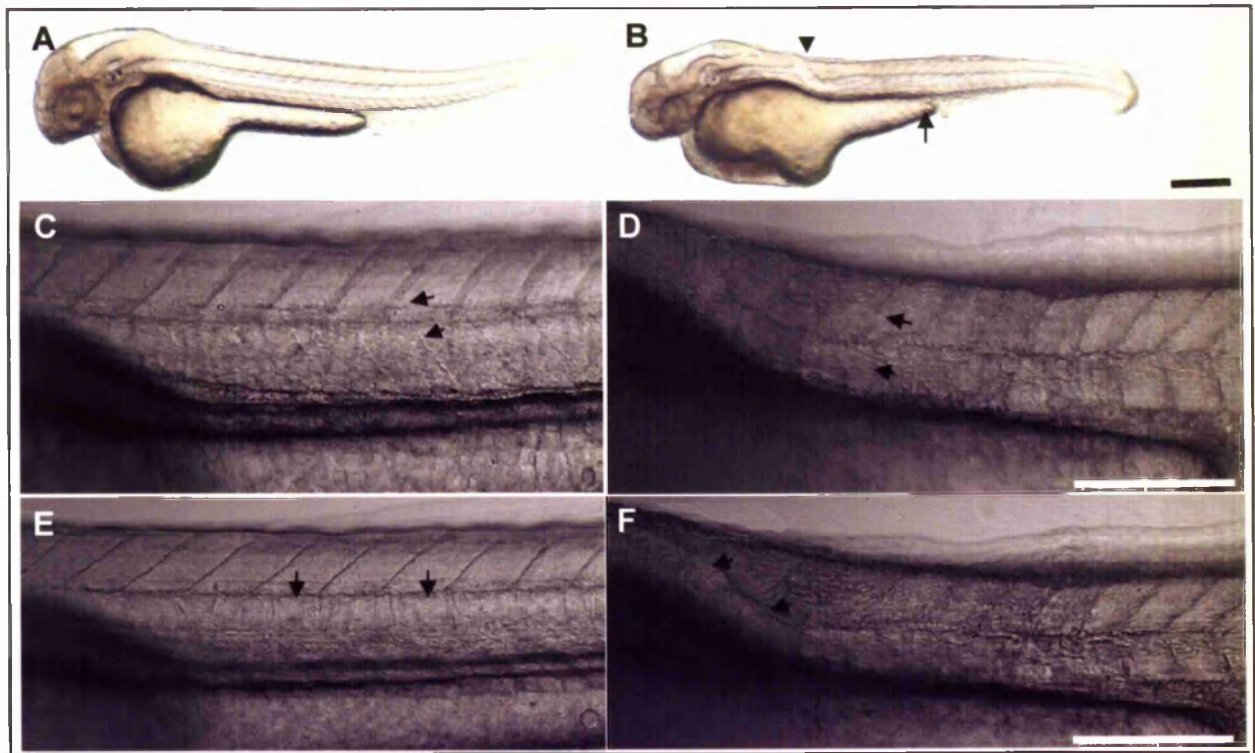


**Figure 7.11: Morphological defects exhibited by mild class *sulf2* morphants.** Embryos were injected at the 1-4 cell stage with S2-SBMO and analysed at 2dpf. Brightfield images of 48hpf S2 mild morphants were taken and compared to control injected embryos. Lateral views of control injected embryo (A) and S2 mild morphants (B) displaying distorted notochord in the anterior of trunk (depicted by black arrowhead) and have a reduced yolk extension (black arrow), morphants also occasionally exhibited pericardial oedema. Higher magnification of the chevron shaped somite boundaries (black arrows) in control anterior trunk (C). Evident in morphants is the loss of chevron shaped somites in the anterior region of the trunk of the mild morphant (D) somites appear more rounded (indicated by black arrows). Patterning of the notochord in control injected embryos (E) and mild morphant (F). The patterning of the notochord mild morphant appears correctly despite the distorted shaped kink in notochord (represented by the blackarrows). in A-F. Higher magnification images are composite image accumulated from a series of z-stacks (1.5 $\mu$ m depth) using normaski optics. Scale bar is 200 $\mu$ m

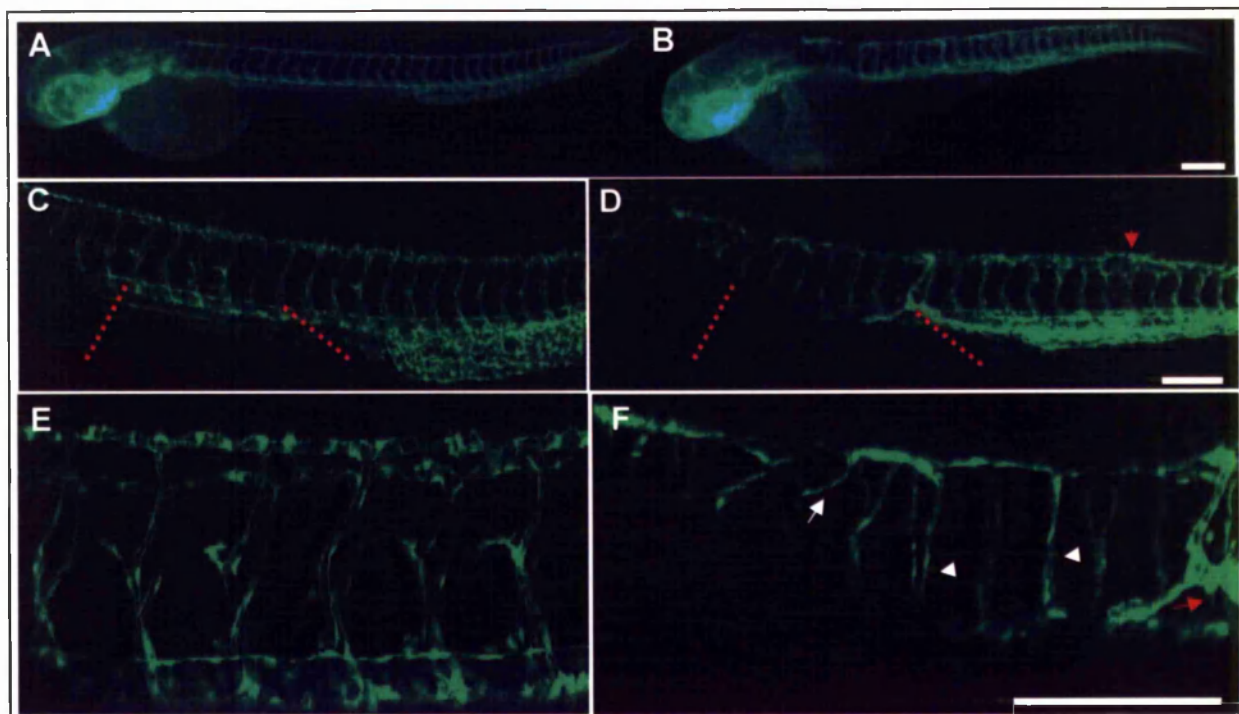


**Figure 7.12: Vascular defects exhibited by the *sulf2* mild class morphants.** *Fli1*:GFP embryos were injected at the 1-4 cell stage with S2-SBMO and analysed at 2dpf. Fluorescent images of 48hpf S2 mild morphants were taken and compared to control injected embryos. Lateral views of the control injected embryo (A), S2 mild morphants (B). Anterior region of trunk in control injected embryo (C) displaying correctly patterned ISVs and fully lumenised axial vessels and caudal plexus. Mild morphants (D) display irregular patterned ISVs in the anterior region of trunk concomitant with ectopic branches sprouting at the most dorsal extent of ISVs (depicted by red arrow). Higher magnification of the ISVs in anterior region of trunk in control injected embryos (E) appear to branch rostrally and caudally following the normal stereotypical intersomitic pathway. Aberrant ISVs present in S2 mild morphants (F) (white arrow heads) following irregular network. Ectopic branching was evident at the most dorsal (white arrow) and ventral roots of ISVs (red arrow). Higher magnification images are composite images accumulated from a series of z stacks (1.5 $\mu$ m depth) Scale bar is 200 $\mu$ m.

majority of non-injected and control injected embryos displayed overall body shape and vasculature network typical to wildtype embryos at the same stage (Fig. 7.10). As described previously with MO knockdown studies, a small percentage of abnormal embryos was present in non-injected, CMO and SBMO injected samples that exhibited developmental abnormalities associated either unhealthy embryos or with non specific gene knockdown. These were classified as non-specific and a higher percentage of these embryos were prevalent in the MO injected samples at 12ng. This is consistent with the idea that MO can induce off-targeting effects<sup>395</sup>. As these apparent off targeting defects were also present in CMO they were excluded from phenotype analyses (Fig. 7.7C).

A subset of embryos was identified at 2dpf in the S2-SBMO injected samples that produced reproducible morphological and vascular defects (referred to S2-SB morphants hereafter). These were grouped into mild and moderate morphants depending on the overall vascular morphology. Mild morphants were separated on the basis of vascular abnormalities in the trunk, and moderate morphants were separated on the basis of vascular abnormalities in the trunk and tail. Phenotypic traits were initially characterised at 1-2dpf and the morphology of these morphants was followed until 3.5dpf. Although a small percentage (10.6%), of morphants was present at the lower concentration of 5ng, a significant percentage of surviving embryos in the 8ng and 12ng injected were classed as morphants with an overall penetrance of 41% and 47% respectively.

The mild class of S2-SB *fli1*:GFP morphants appeared smaller in size compared to the control injected embryos with a reduction also observed in the yolk extension (Fig. 7.11B). Striking in this class of embryos was the mild defect in the anterior region of the notochord displaying two kinks, (Fig. 7.11B,F) while the posterior notochord appeared morphologically normal. Brightfield images of the morphant revealed poor morphogenesis of somite boundaries, with somites no longer retaining their characteristic chevron shape only in mesodermal tissue proximal to the notochord defect (Fig. 7.11D).

On analysis of the trunk vasculature no defects were noted in the formation of the vasculogenic primary axial vessels (Fig. 7.12B) with morphants establishing functional circulation at 28hpf. Initial emergence of intersegmental vessels (ISV's) was delayed at 24hpf (data not shown) in the trunk of S2-SB morphants, however morphants did eventually catch up with their wildtype counterparts by 33hpf. The delay in ISV was not a result of developmental delay as gross morphological landmarks appeared at a normal rate. However in the anterior region of the trunk vasculature the morphants displayed patterning defects in the ISVs. Evident in the first eight ISVs, was the incorrect left-right mirroring (Fig. 7.12D) with some ISVs also possessing either

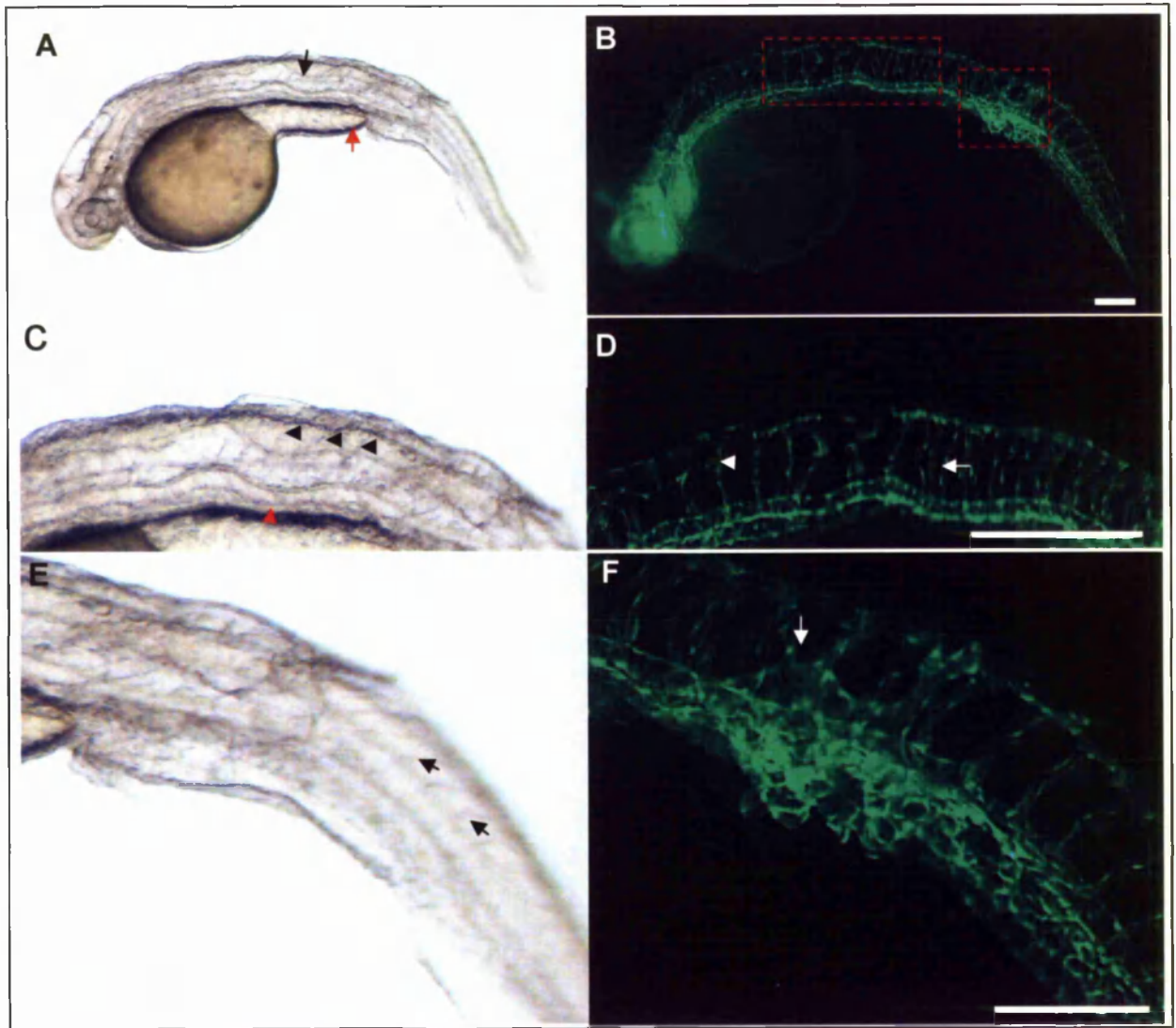


**Figure 7.13: Morphological and vascular defects exhibited by the *sulf2* moderate class morphants.** *Fli1*:GFP embryos were injected at the 1-4 cell stage with S2-SBMO and analysed at 2dpf. Brightfield (A,C,E) and fluorescent images (B,D,F) of 48hpf S2 mild morphants were taken and compared to control injected embryos (Fig. 7.11&7.12). Lateral views of the S2 moderate morphant (A) displaying reduced yolk extension (indicated by red arrow) distorted notochord (indicated by black arrows) and curved body axis. Close up of the mid trunk and tail (C) reveals rounded somites (black arrowheads) and a distorted axial vessel (red arrowhead). However tail somites appear chevron shaped (E) (black arrowheads). Fluorescent image of the whole vasculature of S2 morphant (B). Regions highlighted by the red dotted box are magnified in the images below. ISVs are irregularly patterned (white arrows) and most anterior ISVs appear to form ectopic branches (white arrowhead). The caudal plexus of the morphants (F) display a dense network of ectopic vessels (white arrow). Scale bar is 200µm.

dual ventral roots (Fig. 7.12F red arrow) or forming premature dorsal branches (Fig. 7.12F white arrow). These defects in ISVs were observed at relatively equal frequencies. However the ectopic branching was not only confined to the region of ISV defect but was persistent in the mid region of the trunk (Fig. 7.12D red arrow).

The overall body shape of the moderate morphants appeared to be slightly curved, although the head appeared phenotypically normal these morphants displayed similar notochord and somite defects. The distorted notochord was evident from the anterior trunk to mid trunk with shortening of the yolk extension. In the mesoderm tissue encompassing the notochord defect, the somites appeared to be aberrantly patterned, most boundaries appeared rounded similar to the mild class (Fig. 7.13A,C). However the classic chevron shape of the somitic boundaries was retained in the posterior region of the trunk (Fig. 7.13E). Simultaneous analysis of the vasculature revealed a mis-shaped dorsal aorta (DA) that appeared to follow the structure of the distorted notochord (Fig. 7.13B). Nevertheless the DA was functional providing blood to the trunk and tail. Similarly ISV patterning was also affected in the regions of the notochord defects. ISV's appeared uniformly straight with medial ISVs forming premature dorsal branches, particularly noticeable was the irregular spacing between the anterior-mid ISV's compared to their wildtype counterparts (Fig. 7.13D). These were characteristic of similar patterning defect observed with *sulf2a* morphants. Interestingly the posterior most ISVs appeared correctly patterned and equally spaced. This was consistent with blood flow active in the latter regions of the trunk and only in few medial ISVs. In addition to the alterations in the ISV formation, the anterior region of the caudal plexus also appeared abnormal. Ectopic vessels were observed branching dorsally from the caudal vein and forming aberrant connections with ISVs (Fig. 7.13F).

### 7.3.5 Analysis of ATGMO mediated knockdown of *sulf2a* and *sulf2*

The data presented so far indicates that *sulf2a* and *sulf2* SBMO is capable of knocking down *sulf2a* and *sulf2* mRNA expression and the resulting morphant phenotype are specific to the morpholino sequence. Although the *sulf2a* and *sulf2* morphant phenotypes were evidently reproducible, the seemingly off-target affects described by Robu *et al* (2007)<sup>395</sup> were also evident in the morphant phenotypes. These included notochord defects, abnormal somites, curved body, small head and eyes. To exclude the possibility that these defects were a result of mis-targeting, it was necessary to confirm the reproducibility of the *sulf2a* and *sulf2* morphants. One way to gain additional confidence in the specificity of the morpholino is to design a second,

independent MO and gain a similar phenotype to that induced by the first MO. Gene tools ([www.gene-tools.com](http://www.gene-tools.com)) show that translation blocking MOs (TBMOs) are highly effective at knocking-down a gene of interest and these MOs can show greater specificity for their target than SBMOs. Translational blocking morpholinos (ATGMO/5'UTRMO) were designed to target the translation initiation site of the *sulf2* and *sulf2a* transcript (section 7.2.1). The data discussed with this set of morpholinos was collated by Dr Stringer and Melvin Chua (placement student). Microinjections with the *sulf2a* ATGMO were carried out at 3, 6 and 12ng. Mortality was comparable between the non-injected and ATGMO injected samples, however the survival of the embryos generally decreased with increasing concentration of the ATGMO. The majority of embryos in the ATGMO injected samples displayed characteristics of wildtype embryos at the same stage. Injections at 3ng revealed a small percentage of embryos (7.2%) displaying abnormalities not associated with the *sulf2a* mild/moderate morphant. However with injections at the higher dose, 14% of embryos injected displayed S2a mild/moderate phenotypes described previously. The only striking difference with the mild class of morphants was that the most affected ISV's lay in the posterior region of the trunk, as opposed to defects observed in the mid region of trunk. Moreover injections at the higher dose did not result in higher penetrance of the morphant phenotypes with a significant proportion of the injected embryos displaying wildtype like characteristics. A subset of non-penetrant phenotypes were also present in all ATGMO injected samples that displayed different morphology to the embryos previously described as morphants and were therefore excluded from analysis (Data not shown).

A range of concentrations of the *sulf2* ATGMO were injected into embryos to establish the concentration to be used for future experiments. Preliminary injections were performed at 5, 7 8ng and 10ng. Each experiment was repeated at least twice. At the highest dose of 10ng, S2-ATGMO induced 50% death of embryos. Therefore future injections were carried out at the lower doses. Compared to the non-injected controls, mortality was higher in S2-ATGMO injected embryos and tended to increase with increasing dose. Samples injected at 8ng showed a moderate increase in mortality by 10% however the mortality induced was limited to the first 24hpf. The average survival rate at the three doses was comparable to that of non-injected controls. Surviving embryos were analysed in terms of their overall morphology and vasculature. The majority of embryos in the non-injected, control injected and S2-ATGMO injected samples displayed a body shape and vasculature development typical of wildtype embryos at the same stage. The number of wildtype embryos in the S2-ATGMO injected samples was comparable amongst the different doses. A small subset of embryos was classified as mild and moderate morphants based on the criteria previously mentioned (section 7.3.3). At the lowest

concentration of 5ng, 5% of embryos displayed a phenotype similar to the mild class observed previously in the S2 morphants. In addition to the kinked notochord, and somite patterning defects, these morphants displayed pericardial oedema and inverted tails not previously observed with the S2-SBMO morphants. However injections at the higher dose of 7ng and 8ng did not result in higher penetrance of the previous phenotype, but slightly higher penetrance (12%) of embryos with other abnormalities such as loss of anterior structures i.e. head and eyes, or shorter embryos (Data not shown). On analysis of the vasculature these embryos appeared to show similar ISV and caudal defects despite the different morphologies. Repeat of the doses yielded similar low levels of the mild and moderate phenotype with majority of embryos exhibiting wildtype like morphology. Similar to the results obtained with the S2a-ATGMO, the *sulf2* morphant phenotypes were not reproducible with the S2-ATGMO even at the higher concentration.

Although it was encouraging to observe a low level of the same phenotype from this set of data, the non-penetrant defects led us to question whether the knockdown of the gene target was successful. To test the effectiveness/specificity of a translational blocking morpholino, the protein production is assessed by western blot analysis. Unfortunately there were no antibodies designed to the zebrafish sulfatase proteins that could have allowed for such tests within the time frame of the project. Alternatively the heparan sulphate content of the injected embryos was analysed to test if the weaker phenotype corresponded to smaller changes in the level of disaccharides.

### 7.3.6 HS Disaccharide analysis of *sulf2a* and *sulf2* TBMO injected embryos

As several experiments from *sulf2a* and *sulf2* ATGMO injected embryos did not show a highly penetrant reproducible phenotype, it was decided to test the efficacy of the morpholino by analysing the HS disaccharide content of the injected embryos. It was hypothesised if knockdown of the *sulf2a* and *sulf2* gene is effective then similar changes observed with the SBMO in the expression levels of the 6-O sulfated disaccharides would be expected.

The HS composition of the *sulf2a*-ATGMO injected embryos was analysed at 48hpf and compared to CMO and wildtype (Fig. 7.14A). The six most abundant disaccharides (labelled 1-6) including the three 6-O sulfated disaccharides  $\Delta$ UA-GlcNAc6S,  $\Delta$ UA-GlcNS6S,  $\Delta$ UA2S-GlcNS6S were present in wildtype and S2a-ATGMO injected samples. In the HS profile of S2a-ATGMO morphants there appeared to be a 21% and 18% decrease in the 6-O sulphated  $\Delta$ UA-GlcNAc6S and  $\Delta$ UA2S-GlcNS6S disaccharides respectively, with a 52% increase in  $\Delta$ UA-

GlcNS6S peak compared to control injected (Fig. 7.14B). However these were not statistically significant in either wildtype or CMO injected.

Similarly GAGs were extracted from 48hpf wildtype embryos and live embryos injected with 8ng of S2-ATGMO. The six most abundant disaccharides (labelled 1-6) including the three 6-O sulfated disaccharides  $\Delta$ UA-GlcNAc6S,  $\Delta$ UA-GlcNS6S,  $\Delta$ UA2S-GlcNS6S were present in wildtype, CMO and S2-ATGMO injected samples (Fig. 7.15A). In the HS profile of S2-ATGMO morphants there appears to be minor decreases in the two 6-O sulfated disaccharide peaks  $\Delta$ UA-GlcNAc6S,  $\Delta$ UA2S-GlcNS6S while a large increase was observed in the  $\Delta$ UA-GlcNS6S peak. Although there appeared to be no significant changes in all three of 6-O sulphated disaccharides compared to control, a general trend was observed in the overall NS, 2S and 6S groups. A moderate and minor increase in the 6S (14%) and NS (0.4%) was found compared to control with small a decrease in the 2S groups (3%).

The non-significant changes in 6-O sulphation left undetermined whether the *sulf2a* and *sulf2* ATGMO were effective and the specificity of the phenotypes induced by the S2 and S2a SBMO.

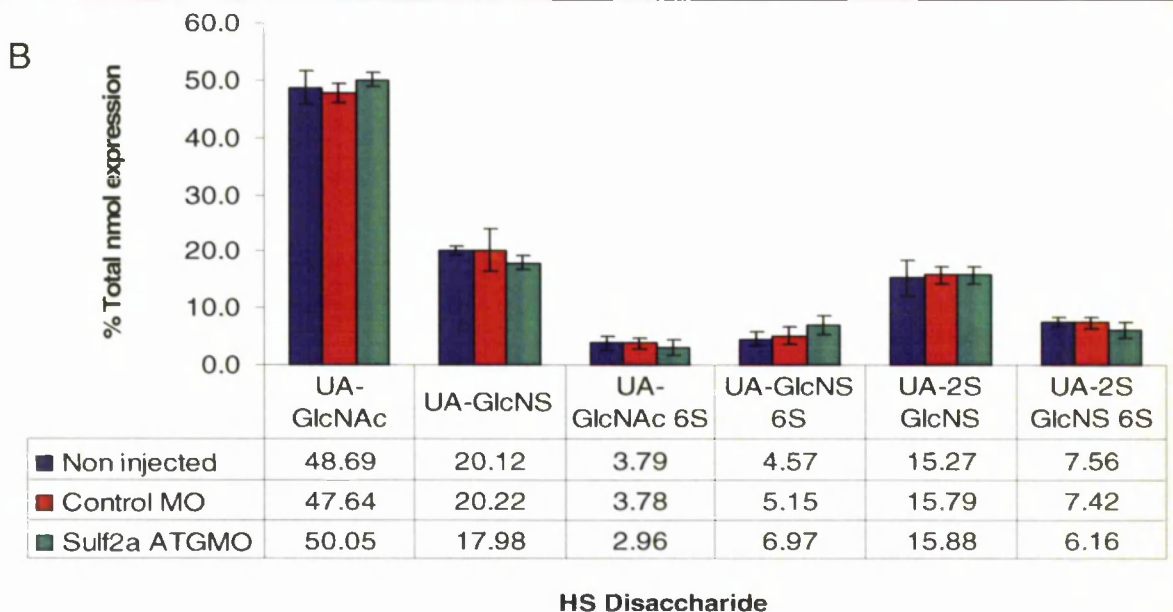
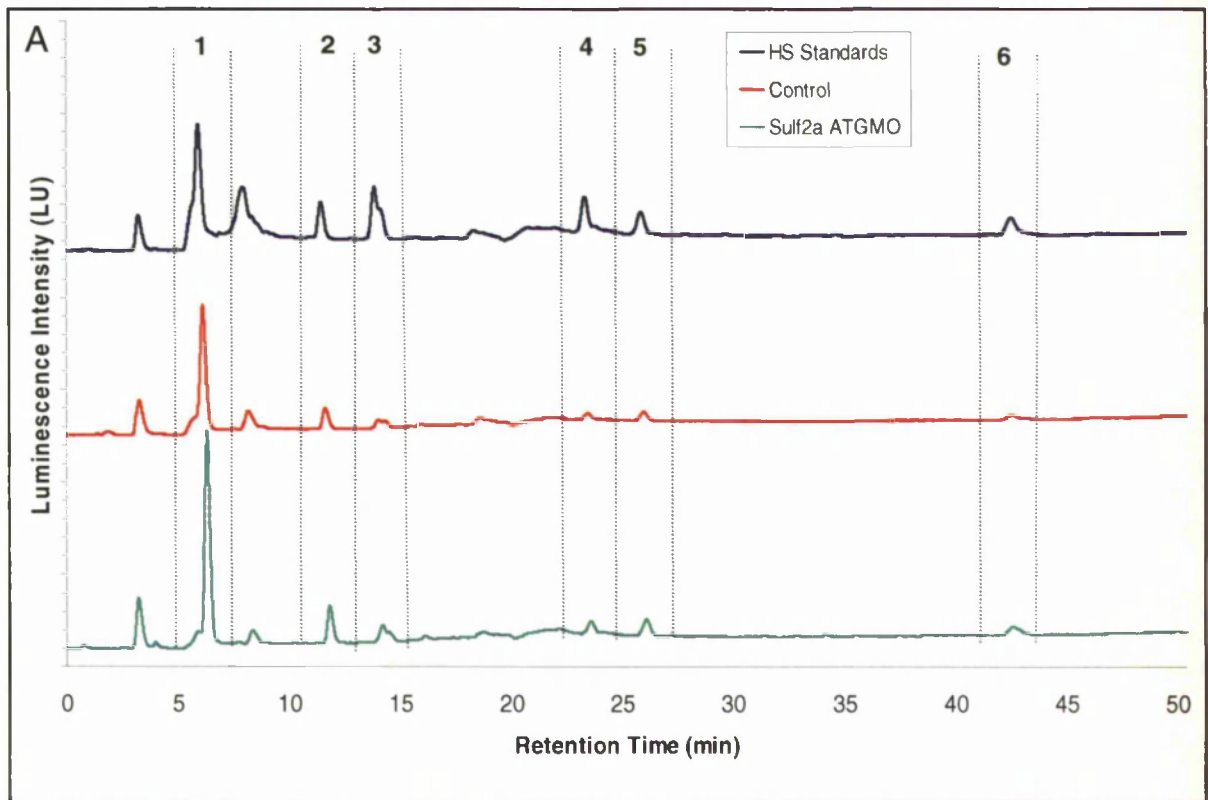
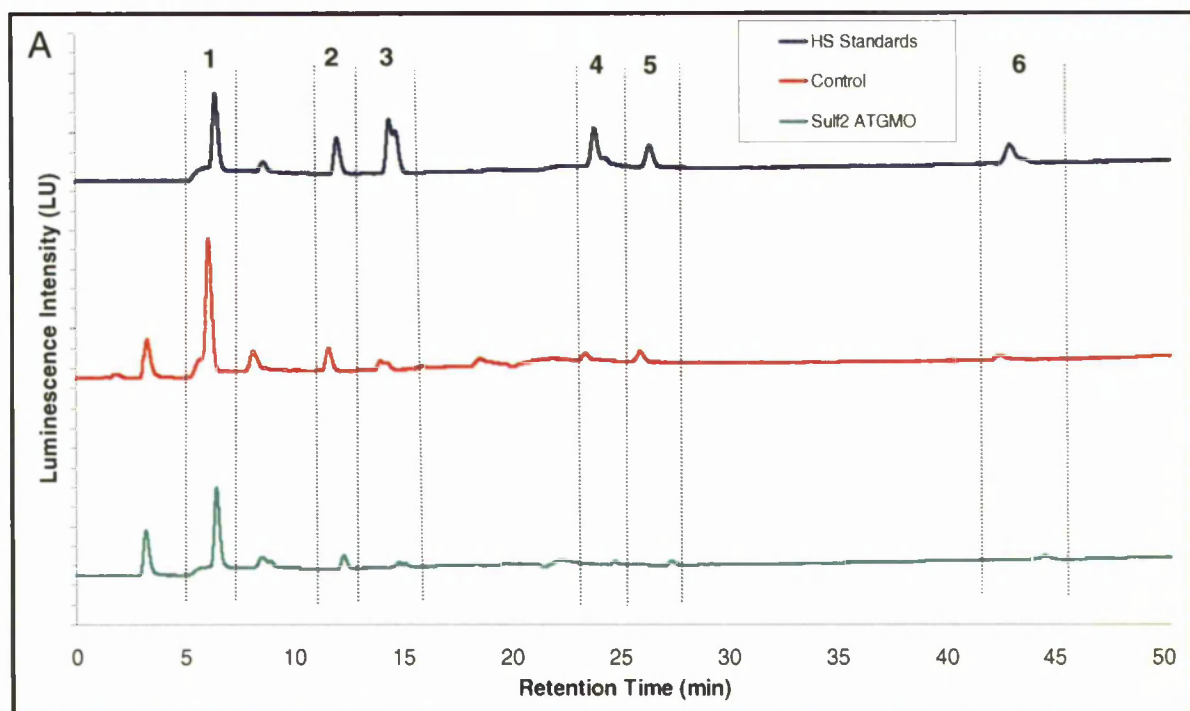


**Figure 7.14: Heparan sulphate profiling of *sulf2a* ATGMO morphant embryos.** **A:** Representative chromatograms of HS standards (blue), non-injected, CMO injected embryos (red) and 8ng of *sulf2a* morphants (green). Six disaccharides were identified by comparison to the elution times of known HS standard peaks; peak 1:  $\Delta$ 4,5 unsaturated hexuronate-*N*-acetyl glucosamine ( $\Delta$ UA-GlcNAc); peak 2:  $\Delta$ UA-*N*-sulfated glucosamine, ( $\Delta$ UA-GlcNS); peak 3:  $\Delta$ UA-6-*O*-sulfated GlcNAc( $\Delta$ UA-GlcNAc6S); peak 4:  $\Delta$ UA-6-*O*-sulfated GlcNS, ( $\Delta$ UA-GlcNS6S); peak 5:  $\Delta$ UA2-*O*-sulfated GlcNS ( $\Delta$ UA2S-GlcNS); peak 6:  $\Delta$ UA2S-GlcNS6S.

**B:** Graphical depiction of disaccharide analysis of HS extracted from 48hpf non-injected, CMO injected embryos and 8ng of *sulf2a*-ATGMO injected embryos, represented as a total percent of heparan sulfate. The six most abundant disaccharides are indicated on the x axis. Average calculated from two individual experiments wildtype n=2, 40-50 embryos per sample, *sulf2a* injected n=2, 45-50 embryos used per sample.



B

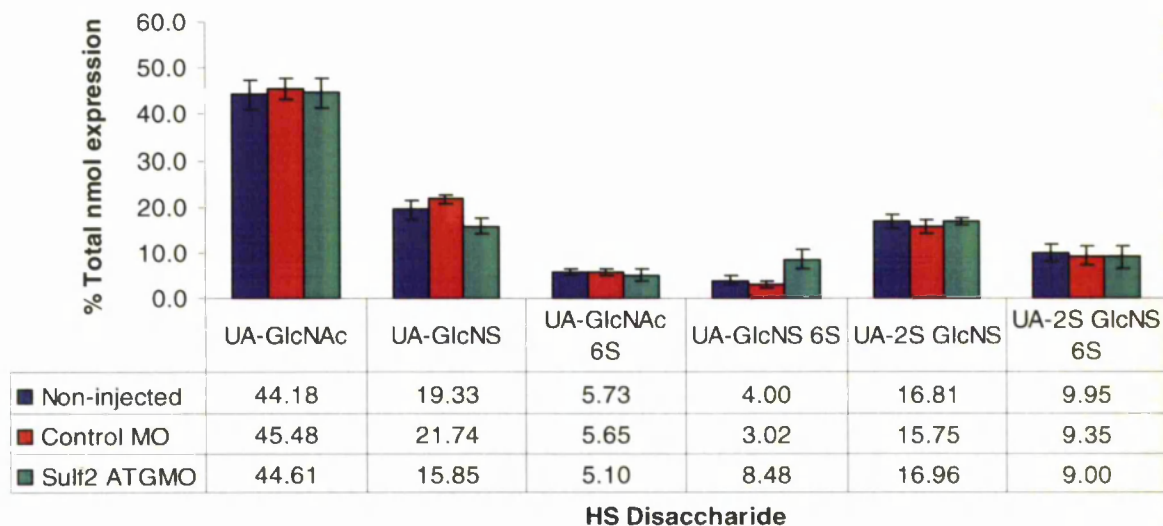


**Figure 7.15: Heparan sulphate profiling of *sulf2* ATGMO morphant embryos. A:** Representative chromatograms of HS standards (blue), non-injected and CMO injected embryos (red) and 8ng of *sulf2* morphants (green). Six disaccharides were identified by comparison to the elution times of known HS standard peaks; peak 1:  $\Delta$ 4,5 unsaturated hexuronate-*N*-acetyl glucosamine ( $\Delta$ UA-GlcNAc); peak 2:  $\Delta$ UA-*N*-sulfated glucosamine, ( $\Delta$ UA-GlcNS); peak 3:  $\Delta$ UA-6-*O*-sulfated GlcNAc ( $\Delta$ UA-GlcNAc6S); peak 4:  $\Delta$ UA-6-*O*-sulfated GlcNS, ( $\Delta$ UA-GlcNS6S); peak 5:  $\Delta$ UA2-*O*-sulfated GlcNS ( $\Delta$ UA2S-GlcNS); peak 6:  $\Delta$ UA2S-GlcNS6S.

**B:** Graphical depiction of disaccharide analysis of HS extracted from 48hpf non-injected, CMO injected embryos and 8ng of S2-ATGMO injected embryos, represented as a total percent of heparan sulfate. The six most abundant disaccharides are indicated on the *x* axis. Average calculated from two individual experiments control injected n=2, 40-50 embryos per sample, S2-MO injected n=3, 35-40 embryos per sample

## Discussion

### 7.4.1 SBMO can reduce the expression of the wildtype *sulf2a* and *sulf2* transcript

*Sulf2a* and *sulf2* morpholinos were designed to target splice acceptor site at intron3-exon4 boundary. Although the expression of the wildtype *sulf2a* and *sulf2* transcript was reduced the predicted aberrant products were not detected in both sets of morphants. In *sulf2a* transcript no short product could be detected, although there may be a possibility like *sulf1c* that the intron is retained in the full length transcript. A shorter product in the *sulf2* morphants was however detected that increased as expression of the wildtype transcript reduced, sequencing of this band revealed a non-specific zebrafish cDNA. Although not proven it is likely that targeting the intron-acceptor site is more complex than anticipated and that intron is retained in the full length transcript. The predicted shorter product was not investigated further. However if the intron was included in both final transcripts the predicted aberrant mRNA would translate a truncated form of the protein lacking the hydrophilic domains and predicted heparin binding sites

### 7.4.2 HS disaccharide and phenotype analysis of *sulf2a* SBMO morphants

HS was extracted from *sulf2a* injected embryos that produced consistent and reproducible phenotypes. Overall total HS content was similar to that observed with *sulf1c* morphants. Although an increase was observed in all three 6-O sulphated disaccharides a statistically significant increase was observed only in the tri-sulphated disaccharide compared to control injected, consistent with *in-vitro* reports of quail and human SULF-2 substrate specificity<sup>347</sup>. This suggests that *sulf2a* activity like *sulf1c* is likely to be conserved from mammals to zebrafish. Consistent with *in-vitro* reports *sulf2* has identical substrate specificity to *sulf1c*. However this contrasts with HS profile of *sulf2* knockout mice that reveal a decrease in the respective tri-sulfated disaccharide and increase in the mono- and di-sulphated disaccharide as this is thought to be due to a overcompensation by increased *sulf1* expression in these mice<sup>349</sup>. Other studies by Ai and Colleagues (2007)<sup>360</sup> have not reported similar findings this could be owed to difference in timepoint of HS extraction especially since the degradation of HS turnover is relatively short. Alternatively subtle differences in substrate specificity may exist *in vivo* however we did not observe such differences. Although more experiments could be done to confirm whether the increases in the mono and di-sulphated disaccharides are statistically significant, we can conclude *sulf2a* is capable of modifying HS structures *in vivo*.

In *sulf2a* injected embryos there did not appear to be a significant increase in mortality compared to control injected embryos. *Sulf2a* mild and moderate morphants displayed correctly formed primary vasculature i.e. axial vessels were correctly assembled however these characteristic morphants displayed defects in intersegmental vessels (ISVs) patterning with moderate morphant displaying also a dilated caudal plexus. Irrespective of these defects under brightfield microscopy the circulation appeared to follow the conventional route. However from our observations it seems unlikely that *sulf2a* is having a direct affect on endothelial cells since defects in the notochord and somite defects were also observed coinciding with the vascular defects. We observed changes in the notochord shape and the loss of chevron shaped somites in the regions coinciding with trunk and tail ISV defects. In support of these observations *sulf2a* expression is strongly detected in the somite boundaries and in the tissue surrounding the notochord. The notochord provides axial support to the growing embryo and serves as an important source of secreting signalling molecules such as *shh* to pattern adjacent neural tube and somites<sup>380,425</sup>. Furthermore large genetic screens have identified a number of notochord mutants that are defective in differentiation, shape and notochord sheath formation<sup>425</sup>. Our *sulf2a* morphant closely resemble mutants with defects in notochord shape such as *tribolite* and *knypek* mutants in which notochord is only affected in the tail of the morphants<sup>411</sup>. Similar to the *sulf2a* morphants the caudal somite patterning is also affected in these notochord mutants. There is a lot of evidence of notochord defects having concurrent affects on somite patterning examples include *floating head*, *bashful* mutants. Interestingly in these morphants both notochord and somite defects have also shown to affect vessel patterning<sup>425</sup>. There are several lines of evidence to suggest that the notochord is important in patterning the vasculature, mutants that display extreme defects in notochord differentiation such as *floating head (flh)* and *no tail (ntl)* mutants show the DA fails to form. Likewise in mutants exhibiting defects in somite patterning such as *out of bounds* display a loss of chevron shaped somites and show irregular ISV formation. Hypothetically it is likely *sulf2a* could be affecting signalling pathways involved in late stage notochord development i.e. the notochord sheath formation. The notochord sheath is surrounded by ECM proteins such as laminin, fibrillin and colleagen that all have the capacity to bind to heparin/HS<sup>426</sup>.

### 7.4.3 HS disaccharide and phenotype analysis of *sulf2* SBMO morphants

HS disaccharide analysis of *sulf2* morphants with consistent and reproducible phenotypes revealed no significant changes in the three 6-O sulphated disaccharides. Although there appeared to be consistent decreases in the mono and di-sulphated disaccharides (UA-GlcNAc6S; UA-GlcNS6S) a trend appeared in the tri-sulphated disaccharide with minor increase and decreases in the UA(2S)-GlcNS6S and UA2S-GlcNS6S this did not appear to be significant. While more experiments could be done, this initial finding suggests potential *sulf2* activity to be similar to *sulf2a* though the concurrent decrease in mono and di-sulphated disaccharides was unexpected. Interestingly though in *sulf2* knockout mice, overcompensation by other sulf enzymes has shown to be a possible mechanism<sup>349</sup>. It would be interesting to confirm in the *sulf2* morphants if a similar theme is occurring here. Although the reduced levels of the *sulf2* transcript does not equate to the changes in HS structure. Further experiments at a higher doses may show significant changes in HS structure.

Similar to *sulf2a* injected embryos, *sulf2* injected embryos did not show any significant difference in mortality despite mortality increasing with increasing dose of S2-SBMO. We also observed similar irregular patterning and ectopic branching of ISVs in the trunk of both mild and moderate *sulf2* morphants. Although not conclusively proven it is likely that the knockdown of *sulf2* transcript is having an indirect affect on endothelial cells as in these morphants notochord and somite also appeared to be affected. In contrary to the *sulf2a* morphants the distorted notochord shape appears only in the anterior and medial regions of the trunk, while the head of the morphants was also affected. Similar to *sulf2a* there maybe a similar role of *sulf2* role in notochord formation. Intriguingly both *sulf2a* and *sulf2* mild morphant phenotypes strike close resemblance to fibrillin morphants<sup>427</sup>. Fibrillins (Fib) are family of glycoprotein residing in the extracellular matrix around the notochord sheath<sup>428</sup>. *Fib-2* morphants exhibit several kinks in the notochord of the similar and *fib-1* and *fib-2* morphants display a dilated caudal plexus. *Fib-1* and *fib-2* are shown to interact genetically, furthermore *fib-1* has several heparan sulphate binding sites and can bind to HS chains on perlecan. *In-vitro* studies have shown heparin may act to prevent binding to magp1 a microfibril glycoprotein important in fibrillin roles. Several lines of evidence suggest that inhibition of sulfation can block microfibril assembly in cell culture<sup>429,430</sup>. This suggests the sulfation status of HS has an important role in *fib-1* function. *Fib-2* morphants however do

not show similar vascular defects and *fib-1* morphants do not display notochord defects. Interestingly the expression patterns of *fib-1* and *fib-2* are consistent with *sulf2a* and *sulf2*, as *sulf2* like *fib-2* is expressed in the hypochord a structure also known to influence axial vessels patterning. It would be interesting to observe the morphant phenotype of the simultaneous knockdown of both *fib-1* and *fib-2* and see whether this coincides with the phenotype of combined *sulf2a* and *sulf2* knockdown. Intriguingly *fibrillin* morphants do not display ectopic branching or irregular intersomitic patterning, likewise screening of all notochord morphants have not yet shown any similar vascular phenotype. The possibility that the notochord and vasculature defects are unlinked with the latter being a more direct affect of *sulf2a/2* deficiency cannot be ruled out. Thus *perlecan* morphants exhibit defects in ISV patterning that are further abrogated with knockdown of VEGF expression<sup>174</sup>. It would be interesting to perform synergy experiments with VEGF to establish if there is connection with the *sulf2a/sulf2* morphant phenotypes. One possible hypothesis is that *sulf2* and *sulf2a* maybe act spatially and temporally at different locations and that knockdown of sulfs may be dose sensitive such that alteration in the balance of 6-O sulphation leads to distinct localised defects in the vasculature.

#### 7.4.4 True morphant phenotypes v, off-target affects

Though possible pathways have been postulated in *sulf2* and *sulf2a* morphants attempts to recapitulate the phenotype with translational blocking MO were unsuccessful. Very low penetrance of the *sulf2* and *sulf2a* mild morphants was observed. There are two possible explanations for this, firstly the SBMO may have relatively easy access to its target site whereby the ATGMO may need a higher dose to induce *sulf1c* knockdown as the MO site maybe buried within the complex secondary structure of pre-mRNA. In support of this the non-significant changes in HS profile further confirms the likelihood the morpholinos may be unsuccessful. Alternatively the notochord defects observed in the SBMO injected embryos may be off-target affects, since kinked notochord and abnormal shaped somites have also been a reported as an off-target affect<sup>395</sup>. It would be important to test the SBMO in the *p53*<sup>-/-</sup> fish (section 4.3.8). However another route to gaining additional confidence is to knockdown the gene using two morpholinos at a dose that individually does not induce a morphant phenotype. Preliminary experiments knocking down *sulf2a* and *sulf2* together using SBMO has shown to recapitulate the irregular patterning of ISV defects however with only altered notochord shape in the tail of the morphants (data not shown).

### 7.5.5 Future work

It is evident that *sulf2a* and *sulf2* morpholinos are capable of reducing the levels of *sulf2* transcript, however only in *sulf2a* morphants this equated to significant changes in HS 6-O sulphation levels. In *sulf2* morphants there appeared to be a general trend in 6-O sulphation levels with a mild increase in the tri-sulfated disaccharide. However these mild changes appeared to reflect a very strong morphant phenotype. It could be concluded changing levels of 6-O sulphation by either *sulf2a* or *sulf2* has drastic effects on the overall morphology. The changes in 6-O sulphation may be dose sensitive. However the specificity of these phenotypes is unclear as we were not able to phenocopy the morphants with a different set of morpholinos. It would be ideal to try and rescue the phenotype with *sulf2* mRNA. The fact that we observe a notochord phenotype in *sulf2* morphants similar to that of *sulf1c* 'overexpression' phenotype is interesting and that it has been shown *sulf1c* is overexpressed in *sulf2* knockout mice to partially compensate for the loss of *sulf2*<sup>349</sup>. Although not proven it would be interesting to assay for *sulf1c* expression in these morphants and perhaps the sulfs maybe acting on a common pathway as *sulf2a* and *sulf2*. A second set of morpholinos would be ideal to use in this experiment to further confirm the phenotype such as the 5'UTRMO. If further experiments revealed true specificity of the *sulf2* and *sulf2a* phenotype then possible candidate molecules including proteins such as fibrillin family of glycoproteins would require further investigation.

## Chapter 8.0 Conclusions

### 8.1 Three sulfatases are differentially expressed during zebrafish development

The data presented in this thesis provide the first insight into the role of 6-O endosulfatases during vascular development in zebrafish. Characterisation of the three zebrafish sulfatase transcripts revealed that the predicted protein sequence of *sulfs*, as well as the spatial and temporal expression pattern of *sulfs* has been highly conserved from zebrafish to mammals. Considering teleosts diverged from human 450 million years ago<sup>431</sup>, the conservation of *sulfs* across a diverse range of species is testimony to the importance of this gene during development. This observation provides an ideal opportunity to study the role of this gene in a range of model organisms; thereby allowing the investigator to move to a different species to ask a question that could not be addressed in another species. Moreover, the conservation of *sulfs* across different species gives the investigator confidence that a finding gained in one species will have relevance to the study of vascular pathological diseases at which the research is ultimately aimed.

Importantly the spatio-temporal expression pattern of *sulfs* in zebrafish correlates with those structures affected in single sulf knockouts in mice and xenopus. *Sulf1*<sup>-/-</sup> mice exhibiting growth defects, limb defects, skeletal tissue and neurological abnormalities, and *sulf1* xenopus morphants exhibit malformed eyes, and loss of floorplate.<sup>352,358,361</sup>

### 8.2 Sulfatases have different roles during vascular development

Zebrafish *sulf1c* and *sulf2a* were found to be expressed in and around the developing vasculature whereas *sulf2* expression was confined to the nervous system. Apart from the role of mammalian *sulfs* in modulating angiogenesis in pathological conditions *in vitro* and *in-vivo* their role in vascular development proceeding in physiological conditions has not yet been characterised. By utilising morpholino knockdown of individual *sulfs* in zebrafish, the data presented in this thesis not only justifies the use of zebrafish as a model in which to study the pathogenesis of vascular diseases in humans but provides the first evidence of the consequence of *sulf* deficiency in zebrafish. A highly specific and reproducible morphant phenotype consisting of vascular morphological defects is induced following morpholino

knockdown of *sulf1c* in zebrafish. *Sulf1c* morphants exhibit defects in arterial venous identity and vascular integrity i.e. central arteries fail to form mature connections contributing to cranial haemorrhage. Importantly these defects can be rescued with *sulf1c* mRNA.

Initial studies of knockdown of *sulf2a* and *sulf2* in zebrafish revealed morphants displaying similar defects in ISV formation though these appear to be region specific, implying sulfs act in a tissue specific manner a common theme amongst HS biosynthesis enzymes. However corresponding morphological defects in notochord and somite formation in the *Sulf2a* and *sulf2* morphants suggests the vascular affect of *sulf2a* or *sulf2* morpholino could possibly be an indirect effect on endothelial cells.

### **8.3 Potential cell signalling molecules affected during vascular development in *sulf1c* morphants**

The data presented in this thesis provide evidence that zebrafish *sulf1c* has a role in arterial venous development and the morphant phenotype bear great resemblance to the zebrafish mutants of components in the VEGF pathway. This data provides evidence that *sulf1c* acts upstream of the notch signalling pathway that leads to activation of EphrinB2a<sup>84</sup>. In zebrafish the arterial venous identity of endothelial cells has been shown to proceed via the Shh-VEGF-Notch signalling cascade<sup>2</sup>. Sulf s can modulate VEGF activity *in-vitro*. Whilst VEGF expression is unaffected in the tail of the sulf morphants, its activity could be hindered by remaining bound to the ECM or retained at the cell surface in a position unable to transduce a signal. On the other hand from our results we observed a decrease in VEGF expression in the head which resulted in a lack of maturation of vessels in this region.

The specificity of both *sulf2a* and *sulf2* morpholino were not tested thoroughly and warrants further investigation before alluding to possible pathways affected in these morphants. However consistent with these morphological vascular defects were the significant changes in the 6-O sulphation content of HS disaccharides in *sulf1c* and *sulf2a* morphants thus implying these changes are specific to *sulf1c* and *sulf2a* activity respectively (Fig. 8.1). The lack of change in 6-O sulphation in the *sulf2* morphants could be one of two reasons, firstly there maybe compensation by other two sulfs enzymes, secondly *sulf2* may be redundant. Although they have not been proven both possibilities are equally likely. The significant change in 6-O sulphation in *sulf1c* and *sulf2a* morphants in combination with their vascular

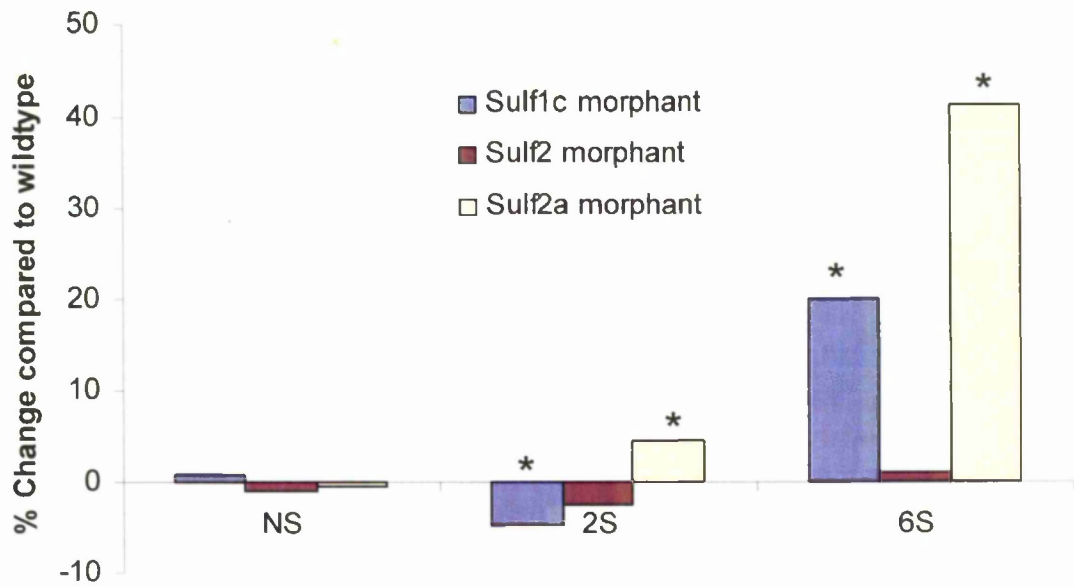


**Figure 8.1: Comparison of HS disaccharide profiling of sulf morphants.** Comparison of the total HS sulfate groups amongst the *sulf1c*ATGMO, *sulf2a* and *sulf2* SBMO morphants. Asterix denotes significant changes compared to wildtype embryos,  $p < 0.05$ .

abnormalities suggest *sulf1c* and *sulf2a* have an important role during vascular development. Interestingly sulf studies in mammals have elucidated an important role of sulfs during normal development thus the lack of a severe phenotype in either zebrafish morphants could be down to functional redundancy amongst the *sulf1c* and *sulf2a* isoform. This is further supported by the overlapping expression patterns between the two sulfs during early through to late somitogenesis stages. The mechanism by which *sulf2a* may affect vascular development is far from completion however analysis of *sulf1c* morphants suggests Shh or VEGF signalling molecules may be affected in this pathway. Considering the context dependent role of sulfs in modulating a number of different signalling molecules, it is conceivable its effects on blood vessels formation could intercept at either shh or VEGF signalling pathways.

To test if sulfs mediate VEGF activity *in vivo* we have constructed a transient VEGF expressing transgenic line in which *sulf1c* morpholino can be injected and morphants assayed for changes in VEGF induced activity. In the short term it would be necessary to assay for activity of downstream targets of VEGF signalling pathway to confirm the ectopic expression and find a suitable region of ectopic vessel quantification. One route to test the affect on VEGF expression is to measure the SIVs basket of the injected embryos since VEGF expression can be controlled spatially and temporally in the HSP70 transgenic line.

However it cannot be ruled out that *sulf1c* maybe acting further upstream of the VEGF pathway possibly affecting the range of *shh* signalling. Continued analysis of *sulf1c* expression in a range of zebrafish mutants such as *sonic you* mutant (deficient in Shh) or a target of shh such as patched (Ptc), would be a useful tool in which to identify the upstream regulators of this gene. Altered expression of *sulf1c* within in a particular mutant does not however provide evidence of whether *sulf1c* is a direct target of the gene/protein in question. Testing the binding affinity of the candidate molecules to HS oligos harbouring different regions of 6-O sulphation in combination with biochemical analyses would help answer these questions.

Finally, the Sanger centre now provide a service whereby a mutant of interest can be searched in the ENU banks. The results presented in this thesis provide the first evidence of the use of zebrafish to study the role of *sulf1c*, and suggest that identification of a *sulf1c* mutant would greatly aid the progress of this research

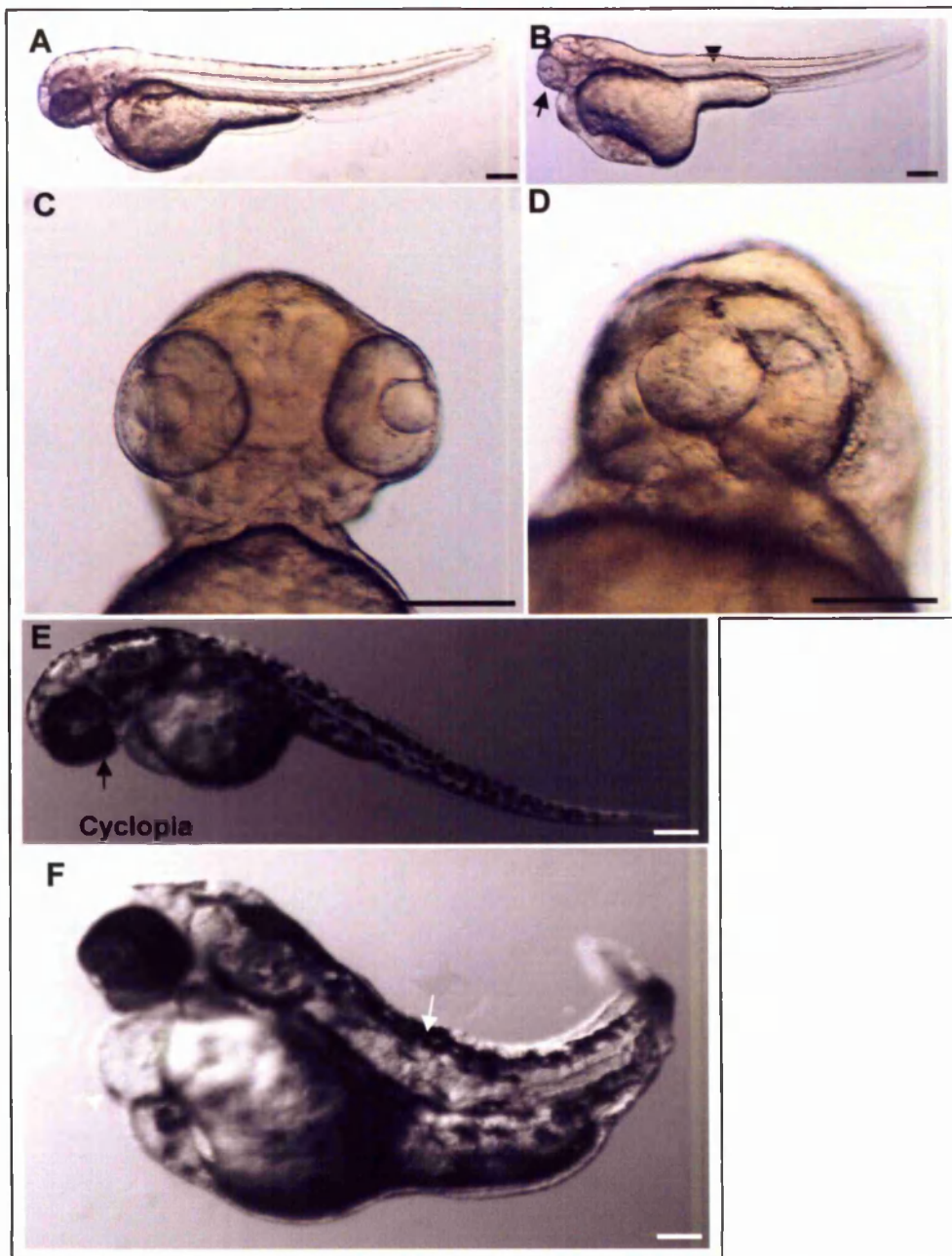
#### 8.4 Microarray analysis of *sulf1/2*<sup>-/-</sup> embryos

To provide a more complex picture of the molecular consequences of ablating Sulf function, generation of sulf knockout in zebrafish can now be performed. Gene targeting using zinc finger nucleases (ZFN) have shown to be useful tools in genome manipulation in invertebrates and cell lines. Recently engineered zinc finger nuclease has been applied in zebrafish to achieve gene targeted inactivation of VEGFR-2 and can introduce heritable mutations in the germ line at high frequency<sup>432</sup>. It would be ideal to generate sulfs transgenic lines to get a comprehensive view of their role in vascular development. Microarray analysis of *Sulf*<sup>-/-</sup> embryos could be performed, such analyses could be performed on the whole embryo or for more precise analyses on FAC sorted *flk1*<sup>+</sup> endothelial cells. By comparison to control, these analyses will provide an insight into the genes affected by complete ablation of *Sulf*. Thus, performing microarray analysis on endothelial cells derived from single and double knockout of sulf would provide information about those genes whose expression is sensitive to *Sulf* dosage.

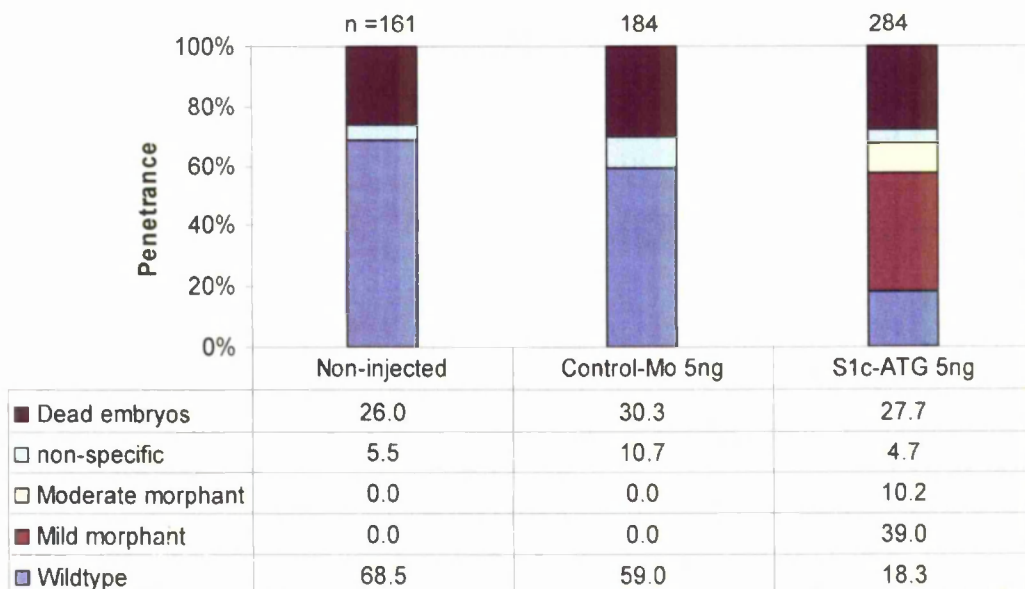
#### 8.5 Summary

Since the discovery of 6-O endosulfatase in 2001 a number of studies have examined its role in development. However few have examined its role in formation of vascular development. The research presented in this thesis provides the first evidence for the role of *sulf1c* in vascular development in zebrafish. This research supports the substrate specificity of the sulfs i.e. *sulf1c* and *sulf2a* selectively removing 6-O sulfated groups from the tri-sulfated disaccharides suggesting sulf function is conserved from mammals to zebrafish.

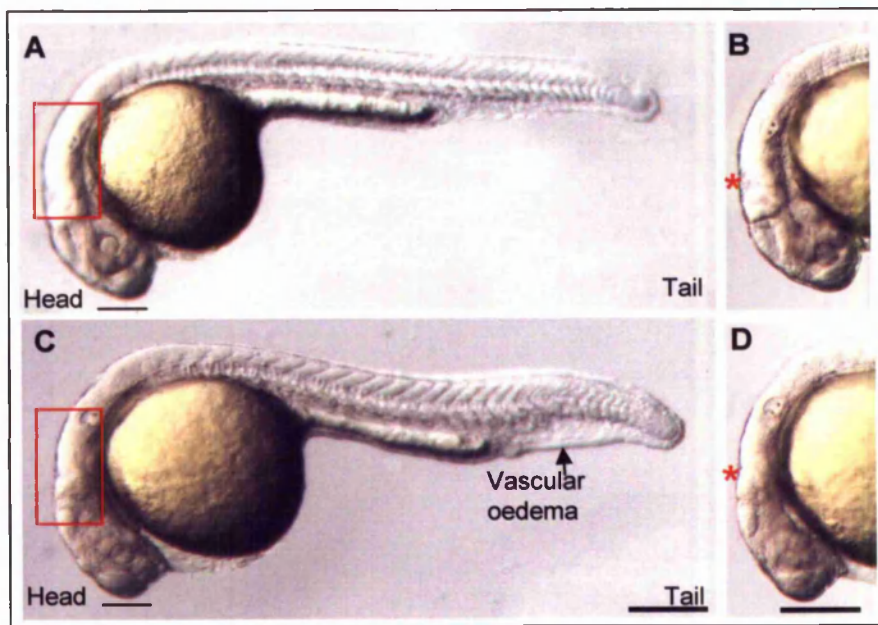
## Chapter 9.0 Appendices



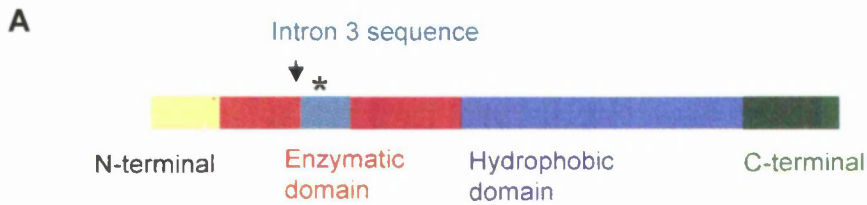
**Appendix I : *sulflc* mRNA injected embryos display cyclopia phenotype.** Embryos injected with varying concentrations (ranging from 100pg-500pg) of *sulflc* mRNA were analysed at 2dpf and scored for percentage of embryos with overall morphology identical to that of wildtype embryos at the same stage. A subset of embryos were present in the injected samples that displayed cyclopia phenotype. The penetrance of the phenotype increased with increasing dose (data not shown). A-F are brightfield images of the different cyclopia mutants present in all the injected samples. Mild cyclopia mutants displayed no abnormalities in the trunk or tail (E), only fusion of the eyes at the midline of the ventral forebrain (shown by the black arrow. Moderate cyclopia mutants displayed mild pericardial oedema and distortions in the notochord, although the overall body shape appeared normal (B,D). Severe cyclopia mutants (F) displayed severe pericardial oedema (white arrowhead) and shortened body axis with distortions in the notochord (white arrow). Scale bar is 200 $\mu$ m. (Note: no pigment defects were observed, images taken A-D were PTU treated for clarity.



**Appendix II : Chart showing the analysis of  $p53^{-/-}$  embryos injected with 5ng of S1c-ATGMO.** Data shown in chart is combined from two experiments and the average penetrance of each category represented as a percentage. Embryos were scored at 24hpf for mortality rate and surviving embryos were analysed at 2dpf. The ATGMO was injected at 5ng and compared to control morpholino and non-injected embryos. Mortality was comparable between non-injected and morpholino injected embryos. A small percentage of non-specific embryos were observed in all samples, and their prevalence decreased in the S1c-ATGMO injected sample. Injection of 5ng of ATGMO resulted in ~36% and 13.2 % of embryo reproducing the characteristic phenotype and severe morphant, previously observed in *fli1:gata* S1c morphants. While 18% embryos retained wildtype morphology observed in the majority of the non-injected and control injected embryos.



**Appendix III : Brightfield images of *p53*<sup>-/-</sup> injected embryos.** Embryos were injected with 5ng of control and S1c-ATGMO and compared at 26hpf. lateral view of CMO injected embryo, red rectangular box denotes the region of hindbrain (A). Close up of the mid-hindbrain region of control embryo, hindbrain develops normally as indicated by width of the blackline (B). Lateral view of *sulf1c* mild morphant showing normal mid-hindbrain boundary highlighted by the red box and vascular oedema in the tail indicated by the black arrow (C). Close up of the mid-hindbrain region of the mild phenotype shows embryos do not display swelling in the hindbrain ventricle (D). Scale bar is 200 $\mu$ m.



**B**

```

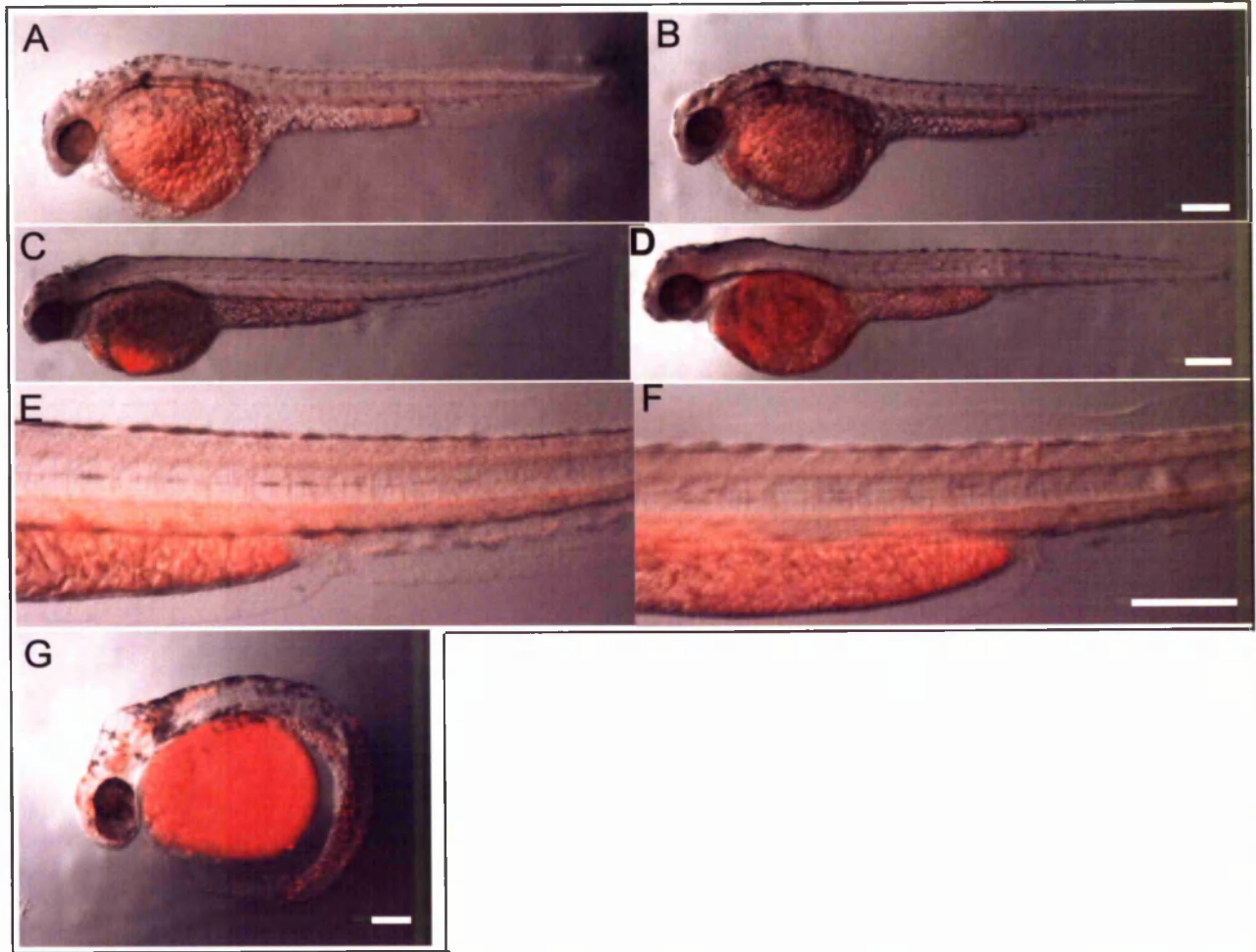
atgatgcagctggtagcctggcttggatgatggctcctggcgcgc
M M Q L V S L A W M M V L A A
cactggctgcttggtttcaccaccgcggtcagggcctgcgt
P L V C F G F T T R G Q G L R
ggcgagttcaagtgaccggaggaacatcagaccaacatcata
G R V Q G D R R N I R P N I I
ctcatcatgacagatgaccaggatgtggagttgggatctttgcag
L I M T D D Q D V E L G S L Q
gtgatgaacaaaaccgcaagatcatggaggatggtaggcacatca
V M N K T R K I M E D G G T S
ttcacgaatgcatttgttactacacccatgtgctgtccttcacga
F T N A F V T T P M C C P S R
tcctctatgctgacggggaagtacgtccacaatcacaacacctac
S S M L T G K Y V H N H N T Y
accaacaatgagaactgctcgtcaccttcatggcaagctcagcat
T N N E N C S S P S W Q A Q H
gagccacgatcttttgcagtttatcttaacaacactggatcatcga
E P R S F A V Y L N N T G Y R
acagctttctttgggaagtacctgaatgagtacaacggcagctac
T A F F G K Y L N E Y N G S Y
atcccacctgggtggcgtgaatgggttgggctgatcaaaaattcc
I P P G W R E W V G L I K N S
cggttctataattacaccgtctgtcggaacgggaataaggagaag
R F Y N Y T V C R N G N K E K
cacggcgcagattatgccaaaggtatgtgtgtgcccgggtcacataa
H G A D Y A K V C V C P V T *

```

→

Start of Intron 3-4

**Appendix IV: Predicted outcome of *sulf1c* protein structure and sequence.** Schematic representation of the truncated protein and the site of intronic amino acid sequence in relation to the full length *sulf1c* protein (A). Characteristic domains of *sulf1c* protein are highlighted in different colours. Asterisk (\*) highlights the site of the stop codon, potentially producing ~ 193aa protein (diagram is not to scale). Predicted protein sequence of aberrant *sulf1c* using open reading finder (B). To test if this would result in an out-of frame *sulf1c* protein sequence, a hypothetical *sulf1c* sequence was entered into an open reading frame finder program (<http://www.ncbi.nlm.nih.gov/gorf.html>) (Wheeler *et al* 2003). cDNA sequences highlighted in small letters, red font denote the start of the intron 3 sequence. Pink asterisk denotes the introduction of a stop codon with the possible inclusion of intron 3.



**Appendix V: Tunel assay of control injected and *sulflc* mild morphant.** *fil:GFP* embryos injected with control morpholino and S1c-ATGMO were fixed at the 35hpf and 72hpf, and then underwent apoptosis assay. Non-injected embryos gave a identical staining to the control injected embryos and therefore are used as a representative for control. Non-specific morphants were used as a positive control. Brightfield and Cy3 channels were selected on stereolumar axiovision software and only overlay of both channels is shown. Stereoimages of control injected embryos (A,C). Whole shot stereoimages of *sulflc* characteristic morphant at 35hpf and 72hpf (B,D). Close magnification of tail control injected embryos (E). Close magnification of tail *sulflc* characteristic morphant (F). Scale bar 200 $\mu$ m

**Appendix VI:** Gorski B, Stringer SE. Tinkering with Heparan sulphate sulphation to steer development. *Trends in Cell Bio.* 2007; 17:173-177.

# Tinkering with heparan sulfate sulfation to steer development

Bushra Gorski and Sally E. Stringer

Division of Cardiac and Endocrine Sciences, University of Manchester, UK, M13 9NT

**Heparan sulfate (HS) proteoglycans, at the cell surface and extracellular matrix, facilitate ligand–receptor interactions crucial to many physiological processes. The distinct sulfation patterns of HS sugar chains presented by their protein core are key to HS proteoglycan activity. Tight regulation of several Golgi complex enzyme families is crucial to produce complex tissue-specific HS sequences. Several *in vivo* models deficient in HS biosynthesis enzymes demonstrate that developmental abnormalities result from modified HS structure. This review will discuss the plasticity of sulfation requirements on HS for activating protein ligands, which might reflect a flexible HS biosynthetic mechanism. In addition, the latest discovery of HS acting enzymes, the Sulfs, responsible for extracellular tweaking of HS sulfation levels subsequent to biosynthesis will be considered.**

## Studies of mutants – an insight into HS function

Heparan sulfate (HS) is a ubiquitous linear glycosaminoglycan with distinct sugar sequences and sulfation patterns. It is found attached to protein cores that can be transmembrane (e.g. syndecans), glycosylphosphatidylinositol (GPI)-linked (e.g. glypicans) or embedded in the matrix (e.g. perlecan). Studies of HS stemmed from the chemically related glycosaminoglycan heparin used widely in the clinic as an anticoagulant. HS is characterized by its long regions of low sulfation and alternating regions of high sulfation [1]. The complex structure of HS enables it to interact with a wide range of proteins influencing many biological processes such as development, angiogenesis, blood coagulation and tumorigenesis. The exact nature of the interactions is a topic of debate, although ionic contacts between the HS sulfate groups and cationic amino acids of protein ligands are thought to have a role in these interactions.

Recent reports of mutations in the HS biosynthetic enzymes in animal model systems have provided important insights into the roles of HS *in vivo*. Mutations that completely prevented formation of HS affected many developmental processes. For example, a mutation in the gene required for production of the UDP-glucuronic acid precursor to HS was found to prevent the initiation of heart valve formation in zebrafish [2] and was crucial for patterning mediated by Wingless (Wnt family member) and Decapentaplegic (related to the bone morphogenic proteins) in *Drosophila melanogaster* (fruitfly) [3–5]. Mutations in

*Drosophila* HS polymerases also affected gradient formation and signalling by Hedgehog (Hh), Wingless and Decapentaplegic crucial for wing patterning [6,7]. Strikingly, it was found that more subtle changes (such as the alteration of the sulfation pattern of the HS chain) controlled specific physiological processes. For example, 2-*O*-sulfation is important for a yet unresolved ligand(s) in kidney development [8] and 6-*O*-sulfation of HS is essential for the fibroblast growth factor-driven formation of the tracheal system in *Drosophila* [9]. The latest reports have described a family of 6-*O*-sulfatase enzymes that are thought to modify further HS structure and function at the cell surface [10]. In quail, *Sulf1* was shown to be important for Wnt-mediated muscle specification [10], whereas no major developmental defects were found in *Sulf2* mutant mice, possibly owing to redundancy in function between *Sulf1* and *Sulf2* [8,11,12]. These findings suggest the exciting possibility that fine-tuning of HS structure through control of the activity of specific enzymes is used to direct individual physiological processes.

In this review, we will explore how recent animal models deficient in specific enzymes of the HS biosynthetic pathway have revealed the genuine functions of HS *in vivo*. We will concentrate particularly on mutants of the later stages of HS biosynthesis, such as the enzymes that create the sulfation patterns, because these provide an insight into ligand-binding criteria and the flexibility of the system.

## HS biosynthesis

HS is produced by many cell types from many different primary structures. Its polysaccharide sequence is not directly encoded by genes but is synthesized by biosynthetic enzymes. Most of the enzymes have been purified, cloned and characterized. The chain is initially polymerized as an *N*-acetyl glucosamine-*D*-glucuronic acid (GlcNAc–GlcA) copolymer attached via a tetrasaccharide linkage region to serine groups of the protein core. A proportion of the GlcNAcs are then *N*-deacetylated and *N*-sulfated, creating sulfated regions that are further modified through epimerization of some of the GlcAs to *L*-iduronic acids (IdoAs), partial 3-*O*- and 6-*O*-sulfation of glucosamines and 2-*O*-sulfation of the uronic acids, thereby creating a complex structure capable of binding a variety of protein ligands.

## Chain initiation and polymerization

HS chain synthesis initiates in the Golgi via formation of tetrasaccharide polymer [GlcA(β1–3)Gal(β1–3)Gal(β1–4)Xyl(β1–4)], where Gal indicates galactose and Xyl indicates

Corresponding author: Stringer, S.E. (sally.stringer@manchester.ac.uk). Available online 21 February 2007.

xylose) attached to the serine residues on the protein core. Polymerization of the GlcNAc–GlcA bipolymer onto this tetrasaccharide is then carried out through the action of glycosyltransferases encoded by a family of tumour suppressor *Exostosin* genes (*EXT*). The importance of these enzymes in HS synthesis has been shown in *EXT1*-deficient mice, which fail to gastrulate and develop deficiencies in bone growth [13]. Even partial loss of HS synthesis in an *Ext1* hypomorphic mutant mouse was found to expand Indian Hedgehog (Ihh) distribution during embryonic chondrocyte differentiation [14]. In humans, mutations in the *EXT1* and *EXT2* genes are linked to hereditary multiple exotoses (HME), a bone disorder that produces benign cartilaginous tumours, possibly caused by the activation of Ihh signalling. Mutations in the *Danio rerio* (zebrafish) exostosin-like genes, *dackel* and *boxer*, homologous to the human *EXT2* and *EXTL3* (*Exostosin-like 3*) genes, respectively, exhibit defects in pectoral fin and branchial arch development [15] possibly from defects in fibroblast growth factor 10 (Fgf10) signalling [16]. This result supports the findings of many biochemical studies suggesting that HS is an essential component of the complex of FGFs with their signalling receptor (reviewed in Ref. [17]).

#### Chain modification

The next step in synthesis is 40–50% of the polymer is *N*-deacetylated and then *N*-sulfated by a bifunctional enzyme *N*-deacetylase/*N*-sulfotransferase (NDST). Four *NDST* genes have been cloned and found to exhibit different acetylation and sulfating activity [18]. *NDST1* and *NDST2* are the most widely expressed with overlapping expression patterns. The enzymes encoded by these two genes create the first blocks of sulfation upon which other enzymes act. Absence of *N*-sulfation in mice and *Drosophila* mutants has serious implications on their development. Several key signalling pathways, such as the FGF, Wnt and Hh pathways, are affected in the *Drosophila sulfateless* mutant defective in the NDST enzyme (reviewed in Ref. [19]), possibly owing to changes in morphogen distribution and receptor-ligand complex formation [20]. *NDST1*-deficient mice die shortly after birth owing to defects in lung development, accompanied by a reduction in *N*- and *O*-sulfation and C5-epimerization of HS [21] (see below). However, *NDST2*-deficient mice exhibit a less severe phenotype characterized by a defect in mast cell differentiation, in response to their inability to synthesize the ubiquitous HS but not the mast cell-based heparin [22]. Different NDST enzymes might have different substrate preferences: for example, *NDST2*, but not *NDST1*, can act on partially *N*-sulfated chains to form the more highly sulfated heparin (reviewed in Ref. [23]). The different substrate preferences of the NDSTs might be key in the formation of the basic domain pattern of the HS on which the other enzymes act, although a more flexible model of enzyme activity has also been proposed (see last section) [23,24].

#### C5-epimerization and 2-O-sulfation

After modification of HS by the NDSTs, specific GlcA units situated between GlcNSO<sub>3</sub> residues or GlcN [25] are epimerized to IdoA by a single C5-epimerase. Studies of this

isolated enzyme have found the reaction to be completely reversible [26] although the action of 2-*O*-sulfotransferases (HS2ST) on the C2 of uronic acid locks the epimerized configuration. Recent work by Feyerabend *et al.* [27] demonstrated in C5-epimerase-deficient mast cells that failure to epimerize GlcA to IdoA distorted the heparin *O*-sulfation pattern.

Several *in vitro* experiments have shown 2-*O*-sulfate groups on HS to be crucial for binding ligands such as FGF-2 [28], but the situation *in vivo* is not clear-cut. Mutations in the HS2ST-encoding gene cause homozygous mice to die at birth; these mice exhibit renal agenesis and abnormalities in the central nervous system [24]. Biochemical analysis of mutant forms of HS shows the expected loss of 2-*O*-sulfation with a concomitant increase in *N*- and 6-*O*-sulfation. Surprisingly, cells deficient in HS2ST show a normal signalling response to FGF-2 [8] suggesting flexibility in the sulfate positional requirements. Similarly, recent studies of *Drosophila Hs2st* and *Hs6st* mutants suggest that 6-*O*-sulfation levels can compensate for losses of 2-*O*-sulfation and vice versa, thus maintaining FGF signaling, which is essential for tracheal development [29]. However, mutants lacking both enzymes exhibited major defects in the FGF pathway. This suggests that the correct positioning of sulfate groups on HS can be bypassed if the overall level of sulfation is maintained; this finding challenges the widely accepted idea that specific sulfation patterns of HS are crucial to ligand-binding [30]. The lack of sulfate groups (for instance in the double mutant) might alter the conformation of HS, which could itself be a crucial component of the binding recognition motif [31].

The C5-epimerase and HS2STs modify only part of the *N*-sulfated regions created by the NDSTs leading to complex HS sequences. The generation of functionally specific and diverse HS sequences is also dependent on the specificity of the next sets of enzymes 6-*O*-sulfotransferases (HS6ST) and 3-*O*-sulfotransferases (HS3ST), which mostly act within the *N*-sulfated regions (Figure 1).

#### 6-O-sulfation

HS6ST transfers sulfate to the C6 position of GlcNSO<sub>3</sub> or any GlcNAc residue adjacent to GlcNSO<sub>3</sub> or IdoA (with or without 2-*O*-sulfation) [32]. As a result 6-*O*-sulfation is potentially restricted within the sulfated regions of HS chains. The HS6ST family consists of at least 3 genes, *HS6ST-1–3*. Although these genes only share 50% homology, the enzymes they encode show similar substrate specificity with only HS6ST1 demonstrating a minor preference towards sequences lacking 2-*O*-sulfation [32]. The addition of 6-*O*-sulfate groups has proved to be vital in the binding of HS to several ligands and has been demonstrated to have functional consequences for several of these proteins such as in FGF-2 activation [9,12].

Several *in vivo* studies have highlighted the regulatory roles of HS6STs in development. Studies in zebrafish [33,34] have identified two important roles for HS6STs in angiogenesis and muscle development reflecting their dynamic temporal and spatial expression patterns. Only *HS6ST-2* expression is detected in cells surrounding the vasculature consistent with the vascular defect in the caudal plexus of morpholino antisense knockdown

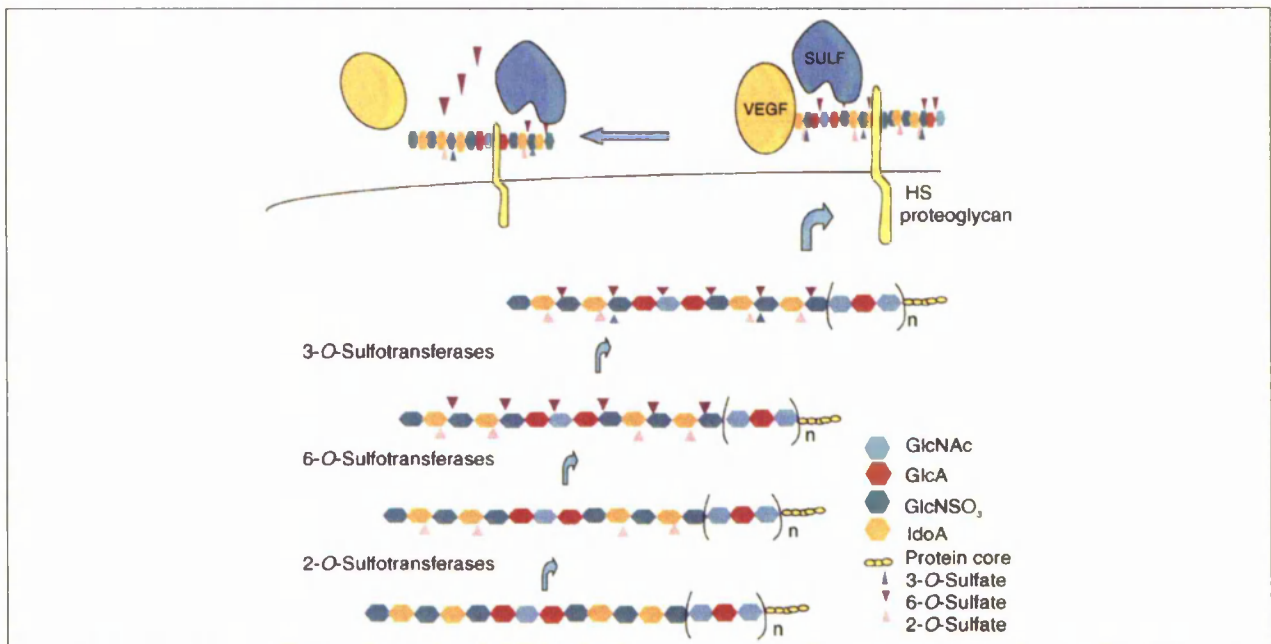


**Figure 1.** The final stages of HS proteoglycan biosynthesis. Following *N*-sulfation and C5-epimerization, the HS chain undergoes further modification by a variety of sulfotransferases (sulfate groups added by their respective enzymes are represented using colour-coded triangles) that generate discrete sulfation patterns. HS chains are translocated to the cell surface whereby the sulfation patterns are remodelled by sulfatases. The end-product is a fairly diverse HS chain structure with distinct sulfation patterns, responsible for interacting with specific ligands. The example presented here depicts VEGF binding to HS; it has been reported that the presence of *N*-, 2-*O*- and 6-*O*-sulfations strongly facilitate this binding [51]. However, overexpression of sulfatase activity can disrupt this interaction [52] and, as a result, can interfere in the biological response mediated by these ligands.

embryos [34]. A separate study by Bink *et al.* [33] has shown that *HS6ST-2* knockdown embryos (morphants) display an abnormal muscle phenotype, as might be expected from its somitic expression. Similarly, in mice, differential expression of *HS6ST* genes during development suggests tissue-specific functional HS is formed [35]. Brain tissue is abundant in *HS6ST-2* mRNA, whereas liver tissue expresses mainly *HS6ST-1* and *HS6ST-3* is expressed in all tissues analysed. Recent *in vitro* studies indicate that high activity of any *HS6ST* gene leads to an altered HS domain structure with the formation of extended 6-*O*-sulfated, predominantly *N*-acetylated domains and a concomitant decrease in 2-*O*-sulfation [36]. This suggests that the strict regulation of *HS6ST* levels is crucial to allow the formation of unique patterns of 6-*O*-sulfation and the overall fine structure of HS. Nevertheless, the role of individual *HS6ST*s remains unresolved.

### 3-*O*-sulfation

*HS3ST*s are thought to be the final elements of the biosynthetic pathway, which merely modify a few sugars per chain (Figure 1), transferring sulfate to the C3 position of the  $\text{GlcNSO}_3$  or  $\text{GlcNSO}_3$  (6-*O*-sulfate). At least six *HS3ST*s have been identified, each differing in their substrate specificity. All except *HS3ST-1* act on  $\text{GlcNSO}_3$  adjacent to 2-*O*-sulfated IdoA or GlcA [37,38] and do not require  $\text{GlcNSO}_3$  to be 6-*O*-sulfated [37], indicating that *HS3ST*s could act before *HS6ST*s. Like *HS6ST* genes, *HS3ST* genes vary in their distribution with brain tissue abundant in *HS3ST-1*, *HS3ST-2* and *HS3ST-4* and liver tissue expressing mainly *HS3ST-3A* and *HS3ST-3B* [37]. The generation of the 3-*O*-sulfate groups (the most infrequent sulfate group

of HS) is crucial for the binding sites of herpes simple virus (HSV) glycoprotein D [38], FGF-7 and its receptor [39] and antithrombin III (reviewed in Ref. [40]). Antithrombin III has an important role in the blood coagulation cascade requiring a well characterized, specific 3-*O*-sulfated pentasaccharide sequence for activity. Mice deficient in the *HS3ST-1* gene do not show a procoagulant phenotype despite a reduction in levels of their antithrombin-binding HS, but die at birth displaying growth retardation in the womb. This result suggests that *HS3ST-1* might have other regulatory roles than those involved in the blood coagulation cascade [41]. Nevertheless, it reiterates the observation that specific sulfation sequences have a key role in certain biological processes.

### Sulfatases

Initially it was thought that sulfation patterns were only created by sulfotransferases. Recently, a group of enzymes, that is the sulfatases, were identified in muscle and neural progenitors of quail by Dhoot *et al.* [10]. These showed distinct activities from lysosomal exosulfatases involved in breakdown of heparan sulfate. In addition to their reported Golgi activity [42] both quail *Sulf* enzymes have been shown to be enzymatically active on the cell surface and in the ECM matrix where they remodel 6-*O*-sulfation levels (Figure 1). *Qsulf1* has an N-terminal signal peptide that directs secretion and a central hydrophilic domain, shown by mutation studies to be important in the anchoring of the *Sulf* proteins to the cell surface as well as in binding substrates [43]. Although both quail enzymes have identical substrate specificity towards tri-sulfated disaccharide units IdoA2S– $\text{GlcNS6S}$  of HS (reviewed in Ref. [43]), studies of

mouse Sulf proteins suggest that specificity is not solely restricted to high regions of HS sulfation [12], giving them greater potential to modify ligand binding sites on HS.

Several studies of Sulf homologues in human, mice, and quail are beginning to show the important role of Sulfs in HS-dependent extracellular signalling. A study by Dhoot *et al.* 2001 showed QSulf1 to promote Wnt1 signalling in developing muscle [10]. Conversely FGF signalling is diminished in the presence of QSulf1 [44]. In both cases the enzymes are thought to interfere with ligand binding sites of HS by removing 6-*O*-sulfation but, although this frees Wnt1 for activity, it disrupts FGF and other growth factors' signalling complexes. Similarly, re-expression of Sulf enzymes that were found to be downregulated in certain cancer lines has been shown to inhibit FGF and hepatocyte growth factor (HGF) stimulation of tumour cell growth and metastasis [45]. However Sulf2 expression was found to be upregulated in breast cancer and has been proposed to stimulate angiogenesis, [46]. In addition to their role in tumour progression, maintenance of 6-*O*-sulfation levels by Sulfs has been shown to regulate vascular smooth muscle cell proliferation and migration [47]. These studies suggest controlling 6-*O*-sulfation levels might be important in vascular development and neoplasia.

#### Flexibility in biosynthesis creates functional sequences

The abnormal phenotypes characterized by mutants deficient in sulfotransferases reflect the importance of the fine structure of HS in regulating a wide variety of biological processes. The action of sulfotransferases is particularly important for the generation of functional HS. The distinct sulfation patterns reflect the tight spatial and temporal regulation of these enzymes during development.

It is widely accepted that the order of HS sulfation depends on the NDST enzymes to produce the substrate for subsequent sulfation. However, *in vivo* studies of mutants deficient for HS biosynthesis enzymes show that mutant HS can still be further modified with increased sulfation at various positions, demonstrating the flexibility in the order of reactions [29]. This flexibility could be achieved through the formation of a 'Gagosome' complex [48] that incorporates specific enzyme family members depending on their abundance in the cell type, and allows them to act at multiple stages of HS biosynthesis. This model was initially put forward to explain the lack of contribution of NDST2, except in the absence of NDST1, to liver HS *N*-sulfation [48]. It was proposed that, normally, NDST1 would be part of the gagosome complex whereas NDST2 (although present) is 'frozen-out' and is only incorporated in the complex in the absence of NDST1 [48]. The NDST enzyme present in the complex might then sulfate HS both before and after other types of chain modifications. The idea of a gagosome complex is further strengthened by interactions of some of the enzymes *in vivo* (i.e. C5-epimerase and HS2ST). Similarly, EXT1 and EXT2 interact to form an HS polymerase complex [49,50].

Whether or not it is the answer to delivering flexibility in the order of HS biosynthesis, a gagosome complex could provide a plausible explanation for the type of HS structures observed in HS enzymes-deficient mutants and the ability

of these structures to function normally in signalling pathways. This compensatory effect of one sulfate type for another also challenges the current selective criteria proposed for protein ligands to bind HS; this raises the question as to whether specific sulfation sequences are important versus overall sulfation content within specific domains. Specifically spaced sulfated domains on HS, separated by *N*-acetylated stretches, appear to be important for binding to multimeric proteins such as VEGF165 and could also be crucial for the HS-mediated formation of multi-protein complexes such as that of the FGF-receptor complex (reviewed in Ref. [30]). The conformation conferred on the HS by the sulfation within these domains might be an important component of the binding motif as opposed to the specific type of sulfation *per se*.

In summary, studies of mutants of HS biosynthetic enzymes have confirmed the importance of HS for the activity of several growth factors such as HH, FGFs, Wnt and VEGF during development, which had originally been suggested by protein-binding and *in vitro* experiments [19]. In certain cases, the mechanism by which HS affects these morphogens was revealed, such as the role of HS in morphogen gradient formation and signalling [6,7]. The structure of the HS chain from NDST mutants reveals a flexibility in the order the enzymes can function; the exact enzymatic sequence remains to be determined [48]. In addition, the compensatory effect, for example of 6-*O*-sulfation for 2-*O*-sulfation required in ligand binding [8,29], was unexpected and opens up questions on what, exactly, constitutes a binding site: spacing of sulfated blocks or chain conformation? Advances in technology such as more powerful spectroscopic methods, might help answer this question. It is clear, however, that tinkering with HS structure steers several developmental processes.

#### Acknowledgements

We acknowledge the British Heart Foundation for funding.

#### References

- 1 Stringer, S.E. and Gallagher, J.T. (1997) Heparan sulfate. *Int. J. Biochem. Cell Biol.* 29, 709–714
- 2 Walsh, E.C. and Stainier, D.Y. (2001) UDP-glucose dehydrogenase required for cardiac valve formation in zebrafish. *Science* 293, 1670–1673
- 3 Binari, R.C. *et al.* (1997) Genetic evidence that heparin-like glycosaminoglycans are involved in wingless signaling. *Development* 124, 2623–2632
- 4 Hacker, U. *et al.* (1997) The *Drosophila* sugarless gene modulates Wingless signaling and encodes an enzyme involved in polysaccharide biosynthesis. *Development* 124, 3565–3573
- 5 Haerry, T.E. *et al.* (1997) Defects in glucuronate biosynthesis disrupt Wingless signaling in *Drosophila*. *Development* 124, 3055–3064
- 6 Han, C. *et al.* (2004) Distinct and collaborative roles of *Drosophila* EXT family proteins in morphogen signalling and gradient formation. *Development* 131, 1563–1575
- 7 Takei, Y. *et al.* (2004) Three *Drosophila* EXT genes shape morphogen gradients through synthesis of heparan sulfate proteoglycans. *Development* 131, 73–82
- 8 Merry, C.L. *et al.* (2001) The molecular phenotype of heparan sulfate in the *Hs2st*<sup>-/-</sup> mutant mouse. *J. Biol. Chem.* 276, 35429–35434
- 9 Kamimura, K. *et al.* (2001) *Drosophila* heparan sulfate 6-*O*-sulfotransferase (*dHS6ST*) gene. Structure, expression, and function in the formation of the tracheal system. *J. Biol. Chem.* 276, 17014–17021
- 10 Dhoot, G.K. *et al.* (2001) Regulation of Wnt signaling and embryo patterning by an extracellular sulfatase. *Science* 293, 1663–1666

- 11 Lum, D.H. *et al.* (2007) Gene trap disruption of the mouse heparan sulfate 6-*O*-endosulfatase, *Sulf2*. *Mol Cell Biol* 27, 678–688
- 12 Lamanna, W.C. *et al.* (2006) Heparan sulfate 6-*O*-endosulfatases: discrete in vivo activities and functional co-operativity. *Biochem. J.* 400, 63–73
- 13 Lin, X. *et al.* (2000) Disruption of gastrulation and heparan sulfate biosynthesis in EXT1-deficient mice. *Dev. Biol.* 224, 299–311
- 14 Koziel, L. *et al.* (2004) *Ext1*-dependent heparan sulfate regulates the range of *Ihh* signaling during endochondral ossification. *Dev. Cell* 6, 801–813
- 15 Schilling, T.F. *et al.* (1996) Jaw and branchial arch mutants in zebrafish I: branchial arches. *Development* 123, 329–344
- 16 Norton, W.H. *et al.* (2005) HSPG synthesis by zebrafish *Ext2* and *Ext13* is required for *Fgf10* signalling during limb development. *Development* 132, 4963–4973
- 17 Ornitz, D.M. (2000) FGFs, heparan sulfate and FGFRs: complex interactions essential for development. *Bioessays* 22, 108–112
- 18 Aikawa, J. *et al.* (2001) Multiple isozymes of heparan sulfate/heparin GlcNAc *N*-deacetylase/GlcN *N*-sulfotransferase. Structure and activity of the fourth member, *NDST4*. *J. Biol. Chem.* 276, 5876–5882
- 19 Bernfield, M. *et al.* (1999) Functions of cell surface heparan sulfate proteoglycans. *Annu. Rev. Biochem.* 68, 729–777
- 20 Lin, X. (2004) Functions of heparan sulfate proteoglycans in cell signaling during development. *Development* 131, 6009–6021
- 21 Forsberg, E. and Kjellen, L. (2001) Heparan sulfate: lessons from knockout mice. *J. Clin. Invest.* 108, 175–180
- 22 Humphries, D.E. *et al.* (1999) Heparin is essential for the storage of specific granule proteases in mast cells. *Nature* 400, 769–772
- 23 Grobe, K. *et al.* (2002) Heparan sulfate and development: differential roles of the *N*-acetylglucosamine *N*-deacetylase/*N*-sulfotransferase isozymes. *Biochim. Biophys. Acta* 1573, 209–215
- 24 Bullock, S.L. *et al.* (1998) Renal agenesis in mice homozygous for a gene trap mutation in the gene encoding heparan sulfate 2-sulfotransferase. *Genes Dev.* 12, 1894–1906
- 25 Jacobsson, I. *et al.* (1984) Biosynthesis of heparin. Substrate specificity of heparosan *N*-sulfate  $\beta$ -glucuronosyl 5-epimerase. *J. Biol. Chem.* 259, 1056–1063
- 26 Hagner-McWhirter, A. *et al.* (2004) Irreversible glucuronyl C5-epimerization in the biosynthesis of heparan sulfate. *J. Biol. Chem.* 279, 14631–14638
- 27 Feyerabend, T.B. *et al.* (2006) Heparan sulfate C5-epimerase is essential for heparin biosynthesis in mast cells. *Nat. Chem. Biol.* 2, 195–196
- 28 Maccarana, M. *et al.* (1993) Minimal sequence in heparin/heparan sulfate required for binding of basic fibroblast growth factor. *J. Biol. Chem.* 268, 23898–23905
- 29 Kamimura, K. *et al.* (2006) Specific and flexible roles of heparan sulfate modifications in *Drosophila* FGF signaling. *J. Cell Biol.* 174, 773–778
- 30 Kreuger, J. *et al.* (2006) Interactions between heparan sulfate and proteins: the concept of specificity. *J. Cell Biol.* 174, 323–327
- 31 Powell, A.K. *et al.* (2004) Interactions of heparin/heparan sulfate with proteins: appraisal of structural factors and experimental approaches. *Glycobiology* 14, 17R–30R
- 32 Habuchi, H. *et al.* (2003) Biosynthesis of heparan sulphate with diverse structures and functions: two alternatively spliced forms of human heparan sulphate 6-*O*-sulphotransferase-2 having different expression patterns and properties. *Biochem. J.* 371, 131–142
- 33 Bink, R.J. *et al.* (2003) Heparan sulfate 6-*O*-sulfotransferase is essential for muscle development in zebrafish. *J. Biol. Chem.* 278, 31118–31127
- 34 Chen, E. *et al.* (2005) A unique role for 6-*O*-sulfation modification in zebrafish vascular development. *Dev. Biol.* 284, 364–376
- 35 Habuchi, H. *et al.* (2000) The occurrence of three isoforms of heparan sulfate 6-*O*-sulfotransferase having different specificities for hexuronic acid adjacent to the targeted *N*-sulfoglucosamine. *J. Biol. Chem.* 275, 2859–2868
- 36 Do, A.T. *et al.* (2006) Overexpression of heparan sulfate 6-*O*-sulfotransferases in human embryonic kidney 293 cells results in increased *N*-acetylglucosaminyl 6-*O*-sulfation. *J. Biol. Chem.* 281, 5348–5356
- 37 Esko, J.D. and Selleck, S.B. (2002) Order out of chaos: assembly of ligand binding sites in heparan sulfate. *Annu. Rev. Biochem.* 71, 435–471
- 38 Shukla, D. *et al.* (1999) A novel role for 3-*O*-sulfated heparan sulfate in herpes simplex virus 1 entry. *Cell* 99, 13–22
- 39 Ye, S. *et al.* (2001) Structural basis for interaction of FGF-1, FGF-2, and FGF-7 with different heparan sulfate motifs. *Biochemistry* 40, 14429–14439
- 40 Petitou, M. *et al.* (2003) 1976–1983, a critical period in the history of heparin: the discovery of the antithrombin binding site. *Biochimie* 85, 83–89
- 41 Hajmohammadi, S. *et al.* (2003) Normal levels of anticoagulant heparan sulfate are not essential for normal hemostasis. *J. Clin. Invest.* 111, 989–999
- 42 Ai, X. *et al.* (2003) QSulf1 remodels the 6-*O*-sulfation states of cell surface heparan sulfate proteoglycans to promote Wnt signaling. *J. Cell Biol.* 162, 341–351
- 43 Ai, X. *et al.* (2006) Substrate specificity and domain functions of extracellular heparan sulfate 6-*O*-endosulfatases, QSulf1 and QSulf2. *J. Biol. Chem.* 281, 4969–4976
- 44 Wang, S. *et al.* (2004) QSulf1, a heparan sulfate 6-*O*-endosulfatase, inhibits fibroblast growth factor signaling in mesoderm induction and angiogenesis. *Proc. Natl. Acad. Sci. U. S. A.* 101, 4833–4838
- 45 Lai, J.P. *et al.* (2006) SULF1 inhibits tumor growth and potentiates the effects of histone deacetylase inhibitors in hepatocellular carcinoma. *Gastroenterology* 130, 2130–2144
- 46 Morimoto-Tomita, M. *et al.* (2005) Sulf-2, a proangiogenic heparan sulfate endosulfatase, is upregulated in breast cancer. *Neoplasia* 7, 1001–1010
- 47 Sala-Newby, G.B. *et al.* (2005) Regulation of vascular smooth muscle cell proliferation, migration and death by heparan sulfate 6-*O*-endosulfatase1. *FEBS Lett.* 579, 6493–6498
- 48 Ledin, J. *et al.* (2006) Enzymatically active *N*-deacetylase/*N*-sulfotransferase-2 is present in liver but does not contribute to heparan sulfate *N*-sulfation. *J. Biol. Chem.* 281, 35727–35734
- 49 Pinhal, M.A. *et al.* (2001) Enzyme interactions in heparan sulfate biosynthesis: uronosyl 5-epimerase and 2-*O*-sulfotransferase interact in vivo. *Proc. Natl. Acad. Sci. U. S. A.* 98, 12984–12989
- 50 Senay, C. *et al.* (2000) The EXT1/EXT2 tumor suppressors: catalytic activities and role in heparan sulfate biosynthesis. *EMBO Rep.* 1, 282–286
- 51 Robinson, C.J. *et al.* (2006) VEGF165-binding sites within heparan sulfate encompass two highly sulfated domains and can be liberated by K5 lyase. *J. Biol. Chem.* 281, 1731–1740
- 52 Uchimura, K. *et al.* (2006) HSulf-2, an extracellular endoglucosamine-6-sulfatase, selectively mobilizes heparin-bound growth factors and chemokines: effects on VEGF, FGF-1, and SDF-1. *BMC Biochem.*, 7, 2 DOI: 10.1186/1471-2091-7-2 (www.biomedcentral.com)

## Endeavour

Coming soon in the quarterly magazine for the history and philosophy of science:

Earthquake theories in the early modern period by F. Willmoth  
 Science in fiction - attempts to make a science out of literary criticism by J. Adams  
 The birth of botanical *Drosophila* by S. Leonelli

**Endeavour is available on ScienceDirect, [www.sciencedirect.com](http://www.sciencedirect.com)**

## Chapter 10.0 References

1. Carmeliet P. Angiogenesis in health and disease. *Nat Med.* 2003;9:653-660.
2. Lawson ND, Vogel AM, Weinstein BM. sonic hedgehog and vascular endothelial growth factor act upstream of the Notch pathway during arterial endothelial differentiation. *Dev Cell.* 2002;3:127-136.
3. Adams RH, Wilkinson GA, Weiss C, et al. Roles of ephrinB ligands and EphB receptors in cardiovascular development: demarcation of arterial/venous domains, vascular morphogenesis, and sprouting angiogenesis. *Genes Dev.* 1999;13:295-306.
4. Gerety SS, Wang HU, Chen ZF, Anderson DJ. Symmetrical mutant phenotypes of the receptor EphB4 and its specific transmembrane ligand ephrin-B2 in cardiovascular development. *Mol Cell.* 1999;4:403-414.
5. Wang HU, Chen ZF, Anderson DJ. Molecular distinction and angiogenic interaction between embryonic arteries and veins revealed by ephrin-B2 and its receptor Eph-B4. *Cell.* 1998;93:741-753.
6. Asahara T, Kawamoto A. Endothelial progenitor cells for postnatal vasculogenesis. *Am J Physiol Cell Physiol.* 2004;287:C572-579.
7. Helisch A, Schaper W. Arteriogenesis: the development and growth of collateral arteries. *Microcirculation.* 2003;10:83-97.
8. Helisch A, Ware JA. Therapeutic angiogenesis for ischemic heart disease. *Adv Exp Med Biol.* 2000;476:327-350.
9. Heil M, Schaper W. Influence of mechanical, cellular, and molecular factors on collateral artery growth (arteriogenesis). *Circ Res.* 2004;95:449-458.
10. Cao R, Brakenhielm E, Pawliuk R, et al. Angiogenic synergism, vascular stability and improvement of hind-limb ischemia by a combination of PDGF-BB and FGF-2. *Nat Med.* 2003;9:604-613.
11. Lutun A, Tjwa M, Moons L, et al. Revascularization of ischemic tissues by PlGF treatment, and inhibition of tumor angiogenesis, arthritis and atherosclerosis by anti-Flt1. *Nat Med.* 2002;8:831-840.
12. Buschmann I, Schaper W. Arteriogenesis Versus Angiogenesis: Two Mechanisms of Vessel Growth. *News Physiol Sci.* 1999;14:121-125.
13. Heil M, Clauss M, Suzuki K, et al. Vascular endothelial growth factor (VEGF) stimulates monocyte migration through endothelial monolayers via increased integrin expression. *Eur J Cell Biol.* 2000;79:850-857.
14. Carmeliet P. Mechanisms of angiogenesis and arteriogenesis. *Nat Med.* 2000;6:389-395.
15. Heil M, Eitenmuller I, Schmitz-Rixen T, Schaper W. Arteriogenesis versus angiogenesis: similarities and differences. *J Cell Mol Med.* 2006;10:45-55.
16. Guttmacher AE, Marchuk DA, White RI, Jr. Hereditary hemorrhagic telangiectasia. *N Engl J Med.* 1995;333:918-924.
17. Johnson DW, Berg JN, Baldwin MA, et al. Mutations in the activin receptor-like kinase 1 gene in hereditary haemorrhagic telangiectasia type 2. *Nat Genet.* 1996;13:189-195.
18. McAllister KA, Lennon F, Bowles-Biesecker B, et al. Genetic heterogeneity in hereditary haemorrhagic telangiectasia: possible correlation with clinical phenotype. *J Med Genet.* 1994;31:927-932.
19. Urness LD, Sorensen LK, Li DY. Arteriovenous malformations in mice lacking activin receptor-like kinase-1. *Nat Genet.* 2000;26:328-331.

20. Irrthum A, Devriendt K, Chitayat D, et al. Mutations in the transcription factor gene SOX18 underlie recessive and dominant forms of hypotrichosis-lymphedema-telangiectasia. *Am J Hum Genet.* 2003;72:1470-1478.
21. Pendeville H, Winandy M, Manfroid I, et al. Zebrafish Sox7 and Sox18 function together to control arterial-venous identity. *Dev Biol.* 2008;317:405-416.
22. Carmeliet P. Angiogenesis in life, disease and medicine. *Nature.* 2005;438:932-936.
23. Hanahan D, Folkman J. Patterns and emerging mechanisms of the angiogenic switch during tumorigenesis. *Cell.* 1996;86:353-364.
24. Neufeld G, Cohen T, Gengrinovitch S, Poltorak Z. Vascular endothelial growth factor (VEGF) and its receptors. *Faseb J.* 1999;13:9-22.
25. Ferrara N. Vascular endothelial growth factor. *Eur J Cancer.* 1996;32A:2413-2422.
26. Carmeliet P, Ng YS, Nuyens D, et al. Impaired myocardial angiogenesis and ischemic cardiomyopathy in mice lacking the vascular endothelial growth factor isoforms VEGF164 and VEGF188. *Nat Med.* 1999;5:495-502.
27. Ferrara N, Carver-Moore K, Chen H, et al. Heterozygous embryonic lethality induced by targeted inactivation of the VEGF gene. *Nature.* 1996;380:439-442.
28. Cleaver O, Tonissen KF, Saha MS, Krieg PA. Neovascularization of the *Xenopus* embryo. *Dev Dyn.* 1997;210:66-77.
29. Dumont DJ, Fong GH, Puri MC, Gradwohl G, Alitalo K, Breitman ML. Vascularization of the mouse embryo: a study of flk-1, tek, tie, and vascular endothelial growth factor expression during development. *Dev Dyn.* 1995;203:80-92.
30. Flamme I, Breier G, Risau W. Vascular endothelial growth factor (VEGF) and VEGF receptor 2 (flk-1) are expressed during vasculogenesis and vascular differentiation in the quail embryo. *Dev Biol.* 1995;169:699-712.
31. Klagsbrun M, D'Amore PA. Vascular endothelial growth factor and its receptors. *Cytokine Growth Factor Rev.* 1996;7:259-270.
32. Enholm B, Paavonen K, Ristimaki A, et al. Comparison of VEGF, VEGF-B, VEGF-C and Ang-1 mRNA regulation by serum, growth factors, oncoproteins and hypoxia. *Oncogene.* 1997;14:2475-2483.
33. Ornitz DM, Itoh N. Fibroblast growth factors. *Genome Biol.* 2001;2:REVIEWS3005.
34. Pintucci G, Moscatelli D, Saponara F, et al. Lack of ERK activation and cell migration in FGF-2-deficient endothelial cells. *Faseb J.* 2002;16:598-600.
35. Ortega S, Ittmann M, Tsang SH, Ehrlich M, Basilico C. Neuronal defects and delayed wound healing in mice lacking fibroblast growth factor 2. *Proc Natl Acad Sci U S A.* 1998;95:5672-5677.
36. Nakamura T, Mochizuki Y, Kanetake H, Kanda S. Signals via FGF receptor 2 regulate migration of endothelial cells. *Biochem Biophys Res Commun.* 2001;289:801-806.
37. Presta M, Rusnati M, Urbinati C, Sommer A, Ragnotti G. Biologically active synthetic fragments of human basic fibroblast growth factor (bFGF): identification of two Asp-Gly-Arg-containing domains involved in the mitogenic activity of bFGF in endothelial cells. *J Cell Physiol.* 1991;149:512-524.
38. Ornitz DM. FGFs, heparan sulfate and FGFRs: complex interactions essential for development. *Bioessays.* 2000;22:108-112.
39. Gerhardt H, Golding M, Fruttiger M, et al. VEGF guides angiogenic sprouting utilizing endothelial tip cell filopodia. *J Cell Biol.* 2003;161:1163-1177.
40. Jain RK, Booth MF. What brings pericytes to tumor vessels? *J Clin Invest.* 2003;112:1134-1136.
41. Hellstrom M, Gerhardt H, Kalen M, et al. Lack of pericytes leads to endothelial hyperplasia and abnormal vascular morphogenesis. *J Cell Biol.* 2001;153:543-553.

42. Maisonpierre PC, Suri C, Jones PF, et al. Angiopoietin-2, a natural antagonist for Tie2 that disrupts in vivo angiogenesis. *Science*. 1997;277:55-60.
43. Carlson TR, Feng Y, Maisonpierre PC, Mrksich M, Morla AO. Direct cell adhesion to the angiopoietins mediated by integrins. *J Biol Chem*. 2001;276:26516-26525.
44. Dumont DJ, Gradwohl G, Fong GH, et al. Dominant-negative and targeted null mutations in the endothelial receptor tyrosine kinase, tek, reveal a critical role in vasculogenesis of the embryo. *Genes Dev*. 1994;8:1897-1909.
45. Rodewald HR, Sato TN. Tie1, a receptor tyrosine kinase essential for vascular endothelial cell integrity, is not critical for the development of hematopoietic cells. *Oncogene*. 1996;12:397-404.
46. Suri C, Jones PF, Patan S, et al. Requisite role of angiopoietin-1, a ligand for the TIE2 receptor, during embryonic angiogenesis. *Cell*. 1996;87:1171-1180.
47. Carmeliet P, Collen D. Molecular basis of angiogenesis. Role of VEGF and VE-cadherin. *Ann N Y Acad Sci*. 2000;902:249-262; discussion 262-244.
48. Visconti RP, Richardson CD, Sato TN. Orchestration of angiogenesis and arteriovenous contribution by angiopoietins and vascular endothelial growth factor (VEGF). *Proc Natl Acad Sci U S A*. 2002;99:8219-8224.
49. Ahmad SA, Liu W, Jung YD, et al. Differential expression of angiopoietin-1 and angiopoietin-2 in colon carcinoma. A possible mechanism for the initiation of angiogenesis. *Cancer*. 2001;92:1138-1143.
50. Holash J, Wiegand SJ, Yancopoulos GD. New model of tumor angiogenesis: dynamic balance between vessel regression and growth mediated by angiopoietins and VEGF. *Oncogene*. 1999;18:5356-5362.
51. Mack CA, Patel SR, Schwarz EA, et al. Biologic bypass with the use of adenovirus-mediated gene transfer of the complementary deoxyribonucleic acid for vascular endothelial growth factor 121 improves myocardial perfusion and function in the ischemic porcine heart. *J Thorac Cardiovasc Surg*. 1998;115:168-176; discussion 176-167.
52. Giordano FJ, Ping P, McKirnan MD, et al. Intracoronary gene transfer of fibroblast growth factor-5 increases blood flow and contractile function in an ischemic region of the heart. *Nat Med*. 1996;2:534-539.
53. Zhang D, Gai L, Fan R, Dong W, Wen Y. Efficacy and safety of therapeutic angiogenesis from direct myocardial administration of an adenoviral vector expressing vascular endothelial growth factor 165. *Chin Med J (Engl)*. 2002;115:643-648.
54. Laham RJ, Sellke FW, Edelman ER, et al. Local perivascular delivery of basic fibroblast growth factor in patients undergoing coronary bypass surgery: results of a phase I randomized, double-blind, placebo-controlled trial. *Circulation*. 1999;100:1865-1871.
55. Symes JF, Losordo DW, Vale PR, et al. Gene therapy with vascular endothelial growth factor for inoperable coronary artery disease. *Ann Thorac Surg*. 1999;68:830-836; discussion 836-837.
56. Tse HF, Kwong YL, Chan JK, Lo G, Ho CL, Lau CP. Angiogenesis in ischaemic myocardium by intramyocardial autologous bone marrow mononuclear cell implantation. *Lancet*. 2003;361:47-49.
57. Asahara T, Bauters C, Zheng LP, et al. Synergistic effect of vascular endothelial growth factor and basic fibroblast growth factor on angiogenesis in vivo. *Circulation*. 1995;92:II365-371.
58. Chae JK, Kim I, Lim ST, et al. Coadministration of angiopoietin-1 and vascular endothelial growth factor enhances collateral vascularization. *Arterioscler Thromb Vasc Biol*. 2000;20:2573-2578.

59. Vincent KA, Shyu KG, Luo Y, et al. Angiogenesis is induced in a rabbit model of hindlimb ischemia by naked DNA encoding an HIF-1 $\alpha$ /VP16 hybrid transcription factor. *Circulation*. 2000;102:2255-2261.
60. Lee JS, Kim JM, Kim KL, et al. Combined administration of naked DNA vectors encoding VEGF and bFGF enhances tissue perfusion and arteriogenesis in ischemic hindlimb. *Biochem Biophys Res Commun*. 2007;360:752-758.
61. Iba O, Matsubara H, Nozawa Y, et al. Angiogenesis by implantation of peripheral blood mononuclear cells and platelets into ischemic limbs. *Circulation*. 2002;106:2019-2025.
62. Kawamoto A, Gwon HC, Iwaguro H, et al. Therapeutic potential of ex vivo expanded endothelial progenitor cells for myocardial ischemia. *Circulation*. 2001;103:634-637.
63. Hiasa K, Ishibashi M, Ohtani K, et al. Gene transfer of stromal cell-derived factor-1 $\alpha$  enhances ischemic vasculogenesis and angiogenesis via vascular endothelial growth factor/endothelial nitric oxide synthase-related pathway: next-generation chemokine therapy for therapeutic neovascularization. *Circulation*. 2004;109:2454-2461.
64. Rafii S, Lyden D. Cancer. A few to flip the angiogenic switch. *Science*. 2008;319:163-164.
65. Carmeliet P, Jain RK. Angiogenesis in cancer and other diseases. *Nature*. 2000;407:249-257.
66. Gupta K, Zhang J. Angiogenesis: a curse or cure? *Postgrad Med J*. 2005;81:236-242.
67. Kabbinavar F, Hurwitz HI, Fehrenbacher L, et al. Phase II, randomized trial comparing bevacizumab plus fluorouracil (FU)/leucovorin (LV) with FU/LV alone in patients with metastatic colorectal cancer. *J Clin Oncol*. 2003;21:60-65.
68. Takano S, Gately S, Neville ME, et al. Suramin, an anticancer and angiosuppressive agent, inhibits endothelial cell binding of basic fibroblast growth factor, migration, proliferation, and induction of urokinase-type plasminogen activator. *Cancer Res*. 1994;54:2654-2660.
69. Kuyu H, Lee WR, Bare R, Hall MC, Torti FM. Recent advances in the treatment of prostate cancer. *Ann Oncol*. 1999;10:891-898.
70. Small EJ, Halabi S, Ratain MJ, et al. Randomized study of three different doses of suramin administered with a fixed dosing schedule in patients with advanced prostate cancer: results of intergroup 0159, cancer and leukemia group B 9480. *J Clin Oncol*. 2002;20:3369-3375.
71. Cherrington JM, Strawn LM, Shawver LK. New paradigms for the treatment of cancer: the role of anti-angiogenesis agents. *Adv Cancer Res*. 2000;79:1-38.
72. Laird AD, Vajkoczy P, Shawver LK, et al. SU6668 is a potent antiangiogenic and antitumor agent that induces regression of established tumors. *Cancer Res*. 2000;60:4152-4160.
73. Roman BL, Weinstein BM. Building the vertebrate vasculature: research is going swimmingly. *Bioessays*. 2000;22:882-893.
74. Jin SW, Beis D, Mitchell T, Chen JN, Stainier DY. Cellular and molecular analyses of vascular tube and lumen formation in zebrafish. *Development*. 2005;132:5199-5209.
75. Lawson ND, Weinstein BM. In vivo imaging of embryonic vascular development using transgenic zebrafish. *Dev Biol*. 2002;248:307-318.
76. Stainier DY, Weinstein BM, Detrich HW, 3rd, Zon LI, Fishman MC. Cloche, an early acting zebrafish gene, is required by both the endothelial and hematopoietic lineages. *Development*. 1995;121:3141-3150.
77. Crosier PS, Kalev-Zylinska ML, Hall CJ, Flores MV, Horsfield JA, Crosier KE. Pathways in blood and vessel development revealed through zebrafish genetics. *Int J Dev Biol*. 2002;46:493-502.

78. Lyons SE, Lawson ND, Lei L, Bennett PE, Weinstein BM, Liu PP. A nonsense mutation in zebrafish *gata1* causes the bloodless phenotype in *vlad tepes*. *Proc Natl Acad Sci U S A*. 2002;99:5454-5459.
79. Brown LA, Rodaway AR, Schilling TF, et al. Insights into early vasculogenesis revealed by expression of the ETS-domain transcription factor *Fli-1* in wild-type and mutant zebrafish embryos. *Mech Dev*. 2000;90:237-252.
80. Thompson MA, Ransom DG, Pratt SJ, et al. The *cloche* and *spadetail* genes differentially affect hematopoiesis and vasculogenesis. *Dev Biol*. 1998;197:248-269.
81. Fouquet B, Weinstein BM, Serluca FC, Fishman MC. Vessel patterning in the embryo of the zebrafish: guidance by notochord. *Dev Biol*. 1997;183:37-48.
82. Gering M, Rodaway AR, Gottgens B, Patient RK, Green AR. The *SCL* gene specifies haemangioblast development from early mesoderm. *Embo J*. 1998;17:4029-4045.
83. Zhong TP, Childs S, Leu JP, Fishman MC. Gridlock signalling pathway fashions the first embryonic artery. *Nature*. 2001;414:216-220.
84. Lawson ND, Scheer N, Pham VN, et al. Notch signaling is required for arterial-venous differentiation during embryonic vascular development. *Development*. 2001;128:3675-3683.
85. Isogai S, Horiguchi M, Weinstein BM. The vascular anatomy of the developing zebrafish: an atlas of embryonic and early larval development. *Dev Biol*. 2001;230:278-301.
86. Childs S, Chen JN, Garrity DM, Fishman MC. Patterning of angiogenesis in the zebrafish embryo. *Development*. 2002;129:973-982.
87. Isogai S, Lawson ND, Torrealday S, Horiguchi M, Weinstein BM. Angiogenic network formation in the developing vertebrate trunk. *Development*. 2003;130:5281-5290.
88. Yaniv K, Isogai S, Castranova D, Dye L, Hitomi J, Weinstein BM. Live imaging of lymphatic development in the zebrafish. *Nat Med*. 2006;12:711-716.
89. Santoro MM, Pesce G, Stainier DY. Characterization of vascular mural cells during zebrafish development. *Mech Dev*. 2009.
90. Georgijevic S, Subramanian Y, Rollins EL, Starovic-Subota O, Tang AC, Childs SJ. Spatiotemporal expression of smooth muscle markers in developing zebrafish gut. *Dev Dyn*. 2007;236:1623-1632.
91. Lawson ND, Mugford JW, Diamond BA, Weinstein BM. phospholipase C  $\gamma$ -1 is required downstream of vascular endothelial growth factor during arterial development. *Genes Dev*. 2003;17:1346-1351.
92. Stainier DY, Fouquet B, Chen JN, et al. Mutations affecting the formation and function of the cardiovascular system in the zebrafish embryo. *Development*. 1996;123:285-292.
93. Torres-Vazquez J, Gitler AD, Fraser SD, et al. Semaphorin-plexin signaling guides patterning of the developing vasculature. *Dev Cell*. 2004;7:117-123.
94. Weinstein BM, Stemple DL, Driever W, Fishman MC. Gridlock, a localized heritable vascular patterning defect in the zebrafish. *Nat Med*. 1995;1:1143-1147.
95. Amsterdam A, Hopkins N. Retroviral-mediated insertional mutagenesis in zebrafish. *Methods Cell Biol*. 2004;77:3-20.
96. Ekker SC, Larson JD. Morphant technology in model developmental systems. *Genesis*. 2001;30:89-93.
97. Golling G, Amsterdam A, Sun Z, et al. Insertional mutagenesis in zebrafish rapidly identifies genes essential for early vertebrate development. *Nat Genet*. 2002;31:135-140.
98. Jin SW, Herzog W, Santoro MM, et al. A transgene-assisted genetic screen identifies essential regulators of vascular development in vertebrate embryos. *Dev Biol*. 2007;307:29-42.
99. Hall CJ, Flores MV, Davidson AJ, Crosier KE, Crosier PS. Radar is required for the establishment of vascular integrity in the zebrafish. *Dev Biol*. 2002;251:105-117.

100. Cleaver O, Krieg PA. VEGF mediates angioblast migration during development of the dorsal aorta in *Xenopus*. *Development*. 1998;125:3905-3914.
101. Ober EA, Olofsson B, Makinen T, et al. Vegfc is required for vascular development and endoderm morphogenesis in zebrafish. *EMBO Rep*. 2004;5:78-84.
102. Schulte-Merker S, van Eeden FJ, Halpern ME, Kimmel CB, Nusslein-Volhard C. no tail (ntl) is the zebrafish homologue of the mouse T (Brachyury) gene. *Development*. 1994;120:1009-1015.
103. Talbot WS, Trevarrow B, Halpern ME, et al. A homeobox gene essential for zebrafish notochord development. *Nature*. 1995;378:150-157.
104. Kusano KF, Pola R, Murayama T, et al. Sonic hedgehog myocardial gene therapy: tissue repair through transient reconstitution of embryonic signaling. *Nat Med*. 2005;11:1197-1204.
105. Pola R, Ling LE, Silver M, et al. The morphogen Sonic hedgehog is an indirect angiogenic agent upregulating two families of angiogenic growth factors. *Nat Med*. 2001;7:706-711.
106. Covassin LD, Siekmann AF, Kacergis MC, et al. A genetic screen for vascular mutants in zebrafish reveals dynamic roles for Vegf/Plcg1 signaling during artery development. *Dev Biol*. 2009;329:212-226.
107. Krebs LT, Xue Y, Norton CR, et al. Notch signaling is essential for vascular morphogenesis in mice. *Genes Dev*. 2000;14:1343-1352.
108. Siekmann AF, Covassin L, Lawson ND. Modulation of VEGF signalling output by the Notch pathway. *Bioessays*. 2008;30:303-313.
109. Carmeliet P, Tessier-Lavigne M. Common mechanisms of nerve and blood vessel wiring. *Nature*. 2005;436:193-200.
110. Tessier-Lavigne M, Goodman CS. The molecular biology of axon guidance. *Science*. 1996;274:1123-1133.
111. Lu X, Le Noble F, Yuan L, et al. The netrin receptor UNC5B mediates guidance events controlling morphogenesis of the vascular system. *Nature*. 2004;432:179-186.
112. Brose K, Bland KS, Wang KH, et al. Slit proteins bind Robo receptors and have an evolutionarily conserved role in repulsive axon guidance. *Cell*. 1999;96:795-806.
113. Lin X, Buff EM, Perrimon N, Michelson AM. Heparan sulfate proteoglycans are essential for FGF receptor signaling during *Drosophila* embryonic development. *Development*. 1999;126:3715-3723.
114. Wang KH, Brose K, Arnott D, et al. Biochemical purification of a mammalian slit protein as a positive regulator of sensory axon elongation and branching. *Cell*. 1999;96:771-784.
115. Bedell VM, Yeo SY, Park KW, et al. roundabout4 is essential for angiogenesis in vivo. *Proc Natl Acad Sci U S A*. 2005;102:6373-6378.
116. Park KW, Morrison CM, Sorensen LK, et al. Robo4 is a vascular-specific receptor that inhibits endothelial migration. *Dev Biol*. 2003;261:251-267.
117. Suchting S, Heal P, Tahtis K, Stewart LM, Bicknell R. Soluble Robo4 receptor inhibits in vivo angiogenesis and endothelial cell migration. *Faseb J*. 2005;19:121-123.
118. Sehnert AJ, Huq A, Weinstein BM, Walker C, Fishman M, Stainier DY. Cardiac troponin T is essential in sarcomere assembly and cardiac contractility. *Nat Genet*. 2002;31:106-110.
119. Sehnert AJ, Stainier DY. A window to the heart: can zebrafish mutants help us understand heart disease in humans? *Trends Genet*. 2002;18:491-494.
120. Chan J, Bayliss PE, Wood JM, Roberts TM. Dissection of angiogenic signaling in zebrafish using a chemical genetic approach. *Cancer Cell*. 2002;1:257-267.

121. Peterson RT, Fishman MC. Discovery and use of small molecules for probing biological processes in zebrafish. *Methods Cell Biol.* 2004;76:569-591.
122. Bayliss PE, Bellavance KL, Whitehead GG, et al. Chemical modulation of receptor signaling inhibits regenerative angiogenesis in adult zebrafish. *Nat Chem Biol.* 2006;2:265-273.
123. Gallagher JT, Turnbull JE, Lyon M. Heparan sulphate proteoglycans. *Biochem Soc Trans.* 1990;18:207-209.
124. Ishihara M, Mamiya G. [Role of heparan sulfate proteoglycan for control of cell growth]. *Tanpakushitsu Kakusan Koso.* 1989;34:853-862.
125. Kramer KL, Yost HJ. Heparan sulfate core proteins in cell-cell signaling. *Annu Rev Genet.* 2003;37:461-484.
126. Rosenberg RD, Shworak NW, Liu J, Schwartz JJ, Zhang L. Heparan sulfate proteoglycans of the cardiovascular system. Specific structures emerge but how is synthesis regulated? *J Clin Invest.* 1997;100:S67-75.
127. Baeg GH, Lin X, Khare N, Baumgartner S, Perrimon N. Heparan sulfate proteoglycans are critical for the organization of the extracellular distribution of Wingless. *Development.* 2001;128:87-94.
128. Lin X, Perrimon N. Dally cooperates with Drosophila Frizzled 2 to transduce Wingless signalling. *Nature.* 1999;400:281-284.
129. Nakato H, Futch TA, Selleck SB. The division abnormally delayed (dally) gene: a putative integral membrane proteoglycan required for cell division patterning during postembryonic development of the nervous system in Drosophila. *Development.* 1995;121:3687-3702.
130. Strigini M, Cohen SM. Formation of morphogen gradients in the Drosophila wing. *Semin Cell Dev Biol.* 1999;10:335-344.
131. Topczewski J, Sepich DS, Myers DC, et al. The zebrafish glypican knypek controls cell polarity during gastrulation movements of convergent extension. *Dev Cell.* 2001;1:251-264.
132. Capurro MI, Xu P, Shi W, Li F, Jia A, Filmus J. Glypican-3 inhibits Hedgehog signaling during development by competing with patched for Hedgehog binding. *Dev Cell.* 2008;14:700-711.
133. Gallet A, Staccini-Lavenant L, Therond PP. Cellular trafficking of the glypican Dally-like is required for full-strength Hedgehog signaling and wingless transcytosis. *Dev Cell.* 2008;14:712-725.
134. Bellaiche Y, The I, Perrimon N. Tout-velu is a Drosophila homologue of the putative tumour suppressor EXT-1 and is needed for Hh diffusion. *Nature.* 1998;394:85-88.
135. Esko JD, Selleck SB. Order out of chaos: assembly of ligand binding sites in heparan sulfate. *Annu Rev Biochem.* 2002;71:435-471.
136. Bernfield M, Kokenyesi R, Kato M, et al. Biology of the syndecans: a family of transmembrane heparan sulfate proteoglycans. *Annu Rev Cell Biol.* 1992;8:365-393.
137. Park PW, Reizes O, Bernfield M. Cell surface heparan sulfate proteoglycans: selective regulators of ligand-receptor encounters. *J Biol Chem.* 2000;275:29923-29926.
138. Beauvais DM, Rapraeger AC. Syndecans in tumor cell adhesion and signaling. *Reprod Biol Endocrinol.* 2004;2:3.
139. Tumova S, Woods A, Couchman JR. Heparan sulfate proteoglycans on the cell surface: versatile coordinators of cellular functions. *Int J Biochem Cell Biol.* 2000;32:269-288.
140. Granes F, Urena JM, Rocamora N, Vilaro S. Ezrin links syndecan-2 to the cytoskeleton. *J Cell Sci.* 2000;113 (Pt 7):1267-1276.

141. Baciuc PC, Saoncella S, Lee SH, Denhez F, Leuthardt D, Goetinck PF. Syndesmos, a protein that interacts with the cytoplasmic domain of syndecan-4, mediates cell spreading and actin cytoskeletal organization. *J Cell Sci.* 2000;113 Pt 2:315-324.
142. Rapraeger AC, Ott VL. Molecular interactions of the syndecan core proteins. *Curr Opin Cell Biol.* 1998;10:620-628.
143. Horowitz A, Tkachenko E, Simons M. Fibroblast growth factor-specific modulation of cellular response by syndecan-4. *J Cell Biol.* 2002;157:715-725.
144. Lim ST, Longley RL, Couchman JR, Woods A. Direct binding of syndecan-4 cytoplasmic domain to the catalytic domain of protein kinase C alpha (PKC alpha) increases focal adhesion localization of PKC alpha. *J Biol Chem.* 2003;278:13795-13802.
145. Ethell IM, Yamaguchi Y. Cell surface heparan sulfate proteoglycan syndecan-2 induces the maturation of dendritic spines in rat hippocampal neurons. *J Cell Biol.* 1999;144:575-586.
146. Kramer KL, Yost HJ. Ectodermal syndecan-2 mediates left-right axis formation in migrating mesoderm as a cell-nonautonomous Vgl cofactor. *Dev Cell.* 2002;2:115-124.
147. Chen L, Klass C, Woods A. Syndecan-2 regulates transforming growth factor-beta signaling. *J Biol Chem.* 2004;279:15715-15718.
148. Chen E, Hermanson S, Ekker SC. Syndecan-2 is essential for angiogenic sprouting during zebrafish development. *Blood.* 2004;103:1710-1719.
149. Fears CY, Gladson CL, Woods A. Syndecan-2 is expressed in the microvasculature of gliomas and regulates angiogenic processes in microvascular endothelial cells. *J Biol Chem.* 2006;281:14533-14536.
150. Noguer O, Villena J, Lorita J, Vilaro S, Reina M. Syndecan-2 downregulation impairs angiogenesis in human microvascular endothelial cells. *Exp Cell Res.* 2009;315:795-808.
151. Jakobsson L, Kreuger J, Holmborn K, et al. Heparan sulfate in trans potentiates VEGFR-mediated angiogenesis. *Dev Cell.* 2006;10:625-634.
152. Conde-Knape K. Heparan sulfate proteoglycans in experimental models of diabetes: a role for perlecan in diabetes complications. *Diabetes Metab Res Rev.* 2001;17:412-421.
153. Iozzo RV. Heparan sulfate proteoglycans: intricate molecules with intriguing functions. *J Clin Invest.* 2001;108:165-167.
154. Bix G, Iozzo RV. Novel interactions of perlecan: unraveling perlecan's role in angiogenesis. *Microsc Res Tech.* 2008;71:339-348.
155. Whitelock JM, Graham LD, Melrose J, Murdoch AD, Iozzo RV, Underwood PA. Human perlecan immunopurified from different endothelial cell sources has different adhesive properties for vascular cells. *Matrix Biol.* 1999;18:163-178.
156. Whitelock JM, Murdoch AD, Iozzo RV, Underwood PA. The degradation of human endothelial cell-derived perlecan and release of bound basic fibroblast growth factor by stromelysin, collagenase, plasmin, and heparanases. *J Biol Chem.* 1996;271:10079-10086.
157. Fuki II, Iozzo RV, Williams KJ. Perlecan heparan sulfate proteoglycan. A novel receptor that mediates a distinct pathway for ligand catabolism. *J Biol Chem.* 2000;275:31554.
158. Arikawa-Hirasawa E, Wilcox WR, Le AH, et al. Dyssegmental dysplasia, Silverman-Handmaker type, is caused by functional null mutations of the perlecan gene. *Nat Genet.* 2001;27:431-434.
159. Nicole S, Davoine CS, Topaloglu H, et al. Perlecan, the major proteoglycan of basement membranes, is altered in patients with Schwartz-Jampel syndrome (chondrodystrophic myotonia). *Nat Genet.* 2000;26:480-483.
160. Arikawa-Hirasawa E, Watanabe H, Takami H, Hassell JR, Yamada Y. Perlecan is essential for cartilage and cephalic development. *Nat Genet.* 1999;23:354-358.

161. Costell M, Carmona R, Gustafsson E, Gonzalez-Iriarte M, Fassler R, Munoz-Chapuli R. Hyperplastic conotruncal endocardial cushions and transposition of great arteries in perlecan-null mice. *Circ Res.* 2002;91:158-164.
162. Gonzalez-Iriarte M, Carmona R, Perez-Pomares JM, Macias D, Costell M, Munoz-Chapuli R. Development of the coronary arteries in a murine model of transposition of great arteries. *J Mol Cell Cardiol.* 2003;35:795-802.
163. Aviezer D, Hecht D, Safran M, Eisinger M, David G, Yayon A. Perlecan, basal lamina proteoglycan, promotes basic fibroblast growth factor-receptor binding, mitogenesis, and angiogenesis. *Cell.* 1994;79:1005-1013.
164. Sharma B, Handler M, Eichstetter I, Whitelock JM, Nugent MA, Iozzo RV. Antisense targeting of perlecan blocks tumor growth and angiogenesis in vivo. *J Clin Invest.* 1998;102:1599-1608.
165. Mongiat M, Taylor K, Otto J, et al. The protein core of the proteoglycan perlecan binds specifically to fibroblast growth factor-7. *J Biol Chem.* 2000;275:7095-7100.
166. Gohring W, Sasaki T, Heldin CH, Timpl R. Mapping of the binding of platelet-derived growth factor to distinct domains of the basement membrane proteins BM-40 and perlecan and distinction from the BM-40 collagen-binding epitope. *Eur J Biochem.* 1998;255:60-66.
167. Aikawa T, Whipple CA, Lopez ME, et al. Glypican-1 modulates the angiogenic and metastatic potential of human and mouse cancer cells. *J Clin Invest.* 2008;118:89-99.
168. Matsuda K, Maruyama H, Guo F, et al. Glypican-1 is overexpressed in human breast cancer and modulates the mitogenic effects of multiple heparin-binding growth factors in breast cancer cells. *Cancer Res.* 2001;61:5562-5569.
169. Gengrinovitch S, Berman B, David G, Witte L, Neufeld G, Ron D. Glypican-1 is a VEGF(165) binding proteoglycan that acts as an extracellular chaperone for VEGF(165). *Journal Of Biological Chemistry.* 1999;274:10816.
170. Nackaerts K, Verbeken E, Deneffe G, Vanderschueren B, Demedts M, David G. Heparan sulfate proteoglycan expression in human lung-cancer cells. *Int J Cancer.* 1997;74:335-345.
171. Gulyas M, Hjerpe A. Proteoglycans and WT1 as markers for distinguishing adenocarcinoma, epithelioid mesothelioma, and benign mesothelium. *J Pathol.* 2003;199:479-487.
172. Volk R, Schwartz JJ, Li J, Rosenberg RD, Simons M. The role of syndecan cytoplasmic domain in basic fibroblast growth factor-dependent signal transduction. *J Biol Chem.* 1999;274:24417-24424.
173. Granes F, Garcia R, Casaroli-Marano RP, et al. Syndecan-2 induces filopodia by active cdc42Hs. *Exp Cell Res.* 1999;248:439-456.
174. Zoeller JJ, Whitelock JM, Iozzo RV. Perlecan regulates developmental angiogenesis by modulating the VEGF-VEGFR2 axis. *Matrix Biol.* 2009;28:284-291.
175. Iozzo RV, San Antonio JD. Heparan sulfate proteoglycans: heavy hitters in the angiogenesis arena. *J Clin Invest.* 2001;108:349-355.
176. Mongiat M, Sweeney SM, San Antonio JD, Fu J, Iozzo RV. Endorepellin, a novel inhibitor of angiogenesis derived from the C terminus of perlecan. *J Biol Chem.* 2003;278:4238-4249.
177. O'Reilly MS, Boehm T, Shing Y, et al. Endostatin: an endogenous inhibitor of angiogenesis and tumor growth. *Cell.* 1997;88:277-285.
178. Sasaki T, Larsson H, Kreuger J, et al. Structural basis and potential role of heparin/heparan sulfate binding to the angiogenesis inhibitor endostatin. *Embo J.* 1999;18:6240-6248.

179. Sasaki T, Fukai N, Mann K, Gohring W, Olsen BR, Timpl R. Structure, function and tissue forms of the C-terminal globular domain of collagen XVIII containing the angiogenesis inhibitor endostatin. *Embo J*. 1998;17:4249-4256.
180. Yamaguchi N, Anand-Apte B, Lee M, et al. Endostatin inhibits VEGF-induced endothelial cell migration and tumor growth independently of zinc binding. *Embo J*. 1999;18:4414-4423.
181. Karumanchi SA, Jha V, Ramchandran R, et al. Cell surface glypicans are low-affinity endostatin receptors. *Mol Cell*. 2001;7:811-822.
182. Yanagishita M, Hascall VC. Cell surface heparan sulfate proteoglycans. *J Biol Chem*. 1992;267:9451-9454.
183. Yanagishita M. Glycosylphosphatidylinositol-anchored and core protein-intercalated heparan sulfate proteoglycans in rat ovarian granulosa cells have distinct secretory, endocytotic, and intracellular degradative pathways. *J Biol Chem*. 1992;267:9505-9511.
184. Manwaring LP, Jamerson PA, Slauch R. Lysosomal storage diseases. *Rn*. 2008;71:33-37; quiz 38.
185. Bernfield M, Gotte M, Park PW, et al. Functions of cell surface heparan sulfate proteoglycans. *Annu Rev Biochem*. 1999;68:729-777.
186. Li J, Partovian C, Li J, et al. Modulation of microvascular signaling by heparan sulfate matrix: studies in syndecan-4 transgenic mice. *Microvasc Res*. 2002;64:38-46.
187. Dhodapkar MV, Kelly T, Theus A, Athota AB, Barlogie B, Sanderson RD. Elevated levels of shed syndecan-1 correlate with tumour mass and decreased matrix metalloproteinase-9 activity in the serum of patients with multiple myeloma. *Br J Haematol*. 1997;99:368-371.
188. Yang Y, Yaccoby S, Liu W, et al. Soluble syndecan-1 promotes growth of myeloma tumors in vivo. *Blood*. 2002;100:610-617.
189. Seidel C, Borset M, Hjertner O, et al. High levels of soluble syndecan-1 in myeloma-derived bone marrow: modulation of hepatocyte growth factor activity. *Blood*. 2000;96:3139-3146.
190. Yang Y, Macleod V, Miao HQ, et al. Heparanase enhances syndecan-1 shedding: a novel mechanism for stimulation of tumor growth and metastasis. *J Biol Chem*. 2007;282:13326-13333.
191. Vlodaysky I, Friedmann Y. Molecular properties and involvement of heparanase in cancer metastasis and angiogenesis. *J Clin Invest*. 2001;108:341-347.
192. Elkin M, Ilan N, Ishai-Michaeli R, et al. Heparanase as mediator of angiogenesis: mode of action. *Faseb J*. 2001;15:1661-1663.
193. Vlodaysky I, Friedmann Y, Elkin M, et al. Mammalian heparanase: gene cloning, expression and function in tumor progression and metastasis. *Nat Med*. 1999;5:793-802.
194. Reiland J, Sanderson RD, Waguespack M, et al. Heparanase degrades syndecan-1 and perlecan heparan sulfate: functional implications for tumor cell invasion. *J Biol Chem*. 2004;279:8047-8055.
195. Gingis-Velitski S, Ishai-Michaeli R, Vlodaysky I, Ilan N. Anti-heparanase monoclonal antibody enhances heparanase enzymatic activity and facilitates wound healing. *Faseb J*. 2007;21:3986-3993.
196. Vlodaysky I, Ilan N, Naggi A, Casu B. Heparanase: structure, biological functions, and inhibition by heparin-derived mimetics of heparan sulfate. *Curr Pharm Des*. 2007;13:2057-2073.
197. Stringer SE, Mayer-Proschel M, Kalyani A, Rao M, Gallagher JT. Heparin is a unique marker of progenitors in the glial cell lineage. *J Biol Chem*. 1999;274:25455-25460.

198. Klein-Soyer C, Archipoff G, Beretz A, Cazenave JP. Opposing effects of heparin with TGF-beta or aFGF during repair of a mechanical wound of human endothelium. Influence of cAMP on cell migration. *Biol Cell*. 1992;75:155-162.
199. Stringer SE, Gallagher JT. Specific binding of the chemokine platelet factor 4 to heparan sulfate. *J Biol Chem*. 1997;272:20508-20514.
200. Lyon M, Deakin JA, Mizuno K, Nakamura T, Gallagher JT. Interaction of hepatocyte growth factor with heparan sulfate. Elucidation of the major heparan sulfate structural determinants. *J Biol Chem*. 1994;269:11216-11223.
201. Abramsson A, Kurup S, Busse M, et al. Defective N-sulfation of heparan sulfate proteoglycans limits PDGF-BB binding and pericyte recruitment in vascular development. *Genes Dev*. 2007;21:316-331.
202. Rolny C, Spillmann D, Lindahl U, Claesson-Welsh L. Heparin amplifies platelet-derived growth factor (PDGF)-BB-induced PDGF alpha-receptor but not PDGF beta-receptor tyrosine phosphorylation in heparan sulfate-deficient cells. Effects on signal transduction and biological responses. *J Biol Chem*. 2002;277:19315-19321.
203. Robinson CJ, Mulloy B, Gallagher JT, Stringer SE. VEGF165-binding sites within heparan sulfate encompass two highly sulfated domains and can be liberated by K5 lyase. *J Biol Chem*. 2006;281:1731-1740.
204. Schlessinger J, Plotnikov AN, Ibrahimi OA, et al. Crystal structure of a ternary FGF-FGFR-heparin complex reveals a dual role for heparin in FGFR binding and dimerization. *Mol Cell*. 2000;6:743-750.
205. Pellegrini L, Burke DF, von Delft F, Mulloy B, Blundell TL. Crystal structure of fibroblast growth factor receptor ectodomain bound to ligand and heparin. *Nature*. 2000;407:1029-1034.
206. Carmeliet P. Fibroblast growth factor-1 stimulates branching and survival of myocardial arteries: a goal for therapeutic angiogenesis? *Circ Res*. 2000;87:176-178.
207. Duan DS, Werner S, Williams LT. A naturally occurring secreted form of fibroblast growth factor (FGF) receptor 1 binds basic FGF in preference over acidic FGF. *J Biol Chem*. 1992;267:16076-16080.
208. Zhang X, Ibrahimi OA, Olsen SK, Umemori H, Mohammadi M, Ornitz DM. Receptor specificity of the fibroblast growth factor family. The complete mammalian FGF family. *J Biol Chem*. 2006;281:15694-15700.
209. Dell'Era P, Presta M, Ragnotti G. Nuclear localization of endogenous basic fibroblast growth factor in cultured endothelial cells. *Exp Cell Res*. 1991;192:505-510.
210. Powers CJ, McLeskey SW, Wellstein A. Fibroblast growth factors, their receptors and signaling. *Endocr Relat Cancer*. 2000;7:165-197.
211. Rusnati M, Dell'Era P, Urbinati C, et al. A distinct basic fibroblast growth factor (FGF-2)/FGF receptor interaction distinguishes urokinase-type plasminogen activator induction from mitogenicity in endothelial cells. *Mol Biol Cell*. 1996;7:369-381.
212. Pantoliano MW, Horlick RA, Springer BA, et al. Multivalent ligand-receptor binding interactions in the fibroblast growth factor system produce a cooperative growth factor and heparin mechanism for receptor dimerization. *Biochemistry*. 1994;33:10229-10248.
213. Ibrahimi OA, Yeh BK, Eliseenkova AV, et al. Analysis of mutations in fibroblast growth factor (FGF) and a pathogenic mutation in FGF receptor (FGFR) provides direct evidence for the symmetric two-end model for FGFR dimerization. *Mol Cell Biol*. 2005;25:671-684.
214. Kan M, Wang F, Xu J, Crabb JW, Hou J, McKeehan WL. An essential heparin-binding domain in the fibroblast growth factor receptor kinase. *Science*. 1993;259:1918-1921.
215. Faham S, Linhardt RJ, Rees DC. Diversity does make a difference: fibroblast growth factor-heparin interactions. *Curr Opin Struct Biol*. 1998;8:578-586.

216. Gallagher JT. Heparan sulphates as membrane receptors for the fibroblast growth factors. *Eur J Clin Chem Clin Biochem.* 1994;32:239-247.
217. Sasisekharan R, Ernst S, Venkataraman G. On the regulation of fibroblast growth factor activity by heparin-like glycosaminoglycans. *Angiogenesis.* 1997;1:45-54.
218. Pellegrini L. Role of heparan sulfate in fibroblast growth factor signalling: a structural view. *Curr Opin Struct Biol.* 2001;11:629-634.
219. DiGabriele AD, Lax I, Chen DI, et al. Structure of a heparin-linked biologically active dimer of fibroblast growth factor. *Nature.* 1998;393:812-817.
220. Goodger SJ, Robinson CJ, Murphy KJ, et al. Evidence that heparin saccharides promote FGF2 mitogenesis through two distinct mechanisms. *J Biol Chem.* 2008;283:13001-13008.
221. Ostrovsky O, Berman B, Gallagher J, et al. Differential effects of heparin saccharides on the formation of specific fibroblast growth factor (FGF) and FGF receptor complexes. *J Biol Chem.* 2002;277:2444-2453.
222. Pye DA, Vives RR, Turnbull JE, Hyde P, Gallagher JT. Heparan sulfate oligosaccharides require 6-O-sulfation for promotion of basic fibroblast growth factor mitogenic activity. *J Biol Chem.* 1998;273:22936-22942.
223. Turnbull JE, Fernig DG, Ke Y, Wilkinson MC, Gallagher JT. Identification of the basic fibroblast growth factor binding sequence in fibroblast heparan sulfate. *J Biol Chem.* 1992;267:10337-10341.
224. Murphy KJ, Merry CL, Lyon M, Thompson JE, Roberts IS, Gallagher JT. A new model for the domain structure of heparan sulfate based on the novel specificity of K5 lyase. *J Biol Chem.* 2004;279:27239-27245.
225. Faham S, Hileman RE, Fromm JR, Linhardt RJ, Rees DC. Heparin structure and interactions with basic fibroblast growth factor. *Science.* 1996;271:1116-1120.
226. Guimond S, Maccarana M, Olwin BB, Lindahl U, Rapraeger AC. Activating and inhibitory heparin sequences for FGF-2 (basic FGF). Distinct requirements for FGF-1, FGF-2, and FGF-4. *J Biol Chem.* 1993;268:23906-23914.
227. Guimond SE, Turnbull JE. Fibroblast growth factor receptor signalling is dictated by specific heparan sulphate saccharides. *Curr Biol.* 1999;9:1343-1346.
228. Kreuger J, Spillmann D, Li JP, Lindahl U. Interactions between heparan sulfate and proteins: the concept of specificity. *J Cell Biol.* 2006;174:323-327.
229. Rudd TR, Skidmore MA, Guimond SE, et al. Site-specific interactions of copper(II) ions with heparin revealed with complementary (SRCD, NMR, FTIR and EPR) spectroscopic techniques. *Carbohydr Res.* 2008;343:2184-2193.
230. Quinn TP, Peters KG, De Vries C, Ferrara N, Williams LT. Fetal liver kinase 1 is a receptor for vascular endothelial growth factor and is selectively expressed in vascular endothelium. *Proc Natl Acad Sci U S A.* 1993;90:7533-7537.
231. Carmeliet P, Collen D. Transgenic mouse models in angiogenesis and cardiovascular disease. *J Pathol.* 2000;190:387-405.
232. Joukov V, Sorsa T, Kumar V, et al. Proteolytic processing regulates receptor specificity and activity of VEGF-C. *Embo J.* 1997;16:3898-3911.
233. Bahary N, Goishi K, Stuckenholtz C, et al. Duplicate VegfA genes and orthologues of the KDR receptor tyrosine kinase family mediate vascular development in the zebrafish. *Blood.* 2007;110:3627-3636.
234. Covassin LD, Villefranc JA, Kacergis MC, Weinstein BM, Lawson ND. Distinct genetic interactions between multiple Vegf receptors are required for development of different blood vessel types in zebrafish. *Proc Natl Acad Sci U S A.* 2006;103:6554-6559.

235. Waltenberger J, Claesson-Welsh L, Siegbahn A, Shibuya M, Heldin CH. Different signal transduction properties of KDR and Flt1, two receptors for vascular endothelial growth factor. *J Biol Chem.* 1994;269:26988-26995.
236. Shalaby F, Rossant J, Yamaguchi TP, et al. Failure of blood-island formation and vasculogenesis in Flk-1-deficient mice. *Nature.* 1995;376:62-66.
237. Fong GH, Zhang L, Bryce DM, Peng J. Increased hemangioblast commitment, not vascular disorganization, is the primary defect in flt-1 knock-out mice. *Development.* 1999;126:3015-3025.
238. Holmqvist K, Cross MJ, Rolny C, et al. The adaptor protein shb binds to tyrosine 1175 in vascular endothelial growth factor (VEGF) receptor-2 and regulates VEGF-dependent cellular migration. *J Biol Chem.* 2004;279:22267-22275.
239. Dayanir V, Meyer RD, Lashkari K, Rahimi N. Identification of tyrosine residues in vascular endothelial growth factor receptor-2/FLK-1 involved in activation of phosphatidylinositol 3-kinase and cell proliferation. *J Biol Chem.* 2001;276:17686-17692.
240. Takahashi T, Yamaguchi S, Chida K, Shibuya M. A single autophosphorylation site on KDR/Flk-1 is essential for VEGF-A-dependent activation of PLC-gamma and DNA synthesis in vascular endothelial cells. *Embo J.* 2001;20:2768-2778.
241. Matsumoto T, Claesson-Welsh L. VEGF receptor signal transduction. *Sci STKE.* 2001;2001:RE21.
242. Hiratsuka S, Minowa O, Kuno J, Noda T, Shibuya M. Flt-1 lacking the tyrosine kinase domain is sufficient for normal development and angiogenesis in mice. *Proc Natl Acad Sci U S A.* 1998;95:9349-9354.
243. Park JE, Chen HH, Winer J, Houck KA, Ferrara N. Placenta growth factor. Potentiation of vascular endothelial growth factor bioactivity, in vitro and in vivo, and high affinity binding to Flt-1 but not to Flk-1/KDR. *J Biol Chem.* 1994;269:25646-25654.
244. Goishi K, Klagsbrun M. Vascular endothelial growth factor and its receptors in embryonic zebrafish blood vessel development. *Curr Top Dev Biol.* 2004;62:127-152.
245. Tammela T, Zarkada G, Wallgard E, et al. Blocking VEGFR-3 suppresses angiogenic sprouting and vascular network formation. *Nature.* 2008;454:656-660.
246. Siekmann AF, Lawson ND. Notch signalling and the regulation of angiogenesis. *Cell Adh Migr.* 2007;1:104-106.
247. Cao Y, Linden P, Farnebo J, et al. Vascular endothelial growth factor C induces angiogenesis in vivo. *Proc Natl Acad Sci U S A.* 1998;95:14389-14394.
248. Jeltsch M, Kaipainen A, Joukov V, et al. Hyperplasia of lymphatic vessels in VEGF-C transgenic mice. *Science.* 1997;276:1423-1425.
249. Oh SJ, Jeltsch MM, Birkenhager R, et al. VEGF and VEGF-C: specific induction of angiogenesis and lymphangiogenesis in the differentiated avian chorioallantoic membrane. *Dev Biol.* 1997;188:96-109.
250. Witzensichler B, Asahara T, Murohara T, et al. Vascular endothelial growth factor-C (VEGF-C/VEGF-2) promotes angiogenesis in the setting of tissue ischemia. *Am J Pathol.* 1998;153:381-394.
251. Dixelius J, Makinen T, Wirzenius M, et al. Ligand-induced vascular endothelial growth factor receptor-3 (VEGFR-3) heterodimerization with VEGFR-2 in primary lymphatic endothelial cells regulates tyrosine phosphorylation sites. *J Biol Chem.* 2003;278:40973-40979.
252. Hamada K, Oike Y, Takakura N, et al. VEGF-C signaling pathways through VEGFR-2 and VEGFR-3 in vasculoangiogenesis and hematopoiesis. *Blood.* 2000;96:3793-3800.
253. Matsumura K, Hirashima M, Ogawa M, et al. Modulation of VEGFR-2-mediated endothelial-cell activity by VEGF-C/VEGFR-3. *Blood.* 2003;101:1367-1374.

254. Kuchler AM, Gjini E, Peterson-Maduro J, Cancilla B, Wolburg H, Schulte-Merker S. Development of the zebrafish lymphatic system requires VEGFC signaling. *Curr Biol.* 2006;16:1244-1248.
255. Soker S, Fidler IJ, Neufeld G, Klagsbrun M. Characterization of novel vascular endothelial growth factor (VEGF) receptors on tumor cells that bind VEGF165 via its exon 7-encoded domain. *J Biol Chem.* 1996;271:5761-5767.
256. Soker S, Takashima S, Miao HQ, Neufeld G, Klagsbrun M. Neuropilin-1 is expressed by endothelial and tumor cells as an isoform-specific receptor for vascular endothelial growth factor. *Cell.* 1998;92:735-745.
257. Woolard J, Wang WY, Bevan HS, et al. VEGF165b, an inhibitory vascular endothelial growth factor splice variant: mechanism of action, in vivo effect on angiogenesis and endogenous protein expression. *Cancer Res.* 2004;64:7822-7835.
258. Bates DO, Harper SJ. Regulation of vascular permeability by vascular endothelial growth factors. *Vascul Pharmacol.* 2002;39:225-237.
259. Tischer E, Mitchell R, Hartman T, et al. The human gene for vascular endothelial growth factor. Multiple protein forms are encoded through alternative exon splicing. *J Biol Chem.* 1991;266:11947-11954.
260. Poltorak Z, Cohen T, Neufeld G. The VEGF splice variants: Properties, receptors, and usage for the treatment of ischemic diseases. *Herz.* 2000;25:126.
261. Houck KA, Leung DW, Rowland AM, Winer J, Ferrara N. Dual regulation of vascular endothelial growth factor bioavailability by genetic and proteolytic mechanisms. *J Biol Chem.* 1992;267:26031-26037.
262. Plouet J, Moro F, Bertagnolli S, et al. Extracellular cleavage of the vascular endothelial growth factor 189-amino acid form by urokinase is required for its mitogenic effect. *J Biol Chem.* 1997;272:13390-13396.
263. Liang D, Chang JR, Chin AJ, et al. The role of vascular endothelial growth factor (VEGF) in vasculogenesis, angiogenesis, and hematopoiesis in zebrafish development. *Mech Dev.* 2001;108:29-43.
264. Stalmans I, Ng YS, Rohan R, et al. Arteriolar and venular patterning in retinas of mice selectively expressing VEGF isoforms. *J Clin Invest.* 2002;109:327-336.
265. Ruhrberg C, Gerhardt H, Golding M, et al. Spatially restricted patterning cues provided by heparin-binding VEGF-A control blood vessel branching morphogenesis. *Genes Dev.* 2002;16:2684-2698.
266. Glass CA, Harper SJ, Bates DO. The anti-angiogenic VEGF isoform VEGF165b transiently increases hydraulic conductivity, probably through VEGF receptor 1 in vivo. *J Physiol.* 2006;572:243-257.
267. Gerber HP, Hillan KJ, Ryan AM, et al. VEGF is required for growth and survival in neonatal mice. *Development.* 1999;126:1149-1159.
268. Shalaby F, Ho J, Stanford WL, et al. A requirement for Flk1 in primitive and definitive hematopoiesis and vasculogenesis. *Cell.* 1997;89:981-990.
269. Clauss M. Functions of the VEGF receptor-1 (FLT-1) in the vasculature. *Trends Cardiovasc Med.* 1998;8:241-245.
270. Dvorak HF, Brown LF, Detmar M, Dvorak AM. Vascular permeability factor/vascular endothelial growth factor, microvascular hyperpermeability, and angiogenesis. *Am J Pathol.* 1995;146:1029-1039.
271. Habeck H, Odenthal J, Walderich B, Maischein H, Schulte-Merker S. Analysis of a zebrafish VEGF receptor mutant reveals specific disruption of angiogenesis. *Curr Biol.* 2002;12:1405-1412.

272. Terman B, Khandke L, Dougher-Vermazan M, et al. VEGF receptor subtypes KDR and FLT1 show different sensitivities to heparin and placenta growth factor. *Growth Factors*. 1994;11:187-195.
273. Cohen T, Gitay-Goren H, Sharon R, et al. VEGF121, a vascular endothelial growth factor (VEGF) isoform lacking heparin binding ability, requires cell-surface heparan sulfates for efficient binding to the VEGF receptors of human melanoma cells. *J Biol Chem*. 1995;270:11322-11326.
274. Ashikari-Hada S, Habuchi H, Kariya Y, Kimata K. Heparin regulates vascular endothelial growth factor165-dependent mitogenic activity, tube formation, and its receptor phosphorylation of human endothelial cells. Comparison of the effects of heparin and modified heparins. *J Biol Chem*. 2005;280:31508-31515.
275. Ruhrberg C. Growing and shaping the vascular tree: multiple roles for VEGF. *Bioessays*. 2003;25:1052.
276. Gengrinovitch S, Greenberg SM, Cohen T, et al. Platelet factor-4 inhibits the mitogenic activity of VEGF121 and VEGF165 using several concurrent mechanisms. *J Biol Chem*. 1995;270:15059-15065.
277. Lee P, Goishi K, Davidson AJ, Mannix R, Zon L, Klagsbrun M. Neuropilin-1 is required for vascular development and is a mediator of VEGF-dependent angiogenesis in zebrafish. *Proc Natl Acad Sci U S A*. 2002;99:10470-10475.
278. Olsson AK, Dimberg A, Kreuger J, Claesson-Welsh L. VEGF receptor signalling - in control of vascular function. *Nat Rev Mol Cell Biol*. 2006;7:359-371.
279. Ashikari- Hada S, Habuchi H, Kariya Y, Kimata K. Heparin regulates vascular endothelial growth factor(165)-dependent mitogenic activity, tube formation, and its receptor phosphorylation of human endothelial cells - Comparison of the effects of heparin and modified heparins. *Journal Of Biological Chemistry*. 2005;280:31508.
280. Kendall RL, Wang G, Thomas KA. Identification of a natural soluble form of the vascular endothelial growth factor receptor, FLT-1, and its heterodimerization with KDR. *Biochem Biophys Res Commun*. 1996;226:324-328.
281. Dougher AM, Wasserstrom H, Torley L, et al. Identification of a heparin binding peptide on the extracellular domain of the KDR VEGF receptor. *Growth Factors*. 1997;14:257.
282. Ono K, Hattori H, Takeshita S, Kurita A, Ishihara M. Structural features in heparin that interact with VEGF165 and modulate its biological activity. *Glycobiology*. 1999;9:705-711.
283. Robinson CJ, Mulloy B, Gallagher JT, Stringer SE. VEGF165 binding sites within heparan sulfate encompass two highly sulfated domains and can be liberated by K5 lyase. *J Biol Chem*. 2005.
284. Presta M, Leali D, Stabile H, et al. Heparin derivatives as angiogenesis inhibitors. *Curr Pharm Des*. 2003;9:553-566.
285. Hricovini M, Guerrini M, Bisio A, Torri G, Petitou M, Casu B. Conformation of heparin pentasaccharide bound to antithrombin III. *Biochem J*. 2001;359:265-272.
286. Maurer AM, Zhou B, Han ZC. Roles of platelet factor 4 in hematopoiesis and angiogenesis. *Growth Factors*. 2006;24:242-252.
287. Eslin DE, Zhang C, Samuels KJ, et al. Transgenic mice studies demonstrate a role for platelet factor 4 in thrombosis: dissociation between anticoagulant and antithrombotic effect of heparin. *Blood*. 2004;104:3173-3180.
288. Deitcher SR, Carman TL. Heparin-induced thrombocytopenia: natural history, diagnosis, and management. *Vasc Med*. 2001;6:113-119.

289. Soker S, Goldstaub D, Svahn CM, Vlodayvsky I, Levi BZ, Neufeld G. Variations in the size and sulfation of heparin modulate the effect of heparin on the binding of VEGF165 to its receptors. *Biochem Biophys Res Commun.* 1994;203:1339-1347.
290. Hasan J, Shnyder SD, Clamp AR, et al. Heparin octasaccharides inhibit angiogenesis in vivo. *Clin Cancer Res.* 2005;11:8172-8179.
291. Jayson GC, Gallagher JT. Heparin oligosaccharides: inhibitors of the biological activity of bFGF on Caco-2 cells. *Br J Cancer.* 1997;75:9-16.
292. Smorenburg SM, Vink R, te Lintelo M, et al. In vivo treatment of rats with unfractionated heparin (UFH) or low molecular weight heparin (LMWH) does not affect experimentally induced colon carcinoma metastasis. *Clin Exp Metastasis.* 1999;17:451-456.
293. Kakkar AK, Levine MN, Kadziola Z, et al. Low molecular weight heparin, therapy with dalteparin, and survival in advanced cancer: the fragmin advanced malignancy outcome study (FAMOUS). *J Clin Oncol.* 2004;22:1944-1948.
294. Sugahara K, Kitagawa H. Heparin and heparan sulfate biosynthesis. *IUBMB Life.* 2002;54:163-175.
295. Habuchi H, Habuchi O, Kimata K. Sulfation pattern in glycosaminoglycan: does it have a code? *Glycoconj J.* 2004;21:47-52.
296. Kokenyesi R, Bernfield M. Core protein structure and sequence determine the site and presence of heparan sulfate and chondroitin sulfate on syndecan-1. *J Biol Chem.* 1994;269:12304-12309.
297. Zhang L, David G, Esko JD. Repetitive Ser-Gly sequences enhance heparan sulfate assembly in proteoglycans. *J Biol Chem.* 1995;270:27127-27135.
298. Lin X, Wei G, Shi Z, et al. Disruption of gastrulation and heparan sulfate biosynthesis in EXT1-deficient mice. *Dev Biol.* 2000;224:299-311.
299. Inatani M, Yamaguchi Y. Gene expression of EXT1 and EXT2 during mouse brain development. *Brain Res Dev Brain Res.* 2003;141:129-136.
300. Nybakken K, Perrimon N. Hedgehog signal transduction: recent findings. *Curr Opin Genet Dev.* 2002;12:503-511.
301. Duncan G, McCormick C, Tufaro F. The link between heparan sulfate and hereditary bone disease: finding a function for the EXT family of putative tumor suppressor proteins. *J Clin Invest.* 2001;108:511-516.
302. Siekmann AF, Brand M. Distinct tissue-specificity of three zebrafish ext1 genes encoding proteoglycan modifying enzymes and their relationship to somitic Sonic hedgehog signaling. *Dev Dyn.* 2005;232:498-505.
303. Norton WH, Ledin J, Grandel H, Neumann CJ. HSPG synthesis by zebrafish Ext2 and Extl3 is required for Fgf10 signalling during limb development. *Development.* 2005;132:4963-4973.
304. Schilling TF, Piotrowski T, Grandel H, et al. Jaw and branchial arch mutants in zebrafish I: branchial arches. *Development.* 1996;123:329-344.
305. Lee JS, von der Hardt S, Rusch MA, et al. Axon sorting in the optic tract requires HSPG synthesis by ext2 (dackel) and extl3 (boxer). *Neuron.* 2004;44:947-960.
306. Aikawa J, Esko JD. Molecular cloning and expression of a third member of the heparan sulfate/heparin GlcNAc N-deacetylase/ N-sulfotransferase family. *J Biol Chem.* 1999;274:2690-2695.
307. Aikawa J. [Functional roles of GlcNAc N-deacetylase/GlcN N-sulfotransferases in the biosynthesis of heparan sulfate/heparin]. *Seikagaku.* 2001;73:479-483.
308. Forsberg E, Pejler G, Ringvall M, et al. Abnormal mast cells in mice deficient in a heparin-synthesizing enzyme. *Nature.* 1999;400:773-776.

309. Aikawa J, Grobe K, Tsujimoto M, Esko JD. Multiple isozymes of heparan sulfate/heparin GlcNAc N-deacetylase/GlcN N-sulfotransferase. Structure and activity of the fourth member, NDST4. *J Biol Chem.* 2001;276:5876-5882.
310. Forsberg E, Kjellen L. Heparan sulfate: lessons from knockout mice. *J Clin Invest.* 2001;108:175-180.
311. Humphries DE, Wong GW, Friend DS, et al. Heparin is essential for the storage of specific granule proteases in mast cells. *Nature.* 1999;400:769-772.
312. Grobe K, Ledin J, Ringvall M, et al. Heparan sulfate and development: differential roles of the N-acetylglucosamine N-deacetylase/N-sulfotransferase isozymes. *Biochim Biophys Acta.* 2002;1573:209-215.
313. Grobe K, Inatani M, Pallerla SR, Castagnola J, Yamaguchi Y, Esko JD. Cerebral hypoplasia and craniofacial defects in mice lacking heparan sulfate Ndst1 gene function. *Development.* 2005;132:3777-3786.
314. Hagner-McWhirter A, Li JP, Oscarson S, Lindahl U. Irreversible glucuronyl C5-epimerization in the biosynthesis of heparan sulfate. *J Biol Chem.* 2004;279:14631-14638.
315. Rong J, Habuchi H, Kimata K, Lindahl U, Kusche-Gullberg M. Substrate specificity of the heparan sulfate hexuronic acid 2-O-sulfotransferase. *Biochemistry.* 2001;40:5548-5555.
316. Feyerabend TB, Li JP, Lindahl U, Rodewald HR. Heparan sulfate C5-epimerase is essential for heparin biosynthesis in mast cells. *Nat Chem Biol.* 2006;2:195-196.
317. Li JP, Gong F, Hagner-McWhirter A, et al. Targeted disruption of a murine glucuronyl C5-epimerase gene results in heparan sulfate lacking L-iduronic acid and in neonatal lethality. *J Biol Chem.* 2003;278:28363-28366.
318. Ghiselli G, Farber SA. D-glucuronyl C5-epimerase acts in dorso-ventral axis formation in zebrafish. *BMC Dev Biol.* 2005;5:19.
319. Kusche M, Oscarsson LG, Reynertson R, Roden L, Lindahl U. Biosynthesis of heparin. Enzymatic sulfation of pentasaccharides. *J Biol Chem.* 1991;266:7400-7409.
320. Safaiyan F, Lindahl U, Salmivirta M. Structural diversity of N-sulfated heparan sulfate domains: distinct modes of glucuronyl C5 epimerization, iduronic acid 2-O-sulfation, and glucosamine 6-O-sulfation. *Biochemistry.* 2000;39:10823-10830.
321. Bullock SL, Fletcher JM, Beddington RS, Wilson VA. Renal agenesis in mice homozygous for a gene trap mutation in the gene encoding heparan sulfate 2-sulfotransferase. *Genes Dev.* 1998;12:1894-1906.
322. Merry CL, Bullock SL, Swan DC, et al. The molecular phenotype of heparan sulfate in the Hs2st<sup>-/-</sup> mutant mouse. *J Biol Chem.* 2001;276:35429-35434.
323. Kamimura K, Koyama T, Habuchi H, et al. Specific and flexible roles of heparan sulfate modifications in Drosophila FGF signaling. *J Cell Biol.* 2006;174:773-778.
324. Habuchi H, Miyake G, Nogami K, et al. Biosynthesis of heparan sulphate with diverse structures and functions: two alternatively spliced forms of human heparan sulphate 6-O-sulphotransferase-2 having different expression patterns and properties. *Biochem J.* 2003;371:131-142.
325. Habuchi H, Tanaka M, Habuchi O, et al. The occurrence of three isoforms of heparan sulfate 6-O-sulphotransferase having different specificities for hexuronic acid adjacent to the targeted N-sulfoglucosamine. *J Biol Chem.* 2000;275:2859-2868.
326. Smeds E, Habuchi H, Do AT, et al. Substrate specificities of mouse heparan sulphate glucosaminyl 6-O-sulphotransferases. *Biochem J.* 2003;372:371-380.
327. Sugaya N, Habuchi H, Nagai N, Ashikari-Hada S, Kimata K. 6-O-sulfation of heparan sulfate differentially regulates various fibroblast growth factor-dependent signalings in culture. *J Biol Chem.* 2008;283:10366-10376.

328. Cadwallader AB, Yost HJ. Combinatorial expression patterns of heparan sulfate sulfotransferases in zebrafish: II. The 6-O-sulfotransferase family. *Dev Dyn*. 2006;235:3432-3437.
329. Chen E, Stringer SE, Rusch MA, Selleck SB, Ekker SC. A unique role for 6-O sulfation modification in zebrafish vascular development. *Dev Biol*. 2005;284:364-376.
330. Bink RJ, Habuchi H, Lele Z, et al. Heparan sulfate 6-o-sulfotransferase is essential for muscle development in zebrafish. *J Biol Chem*. 2003;278:31118-31127.
331. Yabe T, Hata T, He J, Maeda N. Developmental and regional expression of heparan sulfate sulfotransferase genes in the mouse brain. *Glycobiology*. 2005;15:982-993.
332. Liu J, Shriver Z, Blaiklock P, Yoshida K, Sasisekharan R, Rosenberg RD. Heparan sulfate D-glucosaminyl 3-O-sulfotransferase-3A sulfates N-unsubstituted glucosamine residues. *J Biol Chem*. 1999;274:38155-38162.
333. Xia G, Chen J, Tiwari V, et al. Heparan sulfate 3-O-sulfotransferase isoform 5 generates both an antithrombin-binding site and an entry receptor for herpes simplex virus, type 1. *J Biol Chem*. 2002;277:37912-37919.
334. Liu J, Shworak NW, Sinay P, et al. Expression of heparan sulfate D-glucosaminyl 3-O-sulfotransferase isoforms reveals novel substrate specificities. *J Biol Chem*. 1999;274:5185-5192.
335. Liu J, Shworak NW, Fritze LM, Edelberg JM, Rosenberg RD. Purification of heparan sulfate D-glucosaminyl 3-O-sulfotransferase. *J Biol Chem*. 1996;271:27072-27082.
336. HajMohammadi S, Enyoji K, Princivalle M, et al. Normal levels of anticoagulant heparan sulfate are not essential for normal hemostasis. *J Clin Invest*. 2003;111:989-999.
337. Shukla D, Liu J, Blaiklock P, et al. A novel role for 3-O-sulfated heparan sulfate in herpes simplex virus 1 entry. *Cell*. 1999;99:13-22.
338. Chen J, Liu J. Characterization of the structure of antithrombin-binding heparan sulfate generated by heparan sulfate 3-O-sulfotransferase 5. *Biochim Biophys Acta*. 2005;1725:190-200.
339. Kamimura K, Rhodes JM, Ueda R, et al. Regulation of Notch signaling by Drosophila heparan sulfate 3-O sulfotransferase. *J Cell Biol*. 2004;166:1069-1079.
340. Dierks T, Lecca MR, Schlotterhose P, Schmidt B, von Figura K. Sequence determinants directing conversion of cysteine to formylglycine in eukaryotic sulfatases. *Embo J*. 1999;18:2084-2091.
341. Fey J, Balleininger M, Borissenko LV, Schmidt B, von Figura K, Dierks T. Characterization of posttranslational formylglycine formation by luminal components of the endoplasmic reticulum. *J Biol Chem*. 2001;276:47021-47028.
342. von Bulow R, Schmidt B, Dierks T, von Figura K, Uson I. Crystal structure of an enzyme-substrate complex provides insight into the interaction between human arylsulfatase A and its substrates during catalysis. *J Mol Biol*. 2001;305:269-277.
343. Ambasta RK, Ai X, Emerson CP, Jr. Quail Sulf1 function requires asparagine-linked glycosylation. *J Biol Chem*. 2007;282:34492-34499.
344. Ai X, Do AT, Kusche-Gullberg M, Lindahl U, Lu K, Emerson CP, Jr. Substrate specificity and domain functions of extracellular heparan sulfate 6-O-endosulfatases, QSulf1 and QSulf2. *J Biol Chem*. 2006;281:4969-4976.
345. Frese MA, Milz F, Dick M, Lamanna WC, Dierks T. Characterization of the human sulfatase sulf1 and its high-affinity heparin/heparan sulfate interaction domain. *J Biol Chem*. 2009.
346. Tang R, Rosen SD. Functional consequences of the subdomain organization of the sulfs. *J Biol Chem*. 2009.

347. Lamanna WC, Frese MA, Balleininger M, Dierks T. Sulf loss influences N-, 2-O-, and 6-O-sulfation of multiple heparan sulfate proteoglycans and modulates fibroblast growth factor signaling. *J Biol Chem*. 2008;283:27724-27735.
348. Morimoto-Tomita M, Uchimura K, Werb Z, Hemmerich S, Rosen SD. Cloning and characterization of two extracellular heparin-degrading endosulfatases in mice and humans. *J Biol Chem*. 2002;277:49175-49185.
349. Lamanna WC, Baldwin RJ, Padva M, et al. Heparan sulfate 6-O-endosulfatases: discrete in vivo activities and functional co-operativity. *Biochem J*. 2006;400:63-73.
350. Dhoot GK, Gustafsson MK, Ai X, Sun W, Standiford DM, Emerson CP, Jr. Regulation of Wnt signaling and embryo patterning by an extracellular sulfatase. *Science*. 2001;293:1663-1666.
351. Wang S, Ai X, Freeman SD, et al. QSulf1, a heparan sulfate 6-O-endosulfatase, inhibits fibroblast growth factor signaling in mesoderm induction and angiogenesis. *Proc Natl Acad Sci U S A*. 2004;101:4833-4838.
352. Freeman SD, Moore WM, Guiral EC, Holme AD, Turnbull JE, Pownall ME. Extracellular regulation of developmental cell signaling by XtSulf1. *Dev Biol*. 2008;320:436-445.
353. Paine-Saunders S, Viviano BL, Zupicich J, Skarnes WC, Saunders S. glypican-3 controls cellular responses to Bmp4 in limb patterning and skeletal development. *Dev Biol*. 2000;225:179-187.
354. Viviano BL, Paine-Saunders S, Gasiunas N, Gallagher J, Saunders S. Domain-specific modification of heparan sulfate by Qsulf1 modulates the binding of the bone morphogenetic protein antagonist Noggin. *J Biol Chem*. 2004;279:5604-5611.
355. Danesin C, Agius E, Escalas N, et al. Ventral neural progenitors switch toward an oligodendroglial fate in response to increased Sonic hedgehog (Shh) activity: involvement of Sulfatase 1 in modulating Shh signaling in the ventral spinal cord. *J Neurosci*. 2006;26:5037-5048.
356. Uchimura K, Morimoto-Tomita M, Bistrup A, et al. HSulf-2, an extracellular endoglucosamine-6-sulfatase, selectively mobilizes heparin-bound growth factors and chemokines: effects on VEGF, FGF-1, and SDF-1. *BMC Biochem*. 2006;7:2.
357. Holst CR, Bou-Reslan H, Gore BB, et al. Secreted sulfatases Sulf1 and Sulf2 have overlapping yet essential roles in mouse neonatal survival. *PLoS One*. 2007;2:e575.
358. Ratzka A, Kalus I, Moser M, Dierks T, Mundlos S, Vortkamp A. Redundant function of the heparan sulfate 6-O-endosulfatases Sulf1 and Sulf2 during skeletal development. *Dev Dyn*. 2008;237:339-353.
359. Lum DH, Tan J, Rosen SD, Werb Z. Gene trap disruption of the mouse heparan sulfate 6-O-endosulfatase, Sulf2. *Mol Cell Biol*. 2006.
360. Ai X, Kitazawa T, Do AT, Kusche-Gullberg M, Labosky PA, Emerson CP, Jr. SULF1 and SULF2 regulate heparan sulfate-mediated GDNF signaling for esophageal innervation. *Development*. 2007;134:3327-3338.
361. Kalus I, Salmen B, Viebahn C, et al. Differential Involvement of the Extracellular 6-O-Endosulfatases Sulf1 and Sulf2 in Brain Development and Neuronal and Behavioral Plasticity. *J Cell Mol Med*. 2008.
362. Winterbottom EF, Pownall ME. Complementary expression of HSPG 6-O-endosulfatases and 6-O-sulfotransferase in the hindbrain of *Xenopus laevis*. *Gene Expr Patterns*. 2009;9:166-172.
363. Lai JP, Chien JR, Moser DR, et al. hSulf1 Sulfatase promotes apoptosis of hepatocellular cancer cells by decreasing heparin-binding growth factor signaling. *Gastroenterology*. 2004;126:231-248.

364. Lai JP, Sandhu DS, Shire AM, Roberts LR. The Tumor Suppressor Function of Human Sulfatase 1 (SULF1) in Carcinogenesis. *J Gastrointest Cancer*. 2008;39:149-158.
365. Lai JP, Yu C, Moser CD, et al. SULF1 inhibits tumor growth and potentiates the effects of histone deacetylase inhibitors in hepatocellular carcinoma. *Gastroenterology*. 2006;130:2130-2144.
366. Lai JP, Chien J, Strome SE, et al. HSulf-1 modulates HGF-mediated tumor cell invasion and signaling in head and neck squamous carcinoma. *Oncogene*. 2004;23:1439-1447.
367. Narita K, Chien J, Mullany SA, et al. Loss of HSulf-1 expression enhances autocrine signaling mediated by amphiregulin in breast cancer. *J Biol Chem*. 2007;282:14413-14420.
368. Narita K, Staub J, Chien J, et al. HSulf-1 inhibits angiogenesis and tumorigenesis in vivo. *Cancer Res*. 2006;66:6025-6032.
369. Sala-Newby GB, George SJ, Bond M, Dhoot GK, Newby AC. Regulation of vascular smooth muscle cell proliferation, migration and death by heparan sulfate 6-O-endosulfatase1. *FEBS Lett*. 2005;579:6493-6498.
370. Nawroth R, van Zante A, Cervantes S, McManus M, Hebrok M, Rosen SD. Extracellular sulfatases, elements of the Wnt signaling pathway, positively regulate growth and tumorigenicity of human pancreatic cancer cells. *PLoS One*. 2007;2:e392.
371. Dai Y, Yang Y, MacLeod V, et al. HSulf-1 and HSulf-2 are potent inhibitors of myeloma tumor growth in vivo. *J Biol Chem*. 2005;280:40066-40073.
372. Lai JP, Thompson JR, Sandhu DS, Roberts LR. Heparin-degrading sulfatases in hepatocellular carcinoma: roles in pathogenesis and therapy targets. *Future Oncol*. 2008;4:803-814.
373. Morimoto-Tomita M, Uchimura K, Bistrup A, et al. Sulf-2, a proangiogenic heparan sulfate endosulfatase, is upregulated in breast cancer. *Neoplasia*. 2005;7:1001-1010.
374. Backen AC, Cole CL, Lau SC, et al. Heparan sulphate synthetic and editing enzymes in ovarian cancer. *Br J Cancer*. 2007;96:1544-1548.
375. Pinhal MA, Smith B, Olson S, Aikawa J, Kimata K, Esko JD. Enzyme interactions in heparan sulfate biosynthesis: uronosyl 5-epimerase and 2-O-sulfotransferase interact in vivo. *Proc Natl Acad Sci U S A*. 2001;98:12984-12989.
376. Senay C, Lind T, Muguruma K, et al. The EXT1/EXT2 tumor suppressors: catalytic activities and role in heparan sulfate biosynthesis. *EMBO Rep*. 2000;1:282-286.
377. Yue X, Li X, Nguyen HT, Chin DR, Sullivan DE, Lasky JA. Transforming growth factor-beta1 induces heparan sulfate 6-O-endosulfatase 1 expression in vitro and in vivo. *J Biol Chem*. 2008;283:20397-20407.
378. Traver D, Herbomel P, Patton EE, et al. The zebrafish as a model organism to study development of the immune system. *Adv Immunol*. 2003;81:253-330.
379. Cross LM, Cook MA, Lin S, Chen JN, Rubinstein AL. Rapid analysis of angiogenesis drugs in a live fluorescent zebrafish assay. *Arterioscler Thromb Vasc Biol*. 2003;23:911-912.
380. Kimmel CB, Ballard WW, Kimmel SR, Ullmann B, Schilling TF. Stages of embryonic development of the zebrafish. *Dev Dyn*. 1995;203:253-310.
381. Winnier G, Blessing M, Labosky PA, Hogan BL. Bone morphogenetic protein-4 is required for mesoderm formation and patterning in the mouse. *Genes Dev*. 1995;9:2105-2116.
382. Goodwin AM, D'Amore PA. Wnt signaling in the vasculature. *Angiogenesis*. 2002;5:1-9.
383. Habuchi H, Nagai N, Sugaya N, Atsumi F, Stevens RL, Kimata K. Mice deficient in heparan sulfate 6-O-sulfotransferase-1 exhibit defective heparan sulfate biosynthesis, abnormal placentation, and late embryonic lethality. *J Biol Chem*. 2007;282:15578-15588.
384. Morcos PA. Achieving targeted and quantifiable alteration of mRNA splicing with Morpholino oligos. *Biochem Biophys Res Commun*. 2007;358:521-527.

385. Corey DR, Abrams JM. Morpholino antisense oligonucleotides: tools for investigating vertebrate development. *Genome Biol.* 2001;2:REVIEWS1015.
386. Heasman J. Morpholino oligos: making sense of antisense? *Dev Biol.* 2002;243:209-214.
387. Summerton J, Weller D. Morpholino antisense oligomers: design, preparation, and properties. *Antisense Nucleic Acid Drug Dev.* 1997;7:187-195.
388. Summerton J. Morpholino antisense oligomers: the case for an RNase H-independent structural type. *Biochim Biophys Acta.* 1999;1489:141-158.
389. Draper BW, Morcos PA, Kimmel CB. Inhibition of zebrafish *fgf8* pre-mRNA splicing with morpholino oligos: a quantifiable method for gene knockdown. *Genesis.* 2001;30:154-156.
390. Nasevicius A, Ekker SC. Effective targeted gene 'knockdown' in zebrafish. *Nat Genet.* 2000;26:216-220.
391. Lele Z, Bakkers J, Hammerschmidt M. Morpholino phenocopies of the swirl, snailhouse, somitabun, minifin, silberblick, and pipetail mutations. *Genesis.* 2001;30:190-194.
392. Wheeler DL, Church DM, Federhen S, et al. Database resources of the National Center for Biotechnology. *Nucleic Acids Res.* 2003;31:28-33.
393. Desai UR, Wang HM, Linhardt RJ. Substrate specificity of the heparin lyases from *Flavobacterium heparinum*. *Arch Biochem Biophys.* 1993;306:461-468.
394. Nader HB, Porcionatto MA, Tersariol IL, et al. Purification and substrate specificity of heparitinase I and heparitinase II from *Flavobacterium heparinum*. Analyses of the heparin and heparan sulfate degradation products by <sup>13</sup>C NMR spectroscopy. *J Biol Chem.* 1990;265:16807-16813.
395. Robu ME, Larson JD, Nasevicius A, et al. p53 activation by knockdown technologies. *PLoS Genet.* 2007;3:e78.
396. Berghmans S, Murphey RD, Wienholds E, et al. tp53 mutant zebrafish develop malignant peripheral nerve sheath tumors. *Proc Natl Acad Sci U S A.* 2005;102:407-412.
397. Donehower LA, Harvey M, Slagle BL, et al. Mice deficient for p53 are developmentally normal but susceptible to spontaneous tumours. *Nature.* 1992;356:215-221.
398. Nasevicius A, Larson J, Ekker SC. Distinct requirements for zebrafish angiogenesis revealed by a VEGF-A morphant. *Yeast.* 2000;17:294-301.
399. Hentze MW, Kulozik AE. A perfect message: RNA surveillance and nonsense-mediated decay. *Cell.* 1999;96:307-310.
400. Chang YF, Imam JS, Wilkinson MF. The nonsense-mediated decay RNA surveillance pathway. *Annu Rev Biochem.* 2007;76:51-74.
401. Sivasubbu S, Balciunas D, Amsterdam A, Ekker SC. Insertional mutagenesis strategies in zebrafish. *Genome Biol.* 2007;8 Suppl 1:S9.
402. Pfaff KL, Straub CT, Chiang K, Bear DM, Zhou Y, Zon LI. The zebra fish *cassiopeia* mutant reveals that SIL is required for mitotic spindle organization. *Mol Cell Biol.* 2007;27:5887-5897.
403. Owens KN, Santos F, Roberts B, et al. Identification of genetic and chemical modulators of zebrafish mechanosensory hair cell death. *PLoS Genet.* 2008;4:e1000020.
404. Hall TE, Bryson-Richardson RJ, Berger S, et al. The zebrafish candyfloss mutant implicates extracellular matrix adhesion failure in laminin alpha2-deficient congenital muscular dystrophy. *Proc Natl Acad Sci U S A.* 2007;104:7092-7097.
405. Hammerschmidt M, Bitgood MJ, McMahon AP. Protein kinase A is a common negative regulator of Hedgehog signaling in the vertebrate embryo. *Genes Dev.* 1996;10:647-658.
406. Hatta K, Kimmel CB, Ho RK, Walker C. The cyclops mutation blocks specification of the floor plate of the zebrafish central nervous system. *Nature.* 1991;350:339-341.

407. Schier AF, Neuhauss SC, Harvey M, et al. Mutations affecting the development of the embryonic zebrafish brain. *Development*. 1996;123:165-178.
408. Ekker SC, Ungar AR, Greenstein P, et al. Patterning activities of vertebrate hedgehog proteins in the developing eye and brain. *Curr Biol*. 1995;5:944-955.
409. Schier AF, Neuhauss SC, Helde KA, Talbot WS, Driever W. The one-eyed pinhead gene functions in mesoderm and endoderm formation in zebrafish and interacts with no tail. *Development*. 1997;124:327-342.
410. Heisenberg CP, Brand M, Jiang YJ, et al. Genes involved in forebrain development in the zebrafish, *Danio rerio*. *Development*. 1996;123:191-203.
411. Solnica-Krezel L, Stemple DL, Mountcastle-Shah E, et al. Mutations affecting cell fates and cellular rearrangements during gastrulation in zebrafish. *Development*. 1996;123:67-80.
412. Zhao W, Sala-Newby GB, Dhoot GK. *Sulf1* expression pattern and its role in cartilage and joint development. *Dev Dyn*. 2006;235:3327-3335.
413. Bulow HE, Boulin T, Hobert O. Differential functions of the *C. elegans* FGF receptor in axon outgrowth and maintenance of axon position. *Neuron*. 2004;42:367-374.
414. Pratt T, Conway CD, Tian NM, Price DJ, Mason JO. Heparan sulphation patterns generated by specific heparan sulfotransferase enzymes direct distinct aspects of retinal axon guidance at the optic chiasm. *J Neurosci*. 2006;26:6911-6923.
415. Harrington LS, Sainson RC, Williams CK, et al. Regulation of multiple angiogenic pathways by *Dll4* and Notch in human umbilical vein endothelial cells. *Microvasc Res*. 2008;75:144-154.
416. Zhang G, Zhou J, Fan Q, et al. Arterial-venous endothelial cell fate is related to vascular endothelial growth factor and Notch status during human bone mesenchymal stem cell differentiation. *FEBS Lett*. 2008;582:2957-2964.
417. Murayama E, Kissa K, Zapata A, et al. Tracing hematopoietic precursor migration to successive hematopoietic organs during zebrafish development. *Immunity*. 2006;25:963-975.
418. Roman BL, Pham VN, Lawson ND, et al. Disruption of *acvr1l* increases endothelial cell number in zebrafish cranial vessels. *Development*. 2002;129:3009-3019.
419. Ma A, Lin R, Chan PK, et al. The role of survivin in angiogenesis during zebrafish embryonic development. *BMC Dev Biol*. 2007;7:50.
420. Thermes V, Grabher C, Ristoratore F, et al. I-SceI meganuclease mediates highly efficient transgenesis in fish. *Mech Dev*. 2002;118:91-98.
421. Grabher C, Joly JS, Wittbrodt J. Highly efficient zebrafish transgenesis mediated by the meganuclease I-SceI. *Methods Cell Biol*. 2004;77:381-401.
422. Larcher F, Murillas R, Bolontrade M, Conti CJ, Jorcano JL. VEGF/VPF overexpression in skin of transgenic mice induces angiogenesis, vascular hyperpermeability and accelerated tumor development. *Oncogene*. 1998;17:303-311.
423. Phung TL, Ziv K, Dabydeen D, et al. Pathological angiogenesis is induced by sustained Akt signaling and inhibited by rapamycin. *Cancer Cell*. 2006;10:159-170.
424. Rembold M, Lahiri K, Foulkes NS, Wittbrodt J. Transgenesis in fish: efficient selection of transgenic fish by co-injection with a fluorescent reporter construct. *Nat Protoc*. 2006;1:1133-1139.
425. Stemple DL, Solnica-Krezel L, Zwartkruis F, et al. Mutations affecting development of the notochord in zebrafish. *Development*. 1996;123:117-128.
426. Odenthal J, Haffter P, Vogelsang E, et al. Mutations affecting the formation of the notochord in the zebrafish, *Danio rerio*. *Development*. 1996;123:103-115.
427. Gansner JM, Madsen EC, Mecham RP, Gitlin JD. Essential role for fibrillin-2 in zebrafish notochord and vascular morphogenesis. *Dev Dyn*. 2008;237:2844-2861.

428. Gallagher BC, Sakai LY, Little CD. Fibrillin delineates the primary axis of the early avian embryo. *Dev Dyn.* 1993;196:70-78.
429. Cain SA, Baldwin AK, Mahalingam Y, et al. Heparan sulfate regulates fibrillin-1 N- and C-terminal interactions. *J Biol Chem.* 2008;283:27017-27027.
430. Tiedemann K, Batge B, Muller PK, Reinhardt DP. Interactions of fibrillin-1 with heparin/heparan sulfate, implications for microfibrillar assembly. *J Biol Chem.* 2001;276:36035-36042.
431. Kumar S, Hedges SB. A molecular timescale for vertebrate evolution. *Nature.* 1998;392:917-920.
432. Meng X, Noyes MB, Zhu LJ, Lawson ND, Wolfe SA. Targeted gene inactivation in zebrafish using engineered zinc-finger nucleases. *Nat Biotechnol.* 2008;26:695-701.

